Technical Report
TR-23-06
March 2023

Post-closure safety for SFR, the final repository for short-lived radioactive waste at Forsmark

Biosphere synthesis report, PSAR version

SVENSK KÄRNBRÄNSLEHANTERING AB

SWEDISH NUCLEAR FUEL
AND WASTE MANAGEMENT CO

Box 3091, SE-169 03 Solna
Phone +46 8 459 84 00
skb.se

ISSN 1404-0344
SKB TR-23-06
ID 1973884
March 2023

Post-closure safety for SFR, the final repository for short-lived radioactive waste at Forsmark

Biosphere synthesis report, PSAR version

Svensk Kärnbränslehantering AB

Keywords: Post-closure safety, SFR, Final repository, Low- and intermediate-level radioactive waste, Forsmark, Safety assessment, Biosphere object, Discharge areas, Dose assessment, Exposure pathways, Features, events and processes (FEP), Landscape development, Most exposed group, Non-human biota (NHB), Radionuclide transport, Site description, Surface ecosystems.

This report is published on www.skb.se

Summary

The final repository for short-lived radioactive waste (SFR) at Forsmark, Sweden, is used for the final disposal of low- and intermediate-level operational waste from Swedish nuclear facilities. The PSAR assessment of post-closure safety is an important part of the construction license application for the extension of SFR. This report constitutes one of the main references supporting the **Post-closure safety report** and describes the biosphere assessment, which is focused on the surface systems where humans and non-human biota potentially could be exposed to radionuclides released from the SFR repository.

The biosphere assessment is an integrated part of the overall post-closure safety assessment and the methodology is in line with the overall methodology, as well as being compatible with the IAEA BIOMASS methodology. Two methodological aspects that play a central role throughout the assessment are understanding the fate of radionuclides in the surface system and manging identified uncertainties.

As a starting point for the biosphere assessment, the present-day surface system is described in terms of climate, topography, regolith stratigraphy, near-surface hydrological conditions, chemical conditions, ecosystems, land-use and water resources management. This description is primarily derived from the site descriptive model for SR-PSU, i.e. the previous safety analysis for SFR. This description includes for example the digital elevation model (DEM) of the Forsmark area.

The description of the development of the future landscape in Forsmark that was derived in the previous safety assessment is considered to be valid also in the PSAR. This includes the development of topography and regolith, near-surface hydrological and chemical conditions, and the succession of marine, limnic and mire ecosystems. In particular, the site-specific coupled regolith-lake-development model (RLDM) from SR-PSU is used to simulate how shoreline regression and sedimentation/erosion processes shape regolith layers and drive ecosystem succession throughout the assessment period. It also includes a detailed description of the large-scale exchange of water between sea basins, and the flow of ground and near-surface water for a number of shoreline positions.

Areas that are expected to receive a substantial portion of the radionuclides following a release from the repository are identified with the help of the DEM and geohydrological particle tracking simulations that traces flow-paths from the repository. The identified areas are called biosphere objects. Given typical bedrock conditions most of the release from SFR is expected to be discharged into a gently sloping area north of the repository, referred to as biosphere object 157_2.

The biosphere transport and exposure model (BioTEx) is used to describe transport and accumulation of radionuclides in the ecosystems of identified biosphere objects. The model also calculates potential doses to humans and dose rates to non-human biota. Four potentially exposed groups are considered to cover all relevant exposure pathways; Hunter-gatherers, Infield–outland farmers, Drained mire farmers and Garden-plot households. The BioTEx model is similar to the one used in SR-PSU. However, the model was somewhat modified in the safety evaluation for SFL (SE-SFL), and these updates together with a few additional improvements, are included in the model used in the PSAR.

Due to the model updates a number of new parameters are also introduced in the PSAR. Where applicable, central values for these parameters are taken from SE-SFL and probability density functions (PDFs) are added. Collection of new site data (e.g. with respect to chlorine) and revisions of the calculations in SR-PSU also motivate updates of a few additional parameter values.

The joint effects of model and data updates are quantified by model comparisons. For most (80 %) of the radionuclides, the updates affect maximum doses by less than a factor of two, as compared to SR-PSU. However, a finer discretisation of the regolith profile increases the retention in the till, which for some radionuclides may reduce the doses by up to an order of magnitude (e.g. Tc-99 and Zr-93). In the PSAR exposure from a drilled well intersecting the release from SFR is evaluated for a small group. This new exposure pathway, in combination with model and data updates, increases the dose somewhat from radionuclides with a relatively short physical half-life. Finally, it is noted the updated values of plant-related parameters reduces the dose from Cl-36 by a factor of two. This is due to a lower accumulation in peat, which is considered to be in line with the understanding of Cl cycling at the site.

In the PSAR, a set of calculation cases are defined. In all of these, doses are evaluated using probabilistic calculations and a time dependent release from the geosphere. In the main scenario, that is propagated to the risk calculations, there are three calculation cases representing the range of probable future climate evolutions: the *present-day climate calculation case* is the *base case*, the *warm climate calculation case* and the *cold climate calculation case*.

The *base case* provides a reference point for all calculation cases. In this case present-day climate conditions prevail for the entire assessment period, and physical and biological properties of the ecosystems are constant. The geosphere release is discharged into biosphere object 157_2, and transport and accumulations in down-stream objects are simplified. The total annual dose throughout the assessment period is below the dose (14 μSv) that corresponds to the regulatory risk criterion, with a maximum annual dose of 5.6 μSv, occurring around 7000 AD. Draining and cultivation of a mire is the land-use variant resulting in the highest dose, primarily because radionuclides can accumulate in peat over a long period of time prior to exposure, and because the dose-contributing radionuclides predominantly yield dose through ingestion of food. Mo-93 and C-14 contribute most to the total dose from the time of repository closure up until the time around the dose maximum. Ca-41 dominates in the middle of the assessment period, and Ni-59 is most important at the end. The temporal dynamics of radionuclide specific annual doses largely depend on the geosphere release. However, radionuclide specific properties influence retention, decay, transport, accumulation, plant uptake and toxicity and thus affects both the temporal dynamics and the magnitude of the doses. The analysis confirms that the model behaviour is reasonable and conforms with SKB's general understanding of the surface systems at Forsmark.

In the *warmer climate calculation case* a warmer climate leads to a reduction of the maximum dose with respect to the *base case*. This response is primarily an effect of the prolonged period of submerged conditions that delays and reduces the geosphere release of C-14 and Mo-93 due to the lower groundwater flows and decay. In addition, radionuclide specific doses increase modestly due to higher groundwater uptake (C-14), and more accumulation of long-lived radionuclides (Ca-41 and Ni-59) due to dryer summers and lower groundwater flow. However, effects of increased irrigation practices do not increase the dose significantly.

In the *cold climate calculation case,* a colder climate is postulated to cause two periods of periglacial conditions during the second half of the assessment period. During these periods, the temperatures are sufficiently low to induce frozen bedrock and ground conditions so that geosphere releases are either restricted to discharge taliks or completely stopped. Doses during periglacial periods are at least one order of magnitude lower than in the *base case* at the corresponding time. The main reason is that cultivation and extraction of well water is prevented, and hunting and gathering is the main exposure pathway.

Three other (supporting) calculation cases are included in the main scenario to analyse specific uncertainties and evaluate the assumptions in the main scenario: the *timing of shoreline regression calculation case*, the *subhorizontal fracture calculation case*, and the *alternative landscape configuration calculation case*.

The uncertainty in projected global sea-level rise due to global warming is large. The *base case* and the *warm climate calculation case* cover the lower region of this range. The *timing of shoreline regression calculation case* covers the remaining uncertainty by postulating delays in shoreline regression between 0 and 20 000 years relative to the *base case*. As in the *warm climate calculation case*, longer submerged periods result in lower maximum total annual doses. The releases of radionuclides with longer half-lives, like Ca-41, can increase with a longer submerged period and result in higher maximum radionuclide-specific doses. However, such increases of radionuclide-specific doses are limited and maximum total doses do not exceed the maximum dose in the *base case*.

The *subhorizontal fracture calculation case* examines the effects of uncertainties associated with the location of the geosphere release. In this calculation case a hypothetical large subhorizontal fracture distributes the geosphere release between three biosphere objects. The fracture also modifies the discharge of groundwater from the bedrock. The analysis indicates that accumulation of activity after 40 000 AD could result in doses that are higher than in the *base case*. This happens if U-238, U-235 and their decay products accumulate in the relatively thick peat layer in a down-stream mire. However, the effect on the dose is modest, and uncertainties in the distribution of the release to different biosphere objects are unlikely to have any significant effects on the total maximum dose.

The *alternative landscape configuration calculation case* assesses uncertainties with respect to transport pathways and landscape development. Three alternative future landscape variants are analysed. In the *no stream* variant, radionuclides from object 157_2 are transported downstream through the surface regolith layers, and not via stream water as in the *base case*. The analysis indicates that accumulation of Ca-41, U-238, U-235 and its decay products could result in an elevated dose if the release reaches a relatively thick layer of peat in a down-stream mire. However, the effect on the dose is modest and the dose resulting from downstream peat accumulation never exceeds the maximum dose in object 157_2.

In the *release to surface water* variant, the geosphere release reaches surface water in object 157_2 directly and downstream lakes via the stream water. The minimal transport pathways from the geosphere to surface water, would lead to minimal losses of activity due to degassing (C-14) and/or radioactive decay. Doses from C-14, Pu-239 and Pu-240 to hunters and gatherers results in slightly higher doses around 4000 AD than in the *base case*, but never exceed the total maximum dose in the *base case*. Thus, uncertainties with respect to these aspects of transport pathways do not have any significant effect on the maximum dose. The variant also demonstrates that inclusion of the large lake in the *base case* ensures that exposure to C-14 in aquatic ecosystems is adequately assessed and that the rate of lake ingrowth has marginal effect on calculated doses.

Four additional supporting cases are used to further evaluate uncertainties and sensitivity in the parameters related to landscape and hydrology, ecosystem properties and the chemical development: the *alternative delineation calculation case*, the *mire object properties calculation case*, the *ecosystem properties calculation case*, and the *calcite depletion calculation case*. A simplified version of the BioTEx model was used for the first three of these cases. The novel hydrological sub-routine of this model allows for a probabilistic treatment of regolith thickness and groundwater flows that were not varied in the probabilistic simulations of the *base case*.

The *alternative delineation calculation case* assesses uncertainties with respect to the outlining of the original biosphere object 157_2 by comparisons with four alternative sub-areas of the original object. The case also illustrates how the size, position and properties of the biosphere object may affect environmental concentrations and resulting doses. A reduction in area together with low groundwater flow and thick regolith layers results in elevated radionuclide concentrations and doses in drained and cultivated soil. However, areas with such properties are reasonably less likely to receive large radionuclide releases from the geosphere and other counteracting factors tend to further reduce the effect on doses in relation to the differences in object properties.

The *mire object properties calculation case* evaluates the sensitivity of activity concentrations and annual doses to variation in object properties. The properties include object geometries, regolith thickness, and parameters that drive, or modify, groundwater flows. This case is a complement to the *alternative delineation calculation case*, that by varying object properties independently can disentangle the effects of individual properties that are correlated in the landscape. In general, doses are most sensitive to the size of the biosphere object, mainly since the diluting discharge of groundwater from the bedrock increase with size. Properties that control the discharge from the catchment and its vertical distribution also affects most radionuclides through dilution. A thicker till layer tends to decrease the dose from sorbing radionuclides, through the mechanisms of retardation and radioactive decay.

The *ecosystem properties calculation case*, evaluates the sensitivity of radionuclide-specific annual doses to variations in ecosystem parameters, and it identifies key drivers of uncertainty. Ecosystem parameters are used in the broadest sense, including regolith properties (e.g. porosity, density and saturation), characteristics of ecosystems (e.g. biomass density, and rates of primary production and mineralisation) and element-specific properties for regolith layers (sorption, i.e. K_d-values) and organism uptake (including *CR* values). The uncertainty in ecosystem parameters causes a maximum dose variation (90 % confidence interval) of a factor 3, 30, 50 and > 100 for C-14, Mo-93, Ca-41 and Ni-59 respectively. With the exception of C-14, this variation is mainly explained by the uncertainty in uptake in plants (*CR*) and animals (*TC*), and accumulation (i.e. sorption, K_d) in regolith layers that are cultivated. Retention (sorption) in the deep regolith also contributes.

The *calcite depletion calculation case* examines how changes in the future geochemistry may affect calculated doses. This is done by systematically shifting the K_d-values in regolith layers affected by the pH shifts associated with calcite depletion. In this case the mobility of elements that exist as anions (e.g. Mo) and those that form strong mobile complexes with carbonate (e.g. U) is decreased, whereas

the mobility of elements in cationic form is increased (e.g. Ni, Th, Ra, Pb and Cs). The decreased mobility has limited effect on the maximum dose from Mo-93 and U-238. However, retention of U-238 and U-235 becomes an important source of activity for decay products, and the maximum doses from all decay products increase. The increased mobility of cations results in a noticeable reduction of the dose from Ni-59, but has the opposite effect on the dose from Cs-135. The results suggest that while depletion of calcite may influence dose dynamics of individual radionuclides, this will not lead to a total dose that exceed the maximum total dose in the *base case*.

Exposures of non-human biota (NHB) are evaluated by calculating absorbed dose rates for the *base case* the *warmer climate*, the *colder climate* and the *alternative object delineation calculation cases*. For these calculations all concentration ratios (*CR*) are revised in the PSAR, as significant updates have been made to the literature database (Wildlife Transfer Database). As the ERICA methodology has been updated since SR-PSU, new dose conversion coefficients (*DCCs*) and occupancy factors (*OCC*) for NHB are also derived in the PSAR. In all calculation cases, the maximum dose rates are three orders of magnitude below the ERICA screening dose rate (10 μGy h^{-1}) and occur relatively early in the assessment period. The conclusion is that non-human biota will be unaffected by radionuclides released from the repository in the assessed scenarios. Since dose rates are relatively insensitive to the postulated span in climate conditions and object properties this conclusion is robust with respect to uncertainties in the future climate and the development of the landscape.

In summary, the *base case* provides a benchmark for the post-closure safety assessment and, thus, enables straightforward evaluation of differences with respect to other calculation cases. To facilitate efficient computations the representation of the biosphere system is simplified, and the landscape description is deterministic. Supporting calculations demonstrate that the maximum dose is robust with respect to the simplifying assumptions made. Moreover, it is shown that temporal dilution, due to the random shifts in the time for peak maximum, is unlikely to introduce any significant bias in the calculated annual average doses. Taken together, the analyses help to build confidence that the model results from the *base case* are reliable and credible. Thus, it is concluded that the surface system representation in the *base case* is appropriate and fit for purpose with respect to the demonstration of safety.

The results from the *warm climate* and *cold climate calculation case* are reasonable and consistent with SKB's general understanding of how climate affects the surface system. Thus, the two cases, together with the *base case*, adequately address relevant effects of future large-scale climate change that are part of the main scenario. The results from supporting calculation cases show that the maximum dose is relatively insensitive to transport pathways in the landscape, the rate of shoreline regression, the succession of ecosystems, and the leaching of calcite. Object properties clearly influence dose variation, but the responses to uncertainties in regolith thickness and near-surface hydrology are limited. In addition, trends of increasing doses for areas of small size and/or in areas with low bedrock discharge are likely to be counteracted by a reduced geosphere release. Taken together it is concluded that uncertainties in the landscape development and object properties are unlikely to have any significant influence on the calculated dose and the evaluation of the repository safety.

Sammanfattning

Slutförvaret för kortlivat radioaktivt avfall (SFR) i Forsmark, Sverige, används för slutförvaring av låg- och medelaktivt driftavfall från svenska kärntekniska anläggningar. Analysen av säkerhet efter förslutning i PSAR är en viktig del av ansökan om tillåtlighet för utbyggnaden av SFR. Denna rapport utgör en av huvudreferenserna till **Huvudrapporten säkerhet efter förslutning** och beskriver biosfärsanalysen, som fokuserar på de ytnära system där människor och andra organismer potentiellt kan exponeras för radionuklider från slutförvaret.

Biosfärsanalysen är en integrerad del av den övergripande analysen av säkerhet efter förslutning. Metodiken är i linje med den övergripande metodiken, och är kompatibel med IAEA BIOMASS metodiken. Två aspekter i metodiken som spelar en central roll genom hela analysen är förståelsen för radionukliders öde i de ytnära systemen och hantering av identifierade osäkerheter.

Som utgångspunkt för biosfärsanalysen beskrivs dagens ytnära system i termer av klimat, topografi, regolit-lagerföljd, ytnära hydrologiska förhållanden, kemiska förhållanden, ekosystem, markanvändning och hushållning av vattenresurser. Denna beskrivning härrör i första hand från den platsbeskrivande modellen för SR-PSU, det vill säga den tidigare säkerhetsanalysen för SFR. Beskrivningen inkluderar till exempel den digitala höjdmodellen (DEM) av Forsmarksområdet.

Beskrivningen av utvecklingen av det framtida landskapet i Forsmark som togs fram i den föregående säkerhetsanalysen bedöms som giltig även för PSAR. Detta inkluderar utvecklingen av topografi och regolit, ytnära hydrologiska och kemiska förhållanden, och successionen av marina, limniska och våtmarksekosystem. Den platsspecifika utvecklingsmodellen för regolit och sjöar (”regolith-lake development model”, RLDM) från SR-PSU används för att simulera hur strandlinjeförskjutningen och sedimentations-/erosionsprocesser formar regolitlager och driver successionen av ekosystem under analysperioden. Den innehåller också en detaljerad beskrivning av det storskaliga utbytet av vatten mellan havsbassänger och flödet av grundvatten och ytnära vatten för ett antal strandlinjepositioner.

Områden som förväntas ta emot en betydande del av radionukliderna efter utsläpp från förvaret identifieras med hjälp av DEM och geohydrologiska partikelspårningssimuleringar som beskriver flödesvägar från förvaret. De identifierade områdena kallas biosfärsobjekt. Givet typiska berggrundsförhållanden förväntas det mesta av utsläppet från SFR att nå ett svagt sluttande område norr om förvaret, kallat biosfärsobjekt 157_2.

Biosfärsmodellen för transport och exponering (BioTEx) används för att beskriva transport och ackumulering av radionuklider i de identifierade biosfärsobjektens ekosystem. Modellen beräknar också potentiella doser till människor och dosrater till andra organismer (än människa). Fyra potentiellt exponerade grupper bedöms täcka alla relevanta exponeringsvägar; jägare och samlare, inägo-utmarksjordbrukare, jordbrukare på dikad myr och hushåll med kökträdgård. BioTEx-modellen är snarlik den som användes i SR-PSU. Modellen modifierades dock något i säkerhetsvärderingen för SFL (SE-SFL), och dessa uppdateringar, tillsammans med några ytterligare förbättringar, ingår i modellen som används i PSAR.

På grund av modelluppdateringarna introduceras även ett antal nya parametrar i PSAR. När det är möjligt hämtas centralvärden för dessa parametrar från SE-SFL och täthetsfunktioner (PDF) läggs till. Insamling av ny platsdata (t ex med avseende på klor) och revideringar av beräkningarna i SR-PSU leder även till uppdateringar av ytterligare några parametervärden.

Den sammanlagda effekten av modell- och datauppdateringar kvantifieras genom modelljämförelser. För de flesta (80 %) av radionukliderna påverkar uppdateringarna dosmaximum med mindre än en faktor två, jämfört med SR-PSU. En finare diskretisering av regolitprofilen ökar dock kvarhållningen i moränen, vilket för vissa radionuklider (till exempel Tc-99 och Zr-93) kan minska doserna med upp till en storleksordning. I PSAR utvärderas exponeringen från en borrad brunn som korsar utsläppet från SFR för en liten grupp. Denna nya exponeringsväg, i kombination med modell- och datauppdateringar, ökar dosen något från radionuklider med relativt kort fysikalisk halveringstid. Slutligen kan det noteras att de uppdaterade värdena för växtrelaterade parametrar minskar dosen från Cl-36 med en faktor två. Detta beror på en lägre ackumulation i torv, vilket stämmer överens med förståelsen av omsättningen av klor på platsen.

I PSAR definieras en uppsättning beräkningsfall. I alla dessa utvärderas doser med probabilistiska beräkningar och tidsberoende utsläpp från geosfären. Huvudscenariot, vars resultat förs vidare till riskberäkningarna, består av tre beräkningsfall som representerar spannet av en sannolik framtida klimatutveckling: beräkningsfallet med *dagens klimat* är *basfallet*, samt beräkningsfallen med *varmt klimat* och *kallt klimat*.

Basfallet är utgångspunkten för alla beräkningsfall. I detta beräkningsfall råder dagens klimatförhållanden under hela bedömningsperioden och ekosystemens fysikaliska och biologiska egenskaper är oförändrade. Geosfärutsläppet når biosfärsobjekt 157_2 och transport och ackumulering i nedströmsobjekt är förenklade. Den totala årsdosen under hela analysperioden är under den dos (14 μSv) som motsvarar riskkriteriet i föreskrifterna, med en maximal årlig dos på 5,6 μSv, som inträffar omkring 7000 e Kr. Uppodling av en dränerad myr är den markanvändningsvariant som ger den högsta dosen, främst på grund av att radionuklider kan ackumuleras i torv under lång tid före exponering, och för att de dosbidragande radionukliderna främst ger dos genom intag av föda. Mo-93 och C-14 bidrar mest till den totala dosen från tidpunkten för förvarets förslutning fram till tiden kring dosmaximum. Ca-41 dominerar i mitten av analysperioden och Ni-59 är viktigast mot slutet. Tidsdynamiken för den radionuklidspecifika årliga dosen beror till stor del på geosfärsutsläppen men modifieras av radionuklidspecifika egenskaper. Dessa egenskaper påverkar t ex fördröjning, sönderfall, transport, ackumulering, växtupptag och toxicitet. Analysen bekräftar att modellen beter sig rimligt och överensstämmer med SKB:s allmänna uppfattning om de ytnära systemen i Forsmark.

I beräkningsfallet med *varmt klimat* leder ett varmare klimat till en minskning av den maximala dosen i förhållande till *basfallet*. Detta är främst en effekt av den längre perioden av havstäckta förhållanden som fördröjer och reducerar geosfärsutsläppet av C-14 och Mo-93 på grund av de lägre grundvattenflödena och sönderfall. Dessutom ökar de radionuklidspecifika doserna något på grund av högre grundvattenupptag (C-14), och mer ackumulering av långlivade radionuklider (Ca-41 och Ni-59) på grund av torrare somrar och lägre grundvattenflöde. En utökad användning av bevattning leder emellertid inte till någon signifikant ökning av dosen.

I beräkningsfallet med *kallt klimat* postuleras det att ett kallare klimat orsakar två perioder med permafrost under andra hälften av analysperioden. Under dessa perioder är temperaturerna tillräckligt låga för att orsaka frusna förhållanden i berggrunden och i marken så att geosfärsutsläppen antingen begränsas till talikar eller helt avstannar. Doser under permafrostperioder är minst en storleksordning lägre än i *basfallet* vid motsvarande tidpunkter. Främsta anledningen är att odling och uttag av brunnsvatten inte förekommer, och den huvudsakliga exponeringsvägen är via jakt och insamling av föda.

Ytterligare tre (stödjande) beräkningsfall ingår i huvudscenariot. Dessa belyser betydelsen av specifika osäkerheter och utvärderar antaganden i huvudscenariot: beräkningsfallen för *tidpunkt för strandlinjeregression*, *subhorisontell spricka* och *alternativa transportvägar i landskapet*.

Osäkerheten i den uppskattade globala havsnivåhöjningen på grund av den globala uppvärmningen är stor. *Basfallet* och beräkningsfallet för *varmt klimat* täcker den nedre delen av detta spann. Beräkningsfallet *tidpunkt för strandlinjeregression* täcker den återstående osäkerheten genom att postulera fördröjningar i strandlinjeförskjutningen mellan 0 och 20 000 år i förhållande till *basfallet*. Liksom i beräkningsfallet med *varmt klimat* leder längre havstäckta perioder till lägre maximala totala årliga doser. Utsläppen av radionuklider med en längre halveringstid, som Ca-41, kan öka med en längre havstäckt period och leda till högre maximala radionuklidspecifika doser. Sådana ökningar av radionuklidspecifika doser är dock begränsade och maximala totala doser överstiger aldrig den maximala dosen i *basfallet*.

Beräkningsfallet *subhorisontell spricka* utvärderar effekterna av osäkerheter förknippade med platsen för geosfärutsläppet. I detta beräkningsfall fördelar en stor hypotetisk subhorisontell spricka geosfärutsläppet mellan tre biosfärsobjekt. Sprickan modifierar även utströmningen av grundvatten från berggrunden. Analysen pekar på att ackumulering av aktivitet efter 40 000 e Kr kan leda till doser som är högre än i *basfallet*. Detta händer om U-238, U-235 och deras sönderfallsprodukter ackumuleras i ett relativt tjockt torvlager i en myr nedströms. Effekten på dosen är dock ringa, och osäkerheter i den rumsliga spridningen av utsläppet till olika biosfärsobjekt kommer sannolikt inte att ha några signifikanta effekter på den totala maximala dosen.

Beräkningsfallet *alternativa transportvägar i landskapet* utvärderar osäkerheter med avseende på transportvägar och landskapsutveckling. Tre alternativa framtida landskapsvarianter analyseras. I varianten *inget vattendrag* transporteras radionuklider från objekt 157_2 nedströms genom de ytliga regolitlagren och inte via vattendraget som i *basfallet*. Analysen visar att ackumulationen av Ca-41, U-238, U-235 och dess sönderfallsprodukter kan resultera i en förhöjd dos om utsläppet når ett relativt tjockt torvlager i en nedströms myr. Effekten på dosen är dock ringa och dosen till följd av ackumulation i torv nedströms överstiger aldrig den maximala dosen i objekt 157_2.

I varianten *utsläpp till ytvatten* når geosfärutsläppet ytvatten direkt i objekt 157_2 och sjöarna nedströms via vattendraget. De minimala transportvägarna från geosfären till ytvatten leder till ytterst små förluster av aktivitet via frigörelse av gasformigt kol (C-14) och/eller radioaktivt sönderfall. Doser från C-14, Pu-239 och Pu-240 till jägare och samlare resulterar i något högre doser runt 4000 e Kr än i *basfallet*, men överskrider aldrig den totala maximala dosen i *basfallet*. Osäkerheter med avseende på dessa aspekter av transportvägar har således inte någon signifikant effekt på den maximala dosen. Varianten visar också att den stora sjön i *basfallet* säkerställer att exponeringen för C-14 i akvatiska ekosystem är adekvat beräknad och att hastigheten som sjön växer igen med har marginell effekt på beräknade doser.

Ytterligare fyra stödjande fall utvärderar osäkerheter och känslighet i parametrarna relaterade till landskap och hydrologi, ekosystemegenskaper och den kemiska utvecklingen: beräkningsfallen för *alternativa objektsavgränsningar*, *myrobjektegenskaper*, *ekosystemegenskaper* och *kalciturlakning*. En förenklad version av BioTEx-modellen användes för det första av dessa tre fall. Den nya hydrologiska subrutinen i denna modell möjliggör en probabilistisk hantering av regolittjocklek och grundvattenflöden som inte varieras i de probabilistiska simuleringarna av *basfallet*.

Beräkningsfallet för *alternativa objektsavgränsningar* utvärderar osäkerheter med avseende på avgränsningarna av det ursprungliga biosfärsobjektet 157_2 genom jämförelser med fyra alternativa delområden av det ursprungliga objektet. Fallet illustrerar också hur biosfärsobjektets storlek, position och egenskaper kan påverka miljökoncentrationer och resulterande doser. En minskning av arean tillsammans med lågt grundvattenflöde och tjocka regolitlager resulterar i förhöjda radionuklidkoncentrationer och doser i dikad och odlad mark. Det är dock mindre troligt att områden med sådana egenskaper kommer få stora radionuklidutsläpp från geosfären och andra motverkande faktorer tenderar att ytterligare minska effekten på doser i förhållande till skillnaderna i objektets egenskaper.

Beräkningsfallet för *myrobjektegenskaper* utvärderar känsligheten i aktivitetskoncentrationer och årliga doser för variation i objektegenskaper. Egenskaperna inkluderar objektgeometrier, regolittjocklek och parametrar som styr eller påverkar grundvattenflöden. Detta fall är ett komplement till beräkningsfallet för *alternativa objektsavgränsningar*, som genom att oberoende variera objektegenskaper kan isolera effekterna av enskilda egenskaper som är korrelerade i landskapet. Generellt sett är dosen mest känsliga för storleken på biosfärsobjektet, främst eftersom utströmning av utspädande grundvatten från berggrunden ökar med objektstorlek. Egenskaper som styr utströmning från avrinningsområdet och dess vertikala fördelning påverkar också de flesta radionuklider via utspädning. Ett tjockare moränlager tenderar att minska dosen från sorberande radionuklider, genom fördröjningsmekanism och radioaktivt sönderfall.

Beräkningsfallet för *ekosystemegenskaper* utvärderar känsligheten hos radionuklidspecifika årliga doser för variationer i ekosystemparametrar och identifierar nyckelfaktorer för osäkerhet. Ekosystemparametrar används i vid bemärkelse, och inkluderar egenskaper hos regoliten (t ex porositet, densitet och mättnadsgrad), egenskaper hos ekosystemen (t ex biomassadensitet och primärproduktions- och mineraliseringshastigheter) och elementspecifika egenskaper för regolitlager (sorption, K_d-värden) och upptag i organismer (inklusive *CR*-värden). Osäkerheten i ekosystemparametrar leder till en maximal variation i dosen (90 % konfidensintervall) på en faktor 3, 30, 50 och > 100 för C-14, Mo-93, Ca-41 respektive Ni-59. Med undantag för C-14 förklaras denna variation främst av osäkerheten i upptag i växter (CR) och djur (*TC*), och ackumulering (sorption, K_d) i odlade regolitlager. Fördröjning (sorption) i den djupa regoliten bidrar också.

Beräkningsfallet för *kalciturlakning* granskar hur förändringar i den framtida geokemin kan påverka beräknade doser. Detta görs genom att systematiskt ändra K_d-värdena i regolitlager som påverkas av pH-förändringarna i samband med kalciturlakning. I detta beräkningsfall minskas mobiliteten för element som existerar som anjoner (t ex Mo) och de som bildar starka mobila komplex med karbonat

(t ex U), medan mobiliteten för element i katjonisk form ökas (t ex Ni, Th, Ra, Pb och Cs). Den minskade mobiliteten har begränsad effekt på den maximala dosen från Mo-93 och U-238. Ackumulation av U-238 och U-235 blir dock en viktig källa för aktivitet av sönderfallsprodukter, och de maximala doserna från alla sönderfallsprodukter ökar. Katjonernas ökade mobilitet leder till en påtaglig minskning av dosen från Ni-59, men har motsatt effekt på dosen från Cs-135. Resultaten tyder på att även om urlakningen av kalcit kan påverka dosdynamiken för enskilda radionuklider, kommer detta inte att leda till en total dos som överstiger den maximala totala dosen i *basfallet*.

Exponeringar av andra organismer än människa (*non human biota*, NHB) utvärderas genom att beräkna absorberade dosrater för *basfallet*, beräkningsfallen med *varmt klimat*, *kallt klimat* och *alternativa objektsavgränsningar*. Alla koncentrationskvoter (*CR*) är reviderade i PSAR för dessa beräkningar, eftersom betydande uppdateringar har gjorts av litteraturdatabasen (Wildlife Transfer Database). Eftersom ERICA-metodiken har uppdaterats sedan SR-PSU, har nya dosomvandlingskoefficienter (*DCC*) och vistelsefaktorer (*OCC*) för NHB tagits fram i PSAR. I alla beräkningsfall är de maximala dosraterna tre storleksordningar under ERICA-screeningsdosraten (10 μGy h^{-1}) och inträffar relativt tidigt i analysperioden. Slutsatsen är att andra organismer (än människa) kommer att vara opåverkad av radionuklider som släpps ut från förvaret i de utvärderade scenarierna. Eftersom dosraterna är relativt okänsliga för det postulerade spannet i klimatförhållanden och objektegenskaper bedöms slutsatsen vara robust med avseende på osäkerheter i det framtida klimatet och utvecklingen av landskapet.

Sammanfattningsvis utgör *basfallet* en måttstock för analysen av säkerhet efter förslutning och möjliggör en rättfram utvärdering av skillnader mellan beräkningsfall. För att underlätta effektiva beräkningar förenklas representationen av biosfärsystemet i detta fall och landskapsbeskrivningen är deterministisk. Stödjande beräkningar visar att den maximala dosen är robust med avseende på de förenklade antaganden som gjorts. Dessutom har det visat sig att tidsutspädning, på grund av slumpmässiga ändringar i tiden för toppens maximum, sannolikt inte introducerar någon signifikant bias i de beräknade årliga medeldoserna. Sammantaget bidrar analyserna till att bygga upp förtroende för att modellresultaten från *basfallet* är tillförlitliga och trovärdiga. Således dras slutsatsen att representationen av det ytnära systemet i *basfallet* är lämplig och ändamålsenlig med avseende på demonstrationen av säkerhet.

Resultaten från beräkningsfallen med *varmt klimat* och *kallt klimat* bedöms vara rimliga och förenliga med SKB:s allmänna förståelse för hur klimatet påverkar det ytnära systemet. De två fallen, tillsammans med *basfallet*, belyser relevanta effekter av framtida storskaliga klimatförändringar som är en del av huvudscenariot. Resultaten från stödjande beräkningsfall visar att den maximala dosen är relativt okänslig för transportvägar i landskapet, strandlinjeförskjutningens hastighet, ekosystemens succession och kalciturlakning. Objektegenskaper påverkar tydligt dosvariationen, men responsen på osäkerheter i regolittjocklek och ytnära hydrologi är begränsade. Dessutom kommer trender med ökande doser för små områden och/eller i områden med låg utströmning från berget sannolikt att motverkas av ett minskat geosfärutsläpp i sådana områden. Sammantaget dras slutsatsen att osäkerheter i landskapsutvecklingen och objektegenskaperna sannolikt inte kommer att ha någon signifikant inverkan på den beräknade dosen och utvärderingen av förvarets säkerhet.

Contents

1 Introduction

This document is one of the main references to the **Post-closure safety report** that contributes to the preliminary safety analysis report (PSAR) for SFR, the repository for short-lived radioactive waste at Forsmark in Östhammar municipality, Sweden (Figure 1-1). This chapter gives the background and a short overview of the PSAR post-closure safety assessment undertaken as part of the construction license application for the extension of SFR. Moreover, the purpose and content of this report are described.

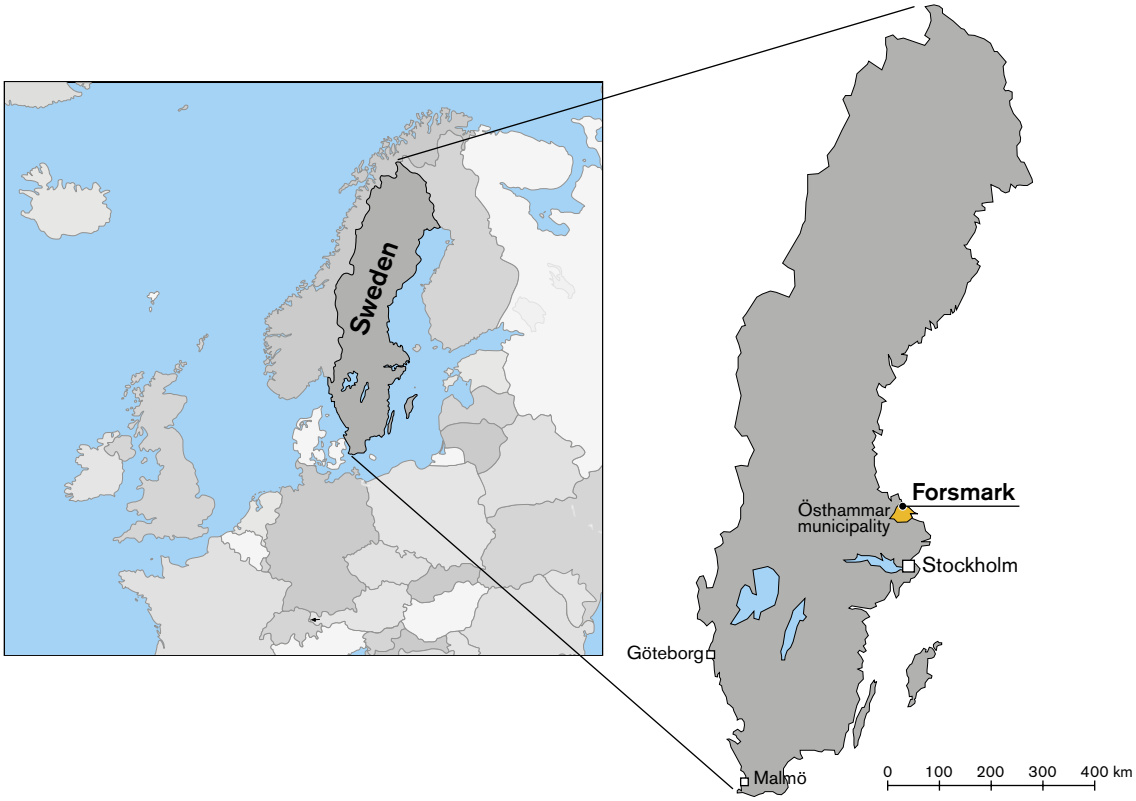

Figure 1-1. *Map showing the location of Forsmark. Forsmark is situated in Östhammar municipality, which belongs to the County of Uppsala.*

1.1 Background

SFR is operated by the Swedish Nuclear Fuel and Waste Management Company, SKB, and is part of the Swedish system for management of waste from nuclear power plants, other nuclear activities, industry, research and medical care. In addition to SFR, the Swedish nuclear waste management system also includes the repository for spent nuclear fuel and the repository for long-lived radioactive waste (SFL) (Figure 1-2).

SFR consists of the existing part, SFR1 (Figure 1-2, grey part), and the extension, SFR3 (Figure 1-2, blue part). SFR1 is designed for disposal of short-lived low- and intermediate-level waste produced during operation of the Swedish nuclear power reactors, as well as waste generated during applications of radioisotopes in medicine, industry, and research. This part was taken into operation in 1988. SFR3 is designed primarily for disposal of short-lived low- and intermediate-level waste from decommissioning of nuclear facilities in Sweden. The extension is called SFR3 since the name SFR2 was used in a previous plan to build vaults adjacent to SFR1. The repository is currently estimated to be closed by year 2075.

The SFR waste vaults are located below the Baltic Sea and are connected to the ground surface via two access tunnels. SFR1 consists of one 70-metre-high waste vault (silo) and four 160-metre-long waste vaults (1BMA, 1–2BTF and 1BLA), covered by about 60 metres of bedrock. SFR3 consists of six waste vaults (2BMA, 1BRT and 2–5BLA), varying in length from 255 to 275 m, covered by about 120 metres of bedrock.

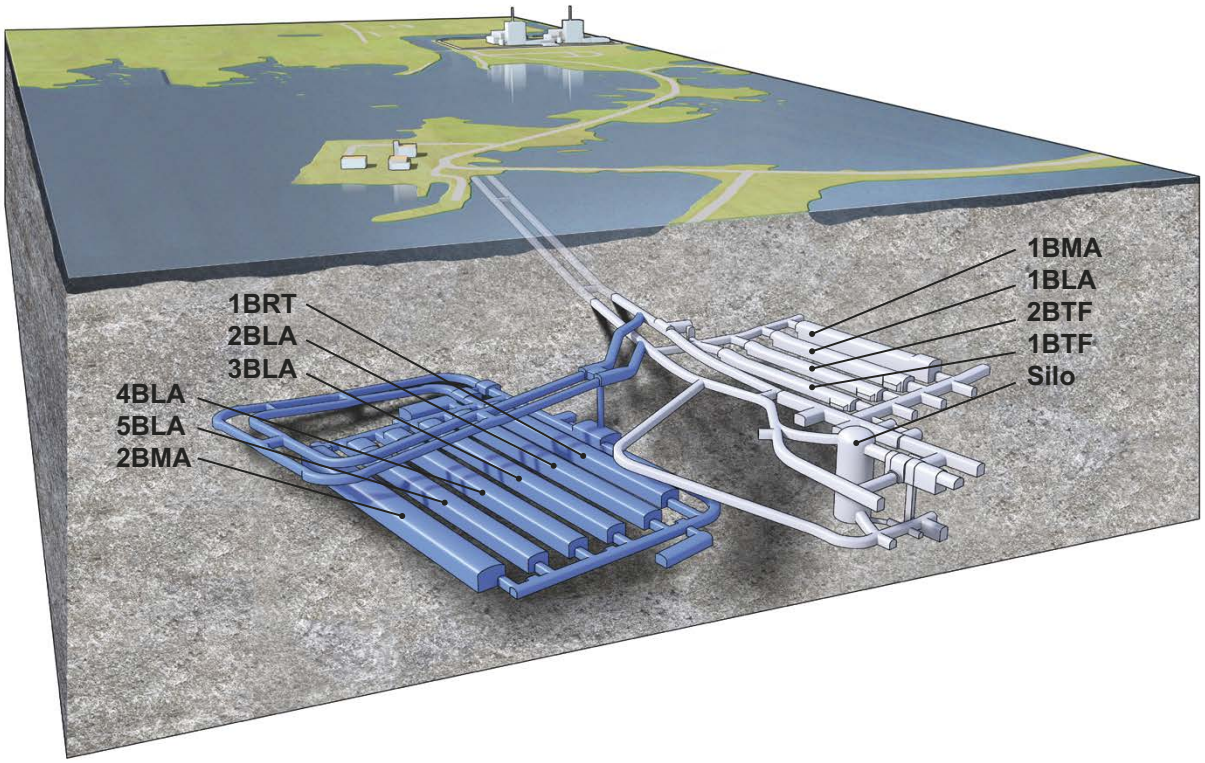

Figure 1-2. *Schematic illustration of SFR. The grey part is the existing repository (SFR1) and the blue part is the extension (SFR3). The waste vaults in the figure are the silo for intermediate-level waste, 1–2BMA vaults for intermediate-level waste, 1BRT vault for reactor pressure vessels, 1–2BTF vaults for concrete tanks and 1–5BLA vaults for low-level waste.*

A prerequisite for the extension of SFR is the licensing of the extended facility. The licensing follows a stepwise procedure. In December 2014, SKB submitted two licence applications to extend and continue the operation of SFR, one to the Swedish Radiation Safety Authority (SSM) for permission under the Act on Nuclear Activities (SFS 1984:3) and one to the Land and Environment Court for permissibility under the Environmental Code (SFS 1998:808). In October 2019 SSM submitted their pronouncement to the Swedish Government and recommended approval of the permission sought by SKB. In November 2019 the Court submitted its statement to the Swedish Government and recommended approval of the licence application. The Swedish Government granted permit and permissibility in December 2021.

The current step in the licensing of the extended SFR is the processing of the construction license application, submitted by SKB to SSM for review under the Act on Nuclear Activities. The licence documentation consists of an application document and a set of supporting documents. A central supporting document is the preliminary safety analysis report (PSAR), with a general part consisting of ten chapters[1]. Chapter 9 of the general part of that report addresses post-closure safety. The **Post-closure safety report** is the main reference to Chapter 9, and this report is a main reference to the **Post-closure safety report**.

1.2 Post-closure safety assessment

1.2.1 Overview

The main role of the post-closure safety assessment is to demonstrate that SFR is radiologically safe for humans and the environment after closure. This is done by evaluating compliance with respect to the Swedish Radiation Safety Authority's regulations concerning post-closure safety and the protection of human health and the environment. Furthermore, the post-closure safety assessment is being successively developed in the stepwise licensing process for the extended SFR, and thus the results from the PSAR assessment[2] provide input to the forthcoming updated assessment to be carried out before trial operation of the facility.

The overall aim in developing a geological repository for nuclear waste is to ensure that the amounts of radionuclides reaching the accessible biosphere are such that possible radiological consequences are acceptably low at all times. Important aspects of the regulations are that post-closure safety shall be maintained through a system of passive barriers. The barrier system of SFR comprises engineered and natural barriers, and the function of each barrier is to, in one or several ways, contribute to the containment and prevention or retention of dispersion of radioactive substances, either directly or indirectly by protecting other barriers in the barrier system. To achieve post-closure safety, two safety principles have been defined. *Limitation of the activity of long-lived radionuclides* is achieved by only accepting waste for disposal that conforms with the waste acceptance criteria for SFR. *Retention of radionuclides* is achieved by the function of the engineered and natural barriers. The two safety principles are interlinked and applied in parallel. The engineered barrier system is designed for an inventory that contains a limited amount of long-lived radionuclides, given the conditions at the selected site and the natural barriers.

The basis for evaluating compliance is a safety assessment methodology that conforms to the regulatory requirements regarding methodology, and that supports the demonstration of regulatory compliance regarding post-closure safety and the protection of human health and the environment. The overall safety assessment methodology applied is described in the **Post-closure safety report**, Chapter 2. The methodology was developed in SR-PSU (SKB TR-14-01[3]) based on SKB's previous safety assessment for SFR1 (SAR-08, SKB R-08-130). Further, it is consistent with the methodology used for the post-closure safety assessment for the final repository for spent nuclear fuel to the extent appropriate given the different nature of the two repositories.

[1] SKB, 2022. PSAR SFR – Allmän del kapitel 1 – Introduktion. SKBdoc 1702853 ver 3.0, Svensk Kärnbränslehantering AB. (In Swedish.) (Internal document.)

[2] For brevity, the PSAR post-closure safety assessment for SFR is also referred to as "the PSAR assessment" or "the PSAR" in the present report.

[3] For SKB reports without named authors, the report number is used instead of publication year when referring to them in the text.

1.2.2 Report hierarchy

The **Post-closure safety report** and main references for the post-closure safety assessment are listed and briefly described in Table 1-1, also including the abbreviated titles (in bold) by which they are identified in the text. Furthermore, there are numerous additional references that include documents compiled either by SKB or other organisations, or that are available in the scientific literature, as indicated in Figure 1-3.

Table 1-2 lists the key background reports used in the PSAR that are related to the biosphere assessment, with a brief description of their content. In addition to regular reports, Table 1-2 also lists the documents that were produced as complementary information to the SR-PSU biosphere assessment as respond to issues raised in the regulatory review. The relationships between the key background reports to the biosphere assessment and the main references are illustrated in Figure 1-4.

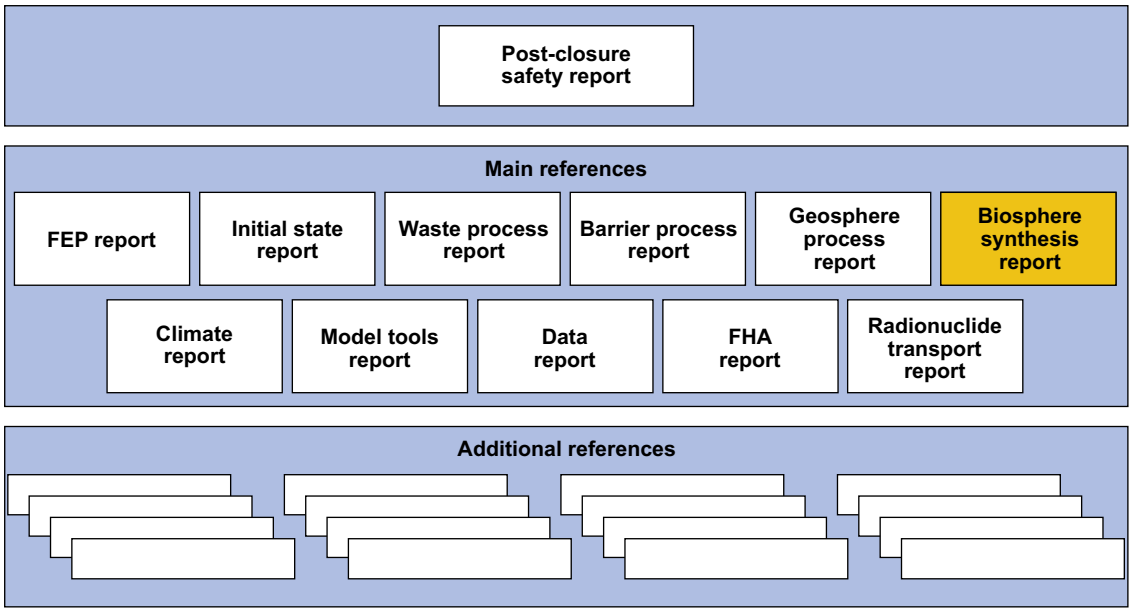

Figure 1-3. *The hierarchy of the Post-closure safety report, main references and additional references in the post-closure safety assessment. The present report is high-lighted in yellow.*

Table 1-1. Post-closure safety report and main references for the post-closure safety assessment. The reports are available at www.skb.se.

Abbreviated title by which the reports are identified in this report Report number	Content
Post-closure safety report SKB TR-23-01	The main report of the PSAR post-closure safety assessment for SFR.
Initial state report SKB TR-23-02	Description of the expected conditions (state) of the repository at closure. The initial state is based on verified and documented properties of the repository and an assessment of its evolution during the period up to closure.
Waste process report SKB TR-23-03	Description of the current scientific understanding of the processes in the waste form and in the packaging that have been identified in the FEP processing as potentially relevant for the post-closure safety of the repository. Reasons are given as to why each process is handled in a particular way in the safety assessment.
Barrier process report SKB TR-23-04	Description of the current scientific understanding of the processes in the engineered barriers that have been identified in the FEP processing as potentially relevant for the post-closure safety of the repository. Reasons are given as to why each process is handled in a particular way in the safety assessment.
Geosphere process report SKB TR-14-05	Description of the current scientific understanding of the processes in the geosphere that have been identified in the FEP processing as potentially relevant for the post-closure safety of the repository. Reasons are given as to why each process is handled in a particular way in the safety assessment.
Climate report SKB TR-23-05	Description of the current scientific understanding of climate and climate-related issues that have been identified in the FEP processing as potentially relevant for the post-closure safety of the repository. Description of the current scientific understanding of the future evolution of climate and climate-related issues.
Biosphere synthesis report SKB TR-23-06 (this report)	Description of the present-day conditions of the surface systems at Forsmark, and natural and anthropogenic processes driving the future development of those systems. Description of the modelling performed for landscape development, radionuclide transport in the biosphere and potential exposure of humans and non-human biota. (This report)
FEP report SKB TR-14-07	Description of the establishment of a catalogue of features, events and processes (FEPs) that are potentially relevant for the post-closure safety of the repository.
FHA report SKB TR-23-08	Description of the handling of inadvertent future human actions (FHA) that are defined as actions potentially resulting in changes to the barrier system, affecting, directly or indirectly, the rate of release of radionuclides, and/or contributing to radioactive waste being brought to the surface. Description of radiological consequences of FHAs that are analysed separately from the main scenario.
Radionuclide transport report SKB TR-23-09	Description of the radionuclide transport and dose calculations carried out for the purpose of demonstrating compliance with the radiological risk criterion.
Data report SKB TR-23-10	Description of how essential data for the post-closure safety assessment are selected, justified and qualified through traceable standardised procedures.
Model tools report SKB TR-23-11	Description of the model tool codes used in the safety assessment.

Table 1-2. Background reports for the biosphere assessment in the PSAR.

Document number	Full title	Brief description and reference in text
Produced within SR-Site Biosphere		
TR-10-01	The terrestrial ecosystems at Forsmark and Laxemar-Simpevarp.	Synthesis of the knowledge of the terrestrial ecosystems, Löfgren (2010)
TR-10-02	The limnic ecosystems at Forsmark and Laxemar-Simpevarp.	Synthesis of the knowledge of the limnic ecosystems, Andersson (2010)
TR-10-03	The marine ecosystems at Forsmark and Laxemar-Simpevarp.	Synthesis of the knowledge of the marine ecosystems, Aquilonius (2010)
Produced within SR-PSU Biosphere		
R-12-03	Digital elevation model of Forsmark. SR-PSU Biosphere.	Presentation of the digital elevation model (DEM), Strömgren and Brydsten (2013).
R-13-01	K_d and CR used for transport calculations in the biosphere in SR-PSU.	Compilation of element-specific parameter values used in the biosphere transport calculations, Tröjbom et al. (2013).
R-13-18	Biosphere parameters used in radionuclide transport modelling and dose calculations in SR-PSU.	Descriptions of all biosphere parameters used in the radionuclide model for the biosphere, Grolander (2013).
R-13-19	Hydrology and near-surface hydrogeology at Forsmark – synthesis for the SR-PSU project. SR-PSU Biosphere.	Modelling results and descriptions of present and future hydrological and near-surface hydrogeological conditions at Forsmark, Werner et al. (2013).
R-13-22	Depth and stratigraphy of regolith at Forsmark. SR-PSU Biosphere.	Presentation of the regolith depth model (RDM), Sohlenius et al. (2013a).
R-13-27	Landscape development in the Forsmark area from the past into the future (8500 BC to 40 000 AD).	Description and results from the regolith-lake development model (RLDM), Brydsten and Strömgren (2013).
R-13-46	The biosphere model for radionuclide transport and dose assessment in SR-PSU.	Description of the model for radionuclide transport and exposure in the biosphere, Saetre et al. (2013a).
R-14-02	Handling of biosphere FEPs and recommendations for model development in SR-PSU.	Descriptions of the handling of Features, Events and Processes (FEPs) in the biosphere assessment, and the exposure pathway analysis, (SKB R-14-02).
Response to regulatory review of SR-PSU		
SKBdoc 1554499	Drainage of runoff water from 157_2 into 157_1 via a stream – Biosphere complementary information for SR-PSU.	A supplementary study of potential effects of the presence of a stream between object 157_2 and 157_1, Saetre and Ekström (2016).
SKBdoc 1571087	Kompletterande beräkningar om biosfärsobjekt (in Swedish).	Additional calculations to evaluate uncertainties in the landscape development modelling, Saetre and Ekström (2017a).
SKBdoc 1581297	Additional considerations for the non-human biota dose assessment in the SR-PSU.	Supplementary information related to effects of various assumptions, and the importance of updates in modelling tool and parameter values, Jaeschke and Grolander (2017).
SKBdoc 1581608	Konvergens av probabilistiska beräkningar (in Swedish).	Study of convergence in probabilistic calculations, Ekström (2017).
SKBdoc 1601415	Svar till SSM på begäran om komplettering av ansökan om utökad verksamhet vid SFR angående konsekvensanalys (in Swedish).	Response to questions related to consequence analsysis, Saetre and Lindgren (2017).
SKBdoc 1610560	Kompletterande beräkningar för gasavgång (in Swedish).	Supplementary sensitivity analysis related to gas transport in agricultural ecosystems, Saetre and Ekström (2017b).
Produced within SE-SFL		
TR-19-05	Biosphere synthesis for the safety evaluation SE-SFL.	Synthesis of the biosphere assessment undertaken as an integral part of the safety evaluation, (SKB TR-19-05).
TR-19-06	Radionuclide transport and dose calculations for the safety evaluation SE-SFL.	Description of the calculations of the release and transport of radionuclides from the waste, via the repository near-field, the geosphere, and through the biosphere, (SKB TR-19-06).
R-19-18	Biosphere parameters used in radionuclide transport modelling and dose calculations in SE-SFL.	Describes all biosphere parameters used in the radionuclide model for the biosphere, Grolander and Jaeschke (2019).
Produced within the PSAR		
P-18-02	SR-PSU (PSAR) Bedrock hydrogeology TD18 – Temperate climate conditions.	Bedrock hydrogeology, Öhman and Odén (2018).

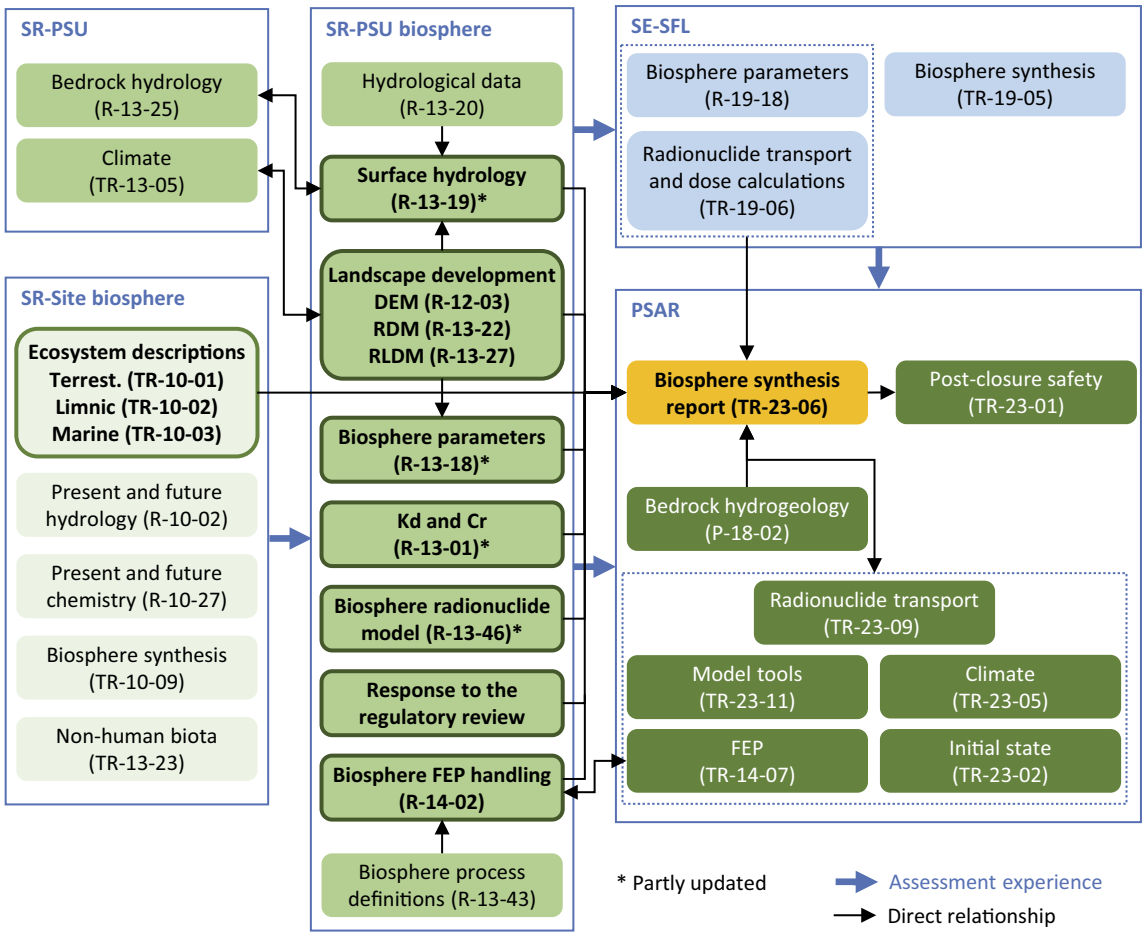

Figure 1-4. *Relationship between reports, relevant for the biosphere assessment, produced in the PSAR and biosphere-related reports produced within earlier SKB biosphere assessments. The present report is marked in orange and bold. Supporting documents produced within other biosphere assessments focusing on the Forsmark site are shown as green boxes (SR-PSU) and light green boxes (SR-Site), and the most recent biosphere assessments for SFL as blue boxes. Reports from earlier assessments used in the PSAR are marked in bold text, and dark green outlines of the boxes.*

1.3 This report

This report is the main document for reporting the work in the PSAR that is related to the surface ecosystems, below denoted the biosphere assessment. As such, this report provides the background information for conclusions on the biosphere assessment communicated in the **Post-closure safety report**. The report gives the context, describes the methodologies, models and data used, and presents the most important results. The findings are synthesised and discussed, and the effects of assumptions and uncertainties on the final results are assessed. All information necessary for a detailed review and for a reconstruction of the work done can be found in the background reports, which communicate primary analyses and results (Table 1-2 and Figure 1-4).

1.3.1 Purpose

The biosphere system, or surface system, is a key part of the system considered in the PSAR, the post-closure safety assessment of the extended SFR. This is where radiological impacts due to potential radionuclide releases from the repository may arise. The main purpose with the PSAR safety assessment is to demonstrate the post-closure safety of the SFR repository, by conducting a safety assessment and evaluate regulatory compliance with criteria concerning safety and protection of human health and the environment in the long-term perspective. The main purpose of the biosphere assessment part of the PSAR is to calculate doses to humans and dose rates to non-human biota to allow estimation of the radiological impact on humans, in terms of radiological risk, and on the environment at Forsmark that reflect a robust description of the biosphere system and a credible handling of associated uncertainties. To meet the intended purpose, the work is divided into four main tasks:

1. Identification of features and processes of importance for modelling radionuclide dynamics in present and future ecosystems in Forsmark.
2. Description of the Forsmark site and its future development with respect to the identified features and processes.
3. Identification and description of areas in the landscape that may be affected by releases of radionuclides from the SFR repository.
4. Calculation of the radiological exposure, in terms of annual doses, to a representative individual of the most exposed group of humans in the future Forsmark landscape, and the radiological exposure to the environment, in terms of absorbed dose rates to non-human biota.

The intention is not to simulate conditions that will necessarily be present in the future, but to capture the main features of transport, accumulation and exposure for a suite of possible future conditions.

The biosphere assessment builds upon previous post-closure safety assessments for the existing and planned radioactive waste repositories in Sweden. Between 2002 and 2008, SKB performed site investigations for a repository for spent nuclear fuel in Forsmark. Data from these site investigations were used to produce a comprehensive, multi-disciplinary site description (SKB TR-08-05). This description has been used as a basis for understanding and modelling the site and its development. The SFR repository has been in operation since 1988. Several post-closure safety assessments, including biosphere assessments, have been performed for the repository since SKB received permission to start building SFR1 in 1983, including the SAFE project (Lindgren et al. 2001, Kautsky 2001), SAR-08 (SKB R-08-130) and SR-PSU (SKB TR-14-01, SKB TR-14-06). Safety assessments have also been performed for the planned repository for spent nuclear fuel, within the SR-Can (SKB TR-06-09) and SR-Site (SKB TR-10-09, SKB TR-11-01) projects, and a safety evaluation for the planned repository for long-lived waste, within the SFL project (SKB TR-19-01, SKB TR-19-05).

Although the safety assessments mentioned above for the various waste types and repository concepts differ in several aspects, the biosphere system is assumed to have the same development and functioning and therefore the development of the biosphere assessment is driven by all safety assessments conducted by SKB. Thus, the biosphere assessment part of the PSAR for SFR is based on extensive knowledge gathered from site data, site modelling and previous safety assessments, together with modelling performed and data collected within the PSAR.

1.3.2 Main developments since the SR-PSU

The biosphere assessment in the PSAR addressed in this report is the next iteration of the biosphere assessment in the SR-PSU (SKB TR-14-06). Although the major approaches, models and data sets from SR-PSU are still valid, there have been many small updates made for the present assessment, of which many of the model updates were introduced in SE-SFL (SKB TR-19-05). This section briefly describes the key updates and improvements made in biosphere assessment in the PSAR, compared with the biosphere assessment in SR-PSU.

The results presented for the calculation cases in this report were all obtained using time-dependent radionuclide-specific releases into the biosphere as input, as opposed to the results presented in SKB (TR-14-06) which are based on constant unit releases of 1 Bq/y into the biosphere. These releases are results from the near-field and geosphere transport modelling for calculation cases in the main scenario, presented in the **Radionuclide transport report**.

The set of calculation cases addressed in the biosphere assessment has been selected to improve the evaluation of key uncertainties, such as in the landscape development and the spatial distribution of the geosphere releases (the *timing of shoreline regression calculation case*, the *subhorizontal fracture calculation case*, the *alternative landscape configuration calculation case* and the *alternative delineation calculation case*).

In SR-PSU, the probability of a drilled well existing within the *well interaction area* was derived as a function of the current well density in the area multiplied by that part of the *well interaction area* that was at least 1 m above sea level. In PSAR, a probability of 1 is assumed for the existence of a drilled well in this area. Then, the well is treated as an exposure pathway, and the dose from the drilled well is assessed for a small group of people getting exposed through ingestion of water and small-scale irrigation of a garden-plot.

The data used in the biosphere assessment has been updated since SR-PSU, and some new parameters have been introduced based on model updates. Details on this are given in Chapter 8. The biosphere transport and exposure model (BioTEx) used in PSAR is largely the same as in SR-PSU. However, several minor modifications have been made, of which most were introduced in SE-SFL. Details on this are given in Chapter 7, below is a brief summary of key updates:

- Instead of treating the two lowermost regolith layers, RegoLow and RegoGL, as two single compartments, they are each divided into five vertical sub-compartments to give a better representation of physical dispersion on the scale of a biosphere object.
- The cultivation of a drained mire is allowed once the highest (rather than the lowest, as in SR-PSU) point of a sloping object is 1 m above sea level.
- In SR-PSU, plant-root uptake of C-14 was regulated by the given concentration of stable carbon dissolved in the pore water (DIC). In the PSAR, this parameter is replaced by model calculations, based on soil respiration and the rate of degassing.
- Plant uptake of radionuclides intercepted on leaves, and subsequent translocation to edible parts, including fodder, is included for agricultural land-use variants with irrigation in the PSAR. Interception of radionuclides on leaves during irrigation is calculated from the activity concentration in the irrigation water, the leaf area index and the leaf storage capacity, and the translocation is represented by an empirical translocation factor.

1.3.3 Contributing experts

Project leader for the PSAR safety assessment has been Jenny Brandefelt (SKB). The work done in the PSAR is based on the experience from SKB's previous safety assessments, and several persons that have contributed to the biosphere assessment have experience from these previous safety assessments. Thomas Hjerpe (Kemakta Konsult AB) was the editor of this report, and the co-authors are listed in Table 1-3.

This report has been significantly improved at different stages by adjustments in accordance with comments provided by informal and factual reviewers. The informal review has been a rather continuous process where most co-authors listed in Table 1-3 have commented on texts written by other co-authors; in addition, Ari Ikonen (EnviroCase, Ltd.), Svante Hedström (SKB), Anna-Maria Jakobsson (SKB), Per-Gustav Åstrand (SKB), and Maria Lindgren (Kemakta Konsult AB) have provided comments. Factual reviewers have been Mike Thorne (Mike Thorne and Associates Ltd.) and Jordi Bruno (Amphos 21 Consulting).

Table 1-3. Names and affiliations of key persons contributing to the Biosphere synthesis report. Each co-author's main contributions are briefly described and references are given to the chapters in the report.

Name	Affiliation	Contribution to the PSAR SFR biosphere synthesis report	Chapter in this report
Thomas Hjerpe	Kemakta Konsult AB	Editor, introduction, assessment context, data evaluation.	Editor, 1, 2, 6, 9
Peter Saetre	SKB	Method development, BioTEX model development, data evaluation, synthesis.	2, 4–11, 13
Olle Hjerne	SKB	Site development, data evaluation, synthesis.	3–5, 10–11, 13
Ulrik Kautsky	SKB	Overall biosphere coordinator at SKB, scientific and method development, data evaluation.	1–13
Johan Liakka	SKB	Climate description, data evaluation.	4, 1
Sari Peura	SKB	Site description and development, assessment data, data evaluation.	3, 4, 8, 11
Jenny Brandefelt	SKB	Overall methodology, introduction.	1–2
Jean-Marc Mayotte	SKB	Hydrology, data evaluation.	3–5, 7, 10–11
Per-Anders Ekström	Kvot AB	BioTEx model development, numerical modelling of radionuclide transport and doses, data evaluation.	7–13
Sara Grolander	Kemakta Konsult AB	Assessment data, element-specific parameters.	8, 12
Mats Tröjbom	MTK AB	Assessment data, element-specific parameters.	8
Mårten Strömgren	Umeå University	GIS analysis, landscape development.	Most figures based on maps
Ben Jaeschke	AFRY	Non-human biota, assessment data.	12
Boris Alfonso	AFRY	Non-human biota, assessment data.	12
Fredrik Lidman	Swedish University of Agricultural Sciences (SLU), Umeå	Geochemistry, behaviour of calcite.	11

1.4 Structure of this report

This report comprises 13 chapters and 8 appendices. Following is a brief description of the contents:

Chapter 1 – **Introduction.** This chapter describes the background to the PSAR post-closure safety assessment, the role and structure of this report, and briefly discusses the key updates and improvements made since SR-PSU.

Chapter 2 – **Assessment methodology.** This chapter presents the biosphere assessment methodology in the PSAR, which is an integrated part of the overall post-closure safety assessment. Details are provided on the main components, or steps, included in the methodology. This includes such aspects as system understanding, the assessment context, representation and modelling of the biosphere system, and evaluation of results.

Chapter 3 – **Site description – present-day conditions at Forsmark.** This chapter provides description of the present-day conditions at Forsmark, which is assumed to be an appropriate representation of the conditions at closure of the repository. The description focuses on features and processes of importance for transport and accumulation of radionuclides. The chapter is structured in terms of descriptions of the Forsmark landscape with respect to climate, topography and regolith, near-surface hydrology, chemistry, marine, limnic and terrestrial ecosystems, and utilisation of the landscape and water resources by humans.

Chapter 4 – **Site development – modelling and description of future conditions and land use.** This chapter gives a short description of the natural processes and possible human impacts driving the development of the Forsmark site. The main processes are described, their implications for the development of topography and regolith, near-surface hydrology and chemistry are outlined and the development of marine, limnic and terrestrial natural ecosystems is presented. The processes are further elaborated to sketch the potential configuration of future landscapes in a regolith-lake-development model (RLDM), and examples of potential future landscapes are described.

Chapter 5 – **Modelling biosphere objects in the landscape.** This chapter identifies the biosphere objects, areas in the modelled landscape that are predicted to receive a substantial portion of the radionuclides following a release from the repository, to use in the transport and exposure modelling. Furthermore, properties of the identified biosphere objects are described and their temporal development.

Chapter 6 – **FEP handling, assessment endpoints and calculation cases.** The handling of features, events and processes (FEPs) important for the evolution of the biosphere system, and transport and accumulation of radionuclides is summarised in this chapter. Furthermore, assessment endpoints for humans and non-human biota are presented, and the calculation cases that are included in the radionuclide transport and dose calculations are summarised.

Chapter 7 – **The biosphere transport and exposure model.** This chapter provides a description of the biosphere transport and exposure model (BioTEx). The BioTEx model describes radionuclide transport and accumulation in the near-surface environment and in ecosystems and calculates potential doses to humans and dose rates to non-human biota (NHB). The structures of the ecosystem models that are part of the BioTEx model for PSAR are summarised, and the model compartments and the processes that transfer radionuclides are outlined. Furthermore, transport and uptake processes, calculations of exposure and the resulting doses to humans are described. In addition, model updates introduced since SR-PSU, and their effects are also discussed.

Chapter 8 – **Data used in the biosphere assessment.** All data used for calculating doses to humans and dose rates to non-human biota are presented here. First, the general principles of how the data have been selected for the BioTEx model used in the PSAR are described. Descriptions are then given of the considerations and calculations underlying the BioTEx parameters that are new or updated since SR-PSU. Furthermore, the quality assurance (QA) process applied to assure that data are complete, correct and traceable is briefly described.

Chapter 9 – **The base case.** The *base case* constitutes the basis for the radionuclide transport and dose calculations in PSAR. This chapter presents the description of the *base case* from a biosphere perspective, including aspects such as the radionuclide releases from the geosphere, the evolution of surface conditions and potentially exposed groups and populations. The outcome from analysing the *base case* with the biosphere transport and exposure model (BioTEx) is also presented and discussed in this chapter, addressing matters such as annual doses, contributions of exposure pathways, and the dynamics of radionuclide transport and accumulation throughout the regolith profile. The chapter also includes more detailed discussions for selected key radionuclides for the total annual dose. These discussions cover how the key patterns in their environmental activity concentrations and annual doses arise from the geosphere release, radionuclide properties and mechanisms such as dilution, retention, retardation, degassing, plant uptake, radioactive decay and radiotoxicity. Finally, this chapter addresses the effect of uncertainties in input parameters on the probabilistically simulated annual doses.

Chapter 10 – **Other calculation cases in the main scenario.** This chapter describes the other calculation cases and supporting calculation cases analysed within the main scenario. Two calculation cases represent a range of probable future evolutions, one with warmer and one with colder climate conditions. In addition, the analysis of the main scenario also comprises three supporting calculation cases, covering potential effects of uncertainties in landscape development and the properties of the discharge area.

Chapter 11 – **Supporting calculation cases for the biosphere.** This chapter presents the four supporting calculation cases that have been formulated to evaluate the sensitivity of calculated doses to uncertainties in the description of the biosphere system. Three cases are presented aiming to evaluate the sensitivity of doses to variations in ecosystem parameters, object properties and the outline of the biosphere object itself. Furthermore, one supporting calculation case addresses potential effects of a change in the mobility of radionuclides due to calcite depletion.

Chapter 12 – **Exposure of non-human-biota.** Exposures of non-human biota (NHB), quantified by calculating absorbed dose rates, are presented in this chapter. Calculations are performed for three calculation cases of the main scenario. In addition, the chapter summarises the method used to derive the dose rates.

Chapter 13 – **Discussion and conclusions.** This chapter discusses the outcomes from the biosphere assessment, focusing on uncertainties and their potential impact on the results of the performed calculations. The discussion is structured according four broad classes of uncertainty: system uncertainty, scenario uncertainty, modelling uncertainty and data uncertainty. Assumptions and reliability with respects to the radionuclides C-14 and Mo-93, which make major contributors to the resulting doses, are discussed in some detail. Finally, the uncertainties from all calculation cases are compared and discussed together and conclusion are drawn.

Appendix A – Terms and abbreviations. The present report contains terms and acronyms that either are rarely used outside SKB or can be regarded as specialised terminology within one or several of the scientific and modelling disciplines involved in the reported work. To facilitate the readability of the report, selected terms and acronyms are explained.

Appendix B – Map of the Forsmark area.

Appendix C – Landscape dose conversion factors, a comparison between PSAR and SR-PSU.

Appendix D – Method to assess exposure of non-human biota.

Appendix E – Updated values for non-human biota concentration ratios, dose conversion coefficients and occupancy.

Appendix F – Hydrological simulations with MIKE SHE.

Appendix G – Multi-model projections and uncertainties of irrigation water demand in a warmer climate.

Appendix H – Parameter files used in the BioTEx model for the *base case*.

2 Assessment methodology

The methodology for assessment of radiological impacts on humans and the environment from potential releases from a radioactive waste repository has been continuously developed internationally during the last few decades, and SKB has been extensively involved in this development.

This chapter first gives an overview of the biosphere assessment methodology in the PSAR and then provides more details on the main components, or steps, included in the methodology. The biosphere assessment is an integrated part of the overall post-closure safety assessment for the PSAR and the methodology applied is in line with the overall safety assessment methodology presented in detail in the **Post-closure safety report**, Chapter 2.

2.1 Overview of the methodology

Several biosphere assessments have been performed by SKB in recent decades, and the development of those assessments has been reported in the RD&D Programme (SKB TR 19-24). Summaries of earlier SKB work and key achievements has been presented in SKB (TR-10-09, TR-14-06, TR-19-05), with SKB (TR-14-06) having presented the latest biosphere assessment undertaken for SFR.

Although SKB's safety assessments for the various waste types and three repository concepts differ in several aspects, the biosphere system is assumed to have the same development and functioning and therefore the development of the biosphere assessment methodology is driven by all safety assessments conducted by SKB. Most of the developments of the methodology and the biosphere modelling introduced in the most recent biosphere assessment, SE-SFL (SKB TR-19-05), were related to issues raised during the regulatory review process of the previous biosphere assessments, to SKB's own development and research programmes, and to international developments. The work performed for SE-SFL can be seen as an iteration of the safety assessment processes for SFR and is accounted for in the present biosphere assessment.

The overall safety assessment methodology applied for the post-closure safety assessment in the PSAR consists of ten main steps, illustrated in Figure 2-1. These ten steps are carried out partly concurrently and partly consecutively.

The biosphere assessment contributes to most of the steps: Features, Events and Processes (FEPs) in the biosphere that can influence post-closure safety for SFR are identified (step 1), and the expected state of the biosphere at closure is described as a part of the initial state of the repository and its environs (step 2). The biosphere system is an integral part of the analysed system, and thus relevant biosphere FEPs are described as internal processes (step 4), and input data for radionuclide transport and dose calculations in surface systems are selected using a structured process (step 6). Given the long timescales considered in the assessment, the surface system is expected to go through significant changes, and this development is captured in the description of the reference evolution (step 7).

Biosphere FEPs are also considered in the selection of calculation cases (step 9). Post-closure safety is evaluated by analysing results from the integrated model chain, that starts with the releases from the waste in the waste vaults and ends with the doses to representative members of potentially exposed groups and dose rates to non-human biota. Finally, the resulting doses and dose rates are used as input in the evaluation of compliance with regulatory requirements.

Uncertainty management is an integral part of the post-closure assessment methodology (**Post-closure safety report**, Section 2.5). An overview of the management of uncertainties in the biosphere assessment is given in Section 2.3.9.

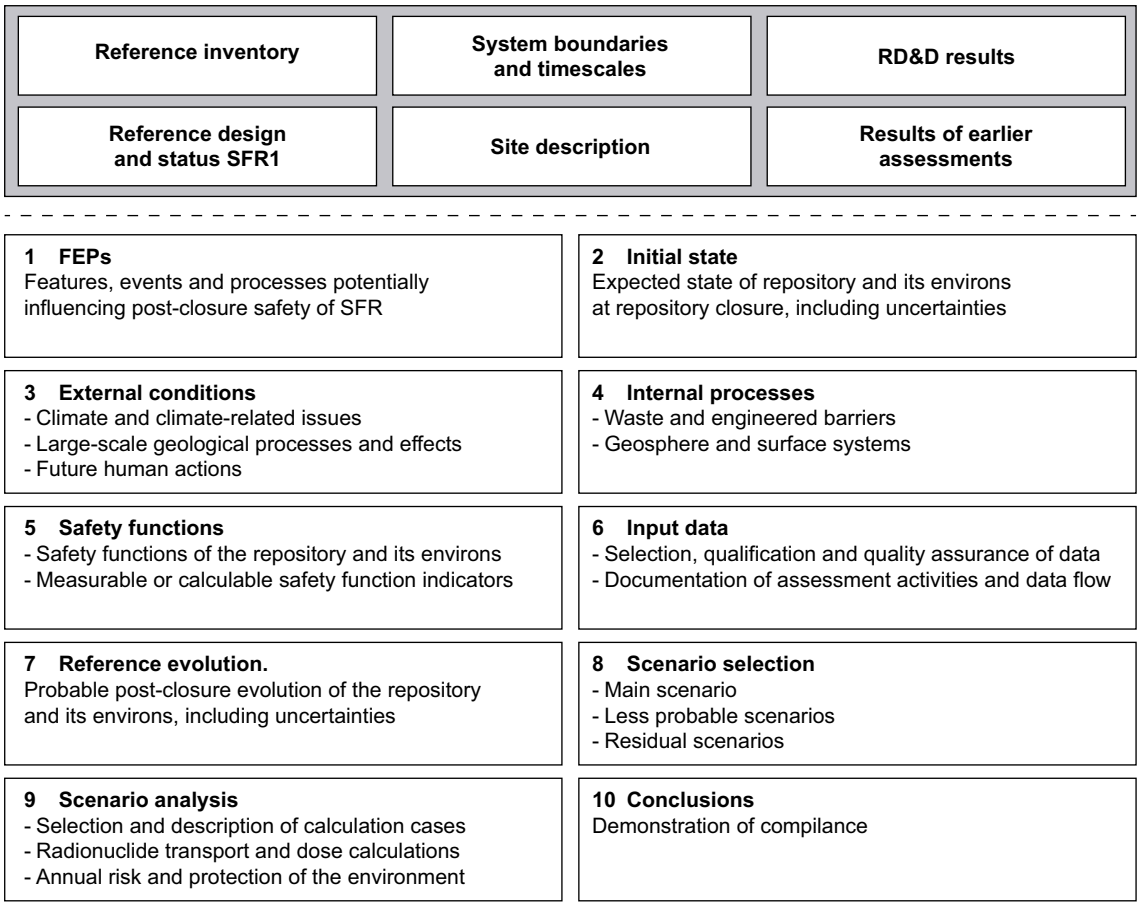

Figure 2-1. *An outline of the ten main steps of the present post-closure safety assessment. The boxes above the dashed line are prerequisites for the methodology and its implementation. The contents of the steps are described in detail in the* ***Post-closure safety report****, Section 2.6.*

In addition to being in line with the overall assessment methodology, the biosphere assessment methodology is also compatible with the IAEA BIOMASS methodology (IAEA 2003, Lindborg 2018, Lindborg et al. 2022). The BIOMASS methodology provides guidance on the treatment of the biosphere in post-closure safety assessments for radioactive waste disposal.

The biosphere assessment methodology applied is illustrated in Figure 2-2. The circle and two-headed arrows indicate that the methodology is essentially iterative in nature. Understanding of the system, including the repository and the bedrock surrounding the repository, plays a central role in the assessment methodology. Building system understanding and a site-specific data basis is an iterative process. For each safety assessment of a disposal facility, the knowledge of the site is increased and refined. The development of the transport and exposure model is an iterative process as well, aiming to ensure that a practicable and justified modelling approach is achieved and maintained. The management of uncertainties is a vital aspect integrated in all steps of the methodology, illustrated in the figure by the circular text. The assessment context is considered the first step in the cycle. The figure is based on the ongoing work of updating the methodological guidance on undertaking post-closure biosphere assessments[4].

[4] The work to update the BIOMASS methodology is the output of Working Group 6 of the second phase of the IAEA project Modelling and Data for Radiological Impact Assessment (MODARIA II), working in collaboration with the international BIOPROTA forum.

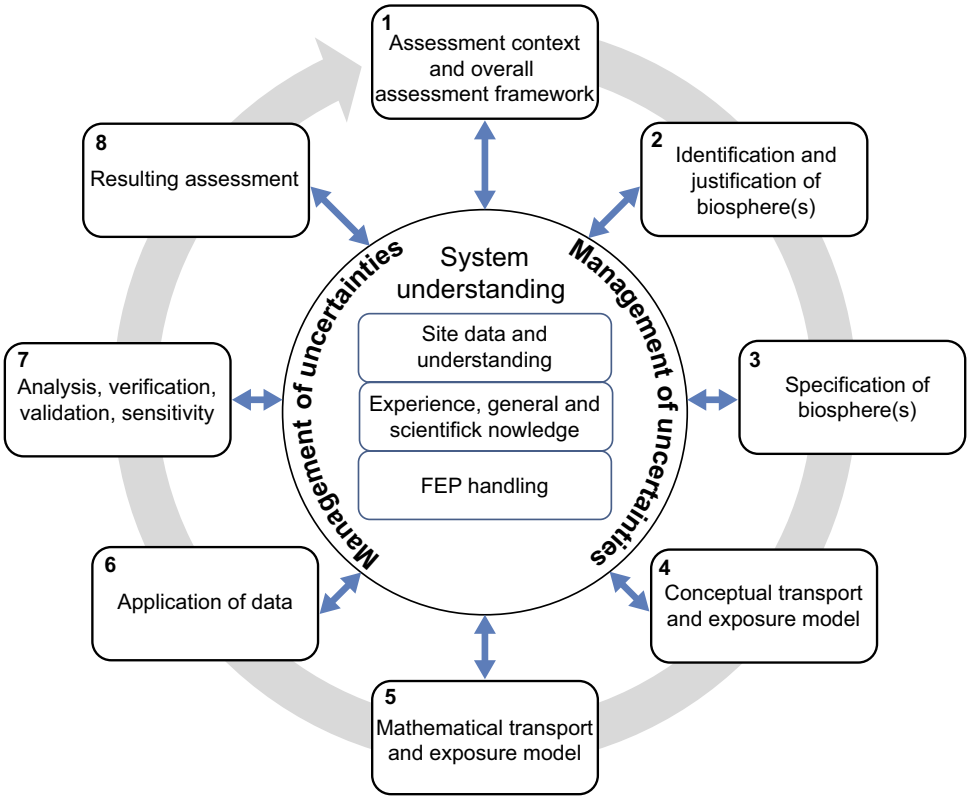

Figure 2-2. *Schematic illustration of the steps in SKB's biosphere assessment methodology. The methodology is presented in a circle to visualise the iterative nature of the safety assessments where knowledge gained during one assessment contributes to the following assessment. Understanding of the surface system plays a central role and interacts with all steps in the assessment methodology. Uncertainties are managed throughout the assessment cycle.*

2.2 System understanding

Understanding of the surface system plays a central role in the biosphere assessment methodology (Figure 2-2). Chapters 3 and 4 provide descriptions of the present-day conditions at Forsmark, natural key processes driving the development of the landscape and resulting spatiotemporal development projections of the landscape for further use in the safety assessment.

Knowledge of the surface system primarily originates from: 1) detailed descriptions of the Forsmark site (e.g. SKB TR-08-05, Lindborg 2008), 2) comprehensive descriptions of terrestrial and aquatic ecosystems that are potential recipients of groundwater discharge at a Swedish Baltic coastal site (Löfgren 2010, Andersson 2010, Aquilonius 2010), and 3) the experience from previous SKB safety assessments related to the Forsmark site, primarily SR-PSU and SR-Site (SKB TR-14-06, SKB TR-10-09).

The understanding from SKB's RD&D programme (e.g. SKB TR-19-24) and the safety evaluation of SFL (SKB TR-19-05) is also used to inform the iterative safety assessment processes, as is the shared experience from international collaboration forums (e.g. IAEA MODARIA II and the BIOPROTA Forum). This system understanding is a key for an adequate representation of the biosphere system, the formulation of an assessment model and the application of data, as well as for addressing key uncertainties in the assessment of environmental and human health impacts.

Identification and handling of biosphere features, events and processes (FEPs), relevant for the post-closure safety of SFR, is an important part of the development of the understanding of the surface system. Lists of FEPs provide a structured way to check that potentially important aspects of the safety assessment have not been overlooked, and a comprehensive analysis of the biosphere interaction matrix facilitates understanding of radionuclide migration and accumulation in surface ecosystems. SKB has long experience of identifying and handling biosphere FEPs, for the previous assessment for SFR this is documented in SKB (R-13-43, R-14-02, TR-14-07). The FEP handling in the present assessment is further addressed in Chapter 6.

2.3 Assessment context and overall assessment framework

In the first step of the methodology (Figure 2-2, step 1), the assessment context is established, which relates to the key aspects relevant for the biosphere part of the PSAR. The overall framework is an aspect of the overall PSAR assessment that affects the biosphere assessment, for example the evolution of the repository and geosphere in various scenarios. The overall framework is addressed in the **Post-closure safety report**. Since the aim is to have a methodology for the biosphere assessment that is compatible and integrated with the overall methodology, it is necessary to have knowledge and understanding of the overall framework when establishing the biosphere assessment context.

2.3.1 Purpose of the assessment

The main role of the post-closure safety assessment, documented in the **Post-closure safety report**, is to demonstrate that SFR is radiologically safe for humans and the environment after closure. This is done by evaluating compliance with respect to the Swedish Radiation Safety Authority's regulations concerning post-closure safety and the protection of human health and the environment (Section 1.2).

The main purpose of the biosphere part of the overall assessment is to calculate annual doses to humans and dose rates to non-human biota to allow estimation of the radiological impact on humans, in terms of radiological risk, and on the environment at Forsmark that reflect a robust description of the biosphere system and a credible handling of associated uncertainties.

2.3.2 Regulatory framework

The form and scope of a safety assessment and the criteria for judging the safety of the repository are defined in regulations issued by the Swedish Radiation Safety Authority, SSM. The regulations are based on various pertinent components of framework legislation, the most important being the Nuclear Activities Act and the Radiation Protection Act. Guidance on radiation protection matters is provided by a few international bodies, and has often, as in the case of Sweden, influenced national legislation.

The main Swedish regulations for the assessments of post-closure safety are SSMFS 2008:37 (SSM 2008a) concerning *the protection of human health and the environment in connection with the disposal of spent nuclear fuel and nuclear waste* and SSMFS 2008:21 (SSM 2008b) concerning *safety in connection with the disposal of nuclear material and nuclear waste*.

According to the Swedish regulations, human health and the environment should be protected from the harmful effects of ionising radiation from the repository. The risk criterion for protection of human health, and other requirements, are important prerequisites when establishing the context for the biosphere assessment.

The regulations also provide guidance on scenarios that should be included in a safety assessment for radioactive waste repositories. Two sections in SSM (2008a) are of specific interest for the biosphere assessment:

Section 10: *"The description shall include a case based on the assumption that the biospheric conditions prevailing at the time when an application for a licence to construct the repository is submitted will not change. Uncertainties in the assumptions made shall be described and taken into account when assessing the protective capability."*

In the general advice to Sections 5–7: *"Taking into consideration the great uncertainties associated with the assumptions concerning climate evolution in a remote future and to facilitate interpretation of the risk to be calculated, the risk analysis should be simplified to include a few possible climate evolutions. A realistic set of biosphere conditions should be associated with each climate evolution."*

The regulatory guidelines thus point out that at least one case where the biosphere conditions of today prevail into the future must be included in the assessment, and that realistic assumptions should be applied for the description of the biosphere under different climatic evolutions.

2.3.3 Scenarios and calculation cases

The selection of scenarios is part of the overall safety assessment methodology (Figure 2-1, step 8). The set of scenarios aims to illustrate the most important courses of development of the repository and its environs. In practice, the scenario selection is mainly driven by the development of the repository (the waste packages, and the engineered barriers and other repository structures), accounting for uncertainties in external conditions, especially in the development of the climate. Hence, the scenario selection can be seen as a prerequisite for the biosphere assessment, where the development of the biosphere system in the scenarios is addressed in steps 2 and 3 in Figure 2-2. In line with the general advice associated with SSMFS 2008:21 (SSM 2008b), three types of scenarios are considered in the PSAR:

- The *main scenario* (**Post-closure safety report**, Chapter 7) takes into account the most probable changes within the repository and its environs, based on the initial state, the reference external conditions, and the reference evolution. It is used as the starting point for the analysis of the impact of uncertainties and is included in the calculation of radiological risk (**Post-closure safety report**, Chapter 10).
- *Less probable scenarios* (**Post-closure safety report**, Chapter 8) evaluate scenario uncertainties and other uncertainties that are not evaluated within the framework of the main scenario. These scenarios are also included in the calculation of radiological risk, albeit with a lower probability to occur than the main scenario (**Post-closure safety report**, Chapter 10).
- *Residual scenarios* (**Post-closure safety report**, Chapter 9) are selected to illustrate the significance of individual barriers and barrier functions, detriment to humans intruding into the repository, and the consequences of an unsealed repository that is not monitored. These scenarios typically comprise sequences of events and conditions that are selected and studied independently of probabilities, and the results from the residual scenarios are thus not considered in the calculation of radiological risk.

The scenarios are the basis for assessing the protective capability of the repository and potential environmental consequences. This assessment is quantitatively done by identifying and analysing one, or more, calculation cases for each selected scenario. The endpoint of a calculation case is typically described in the form of radiological consequences, i.e. doses to humans and dose rates to NHB (see Section 2.3.5). An overview of the scenarios and calculation cases in the PSAR is given in the **Radionuclide transport report**, Table 2-1. The calculation cases included in this report are all related to the main scenario and are further discussed in Section 6.4.

2.3.4 Time frames

The regulations (SSM 2008a) require that an assessment of a repository's protective capability for the first thousand years after repository closure should be based on quantitative analyses of the impact on human health and the environment. For a longer period, the assessment of the repository's protective capability shall be based on various possible sequences for the development of the repository's properties, its environment and the biosphere. In the general advice associated with the regulation (SSM 2008a), it is clarified that for a repository of SFR type the longer time frame should at least cover the period of time until the expected maximum consequences in terms of risk and environmental impact have taken place, although for a maximum time period of up to one hundred thousand years. In the PSAR, the safety of the repository is evaluated over a period of 100 000 years.

The biosphere assessment for the PSAR is not subdivided into different time frames; instead, it is modelled in a continuum. However, three main time periods are identified as relevant for different purposes, discussed below.

The first of these time periods concerns the initial period when the area above the repository is still submerged beneath the sea. The duration of this period is determined by the opposing contributions from future sea-level rise and post-glacial isostatic rebound. The duration may exceed 10 000 years if the contribution from future sea-level rise is large. A lower limit for the duration, corresponding to a negligible sea-level rise, is approximately 1 000 years (**Climate report**). This lower value was used to define the initial duration of the submerged period in the main and less probable scenarios in SR-PSU and is also chosen for most calculations in the present safety assessment. This is a cautious

approach as doses during the submerged period tend to be orders of magnitude lower than doses resulting from human utilization of land resources. Thus, regardless of the outcome of future sea-level rise, the submerged period is considered to encompass the first 1 000 years that are specified by the regulations as of special importance with requirements for detailed analysis.

The second period concerns, approximately, the 10 000 years following the emergence of the repository area above the sea level. During this period, all objects considered in the biosphere analyses (Chapter 5) are turned into terrestrial areas. The end of this period also approximately corresponds to the time when the sea leaves the site development model area (Chapter 4).

The third period starts from the time when the sea leaves the model area and extends until the end of the assessment period 100 000 years after closure. During this period, the shoreline has left the model area, and hence the biosphere development is dominated primarily by climate changes.

2.3.5 Radiation protection criteria and assessment endpoints

Risk criteria for protection of human health

The regulations state that "*A repository for spent nuclear fuel or nuclear waste shall be designed so that the annual risk of harmful effects after closure does not exceed 10^{-6} for a representative individual in the group exposed to the greatest risk.*" (SSM 2008a).

Furthermore, in the general advice on the application of the regulations, it is stated that *"if the exposed group only consists of a few individuals, the criterion of the regulations for individual risk can be considered as being complied with if the highest calculated individual risk does not exceed 10^{-5} per year. An example of a situation of this kind might be if consumption of drinking water from a drilled well is the dominant exposure pathway."* (SSM 2008a).

Moreover, it is stated that the recommendations of the International Commission on Radiological Protection (ICRP) Publication No. 60 (ICRP 1991) are to be used for calculation of the harmful effects of ionizing radiation. According to ICRP Publication No. 60, the factor for conversion of effective dose to risk is 7.3 % per Sievert[5].

Protection of the environment

For the protection of the environment, no risk criteria exist in the Swedish legislation. However, SSM (2008a) states in Sections 6 and 7:

"The final management of spent nuclear fuel or nuclear waste shall be implemented so that biodiversity and the sustainable use of biological resources are protected against the harmful effects of ionising radiation. Biological effects of ionising radiation in the habitats and ecosystems concerned shall be described. The report shall be based on available knowledge on the ecosystems concerned and shall take particular account of the existence of genetically distinctive populations such as isolated populations, endemic species and species threatened with extinction and in general any organisms worth protecting."

"The assessment of effects of ionising radiation in selected organisms, deriving from radioactive substances from a repository, can be made on the basis of the general guidance provided in the International Commission on Radiological Protection's (ICRP) Publication 91 (ICRP 2003). The applicability of the knowledge and databases used for the analyses of dispersion and transfer of radioactive substances in ecosystems, and for analysing the effects of radiation on different organisms, should be assessed and reported on."

[5] The 2007 Recommendations of the International Commission on Radiological Protection, Publication No. 103 (ICRP 2007), formally replace the Commission's previous, 1990, Recommendations in Publication No. 60. However, until SSM state otherwise, the recommendations in Publication No. 60 are valid. SKB interprets 5§ in the consolidated version of SSMFS 2008:37 that it is SSMs intention to apply the recommendations in ICRP Publication No. 103 in the future, but since this is not mentioned in the amending regulation 2018:19, SKB will continue to apply the recommendations in ICRP Publication No. 60 until all regulations are uniformly updated.

Assessment endpoints

The methodology for the estimation of the annual radiological risk is part of the overall assessment methodology (Figure 2-1 and **Post-closure safety report**, Section 2.6.9). The individual risk should be "*calculated as an annual average on the basis of an estimate of the lifetime risk for all relevant exposure pathways for every individual. The lifetime risk can be calculated as the accumulated lifetime dose multiplied by the conversion factor of 7.3 per cent per sievert.*" (SSM 2008a). In the case where dose may be incurred in the far future over the entire life of the individual, ICRP (2000, §46) states that "*…it could be assumed that radioactive contamination of the biosphere due to releases from the repository is likely to remain relatively constant over periods that are considerably longer than the human life span. It is then reasonable to calculate the annual dose/risk averaged over the lifetime of the individuals, which means that it is not necessary to calculate doses to different age groups; this average can be adequately represented by the annual dose/risk to an adult*.

The endpoint for humans is the *annual dose*, calculated as the annual effective dose to an adult, where the annual effective dose is defined as the effective dose from external exposure in a year, plus the committed effective dose from intakes of radionuclides in that year. The annual dose is deemed appropriate to use as a basis for estimating the radiological risk for the assessment of the protection of human health.

The dose coefficients for intake used in the calculations of effective dose account for retention of radionuclides in the human body and exposure from radioactive decay products produced in the body, as well as the different radiation sensitivities of various tissues and organs. Doses calculated using these coefficients are committed effective doses from intake in a single year. According to ICRP (2006, §78), "*this conservative accounting of dose ensures that individuals are protected over a lifetime of exposure, regardless of the number of years for which they are exposed*".

The annual dose is calculated by running 1 000 simulations with different randomly drawn sets of ecosystem parameters (Section 6.4.1). The dose is calculated for each point in time by summing the dose over all simulations, giving each realisation the probability of 0.001. This time-dependent probability weighted average is the expected value of the dose for each fixed point in time. As it is equivalent to the mean of the 1 000 simulations, it is referred to as the mean total (or radionuclide specific) annual dose.

Predictions of future human behaviour are inherently uncertain, especially on the timescales addressed in the present assessment (Section 2.3.4). In SR-PSU, exposure pathways of relevance within ecosystems of interest were reviewed. Land-use variants, which resulted in relatively high exposure, and the associated potentially exposed groups (PEGs) were then identified from historically self-sustainable communities (SKB R-14-02). Following this approach, ecosystems created by humans have a more simplified representation than natural ecosystems, and potentially exposed groups are to be interpreted as credible bounding cases with respect to the identified exposure pathways. The potentially exposed groups used in this assessment are further described in Chapter 6.

Regarding endpoints related to the protection of the environment, there are, at present, neither any risk criteria nor limiting exposure values for non-human biota (NHB) stipulated in SSM's regulations. However, there has been a substantial development of the framework aiming at protection of NHB that post-dates the basis for SSM (2008a). As in SR-PSU, the ERICA methodology is applied in the current assessment (Beresford et al. 2007, Brown et al. 2008). This methodology recommends a screening value for the absorbed dose rate at the ecosystem level of 10 μGy h^{-1}. This value has been endorsed by the EU PROTECT project (Andersson et al. 2009), and the ERICA methodology is in line with the ICRP recommendations on environmental protection (ICRP 2008) (for the screening value, see below).

Hence, the primary endpoint selected by SKB for demonstrating protection of non-human biota is absorbed dose rates to a set of reference organisms, in the following referred to as dose rates. The ERICA screening dose rate was originally derived as a predicted no-effect-dose-rate value for ecosystems, based on a distribution analysis of mortality and reproduction response to chronic exposure in a broad range of organisms (Garnier-Laplace and Gilbin 2006). In subsequent analyses restricted to vertebrates, invertebrates, and plants, the use of this screening dose rate was further supported, and it can be interpreted as the dose rate where 5 % of species are expected to have a 10 % reduction in reproductive rate, accounting for data uncertainties (Andersson et al. 2009, Garnier-Laplace et al. 2010). If a dose rate in an assessment exceeds the screening dose rate, then a more detailed investiga-

tion of exposure parameters and uncertainties, and/or some investigation into the radio-sensitivity of specific organisms, should be performed. If dose rates are below this screening value it follows that a potential release from the repository is highly unlikely to cause detrimental effects on the survival and reproduction of individual organisms. As no effects are expected at the level of the individual organism, effects at the levels of populations, communities, and ecosystems are also highly unlikely.

It is worth mentioning that this screening dose rate is well below the screening dose rates used by some other agencies, for instance the US Department of Energy. US DoE suggests using a screening dose rate of 400 μGyh^{-1} for native aquatic animals, and screening dose rates of 400 and 40 μGyh^{-1} for terrestrial plants and terrestrial animals, respectively (US DOE 2002). Furthermore, UNSCEAR concluded that chronic dose rates less than 100 μGyh^{-1} to the most highly exposed individuals would be unlikely to have significant effects on most terrestrial communities, and that maximum dose rates of 400 μGyh^{-1} to any individual in aquatic populations of organisms would be unlikely to have any detrimental effect at population level (UNSCEAR 2011). ICRP recommends the lower band of the derived consideration reference level (DCRL) as a benchmark against which the acceptability, in terms of environmental impacts, of planned activities may be gauged (ICRP 2014). Consideration is therefore also given to relevant DCRLs where these are more restrictive than the generic ERICA screening value. The development of the non-human biota framework at SKB is further described in Jaeschke et al. (2013). Handling of dose rates to non-human biota in SR-PSU is described in Chapter 12.

2.3.6 Repository system and site context

Information on the repository system and the disposal site context set key boundary conditions for the biosphere assessment. In this safety assessment, repository system includes both the repository and its environs. SFR was built between 1983 and 1988, to receive, and after closure serve as a final repository for, low- and intermediate-level radioactive waste. The five waste vaults in SFR1 (the existing part of SFR) are situated in rock beneath the sea floor and are currently covered by about 60 metres of granitoid rock, a few metres of regolith and 6–10 m seawater (Kautsky 2001). The waste vaults contain different types and amounts of waste (**Initial state report**). The underground part of the facility is reached via two tunnels (Figure 1-2). The extension of SFR (SFR3) will function in the same way as the existing, but the six waste vaults will be situated deeper, at a depth of about 120 m. In addition to similar wastes as those held at the existing SFR, decommissioning waste, including the reactor pressure vessels from Swedish boiling water reactors, are also to be disposed in the extended facility (**Post-closure safety report**, Section 4.3).

SFR is situated in Forsmark, which is located on the coast of the Bothnian Sea (a part of the Baltic Sea) in Östhammar municipality, about 120 km north of Stockholm, Sweden (Figure 1-1). SFR is situated in the vicinity of the nuclear power plant in Forsmark. The surroundings show small-scale topographic variations of less than 20 metres (Figure 2-3).

The land at the site is young and several recently isolated lakes and wetlands are scattered in the landscape. New land and lakes are continuously formed as a consequence of the regressing shoreline (see Chapter 3). The coastline consists of sheltered shallow bays and small islands. The present-day conditions of the site are described in Chapter 3.

Figure 2-3. *The coastal area in Forsmark, characterised by low topographical relief, shallow coastal bays and recently isolated shallow lakes and wetlands.*

2.3.7 Source term and radionuclide releases from the geosphere

The key aspect of the source term for the assessment context is the physico-chemical form of the waste, especially the activity of the radionuclides, and the way in which it is conditioned and packaged. The activity and other characteristics of the radionuclide inventory to be applied in the safety assessment are presented in the **Initial state report**.

The activity of radionuclides in the waste to be disposed in SFR is dominated by short-lived radionuclides, e.g. Fe-55 and Co-60, and a large part of the total activity disposed in SFR will decay substantially prior to closure of the repository. The activity of the radionuclides in the waste from the time of repository closure up to around 100 000 years after closure is presented in the **Post-closure safety report**, Figure 1-4. The total activity 100 years after closure is about 40 % of its initial value, and about 1.5 % remains after 1 000 years. Initially, Ni-63 dominates the activity, then, after about 1 000 years, Ni-59 and C-14 dominate. The radionuclides with the highest activity are not necessarily those that contribute most to the radiotoxicity of the waste. Ingestion radiotoxicity, below denoted radiotoxicity, serves to quantify the radiological hazard from individual radionuclides in a simple way. The radiotoxicity is here defined as the product of the activity of a radionuclide and its corresponding ingestion dose coefficient. Hence, radiotoxicity is the effective dose one would receive from ingesting a that activity of the radionuclide. The radiotoxicity of the waste as a function of time after closure is presented in the **Post-closure safety report**, Figure 1-5. The radiotoxicity is initially dominated by Cs-137 and Ni-63. The total radiotoxicity 100 years after closure is less than 20 % of its initial value, and decreases to about 2.5 % after 1 000 years, and to about 1 % after 10 000 years. By the end of the assessment period, after 100 000 years, less than 0.2 % of the initial radiotoxicity remains.

The radionuclide release from the geosphere is a key input to the biosphere assessment. Two aspects of the release are particularity important. Firstly, how much activity is transported from the waste, through the near-field and geosphere, and at what time it reaches the biosphere system. This is addressed in the **Radionuclide transport report** and the time series of the activity reaching the biosphere system is used as direct input to the biosphere calculations. The second aspect is the spatial distribution of the geosphere release. The location of the release depends on the flow paths of deep groundwater passing the repository and on the location of deformation zones above, and the position of the release changes in response to the emergence of land above the repository. The results from hydrogeological particle

tracking studies (Odén et al. 2014, Öhman and Odén 2018) are used to outline surface ecosystems expected to have relatively high concentrations of radionuclides. These areas are used to evaluate potential doses to humans and dose rates to non-human biota.

2.3.8 Approach for calculating the assessment endpoints

The assessment endpoints in the biosphere assessment are annual dose (derived as the effective dose from external exposure in a year, plus the committed effective dose from intakes of radionuclides in that year) to adults, and dose rates to a set of reference organisms for non-human biota (Section 2.3.5). Furthermore, the regulatory criterion for annual risk of harmful effects relates to a representative individual in the group exposed to the greatest risk (Section 2.3.5, SSM 2008a). To enable the demonstration of compliance with regards to this risk criterion, annual doses are calculated to groups of individuals likely receiving the higher exposures (denoted potentially exposed groups). When selecting the groups, all relevant pathways of exposure are addressed, and the spatial distributions of radionuclides are considered by identifying areas with the highest concentrations of radionuclides. The habits of the groups reflect land-use that results in relatively high exposure and are selected to be reasonable and sustainable. This approach to selecting potentially exposed groups is consistent with how ICRP defines the *representative person* to be used for determining compliance with dose constraints (ICRP 2006, Chapter 3).

The assessment context described above includes aspects related to requirements set by the authorities, conditions imposed by the repository system and the site, as well as requirements and prerequisites from the overall safety assessment. The approach[6] for calculating the assessment endpoints is chosen to meet these requirements and prerequisites and adequately represent conditions imposed by the repository system and site.

The approach to the radionuclide transport modelling of natural ecosystems is to be as comprehensive and realistic as possible, with respect to model structure, primary transport pathways, landscape development and the associated parameters. However, the uncertainties with respect to the characteristics of future human inhabitants of the area are large and essentially irreducible. Thus, the description of exposure is based on the analysis of potential exposure pathways (conducted in SR-PSU) and cautiousness/pessimism, rather than on an attempt to explicitly predict living conditions and habits of generations to come in the Forsmark area.

In the PSAR, a probabilistic approach is applied in the calculation of doses, and parameters that describe ecosystem properties are represented by probability density functions. However, best estimates of parameters are used to describe landscape geometries and the associated hydrology. Parameters describing potentially exposed groups for humans (Section 6.2) and reference organisms for non-human biota (Section 6.3) are based on cautious or pessimistic assumptions. Fully deterministic calculations are only used for evaluation of model performance (Chapter 7, Appendix C). The assessment endpoints primarily feeding into the risk estimation (**Post-closure safety report**, Chapter 10) are selected to be the mean values of calculated annual doses and dose rates.

2.3.9 Management of uncertainties

The management of uncertainties is an important aspect of any safety assessment. There is no unique way in which to classify uncertainties. Here the classification is adopted and described that is suggested in the general advice to SSMFS 2008:21 (SSM 2008b). Thus, it captures relevant aspects that also relate to the recommendations described in the general advice to SSMFS 2008:37 (SSM 2008a) as well as international practice in this type of analysis (NEA 2012, IAEA 2012). The following broad definitions are used (**Post-closure safety report**, Section 2.5):

- *Scenario uncertainty* refers to uncertainty with respect to external conditions and internal processes in terms of type, degree and time sequence, resulting in an uncertainty in the future states of the repository system. It includes uncertainty for example in the evolution of the repository system, human habits, and climatic and other long-term processes.

[6] In the BIOMASS methodology, the term *assessment philosophy* is used to describe the approach selected for calculating the assessment endpoints.

- *System uncertainty* concerns comprehensiveness issues, i.e. the question of whether all aspects important for the safety evaluation have been identified and whether the analysis is capturing the identified aspects in a qualitatively correct manner. In short, have all factors, features, events and processes been identified and included in a satisfactory manner or has their exclusion been appropriately justified?
- *Modelling uncertainty* arises from a necessarily imperfect understanding of the nature of processes involved in repository evolution which leads to imperfect conceptual models. The mathematical representations of conceptual models will have involved some simplification, also contributing to modelling uncertainty. Imprecision in the numerical solution of mathematical models is another source of uncertainty which fall into this category.
- *Data uncertainty* concerns all quantitative input data, i.e. parameter values used in the assessment. There are several aspects to consider in the management of data uncertainty. These include correlations between data, the distinction between uncertainty due to lack of knowledge (epistemic uncertainty) and due to natural variability (aleatoric uncertainty) and situations where modelling uncertainty is treated by broadening the range of input data. The input data required by a particular model is in part a consequence of the conceptualisation of the modelled process, meaning that modelling uncertainty and data uncertainty are to some extent intertwined.

The strategy for managing uncertainties in the present safety assessment includes several elements. System uncertainty is dealt with in the FEP analysis, which in turn emerges from a system understanding (Section 2.2). Scenario, modelling and data uncertainties are handled primarily in steps 2 to 6 of the biosphere assessment methodology, as described in Sections 2.4 to 2.6 below.

2.4 Representation of the biosphere

These steps of the methodology (Figure 2-2, steps 2 and 3) refer to identifying and describing (or specifying) the set of biosphere systems that are needed to support the safety assessment.

Based on previous assessments related to the Forsmark site, coastal sea basins, lakes and wetlands are the three natural ecosystems that are expected to occur in areas where deep groundwater is discharged (e.g. SKB TR-10-09, SKB TR-14-06). Two versions of agricultural land use were used in SR-PSU to evaluate effects from draining and cultivating natural ecosystems, and from using wetlands for haymaking (SKB TR-14-06). In addition, a garden plot system was used to assess consequences from exposure routes considered to be relevant on a smaller scale (e.g. irrigation and fertilisation with algae or ash). The same set of biosphere systems are deemed appropriate for the present assessment.

The principal characteristics of the biosphere at the present day are presented in Chapter 3. Chapter 4 then gives short descriptions of natural processes driving the development of the Forsmark site, and of the regolith-lake development model (RLDM) used to describe potential future landscapes.

Management of uncertainties

The uncertainties regarding the representation of the biosphere are classified as scenario and modelling uncertainties. The scenario uncertainty is related to landscape development, ecosystem succession, changes in the soil chemical environment and the future climate evolution. This uncertainty is accounted for mainly by defining several future representations of the biosphere, corresponding to a range of probable evolutions of external conditions (Chapter 4). Effects of these uncertainties are evaluated by a set of calculation cases within the main scenario, and by supporting calculation cases.

The modelling uncertainty, in steps 2 and 3, relates to an imperfect understanding of the nature of processes involved, which is propagated into modelling of present-day and future conditions of the biosphere. These include, for instance, uncertainties in modelling of the locations of the primary future discharge areas and the associated properties with respect to geometries, regolith stratigraphy and hydrology (Chapter 5). Effects of these uncertainties are evaluated by including several supporting calculation cases that are based on alternative assumptions.

2.5 Biosphere assessment model

To simulate radionuclide transport, accumulation and potential exposure in the biosphere, conceptual and numerical models of identified ecosystems have been developed in step 4 and 5 of the methodology (Figure 2-2). The biosphere model for transport and exposure (BioTEx) used in the present assessment is in essence the same as the one used in SR-PSU (Saetre et al. 2013a) and further developed in SE-SFL (SKB TR-19-05). The BioTEx model handles coupled terrestrial and aquatic ecosystems, and their temporal development, agricultural systems and dose calculations. It has been verified by code comparisons, and part of the model has been validated (SKB TR-13-18). Moreover, it has proven to be useful through experience (SKB TR-14-06, SKB TR-19-05) and has been judged to give a good description of the biosphere system and to yield reasonable results (e.g. SSM 2019).

The conceptual structure of the BioTEx model reflects the outcome of the FEPs analysis, where biosphere FEPs that are potentially important for post-closure safety have been identified and the biosphere interaction matrix developed (SKB TR-11-01, SKB R-13-43). It further reflects previously established conceptual models of aquatic and terrestrial ecosystems (Andersson 2010, Aquilonius 2010, Löfgren 2010), a conceptual landscape model (Lindborg 2010), and potentially exposed groups identified through a comprehensive exposure pathway analysis (SKB R-14-02). The BioTEx model is described in more detail in Chapter 7. Supporting modelling activities that provide input to the BioTEx model are, for example, modelling of regolith and lake development (Chapter 4) and surface/near-surface hydrogeology modelling (Chapter 5).

Management of uncertainties

Improvements of the BioTEx model were made in SE-SFL (SKB TR-19-05), and are related to e.g. higher vertical discretisation of the lowermost regolith layers and improved representation of terrestrial carbon (stable and C-14). These updates are included in the model together with a few additional changes (see Chapter 7). The effects of updates are examined and evaluated in the PSAR. The uncertainty introduced by using the BioTEx model can be classified as modelling uncertainty. Uncertainties with respect to the contribution of decay products in agricultural systems are addressed by comparisons of calculation methods.

2.6 Application of data

An important and challenging task in the biosphere assessment is gathering appropriate and internally consistent data sets for the mathematical models (Figure 2-2, step 6). This task includes definitions of uncertainty bounds or distributions to be used in probabilistic simulations. The challenge is not only compiling data representing the present-day biosphere systems, but also to specify data that are representative of conditions that may prevail in the future.

The main approach in the biosphere assessment in the PSAR is to, as far as possible, utilise site-specific information for Forsmark, both for describing the parameters to be modelled and for selecting parameter values and their probability density functions. However, in some cases site data are not available. In these cases, the parameter values are estimated from literature data, or by using analogues.

In the biosphere modelling, radionuclide fluxes are linked to natural processes (e.g. fluxes of water, solids or gas, diffusion and plant uptake) to make it possible to derive parameter values from conditions measured at the site or modelled based on site data. The use of real site data means that model assumptions and parameter values are transparent and can be traced back to the site description. Moreover, using a representative data set, where the measured parameters are sampled at the same site during the same period, gives internally consistent data. Thus, it is possible to make a scientifically underpinned and coherent assessment that is relevant for Forsmark.

The assessment is based on substantial knowledge of present-day conditions at Forsmark and its Holocene history. The uncertainty in assumptions and parameters describing the succession of natural ecosystems is relatively low for current conditions. However, uncertainties in biosphere properties in the future increase gradually with time, such as for properties of future terrestrial conditions not currently found at Forsmark, and thus it is inevitable that some cautious assumptions must be introduced to handle these uncertainties.

In addition to using a sound data basis for collating the data to be used in the modelling, a quality assurance procedure has been developed to ensure a controlled handling of data and workflow to guarantee the quality of data and model results (Chapter 8).

Management of uncertainties

The uncertainty in parameter values naturally relates to data uncertainty. In the PSAR, parameters that describe ecosystem properties are represented by probability density functions that are aimed at capturing natural variability. However, when measurements are few (or lacking), cautious assumptions with respect to the typical values and the spread of the data are used to deal with uncertainties due to lack of data. In addition, the sensitivity of the calculated dose to changes in the values of ecosystem parameters is examined in separate calculations.

The uncertainties with respect to the characteristics of future human inhabitants of the area are large and essentially irreducible. Parameters describing potentially exposed groups are therefore represented by cautious or pessimistic assumptions. The parameters describing landscape geometries and the associated hydrology are not assigned any uncertainty in the main scenario. However, landscape modelling on such timescales is intrinsically uncertain, and the effects of variation in parameters describing biosphere object properties are illustrated with supporting calculations, including a sensitivity analysis.

2.7 Analysis and verification

When implementing the mathematical models for the biosphere assessment, considerations is given to ensuring that selected modelling tools are fit-for-purpose and that the resulting implementations of mathematical models are, as far as reasonable, verified (Figure 2-2, step 7).

The modelling tools used in the present biosphere assessment are the same as used in previous assessments for SFR and for SFL, and the models are to a large degree the same. The BioTEx model has previously been evaluated and deemed fit-for-purpose for use in the biosphere assessments (Section 2.5), and since there are only minor changes in assessment context and in the mathematical models, this still stands for the present assessment.

All model updates introduced in the PSAR have been verified by code auditing, and the effects of the updates are quantified by model comparisons (Appendix C). Differences in model results, as compared with the SR-PSU model, are in line with a-priori expectations, building confidence that the model modifications are implemented as intended.

In Chapter 9, the results from the *base case* are examined in detail. The chapter covers in-depth analyses of the annual doses to different potentially exposed groups, contributions of exposure pathways and the dynamics of radionuclide transport and accumulation throughout the regolith profile. The fate of accumulated radionuclides upon draining and cultivation of a mire is also analysed. Patterns in annual doses are deduced from the geosphere release, radionuclide properties and mechanisms such as dilution, retention, retardation and radioactive decay. In this way, key radionuclides are identified, and their main exposure pathways, transport mechanisms and timescales are characterised. Conclusions with respect to mechanisms controlling transport and accumulation of key radionuclides are further supported by the results from the sensitivity analysis of ecosystem parameters. Finally, the effects of data uncertainties on the results are evaluated.

This step in the methodology demonstrates SKB's understanding of the BioTEx model and helps build confidence that the model results are plausible and reliable. Sense-checks and comparisons of model outputs with results and understanding from analytical solutions for steady-state conditions are also used to assure that the model performs as intended and that results are reasonable. In SKB's experience this type of high-level verification has proved to be very efficient for identifying inconsistencies in the data and/or problems with the mathematical implementation of the model that have effects on the model outcome.

2.8 Results for evaluation of safety

As a part of the radionuclide transport model chain in the PSAR, the BioTEx model is applied to all relevant calculation cases in the overall assessment (Figure 2-2, step 8).

A strategy in the PSAR has been to improve the integration of the biosphere assessment with the overall safety assessment. Members of the biosphere team have worked closely with experts from other disciplines as a part of the radionuclide transport team. The integration has been facilitated by, for example, applying a biosphere assessment methodology that is compatible with the overall assessment methodology, common and consistent comprehensive descriptions of the initial state of the repository, geosphere and biosphere and of the evolution of the repository and its environs. The interpretation, presentation and communication of results produced within the biosphere assessment are also improved. Discussions about and iterations between identification and definition of calculation cases and the interpretation of results have improved the internal consistency of calculation cases, and have resulted in a better balance between simplifications made in the different domains (e.g. climate, near-field, geosphere and biosphere). The results from the probabilistic simulations conducted for the main scenario (Chapters 9 and 10) are part of the process of selecting the calculation cases presented in the **Radionuclide transport report**, and further propagated to the **Post-closure safety report**. Thus, interpretations of results presented here are directly applicable to the results that underpins the risk assessment.

A comprehensive understanding of results also helps to build confidence in the reliability of the results of individual calculation cases, confirming that the model responses to changes in conditions are reasonable. Results from the supporting calculation cases presented in Chapter 11 are only presented in this report. These calculations are designed to address scenario, model and data uncertainties that are biosphere-specific. However, where applicable, conclusions drawn from these cases are referred to in the discussion of risk and the evaluation of safety (**Post-closure safety report,** Chapters 10 and 11).

3 Site description – present-day conditions at Forsmark

The initial state of the repository and its environs is defined as the expected state at closure of the repository and is one of the fundamentals for the safety assessment (**Post-closure safety report**, Chapters 2 and 4). For the surface system, the initial state is assumed to be similar to the present-day conditions at Forsmark presented in this chapter in terms of climate (Section 3.1), topography and regolith (Section 3.2), surface hydrological conditions (Section 3.3), chemical conditions (Section 3.4), marine, limnic and terrestrial ecosystems (Section 3.5), human population and land use (Section 3.6) and wells and water resources management (Section 3.7). Most data and models for the description of the surface systems presented were included in the site descriptive model (SDM) for SR-PSU (SKB TR-11-04), but the main part of the information was produced as part of SDM-Site (SKB TR-08-05), i.e. the site description for the repository for spent nuclear fuel at Forsmark. A relatively large area (the Forsmark area, see the overview map in Appendix B) was therefore included in the underlying site description. Here in the PSAR, the main focus has been on the smaller area downstream of SFR, which already in earlier assessments was identified as the potential area for release from SFR (release areas, so called biosphere objects, are further described in Chapter 5). The site description was updated with knowledge from new investigations performed after SR-PSU, whereas other recent studies are still being processed or analysed for use in future safety assessments.

3.1 Climate conditions

The recent and present climate in the Forsmark area has affected and continues to affect the development and structure of the regolith and topography, hydrology, chemistry, ecosystems as well as potential human land-use activities. The average surface air temperature and precipitation during the IPCC (Intergovernmental Panel on Climate Change) 1986–2005 reference period (IPCC 2013) can be used to describe present-day climate conditions at Forsmark (**Climate report**, Section 3.3). This period is also used as a baseline in most of the future climate and sea-level projections in this safety assessment (**Climate report**, Sections 3.4 and 3.5). The Forsmark mean annual air temperature during the reference period is estimated as 6.1 °C (**Climate report**, Section 3.3). This is about 0.6 °C higher than the average air temperature during the 1961–1990 reference period used in SR-PSU (SKB TR-14-06, Section 3.2) and is thus consistent with the overall warming trend observed in the region.

The vegetation period, broadly defined as the interannual period during which the mean air temperature is above 5 °C, is approximately 6 months (May to October) according to temperature data in the 1986–2005 reference period. The prevailing wind direction is from the southwest and the mean annual precipitation is estimated to 612 mm during this period (**Climate report**, Section 3.3). This is about 10 % higher than the mean annual precipitation calculated for the 1961–1990 SR-PSU reference period (Johansson et al. 2005). Precipitation at Forsmark is unevenly distributed over the year. Most precipitation in the reference period occurred during the summer period of June–August with an average of 203 mm and the least precipitation occurred during the spring period of March–May with an average of 112 mm. According to the meteorological and hydrological monitoring programme conducted at Forsmark (Berglund and Lindborg 2017), which includes data from surrounding stations operated by the Swedish Meteorological and Hydrological Institute (SMHI), ~75 % of the precipitation returns to the atmosphere via evapotranspiration and ~25 % is converted to runoff (Johansson et al. 2005, Werner at al. 2013).

3.2 Topography and regolith

For historical and practical reasons, the safety assessment is mainly described and modelled separately for the near-field, the geosphere and the surface system. The surface system contains the bedrock surface in rock outcrops, the regolith, i.e. unconsolidated deposits on top of the bedrock, the surface groundwater within the regolith, waterbodies, and the adjacent atmosphere, including the organisms in these media. However, the geosphere and surface hydrological models underlying the transport modelling overlap across this somewhat arbitrary border to ensure consistency of assumptions and boundary conditions.

The bedrock surface in the Forsmark region is a part of the sub-Cambrian peneplain in southeast Sweden. This peneplain represents a relatively flat topographic surface with a gentle slope towards the northeast that formed more than 540 million years ago (SKB TR-08-05). The Forsmark area is characterised by a small-scale topography (Figure 3-1). Most of the area studied in detail in the site investigations for the planned spent nuclear fuel repository is below 20 metres above the current sea level (Johansson 2008).

Figure 3-1. *The Forsmark area seen from the southeast, with the only larger arable land area, Storskäret, in the foreground, and the Forsmark nuclear power plant in the background (cf Appendix B).*

The whole area is located below the highest coastline associated with the last deglaciation and large parts of the area emerged from the Baltic Sea only during the last 2 000 years (Section 4.6.2). Despite the relatively flat topography, the upper surface of the bedrock undulates over small distances, but this variation is partly evened out by variations in thickness of the regolith, i.e. unconsolidated deposits above the bedrock (SKB TR-08-05 and see Figure 3-4).

A Digital Elevation Model (DEM) describes the topography (including bathymetry which is the underwater equivalent to topography) of the Forsmark area (Figure 3-2). The DEM, which has a horizontal resolution of 20 m, is a central data source for the site characterisation, and it is used as input to hydrogeological descriptions and models, as well as to most of the descriptions and models of the surface system. In the terrestrial areas, the DEM is based on aerial stereo-photographs taken from an altitude of 2 300 m. In the marine areas, the DEM is constructed using a combination of nautical charts, supplementary depth probing and marine-geological surveys. A detailed description of the DEM is provided in Strömgren and Brydsten (2013). The elevation differences are small in the terrestrial parts of the Forsmark area, especially near the coastline, and also in the marine areas in the vicinity of SFR. Prominent topographical features of the landscape are glacial landforms such as eskers. The highest overall areas are located in the southwestern part of the area (Figure 3-2). A deep trough (Gräsörännan) runs in the NNW–SSE direction in the eastern part of the embayment, and the lowest point (−55 m elevation) is in the northernmost part of this trough.

In the Forsmark area, as common in Sweden, almost all the regolith was formed during or after the final phase of the latest glaciation, which in Forsmark occurred at around 8800 BC. Since it was formed during the Quaternary period, the regolith is commonly denoted Quaternary deposits. Soils, i.e. the upper part of the regolith in terrestrial systems and the uppermost sediments in aquatic systems, are affected by a number of processes, e.g. deposition, decomposition of organic material, bioturbation, erosion, and in terrestrial areas also frost action and weathering. Data describing regolith properties are an important input when modelling the hydrology and transport of elements and various compounds within the biosphere and between the geosphere and the biosphere. Soil properties are also strongly associated with vegetation types and land use in terrestrial ecosystems.

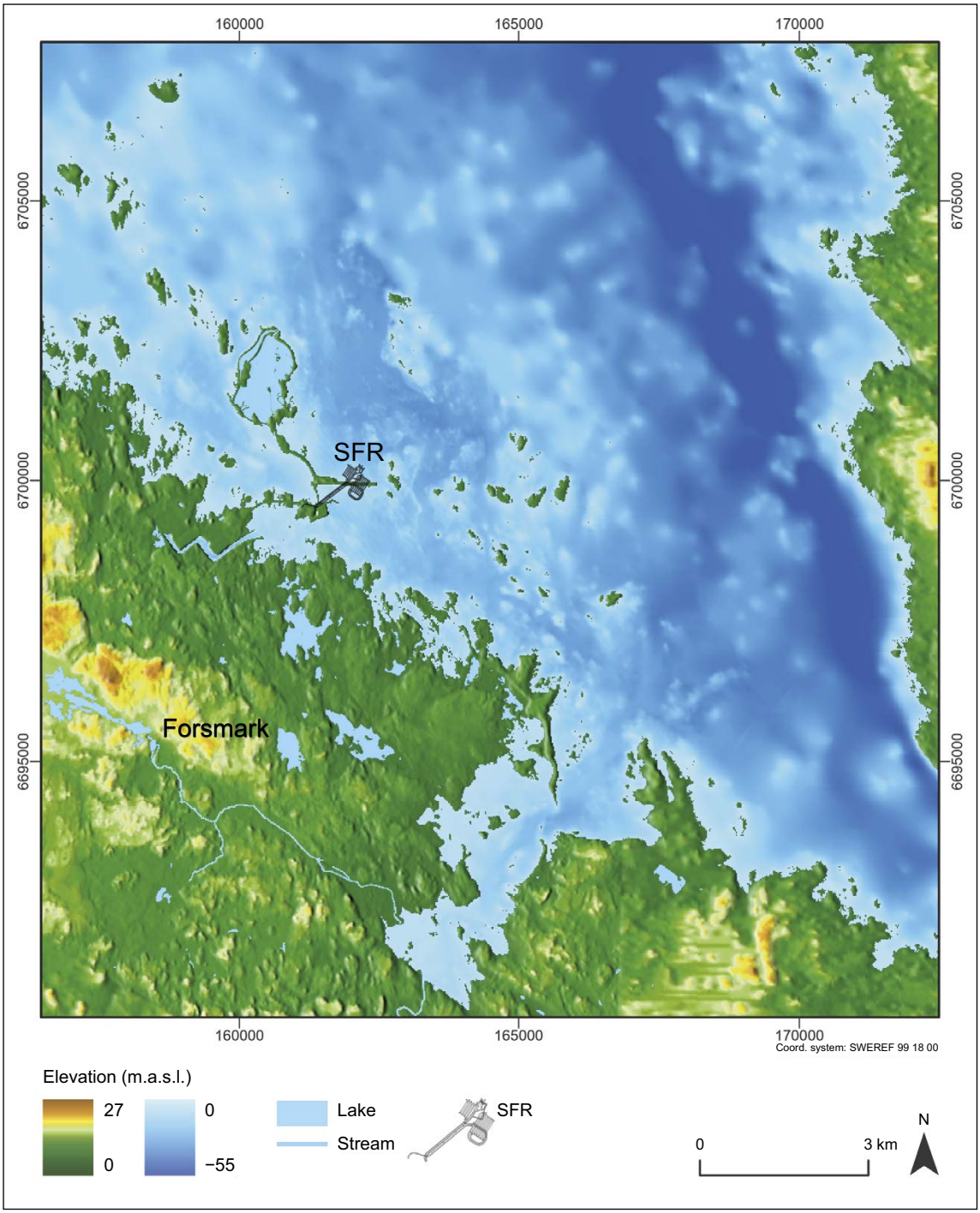

Figure 3-2. *The digital elevation model (DEM) of the Forsmark area, including the bathymetry of the sea (Strömgren and Brydsten 2013). The DEM has a horizontal resolution of 20 m. The map also shows the location of the existing and planned extension of SFR.*[7]

[7] On the maps produced for this report, horizontal coordinates are generally given in the coordinate system SWEREF 99 18 00, where numbers approximate meters. Maps copied from, and produced for, SR-PSU (e.g. SKB TR-14-06) use RT 90 2,5 gon V/0:15. Information about the coordinate system is given in figure legends or captions. Elevation is expressed as meters above the sea level 1970 (RHB 70 datum).

The descriptions of the spatial distribution of regolith (Figure 3-3) and its properties are based on the map of regolith and primary data obtained from extensive field mapping, investigations in the form of drilling, excavations and geophysics, and physical and chemical laboratory tests. For further details on the availability of primary data associated with regolith and soil and evaluations of such data, see Lundin et al. (2004), Hedenström and Sohlenius (2008), Nyberg et al. (2011), and Sohlenius et al. (2013a).

The distribution of regolith types in Forsmark (Figure 3-3) is typical for areas located below the highest coastline. Exposed bedrock occurs in locally high topographical terrestrial areas and along the shoreline. Till is the dominant type of regolith and occupies about 65 % of the surface in terrestrial areas and 30 % of the sea floor. A glaciofluvial deposit, Börstilåsen, has N–S and NW–SE directions along the coast of the mainland, and a continuation at the sea floor east of SFR. Glacial clay occurs primarily below present lakes and in depressions on the sea floor. Postglacial sand often covers the glacial clay. Postglacial clay gyttja, rich in organic material, is predominantly found and is presently being deposited in shallow bays and in the deepest parts of the sea floor. Gyttja mainly consists of organic material and is currently being deposited in the lakes. Peat accumulates in fens and along the lakeshores. The sea floor in the close vicinity to SFR is dominated by till and, in the lower topographical areas, by glacial clay partly covered with sand. The shallowest areas and islands have a high proportion of exposed bedrock.

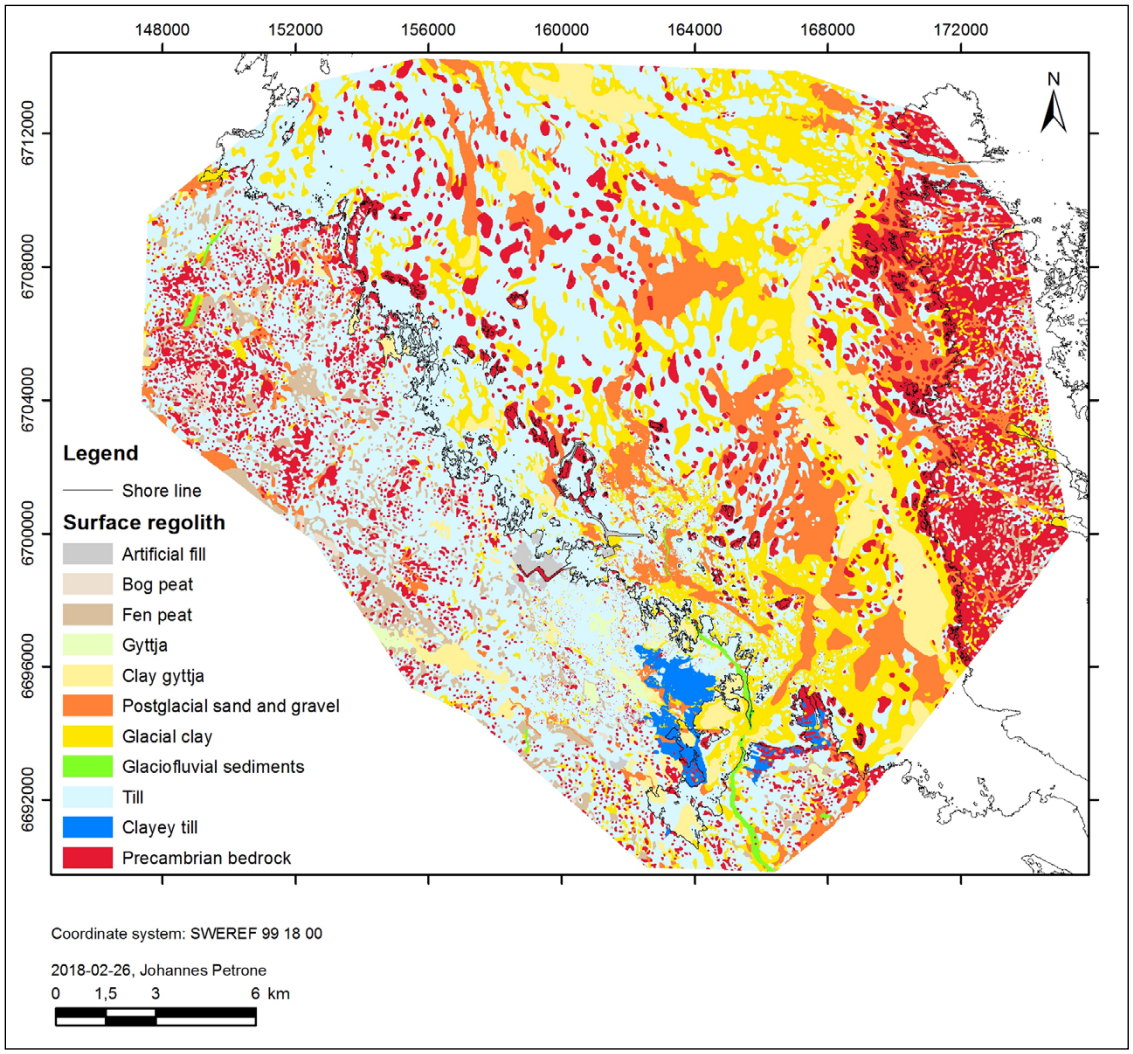

Figure 3-3. *Surface distribution of regolith with a minimum thickness of 0.5 m and areas with exposed bedrock in the Forsmark area (note that lakes and the sea are shown without surface water). Figure modified from Petrone et al. 2020.*

Soil-type classifications were conducted in pits dug in each land use type (forest, wetland, arable land). Compared with most other parts of Sweden, regolith in the Forsmark area has been subjected to soil-forming processes only for a relatively short time and most of the soils are therefore immature and lack distinct soil horizons (Lundin et al. 2004). Till and glacial clay in Forsmark have high contents of calcite (calcium carbonate, $CaCO_3$) and originate from Palaeozoic limestone that outcrops on the sea floor north of the Forsmark area (e.g. Figure 4-12 in Hall et al. 2019). The high content of $CaCO_3$ in the soils strongly affects their chemical properties.

A regolith depth and stratigraphy model (RDM) has been developed to provide a geometric model of the thickness and surface distribution of regolith layers at a landscape level. The RDM is based on the general top-down stratigraphy for the Forsmark area, consisting of peat, gyttja and clay gyttja, postglacial sand/gravel, glacial clay, glaciofluvial sediments, and till (Sohlenius et al. 2013a).

The total regolith thickness varies between 0 and 47 m. The coastal zone and the islands (including the coastal zone of the island of Gräsö) are characterised by thin regolith and frequent bedrock outcrops. Generally, the regolith is thicker in the marine area, with an average thickness of c 8 m, whereas the average thickness in the terrestrial area is c 4 m. The regolith thickness on the sea floor (excluding the long pier clearly visible in the shoreline contours of the maps) above the SFR repository and in the primary release area (biosphere object 157_2, see Chapter 5) is mostly 1–5 m (Figure 3-4).

A new DEM (Petrone and Strömgren 2020) and a new RDM (Petrone et al. 2020) have recently been published but they are not yet incorporated in the safety assessment for SFR.

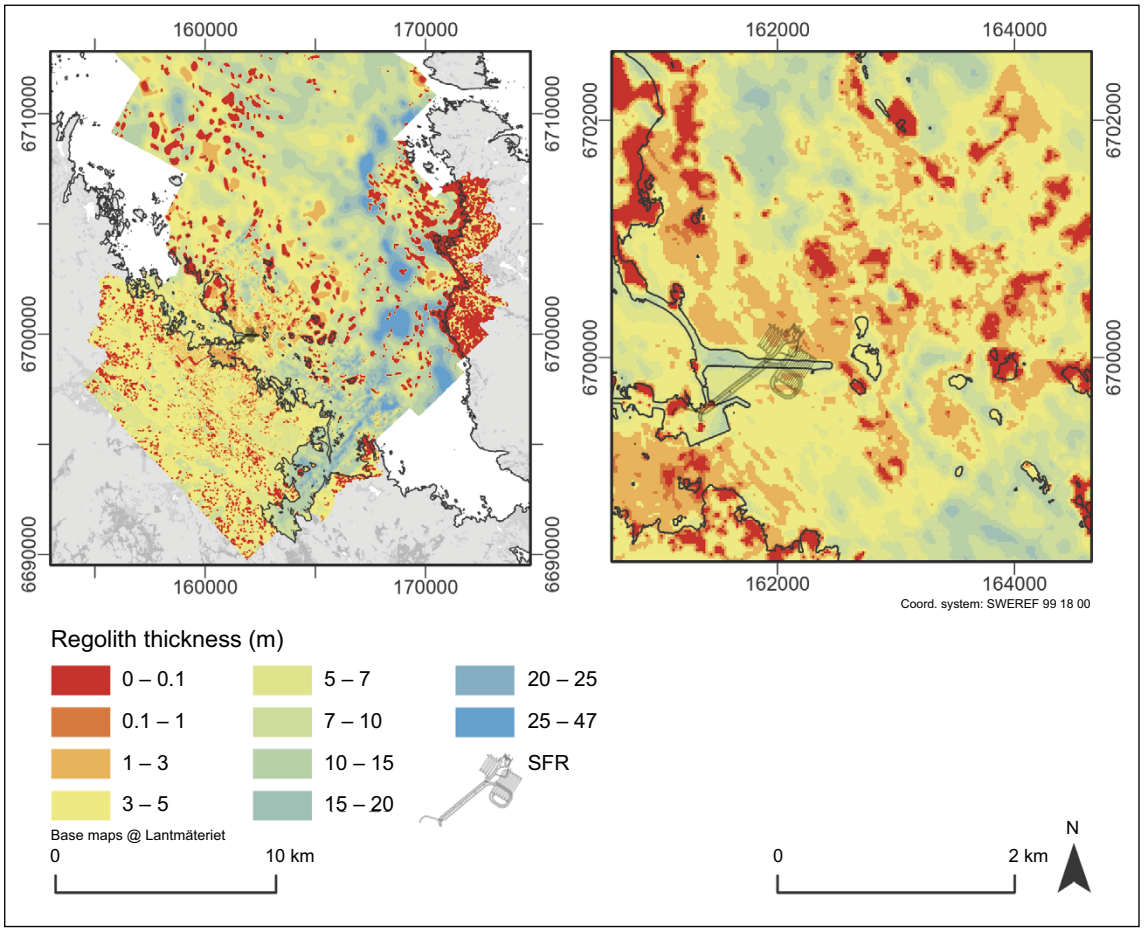

Figure 3-4. *Modelled total regolith thickness, left) in the Forsmark area and right) closest to SFR (Sohlenius et al. 2013a). Bedrock outcrops are shown as areas with regolith depth 0–0.1 m.*

3.3 Hydrological conditions

3.3.1 Surface hydrological conditions

The marine area at Forsmark consists of the open-ended embayment Öregrundsgrepen, with a wide and deep boundary towards the north and a narrow and shallower strait towards the south. Based on the sea bathymetry according to the DEM (Strömgren and Brydsten 2013), the present-day marine area outside Forsmark was divided into 38 basins (Figure 3-5). Most of this coastal area is shallow (sea depth less than 10 m), except for Gräsörännan with sea depths exceeding 50 m. The salinity stratification in Öregrundsgrepen is generally weak. Local freshwater runoff results in a slightly lower salinity compared with the Bothnian Sea (Aquilonius 2010). The direction of the flow through Öregrundsgrepen varies with time, but on an annual basis there is a net flow directed from north to south (Karlsson et al. 2010).

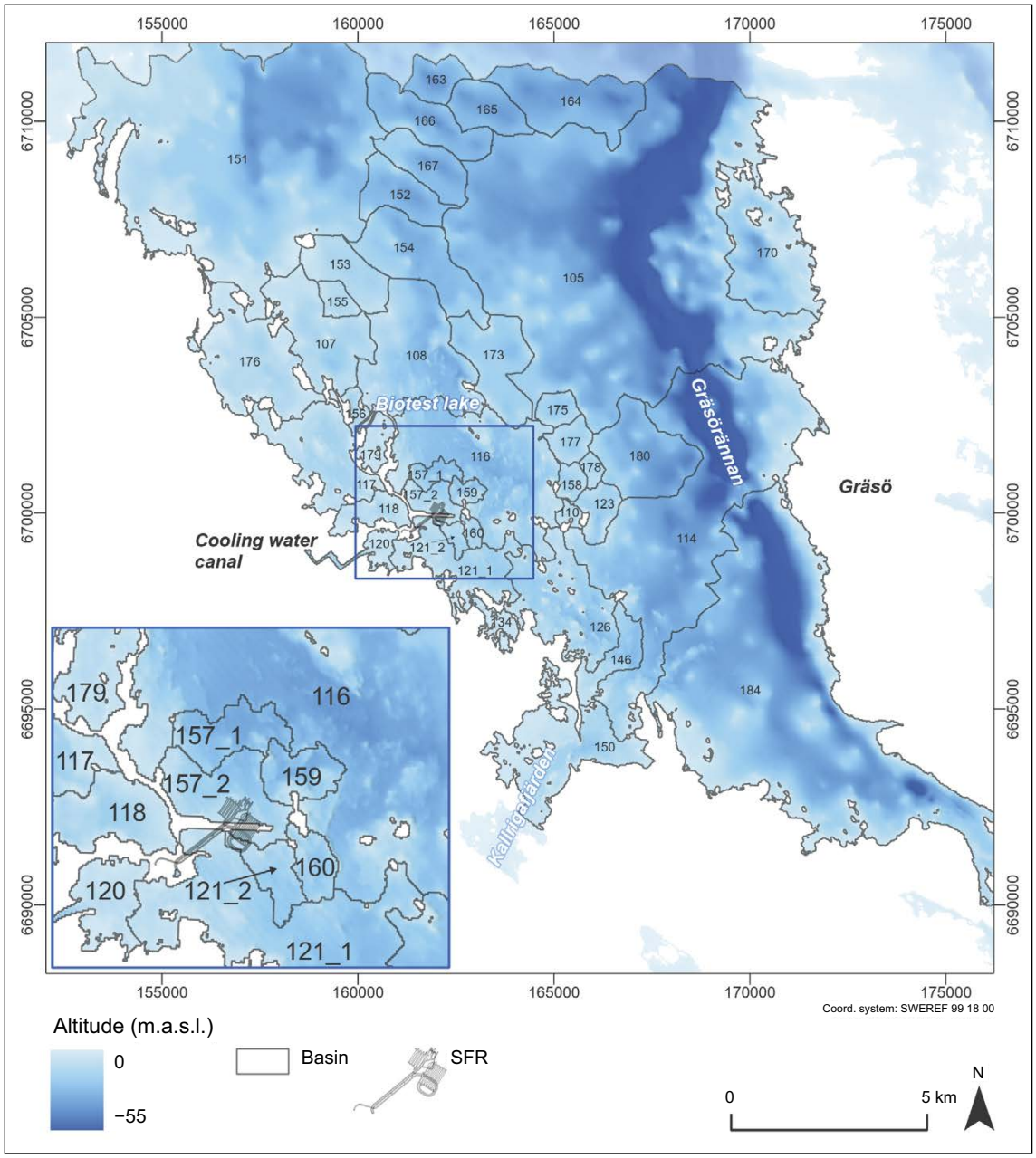

Figure 3-5. *Coastal basins (delineated based on the DEM) outside Forsmark. The inlet to the cooling-water canal for the Forsmark nuclear power plant is visible in basin 120, and the location of SFR is indicated on the map.*

The calculated average residence time (‘average age of the water’, AvA) for the individual basins varies between 13 and 29 days with an average of 19 days (Werner et al. 2013). AvAs are generally smaller in the deeper areas close to the open Bothnian Sea and generally larger in the shallow, isolated coastal basins. For basin 157, directly above SFR, the AvA is 20 days. Most of the sea bottom consists of shallow and exposed semi-hard (till, sand and gravel) and hard bottoms (boulders or bedrock) interspersed by valleys with soft bottoms (cf Figure 3-3).

A total of 25 present and future (currently sea-covered) lake catchments and sub-catchment areas, with sizes ranging from 0.03 to 8.67 km^2, have been delineated within the Forsmark area (Brunberg et al. 2004, Andersson 2010). Lake Fiskarfjärden, Lake Bolundsfjärden, Lake Eckarfjärden and Lake Gällsboträsket are the largest present lakes in the area (Figure 3-6 and Figure 3-7), but they all have a surface area of less than 1 km^2. The average depth of the lakes in the Forsmark area is less than one metre. Wetlands cover 10–20 % of the Forsmark area (Löfgren 2010). Many wetlands contain ecologically important ponds, whose depths and extents vary with wetter and drier periods. Forsmarksån and Olandsån are the largest streams around Forsmark (Figure 3-6) and other streams in the area are small with highly seasonal flows; several sections of these streams are often dry during the summer (Figure 3-8).

The infiltration capacity of the regolith in the Forsmark area generally exceeds rainfall and snowmelt intensities, and groundwater recharge is dominated by precipitation and snowmelt (Johansson 2008). This suggests that surface runoff in the area is relatively low and that the waterways in Forsmark receive much of their water from the near-surface groundwater. For example, lakes in the area are generally considered to be groundwater discharge areas. However, some lakes may periodically switch to recharge areas during the summer months as groundwater levels decrease to levels below the surface water levels in the lakes. Fluxes of deep groundwater through the lake bottoms are assumed to be small relative the fluxes from the near-surface groundwater due to the relatively low hydraulic conductivity of the lake sediments.

The groundwater table in the regolith tends to follow the surface topography and is generally within one metre of the ground surface (Figure 3-9) and groundwater divides in the regolith are therefore assumed to coincide with the topographical surface-water divides. The close correlation between the landscape topography and the near-surface groundwater results in the locally varying groundwater system with a small spatial scale in relation to the groundwater flow systems of the bedrock.

The hydrological and hydrogeological system at Forsmark is complex. Detailed numerical hydrological models were needed in order to help predict how the system would respond to future conditions. Hydrological/hydrogeological models for Forsmark were constructed using the MIKE SHE modelling tool during SR-PSU (Werner et al. 2013). These models were calibrated against the present understanding of Forsmark (i.e. measured data) and then used to predict the future hydrological and hydrogeological conditions of the area as affected by projected changes in the landscape, primarily driven by the shoreline displacement and climate (further described in Section 4.3).

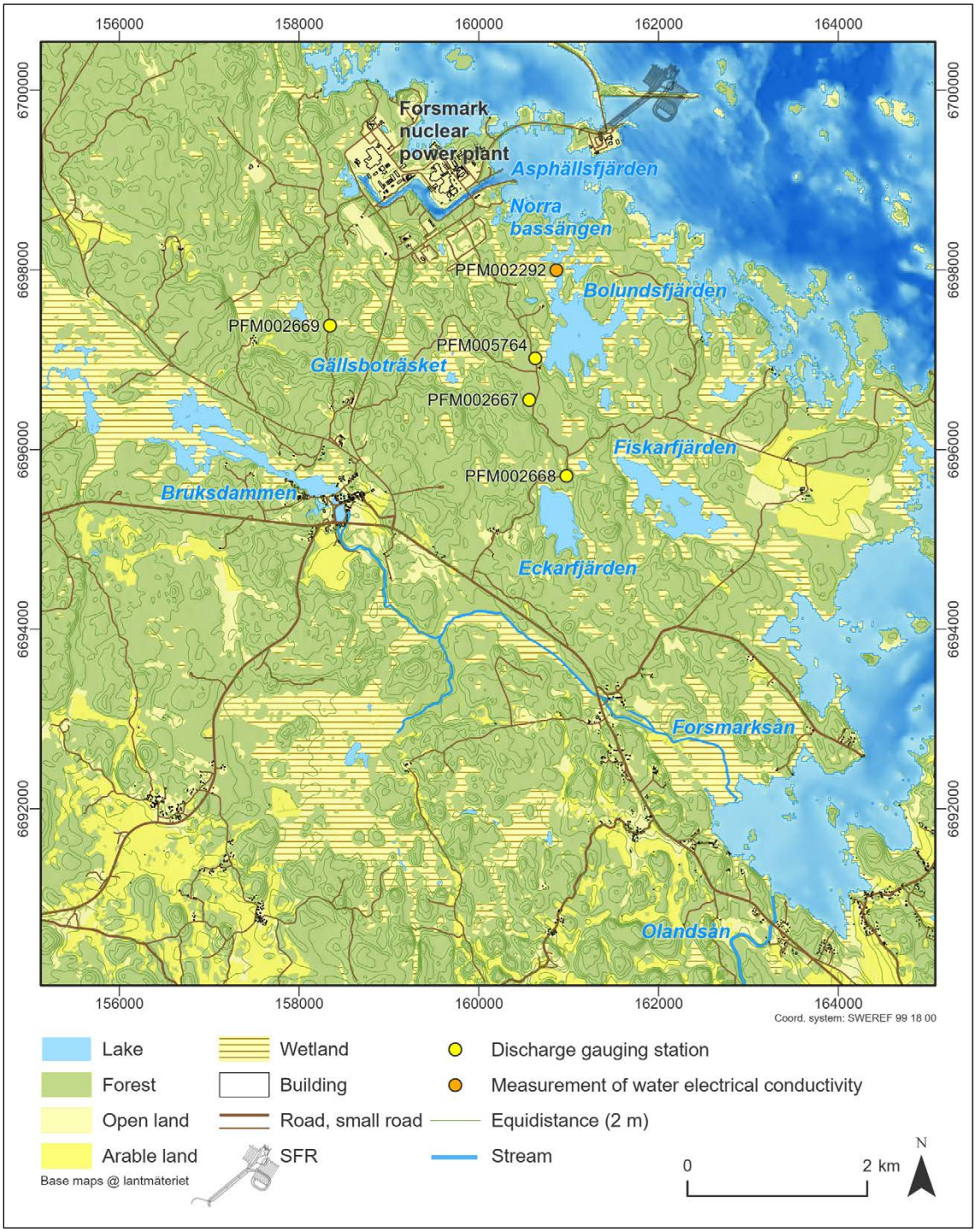

Figure 3-6. *Overview map of lakes, streams and some monitoring stations.*

Figure 3-7. *Lake Eckarfjärden (see also Figure 3-6), one of the larger lakes in the Forsmark area. As with other lakes in the area, Lake Eckarfjärden is a shallow oligotrophic hardwater lake, with dense Chara stands on the lake bottoms and the shoreline dominated by reed belts.*

Figure 3-8. *Photos showing (left) the largest stream in the Forsmark area (excluding Forsmarksån and Olandsån), near the inlet to Lake Bolundsfjärden (see Figure 3-6) and (right) a stream section that is dry in the summer, a common sight in the Forsmark area.*

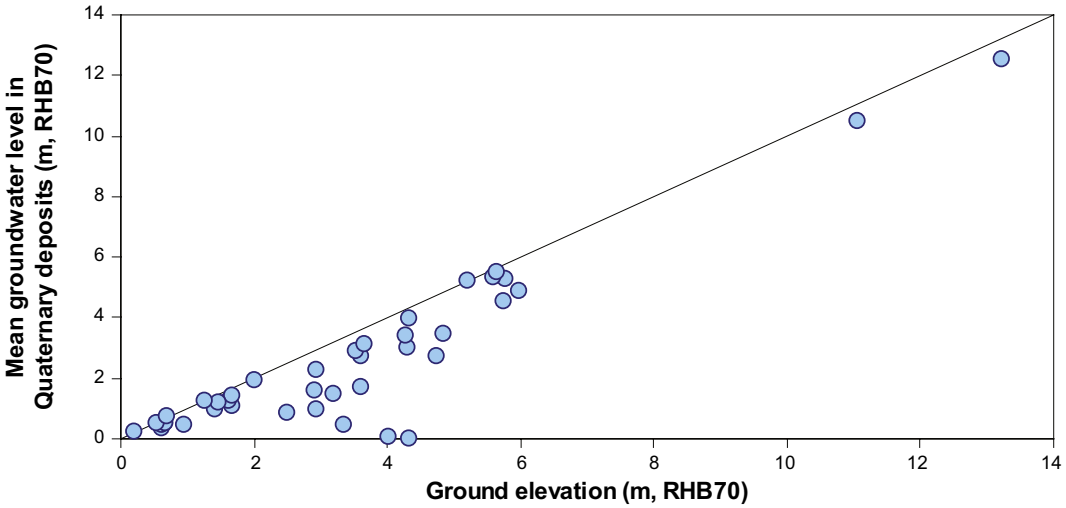

Figure 3-9. *Cross plot and 1:1 line (solid black line) of average groundwater level in regolith (blue dots) against the ground elevation at the location of the measurement. The figure is produced using data from Johansson (2008).*

3.3.2 Bedrock hydrogeological conditions

The bedrock hydrogeological system surrounding SFR is an important part of the total hydrological system within the context of the PSAR: it is primarily the bedrock hydrogeological system that governs where radionuclides are predicted to reach the surface following a potential release from the repository level. A conceptual model of the bedrock hydrogeological features surrounding SFR (Figure 3-10) was used in the safety analyses presented in SR-PSU (see Odén et al. 2014). This conceptual model is also used in the PSAR. The model was built using borehole data, measurements of the magnetic total field at the surface (i.e. magnetometry data), hydrogeological testing data, and data gathered during the tunnelling and construction of the SFR repository. Presentation of the conceptual model as well as the data used in its construction was presented in Öhman et al. (2012).

Two relatively wide deformation zones, known as the "Northern boundary belt" and the "Southern boundary belt" bound the SFR site to the northeast and southwest respectively (see Figure 3-11). Within the context of these analyses, the deformation zones are areas in the earth's crust where shear forces in two or more rock masses can cause a ductile and/or brittle failure of the rock along the shear plane (i.e. a fault line). Between these boundary belts is located a rock volume that is significantly less affected by deformation, called the "Central block". SFR, including the planned extension, will is located entirely within the Central block. A series of smaller deformation zones run perpendicular to the bounding belts within the rock volume for the planned SFR extension. Observation of these deformation zones was done primarily via the analysis of borehole and magnetometry data. A total of forty deformation zones are accounted for in the bedrock conceptual model with varying levels of confidence in their existence (Odén et al. 2014). Three of these deformation zones are modelled as gently dipping (i.e. the inclination of the formation relative the horizontal plane is < 45°) with the remainder being either steeply dipping (i.e. the inclination of the formation relative the horizontal plane is > 45°) or vertical (see Stephens et al. 2007 and Odén et al. 2014). The deformation zones are characterized by brittle, ductile and highly conductive rock and are referred to as hydraulic conductor domains (HCDs) in the conceptual model, (Figure 3-10). The conductivities within the deformation zones are several orders of magnitude higher than in the surrounding rock which allows for substantially larger flows within these zones. This implies that the bulk vertical transport of radionuclides to the surface is likely to occur within a deformation zone following a release of radionuclides from SFR. For more information regarding the identification and modelling of the deformation zones (see Rhén et al. 2003).

Some borehole sections showed bedrock with characteristics similar to those found in a deformation zone (i.e. a highly transmissive section of rock), but these deformations could not be linked to a surface geological feature thus making them "unresolved". This means that although the existence of these deformation zones is supported by measurements there is less confidence in their size and position relative the deformation zones discussed above. These unresolved deformation zones are referred to as potential deformation zones (PDZs), see Figure 3-10, and they are stochastically represented in the conceptual model (see Öhman et al. 2012, Appendix A).

Transmissivity measurements in the upper 200 m of bedrock within the boundaries of the SFR regional model (Figure 3-11) indicate that there likely exists a network of water-bearing structures with heightened transmissivities with an orientation ranging from gently-dipping to horizontal. The most transmissive fractures are generally gently dipping to horizontal which play an important role in the hydrogeology of the fractured rock at these depths. In the top 60 m of the bedrock, measurements indicate that the rock mass is highly transmissive relative the average transmissivity of the bedrock volume below 60 m. This heightened transmissivity appears to be spatially independent within the SFR regional model area. Between 60 and 200 m depth, transmissivity measurements indicate that bedrock structures with heightened transmissivities exist near the Northern and Southern boundary belts but not within the Central block (see Öhman et al. 2012, Section 5.3.1). These high-transmissivity structures are referred to as "Shallow Bedrock Aquifer" SBA) structures are represented deterministically in the conceptual geological model used in the PSAR even though their existence is uncertain (Figure 3-10). For more information on the realization of these structures in the conceptual model see Appendix B in Öhman et al. (2012).

Current limitations in measurement techniques prevent the observation of every water-bearing structure relevant for SFR. However, it is understood that there certainly exist structures in the bedrock that we have not observed but will certainly affect the regional and local hydrogeology relevant for SFR. In the conceptual model, these unobserved structures are represented by a stochastically generated "discrete fracture network (DFN)". While much of the DFN is randomly generated, parametrization of the hydraulic properties of the DFN are largely based on observations like fracture statistics from boreholes and surface outcroppings. For more information regarding the generation and parametrization of the DFN see Appendix G in Öhman et al. (2012).

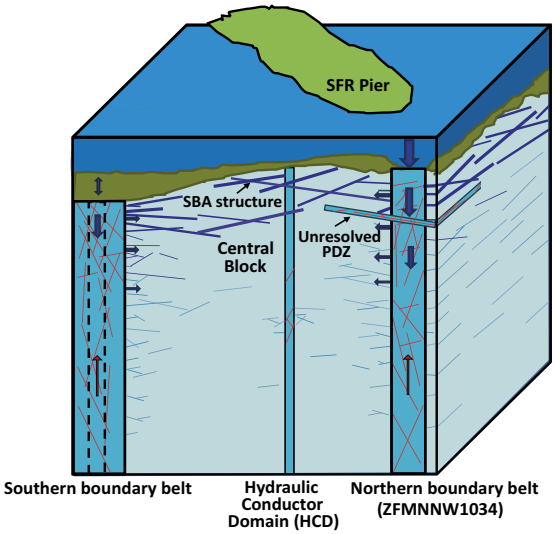

Figure 3-10. *Side view facing west showing the conceptual model of hydrogeological features relevant for the PSAR including the Northern and Southern boundary belt. The horizontal and vertical dimensions of the conceptual model are approximately 1.5 km and 1.1 km respectively. Figure modified from SKB TR-11-04.*

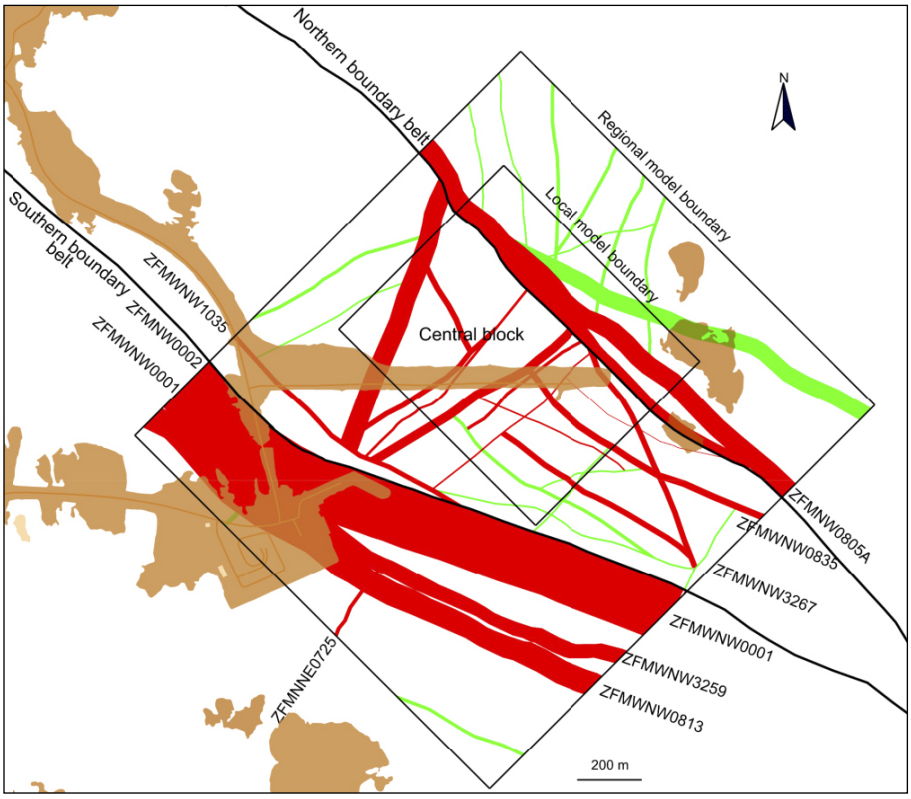

Figure 3-11. *A top-down view of the intersection, the deformation zones inside and the current ground surface within the PSAR regional and local model area. Deformation zones with a "high confidence in existence" are displayed in red. Deformation zones with a "medium confidence in existence" are displayed in green. Names of individual deformation zones are also noted; names of deformation zones use the notation "ZFM" followed by a unique ID. The domain boundaries of regional deformation zones ZFMWNW0001 and ZFMN20805A form the Southern respective Northern belt boundaries of the Central block.*

3.4 Chemical conditions

The chemistry of the surface systems (surface water, groundwater, regolith, soils, sediments and biota) at Forsmark has been the subject of various site investigation and modelling activities, including studies of the water chemistry of limnic and marine systems (e.g. Sonesten 2005, Tröjbom and Söderbäck 2006, Tröjbom et al. 2007, Andersson 2010, Aquilonius 2010, Qvarfordt et al. 2010), the chemistry of terrestrial systems including regolith and sediments (Hedenström and Sohlenius 2008, Löfgren 2010, Sheppard et al. 2009, 2011), the chemistry of biota (Sheppard et al. 2009, 2011), and synthesis reports concerning the chemistry of the surface system (Tröjbom and Grolander 2010, Tröjbom and Nordén 2010, Löfgren 2011). Since 2002 there has been an ongoing long-term chemical monitoring programme at the site, comprising surface water and groundwater from regolith and bedrock (SKB R-07-34, Berglund and Lindborg 2017).

The high content of calcium carbonate (calcite) in the regolith and the recent emergence of the Forsmark area above sea level affect the chemistry of surface waters and shallow groundwater (Tröjbom et al. 2007). Specifically, surface water and shallow groundwater in Forsmark are generally slightly alkaline (pH 7–8) and have high concentrations of major constituents due to marine relics since the area was covered by sea water and due to glacial remnants deposited during the latest glaciation. The high calcite content of the till (c 20 wt% Hedenström and Sohlenius 2008) has had strong effects on the development of the terrestrial and limnic ecosystems at the site. Secondary calcite precipitation and co-precipitation of phosphate contribute to the development of the nutrient-poor oligotrophic hardwater lakes that are characteristic of the Forsmark area (Andersson 2010). The rich supply of calcium also influences soil formation and the development and structure of the terrestrial ecosystems, for example by the formation of rich fens with lime-favoured flora (Löfgren 2010).

The distribution of elements among biotic and abiotic pools within the surface systems gives, together with estimates of element fluxes into and out of these pools, an overall picture of major sources and sinks of elements in the landscape. For most elements, the dominant fraction of the total content is found in the regolith of both the terrestrial and limnic ecosystems. Carbon, main nutrients and some essential trace elements are also found in significant fractions in the organic soil and biota pools (e.g. N, P, K, S, Ca, Zn, Cu and Cl). This pattern is most pronounced for the terrestrial ecosystem due to the significantly larger biomass compared with the limnic ecosystem in Forsmark (Tröjbom and Grolander 2010). Recent studies have shown that a significant fraction of the Cl is bound into the biomass of the terrestrial system and that this pool has a high turnover rate (Svensson et al. 2021).

The mobility and retention of elements in the landscape are the basis for the radionuclide transport modelling of the biosphere. Empirical models based on sorption coefficients (K_d) and concentration ratios (*CR*) are applied to model the transport, retention and uptake of radionuclides in water, regolith and biota (Tröjbom and Nordén 2010, Tröjbom et al. 2013). The mobility of specific elements has been studied by statistical and geochemical models to further support the assumptions of the radionuclide transport model (Jaremalm et al. 2013, Sohlenius et al. 2013b, Erichsen et al. 2013, Lidman et al. 2017, Lidman 2022). These investigations illustrate the importance of understanding the modelled environment regarding chemical, physical and geometrical aspects to adequately model the speciation and fate of radionuclides released to the biosphere.

3.5 Ecosystems

One use of the description of the present-day surface ecosystems, together with scientific knowledge, is to identify processes potentially affecting transport and accumulation of elements to account for in the radionuclide transport modelling and safety assessment. This is done in a systematic manner by developing an interaction matrix for the surface system and FEP identification (see Chapter 6). The most important processes affecting transport and accumulation of elements in marine, limnic and terrestrial ecosystems, respectively, are summarized below (Figure 3-12 and Figure 3-13).

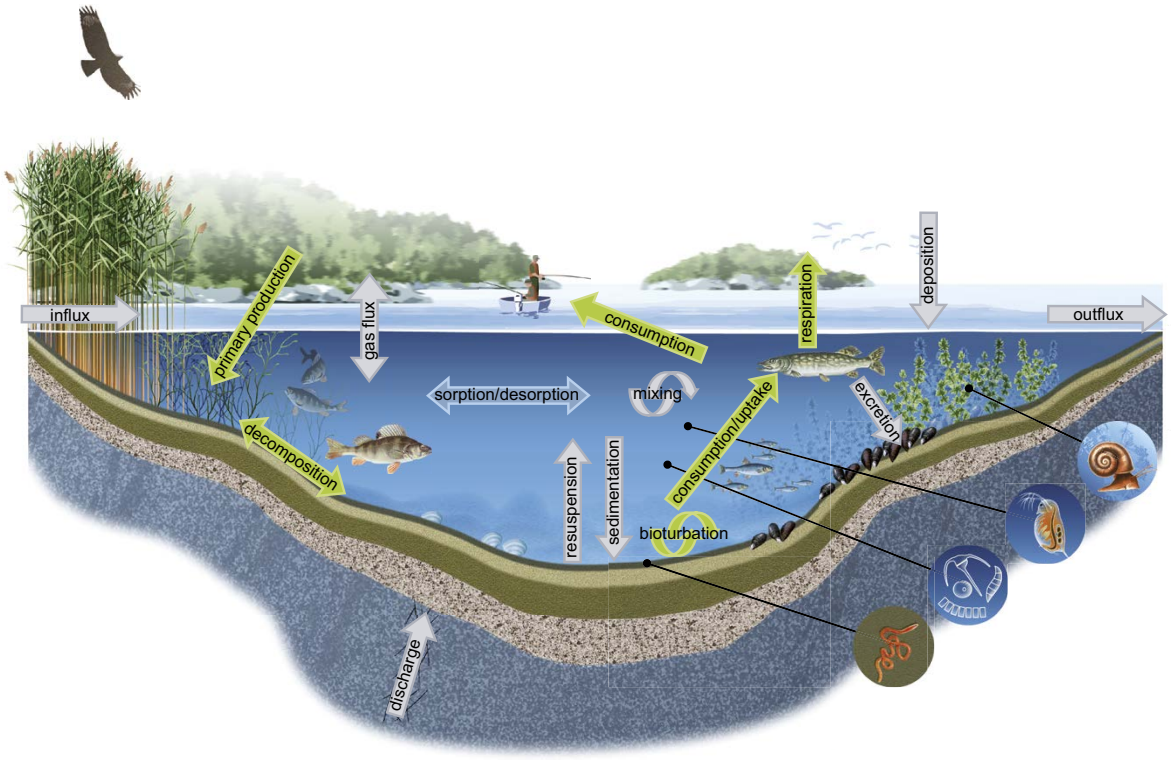

Figure 3-12. *Conceptual model of functional groups and important fluxes affecting transport and accumulation of elements in aquatic (i.e. limnic and marine) ecosystems. Green arrows are fluxes mediated by biota (including consumption of fish by humans), grey arrows are fluxes of water, particles and gas, and the blue arrow represents sorption/desorption processes. The symbols to the right are examples of the smaller-bodied flora and fauna in aquatic ecosystems.*

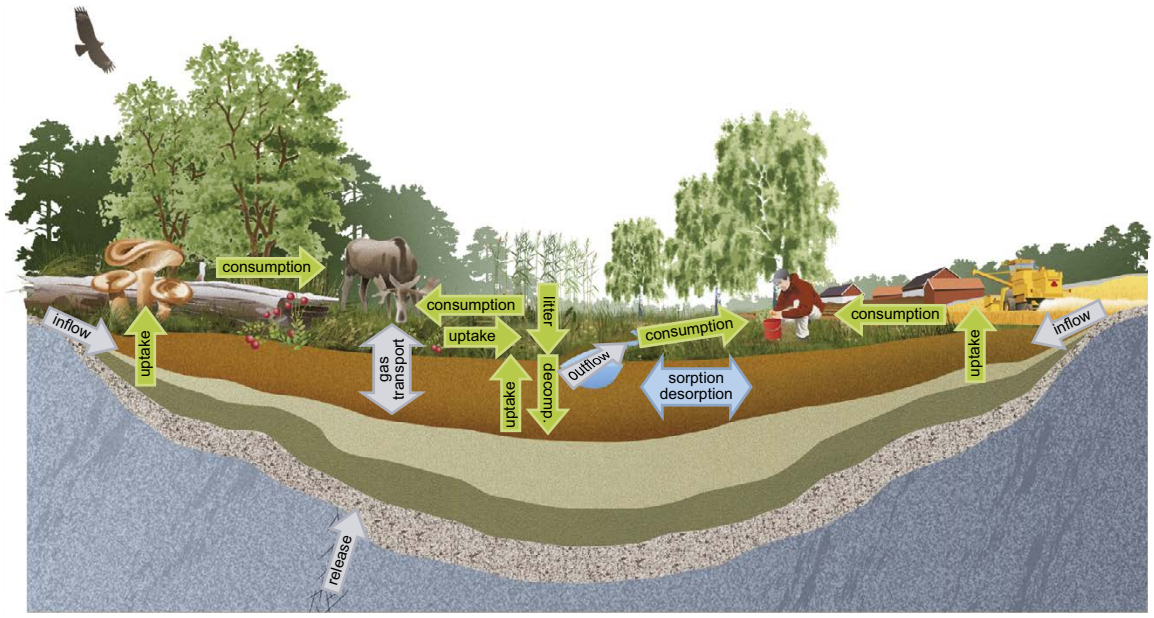

Figure 3-13. *Conceptual model of important fluxes affecting transport and accumulation of elements in a wetland ecosystem and arable land on a drained part of a mire (Löfgren 2010). Green arrows are fluxes mediated by biota (the uptake includes also the water for drinking), grey arrows are water and gas fluxes, and the blue arrow represents sorption/desorption processes. "Release" indicates a hypothetical release of groundwater from bedrock containing repository-derived radionuclides. The mire was preceded by a lake stage and a marine stage, in which gyttja/clay and postglacial clay (shown as the greenish regolith layers) were deposited prior to the peat (uppermost, brown layer).*

3.5.1 Marine ecosystems

The salinity in the Bothnian Sea outside Forsmark is low due to a large freshwater supply from terrestrial areas to the Gulf of Bothnia and Baltic Sea and limited mixing with the North Sea. This results in a low species diversity as few organisms are adapted to such brackish conditions. Shallow waters, subdued bathymetry, restricted light penetration and upwelling along the coast also characterise the marine ecosystems at Forsmark. Together, these factors result in a high primary production of primarily benthic vegetation in the near-shore zone, in a region of otherwise fairly low production (Aquilonius 2010). The primary production is lower in deeper areas and is there dominated by planktonic organisms due to limitation of light at the bottoms. In agreement with the general eutrophication of the Baltic Sea (Larsson et al. 1985, Andersen et al. 2017) and the Bothnian Sea (Lundberg et al. 2009) during the last century, the primary production has most likely increased in the Forsmark area. The biomass of primary producers is dominated by benthic organisms such as microalgae, vascular plants and benthic macroalgae and the fauna are dominated by detritivores (i.e. snails and mussels feeding on dead organic material) on both hard bottom (Figure 3-14) and soft bottom substrates. The fish community is generally dominated by the marine species herring (*Clupea harengus membras*) in the pelagic zone, whereas limnic species (especially Eurasian perch, *Perca fluviatilis*) dominate in near-shore areas and in secluded bays. Three-spined sticklebacks (*Gasterosteus aculeatus*) have increased considerably lately and dominate the fish community numerically (Adill et al. 2021).

Comparison between results from sampling of marine vegetation and the GIS model (Geographic Information System) used to model biomasses of marine basins (Aquilonius 2010) indicates that the GIS model predicts total biomass fairly well, with 1.4 times higher biomass in field investigations compared with modelled estimates (Aquilonius et al. 2011). Data from the mapping of reed beds in shallow bays in the Forsmark area (Strömgren and Lindgren 2011) have been used to improve the understanding of terrestrialisation, i.e. infilling of ecosystems transforming from marine basins into lakes and wetlands.

Both abiotic and biotic processes influence transport and accumulation of elements in marine ecosystems (Figure 3-12). However, carbon budgets (Aquilonius 2010) show that in marine ecosystems advective fluxes (water exchange) rather than biotic fluxes (e.g. primary production and consumption within the basins) often regulate transport and accumulation of elements (in particular in open and more offshore basins).

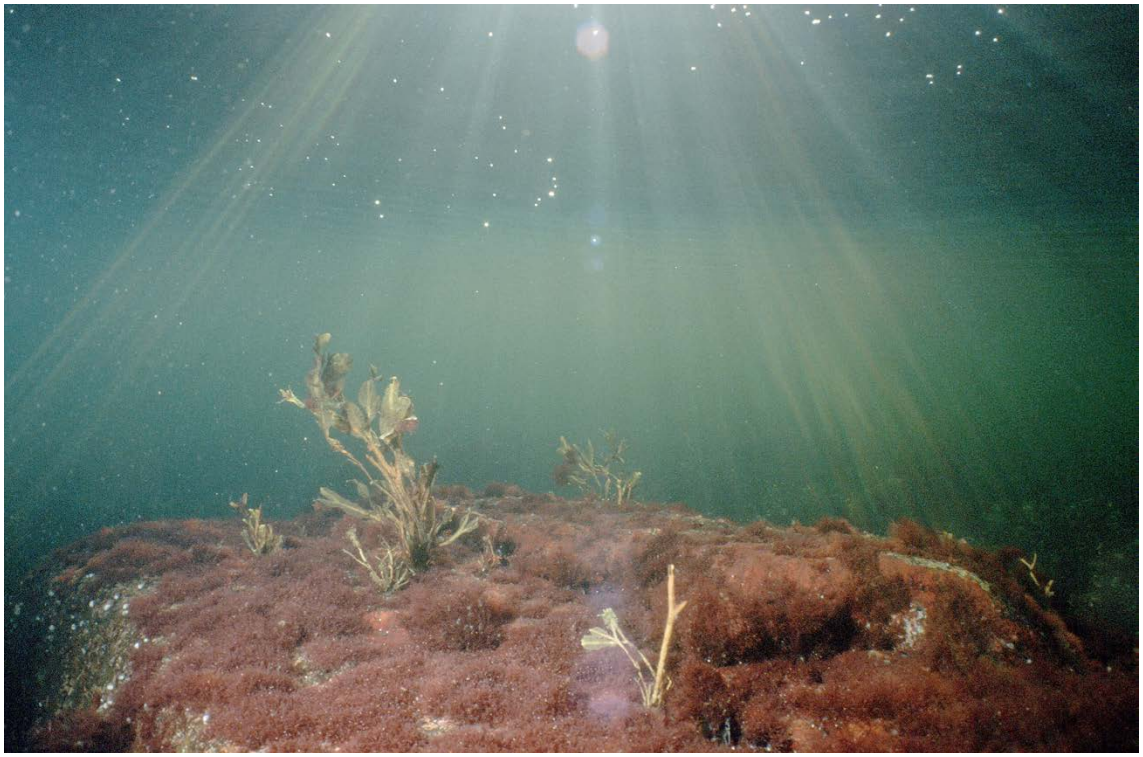

Figure 3-14. *Hard bottom with red algae and bladder wrack at Forsmark.*

The modelling of delineated marine basins shows that the whole marine area as an average has positive net ecosystem production (NEP), meaning that the primary production is higher than the decomposition. Specifically, shallow areas near the coastline have positive NEP and export of organic matter to more offshore areas that in turn have negative NEP, mainly due to the large contribution from benthic macroalgae in shallow areas. Further details on the availability of primary data associated with marine ecosystems and evaluations of such data are provided in Aquilonius (2010).

3.5.2 Limnic ecosystems

Present-day lakes in the Forsmark area (Figure 3-6) are small and shallow (mean depth is typically below 1 m). They are characterised as oligotrophic hardwater lakes, with high calcium and low nutrient levels (Andersson 2010). This lake type (exemplified in Figure 3-7) is common along the coast of northern Uppland region where Forsmark is situated, but rare in the rest of Sweden (Brunberg et al. 2002, Hamrén and Collinder 2010).

Shallow depths and relatively clear waters allow photosynthesis in the entire benthic habitat, and the lake bottoms are covered by dense stands of macrovegetation and a thick layer of microphytobenthos (microscopic algae and cyanobacteria). These two types of primary producers dominate the biomass and primary production, making phytoplankton biomass and production less important.

The shorelines are dominated by reed belts, which are extensive especially around the smaller lakes. The fish communities in the lakes of Forsmark are dominated by perch (*Perca fluviatilis*), roach (*Rutilus rutilus*), tench (*Tinca tinca*) and crucian carp (*Carassius carassius*), of which the latter two species are resistant to the low oxygen concentrations that could occur during winter under the ice.

The streams in the Forsmark area are small and many stream stretches dry out during summer (Figure 3-8). However, some streams close to the coast carry water for most of the year and function as passages for migrating spawning fish. Extensive spawning migration has been observed between the sea and Lake Norra Bassängen (Loreth 2005). The two large streams Olandsån and Forsmarksån, located just south of the Forsmark area, carry water during the whole year and discharge into the sea bay Kallrigafjärden. The vegetation in the streams is highly variable, between 0 and 100 % coverage of the streambed, but with some longer parts with intense growth (75–100 % coverage, Andersson et al. 2011).

As for marine systems, both abiotic and biotic processes influence transport and accumulation of elements in limnic ecosystems (Figure 3-12). Modelling of carbon dynamics in limnic ecosystems shows that, contrary to typical Swedish lakes, primary production exceeds respiration in many lakes in the Forsmark area (Andersson 2010). In some of the larger lakes in the area (e.g. Lake Bolundsfjärden and Lake Eckarfjärden, Figure 3-6), the primary production involves large fluxes of carbon compared with the amounts that are transported from the surrounding catchment area. Consequently, there is a large potential for inorganic carbon entering the lakes to be incorporated into the lake food web via primary producers. However, much of the primary produced carbon is circulated within the microbial food web and transferred back to abiotic pools or sequestered in sediments (Andersson 2010, Chapter 5).

In the larger lakes, there is a relatively large deposition in sediments, which can be a permanent sink for elements. In smaller lakes and ponds, the amounts of carbon involved in the primary production and deposited in sediments are small compared with the amounts of carbon transported from the surrounding catchment area. According to ecosystems modelling, these lakes hence function more as through-flow systems (Andersson 2010). The chemical properties of the elements, the size of the lake and its location in the catchment area determine the fate of elements entering lake systems. Further details on the availability of primary data associated with limnic ecosystems and evaluations of such data are provided in Andersson (2010).

3.5.3 Terrestrial ecosystems

The present-day terrestrial vegetation is strongly affected by topography, regolith characteristics and human land use. Some three quarters of the land area in Forsmark is covered by forests, dominated by Scots pine (*Pinus sylvestris*) and Norway spruce (*Picea abies*) (Löfgren 2010). Due to the calcareous regolith, the field layer is characterised by herbs, broad-leaved grasses and many orchid species. The area has a long history of forestry, with a large percentage of younger and older clear-cuts in different succession stages. Most of the frequent wetlands are coniferous forest swamps or open mires (Figure 3-15). Less mature wetlands consist of rich fens due to the high calcareous content of the regolith. In this report, the term mire is generally used for peat-accumulating wetlands, including both fens and raised bogs, of which especially fen mires can be suitable for drainage and cultivation. Agricultural land (arable land and grassland) only covers a minor part of the land area of Forsmark.

The most common large mammal species in the Forsmark area are roe deer (*Capreolus capreolus*) and moose (*Alces alces*). In total, 139 bird species have been found in the Forsmark area (Green 2019), and the most common species are, as in comparable regions of Sweden, chaffinch (*Fringilla coelebs*) and willow warbler (*Phylloscopus trochilus*) (Löfgren 2010). The area is interesting from a nature conservation point of view, where the highest nature values are associated with wetlands and forests containing red listed and/or legally protected species (Hamrén and Collinder 2010). Two such rare species are the wetland species fen orchid (*Liparis loeselii*) and the pool frog (*Rana lessonae*), which both have a restricted national distribution range along the coast around Forsmark within the north of Uppland and are found in this area.

Modelling of carbon dynamics for two conifer forest stands (i.e. the dominant vegetation type in Forsmark) and one forested wetland shows that the largest carbon flux in terrestrial ecosystems is the uptake of carbon by primary producers, and that the vegetation at all the investigated localities today acts as a carbon sink (Löfgren 2010). The net primary production sets the upper limit for the potential uptake of different elements into biomass, which in turn limits the extent of further propagation up the food web. Eventually, biomass reaches the soil compartment as litter and is mineralised. The balance between litter production and heterotrophic respiration determines to what extent organic material (and incorporated elements) can be accumulated in the soil, with generally higher accumulation in wet (and anoxic) conditions.

Figure 3-15. *A wetland in Forsmark dominated by common reed (Phragmites australis).*

Dynamic vegetation modelling based on site data shows that other vegetation types (e.g. deciduous trees, meadows and arable land) also are carbon sinks, with the exception of clear-cut forests that act as carbon sources (Löfgren 2010). Figure 3-13 illustrates a compilation of important processes for a mire ecosystem. Further details on the availability of primary data associated with terrestrial ecosystems and evaluations of such data are provided in Löfgren (2010).

3.6 Human population and land use

At the site, the Forsmark nuclear power plant is a large industrial activity in an otherwise relatively undisturbed area. There are no residents or holiday houses within a 3 km radius from SFR. Within a 5 km radius from SFR there are a few permanent residents and holiday houses and one farm (situated at Storskäret, Appendix B). The Forsmark area is used for hunting and fishing (outside the protected area around the nuclear power plant), but only occasionally used for other recreational activities due to the small local population, the relative inaccessibility of the area and the distance from major urban areas. Land use has previously been dominated by commercial forestry, and timber extraction has been the only significant man-made export of biomass from the area.

Despite the lack of farming close to SFR, present agricultural activities in the areas around Forsmark are described here in more detail due to the importance of cultivated land for potential future radionuclide exposure (see Sections 6.2.1 and 9.3). Currently most arable land in the region around Forsmark, as generally in the county of Uppsala, is situated in areas with water-deposited clays (glacial and post-glacial) and other fine-grained deposits, formed in topographical depressions when the area was covered by the Baltic Sea (Lindborg 2010). These deposits are, however, almost lacking in the terrestrial part of the present Forsmark area and the proportion of arable land is therefore low. That can, however, change in the future when the fine-grained deposits situated at shallow water depths around SFR become available for cultivation through the shoreline displacement (further discussed in Sections 4.6 and 4.7).

According to the land use data, the agricultural land in the Forsmark model area comprises 84 ha, of which 34 ha is arable area and 50 ha is classified as semi-natural grasslands or pastures (Löfgren 2010). Only around 10 % of the earlier used total agricultural area (arable area and pasture) is today used for production of grain and vegetables. This is in line with the agricultural practises in Sweden, where 3/4 of the agricultural area is used for fodder production and 1/4 for production of grain and vegetables for human consumption.

A smaller fraction of the arable land in the region around Forsmark is situated in areas with till and peat. The till in most areas has a high content of boulders and stones and is therefore not suitable for cultivation. The proportion of organic deposits used for cultivation in the whole of Sweden has decreased significantly during the last 60 years (cf Lindborg 2010). The present proportion of cultivated peat deposits in the County of Uppsala (5 %) is close to the Swedish average (Berglund et al. 2009). Today it is generally not allowed to make new ditches in areas unaffected by ditches, and peat-covered wetlands (i.e. mires) are at present not converted to arable land in Sweden. However, a larger proportion of the Swedish peatland could potentially be used for cultivation in the future.

Many of the wetland areas in the County of Uppsala have been drained for improving forest growth. This has caused subsidence and oxidation of peat in large areas. These processes are, however, much slower in forested areas than in areas used as arable land (Maljanen et al. 2010). Additionally, some wetlands have been drained for exploration of fuel peat or peat used for soil improvement. The peat in the Forsmark regional model area is at present not suitable for use as fuel, due to high sulphur and ash contents and to relatively small and shallow peat deposits (Lindborg 2010, Fredriksson 2004). Historical land use in the region, in particular cultivation of peat, is further described in Section 4.6.

3.7 Wells and water-resources management

All public water supply in the Municipality of Östhammar is based on groundwater (Werner et al. 2010). The public water supply closest to SFR is located at the Börstilåsen esker, several kilometres southeast of SFR.

At present, c 30 % of the inhabitants in Östhammar obtain their drinking water from private wells. Today, there are some private wells (dug in regolith or drilled in bedrock) in land areas along the coast. Analyses of the well water show that the water quality varies from potable to non-potable. Consequently, some wells are not used as drinking-water supplies but instead for other purposes, e.g. irrigation of garden plots.

According to an analysis of regional well density (both dug and drilled wells), the current well density varies between c 0.2 and 2 wells per km^2 depending on the size and location of the analysed area (Kautsky 2001). The well density varies between 0.2 and 0.9 wells per km^2 in different sub-areas within an area close to SFR (size 400 km^2) and between 0.5 and 2 wells per km^2 in different sub-areas within northern Uppland (size 3 300 km^2).

According to an analysis of data from the SGU Well Archive (Geological Survey of Sweden, SGU) on more than 5 000 private wells drilled in bedrock in northern Uppland (cf Gentzschein et al. 2007), a typical well depth in bedrock is c 60 m. For further descriptions of dug and drilled wells, see Werner et al. (2013).

Current water management activities in Forsmark include pumping groundwater out from SFR, a cooling-water canal from the sea to the Forsmark nuclear power plant, the use of Lake Bruksdammen (c 4 km southwest from Forsmark) as a water supply, and a groundwater-drainage system at the power plant (Werner et al. 2013). There are no land improvements or drainage activities registered in public records. However, there are shallow drainage ditches in the forests, and the level of Lake Eckarfjärden has previously been artificially lowered. Some minor natural springs have been observed in the area (see, for example, Nilsson and Borgiel 2005). None of these springs are registered in public records, and they have not been used according to the available information.

In Sweden today, the proportion of the arable land that is irrigated is small, 3–4 % (Bergström and Barkefors 2004). The irrigated land is primarily located in the county of Skåne (southern Sweden) and the use of irrigation is less common in northern regions. In Uppsala County, the total irrigated area was estimated to be below 100 ha in 2006 and irrigated areas thus make up less than 0.1 percent of the total arable land in the county (Brundell et al. 2008, see also Löfgren 2010 for a discussion). Irrigation of cereals and fodder is very rare, and instead it is primarily potatoes and horticultural products that are irrigated. Between 14 % and 28 % of the land used to produce these crops is irrigated in the Uppsala County, which is below the national average (Brundell et al. 2008). For the last 40 years surface water has been the primary source for irrigation in Sweden, and it covers approximately 85 % of the water used (Johansson and Klingspor 1977, SCB 2017).

4 Site development – modelling and description of future conditions and land use

As the safety assessment spans a large time scale, it is necessary to acknowledge factors that influence the development and properties of the future landscape. This chapter gives a short description of the natural processes and possible human impacts driving the development of the Forsmark site. The focus in this chapter is on the landscape features that are likely to have the largest impact on human exposure to radionuclides originating from the repository, and landscape features that historically have been affected by human utilisation.

The main processes such as climate and climate-related processes that affect the landscape succession, including a description of shoreline displacement, are described (Section 4.1). Their implications for the development of topography and regolith (Section 4.2), surface hydrological conditions (Section 4.3) and chemical conditions (Section 4.4) are outlined and the development of marine, limnic and terrestrial natural ecosystems under present-day, global warming and periglacial conditions is presented (Section 4.5).

Knowledge of historical land use is then described and used to sketch future landscapes. Agricultural land is the most intensively managed part of the landscape (Section 4.6). This includes the cultivation of organic soils situated in discharge areas for groundwater, where there is a potential for radionuclides to accumulate for a long period of time prior to drainage and cultivation (SKB TR-10-09, Saetre et al. 2013b). Special effort has therefore been put on estimating characteristics of lakes, mires, and cultivated peat deposits.

Finally, the processes driving the landscape development are further elaborated to sketch the potential configuration of future landscapes in a regolith-lake-development model (RLDM, Section 4.7). Examples of potential future landscapes are described based on the RLDM and knowledge from the present landscape, climate modelling, historical data and historical land use. Finally, the uncertainties in the future landscape descriptions and the application of the results from regolith-lake development model in the safety assessment are discussed.

4.1 Climate and climate-related processes

The long-term development of the future landscape in the Forsmark area is mainly controlled by two partly interdependent factors: climate variations and shoreline displacement. These two factors in combination strongly affect many of the processes determining the development of ecosystems and future conditions of importance for radionuclide transport and exposure. Examples of such processes are erosion and sedimentation, groundwater recharge and discharge, soil formation, primary production, and decomposition of organic matter.

4.1.1 Future climate evolution

The climate evolution of the next 100 000 years will be primarily determined by changes in the incoming solar radiation (insolation) during the boreal summer season, current levels of atmospheric CO_2 and future emissions of anthropogenic greenhouse gases (**Climate report**, Sections 3.4.5 and 4.3). Future changes in insolation to the Earth can be predicted with high accuracy. These show that the summer insolation over the *next* 100 000 years will be associated with considerably less variability than during the *past* 100 000 years when the Fennoscandian climate was dominated by major glaciations (**Climate report**, Chapter 3). As a result, it is likely that the current interglacial, the Holocene, will be significantly longer than the previous interglacials. However, the length of the current interglacial is also dependent on the amount of anthropogenic greenhouse gases emitted to the atmosphere. Specifically, it will last at least for another 50 000 years even if the anthropogenic greenhouse gas emissions are substantially reduced within the coming decades, but likely for another 100 000 years or longer if current, or higher, levels of anthropogenic emissions continue over the next few decades (**Climate report**, Sections 3.4.5 and 4.3).

Taking these projections about future climate evolution as well as the results from SR-PSU into account, three post-closure climate developments are selected as *variants* of reference external conditions in the PSAR: the *present-day climate variant*, *warm climate variant* and *cold climate variant*. Collectively, these variants define the range of probable climate developments at Forsmark over the next 100 000 years, and thus constitute the range of external conditions considered in the main scenario (see further the **Post-closure safety report**, Section 2.6.3). The conceivable climate-related conditions can be represented as climate-driven process domains, typically referred to as *climate domains* (**Climate report**, Section 1.4.3). At Forsmark, characteristic climate-related conditions of importance for repository safety can be represented by the temperate, periglacial and glacial climate domains. In summary, the temperate climate domain is defined as periods without the presence of permafrost or ice sheets, whereas the periglacial climate domain is defined as periods that contain permafrost but no ice sheets at the Forsmark site. Periods defined as the glacial climate domain are characterised by ice-sheet coverage at Forsmark that may, or may not, also contain permafrost.

In addition to the climate domains, the description of the post-closure climate evolution also includes information as to whether the Forsmark site is submerged beneath the Baltic Sea or not. Submerged conditions are defined to prevail when the relative sea level is above −5.6 m (in the Swedish national reference height system RH2000 (SMHI 2020). This corresponds approximately to 5.8 m below the present sea level at the site[8]. At this height, 75 to 100 % of the surface above the repository is land. Furthermore, a decrease of the relative sea level to this height has a large effect on several features of importance for the safety assessment, e.g. the groundwater flow, discharge areas and land use (see further Chapter 5).

The succession of climate domains in the three variants, including periods of submerged conditions, is shown in Figure 4-1. These variants are briefly discussed in the following, whereas a more comprehensive description is provided in the **Climate report**, Chapter 5.

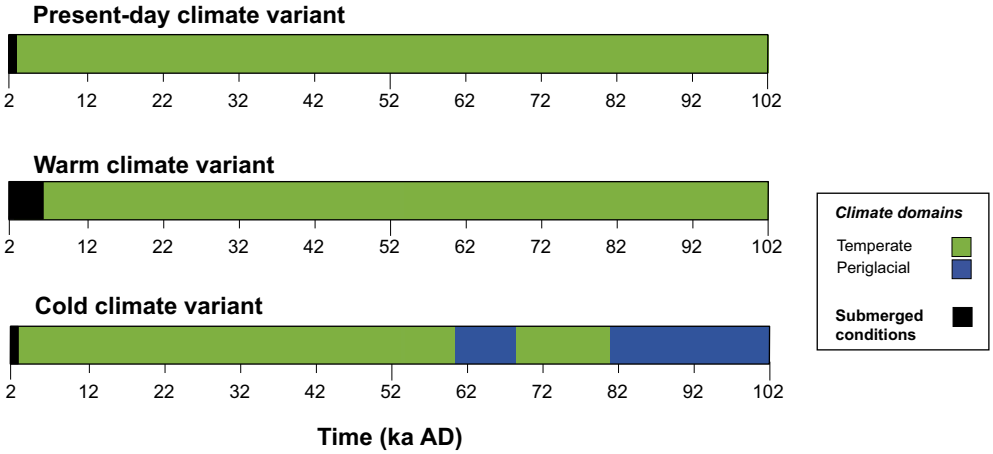

Figure 4-1. *Succession of climate domains, including periods of submerged conditions, of the climate developments considered in this report.*

[8] The present-day mean relative sea level at Forsmark is approximately +0.2 m in the RH2000 reference system (**Climate report**, Section 3.4).

Present-day climate variant

The *present-day climate variant* represents a future development where present-day climate conditions prevail for the complete assessment period. This results in 100 000 years of continued temperate climate conditions at Forsmark, consistent with the *warm climate variant* which represents the anticipated future climate evolution under "business as usual" global warming (see below).

The present-day climate is represented by locally measured meteorological data during a standardized one-year period (October 2003 to September 2004), referred to as the "normal" year (Bosson et al. 2010), see Table 4-1. During this year, the average air temperature was 6.4 °C and the accumulated precipitation was 583 mm. These values are similar to the average annual air temperature and precipitation during the 1986–2005 reference period (Section 3.1) as well as the period 2004–2010 when the site investigations were carried out (Bosson et al. 2010, Werner et al. 2013). The estimated annual potential evapotranspiration of the standardized normal year is 421 mm.

Table 4-1. Characteristics of the climate in the present-day climate variant. Annual (without a subscript) and summer (June, July and August; denoted JJA) values are given for temperature (T), precipitation (P), and potential evapotranspiration (PET). Present-day characteristics are taken from the normal year which has been used in SKB's description of the future hydrology in Forsmark in SR-Site and SR-PSU (Bosson et al. 2010). PET was calculated in Johansson (2008).

	Air temperature		Precipitation		Pot. Evapotransp.	
	T (°C)	T_{JJA} (°C)	P (mm)	P_{JJA} (mm)	PET (mm)	PET_{JJA} (mm)
Present day	+6.4	+16	583	186	421	244

Warm climate variant

The likely developments of external conditions over the next 100 000 years are represented by the *warm climate variant* and the *cold climate variant*. The *warm climate variant* assumes that anthropogenic greenhouse gas emissions comparable to present-day levels will continue for the next few decades, followed by a gradual decline towards net-zero emissions by the beginning of the 22nd century. Hence, this variant represents a likely scenario in line with recent projections of "business as usual" emissions as well as the Intergovernmental Panel on Climate Change (IPCC) medium emissions scenarios RCP4.5 and RCP6.0[9] (**Climate report**, Section 4.2). Most modelling studies on the long-term future climate evolution project that the current interglacial will be prolonged for at least 100 000 years under these emissions (**Climate report**, Section 4.3). As a result, as with the *present-day climate variant*, the *warm climate variant* is characterised by temperate conditions at Forsmark for the complete analysis period of 100 000 years.

In the *warm climate variant*, the air temperature at Forsmark is assumed to increase by a maximum of 5 °C above the present level within the current millennium (Table 4-2), after which it will slowly decline over the following tens of thousands of years. The maximum temperature increase corresponds, approximately, to the mean value in future warming at Forsmark considering the amount of emissions assumed in the *warm climate variant* (**Climate report**, Section 3.4.4). Annual precipitation is projected to increase with higher temperatures. For a warming of 5 °C, the corresponding precipitation at Forsmark is estimated to increase by c 10–20 % relative to present day precipitation (Table 4-2 and **Climate report**, Section 3.4.4). However, the corresponding precipitation response during the summer months (June to August) may either increase or decrease, where the higher annual precipitation corresponds to an increase also in summer precipitation, but the lower value corresponds to a decrease in the summer precipitation relative to present (Table 4-2 and **Climate report**, Appendix B). The annual potential evapotranspiration is also expected to increase with higher air temperatures. The change in potential evapotranspiration due to a warmer climate is calculated using the temperature-based methodology described in Pereira and Pruitt (2004) (**Climate report**, Appendix D). Using this methodology, the maximum increase of annual potential evapotranspiration, resulting from a 5 °C warming, is estimated to be c 34 %, compared to that of the present-day (Table 4-2). The projected

[9] Nomenclature adopted from IPCC's fifth assessment report (IPCC 2013). In the most recent, sixth, IPCC assessment report, emissions scenarios denominated SSPs rather than RCPs (see **Climate report**, Section 4.2.1).

changes in precipitation and PET indicate the moisture in future Forsmark terrestrial landscape with the *warm climate variant* would range from similar to present conditions to considerably dryer. As the potential evapotranspiration increases more than precipitation in summers, and summers may be relatively dry, the crop water demand is expected to increase in the *warm climate variant.*

Table 4-2. Maximum changes from present-day (Table 4-1) in the warm climate variant. Annual (without a subscript) and summer (June, July and August; denoted JJA) changes are given for temperature (ΔT), precipitation (ΔP), and potential evapotranspiration (ΔPET). Note that the warm climate variant describes two different representations of summer precipitation, see the text for further details.

	Air temperature		Precipitation		Pot. Evapotransp.	
	ΔT (°C)	ΔT_{JJA} (°C)	ΔP (mm)	ΔP_{JJA} (mm)	ΔPET (mm)	ΔPET_{JJA} (mm)
Warm climate	+5.0	+4.0	+19 %	+17 %	+34 %	+18 %
Warm climate with dry summer			+10 %	−13 %		

Cold climate variant

The *cold climate variant* represents a future development characterised by substantial reductions in anthropogenic greenhouse gas emissions and/or removal of atmospheric CO_2 by technological measures. Under these developments, atmospheric CO_2 is projected to have returned to pre-industrial levels within the first 50 000 years (**Climate report**, Sections 3.4.1 and 4.3), resulting in growth of Northern Hemisphere ice sheets in response to the next substantial minimum in summer insolation around 56 000 AD (**Climate report**, Section 3.4.5). This development is envisaged to result in two ensuing periods of periglacial conditions at Forsmark during the second half of the assessment period. Regional climate modelling indicates somewhat wetter conditions in Forsmark in a periglacial climate as the evapotranspiration is estimated to decrease more (50 %) than the precipitation (30 %), resulting in a higher runoff (Table 5.3 in Werner et al. 2013 based on input from Kjellström et al. 2009).

4.1.2 Shoreline displacement

Changes in the shoreline displacement, i.e. the relative sea level, in the Forsmark area are determined by the opposing contributions of eustasy and isostasy. Eustasy represents changes in sea level due to e.g. changes in the volume and spatial distribution of sea water in the world's oceans, whereas isostasy describes the vertical movement of the Earth's crust (i.e. bedrock), which in the Forsmark area is currently dominated by rebound following the latest glaciation. If the rate of isostatic rebound exceeds the eustatic contribution, the relative sea level will decrease and the resulting shoreline regression will contribute to a gradual exposure of new land areas. Conversely, if the eustatic contribution exceeds the rate of isostatic rebound, the relative sea level will increase and the resulting shoreline transgression will contribute to a gradual disappearance of land areas beneath the sea.

In the past, shoreline displacement has strongly affected the Forsmark area, both before and after the latest deglaciation. The ongoing shoreline regression creates an altitude gradient from coast to inland that represents a timeline in landscape development from the last deglaciation. At the end of the latest deglaciation around 8800 BC, the area was covered by approximately 150 m of glacial lake water and the nearest shoreline was situated some 100 km west of Forsmark (see Chapter 3 in Söderbäck 2008). Thereafter, the isostatic rebound has been continuous and slowly declining in rate. The rate of rebound in Forsmark has decreased from c 35 mm a^{-1} directly after the deglaciation to a present rate of c 6.7 mm a^{-1}. At present, the rate of isostatic rebound is also compensated by an eustatic contribution (sea-level rise) amounting to a rate of about 2.6 mm a^{-1}. These combined contributions result in a present-day decrease of the relative sea-level, i.e. shoreline regression, of about 4.1 mm a^{-1} (**Climate report**, Section 3.5).

The uncertainty in future global sea-level rise over the next thousands of years is very large, with increases in sea level ranging from a few metres to several tens of metres depending on the degree of global warming and how Earth's ice sheets and glaciers will respond to that warming (**Climate report**, Section 3.5.3). At Forsmark, this uncertainty translates into either a shoreline transgression

or a continued shoreline regression. Owing to the large uncertainty of future sea-level rise, multiple variants of relative sea-level change are described in the PSAR, see Section 6.2 of the **Post-closure safety report**.

In the *present-day climate variant* and *cold climate variant*, the contribution of future sea-level rise is for simplicity assumed to be negligible. Thus, the initial shoreline displacement at Forsmark in these variants is comparable to the glacial isostatic adjustment (Brydsten and Strömgren 2013). Since earlier safety assessments (e.g. SR-PSU) show that doses are generally higher in terrestrial systems, this simplification is assumed to be pessimistic as it results in a faster emergence of new land areas than when an expected sea-level rise is considered. Further, it facilitates comparison with the results of the main scenario in SR-PSU where the same representation of future shoreline displacement was used (SKB TR-14-01). The resulting initial duration of submerged conditions in these variants is 1 000 years.

In the *warm climate variant*, the climate warming is assumed to result in an increased rate of sea-level rise over the initial thousands of years, resulting in a delayed shoreline regression compared with the other variants. As a result, the initial duration of submerged conditions is prolonged by 3 500 years in the *warm climate variant* compared with the other variants. Further details about the shoreline displacements included in the climate variants are given in the **Climate report**, Chapter 5.

The shoreline regression will expose sediments to wave erosion and resuspended fine-grained particles will be transported out of the area into the Bothnian Sea, or re-settle on deeper bottoms within the study area (Brydsten and Strömgren 2010, 2013). Accordingly, the relocation of sediments may have implications for transport and accumulation of radionuclides potentially originating from the repository. The shoreline displacement will also cause a continuing and predictable change in the abiotic environment, e.g. in water depth, hydrology and availability of terrestrial ecosystems e.g. suitable for cultivation and extraction of well water. These factors influence transport and potential exposure to radionuclides and it is therefore appropriate to describe the origin and succession of ecosystems in relation to shoreline displacement.

4.2 Development of topography and regolith

The distribution of regolith in the Forsmark area will change throughout the period considered in the safety assessment. In the present terrestrial area, the proportion of peat-covered areas will increase as the shallow lakes are infilled, and the low-lying wetlands are covered by a layer of peat (i.e. mires). New lakes will form when the present sea floor becomes exposed with the land uplift and these lakes will successively be filled with gyttja and peat (see Section 4.5) that can be drained and cultivated. The proportion of land suitable for agriculture is likely to increase significantly in the far future as the areas with water-deposited clay and sand at the floor of Öregrundsgrepen become exposed from the sea (Figure 3-3). Areas with such minerogenic deposits can likely be cultivated for many thousands of years. However, importantly for the safety assessment, discharge of groundwater occurs only in limited parts of these areas (Werner et al. 2007).

In addition to some forested areas situated on sand and clay, a large proportion of the present mainland is covered by till and forests. These till areas typically have a normal frequency of surficial boulders (5–30 boulders/100 m^2) and may be used as arable land in the future. However, based on current and historical practices it is unlikely that there will be any extensive cultivation of these areas (Lindborg 2010). Glaciofluvial deposits and till with a high frequency of boulders, and outcrops are not suitable for cultivation and will probably remain forested.

The accumulation of sediment and peat as well as the erosion of sediment on the sea floor will continue in the future. Some parts of the sea floor are likely to become shallow lakes and mires and will eventually be covered by a layer of fen peat. Many of the mires that will form directly upon the clay, sand or after a lake state can probably relatively easily be drained and used as arable land.

However, due to fast subsidence of peat, it may be difficult to maintain the drainage of many areas with lake and wetland deposits, and these may be used for cultivation only for a relatively short period of time (< 100 years). This affects especially fen mires developed in former lakes and often underlain by thick layers of gyttja sediments, which are sensitive to compaction. Future locations with relatively thin peat layers that will form in the clay- and sand-dominated areas, however, may be suitable for

cultivation for a longer period of time. This is because these areas are underlain by deposits that are not sensitive to compaction, and, thus, are suitable for cultivation even when the peat has disappeared. The accumulation rate of fen peat is often below 1 mm y^{-1} (Sohlenius et al. 2013c) and peat suitable for cultivation is consequently not available in recently uplifted areas.

Unlike fen peat, bog peat is low in nutrients and it is therefore not likely that bogs will be drained for agricultural purposes. Moreover, raised bogs, with rain-fed production on the bog plane (see Figure 4-4), are of limited interest in a safety assessment where the radionuclides enter the ecosystem from below. Consequently, a higher degree of *Sphagnum* peat in a raised bog will both make the mire less suitable for cultivation, decrease or prevent further discharge of deep groundwater and continue to dilute the content of radionuclides originating from the deep groundwater. Based on this argument, a sufficiently deep layer of bog peat would restrict both the potential contamination from deep groundwater and the use as arable land.

The onset of bog peat accumulation varies due to local conditions, and, in many fens, bog peat starts to form after a fen stage of several thousand years (Lundqvist 1963). The estimates on the accumulation of peat on a bog vary, from the accumulation of 1 m of peat in 1 500 years (0.64 mm y^{-1}, Mäkilä and Goslar 2008), to 1.5 m of peat developing during 850 years (1.8 mm y^{-1}, Sternbeck et al. 2006). Consequently, it seems that the window of opportunity for agriculture on mires may be variable depending on size, age, local hydrological conditions and climate. Further, although it is likely that the peat in the area generally does not fulfil the demands of the present peat industry, it is still possible that peat will be used to heat individual households, as litter peat to absorb animal excrements, and as soil conditioner in the future. For more details on the processes related to regolith development and how those have been modelled in Forsmark, the reader is referred to Lindborg (2010) and the references therein.

4.3 Development of surface hydrological conditions

Hydrological processes play a role in the development of surface systems, primarily by regulating the water availability and exchange in limnic and terrestrial ecosystems. Water also acts as a medium for transport of dissolved substances and particles, including radionuclides. Conceptual and numerical models describing present and future hydrology were developed (Werner et al. 2013), based on SDM-Site (Bosson et al. 2008) and SR-Site (Bosson et al. 2010).

For the marine basins, the major factor influencing changes in the ‘average age of the water’ (AvA) in the marine basins included the PSAR is the interchange of the water between Öregrundsgrepen and the Baltic Sea: in the future, surface-water exchanges across the strait in the south (between basin 184 and the Baltic Sea, see Figure 3-9), as well as inter-basin exchanges, will continually decrease as the shoreline recedes and the basins are isolated from the sea. At 3000 AD (in the *present-day climate variant*), the strait is expected to close and Öregrundsgrepen will turn into a bay and the only connection between the marine basins and the open water of the Baltic Sea will exist in the northern part of Öregrundsgrepen (Karlsson et al. 2010, Werner et al. 2013). At 9000 AD, only one marine basin is in contact with the Baltic (basin 105). By 11 000 AD there is no sea within the PSAR regional model area (Brydsten and Strömgren 2013). However, a small sea area is kept in the northern reaches of the regional model area to be used as a boundary condition in the numerical modelling (see Werner et al. 2013, Figure 3-3). For more information on the development of the landscape with regards to the retreat of the shoreline, see Brydsten and Strömgren (2013). For more information on the modelling used to predict the inter-basin exchanges between marine basins, as well as the exchanges between marine basins and the Baltic Sea, see Section 5.6 in Werner et al. (2013).

The numerical modelling, using the MIKE SHE hydrological modelling tool, was conducted in order to estimate the future hydrological conditions at Forsmark (Werner et al. 2013). Local, high-resolution models were constructed to examine hydrological conditions on the scale of the biosphere objects (e.g. release areas, further described in Chapter 5). Regional models with a relatively lower resolution were used to examine the basin-scale hydrology of Forsmark and to provide the local models with time-varying boundary conditions. Hydrological models were developed for the times 2000 AD (present conditions), 3000, 5000 (see Figure 4-2) and 11 000 AD. The characteristics of the hydrological models vary over time due to shoreline displacement, redistribution of regolith materials due to erosion as

well as the by-products of these phenomena (e.g. changes in topography and vegetation coverage), see Brydsten and Strömgren (2013). The meteorological data and projected shoreline regression used for these time periods are based on the *present-day climate variant* described in Section 4.1.

Figure 4-2 shows model results for the average vertical head differences between the rock and regolith within the local model area at 5000 AD as forced by the "normal-year" meteorological conditions (see Section 4.1.1). When viewed in this fashion, results can help indicate within which parts of the modelled landscape the bedrock groundwater, i.e. modelled groundwater which has passed through the bedrock volume for the current repository and its planned extension, discharges up into the regolith (negative differences Figure 4-2) or where the regolith groundwater recharges the bedrock groundwater (positive differences). By comparing results for all modelled time periods (i.e. normal-year meteorological conditions for 2000, 3000, 5000 and 11 000 AD, Odén et al. 2014) it is possible to denote how changes in the landscape may affect the magnitude and location of the bedrock groundwater discharge zones.

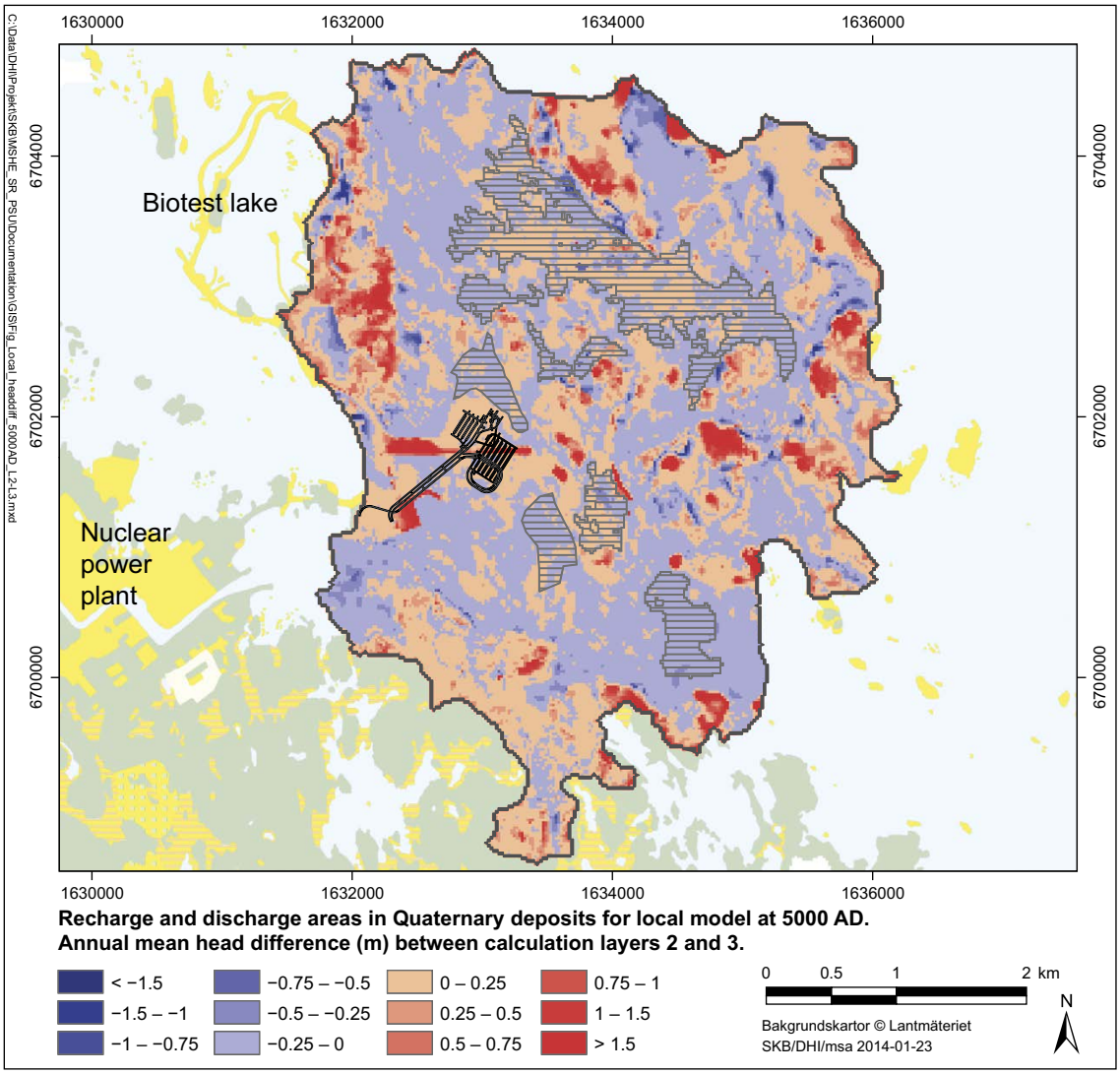

Figure 4-2. *MIKE SHE-calculated annual average vertical hydraulic-head differences in the regolith at 5000 AD in the local model (modified from Figure 5-3 in Werner et al. 2013, the coordinate system is RT 90 2,5 gon V/0:15). Blue colours represent areas with upward flow (discharge) and red colours are areas with downward flow (recharge). Dashed areas indicate the delineated biosphere objects (see Chapter 5).*

Results from the particle transport modelling conducted for SR-PSU presented in Odén et al. (2014) indicate that with the receding shoreline, discharge areas for bedrock groundwater tend to advance towards the new and relatively low elevation areas along the shoreline in the emerging landscape. The results show that, in addition to the position of the shoreline, the general locations of discharge and recharge areas are also strongly dependent on the relative elevation differences in the landscape topography. However, the regolith stratigraphy and depth may affect recharge and discharge patterns on the local scale. This indicates that while the topography of the landscape dictates where, in general, the discharge and recharge areas are located, the regolith stratigraphy and depth in these areas (see Section 4.3) influence how groundwater and dissolved substances are transported through the regolith.

Werner et al. (2013) examined the water balances for several groundwater discharge areas in the future landscape. In the context of the safety assessment, these discharge areas are referred to as "biosphere objects" (see Chapter 5 for a description of biosphere objects). Results indicated that the yearly groundwater discharge rate from the bedrock to the regolith increases over time as the hydraulic gradient between the terrestrial groundwater and open sea increases with the shoreline regression. This is especially evident when comparing the results of the 3000 and 5000 AD realisations; it is between these two periods that the Forsmark landscape changes from a terrestrial-and-sea landscape to a largely terrestrial landscape. An increase in the magnitude of the groundwater discharges within the local model area was also observed when comparing results of the 5000 and 11 000 AD simulations. However, there was a significant deceleration of the changes between these periods due to the fact that the modelled area was entirely terrestrial by 5000 AD, thus resulting in a reduced effect of the position of the shoreline on the groundwater hydraulic gradients until 11 000 AD. By 11 000 AD, all lakes within the local model area have been transformed to terrestrial areas, resulting in a reduction of the bulk evapotranspiration, due to a reduction in the open-water surface area, and higher annual average stream discharges than those observed in the model results from 5000 AD.

The influence of a warmer climate on surface hydrology was investigated using the 5000 AD model (Sassner et al. 2022). The hydrological simulations were based on the climate conditions described for the *warm climate variant* (Section 4.1.1 and Table 4-2), with higher mean annual temperatures and potential evapotranspiration than in the *present-day climate variant*. In one simulation a higher precipitation than at present was assumed for all seasons and a second simulation assumed higher precipitation for the winter, spring and fall seasons but lower precipitation for the summer season (**Climate report**, Section 3.4). In short, the *warm climate variant* is characterised by more annual precipitation and a higher potential evapotranspiration than that of the normal year variant. According to the results of the hydrological modelling presented in Sassner et al. (2022), the increased precipitation does not compensate for the higher evapotranspiration in a warmer climate. The influence of the warm climate is comparatively large on surface water flows, which are directly affected by increases in potential evapotranspiration. However, the effects on deeper groundwater flows are limited. Thus, the location of discharge areas and the groundwater level in these areas are expected to be similar to those in temperate conditions (Sassner et al. 2022, Werner et al. 2013). However, for upland areas a warmer climate is expected to result in an increased water deficit during the summer months.

Periglacial conditions, featured in the *cold climate variant*, influence the hydrology and were described and analysed in Werner et al. (2013). Periglacial environments are typically characterised by permanently frozen ground, known as permafrost, that controls the general distribution and routing of surface water across the landscape. There is a relatively short hydrologically active period in the spring and summer months. At the top of the permafrost there is a relatively thin, hydrologically active layer which undergoes a seasonal freeze-thaw cycle. A large part of the snowmelt occurs when the active layer is still frozen thus preventing infiltration into the groundwater. Once the active layer is thawed it is quickly water-saturated, which promotes ground-surface storage, pond formation and surface-water runoff. In discontinuous permafrost, most groundwater recharge is assumed to occur via through taliks that connect the unfrozen groundwater flow system under the permafrost to the active layer on the ground surface (Figure 4-3). In a periglacial environment without permafrost near the surface, groundwater flow in the uppermost regolith is the largest part of the runoff, whereas with permafrost the surface runoff makes the largest contribution to runoff.

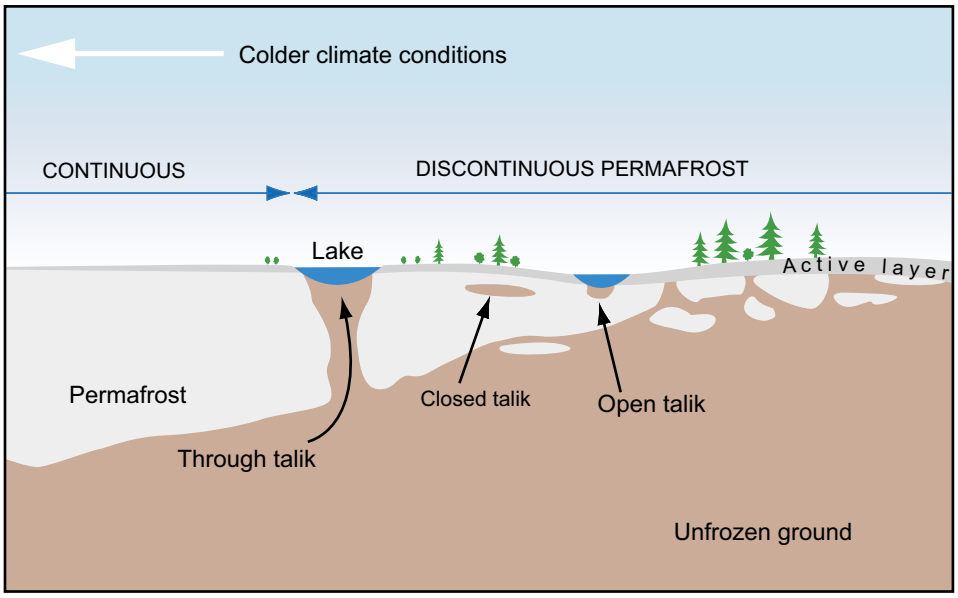

Figure 4-3. *A schematic profile through a permafrost area with an active layer and different types of taliks (Bosson et al. 2010).*

4.4 Development of chemical conditions

The chemical conditions in the regolith and surface waters affects element transport and accumulation as well as the species communities, productivity and development of ecosystems. Present chemical conditions in the Forsmark area are a consequence of past glaciation and deglaciation, past climate changes, past landscape development, past and present land use, and anthropogenic inputs. Several factors will influence the development of the future chemical environment, where external abiotic factors, such as shoreline displacement, climate and atmospheric deposition, set the limits, while internal factors, such as primary production and land use, may further modify the environment. The minerogenic material dominating the agricultural lands in Forsmark is subject to erosion and weathering. Erosion is expected to be a slow process in the flat landscape of Forsmark (Cerdan et al. 2010). Chemical weathering releasing nutrients needed for primary production is also a slow process.

The Forsmark region is rich in calcite and calcite-bearing till deposits that have a marked influence on the hydrochemistry in the area. When new areas of the present sea floor rise above the sea level, weathering of the calcite is initiated, releasing Ca^{2+} and CO_3^{2-}/HCO_3^- ions. This process increases the alkalinity in the shallow groundwater, streams and lakes, affecting also the soil pH and can thus influence the sorption and transport of many elements, including radionuclides. In the soil horizons farther away from Forsmark, calcite has been depleted down to considerable depths and there is a clear gradient with shallower depths towards the coast (Ingmar and Moreborg 1976). Estimates based on soil calcite inventories and present weathering rates suggest that the calcite in the regolith layers might be depleted within a time span of some 1 000 (Tröjbom and Grolander 2010) to more than 50 000 years (preliminary results from ongoing analyses[10]). The high calcite levels elevate the soil pH, which means highly fertile soils, but the calcite dissolution will in the long run lead to a lower pH and potentially a decreased productivity in unmanaged soils. Possibly, weathering rates of less readily weathered minerals such as silicates will increase in the future when the calcite in the regolith is depleted and pH decreases (Lindborg 2010). The release of major constituents originating from these types of minerals (e.g. Al, Na and Mg) as well as release of trace elements incorporated in the bulk minerals (e.g. Th and rare earth elements) are thus assumed to increase in the future.

[10] The time for depletion of the calcite content in the till (640 kg m^{-2}) was estimated assuming an average till thickness of 4 m on 65 % of the terrestrial surface area, ~8 % calcium content and ~2 000 kg m^{-3} bulk density of the till (Hedenström and Sohlenius 2008) and a constant area-specific transport of calcium of ~8 g/m^2/a in the Forsmark area (Tröjbom and Grolander 2010).

In the wetlands and lakes, the ample supply of Ca^{2+} ions and the high alkalinity facilitate chemical precipitation of calcite forming calcareous sediments (Hedenström and Sohlenius 2008). As observed in the lakes farther to the inland, the oligotrophic hardwater stage usually persists a few thousand years followed by the development of brown-water lakes with higher concentrations of humic substances and finally mire formation (Andersson 2010). These observations imply that the calcite influence on lakes and streams at the Forsmark site will diminish in a 10 000-year perspective.

The present distinctive conditions of the Forsmark area will change towards the hydrochemical environment seen in most other parts of Sweden, but the quantitative effects of calcite leaching on the chemistry of surface water and regolith are hard to predict. However, by contrasting the water and soil chemistry of Forsmark with that of similar coastal sites without the calcite influence (e.g. Laxemar) or older sites farther inland, effects of calcite depletion can be estimated. Such a comparison suggests that the pH of lake water may decrease by one unit or less (Andersson 2010). Similarly, the pH of regolith layers is likely to decrease, but probably not more than two units (Sheppard 2011, Lundin et al. 2004, Löfgren 2011). One important effect of calcite depletion and decreasing pH will be changes in sorption strength of different elements and would thus also affect the transport and accumulation of radionuclides from the repository within the regolith.

In the long term, weathering has implications on the magnitude of processes such as chemical co-precipitation and primary production in limnic and mire ecosystems. Whereas dissolved calcium, pH and alkalinity drop, the availability of phosphorus increases. When the surface water composition in the Forsmark area approach inland brown-water systems, a relative shift from benthic to more pelagic primary production is expected in lakes (Andersson 2010).

Typically, the mire formation in Forsmark initially results in a fen, i.e. a groundwater influenced mire, and could eventually succeed into formation of a raised bog. The typical fen mire in the Forsmark area has a high pH and will undergo a natural long-term acidification when turning into a more bog-like mire (Löfgren 2010, Section 10.4).

4.5 Ecosystem development

In this section, the potential ecosystem development is described for three different climates; under present-day temperate, global warming and periglacial conditions. The ecosystem development is strongly affected by the shoreline displacement that turn the sea bottom into terrestrial areas. Relatively enclosed sea bays may become isolated and gradually turn into lakes. After isolation from the sea, sedimentation of matter produced within the lake or originating from the catchment and ingrowth of vegetation, gradually transform the lake ecosystem into a mire system (Figure 4-4 and further discussed Section 8.2 in Andersson 2010 and in the summary description in Lindborg 2010). More open bays can turn directly into mires, without intermediate lake stages and more exposed bottoms often become forested.

4.5.1 Ecosystem development under present-day temperate conditions

Marine

Future temperate brackish water and marine ecosystems are expected to be similar to those at present (Aquilonius 2010, Lindborg 2010). However, the gradual sea regression will alter the functional group composition and the magnitude of the fluxes within the ecosystems. One major change will be the deeper offshore ecosystem shifting from pelagic-dominated to benthic-dominated primary production along with the uplift of the sea floor. However, the magnitude of the primary production in these altered habitats will likely be similar to the shallow coastal areas existing today. At present, the whole marine area in Forsmark is net autotrophic (i.e. more production than consumption) due to the high primary production in the shallow areas, and it is likely that the marine ecosystem will continue to be net autotrophic in the future. Assuming present day runoff and global sea level, the continued shoreline regression due to the isostatic rebound would lower the salinity in the Bothnian Sea. The species composition would shift from a mix of freshwater and marine species towards higher dominance of freshwater species. According to the landscape modelling, the marine area in Forsmark has almost completely retreated from the model area at 11 000 AD (Section 4.7), and the salinity in

the remaining basins in the model area will have decreased to between 2 to 3 ppm (concluded from Gustafsson 2004), which is similar to the present conditions in the Bothnian Bay. The Bothnian Sea would be isolated from the Baltic Proper around 25 000 AD and then become a large freshwater lake (Påsse 2001, see also Posiva 2013).

Limnic

In the future, shoreline displacement will isolate both shallow and deeper marine basins and turn them into lakes (Andersson 2010). Most of the emerging lakes are assumed to closely resemble the present-day shallow oligotrophic hardwater lakes in Forsmark with high benthic primary production. However, if the calcite is depleted from regolith layers, it is possible that future lakes will be dystrophic (i.e. brown-water lakes) dominated by respiration of the material produced in and discharged from the surrounding terrestrial catchment.

Three of the future lakes, located farther away from the repository, will be more than 10 metres deep at isolation from the sea. These deeper lakes will differ from the shallow lakes in a number of aspects and are assumed to more closely resemble other deep lakes in surrounding areas. They will be deep enough to allow for thermal stratification during both summer and winter. A larger pelagic production in these lakes may be utilised directly in the pelagic habitat by zooplankton. Losses through the outlet will probably be large due to the large catchment areas resulting in relatively a rapid water exchange. In addition to lakes, ephemeral pools like the small ponds found in Forsmark today, will most likely be formed also in the future. However, due to the size of the ponds, they will be transformed into mires relatively quickly.

In the future, small streams closely resembling the streams in the Forsmark area today (cf Section 3.3 and 3.5.2) will form in the area close to SFR. Further downstream in the model area, somewhat larger streams, more similar to the nearby Forsmarksån (Figure 3-6), will be formed. The water retention time in those larger future streams will be shorter than in the present smaller ones, due to their larger catchment areas.

Terrestrial

Several natural terrestrial ecosystem types, with different properties in terms of dominating functional groups, biomass, net primary production (NPP) and groundwater availability, are found in the Forsmark region and farther inland. Forests are most common, but fen mires have been identified as the terrestrial ecosystem type where deep groundwater (e.g. from a repository) most likely will discharge (SKB TR-10-09, Section 7.1.1 and Saetre et al. 2013a, Chapter 6). Consequently, the focus here is on these mire ecosystems and their potential use as agricultural land after drainage.

Mires are formed through three different processes: terrestrialisation, primary mire formation and paludification (Löfgren 2010). Terrestrialisation is the infilling of shallow lakes by sedimentation and establishment of vegetation. Primary mire formation is when peat is developed directly on fresh soils after emergence from water or ice. Paludification, which is the dominant process of mire formation in more humid parts of Sweden, is peat formation on mineral soils that become saturated due to changed hydrological conditions or expanding mires. All three processes are likely to occur in Forsmark, but today terrestrialisation and the consecutive development of fen mires are probably most important in the area that emerged from the sea relatively recently (Section 4.1.1 in Löfgren 2010).

The first stage in the wetland ontogeny of the Forsmark area is today characterised by rich fen mires dominated by mosses of the *Bryales* family. As the mire development proceeds and the influence of mineral-enriched groundwater diminishes over time, these become replaced by nutrient poor fen communities dominated by the *Sphagnum* mosses (e.g. Löfgren 2011). This development can be seen already after 2 000 years for catchments located higher in the landscape (e.g. at Rönningarna, c 1.5 km southwest of Lake Bolundsfjärden). This transition may take longer if a larger amount of groundwater is directed into the mire (i.e. if the catchment is larger as they often are on a lower ground). Eventually, a rain-fed raised bog will typically develop, but large bogs are rare in Forsmark today because they have had too little time to develop in this young terrestrial environment (Figure 4-4 and Löfgren 2010, Section 10.4).

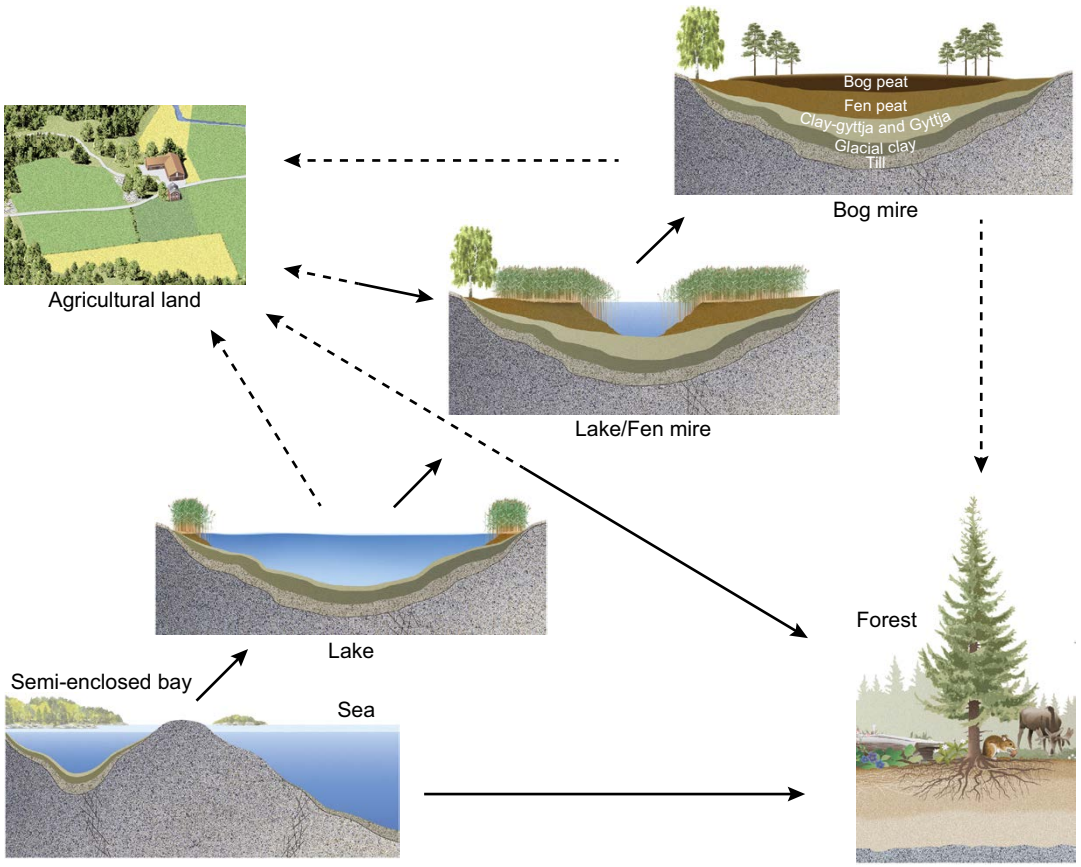

Figure 4-4. *A schematic illustration of the major ecosystems that may be found during a temporal sequence at the Forsmark site, where the original sea bottom slowly becomes land due to shoreline displacement. Black-line arrows indicate natural succession, while dashed arrows indicate human-induced changes to provide new agricultural land or improved forestry. Agricultural land may be abandoned and will then develop into forest or, if the hydrological conditions are suitable, into a fen. A forest may be "slashed and burned" and used as agricultural land. Through primary mire formation, some ecosystems transform from a sea bay directly into a mire without an intermediate lake stage (not illustrated in the figure).*

4.5.2 Ecosystem development under global warming conditions

Marine

Under global warming conditions, changes in precipitation and runoff may affect the load of nutrients and particulate matter in the marine area. Decreased duration and extent of sea ice, increased water temperature, and changes in freshwater input and wind stress will affect vertical mixing, upwelling and ultimately the nutrient supply. These changes in turn affect the growth dynamics, location, and species composition of phytoplankton, benthic primary producers as well as zooplankton and fish communities. The increased temperature increases bacterial respiration, that can lead to bottom anoxia which constrains benthic fish and other fauna. Changes in temporal overlap between primary producers and consumers may occur and effects on the whole food chain and fish productivity are possible (BACC 2008) but difficult to predict. Along with warmer conditions and a deeper summer thermocline in most coastal areas, warm-water species will extend their habitats at the expense of the cold-water species. Similar shifts are expected for other organism groups, for example a reduced reproduction of Baltic ringed seals (*Phoca hispida botnica)*, since they need ice cover to breed their pups (BACC 2008).

Limnic

Lakes have been proposed to serve as sentinels of climate change due to their rapid and observable responses (Adrian et al. 2009). However, the responses of lakes to global warming are affected by individual catchment characteristics, lake morphometry and food-web interactions. Thus, the response of lakes to global warming is more variable than effects on terrestrial ecosystems (see Andersson (2010)

for a discussion). Generally, the effects on abiotic parameters, such as the duration of ice cover, are relatively easily foreseen, whereas effects on biotic parameters, such as biomass of different organism groups, are more difficult to predict.

An increased air temperature will lead to a longer thermal stratification period in summer and shorter period with sea-ice coverage. Since the winter temperature under a "business as usual" global warming will likely be several degrees higher than 0 °C (Section 4.1.1 and the **Climate report**), the duration of ice cover is expected to decrease and to be interrupted by longer periods of open water. This has implications for other abiotic and biotic parameters in the lakes, such as mixing, light conditions, biomass and production. Runoff patterns will change in a warmer climate, which will influence nutrient concentrations in lakes and streams, both through altered input loads and altered retention times. Furthermore, within-lake factors, such as mixing and anoxia, may influence the future nutrient concentrations in the water column. In most lakes, brownification and dissolved organic carbon (DOC) is expected to increase due to global warming (Weyhenmeyer et al. 2016, Meyer-Jacob et al. 2019), but the response of the lakes in Forsmark with respect to DOC is somewhat uncertain due to their presently high DOC concentrations.

There may be a shift in occurrence of anoxia from winter to summer. At present, anoxia occurs in the shallow lakes in Forsmark during winter. A shortened period with ice coverage reduces the risk of anoxia in winter. On the other hand, increased production in summer can lead to increased amounts of degradable matter, resulting in increased respiration and increased anoxia during the summer thermal stratification. The effects on biotic components in lakes are difficult to foresee and there may, for example, be an increase or decrease in phytoplankton biomass. For a more comprehensive discussion on possible effects of global warming on the Forsmark lakes, see Andersson (2010).

Terrestrial

A warmer climate is typically associated with increased biomass and net primary production (NPP), as well as increased respiration rates and thus reduced storage of organic matter in the short term (Chapin et al. 2002, BACC 2008). Potential plant functional types under warmer climate conditions were simulated with the dynamic global vegetation model LPJ-GUESS (Sitch et al. 2003). The modelling result suggests that Forsmark would be dominated by broad-leaved trees, with a larger biomass but with an NPP similar to that of today.

Other modelling approaches, e.g. BACC (2008), suggest that in forests both the productivity and the biomass increase in response to a warmer climate. They also highlight the uncertainties concerning the carbon dynamics in wetlands. A warmer and possibly drier future climate (see Section 4.1.1) may affect the properties of peat-covered areas. An increased temperature, with a corresponding increase in evapotranspiration, will likely lower the groundwater table and increase heterotrophic respiration. This may prevent the development of fens into bogs. However, in wet environments, drying conditions may enhance plant production and initially result in a faster carbon storage (Strack et al. 2008).

4.5.3 Ecosystem development under periglacial conditions

Marine

Marine primary production is largely determined by light, water mixing and nutrient conditions, rather than directly by temperature, and it is thus hard to predict how it will change in a future periglacial climate. It is likely that respiration rates will decrease along with temperature. For marine areas, higher organisms at Forsmark are expected to remain quite similar to those currently present, although species abundance and composition may be altered. For example, marine mammals are already present in the Baltic, but the growing season will be shorter and the ice cover will provide an increased habitat for breeding of some marine mammals (i.e. seals), which therefore may increase in abundance. As under temperate present-day conditions, a shift towards more benthic production and freshwater species is expected along with the continued shoreline regression, but also a shift towards more cold-water adapted species. The bird community has been very stable around the Baltic Sea during the recent interglacial (BACC 2008) and will probably remain so also under colder conditions.

Limnic

A large difference between present lakes in Forsmark and future periglacial lakes is that there will be no reed dominating the shores of the periglacial lakes (Andersson 2010). The lake shores may instead be covered by bryophytes or other vascular plants that lack some of the reed properties in terms of providing sheltered breeding areas for aquatic organisms and influencing the composition of water entering the lake from the catchment. Lake ice cover will be thicker and persist longer. This affects light penetration as well as the mixing and transport of nutrients and ultimately primary producers. Nutrient concentrations may be lower due to a shorter runoff season, altered weathering, production and retention in the soil surrounding the lakes, as well as altered internal circulation of nutrients. There is an increased risk of oxygen depletion during the winter due to longer periods with ice cover.

Species composition will probably change towards more cold-water adapted species, but the biomass and production of benthic primary producers under periglacial conditions will not necessarily be lower than during temperate conditions, despite a shorter growing season. Phytoplankton biomass is relatively low in present-day Forsmark lakes and will likely be low also in a periglacial climate (Andersson 2010). However, fish production and biomass will probably decrease (Andersson 2010).

In addition to existing and future lakes defined by bedrock depressions, there will be temporary, so called thermokarst lakes, that develop in a cyclic pattern where permafrost freezes and thaws in a periglacial system. However, thermokarst lakes do not have a connection to deep groundwater flow and are therefore not important in the context of radionuclide transport directly from a geological repository.

Terrestrial

The potential species present at Forsmark under a periglacial climate domain have been evaluated using the information gained in the SKB assessment for the Greenland Analogue Surface Project (GRASP, see SKB TR-13-18, Lindborg et al. 2016, 2020). In the GRASP area, large trees, gastropods, amphibians and reptiles are absent, and these organism types are also expected to be absent at the Forsmark site under periglacial conditions. Apart from these organisms, the functional groups are expected to be similar to those occurring presently at Forsmark, although a shift in species composition from temperate to arctic species is expected.

The areas that have been classified as mires during periods of temperate conditions will also be likely to be mires in a periglacial landscape. The mires formed in a colder climate are often a mixture of fen and bog areas and are dominated by sedges and mosses. This is a general description and several factors, such as topography and wind stress, influence where the vegetation types are found (see Löfgren 2010). Moreover, a prevailing permafrost regime, together with the lower evapotranspiration, suggests larger areas being partially or periodically water-inundated than in the current landscape.

A sufficiently reduced temperature will eventually change a temperate or boreal environment to a more tundra-like environment. This will lead to lower biomasses and net primary production (NPP) in both forested taiga and tundra peatlands. Despite lower respiration and decomposition rates, carbon storage, e.g. as peat, will most likely be lower than under present conditions. A lower mean annual temperature will reduce the yield of crop production and dramatically change the potential for cultivation. For a detailed discussion on terrestrial ecosystems and how they are expected to change under different climate conditions, see Löfgren (2010); a summary is provided in Lindborg (2010).

4.6 Land use and human influence on landscape development

In this section, the historical, present and future landscapes of Forsmark are discussed. For a more comprehensive description of the past and present land use and historical development of the Forsmark region, the reader is referred to Söderbäck (2008) and Lindborg (2010).

4.6.1 Historical land use

A major part of the Forsmark area was completely covered by water until c 1500 BC. The earlier development of human land-use is therefore based on information from other parts of Sweden. Before the Younger Stone Age in the region (Neolithic, 4000–1800 BC), the impact of human activities on the natural landscape was small and almost all terrestrial areas in south and mid Sweden were covered by forest. The early inhabitants constituted hunting, fishing and gathering societies similar to the potentially exposed group hunter-gatherer (HG, Section 6.2.1) for which doses are estimated in the safety assessment (e.g. Section 9.3). In southern Sweden, the dense forests were cleared during the first phase of the Younger Stone Age (Hyenstrand 1994), often by burning, and the created open areas were first cultivated for some years and then used as grazing land. During the Bronze Age (1800–300 BC) and the Iron Age (300 BC–1100 AD[11]), the areas with cultivated soils gradually increased. These societies resembled the potentially exposed group Inland-Outland farmers (IO, described in Section 6.2.1). Iron mining has had an important role in the Forsmark region since the Iron Age. As the iron industry became more organised in the 16th century, forests were cut down to feed furnaces and mines with wood and charcoal. The region around Lake Mälaren in south-central Sweden, about 100 km south of Forsmark, was almost depleted of trees at the end of this period (Welinder et al. 1998).

Before the modernisation of agriculture, only fairly dry soils could be cultivated. Heavy clays (soil with > 50 % clay particles) and mires were used for haymaking, and stone-ridden tills and bedrock with some surficial soil were grazed. The modernisation of agriculture made it possible to drain peat and heavy-clay areas for cultivation. Extensive draining of mires started a bit over one hundred years ago and peaked in Sweden in the 1930s (Eliasson 1992). This was done by lowering the groundwater table in mires and lakes by ditching. From the 18th to the 20th century there was an increasing demand for food production since the population was growing. This resulted in extensive ditching of mires and lowering of lakes, considerably changing the landscape. As a result, up to 90 % of the mire area has been drained in some parts of Sweden (Svanberg and Vilborg 2001). The proportion of open landscape was largest in the late 19th century. This trend came to an end as agricultural management was rationalised by the use of fertilisers and better equipment in the early 20th century. Drained-mire farmers (described in Section 6.2.1) is the potentially exposed group that generally receive the highest doses in the dose assessment (e.g. Figure 9-4 in Section 9.3, Section 10.2.2 and 10.3.2) and cultivation of peat is thus described in more detail below.

Cultivation of peat – patterns and boundaries

The thickness and properties of peat and the underlying regolith are of importance for the possibility to drain a mire and use it for agricultural purposes. Peat may accumulate in either fens or bogs, the former usually being discharge areas for groundwater. As peat continues to accumulate, the fen can at a certain point develop into a bog where the surface of the mire becomes ombrotrophic, i.e. hydrologically independent of the landscape and the vegetation is all rainwater-fed. The peat developed during such ombrotrophic conditions has low nutritious value (i.e. the C:N ratio is high, Osvald 1937) and low pH, and is therefore less suitable for agricultural purposes (Berglund 1996). Moreover, the potential accumulation in vegetation and peat of radionuclides entering from below will level off as the bog plane rises and the influence of deep groundwater decreases. During the mid-20th century the most commonly cultivated peat types in the County of Uppsala (including the Forsmark area) were *Carex* sedge peat and *Bryales* moss peat (Hjertstedt 1946), which are both formed in fens. However, but a small proportion of nutrient-poor bog peat (*Sphagnum* moss peat and forest bog peat) was also cultivated.

Due to oxidation and compaction, peat subsides considerably when the groundwater is lowered after draining (discussed in Sohlenius et al. 2013c). Subsidence of peat is a fast process and sustainable cultivation for longer periods is possible only if the underlying deposits are suitable for cultivation. In the County of Uppsala about half of the cultivated peatlands appear to have gone through a lake stage and generally have larger peat depths than the other half of the peatlands (Sohlenius et al. 2013c).

[11] The second half of this is period is also known as the Viking Age.

All studied cultivated peatlands were underlain by fine-grained minerogenic material and none were directly underlain by till. However, the highest doses from a drained mire are expected directly after drainage (the first fifty years after drainage are evaluated in the dose assessment, Section 6.2.2 and 9.3). Therefore, mires with relatively thin peat layers covering till should not be ignored in the dose assessment if radionuclide releases to such areas are possible.

4.7 Modelling of the future landscape at Forsmark

Already earlier, in SR-PSU, a regolith-lake development model (RLDM) was used to describe the future landscape development in Forsmark (Brydsten and Strömgren 2013). Output from the model included time-dependent parameters describing average landscape geometries and three-dimensional regolith models for specific time steps. In addition, different sets of assumptions on land use and climate were applied to the RLDM output to produce illustrations of potential future landscape configurations. No additional landscape modelling has been performed in the PSAR, so this section summarises the previous work. It briefly describes the RLDM, the results and its application in the PSAR, discusses the uncertainties in landscape development projections and the use of such projections in dose assessments.

4.7.1 Regolith-lake development model

The RLDM simulates the surface geology, stratigraphy, and thickness of various regolith strata for the period considered in a safety assessment (Brydsten and Strömgren 2013). The model is divided into two modules: a marine module that simulates the sediment dynamics caused by wind waves and a lake module that simulates the lake infilling processes.

The marine module starts when the area has recently been deglaciated (8500 BC). The entire area is cover by the sea and all regolith materials are of glacial origin. The starting conditions are generated using the bedrock surface, the till layer and the glacial clay layer from the regolith depth and stratigraphy model (RDM, Sohlenius et al. 2013a) in combination with an assumption that the glacial clay layer is at least 2 m thick over the entire sea bottom. The sediment dynamic subroutine model, determined sedimentation of postglacial fine-grained sediments or erosion of those sediments and glacial clay in each raster cell based on the modelled wind wave driven water movement at the sediment surface (Brydsten 2009). For each time step of 500 years, the marine module outputs are raster maps of regolith layer thicknesses and bathymetry (i.e. a DEM for the sea, see Section 3.2).

When enclosed sea bays become isolated as a result of the shoreline regression, the regolith development of each lake is modelled separately with the lake module. The DEM from the time step prior to the lake isolation is used as input to the module, in combination with an assumption that the thresholds of future lakes are lowered to the upper surface of the till layer. The lake module initially estimates the vegetation ingrowth in the sea bay prior to isolation and then estimate sedimentation and ingrowth by vegetation in 100-year time steps until the lake is completely infilled (Brydsten and Strömgren 2013). Raster maps of regolith layer depths limnic sediments (i.e. clay gyttja) and peat, and an updated DEM are outputs from the lake module for each time step. In a post-processing routine, the outputs from the marine and lake modules are merged into combined raster maps of the regolith layers (till, glacial clay, combined post-glacial marine and limnic sediments, and peat) and an updated DEM for each time step.

The output from the RLDM was used to extract time-dependent parameters describing geometries of specific biosphere objects for the calculations in the BioTEx model (Grolander 2013, Chapter 4). These include average water depths, average regolith thicknesses and sedimentation rates (see Chapter 5 for a description of biosphere objects and their properties). The output from the RLDM was also used to export three-dimensional regolith models used for the hydrological modelling at different stages for the landscape above the repository (Werner et al. 2013, Section 2.2.2). These included submerged conditions (3000 AD), terrestrial conditions with open lakes (5000 AD) and terrestrial conditions with all lakes infilled with mires (11 000 AD), discussed in Section 4.3 above.

Note that only one realisation of the landscape development in Forsmark was derived with the RLDM. As all lakes close to the repository are projected to be infilled before the first permafrost, there was no need to reduce the rate of ingrowth during periods with periglacial climate. Moreover, for variants

where submerged conditions were prolonged (i.e. in a considerably warmer climate), or occurred after a passage of an inland ice sheet, the same landscape projection was used, but the development was shifted forwards in time (SKB TR-14-06, Chapter 7).

4.7.2 Landscape development in the present-day climate variant

To illustrate potential future landscapes at Forsmark, covering different climate conditions and land-uses, maps of five different variants were presented in SR-PSU (SKB TR-14-06, Section 5.5). These were constructed by coupling the RLDM output with different sets of assumptions with respect to the links between regolith, ecosystems and potential land use. Below is a summary of the results presented for the variant that assumes intensive cultivation and present-day climate conditions.

In this variant, the rate of shoreline regression corresponds to that used in the *present-day climate variant* in the PSAR (Section 4.1.2). In short, the rules relating regolith types to terrestrial ecosystems were as follows: rock outcrops were assigned pine forest, peats were assigned mires, and all other regolith types were assigned mixed coniferous forest. However, if the total thickness of cultivatable regolith layers (excluding till with a normal or high frequency of boulders but including clayey till) was sufficient for cultivation (> 0.5 m depth after soil subsidence), the area was larger than 0.24 ha, and located outside a lake basin with open water, then it was outlined as potential arable land (for details on the rules, see Table 5-1 in SKB TR-14-06).

Applying these rules to the output from the RLDM, the distributions of ecosystems in the landscape were derived for the period between 1500 BC (i.e. −1500 AD in the figure) and 40 000 AD (Figure 4-5). With the assumed rate of sea-level change, the shoreline will regress relatively fast for the next 5 000 years, resulting in an increase of the terrestrial ecosystems, including the area of potential arable land. Potential arable land will further increase when the lakes have been filled in with sediment and peat.

The proportion of mires (wetlands in Figure 4-5) increases over time from 500 BC to 8500 AD, when it represents c 10 % of the modelled area. After 8500 AD, the proportion of mires decreases, as they become potential arable land by the assignment rules above. The total lake area is largest at 5500 AD (almost 6 % of the modelled area). At 15 000 AD, only 6 out of the 48 lakes remain. However, as these lakes are large and deep, the lake area still makes up 2 % of the total area. At 20 000 AD, no lakes remain in the area above repository. At the end of the simulation (40 000 AD), all lakes are projected to be filled with sediment and peat and most of them are classified as potential arable land.

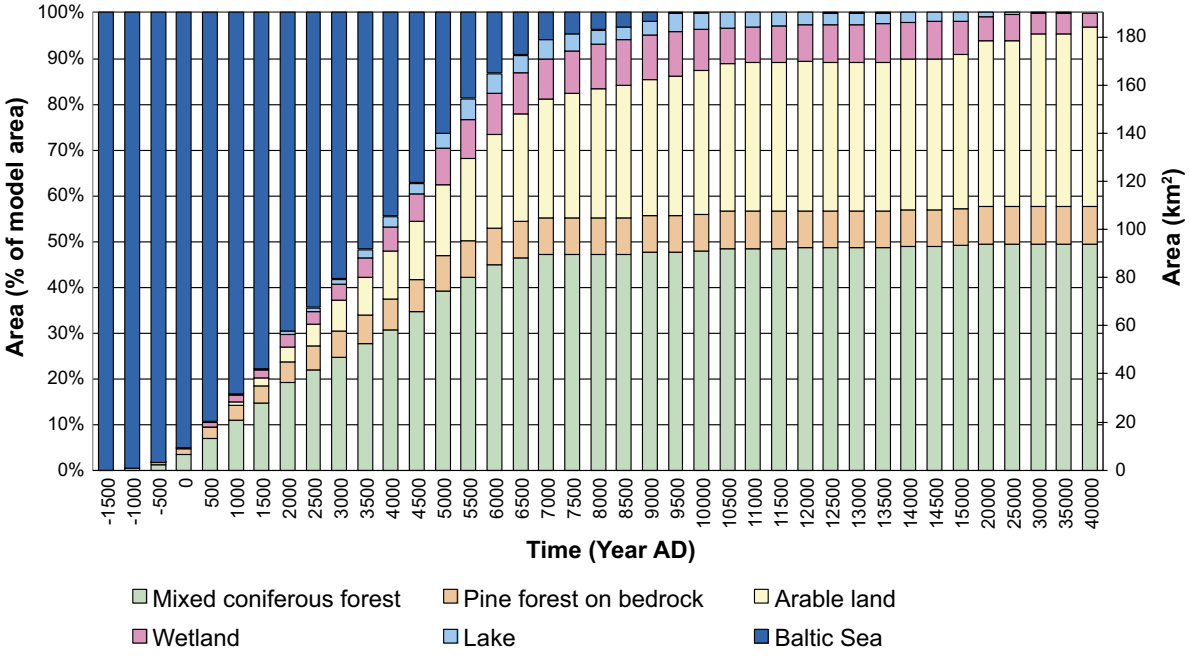

Figure 4-5. *Proportions of different ecosystems as a function of time, assuming intensive cultivation and present-day climate conditions. The time scale is in 500-year intervals from –1500 AD to 15 000 AD and 5000-year intervals from 15 000 AD to 40 000 AD.*

It should be noted that the land assigned as potential arable land corresponds to an upper estimate of cultivable land (about 40 % at 40 000 AD). However, it is unlikely that all this land would be cultivated simultaneously. For example, many of the mires can only be cultivated for a short period of time as the peat layers are likely to subside relatively fast (Section 4.6.1 and e.g. Chapter 6 in SKB R-14-02). The corresponding landscapes above the repository for the time steps 2000, 3000, 5000, and 20 000 AD are shown in Figure 4-6.

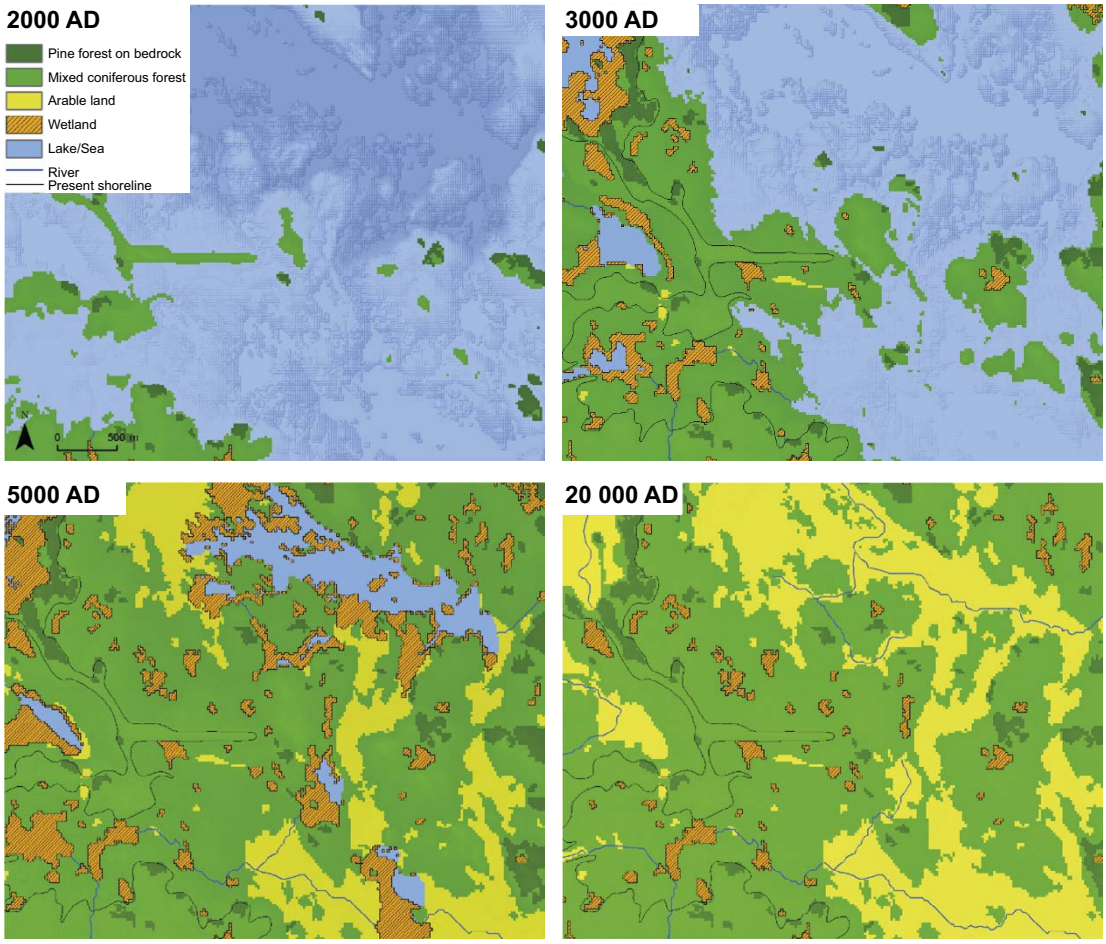

Figure 4-6. *Illustration of the landscape development using the time steps 2000 AD, 3000 AD, 5000 AD and 20 000 AD assuming the shoreline regression based on the present-day climate variant and intensive cultivation. The yellow colour represents land that could potentially be cultivated. Note that in this projection, mires within lake basins are not marked as potential arable land until the lake has been completely infilled.*

4.7.3 Comparing landscape projections with the present area in Forsmark

In SR-PSU, the landscape projected by the RLDM at 2000 AD was compared with a corresponding map of the area today (Figure 4-7, and Section 5.6.2 in SKB TR-14-06). For a better comparison, present land-use practises were used to assign areas suitable for cultivation in the simulated landscape. That is, vegetation types were assigned as described above, with the exception that areas had to be at least 1 ha (not 0.24 ha) to be considered suitable for agriculture, and draining of peat soil was not considered, as this is not part of present agricultural practices in the Forsmark area. The map of the present distribution of ecosystems was retrieved from Lantmäteriet and from the Swedish Board of Agriculture (http://www.jordbruksverket.se, accessed 2013-12-01).

The comparison showed that RLDM captured many features of the present landscape. For example, the distribution of large lakes and the mires in the vicinity of the lakes were in good agreement with the present conditions. However, some of the small lakes are missing and covered by peat in the model. This is primarily because the model does not describe the development of lakes with an area less than 4 ha. Such structures are considered to be colonised with mire vegetation within a relatively short time, and in the RLDM they are instantaneously filled with peat (Brydsten and Strömgren 2010, 2013). In some cases, small mires present in the landscape of today have also been missed. This could be due to small-scale deposits of semi-permeable fine-grained material that are not captured by the RLDM.

Today, the largest cultivated area is situated at Storskäret (Figure 4-7), which also is reflected in the model (2000 AD). In the model, the corresponding area reflects the distribution of clayey till, but all of the potentially arable land is not cultivated presently. Moreover, in some areas, the modelled shoreline is situated clearly outside the present location. This indicates that it is difficult to make precise predictions of the shoreline position on a flat landscape.

A comparison between the modelled distribution of glacial clay and postglacial gyttja clay (Brydsten and Strömgren 2013) and the present clay distribution, as indicated by the site descriptive regolith map (Sohlenius et al. 2013a), also showed some discrepancies (data not shown here). For example, smaller areas on the regolith maps are missing in the RLDM output, and in other instances the model predicts water-deposited clays in areas where there presently are none. This is not surprising as erosion and sedimentation in the sea are difficult to predict. However, this implies that the future distribution of small areas suitable for cultivation may only be partly realistic, and that the thickness of clay layers in such areas may be associated with considerable uncertainties.

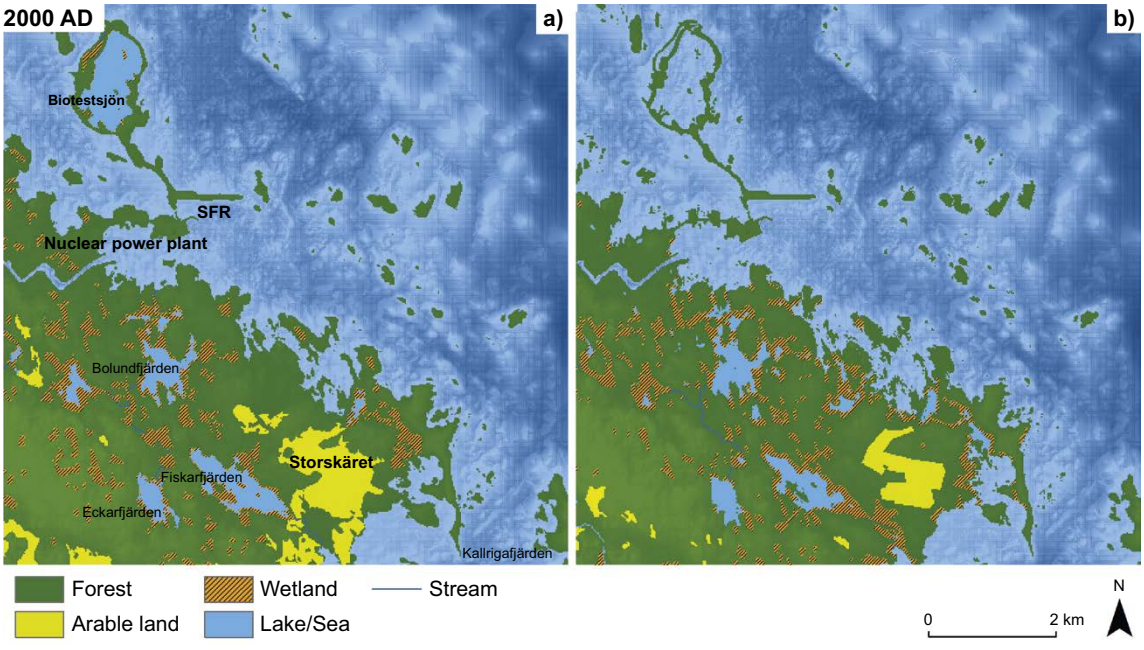

Figure 4-7. *Close-up of the RLDM with (a) modelled land use for the year 2000 AD, compared with (b) the present map of Forsmark showing the distribution of five different ecosystems. Note that yellow areas in the RLDM represent potential arable land, assuming present land-use practices.*

4.7.4 Conclusion from the landscape modelling

The safety assessment is performed for long timescales during which processes such as climate change, shoreline displacement and ecosystem succession may have a significant impact on the development of the landscape. Uncertainties with respect to the future climate and the effect of the relative sea-level change are described and addressed in the **Climate report**. In short, these uncertainties are captured by the definition of several post-closure climate developments (Section 4.1.1 and the **Climate report**, Chapter 5). For example, as global warming may cause sea levels to rise, due to an increased melting of inland ice sheets and glaciers and an accentuated effect of sea-water thermal expansion, the submerged period is extended by 3 500 years in the *warm climate variant*. Moreover, the effect of a prolonged submerged period is considered to primarily change the timing of transitions between sea, lake and mire ecosystems.

The regolith-lake development model (RLDM) is used to describe a potential future landscape based on physical constraints and knowledge of the historical processes that have shaped the Forsmark landscape. The model is based on data that describe the elevation, the relative sea-level change, the present distribution of till, sedimentation and erosion processes for glacial and postglacial deposits, lake ingrowth (terrestrialisation), and primary mire formation. All these data sources are associated with uncertainties, and for practicality, the landscape development simulated with the RLDM is currently based on one realisation which is further modified in postprocessing to analyse other variants.

The resulting topography and regolith stratigraphy from the RLDM have been used to identify ecosystems that are potential recipients for deep groundwater, e.g. shallow bays, lakes, mires and streams. The identification of these areas is based on the present DEM, which is relatively reliable for present conditions in the area above the repository. However, the size of the identified ecosystems and their temporal development are more uncertain. For example, the spatial extent of a future lake is dependent on the presence of the lake threshold, which may be subject to erosion, draining or damming activities. Moreover, small mires and lakes may be overlooked, and the projections of the thickness of the clay layers may not be reliable at finer scales.

Thus, although the results from the RLDM give a comprehensive example of landscape development, it is important to account for uncertainties when results are used at the level of individual biosphere objects. As the development of the future landscape is presently described by a single realisation, parameters extracted from the model do not have any explicitly expressed uncertainty. To not constrain the representation of the landscape, a suite of examples is used to illustrate reasonable alternative landscape configurations and discharge area properties in the dose assessment. This is mainly addressed by the *alternative landscape configuration calculation case* (Section 10.6) and *the alternative delineation calculation case* (Section 11.3), but the *timing of shoreline regression calculation case* (Section 10.4) and the *subhorizontal fracture calculation case* (Section 10.5) add further insights related to the uncertainty in the landscape development and the future landscape characteristics. Moreover, to clarify how projected properties like the size of a discharge area and the thickness of regolith layers affect the calculated dose, sensitivity analyses were performed (the *mire object properties calculation case*, Section 11.4).

5 Modelling biosphere objects in the landscape

This chapter describes the identification and development of biosphere objects. A biosphere object is an area in the modeled landscape that is predicted to receive a substantial portion of the radionuclides following a release from the repository. Radionuclides may arrive via discharge of groundwater from the geosphere and/or indirectly via lateral transport of surface and near-surface groundwater. A biosphere object is used as the spatial unit for the coupled aquatic-terrestrial ecosystem that is used in the BioTEx model (Chapter 7). Thus, the spatial information from the landscape-level modelling (Chapter 4) is extracted and applied to specific biosphere objects. The main tools used to outline a biosphere object are the digital elevation map (DEM) and results from the geohydrological flow-path (or particle tracking) analyses. The surface hydrological descriptions of the watershed containing the biosphere object are also used in the delineation of the biosphere objects.

The biosphere objects identified in SR-PSU (SKB TR-14-06) are also used in the PSAR. The methodology applied in the delineation of the biosphere objects is summarized in Section 5.1. Discharge locations from the latest hydrogeological simulations of SFR are also examined in Section 5.1. The properties of biosphere objects are outlined in Section 5.2; special attention is paid to the description of object 157_2 because prior analyses have indicated this area as being the primary receiver of radionuclides. The temporal evolution of the biosphere objects is described in Section 5.3. Cold climate and permafrost conditions for the biosphere objects are examined in Section 5.4. Lastly, the potential effects of groundwater pumping wells on radionuclide transport and radiation doses are discussed in Section 5.5.

5.1 Methodology

5.1.1 Geometrical features of the biosphere objects

The process of defining the geographical boundaries of a biosphere object is essentially an exercise in identifying the area of the landscape capable of contributing surface and subsurface runoff to a location in the modelled landscape that is predicted to receive a substantial portion of radionuclides following a release from the repository. It is here, within the boundaries of the biosphere object, that exposure of humans and non-human biota is expected to be highest.

Three landscape features are of particular interest when calculating the water fluxes affecting radionuclide transport and exposure calculations in the biosphere system. The first landscape feature is the general area, or areas, in the landscape where radionuclides are expected to reach the surface. These areas often coincide with local depressions, or low points, in the landscape. As the shoreline retreats due to land uplift, these low points are assumed to be transformed into a mire ecosystem, either with or without an associated lake. These low points are therefore referred to as a lake–mire (or mire) ecosystem in the context of the PSAR. The boundary of the lake-mire ecosystem is most often defined by the surrounding topography. For example, the delineation of the area might be the first isometric contour which entirely encompasses the lake–mire ecosystem. It is this boundary that serves as the spatial delineation of the biosphere object. However, it should be noted that this applies only after the entire object has fully emerged from the sea, i.e. the terrestrial period. The delineation of the biosphere object during the marine and transition phases is discussed below. For the PSAR, all lake–mire (or mire) ecosystems are assumed to have an accompanying stream and all surface discharge is assumed to exit the stream outlet (see Figure 5-1).

The second landscape feature is the “basin”, which equals the catchment that contributes runoff to the lake–mire ecosystem. Runoff from the basin is contributed either directly, via overland and sub-surface flow, or routed through a stream. All runoff from the basin is routed through the stream outlet of the basin. This stream outlet also coincides with the stream outlet of the lake–mire ecosystem. Delineation of the basin is done using the DEM. The boundaries of the DEM are constant regardless of whether the basin is in marine or terrestrial conditions. The part of the watershed where runoff is routed directly to the biosphere is the third landscape feature of interest; this feature is referred to as the “sub-catchment”. The sub-catchment is a sub-area of the basin. If there exists a stream inlet to the ecosystem, then a part

of the runoff in the basin is routed into the biosphere object via the "stream-inlet" (see Figure 5-1). If the stream-discharge of a biosphere object is routed downstream to another biosphere object, then the basin for the downstream object begins immediately downstream of the stream outlet of the upstream object (i.e. all basin, sub-catchment and lake–mire ecosystem areas are mutually exclusive).

While the landscape is in submerged condition (Section 4.1.1), the whole basin, or parts of it, is covered by the sea. The portion of the basin covered by water is defined as the aquatic ecosystem and the boundary of the biosphere object coincides with the area of the basin covered by water. It is here, in the aquatic ecosystem, where humans and non-human biota may be most exposed to radionuclides. As the shoreline retreats, due to land uplift, the aquatic ecosystem transitions to a lake–mire or mire ecosystem within the basin (see Figure 5-1). The area of the aquatic ecosystem will decrease in proportion to the area of the basin no longer covered by the sea as the shoreline retreats.

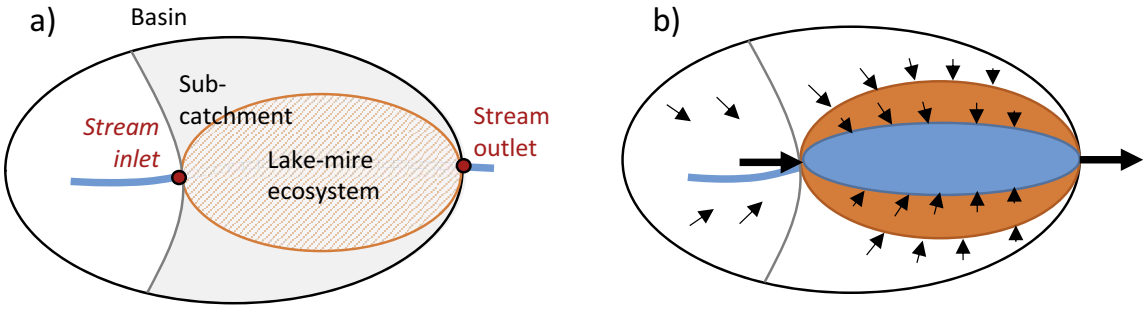

Figure 5-1. *a) Conceptual illustration of geometrical areas and flows of runoff associated with a biosphere object in the terrestrial stage (with no upstream object). Black ellipse represents the basin which is also the catchment. The grey line divides the basin into the catchment of the inlet (left) and the sub-catchment (right, shaded). The sub-catchment includes the biosphere object (hatched area). b) Black arrows represent the flow of runoff, either as streaming water (large arrow) or as surface and subsurface runoff (small arrows). Blue oval represents a lake, surrounded by a mire (orange). All runoff in the basin will be discharged through the stream outlet. Figure modified from Grolander and Jaeschke (2019).*

5.1.2 Identification of biosphere objects

The biosphere objects identified in SR-PSU (SKB TR-14-06) are used also in the PSAR (Figure 5-2). The methodology used in their identification is summarised as follows: Future lakes and lake catchment geometries were first identified using the digital elevation model (DEM) presented in Section 4.7 and Strömgren and Brydsten (2013) (Figure 5-2). Areas where deep groundwater discharges from the bedrock into the regolith were then identified using results from non-reactive particle tracing simulations, imposed on the flow-field calculated by the geohydrological model, to trace flow-paths from the repository (Odén et al. 2014). The estimated locations of the future lakes and catchment geometries and the deep groundwater discharge areas was then examined simultaneously in order to identify where surface hydrological processes, such as runoff and near-surface groundwater movement, will likely interact with deep groundwater flow paths originating from the repository. It is in these areas, where the deep groundwater discharges are likely to interact with the surface water hydrology at the surface, where focus is given when defining most of the biosphere objects in the PSAR. It is these areas where the sub-basin (see Section 5.1.1) is defined, and therefore the lateral boundary of the biosphere objects. For the PSAR, the location of all biosphere objects was defined in this fashion with the exception of biosphere object 157_2.

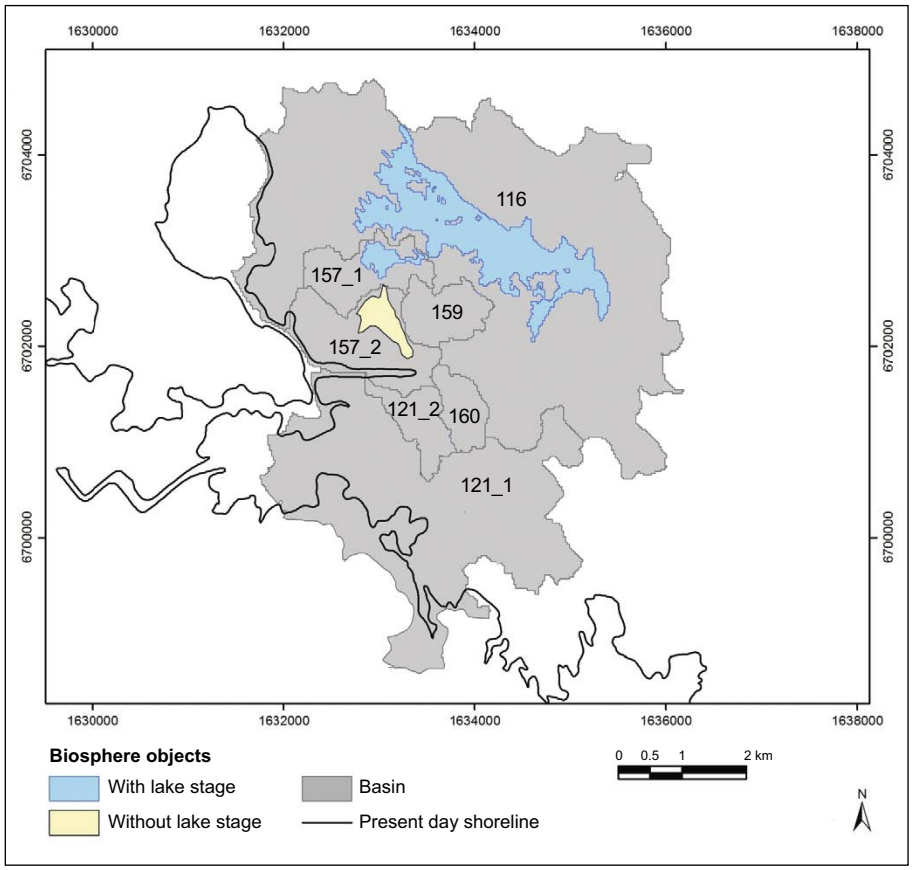

Figure 5-2. *Biosphere objects in the PSAR. When the area is under the sea, the biosphere objects are in their marine stage and all of the delineated objects are used simultaneously in order to assess the potential exposure dose from the marine object. However, significant fractions of the geosphere release are only expected to be discharged to basins 157_2 in the base case, and to 157_1, 157_2 and 116 given the presence of an atypical horizontally sloping fracture (Section 5.2). Thus, these three objects were considered sufficient for assessing dose in the terrestrial stage. In the terrestrial stage, the biosphere object is defined as the original lake basin (blue) or the mire (yellow). The coordinate system is RT 90 2,5 gon V/0:15. Figure modified from SKB TR-14-06.*

For biosphere object 157_2, a gently sloping local topography without any pronounced depressions within the focus area prevented the formation of an inland lake during the transition from a marine to a terrestrial basin. However, results from the future hydrological modelling predicted that the annual average groundwater table would be near the ground surface producing conditions conducive of wetland formation (Werner et al. 2013). It was therefore assumed that the object would bypass a lake stage during its isolation from the sea and transition directly to a wetland stage. This meant that it was not possible to define the boundaries enveloping the mire ecosystem solely based on the position of a stream outlet Instead, the object was delineated by enveloping the majority of discharge points that were modelled for the terrestrial stage of the basin (see Figure 6-12 in SKB TR-14-06). The spatial boundary of the biosphere object was defined by generally following the isoline enveloping the majority of the discharge points while avoiding the water divide for basin 159. Special attention was paid to ensure that the drainage outlet of biosphere object 157_2 matched that of the larger basin (Figure 5-3).

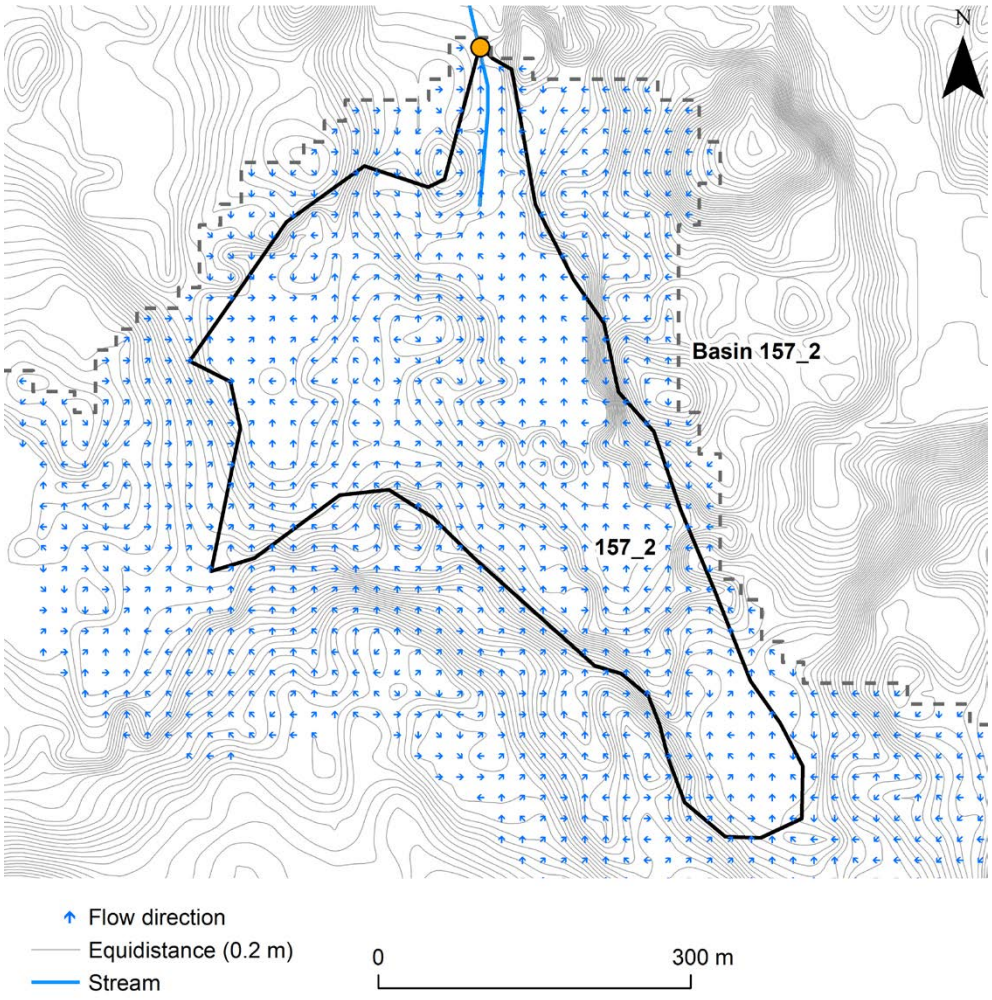

Figure 5-3. *Flow routed over biosphere object 157_2. The flow direction from the watershed converges into the object, whereas the flow within the object is directed to the stream outlet. Dashed line shows the watershed of the object and the orange circle the stream outlet. Grey lines represent topographic contours (elevational equidistance of 0.2 m).*

5.1.3 Analysis of potential areas for discharge from SFR

The first, and arguably most important step in the identification and delineation of the biosphere objects in the PSAR is the estimation of the discharge points at the surface. Hydrogeological models of the Forsmark landscape were developed for multiple future time steps for SR-PSU. For each time step, a steady-state flow field was generated and used for particle tracking simulations (Odén et al. 2014). Results from these simulations show where groundwater from the repository could enter the biosphere, and which areas of the biosphere may therefore contribute to a release of radionuclides from SFR to the biosphere.

After SR-PSU, complementary studies examined uncertainties in the parameterization and structure of the bedrock hydrogeological models. Öhman and Odén (2017) and Saetre and Ekström (2017a) examined a postulated, large, horizontally sloping fracture in the bedrock below biosphere object 157_2 and how it may affect future groundwater discharges. Öhman and Odén (2018) built on these studies and examined how uncertainties in the model parameterization, structure and heterogeneity of the bedrock model affected modelled discharge locations. Results from these studies were then compared with the discharge locations produced in Odén et al. (2014) in order to assess if the biosphere objects used in the SR-PSU work were relevant for the PSAR.

Results from Öhman and Odén (2017) (see *subhorizontal fracture calculation case*, Section 10.5) largely confirmed the pattern of discharge locations reported by Odén et al. (2014) in SR-PSU in spite of the uncertainties of the bedrock model; these results help support the conclusion that the biosphere objects defined in SR-PSU are also appropriate to the PSAR, i.e. objects 157_2, 157_1 and 116. Moreover, it was found that in most cases it is sufficient to use biosphere object 157_2 as the primary discharge area for the geosphere release. For 22 of the 30 bedrock cases examined in Öhman and Odén (2018), almost all particles released from SFR1, and most particles from SFR3 were discharged into biosphere object 157_2 (Table 5-1, Figure 5-4). In the marine period, the surface water in all seven basins will receive radionuclides via advective fluxes of the surface water across the basin boundaries (see Section 5.3.1). In the terrestrial period, objects 157_1 and 116 will receive radionuclides via surface or groundwater flows from object 157_2. Descriptions of objects 157_1 and 116 are also required to assess the consequences of a geosphere release that is distributed via the horizontally sloping fracture examined in Öhman and Odén (2017) and Saetre and Ekström (2017a).

Table 5-1. Location of released particles at the bedrock-regolith boundary. The result is presented as fraction of the total number of released particles from SFR1 and SFR3 (10 000 per waste vault and bedrock case); a blue-to-yellow (0–100 %) gradient is used to visually emphasize the results. "Object" refers to the biosphere object itself, and "Basin" refers to the larger basin within which the "Object" is located. 'Mean' refers here to the mean fraction of 22 typical bedrock cases (including "base case" BC1, results for which are displayed also separately). The mean for the eight bedrock realisations for the atypical realisation with a large horizontally sloping fracture underneath object 157_2 is reported separately (R02). Note that most released particles reach the basin of 157_2 in the marine stage (~ 98 %, 3000 AD), and the object area in the terrestrial stage (> 90 %, 5000 and 9000 AD), but that a large fracture may alter this pattern (see text for details). Data from Öhman and Odén (2018).

Time (AD)		3000			5000			9000		
Area		BC1	Mean	R02	BC1	Mean	R02	BC1	Mean	R02
157_2	Basin	100 %	98 %	97 %	97 %	94 %	57 %	98 %	96 %	66 %
	Object	83 %	79 %	77 %	94 %	92 %	56 %	95 %	94 %	64 %
157_1	Basin	0 %	0 %	0 %	2 %	4 %	25 %	2 %	3 %	24 %
	Object	0 %	0 %	0 %	2 %	2 %	11 %	1 %	2 %	10 %
116	Basin	0 %	0.1 %	0.1 %	1 %	2 %	17 %	0 %	1 %	10 %
	Object	0 %	0 %	0 %	0 %	1 %	9 %	0 %	1 %	5 %

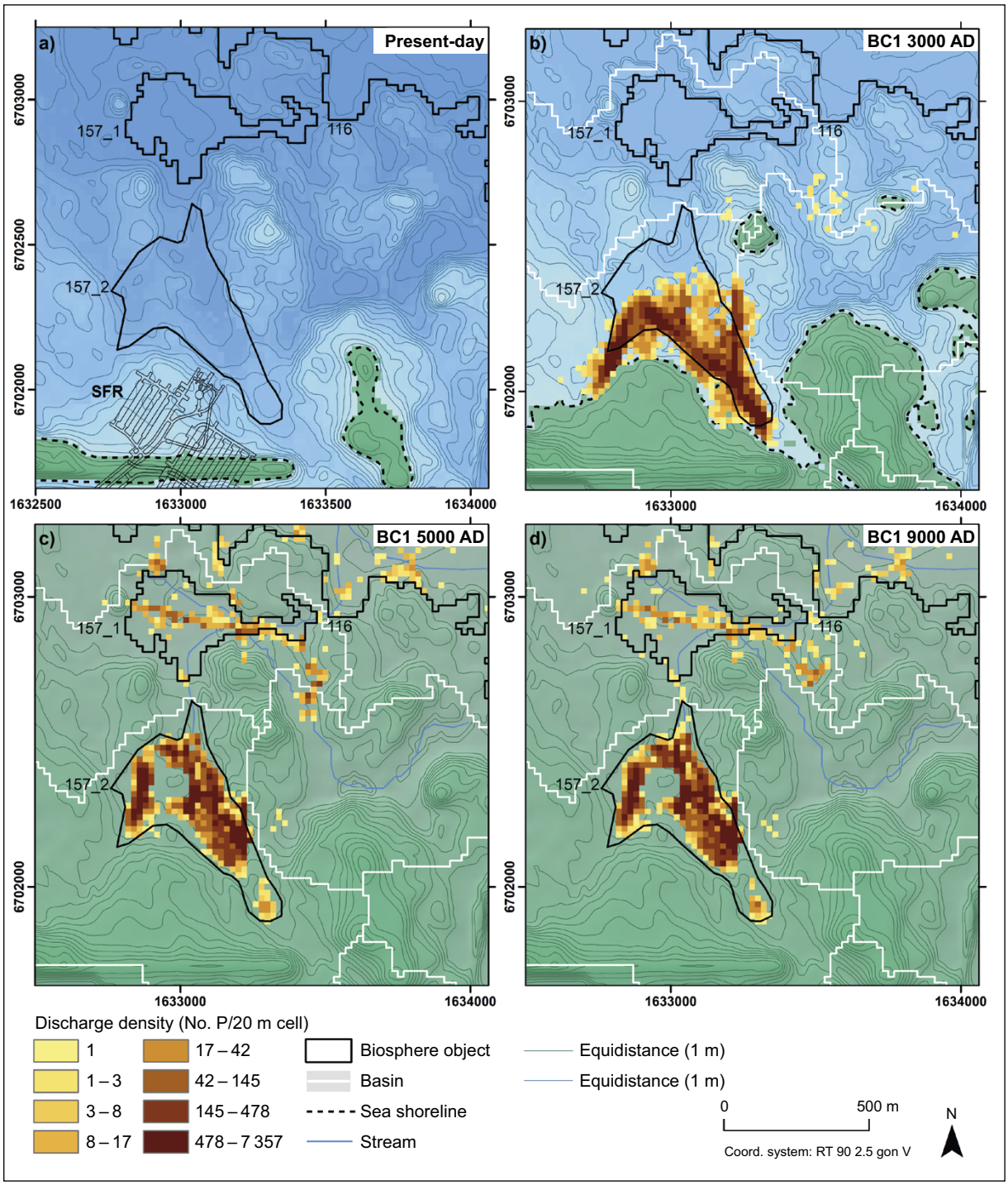

Figure 5-4. *Spatial distribution of discharge locations for particles released from SFR as reported in Öhman and Odén (2018) (110 000 particles and bedrock case BC1) in relation to basins and biosphere objects used in SR-PSU. The discharge density is expressed here as the number of particles per each 20 x 20 m² model cell. The upper left panel shows the present bathymetry for the sea floor north of SFR. Note that the object outline broadly follows the topography of the sea floor; the original outline of 157_2 was defined using a map of a coarser scale and therefore there are somewhat larger differences between the object borders and the topography contours. The other three panels show particle densities (number of points per 400 m²) for three timesteps, representing the sea stage (3000 AD) and the terrestrial stage (5000 and 9000 AD). The released particles are primarily discharged into biosphere object 157_2. Objects 157_1 and 116 are included for orientation. Corresponding fractions for particles discharged into the three objects are shown in Table 5-1.*

5.2 Properties of biosphere objects

This section describes the properties of biosphere objects that are of importance for modelling the transport and accumulation of radionuclides. These include geometrical features, water exchange during the marine stage, regolith depth and ground- and surface-water flows.

5.2.1 Properties of marine basins

At 3000 AD, at least some portion of every sea-basin is predicted to have emerged from the sea due to land uplift. However, most of each basin is predicted to still be covered by surface water; all basins are, at this time, considered to be in the marine stage. All seven sea-basins and Öregrundsgrepen (i.e. the open water between Forsmark and present-day Gräsö) are used to assess the repository safety in the marine stage (3000 AD in Figure 5-4 and Figure 5-5) as all basins are in direct, or indirect, contact with object 157_2 via surface water exchange (Figure 5-5). During the marine stage, it is the sea-basins that are used to delineate the biosphere object used in the dose calculations. For the objects, or sea-basins, that do not contain groundwater discharge areas (i.e. all basins except for 157_2, 157_1 and 116) it is assumed that radionuclides may be transported to these objects via surface water exchange and sedimentation mechanisms only. The amounts of accumulated radionuclides in the regolith within the objects/basins that do not contain discharge areas are therefore expected to be orders of magnitude lower than the amounts of radionuclides accumulated in the regolith of the objects which contain groundwater discharge areas. Thus, in order to simplify the analyses performed during the marine stage, the assessment of all objects other than 157_2 (i.e. the object within which the primary groundwater discharge area is located) is restricted to the area of the basin which is covered with water (see Section 9.2 and Figure 5-5). Consequently, it is only the object properties that are associated with the open water that are utilized in the PSAR for these objects during the marine stage. The most important of these properties include the surface water area, the water depth, and the horizontal flows of water between the objects. The concentration of particulate matter, mineralization rate, biomass and primary production are also properties of the basins that are described in the analyses, but these properties are considered to be of less importance in the dose calculations in comparison to properties affecting the advective transport of radionuclides. The DEM (Strömgren and Brydsten 2013) was used to define the water surface area and water depth (Brydsten and Strömgren 2013). The biotic properties were derived from the morphometry of the basin (Grolander 2013). The horizontal water exchange between the objects was calculated using the MIKE 3 FM modelling tool (Werner et al. 2013).

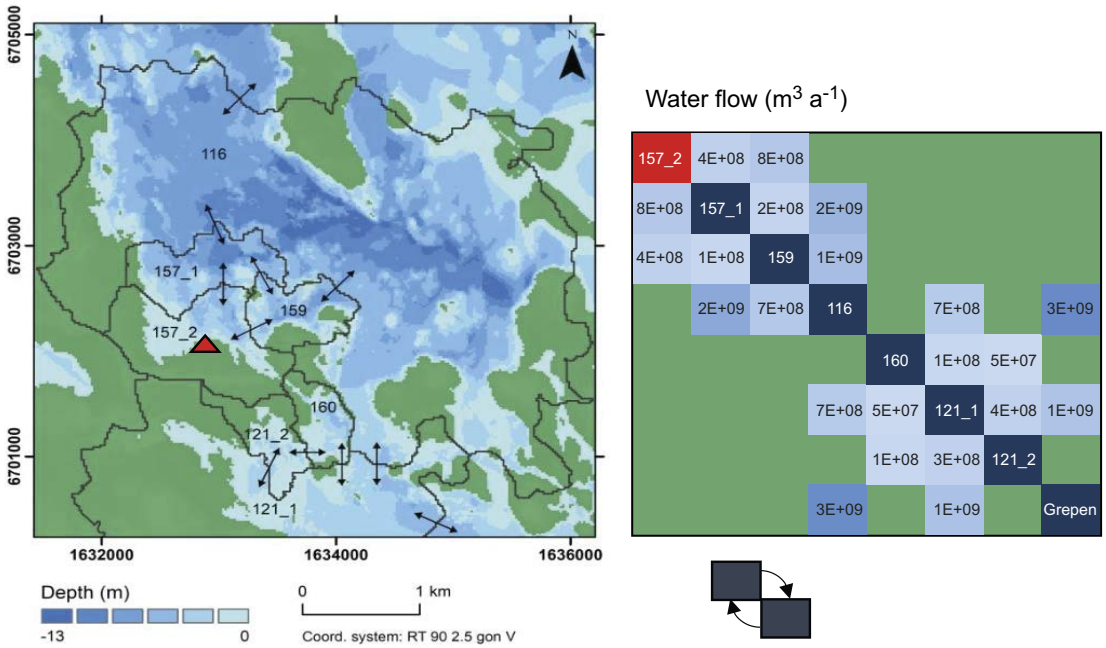

Figure 5-5. *Physical properties and water exchange of marine basins. Left: depth map over the Forsmark area at 3000 AD. Basin boundaries are outlined with black lines. The red triangle marks the primary groundwater discharge from the repository within object 157_2. The arrows indicate straits that are open for exchange of water. Right: water flows between connected biosphere objects (m^3 a^{-1}). Biosphere objects are positioned on the lead diagonal including the object "Grepen" which is added to represent the exchange between the object and the open-water of Öregrundsgreppen. The flow directions between the objects along the lead diagonal are given in a clock-wise direction (see the diagram directly below the figure). Higher flows correspond to darker blue colours. Flows were calculated with MIKE 3 FM (Werner et al. 2013).*

5.2.2 Regolith depth of terrestrial objects

The thickness of the regolith layers was calculated using the regolith–lake development model (RLDM), a landscape development model that examines how processes such as erosion and land uplift may affect the landscape of Forsmark. For the till, a regolith layer that is assumed to not be affected by interglacial erosion processes, the thickness is described using the regolith depth model (RDM), a geospatial dataset describing the current state of the regolith at Forsmark (see Section 4.7.1 for a brief explanation of the RLDM).

Biosphere objects 157_2, 157_1 and 116 all have similar till thicknesses ("RegoLow" in Figure 5-6). The organic regolith layers (post-glacial clay-gyttja and peat) accumulate over time (see Section 5.4) and are assumed to reach a steady-state once the object is in its the mire stage. Object 157_2 is located on a gentle hillslope and is not predicted to contain a lake basin. In this object, regolith layers on top of the till are estimated to be relatively thin (> 0.3 m) (Figure 5-6). Local depressions within object 157_2 are estimated to be partly filled with inorganic deposits (e.g. Figure 5-7). Regolith thickness varies across the landscape with generally thicker sedimentary deposits in local depressions and in down-stream portions of each basin (see Section 11.3.1). Objects 157_1 and 116 are situated downstream of 157_2 and they have deeper lake basins than that of object 157_2. These objects are predicted to have more sedimentary deposits on top of the till, with object 116 projected to have the thickest layer of sedimentary deposits (Figure 5-6).

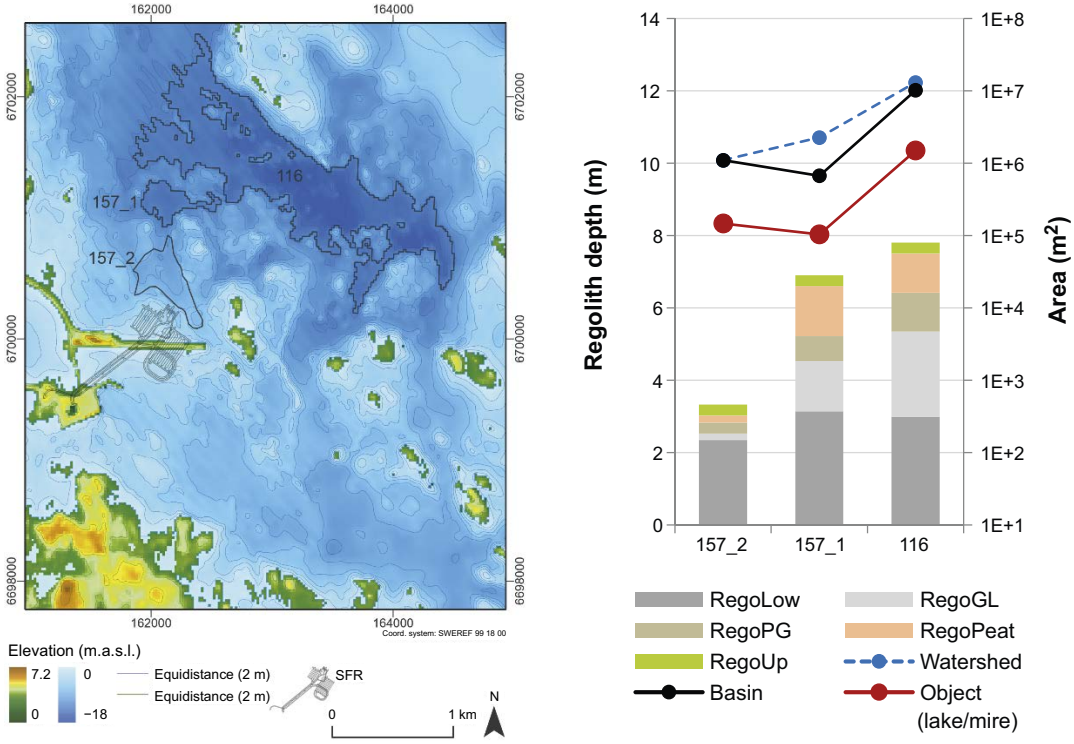

Figure 5-6. *Object boundaries and regolith thicknesses of biosphere objects 157_2, 157_1 and 116 during their terrestrial period. Left: digital elevation model (DEM) of the area around SFR with the three biosphere objects outlined in black. Right: regolith stratigraphy of the biosphere objects at the mire stage (bar chart, left vertical axis) and sizes of object, basin and watershed (right vertical axis, note the logarithmic scale).*

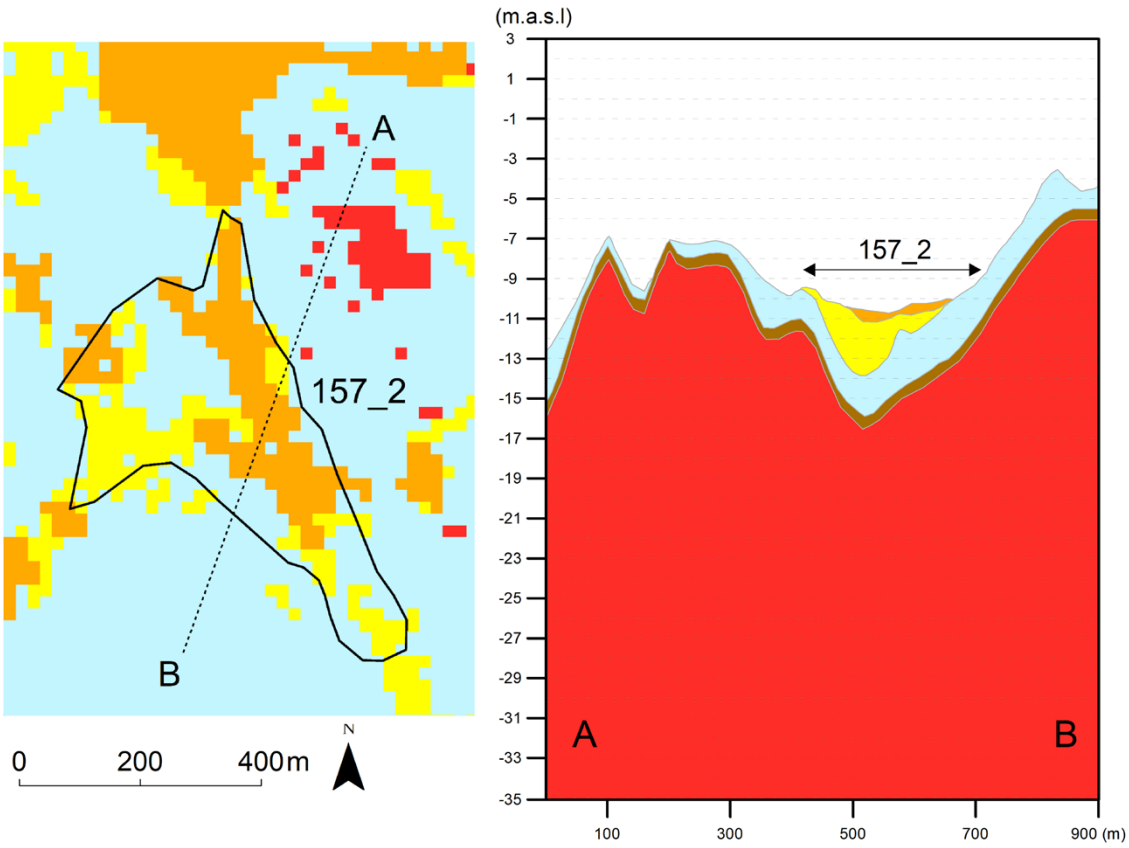

Figure 5-7. *Regolith distribution and stratigraphy in object 157_2 according to the regolith depth model (RDM). Left: surface distribution of regolith layers with a minimum thickness of 0.5 m. Position of the transect shown on the right-hand panel is indicated by the dotted black line. Right: vertical profile showing stratigraphy and total regolith thickness along a transect that intersects object 157_2 (indicated by the double-ended arrow) and beyond. The vertical axis shows the altitude in relation to the sea level (m a.s.l.), and the upper surface of the profile coincides with the digital elevation model (DEM). Orange represents post-glacial sand deposits, yellow is different types of clay, blue is till and red is bedrock with the uppermost bedrock layer in brown. Figure updated from Sohlenius et al. (2013a).*

5.2.3 Surface hydrology

Surface hydrological characteristics and water balance components were derived for biosphere objects 157_2, 157_1 and 116 using a distributed hydrological model implemented in MIKE SHE (Werner et al. 2013). Simulations were carried out for four shoreline positions as denoted by the time period of the simulation. For “present day” and 3000 AD simulations, all objects are in their marine stage (i.e. covered by sea) and in the 5000 and 11 000 AD models the objects are in their terrestrial stage (i.e. isolated from the sea) (Figure 5-4). According to the hydrological modelling (Werner et al. 2013) all of object 157_1 and most of object 116 are below the piezometric water surface in the wet period of the year thus indicating that these portions of the object are under water (Figure 5-8). This is also the case for object 157_2 but to a lesser spatial extent. This indicates that primary mire formation is likely to occur within object 157_2, even in the absence of a lake basin during the terrestrial stage, which indicates that this future hillslope will likely have wetland characteristics.

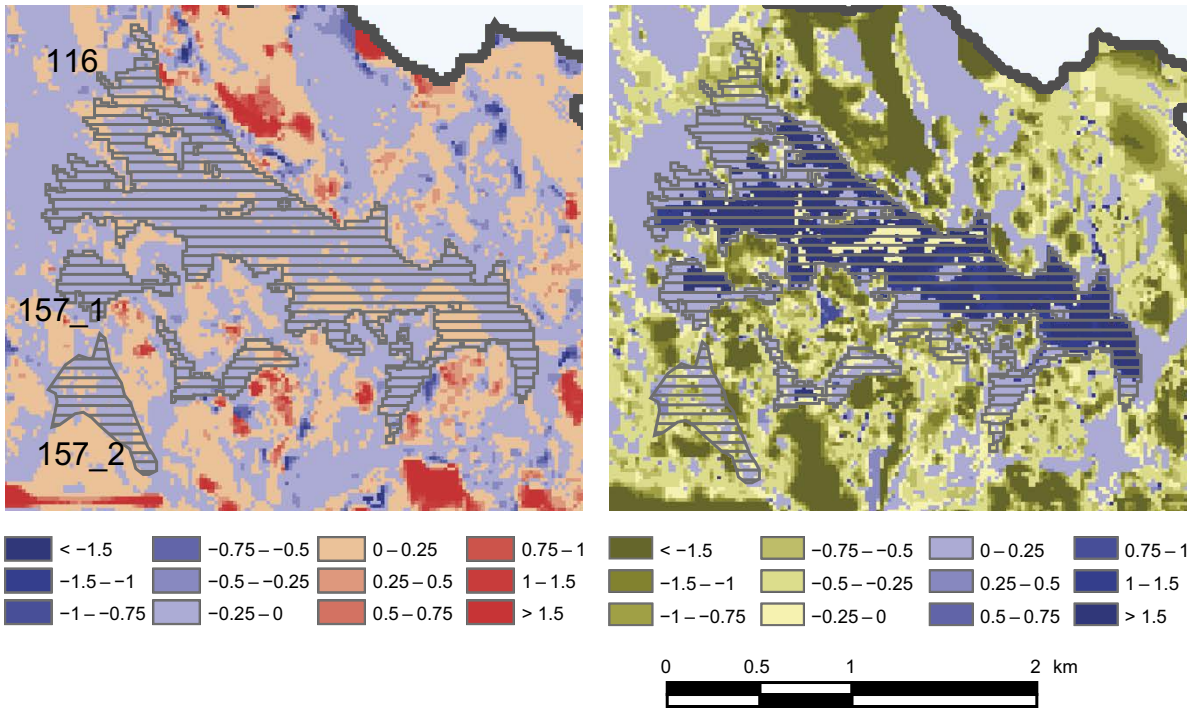

Figure 5-8. *Surface hydrological characteristics of the area surrounding the biosphere objects. Results from simulations with the shoreline position of 5000 AD and a temperate climate (normal year). Striped areas indicate the three biosphere objects and the small lake in basin 159. Left: annual average hydraulic-head differences (m) in the regolith at ~4 m below ground surface (i.e. between calculation layers 2 and 3 in the model). Labels of the biosphere objects appear to the left of the object; the small lake basin in basin 159 is east, north–east of object 157_2 and is not labelled. Blue colours indicate a negative pressure change in the vertical direction (pressure decreases as elevation increases) thus implying an upward flow of groundwater in these areas. Red colours indicate a positive pressure gradient in the vertical direction (pressure increases as elevation increases) thus implying a downward flow of groundwater in these areas. Right: depth to the groundwater table (m) during a wet period (March). Blue colours indicate areas where the modelled groundwater level is above the ground surface thus implying the presence of surface water in these areas. Green/brown colours indicate areas where the modelled groundwater head is below the surface thus implying that these areas consist of "dry land". Panels are details from Figures 5-3 and A1-15 in Werner et al. (2013).*

Water balances derived from the MIKE SHE modelling results presented in Werner et al. (2013) are used to calculate the surface and sub-surface water fluxes in and out of the biosphere objects that are later used in the BioTEx model (Chapter 7)[12]. Key parameters of these water balances are the vertical water flows between the bedrock and the regolith within the biosphere object, and the vertical fluxes between the different layers[13] within the regolith profile (Figure 5-9). During the terrestrial periods (i.e. 5000 and 11 000 AD), the water balances included horizontal flows into and out of each object, as well as flows across the boundary of mire and lake/stream parts of the objects (Figure 5-9).

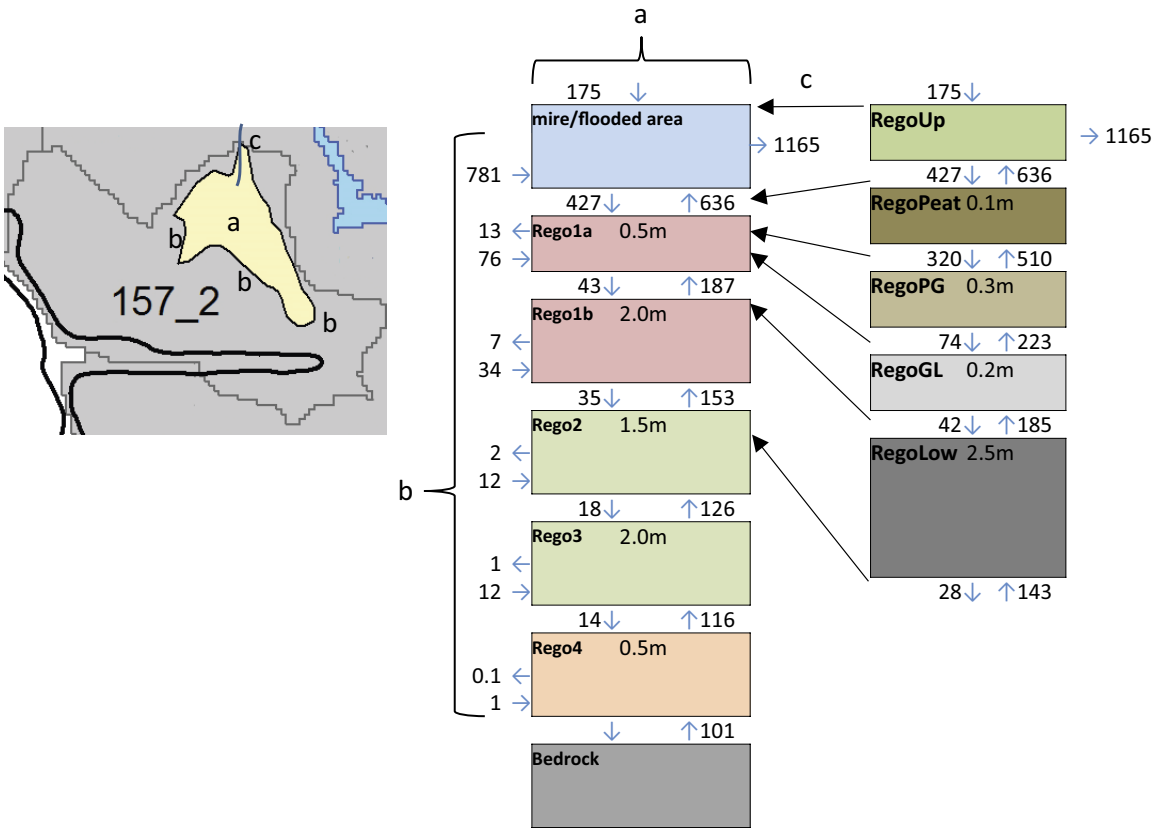

Figure 5-9. *Water balances for terrestrial conditions of biosphere object 157_2. Left: map of the biosphere object (yellow) and its catchment. The grey line outlines the borders of the basin. The blue line represents a stream. The present shoreline is outlined in black for reference. Middle: stacked boxes represent MIKE SHE model calculation layers within the object, and the arrows represent water flows across object boundaries (horizontal) or the regolith layers (vertical). Right: upward and downward flows between regolith layers in the BioTEx model (Chapter 7), as estimated by linear interpolation between the boundaries of the MIKE SHE calculation layers. The flows in the water balances are normalized to the area of the object (i.e. being in terms of area-specific flows) and are expressed as mm* a^{-1} *(equivalent to* 10^{-3} m^3 *per* m^2 *and year). Regolith thicknesses for the calculation layers are given in both stacks of boxes. The head of the arrows (connecting the middle and right panels) indicate the approximate vertical locations of regolith layer boundaries in the corresponding MIKE SHE calculation layers. For example, the boundary between RegoGL and regoLow is located 0.1 m into the Rego1b layer. For details on the methodology see Section 7.2 in Werner et al. (2013). Letters are used to link components in the left and middle panels.*

[12] Sassner, 2022. Framtagande av vattenbalanser från MIKE SHE till radionuklidtransportmodellering. SKBdoc 1987268, ver 1.0, Svensk Kärnbränslehantering AB. (In Swedish.) (Internal document)

[13] In MIKE SHE, there is a distinction between calculation layers for which flow calculations are made and regolith layers to which hydrogeological parameters are assigned. At positions where more than one regolith layer overlaps with a calculation layer, the properties of the calculation layer are obtained by spatial averaging of the regolith-layers properties (using harmonic mean for vertical conductivity, see Bosson et al. 2010, Section 4.1.1). As the boundaries of the calculation layers do not coincide with those of the regolith layers, linear interpolation was used to calculate upward and downward flows at vertical positions corresponding to the boundaries of the regolith layers (Section in 7.6 in Werner et al. 2013, see also Figure 5-8).

A comparison of the modelled vertical flows within the objects indicates that the area-specific groundwater discharge is expected to be higher in object 157_2 than in the other two biosphere objects (Figure 5-10). This is due to the thinner regolith layers (Figure 5-6) and a larger discharge from the bedrock within the object. The area-specific bedrock discharge is an order of magnitude larger in object 157_2 than for the other two objects. This is due in large part to the structure of the bedrock directly under object 157_2 as discussed in Öhman and Odén (2017) and Saetre and Ekström (2017a).

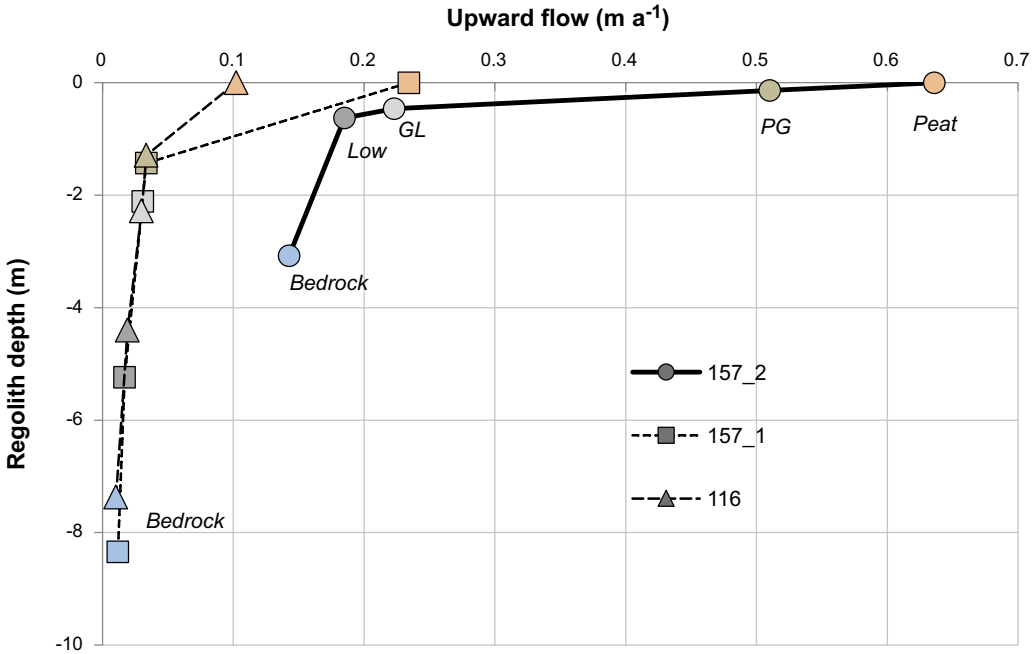

Figure 5-10. *Upward flows leaving the top of the specified layers as a function of soil depth in biosphere objects 157_2, 157_1 and 116 normalized by the area of the object. Marker colour indicates the layer from which the flows are leaving: top of the bedrock (blue), top of till (Low, dark grey), top of glacial clay (GL, light grey), top of postglacial clay-gyttja (PG, light brown) and top of deep peat (orange).*

5.3 Temporal development of biosphere objects

The spatial boundaries of a biosphere object are largely defined according to the surface topography. Surface topography is, in large part, dictated by the topography of the bedrock and the deposition pattern of the overlying till. These geological layers are expected to undergo marginal/negligible changes during an interglacial period due to the relatively large amount of energy and/or time required to displace these materials.

In contrast, the glacial clay and postglacial sedimentary materials are lighter and are therefore more susceptible to displacement via interglacial erosion mechanics. Shoreline regression, wave erosion and sedimentation, lake infilling and ecosystem succession are all expected to shape the landscape during the interglacial periods. Thus, the regolith–lake development model (RLDM, see Chapter 4) was used to describe the temporal development of the biosphere objects in SR-PSU over the interglacial time-period considered in these analyses (i.e. up to 11 000 AD).

5.3.1 Stylised development of biosphere objects used in the assessment

Biosphere object 157_2

Object 157_2 is located north of SFR. Currently, the object sits under the sea on a gentle slope (~0.5 %) which generally points downward to the north (Figure 5-4). Within the present modelling framework, the rate of shoreline regression corresponds to the present rate of isostatic rebound (Brydsten and Strömgren 2013). At this rate, the shallowest (southern) parts of the object will emerge from the sea ~1 000 years into the future (3000 AD) and the object will become fully isolated from the sea in ~2 500 years (4500 AD). These time horizons are considered to be early estimates as they do not account for the current and future rate of sea-level rise associated with a warming climate which would delay the terrestrial isolation of the object.

There are four local depressions within object 157_2 which, in total, cover about a third of the object's area, see Saetre and Ekström (2017a). These depressions may form shallow pools during the object's isolation from the sea which will eventually be overtaken by mire vegetation. The effect of these pools on dose calculations was examined in Saetre and Ekström (2017a). Results from this study indicated that the existence of these pools had no noticeable effect on the modelled radionuclide doses. It was therefore decided to model these depressions as being filled with peat during all stages of the object's isolation in order to simplify the hydrological and radionuclide transport models.

A stream is assumed to carry the runoff from object 157_2 to the downstream object 157_1 (see Section 7.5.2 in Werner et al. 2013 for details). This stream was not accounted for in SR-PSU. This stream was added for the PSAR as its formation is consistent with other small streams postulated in the stream network (e.g. streams in basins 159 and 157_1). The inclusion of this stream also ensures that exposure to organisms in an aquatic habitat can be appropriately assessed even though the shallow pools that are predicted to exist during the object's isolation from the sea are not explicitly modelled[14].

The regolith description of object 157_2 suggests that much of the object's area would be suitable for cultivation due to extensive glacial clay and post-glacial sand deposits (Figure 5-7). It is therefore assumed that cultivation will be possible within the object areas assuming the wetland areas are properly drained.

Biosphere object 157_1

Biosphere object 157_1 is located directly to the north and downslope of 157_2. The assumptions inherent to the modelling of shoreline regression indicate that object 157_1 will become isolated from the sea a few hundred years after the isolation of object 157_2. Once isolated, object 157_1 will be a lake with a mean depth of approximately 2 metres. Mire vegetation will begin to colonize the lake thus accelerating the accumulation of sediment. Peat accumulation begins once the lake is completely filled

[14] Calculated activity concentrations in surface water will be similar in pools and streams, as the dilution with surface water is primarily determined by the size of the watershed. For C-14 this is not true, due to losses from degassing in the mire. Therefore, dose rates to non-human biota (NHB) are also cautiously evaluated postulating a release to surface water with no prior degassing (Chapter 12).

with sediment. The lake is considered to be completely filled ~1 000 years after its isolation, assuming no anthropogenic intervention. Given the clay deposits and the expected future accumulation of organic deposits (i.e. clay-gyttja and peat) within the object, it is plausible to assume that object 157_1 could be cultivated in the future if it is drained.

Biosphere object 116

Biosphere object 116 is the largest of the three objects considered. The object is currently a sea basin with an average depth of 10 metres and it is expected to be a lake once it is isolated from the sea. The lake threshold of object 116 is less than a metre below that of upstream object 157_1; lake isolation is predicted to occur less than a hundred years after the isolation of object 157_1. The mean depth of the lake comprising object 116 is estimated to be ~2 metres with some parts as deep as 5 metres. The time required for complete terrestrialisation of object 116 is expected to be substantially longer than that estimated for 157_1. Via extrapolation of the ingrowth rates for present lakes in the region, it is estimated that the lake comprising object 116 could stay open for thousands of years in the absence of anthropogenic intervention. This is due to the presence of relatively deep local depressions within the lake and the lake's relatively large size. Object 116 is also assumed to be well suited for cultivation in the future due to the relatively thick layer of glacial clay in the area, the accumulation of organic deposits (i.e. clay-gyttja and peat) that is expected during the infilling of the object and assuming the object is properly drained.

5.3.2 Projected change in biosphere objects according to the RLDM

Quantitative properties describing the development of biosphere objects were extracted from the RLDM for each of the three biosphere objects as part of the parametrisation of the assessment model in SR-PSU (Grolander 2013). These properties are also used in the *base case* of the PSAR assessment in this report. However, as previously noted, uncertainty with respect to object properties and the time of emergence are handled in separate calculation or sensitivity cases (see Chapter 6 for an overview).

If the climate gets significantly warmer than postulated in the RLDM, changing sea levels may delay the isolation of the biosphere objects from the sea. The transition of the biosphere object from its lake to its peat stage is not expected to be significantly different from the conditions postulated in the RLDM when considering a warmer climate. Thus, it is considered reasonable to shift the times of the isolation events to account for a postulated sea level rise while keeping the projected timing of the transitioning between lake- and peat-stages constant.

Regolith characteristics for all biosphere objects will change on the timescale considered in the analyses. The RLDM is used to calculate the development of regolith of the biosphere objects over time, and to describe their transition from marine to terrestrial objects. An example of these results is illustrated in Figure 5-11.

Ground- and surface-water fluxes in and out of the biosphere objects will change along with the development of the landscape. To account for this, snapshots in time were taken to represent stages of the aquatic (3000 AD) and terrestrial (5000 and 11 000 AD) ecosystems. Linear interpolation was used to calculate flows in the interim periods. This simple method is considered adequate as the largest, most significant changes in the flows are assumed to occur in the time period surrounding the emergence of the object from the sea. A more detailed explanation of flux calculations is presented in Section 8.2.4.

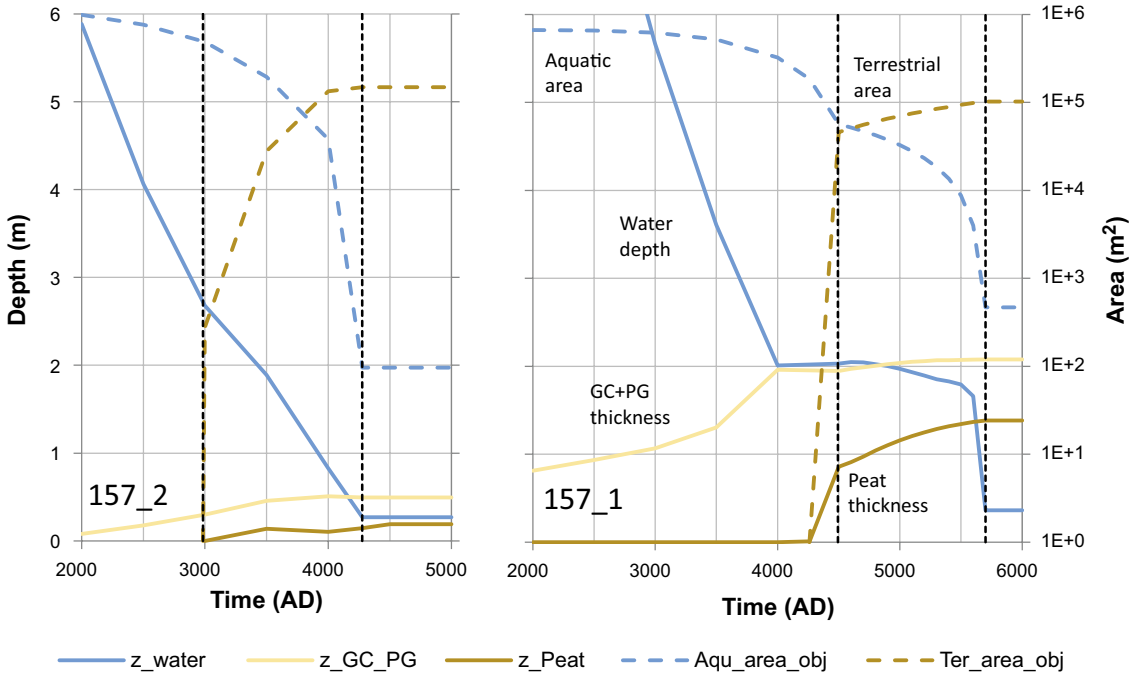

Figure 5-11. *Example of object properties that change in accordance with the development projected in the RLDM. Left panel: development of mire object 157_2, with no lake stage. Dashed coloured lines represent the area of the aquatic object (blue) and the mire (dark brown). Solid coloured lines represent the average thickness of glacial clay and post-glacial clay gyttja (GC+PG, light brown), of deep peat (dark brown) and the average water depth (dark blue). Left panel: The upper parts of the hill-slope starts to emerge ~3000 AD (first vertical line), and the mire object is fully emerged ~4500 AD (second vertical line). Right panel: development of lake object 157_1. The lake is isolated from the sea ~4500 AD (first vertical line) and it has been filled with sediments and peat ~5700 AD (second vertical line). The end stage of both objects is a mire with a central stream.*

5.4 Discharge locations in periglacial conditions

Hydrological models of periglacial conditions were examined by Bosson et al. (2010, 2013). Results from particle tracking simulations indicated several potential areas for discharge given permafrost extending down to a depth of 100 m (Odén et al. 2014). Results from these studies supported the choice of object 157_1 and lake 114 as potential through taliks under periglacial conditions (see Figure 5-12). These objects are also used in the PSAR to examine radionuclide transport in the biosphere system under periglacial conditions.

The current interglacial is projected to prevail for at least another 50 000 years (Section 4.1.1). During periglacial conditions, ingrowth of mire vegetation and accumulation of lake sediment are expected to be slower than during temperate conditions (Brydsten and Strömgren 2010). However, it is assumed that all lakes above the repository, including object 157_1, will be infilled already by this time. Therefore, the periglacial conditions are assumed to not considerably affect the projected natural development of these objects and object 157_1 is assumed to be a mire talik.

Object 114 is positioned among the string of narrow sea bays and lakes that are projected to be the last to remain in the Forsmark landscape (Brydsten 1999). The main stream in the Forsmark landscape is expected to flow through this chain of lakes in the future valley, resulting in a catchment that is significantly larger than those for the biosphere objects in the vicinity of the repository. Due to the present topography and long-lasting availability of the lakes for sediment accumulation, the regolith layers in these lakes are expected to be significantly thicker than those above the repository. For the periglacial hydrological simulations, ~40 % of the lake basin of object 114 is assumed to be covered by a mire (Werner et al. 2013).

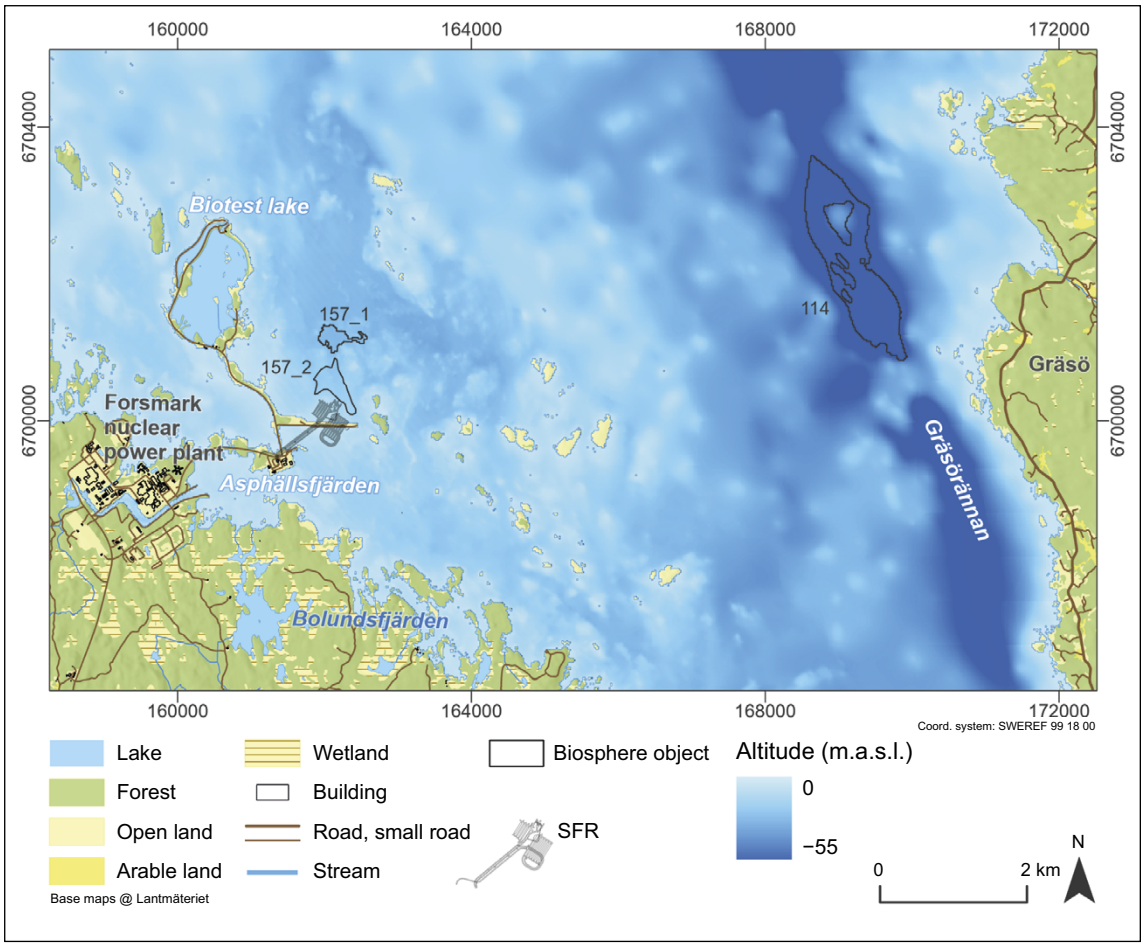

Figure 5-12. *Biosphere objects utilised for hunting and gathering during periglacial conditions outlined on the map of today's landscape. Objects 157_1 (mire) and 114 (lake) are assumed to form through taliks during periglacial conditions and, thus, receive direct discharge of deep groundwater from the repository No through talik and corresponding radionuclide releases are assumed in biosphere object 157_2, but the object could be utilised for hunting and gathering and radionuclides that have accumulated in earlier temperate periods would then contribute to exposure.*

5.5 Well interaction area

Both dug and drilled wells are considered in the PSAR. Dug wells are considered as an exposure pathway for agricultural, self-sustained communities in the biosphere objects and are included in the assessment (Chapter 6). A drilled well is treated as a separate exposure pathway and the dose from this pathway is evaluated according to a small, exposed group that uses the water for household needs (see Section 7.5.4). The effects of wells on local hydrology and hydrogeology are considered in the assessment of bedrock-drilled wells (Werner et al. 2013, Section 6.4). Drilled wells that penetrate the repository are not included in the biosphere assessment; See the **FHA report** for a description of these wells.

Earlier in SR-PSU, two types of drilled well locations were examined: drilled wells within potential agricultural settlements and wells drilled in the path of the contaminant plume originating from SFR. The locations of wells within potential agricultural settlements were estimated based on current and historical information regarding well placement relative to the distance from arable land and sea. Based on an analysis of the historical information, bedrock wells were considered to be within 100–200 m from arable land at points with a ground surface elevation at least 1 m above sea level in order to avoid sea-water intrusion (Werner et al. 2013, Section 6.4.2).

In addition, a "well interaction area" was used to assess the potential contamination of bedrock wells drilled within the path of the contaminant plume (Figure 5-13). The well interaction area was defined as the volume of bedrock between −10 and −80 m depth (below bedrock surface) within which the majority of particles released from SFR passes through; the volume is then projected on the topographical surface producing a 2D area. The outlined well interaction area has a size of 0.26 km^2, and the density of wells in the region ranges between 0.5–2 wells per km^2 (Werner et al. 2013, Section 6.4). Thus, simultaneous exposure from the use of more than one well in the area is not considered reasonable.

Werner et al. (2013) used particle tracking studies to estimate the potential contamination of these wells due to a release of radionuclides from the repositories. Hypothetical wells placed within the well interaction area were pumped at a rate consistent with the projected water demands of a future agricultural settlement and covering the irrigation demand for a garden plot in a warmer climate (Werner et al. 2013, Section 6.4, this report, Section 8.3.3). Most of the wells in potential agricultural settlements, outside of the well interaction area (cf above), received no particles during the simulations. For the minority of the wells that did receive particles, 0.05 % of the total particles released from SFR1 were captured, and 0.004 % of the total particles released from SFR3 were captured in these wells. The number of particles captured by wells drilled within the well interaction area was significantly higher. Within the well interaction area, the average fraction of released particles reaching a well ranged from 2 % of the total particles released (SFR3, particles originating in vault 5BLA) and 8 % (SFR1, particles originating from the silo), see Section 6.4 in Werner et al. (2013) for a more in-depth explanation.

In SR-PSU effects from a potential release to wells drilled by agricultural settlements within a few kilometres of the repository was also investigated (Werner et al. 2013, Sections 6.4.2 and 6.6.4). Particle tracking studies suggested that most of these wells are unlikely to receive any radionuclides from the repository (Werner et al. 2013, Table A3-1). The three wells that did receive particles were located close to SFR, and the fraction of the release was two orders of magnitude lower than expected for wells located in the well interaction area (i.e. typical fractions for SFR1 and SFR3 were 1×10^{-5} and 3.5×10^{-5} as compared to a few percent, Table 8-4). Thus, the potential dose to a farming population utilizing drilled wells in the vicinity of SFR is considered to be small as compared to potential doses from a well in the well interaction area. Consequently, wells in the well interaction area are the only type of drilled well considered in the PSAR. The probability of drilling a well into the well interaction area is not accounted for in the PSAR. Instead, the drilled well is treated as a separate exposure pathway with a probability of 100 %, and the dose from this pathway is evaluated considering a small exposed group, that uses the water for household needs (see Section 7.5.4).

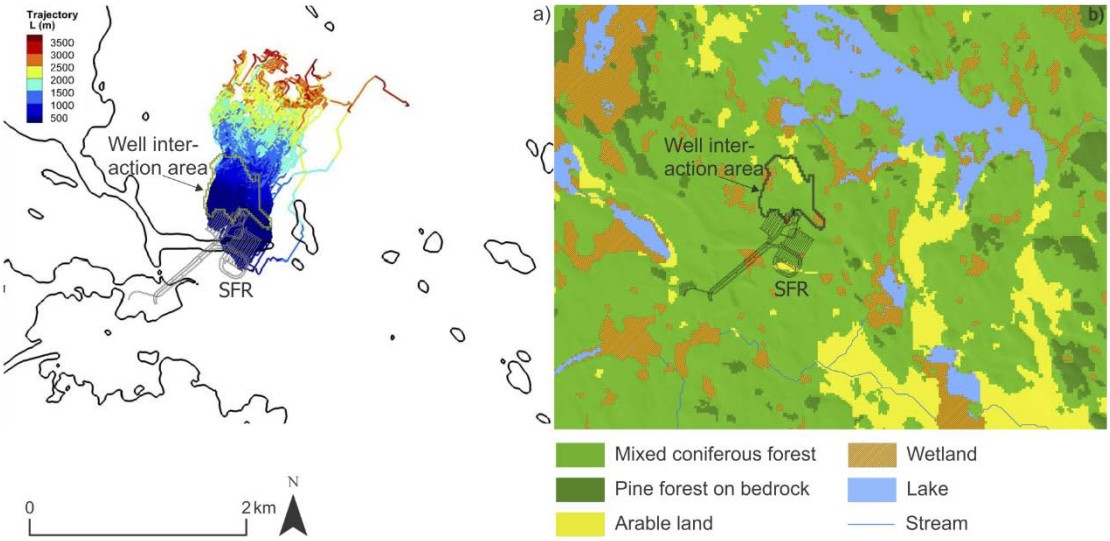

Figure 5-13. *The well interaction area superimposed on particle trajectories from SFR (left panel) and the 4500 AD landscape map (right panel). Figure modified from Werner et al. (2013).*

6 FEP handling, assessment endpoints, and calculation cases

In this chapter, SKB's work in identifying features, events and processes (FEPs) important for the evolution of surface ecosystems, and transport and accumulation of radionuclides are described in Section 6.1. The incorporation of these FEPs in different parts of the biosphere modelling is also described in Section 6.1. Sections 6.2 and 6.3 summarise the (human) exposure pathways and the identification of assessment endpoints for human and non-human biota. The last section, Section 6.4, presents the calculation cases used in the radionuclide transport and dose calculations described in this report.

6.1 FEP handling

A FEP is a feature, an event or a process that is potentially relevant to post-closure safety and hence needs to be addressed in the assessment. Earlier in SR-PSU, a major effort on the identification and handling of FEPs related to the biosphere system was carried out (SKB TR-14-06, SKB R-14-02). The PSAR FEP catalogue has been established by performing a validity check of the SR-PSU FEP catalogue, accounting for new knowledge, and a check against new international FEP lists; this review did not lead to any change in the set of FEPs included in the catalogue (**Post-closure safety report**, Section 3.4). Also, the FEP handling described below is mainly the same as in SR-PSU.

Ecosystems are dynamic systems that continuously evolve because of a complex interplay of internal and external factors linked to each other through many interacting processes. A systematic approach is taken to i) identify and analyse the ecosystems that are likely to receive discharges of deep groundwater, ii) their internal components (where radionuclides may accumulate), and iii) the internal and external processes that affect the transport, accumulation and exposure to radionuclides of organisms and humans. The PSAR assessment period spans over 100 000 years. Thus, effects of landscape development and ecosystem succession on transport, accumulation and exposure also need to be considered, as well as the effects of large-scale climate change.

To facilitate traceability in this chapter, identifiers in the PSAR FEP catalogue (**FEP report**, Chapter 5 and Appendix 2) are given in parentheses. Biosphere components are identified as CompBio*nn*, processes are identified as Bio*nn*, and variables[15] are identified as VarBio*nn* (where *nn* is the number assigned to the component/FEP/variable).

6.1.1 Identification of important components, processes and conditions

An interaction matrix (IM) is a practical tool to transparently visualise identified components and pathways that may potentially affect radionuclide transport, accumulation and exposure. It can be used to list the rationale for dismissing identified processes as being of little or no quantitative importance in a particular safety assessment (see for example Avila and Moberg 1999, Harrison and Hudson 2006, Velasco et al. 2006). The major components (CompBio*nn*) of the system are listed along the lead diagonal of the matrix, each representing a physical feature of the system. The dynamics of the system are then described in terms of processes (Bio*nn*) directly acting between the major components, displayed as off-diagonal elements in the matrix.

IMs have been used by SKB to describe the effects of a potential release of radionuclides from deep repositories since the early 1990s (Eng et al. 1994, Skagius et al. 1995, Pers et al. 1999). An early version of an IM for the biosphere system was presented in 2001 (Kautsky 2001, SKB R-01-13), which has been further developed and updated to reflect the current understanding of ecosystem processes and radionuclide behaviour (SKB R-13-43).

[15] Defined as features, or internal conditions, related to the initial state of components, or features that influence, or are influenced by, processes.

Ten physical components, two boundary components (geosphere (CompBio01) and external conditions (CompBio12)), six variables (features), and 50 processes were identified in the biosphere IM in SR-PSU (SKB R-13-43). Four components represent different environmental media: regolith (CompBio02), soil water (CompBio03), surface water (CompBio04), and atmosphere (CompBio05), Six components represent organism groups that are exposed, directly or indirectly, through these media: primary producers (CompBio06), decomposers (CompBio07), filter feeders (CompBio08), herbivores (CompBio09), carnivores (CompBio10), and humans (CompBio11). The variables (VarBio*nn*) represent features of these components (geometry, material composition, water composition, temperature, stage of succession, and radionuclide inventory).

Not all processes between the components in the IM are expected to be significant for the transport and accumulation of radionuclides from a geological repository at Forsmark. Of the 50 initially identified processes, 45 were considered relevant and sufficient for assessing the safety of human health and the environment (Table 6-1). The processes judged to be insignificant and not necessary to be included in the safety assessment are movement (Bio11), change of pressure (Bio20), loading (Bio23), irradiation (Bio44), and radiolysis (Bio46). Justification for the exclusion of these five processes is provided in SKB (R-13-43, Chapter 7).

The processes have been grouped into six broad categories: 1) biological processes, 2) processes related to human behaviour, 3) chemical, mechanical and physical processes, 4) transport processes, 5) radiological and thermal processes, and 6) landscape-development processes. In the text below, these process categories are defined, and key processes for the modelling are briefly described. In addition, internal conditions (variables) that affect the components and/or processes are also briefly described. A detailed description of all processes and variables is given in SKB (R-13-43).

Biological processes

Biological processes are those that are dependent on organisms. One pathway of exposure to radionuclides is via intake of water and food, and thus the distribution of biota and food-web interactions are important. In addition, biota may influence the distribution of radionuclides in abiotic pools by, for example, disturbing sediment or affecting water composition. The biotic processes are general and may involve both humans and other organisms. Processes that are strictly related to humans are categorised as processes related to human behaviour (see below). Consumption (Bio02), decomposition (Bio04), excretion (Bio05), food supply (Bio06), growth (Bio07), habitat supply (Bio08), primary production (Bio13), stimulation/inhibition (Bio14), and uptake (Bio15) are biotic processes that influence the distribution of radionuclides in biota and the transport of radionuclides in food webs. The processes decomposition and excretion also affect the transformation of radionuclides from organic to inorganic form.

The processes bioturbation and (Bio01) particle release/trapping (Bio12) are biotic processes that influence the abiotic compartments of the environment. Bioturbation influences the properties of the regolith and thereby affects the accumulation of radionuclides in the regolith. Particle release/trapping influences the amounts of particles in water and air, which is important for the transport of radionuclides adhering to particles.

Processes related to human behaviour

Human behaviour may have a large effect on the surface ecosystems, for example by introducing chemical elements or radionuclides. Water use such as irrigation (Bio19), anthropogenic release for example via fertilisation (Bio16), and species introduction/extermination (Bio18) are key processes related to human behaviour that need to be considered in the safety assessment.

Chemical, mechanical and physical processes

Chemical, mechanical and physical processes can influence the state of elements and compounds, which can be important for the transport and accumulation of radionuclides. For example, elements are tightly bound to particles in some oxidation states, whereas in other states they may be easily dissolved and transported by water. Chemical, mechanical and physical processes that need to be considered in the safety assessment are, for example, element supply (Bio22), phase transitions (Bio24) and sorption/desorption (Bio27). Element supply is the amount of an element available for use by biota, and a low

element supply may limit biotic production. The process phase transition is important, among others, for transport of C-14 from water to air (i.e. degassing). The process sorption/desorption determines whether radionuclides are bound to surfaces or dissolved in water. This process is crucial to consider when determining the transport of radionuclides. Sorption/desorption is typically affected by properties of the local environment such as pH and Eh (redox potential).

Transport processes

Transport processes are those whereby elements and other substances are transported from one point to another in a system. Key processes assigned to this category include: convection (Bio32), deposition (Bio34), import (Bio36), relocation (Bio38), resuspension (Bio39) and water saturation (Bio40). The latter two are not transport processes per se but are included in the category because they are the result of, or affect, transport.

Convection concerns the transport of a substance (e.g. water) or a conserved property in a liquid or gas. The process includes advection/dispersion through surface- and groundwater flows, as well as water-mediated element transport (e.g. diffusion and transport through capillary rise). Deep groundwater discharge is especially important for the transport upwards from a repository to the surface environment. Surface water flow is also important for relocation of radionuclides, i.e. transport of solid matter and sessile organisms, and it may affect the retention time and dilution of radionuclides in surface-water bodies. Advection and diffusion of gas are important for the transport and dilution of C-14.

The processes resuspension, relocation and deposition are important to describe the transport from sediment to a water column and vice versa. Deposition relates, in addition to sedimentation, also to precipitation (rain- and snowfall), which is important for water balances and water flows. Import and water saturation are processes not occurring within the biosphere system. However, import has been assigned to this category as it, by definition, is the result of transport into the biosphere system (SKB R-13-43). Saturation refers to changes in water content of the regolith, which is important for the properties of the regolith, which in turn, affect convection as well as living conditions for biota.

Radiological and thermal processes

Radiological and thermal processes are those processes that concern radionuclides, solar insolation and temperature. Important processes to consider here are: radionuclide release (Bio47), radioactive decay (Bio41), exposure (Bio42), light-related processes (Bio45) and heat storage (Bio43).

Radionuclide release refers to the amounts of radionuclides, originating from the disposed waste, that are released from the geosphere to the biosphere system per unit time. This is strictly speaking not an internal process of the biosphere system, but it is included as it is a fundamental prerequisite for the analysis. Radioactive decay is a physical phenomenon acting as a removal mechanism for the released activity, as well as a source for decay products. Exposure is the process whereby living or dead organisms/matter are exposed to ionising radiation. It can either be external from sources outside the body or internal from sources inside the body. The handling of exposure is described in Section 6.2. Light-related processes include insolation, light absorption, light reflection and light scattering, all of which influence primary production in both aquatic and terrestrial ecosystems. Heat storage has a strong influence on both biotic and abiotic components of aquatic ecosystems, and influences, for example, the distribution of biota, mixing of the water column, and occurrence of ice cover (which in turn limits exchange across the air-water interface).

Landscape development processes

The type of ecosystem (marine, limnic or terrestrial) influences transport and accumulation of radionuclides. Thus, processes affecting landscape development, and transitions from one type to another type of ecosystem, need to be considered. Processes important to consider here are change in rock-surface location (Bio48), sea-level change (Bio49), and thresholding (Bio50). Thresholding is the occurrence and location of thresholds that delimit water bodies like lakes and sea basins. The processes change in rock-surface location, sea-level change, and thresholding determine the sizes and types of ecosystems at the site.

Internal conditions (variables)

The variables representing internal conditions of the biosphere system may have a significant influence on biosphere components and their interactions, and thus their effects on transport and accumulation need to be considered. The geometry (VarBio01) of the landscape and of individual biosphere components affects both transport rates and the potential for accumulation of radionuclides in the environment. It includes, for example, topography and bathymetry, the size of a biosphere object, the thickness of regolith layers and the shapes of organisms. Material composition (VarBio02) and water composition (VarBio06) include chemical composition (e.g. salinity and the concentrations of minerals and nutrients) as well as physical features (such as grain size and porosity). These conditions, together with temperature (VarBio03), strongly influence biogeochemical processes and process rates. The successional stage of a biosphere object (VarBio04) determines the type of ecosystem that occurs at a given time and thereby affects the processes at the site. In addition to natural successional stages, it is also important to consider human activities, e.g. draining activities that convert lakes and/or mires to agricultural land. Radionuclide inventory (VarBio03) is the amount of a radionuclide stored within a physical component. However, in most instances the concentration of radionuclides resulting from a release from a geological repository is expected to be too small to influence processes and reactions in the biosphere system (SKB R-13-43).

6.1.2 Handling of potentially safety-relevant biosphere FEPs

Earlier in SR-PSU, 45 out of 50 processes and variables were identified as relevant and sufficient to consider for a safety assessment of a geological repository (SKB R-13-43). Identification of relevant FEPs and model development have been going on in parallel at SKB for the last 25 years. Thus, knowledge of important FEPs has been considered in the development and improvements of the biosphere transport and exposure model, and more experience in the importance of FEPs has been gained. Consequently, many relevant FEPs are included as components and/or processes in this dynamic model (Chapter 7). However, not all the FEPs are explicitly included in the model, some are accounted for in the supporting modelling of hydrology and landscape development (Chapter 4), others underlie the derivation of parameter values for the model (Chapter 8). To ensure that the relevant FEPs have been included/represented in an appropriate manner in the assessment, the FEPs have been mapped to the different modelling activities in the PSAR where they are considered (Table 6-1). A check against internationally identified FEPs related to the biosphere, which confirmed that no FEPs of potential significance were identified as having been omitted, is reported in the **FEP report**.

Table 6-1. Handling of biosphere FEPs in the different model activities in the PSAR. Aqua, Mire, and Agri represents the three ecosystems included in the modelling, i.e. aquatic (sea, lake and stream), mire (wetland), and agricultural land. NHB is short for non-human biota, K_d/*CR* represents sorption coefficients and concentration ratios and X indicates inclusion in the model activity.

Process and Variables		Transport and exposure modelling					Supporting activity						
		Transport modelling			Dose calculations		Landscape modelling	Hydrological modelling	Ecosystem-specific parameters				
		Aqua	Mire	Agri	Humans	NHB			Aqua	Mire	Agri	K_d/CR	Humans/NHB
Biological processes													
Bio01	Bioturbation	X		X					X		X		
Bio02	Consumption	X	X		X	X	X		X	X	X		X
Bio03	Death	X	X				X		X	X			
Bio04	Decomposition	X	X	X			X		X	X	X		
Bio05	Excretion	X	X						X	X	X	X	
Bio06	Food supply				X		X		X	X	X		
Bio07	Growth						X				X		
Bio08	Habitat supply				X	X	X		X	X	X		X
Bio09	Intrusion			X	X								X
Bio10	Material supply				X		X		X	X	X		X

Table 6-1. Continued.

Process and Variables		Transport and exposure modelling					Supporting activity						
		Transport modelling			Dose calculations				Ecosystem-specific parameters				
		Aqua	Mire	Agri	Humans	NHB	Landscape modelling	Hydrological modelling	Aqua	Mire	Agri	K_d/CR	Humans/NHB
Bio12	Particle release/trapping	X	X						X	X	X		
Bio13	Primary production	X	X				X		X	X	X		
Bio14	Stimulation/inhibition						X		X	X	X		
Bio15	Uptake	X	X		X	X			X	X	X	X	X
Processes related to human behaviour													
Bio16	Anthropogenic release			X	X						X		X
Bio17	Material use			X	X						X		X
Bio18	Species introduction/extermination				X	X			X		X		
Bio19	Water use			X	X			X					X
Chemical, mechanical and physical processes													
Bio21	Consolidation			X							X		
Bio22	Element supply						X		X	X	X	X	
Bio24	Phase transitions	X	X	X				X	X	X	X		
Bio25	Physical properties change	X	X	X				X	X	X	X		
Bio26	Reactions	X	X	X					X	X	X	X	
Bio27	Sorption/desorption	X	X	X	X	X						X	
Bio28	Water supply				X	X	X	X					X
Bio29	Weathering								X	X	X	X	
Bio30	Wind stress						X		X	X	X		
Transport processes													
Bio31	Acceleration							X					
Bio32	Convection	X	X	X				X	X	X	X		
Bio33	Covering	X	X				X	X	X	X			
Bio34	Deposition	X	X				X	X	X	X			
Bio35	Export	X	X	X			X	X					
Bio36	Import	X	X	X			X	X					
Bio37	Interception			X				X			X		
Bio38	Relocation			X			X				X		
Bio39	Resuspension	X			X		X		X				
Bio40	Saturation						X	X			X		
Radiological and thermal processes													
Bio41	Radioactive decay	X	X	X	X	X							X
Bio42	Exposure				X	X							X
Bio43	Heat storage								X	X			
Bio45	Light related processes								X	X	X		
Bio47	Radionuclide release	X	X	X									
Landscape development processes													
Bio48	Change in rock-surface location						X	X					
Bio49	Sea level change						X	X					
Bio50	Thresholding						X	X					
Variables													
VarBio01	Geometry	X	X	X	X	X	X	X	X	X	X		X
VarBio02	Material composition	X	X	X			X	X	X	X	X	X	
VarBio03	Radionuclide inventory	X	X	X	X	X							
VarBio04	Stage of succession	X	X	X	X	X	X	X	X	X	X		X
VarBio05	Temperature	X	X	X	X	X	X	X	X	X	X		
VarBio06	Water composition	X	X	X	X	X			X	X	X	X	

6.2 Assessment endpoints for humans

The assessment endpoint for humans in the biosphere assessment is the annual dose, calculated as the annual effective dose to an adult, where the annual effective dose is defined as the effective dose from external exposure in a year, plus the committed effective dose from intakes of radionuclides in that year (Section 2.3.5). The approach in the assessment is to calculate annual doses to a set of potentially exposed groups (PEGs). When selecting the groups, all relevant pathways of exposure with respect to the use of the areas with the highest concentrations of radionuclides are considered. The habits of the groups reflect land-uses that result in relatively high exposure, and are selected to be reasonable and sustainable with respect to physical constraints of the landscape, to human needs for nutrients and energy, and to present and/or historical land use.

A comprehensive pathway analysis for exposure of humans was conducted in SR-PSU (SKB R-14-02) and is valid also for the present assessment. A set of exposure route cases was identified, considering the modes of exposure (such as ingestion or inhalation) combined with environmental media that may receive repository-derived radionuclides (such as surface waters or regolith). A screening evaluation was performed on each exposure route case, either qualitatively or quantitatively, to determine if its contribution is insignificant for post-closure safety and hence if it can be excluded from the safety assessment.

The outcome of the exposure pathway analysis was that 22 exposure route cases were screened in, and that they could be covered in the dose calculations by establishing four potentially exposed groups (PEGs): Hunter-gatherers (HG), Infield-outland farmers (IO), Drained-mire farmers (DM), and Garden-plot households (GP). These groups are described in SKB (TR-14-06) and the parameter values used to characterise them are addressed in Chapter 8 below. Figure 6-1 illustrates the exposure pathways included in the dose calculations. When characterising the most exposed groups, physical and biological characteristics of the biosphere objects, human requirements for energy and nutrients, and habits from historical and present societies have been considered (Saetre et al. 2013a, b).

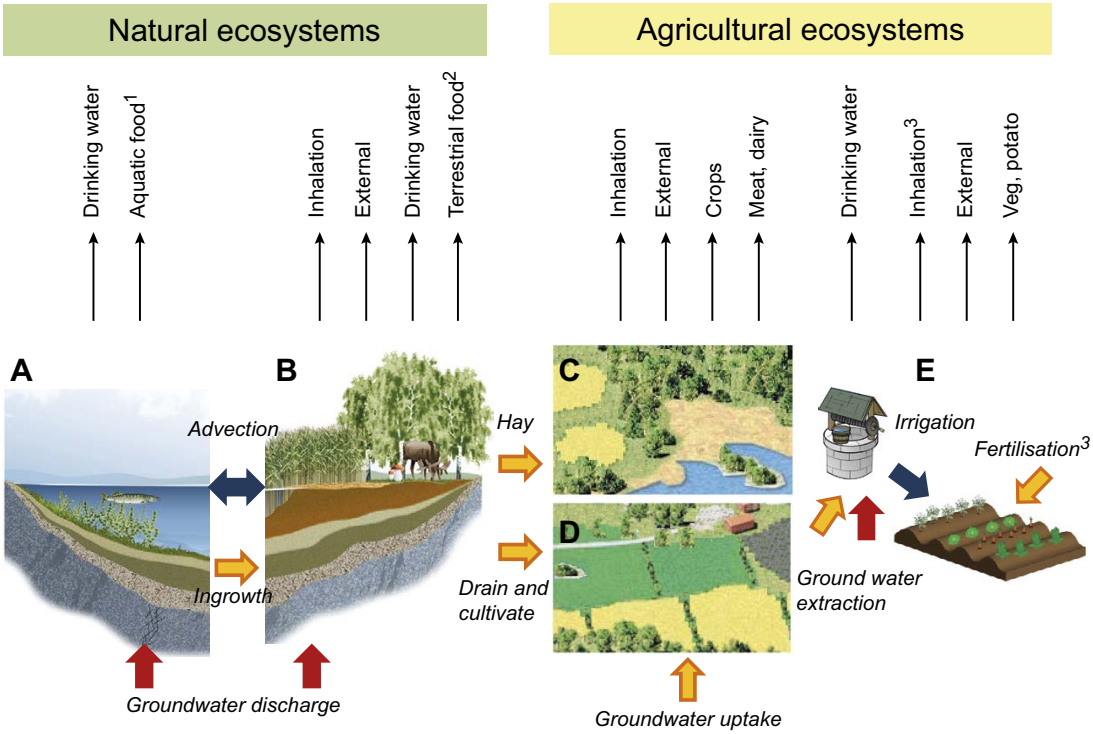

Figure 6-1. *Exposure pathways included in the dose calculations for exposed populations using natural resources and/or living in biosphere objects. Hunter-gatherers use natural aquatic (A) and mire (B) ecosystems. The other three exposed populations represent different uses of arable land, namely infield-outland agriculture (C), draining and cultivating the mire (D) and small-scale horticulture on a garden-plot (E). Bold arrows represent input of radionuclides from the bedrock (red), from natural ecosystems or deep regolith deposits (orange), or water-bound transfer of radionuclides within the biosphere (blue). The thin black arrows represent exposure routes: [1]fish and crayfish, [2]game, berries and mushroom, [3]inhalation and fertilisation that include radionuclides from combustion of biofuel.*

The PEGs are briefly described below and are considered credible to use as bounding cases for a representative individual in the group exposed to the greatest risk, with respect to exposure through all relevant exposure pathways.

6.2.1 Potentially exposed groups

Hunter-gatherers (HG)

A hunting-gathering society has been identified to serve as a local reference for the most exposed group with respect to radiation exposures from the natural environment, i.e. essentially undisturbed by humans, and intakes of surface water and aquatic and terrestrial natural foods. The major exposure pathways to a hunter-gatherer are related to foraging discharge areas in the landscape (fishing, hunting, and collecting berries and mushrooms), and from drinking water from surface water (streams or lakes). Land use and habits of a typical hunter-gatherer community have been extracted from historical records (Saetre et al. 2013b and the associated electronic supplementary material), and the group is considered to be made up of 30 individuals that forage an area of approximately 20 km^2, as illustrated in Figure 6-2.

Infield-outland farmers (IO)

This self-sustained agrarian system is characterised by fertilised arable fields and enclosed meadows (infield) on one hand, and by livestock grazing nearby pastures and forests (outlands) on the other hand. The key principle is to fertilise the arable land with the nutrients from outlands, using animal manure as organic fertiliser. This basic principle more or less characterised agricultural practices in Scandinavia well into the 18th century (Welinder et al. 1998). Radionuclides in wetland hay reach the cultivated soil through fertilisation with manure. The major exposure pathways are from growing food and raising livestock, and from drinking water either from a dug well or surface water. A self-sufficient community of infield-outland farmers is assumed to be made up of 10 persons. A wetland area of 0.1 km^2 (10 ha) is needed to supply winter fodder to the herd of livestock corresponding to the amount of manure needed to support infield crop production for this group.

Drained-mire farmers (DM)

Agricultural practice changed dramatically during the 19th century in Sweden. The amount of arable land increased and the use of large-scale drainage to increase the land available for cultivation was first observed. At the turn of the 19th century, most of the farming population was found on self-sufficient small-scale farms. These are considered to serve well as a reference for the most exposed group with respect to exposure from draining and cultivating contaminated lake–mire systems. The radionuclides reach the cultivated soil through groundwater uptake, and radionuclides that have accumulated for an extended time prior to drainage of the mire are also considered. The major exposure pathways are from growing food and raising livestock, and from drinking water from a dug well (or from surface water). A self-sufficient community of drained-mire farmers is assumed to be made up of 10 persons. A wetland area of 6 ha is needed to support food production for this group, assuming a level of technology similar to that from the turn of the nineteenth century.

Garden-plot households (GP)

There are several possible exposure pathways that are likely to affect a small group of future permanent residents who are not necessarily entirely self-sustained with respect to food production. Such possible exposure pathways include particularly irrigation and fertilisation. A garden-plot household is a reasonable reference for a family that is self-sustained with respect to vegetables and root crops produced through small-scale horticulture. Hence the garden-plot household serves well as a reference for the most exposed group with respect to radionuclides from intake of irrigated crops and external exposure from soils contaminated due to irrigation. In the assessment, a garden-plot household is also suitable for covering exposure pathways related to using seaweed or fly ash as soil fertilisers. Radionuclides reach the cultivated soil through fertilisation and irrigation. The major exposure pathways are from growing food and from drinking water from a dug or drilled well (or from surface water). A garden-plot household is assumed to be made up of five persons and a 270 m^2 area garden plot is assumed to be sufficient to support the family with vegetables and root crops. The garden-plot is also associated

with support areas providing fertilizers. These depend on the productivity of seaweed, the productivity of wood, or the depth of the peat layer in the biosphere object. The productivity of the garden-plot and the diet for this group have been determined from present-day habits.

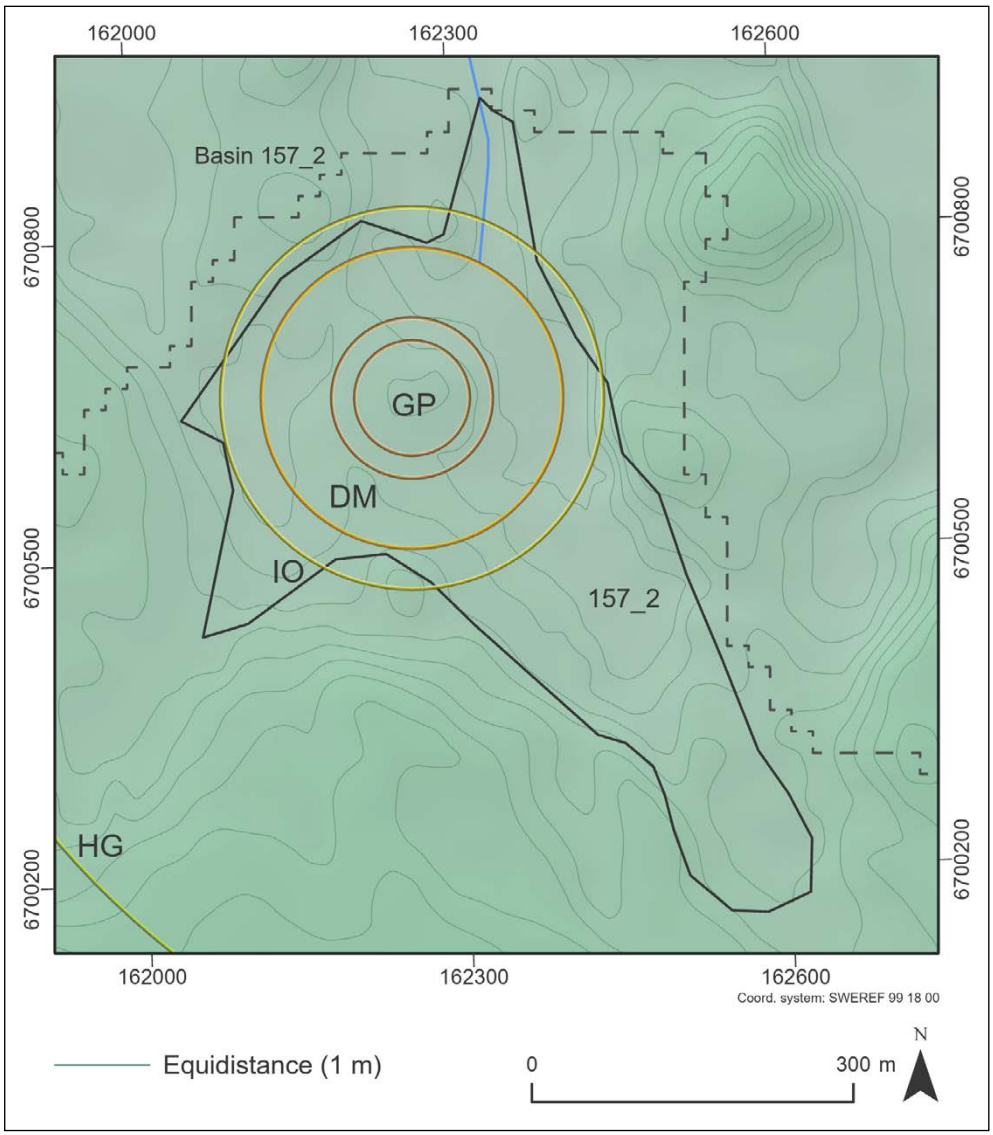

Figure 6-2. *Support areas for the potentially exposed groups superimposed on biosphere object 157_2. Only part of the perimeter of the 20 km^2 foraging area supporting a typically sized group of hunter-gatherers is shown (HG, in the left lower corner). The area for the infield-outland farmers (IO) corresponds to the size of a mire that could produce the winter fodder for the herd of livestock supporting the group. The area for drained-mire farmers (DM) corresponds to the arable land needed to support the group with crops and fodder. The two areas for the garden-plot household (GP) correspond to the areas of a mire that could support biofuel for heating a house by combustion of fire-wood (outer circle, sustainable yearly production) or harvesting of peat (inner circle, given a 50-year period and the average depth of peat in object 157_2).*

6.2.2 Remarks on the potentially exposed groups

The annual dose (see Section 2.3.5) is calculated for all potentially exposed groups. Doses are evaluated continuously over the assessment period, but for the drained-mire farmers, doses arise from an event (the draining and cultivation of a natural wetland). Exposure is evaluated and averaged over a 50-year period following the drainage event, assuming that the mire has not been drained previously. However, the consequences of draining the mire are cautiously evaluated for all times when cultivation is feasible.

The hunter-gatherer community uses undisturbed ecosystems, whereas the other three groups actively cultivate the land. For hunter-gatherers and drained-mire farmers, exposure occurs within the boundaries of the biosphere object or objects. However, for infield-outland farmers and garden-plot households, exposure occurs due to utilising resources from the biosphere object (e.g. organic fertilisers, biofuel or irrigation water) and the location of the cultivated land is not explicit.

During marine conditions, natural ecosystems can be used for food gathering (fishing) and as a source for organic fertilisers (seaweed), but cultivation of crops is not possible in the biosphere object. The possibility to drain and cultivate the biosphere object and to extract water from a well increases as more land becomes available due to the shoreline regression. Hay and surface waters can be used as soon as an object has been isolated from the sea. Wells can be dug, and mires can be drained when the risk of saltwater intrusion has been reduced, which is assumed to occur when the land is at least 1 m above sea level.

It follows from the description above that the four potentially exposed groups represent four different types of future land use. In the remaining of the report, especially in the description of modelling results, the groups are frequently referred to as “land use variants”.

6.3 Assessment endpoints for non-human biota

The primary endpoint selected for demonstrating protection of non-human biota is absorbed dose rate (Section 2.3.5). As for humans, an exposure pathway analysis was conducted earlier for SR-PSU for non-human biota (SKB R-14-02), which is valid also for the present assessment. In a similar manner, exposure route cases relevant to include in the post-closure safety assessment were identified. Three relevant exposure modes by which biota may be exposed to radionuclides was identified: through the respiratory tract (inhalation), through the digestive tract (ingestion) and via external irradiation (SKB R-14-02). However, exposure via ingestion and inhalation are not modelled separately as an organism is modelled as one unit and not characterised in terms of tissues and organs. Hence, the exposure modes for non-human biota are only divided into internal (via inhalation and ingestion) and external exposure.

The outcome of the exposure pathway analysis was that eight exposure route cases were screened in: internal exposure due to seawater, lake/stream water or peat, and external exposure from seawater, lake/stream water, sea sediment, lake/stream sediment or peat (SKB R-14-02, Table 3-9).

6.3.1 Organism types in the assessment

Concerning exposure estimates to biota, it is practically impossible to consider and ensure protection of every single population of organisms at the site, so generalisations are necessary to allow assessments to focus on a few representative targets characterising the range of species and their habitats present. The challenge is thus to identify a small enough number of targets to make assessments manageable without reducing the information value of the assessment beyond credibility. This is discussed in more detail in Jaeschke et al. (2013).

Species at the site are represented by a number of reference organisms included in ERICA, in terrestrial, freshwater and marine ecosystems. Reference organisms are a set of organism types selected as assessment targets in order to represent organisms that are likely to get the highest exposure in the ecosystems of relevance, thus mirroring the reference man concept employed in human dose calculations. Since SR-PSU, the reference organisms have been updated (Brown et al. 2016), along with updates to the ERICA tool (the present assessment is based on the updated version, that is v2.0).

Key changes included removal of the “Bird-egg” organism type, as it was deemed inconsistent with the general protection strategy, while adding the freshwater “Reptile”, as some protected reptile species in Europe were identified.

As described in SKB (R-14-02), the reference organism concept was acceptable to represent species at the Forsmark site in most cases, and only a few changes and additions have been made to capture important site-specific aspects. For example, one small benthic limnic primary producer has been added to represent the microphytobenthos present in thick layers in the lake sediment in many of the lakes in the Forsmark area today (Andersson 2010). Marine reptiles and sea anemones/corals are not deemed relevant to the site, at present or in the future, and so the corresponding reference organism types were excluded from the assessment.

The types of ecosystems included are sea, lake/stream and wetlands. Agricultural ecosystems have not been considered relevant in the analysis because future discharge areas are expected to be marine areas, lakes/streams or wetlands. Even though wetlands may be drained and cultivated, these agricultural soils are expected to be productive (and thus provide a stable environment) for 100 years or less (Lindborg 2010). Species associated with this land would either be introduced by humans (crops or livestock) or immigrate from adjacent land and consequently they would be part of larger and more stable biological populations. The populations would also be actively manipulated by humans. The exclusion of farmed animals from the assessment is consistent with the ICRP view that the protection of humans themselves is probably sufficient for such managed environmental or ecological situations (ICRP 2008).

In total, 38 organism types have been included in the safety assessment: 13, 14 and 11 for terrestrial, freshwater and marine ecosystems, respectively (Table 6-2).

Table 6-2. Organism types included in the assessment of non-human biota in the PSAR.

Terrestrial ecosystem	Freshwater ecosystem	Marine ecosystem
Amphibian	Amphibian	Benthic fish
Annelid	Benthic fish	Bird
Arthropod – detritivorous	Bird	Crustacean
Bird	Crustacean	Macroalgae
Flying insects	Insect larvae	Mammal
Grasses & herbs	Mammal	Mollusc – bivalve
Lichen & bryophytes	Microphytobenthos	Pelagic fish
Mammal – large	Mollusc – bivalve	Phytoplankton
Mammal – small-burrowing	Mollusc – gastropod	Polychaete worm
Mollusc – gastropod	Pelagic fish	Vascular plant
Reptile	Phytoplankton	Zooplankton
Shrub	Reptile	
Tree	Vascular plant	
	Zooplankton	

6.4 Calculation cases

Radionuclide transport and dose calculations are performed to provide a basis for estimation of radiological risks for various scenarios assessed in the PSAR. As described in Section 2.3.3, there are three types of scenarios: the main scenario that represents a probable future evolution of the repository and its environs; less probable scenarios to evaluate scenario uncertainties that are not evaluated within the framework of the main scenario; and residual scenarios to primarily illustrate the significance of individual barriers and barrier functions independently of risk.

Calculation cases provide quantitative assessment of radiological consequences for scenarios. Often only a single calculation case is defined per scenario. For some scenarios, however, more than one calculation case is defined to evaluate specific uncertainties in initial state and future evolution of external (climate) conditions and internal (repository and its environs) processes. A calculation case may also include variants to evaluate the effect on the outcome due to alternative assumptions related to different aspects within the framework of the calculation case description. An overview of all the scenarios and calculation cases in the PSAR is given in the **Radionuclide transport report**, Table 2-1, and the calculation cases described and analysed in this report are summarised in Table 6-3.

The main scenario includes three calculation cases based on the three variants of the reference evolution (**Post-closure safety report**, Chapter 7). These include the present-day climate calculation case, which is defined as the *base case* in the PSAR, and two cases, *warm climate calculation case* and *cold climate calculation case*, representing a range of probable future climate evolutions for the assessment period. The *base case* provides a benchmark for the post-closure safety assessment and, thus, enables straightforward evaluation of differences with respect to other calculation cases. To this end, models built for the other calculation cases typically are only described if they deviate from the *base case*, and results are typically compared with those for the *base case*.

The three calculation cases of the main scenario are complemented with a set of supporting calculation cases. These provide sensitivity analyses of specific uncertainties in external conditions and the description of transport and accumulation of radionuclides in the future Forsmark landscape. The objective of these calculations is to support the selection of assumptions for the calculation cases of the main scenario, and they are consequently not included in the radiological risk evaluation. Due to the long timeframe of the assessment, the landscape will change considerably throughout the assessment period (Chapter 4). The location of a future discharge area depends on the description of the bedrock hydrogeology (Öhman and Odén 2018), and the ecosystem state of the area will be affected by the rate of change in the relative sea-level (Chapter 5). The local topography and the position in the landscape affect the regolith stratigraphy and groundwater-flow patterns. Thus, the location, size and properties of a discharge area are important characteristics that influence transport, accumulation and dilution of radionuclides.

To cover the potential effects of uncertainties in landscape development and the properties of the discharge area, four supporting calculation cases have been designed: the *timing of shoreline regression calculation case*, the *horizontally sloping bedrock fracture calculation case*, the *alternative landscape configuration calculation case* and the *alternative delineation calculation case*. The first of these calculation cases is identified in the overall safety assessment (**Post-closure safety report**, Chapter 7). The other three cases, which were identified already in SR-PSU (Saetre and Ekström 2016, Saetre and Ekström 2017a), are relevant and appropriate for evaluating potential effects of uncertainties associated with the future discharge area.

A few additional supporting calculations have also been formulated. These include two sensitivity analyses where the impact of changes in *ecosystem properties* and in *object properties* (including hydrology) on doses are evaluated. In addition, one case is designed to evaluate the potential effects of *calcite depletion* in regolith layers of Forsmark.

Four potentially exposed groups are used in the *base case* and in most other calculation cases, including different exposure pathways related to land use of the discharge area (Section 6.2.1). In the PSAR, the use of water from a well drilled into the bedrock is evaluated independently of other exposure pathways (Section 5.6).

The 11 calculation cases described and analysed in this report (Table 6-3), include three cases of the main scenario and eight supporting cases. In the supporting calculations cases, biosphere conditions are altered as compared with present-day conditions in the *base case*. Detailed descriptions and selection of parameter ranges/values are presented together with the results of the calculations in Chapters 9, 10 and 11. The calculation cases analysing less probable scenarios and most of the residual scenarios are described in the **Radionuclide transport report**. These descriptions also include the handling in the biosphere models and the resulting dose consequences. Residual scenarios related to future human actions with potential to impair the repository performance and/or lead to radiological consequences to humans are described in the **FHA report**.

Table 6-3. Calculation cases analysed in this report. Calculation cases included in the main scenario are marked in orange. Supporting calculation cases for the main scenario only presented in this report are marked with solid green, and supporting calculation cases presented in this report and in the Radionuclide transport report are marked in green stripes.

	Calculation case	Variants	Geosphere release	Discharge area	BioTEx Model	Parameter set			NHB
						Landscape	Hydrology	Ecosystem	
Main scenario	*Base case* (Present-day climate)		Time-dependent, probabalistic	157_2	Full representation of 157_2, other objects	Present development	Present, stream in 157_2	Present	Yes
	Warm climate[a]	High summer precipitation	Modified with delayed shoreline regression	*base case*	*base case*	Delayed emergence	Warm	Warm	Yes
		Low summer precipitation					Warm and dry	Warm and dry	
	Cold climate	Continuous permafrost	*Base case*, no release during periglacial	*base case*	*base case*	*base case*	*base case*, restricted to active layer in permafrost	*base case*, cold in permafrost periods	Yes
		Permafrost with talik	*base case*	*base case*, 157_1, 114 in permafrost	Full representation of 157_2, 157_1, 114		*base case*, + taliks in permafrost		
Supporting calculation cases	Timing of shoreline regression	Four variants	Deterministic, modified with timing of shoreline regression	*base case*	*base case*	*Delayed emergence*	*base case* (timing adjusted)	*base case*	
	Subhorizontal fracture	Distributed release	*base case* (distributed)	157_2, 157_1, 116	Full representation of all objects	*base case*	*base case*	*base case*	
		+ modified discharge					Adjusted bedrock discharge		
	Alternative landscape configuration	No stream	*base case*	*base case*	Full representation of all objects	*base case*	no stream in 157_2	*base case*	
		Release to surface of water		Stream			*base case*		
		+ open lake							
	Alternative delineation	Upward gradient	*base case*	Upward gradient	No downstream objects	Mire object (mature state)	Upward gradient	Sea ecosystem excluded	Yes
		Wetland		Wetland			Wetland		
		Up-hill		Up-hill			Up-hill		
		Agriculture		Agriculture			Agriculture		
	Ecosystem properties	Sensitivity analysis	*base case* (mean)	*base case*	No downstream objects	Mire object (mature state)	Mire sub-model	Sea ecosystem excluded	
	Mire object properties	Sensitivity analysis	*base case* (mean)	Stochastic	No downstream objects	Mire object (mature state)	Mire sub-model Stochastic	Sea ecosystem excluded	
	Calcite leaching	ΔpH −1 in 3 000 y	*base case*	*base case*	*base case*	*base case*	*base case*	K_d shift for pH sensitive elements	
		in 50 000 y							
		ΔpH −2 in 3 000 y							
		in 50 000 y							

a) Doses are evaluated to drained-mire farmers with and without large-scale irrigation.

6.4.1 Probabilistic simulations

The approach to the radionuclide transport modelling of natural ecosystems is selected to be as comprehensive and realistic as possible, with respect to model structure, primary transport pathways and landscape development (Section 2.3). Accordingly, most ecosystem parameters are described with probability density functions (PDFs) that reflect natural variation (Section 8.1). In the transport calculations, parameter uncertainties are propagated to the assessment endpoints by probabilistic Monte Carlo simulations. In practice, this is done by applying a Latin hypercube sampling scheme to randomly and independently draw values from the specified PDF, and then applying each parameter set to the full simulation period.

For some parameters, this approach is not applicable. For example, parameters associated with the shoreline regression change in a co-ordinated manner in response to ecosystem succession (e.g. the size and volume of water bodies decreases and the area of the mire increases with land emergence and expansion of mire vegetation, and the thickness of regolith layers increases with sedimentation and peat accumulation). The values of other parameters are directly dependent on an explicit description of the landscape (e.g., surface and groundwater flows), and it would be unrealistic to change the values of geometrical and hydrological parameters independently. Thus, uncertainties in time- and landscape-dependent parameters are not included in the *base case*. The potential effects of uncertainties in these parameters are instead examined in separate supporting calculation cases where transport is described with a time-independent mire ecosystem model (i.e. the object delineation case and the mire object properties case).

The habits of the potentially exposed groups described in Section 6.2.1 are based on cautious assumptions with respect to the use of the areas with the highest concentrations of radionuclides, and the groups are considered credible bounding cases for exposure calculations. The parameter values describing the groups are selected to reflect a reasonable and sustainable use of land and natural resources in the biosphere object, but no uncertainties are assigned to the exposure calculations. Following SKB practice, in agreement with international recommendations (e.g., ICRP 2006), parameters describing human characteristics and conversion factors from exposure to dose (i.e., dose coefficients) are considered as reference values, and are accordingly also kept fixed.

To avoid negative flows of carbon and radionuclides from the upper peat to the deeper peat layer the uncertainty of the parameters describing the processes *burial* are re-examined in the PSAR[16]. Accounting for the fact that a fraction can only take values between 0 and 1, the PDF for the parameter f_refrac_ter is now described by a probit distribution (see Section 8.1.2). Moreover, using literature data, a lower boundary is specified for the function describing *burial* (see Section 9.2.2). By these adjustments, no parameter sets need to be disregarded, and thus the potential bias introduced by exclusion of samples has been avoided.

[16] The rate of burial is calculated as the difference between the input and loss of refractory organic matter from the upper peat layer. The parameters associated with this mass balance calculation include *NPP_ter*, *f_ refrac_ter*, *z_regoUp_ter*, *f_C_peat, dens_regoUp_ter and minRate_regoUp_ter* (Section 6.2.4 in Saetre et al. 2013a).

7 The biosphere transport and exposure model

This chapter provides a description of the biosphere transport and exposure model (BioTEx) which is the last link in a chain of models used to simulate radionuclide transport from a repository to the surface. The BioTEx model describes radionuclide transport and accumulation in the near-surface environment and in ecosystems; it also calculates potential doses to humans and dose rates to non-human biota (NHB).

This chapter summarises the structure of the ecosystem models that are part of the BioTEx model for the PSAR. The model compartments and the processes that transfer radionuclides are outlined for each ecosystem (Section 7.2). The model is in most parts the same as used earlier in SR-PSU; for details on approaches, assumptions and the mathematical representation the reader is referred to the original model report (Saetre et al. 2013a). Transport and uptake processes are described in Section 7.3. Calculations of exposure and the resulting doses to humans are then described in Section 7.4. Model updates introduced since SR-PSU are described in Section 7.5 and the effects of these updates are discussed in Section 7.6.

The model described in this chapter is used for the modelling in the calculation cases within the main scenario (i.e. the *base case*, the *warm climate calculation case*, and the *cold climate calculation case)*. Modelling aspects related to the implementation used in supporting calculation cases are described in Chapters 10 and 11. The calculations of dose rates to NHB follows the ERICA methodology, and the application of this methodology in the PSAR is described in Chapter 12.

7.1 Model approach and overview

Given the requirements of the safety assessment (Chapter 2), the biosphere model needs to handle relevant features, events and processes for transport and accumulation of radionuclides, and address important exposure pathways (Chapter 6) so that it is consistent with the descriptions of the site and its development (Chapters 3, 4 and 5). Moreover, transport, accumulation and decay of radionuclides (including in-growth of decay products) with different biogeochemical behaviour needs to be handled consistently. As SFR is located in a coastal area, and because the evaluation period covers one hundred thousand years, both aquatic and terrestrial ecosystems need to be represented by the model, and capabilities are needed to handle temporal development of the system.

The biosphere model used in SR-PSU, which was developed from the model used in SR-Site (Avila et al. 2010) has the above-mentioned capabilities. However, as a result of reviews of SR-Site and SR-PSU by SSM (e.g. SSM 2017, 2018, Walke et al. 2017), as well as SKB's own development and research programmes, the BioTEx model was somewhat modified in SE-SFL (SKB TR-19-05). Most of these updates are included the BioTEx model adopted for the PSAR.

The mathematical approach used in the BioTEx model is that of compartment modelling. This approach has been described in detail by Saetre et al. (2013a). It assumes that a system can be adequately represented by a limited number of compartments ('pools'), each of which is homogeneous and connected to other compartments. Discharge of radionuclides into the biosphere system is evaluated over thousands of years. The discharge area is considered at the scale of a coastal basin or a lake–mire complex (Chapter 5) and annual effective doses to adults are calculated for future inhabitants (Section 2.3.5). At these temporal and spatial scales, it is assumed that most biogeochemical interactions can be approximated by equilibrium or steady-state conditions. Thus, ecosystem states are represented by average conditions, and fluxes of water, solid matter and gas are typically described as functions of empirical parameters that capture the combined outcome of the underlying processes.

In the calculation cases (see Table 6-3), radionuclides released from the repository enter the surface system through deep groundwater discharge and then reach the soil, sediments, water and air. Two main types of ecosystems are simulated, namely aquatic ecosystems (including sea basins, lakes and streams) and terrestrial ecosystems (including mires and agricultural land). In addition, a garden plot is used to evaluate consequences of irrigation with water from a drilled well in the bedrock and

combustion of wood and peat. In the BioTEx model, each compartment represents a radionuclide inventory associated with a physical (or biological) component in the surface ecosystems (Figure 7-1). The dynamic change in the radionuclide content of each compartment is the result of ingrowth/decay, radionuclide flows, which are associated with mass flows of water, solids (including organic matter) or gas, together with diffusion and/or with the transformation between inorganic and organic forms.

The endpoints of the transport calculations are the concentrations of radionuclides in environmental surface media. The identification of potential areas reached by radionuclides (i.e. biosphere objects; Chapter 5) is a prerequisite for this modelling. Parameters, and their values, describing the properties of biosphere objects were derived from site investigations and modelling of the development of the Forsmark area (Chapters 4, 5 and 8). The final step in the biosphere modelling consists of calculating annual doses to humans and dose rates to NHB that are exposed to repository derived radionuclides in the environment. These calculations depend on the environmental concentrations and exposure pathways and habits identified as relevant for post-closure safety (Chapters 6 and 12). The BioTEx model is implemented in the Ecolego 6.5 compartment modelling software[17] (see also **Model tools report**).

7.2 Model compartments

The model compartments in the BioTEx model for the PSAR are identical to those of the earlier SR-PSU model. The compartment structure was designed based on the previously established understanding of (i) ecosystems (Chapter 3), (ii) landscape and landscape development (Chapter 4), as well as on (iii) previously identified biosphere components that have been found to be important for assessing post-closure safety for SKB's radioactive waste repositories (SKB TR-10-09, SKB TR-14-06, SKB TR-19-05). However, the two lowermost regolith layers have now been subdivided into five sub-compartments each (Section 7.5).

The compartments in the model are considered to capture radionuclide accumulation at an appropriate spatial scale given the underlying assumption of homogeneity with respect to physical, chemical and biological properties. Thus, as compared with earlier conceptual models for aquatic and terrestrial ecosystems, highly aggregated biosphere components (like regolith) are split into smaller parts. On the other hand, components that were considered to have small or insignificant radionuclide inventories are excluded from the transport part of the model (e.g. consumers). Compartments with a fast turnover of radionuclides (e.g. liquid phases), are, in many cases, combined with compartments having slower dynamics (e.g. solid phases), assuming that equilibrium would be approached within each time step of the simulation. The model compartments used for aquatic, mire and agricultural systems are described below (Sections 7.2.1 to 7.2.3) and summarised in Table 7-1, and the conceptual model (including radionuclide fluxes) is presented in Figure 7-1.

7.2.1 Aquatic ecosystems

As earlier in SR-PSU, two types of aquatic ecosystems are recognised, namely marine and limnic ecosystems. These two systems are regarded as structurally and functionally similar, and consequently a common set of physical compartments is identified for all aquatic ecosystems. The main considerations and assumptions underlying the modelling of aquatic ecosystems at Forsmark are summarised as follows.

All aquatic organism compartments identified in SKB (R-13-43) are considered to have fast dynamics, and the amounts of elements in consumers are considered small in relation to inventories in sediment and water. Consequently, filter feeders, herbivores, carnivores and decomposers are not included as dynamic model compartments. For a few elements the inventory in primary producers makes up a substantial fraction of that in water, e.g. Mn in the sea ecosystems (Aquilonius 2010). Primary production is also the main source of organic carbon (and C-14) in sediments. Thus, primary producers (PrimProd, cf Figure 7-1) are included as a separate model compartment.

[17] As the model has now been migrated to Ecolego 6, the enhanced functionality in this tool is utilised. For example, in the present version of the model, linear interpolation in transition periods is done with inbuilt interpolation routines, rather than by user-defined functions (as was done in SR-PSU, appendix G in Saetre et al. 2013a).

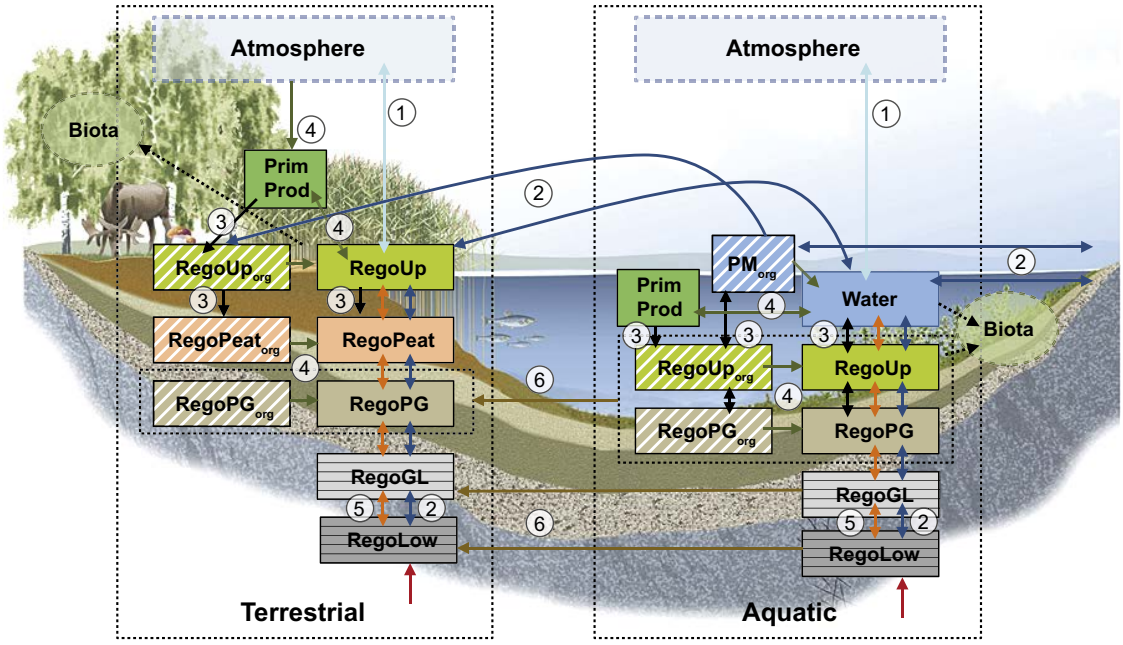

Figure 7-1. *Conceptual model corresponding to the BioTEx model used to simulate transport and accumulation in a discharge area with two natural ecosystems (delimited by thin dotted black lines). Each box in the two ecosystems corresponds to a radionuclide inventory associated with a physical or biological compartment. Note that now in the PSAR the two lowermost regolith layers are represented by five compartments each. Arrows represent flows of radionuclides between compartments and flows into and out of the system. Radionuclide flows are linked to mass flows of gas (1, light blue), water (2, dark blue) and solid matter (3, black), to transformation between inorganic and organic forms of radionuclides (4, green), to diffusion in soil pore water (5, orange), and to ingrowth of wetland vegetation (6). The red arrow indicates that the geosphere release enters the biosphere system via groundwater discharge to the till layer (compartments RegoLow). Dotted boxes (atmosphere and biota) are assumed to be in equilibrium with the corresponding environmental media, and the uptake of radionuclides into biota (dotted arrow) is not included in the mass balance of the BioTEx model. Figure from SKB (TR-19-05).*

To represent the radionuclide fluxes associated with sedimentation, radionuclide concentrations on suspended particulate matter needed to be estimated. Due to the temporal resolution of the model, it is considered reasonable to represent dissolved and adsorbed radionuclides within one compartment (Water), and by partitioning radionuclides assuming equilibrium. However, the radionuclide concentrations in refractory particulate organic matter are not necessarily in equilibrium with those in surface water. Therefore, a compartment representing radionuclides stored in refractory particulate organic matter in the water column is represented by a separate compartment (PM_{org}).

For the modelling of radiocarbon (C-14), a single compartment is deemed not to be sufficient to represent storage (and subsequent release) of radionuclides in aquatic sediments. Compartments representing radionuclides stored in organic matter are identified as essential in order to describe the accumulation in aquatic sediments. The storage of carbon in sediments is a function of organic matter input and mineralisation. Mineralisation rates are highly dependent on oxygen, and in oxygen-depleted environments even decomposable (labile) organic matter will accumulate. This implied a need for a vertical stratification of the aquatic sediments into oxygenated top sediments and oxygen-depleted deep sediments. It is assumed that radionuclides in pore water are in equilibrium with radionuclides adsorbed on solids, and consequently the inventory of inorganic radionuclides is described with one compartment per layer and a layer-specific sorption coefficient (K_d).

The oxygenated top sediments are represented by two compartments, one representing radionuclides adsorbed on solids/dissolved in pore water (RegoUp), and one representing radionuclides in organic matter ($RegoUp_{org}$). The sum of these two inventories reflects the total radionuclide contents in the biologically active aquatic sediment, wherein fauna can be exposed to ionising radiation.

Below the oxygenated layer, decomposition rates slow and organic matter builds up in aquatic sediments. These regolith layers correspond to marine or lacustrine gyttja, and the build-up of these sediments started after the last glaciation (i.e. they are post-glacial sediments). As with the oxygenated layer (see above), radionuclides stored in post-glacial sediments are represented by two compartments, i.e. one that represents radionuclides adsorbed on solids/dissolved in pore water (RegoPG) and one that represents radionuclides in organic matter ($RegoPG_{org}$).

The older sediments buried under post-glacial gyttja are depleted of organic matter and the amount of radionuclide activity stored in organic matter in these layers is considered quantitatively insignificant. Older deposits at the site consist primarily of two classes, glacial clay and till. The ontogeny and physical properties are different for these two geological layers, and thus minerogenic sediments are split into two different types of compartments, glacial clay (RegoGL) and till (RegoLow). Both these compartments themselves account for radionuclides adsorbed on solids and radionuclides dissolved in pore water. However, to better represent transport and accumulation in these compartment types they are further divided into five sub-compartments each in the mathematical model in the PSAR (Section 7.5.1).

The last physical biosphere component identified is the atmosphere. The BioTEx model allows a separation between near-surface and higher layers of the atmosphere (Saetre et al. 2013a). The dynamics in the atmosphere are fast (hours) compared with the dynamics in water (weeks/months) and regolith (years or more), and the transport times in the upper atmospheric layers are much faster than the transport times in the surface water. Thus, the atmosphere is treated as a dynamic equilibrium component in the model, and concentrations of volatile radionuclides are calculated using a steady-state solution (Saetre et al. 2013a, Section 8.2).

7.2.2 Mire ecosystem

As earlier in SR-PSU, two major types of terrestrial ecosystems are likely to be affected by radionuclides originating from SFR, namely mire ecosystems and agricultural ecosystems (Löfgren 2010). SKB has previously identified several biosphere components that should be considered in a post-closure safety assessment of a geological repository in the Forsmark area (SKB R-13-43). Considerations and assumptions related to the modelling of the mire ecosystem are summarised in the following, and those related to the agricultural system in Section 7.2.3.

Site and literature data indicate that inclusion or exclusion of organism compartments is not likely to affect simulated dynamics and concentrations of radionuclide inventories in regolith layers. Consequently, terrestrial herbivores (incl. humans and livestock), carnivores (incl. humans) and decomposers are not included as separate model compartments in the dynamic model. However, they are included in the exposure part of the model. For a few elements (e.g. non-metals like Br and Cl) the inventory in primary producers in wetlands is substantial (Löfgren 2010). Primary production is also the main source of organic carbon for peat formed in wetlands, and thus terrestrial primary producers (PrimProd) are included in the sub-model of the mire ecosystem.

With the modelling of radiocarbon (C-14) and other radionuclides incorporated into organic matter (e.g. Cl-36 and Ca-41) in mind, the need for separate compartments reflecting storage (and release) of radionuclides in organic matter was identified in SR-PSU. The accumulation of carbon in peat is a function of organic matter input and mineralisation. Mire peat is usually characterised by strong vertical gradients with respect to oxygen content, hydraulic conductivity and organic matter quality, and thus the oxygenated top layer and the oxygen-depleted deep layer of peat are represented by separate compartments. Radionuclides in pore water and radionuclides adsorbed on solids are assumed to be in equilibrium, and thus the two inventories are described with one compartment and an equilibrium sorption coefficient (K_d).

The oxygenated surface peat is modelled using two sub-compartments, one representing radionuclides adsorbed on solids/dissolved in pore water (RegoUp), and one representing radionuclides in organic matter ($RegoUp_{org}$). The sum of these two inventories reflects radionuclides in the biologically active peat, where roots take up elements and mire-dwelling organisms can be exposed to ionising radiation. Below the oxygenated layer, decomposition rates slow and organic matter accumulates in peat that may

grow to a thickness of several metres below the groundwater table, given sufficient time. Radionuclides in deep peat are also modelled using two sub-compartments, one for radionuclides adsorbed on solids/ dissolved in pore water (RegoPeat), and one for those in organic matter ($RegoPeat_{org}$).

Mire peat develops on top of layers that were deposited when the discharge area was covered by water (i.e. when the area was a sea basin or a lake). To also account for radionuclides that accumulated in earlier successional stages or those accumulated during transport through these layers, the need is recognised for representing radionuclides stored in organic matter of marine and lacustrine sediments ($RegoPG_{org}$) and radionuclides adsorbed on solids/dissolved in pore water of the same layer (RegoPG), and the underlying minerogenic layers of glacial clay (RegoGL) and till (RegoLow). New since SR-PSU is that the lower compartments RegoGL and RegoLow are further divided into five sub-compartments each in the mathematical model to better represent transport and accumulation.

As for aquatic ecosystems, the atmosphere in a mire ecosystem is treated as being in dynamic equilibrium, and the concentrations of volatile radionuclides in the canopy atmosphere (and layers above) are calculated using a steady-state solution (Saetre et al. 2013a, Section 8.1).

7.2.3 Agricultural system

Agricultural ecosystems are simulated in order to calculate the potential exposure of future human inhabitants. Discharge of deep groundwater is unlikely to cause long-term accumulation of radionuclides in existing agricultural ecosystems resulting from draining former mires or lakes, as organic soils have a limited sustainability due soil subsidence (Sohlenius et al. 2013c). Instead, three stylised agricultural land-use variants are used to calculate dose to future human inhabitants (cf Section 6.2). These are: draining and cultivating a mire (over a human lifetime), irrigating and fertilising a garden plot (over a human lifetime), and long-term fertilisation of a cultivated clay soil due to infield-outland agriculture (over 500 years). In the first variant, radionuclide accumulation in lake and mire regolith layers is included in the initial conditions for agricultural soil. In addition, radionuclides enter the cultivated soil through groundwater uptake. In the other two variants, radionuclides enter cultivated soil from above with irrigation water and/or fertilisers. In these settings, it is considered sufficient for dose calculations to represent the dynamics of radionuclides in the soil-plant system with two regolith compartments, representing radionuclides in the upper biologically active layers of cultivated soil (Figure 7-2).

Elemental pools in decomposers and consumers (herbivores and carnivores) are expected to be small in relation to the pools in the uppermost layers of cultivated soil. The turnover of soil animals and microbiota is typically very fast. Also, the majority of plant biomass is expected to have a relatively fast turnover due to the cultivation of annual crops (cereals, root crops and vegetables). For simplicity, organism components are therefore not included as separate compartments in the agricultural ecosystem sub-models, and consequently radionuclide concentrations in crop, and livestock and dairy products are calculated assuming they are in equilibrium with soil and fodder concentrations, respectively.

The oxygenated and unsaturated layer of cultivated soil is represented by two compartments, one representing radionuclides adsorbed on solids and dissolved in pore water (RegoUp), and one representing radionuclides in soil organic matter ($RegoUp_{org}$). The sum of these inventories reflects radionuclides in the biologically active layer of cultivated soil where roots take up elements.

As for aquatic and mire ecosystems, the atmosphere in agricultural ecosystem is treated as a dynamic equilibrium, and the concentrations of volatile radionuclides in the canopy atmosphere (and layers above) are calculated using a steady-state solution (Saetre et al. 2013a, Section 8.1).

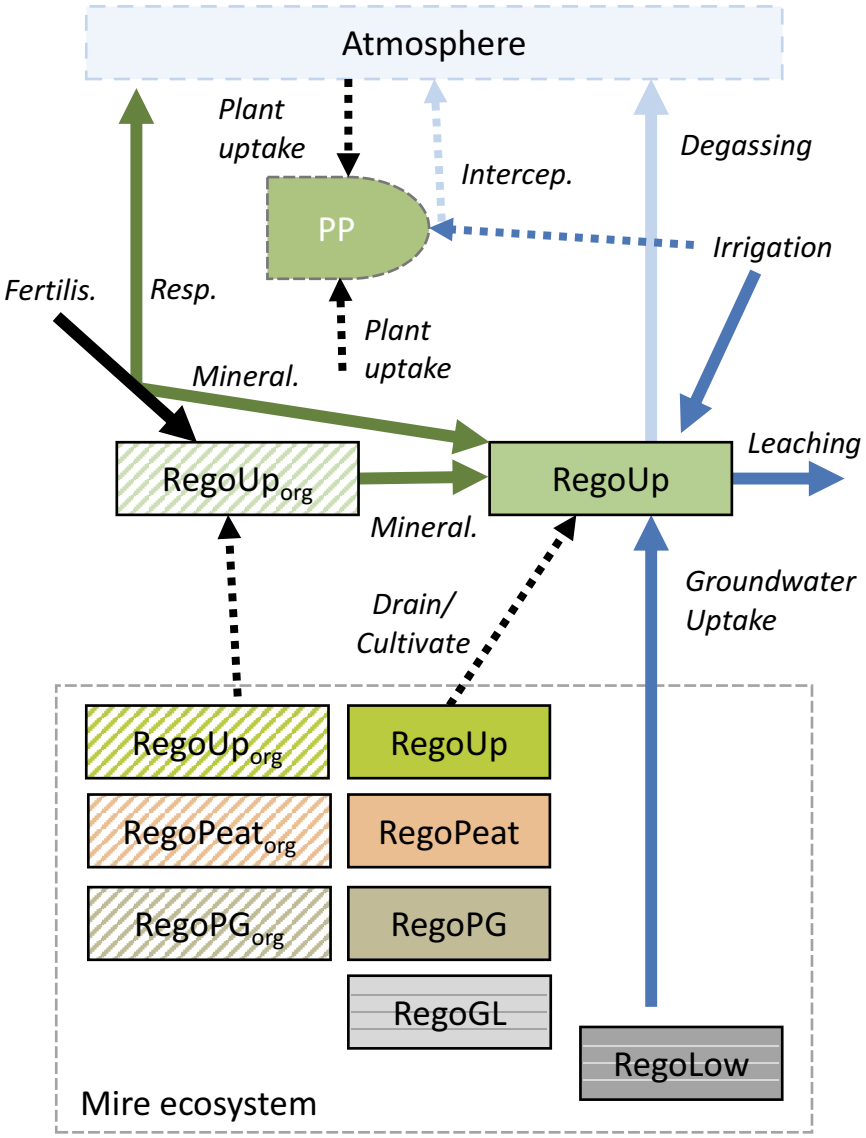

Figure 7-2. *A conceptual model of radionuclide transport in agricultural ecosystems. Each box corresponds to a radionuclide inventory associated with a physical compartment. Solid arrows represent radionuclide flows between compartments and flows into and out of the system. Radionuclide flows are linked to diffusion of gas (light blue), to mass flows of water (dark blue) and solid matter (black), and to mineralization (green). Four sources of radionuclides are represented: 1) irrigation, 2) fertilisation, 3) draining and cultivation of a lake–mire system and 4) groundwater uptake. The activity concentration in crop is calculated assuming that the plant is in equilibrium with radionuclides in soil and the canopy atmosphere (plant uptake), and that radionuclides in irrigation water are intercepted by the canopy. Note that each land-use variant uses a different set of source terms (see text and Saetre et al. 2013b).*

Table 7-1. Summary description of compartments representing radionuclide inventories in the BioTEx model (see also Figure 7-1).

Ecosystem/Name	Description
Aquatic	
Water	Radionuclides in open water of sea basins, lakes and streams, including radionuclides dissolved in water and adsorbed to particulate matter.
PM_{org}*	Radionuclides stored in refractory organic particulate matter suspended in the water column.
PrimProd	Radionuclides stored in aquatic primary producers, including radionuclides in pelagic, microbenthic and macrobenthic primary producers.
RegoUp	Radionuclides in the upper oxic and biologically active layer of aquatic sediments, including radionuclides in pore water and adsorbed on sediment particles.
$RegoUp_{org}$	Radionuclides incorporated into organic particulate matter in the upper oxic and biologically active layer of aquatic sediments.
RegoPG	Radionuclides in post-glacial aquatic sediments (clay gyttja) below the biologically active layer, including radionuclides in pore water and adsorbed on sediment particles.
$RegoPG_{org}$	Radionuclides incorporated into organic particulate matter in post-glacial aquatic sediments (clay gyttja) below the biologically active layer.
RegoGL	Radionuclides in glacial clay (typically overlaid by post-glacial deposits), including radionuclides in pore water and adsorbed on sediment particles. Note that this layer is vertically discretised and represented by five sub-compartments in the PSAR.
RegoLow	Radionuclides in till (typically overlaid by glacial clay), including radionuclides in pore water and adsorbed on sediment particles. Note that this layer is vertically discretised and represented by five sub-compartments in the PSAR.
Mire	
PrimProd	Radionuclides stored in mire vegetation biomass, including both above- and below-ground biomass of bryophytes and vascular plants.
RegoUp	Radionuclides in the upper oxic and biologically active layer of peat (acrotelm peat), including radionuclides in pore water and adsorbed on peat.
$RegoUp_{org}$	Radionuclides incorporated into organic matter in the upper aerobic and biologically active layer of peat (acrotelm peat).
RegoPeat	Radionuclides in deep, permanently anoxic peat (catotelm peat), including radionuclides in pore water and adsorbed on peat.
$RegoPeat_{org}$	Radionuclides incorporated into organic matter in the deep, permanently anoxic peat (catotelm peat).
RegoPG	Radionuclides in post-glacial sediments (clay gyttja) overlaid by peat, including radionuclides in pore water and adsorbed on sediment particles.
$RegoPG_{org}$	Radionuclides incorporated into particulate organic matter in post-glacial sediments (clay gyttja) overlaid by peat.
RegoGL	Radionuclides in glacial clay buried under peat and typically overlaid by post-glacial deposits. Inventory includes radionuclides in pore water and adsorbed on sediment particles. Note that this layer is vertically discretised and represented by five sub-compartments in the PSAR.
RegoLow	Radionuclides in till, buried under peat and typically overlaid by glacial clay. Inventory includes radionuclides in pore water and adsorbed on sediment particles. Note that this layer is vertically discretised and represented by five sub-compartments in the PSAR.
Agricultural	
RegoUp	Radionuclides in the upper (ploughed) unsaturated soil layer of cultivated land, including radionuclides in pore water and adsorbed on soil.
$RegoUp_{org}$	Radionuclides incorporated into organic matter in the upper aerobic and biologically active layer of the soil.

* PM_{org} compartment is also referred to as $Water_{org}$ in the earlier technical description (Saetre et al. 2013a).

7.3 Transport and uptake processes

7.3.1 Process identification

Earlier in SR-PSU, SKB identified processes important for transport and accumulation of radionuclides in natural and agricultural ecosystems by considering conceptual models for aquatic and terrestrial ecosystems. In all ecosystems, flows of radionuclides are associated with mass flows (of water, solid matter and gas) or with transformations between inorganic and organic forms of radionuclides (i.e. primary production and mineralisation of organic matter). The exchange of radionuclides between solid and liquid states was also highlighted as a key process for radionuclide transfer in all types of ecosystems (Saetre et al. 2013a).

In the next step, it was assessed which of these processes may be of quantitative importance for the flow of radionuclides between the identified model compartments, and the identified processes were checked against the processes in the SKB FEP list (SKB R-13-43, Chapter 6). The processes identified in SR-PSU are still considered valid. Below is a brief description of the processes that are represented by a flow of radionuclides in the transport model (see also Table 7-2 for an overview)[18].

Bioturbation

Bioturbation refers to translocation of radionuclides by mixing of sediment and soil particles in aquatic and terrestrial regolith layers. Mixing of aquatic sediments by, for example, organisms living in or on the sediments leads to improved oxygenation. When the depth of the upper sediment layer is reduced during episodes of resuspension, bioturbation causes the oxygen front to penetrate the underlying sediments, resulting in an apparent translocation of radionuclides from anoxic regolith layers to the upper, biologically active, sediment layer. A further example is that the combined effect of ploughing and soil fauna activity (e.g. earthworm burrowing) mixes cultivated soil. When drained mire and lacustrine sediments are cultivated, radionuclides from deeper regolith layers are redistributed and mixed with radionuclides in the upper soil horizon.

Plant uptake

Plant uptake is fixation of inorganic radiocarbon and other radionuclides into plant biomass, as a result of primary production. In aquatic ecosystems, plants take up dissolved radionuclides from the surrounding water. In terrestrial (mire and agricultural) ecosystems, plants take up radionuclides from the upper soil layers through root uptake, and from the canopy atmosphere through atmospheric fixation (C-14 only)[19].

Leaf retention

Leaf retention refers to the temporary retention of radionuclides in intercepted irrigation water on the surface of crop leaves. Losses due to rain and wind are accounted for, but losses from external parts during food processing are cautiously neglected. The resulting activity concentration is added to the internal activity concentration of the edible parts of crops to calculate the dose from ingestion.

Litter respiration/release

When organic matter is metabolised by decomposers and grazers, labile organic carbon is transformed to inorganic carbon. Litter respiration/release refers to the release of radionuclides from fast (within a year) decomposition of aquatic and wetland net primary production. Through this process radionuclides stored in plant biomass are released to the water column and to the upper peat layer in aquatic and mire ecosystems, respectively. The inventory in plants is not modelled dynamically in agricultural ecosystems (Section 7.2.3), but litter respiration/release affects the form of radionuclides originating from organic fertilizers.

[18] A comprehensive audit of identified processes in Chapter 6 with respect to the representation in the BioTEx model is presented in Table E-1 in Saetre et al. 2013a.

[19] Rooted plants growing at the margins of aquatic ecosystems are considered to be part of the mire ecosystem.

Litter production

Most of the biomass produced annually is metabolised by grazers and decomposers (see litter respiration, above). However, a part of the biomass production is made up of refractory organic matter. This decomposes much more slowly, and consequently a fraction of the biomass production will contribute to the build-up of organic matter in the upper regolith layer. Litter production thus represents the transfer of radionuclides stored in plant biomass to the organic component of the upper regolith layers in aquatic and mire ecosystems, respectively.

Regolith mineralisation

When refractory organic matter is metabolised by decomposers, organic carbon is transformed to inorganic carbon. Regolith mineralisation refers to the release of radionuclides from slow decomposition of organic matter in soil and sediments. Through this process, radionuclides stored in organic regolith layers are released to the pore water of the corresponding regolith layer in aquatic, mire and agricultural ecosystems, respectively.

Vegetation ingrowth

Wetland vegetation will colonise shores and bottoms of sea basins and lakes. The establishment of mosses, emergent and floating-leaved vegetation is associated with soft bottoms, where organic matter from refractory litter accumulates, ultimately forming a peat layer that will cover the aquatic sediments. The process, vegetation ingrowth[20], thus represents the translocation of radionuclides in aquatic regolith layers to the corresponding mire regolith layer, caused by peatland succession.

Horizontal advection

This process represents advective transport of radionuclides by lateral bulk movement of water. In the submerged period, horizontal transport of radionuclides by advection occurs through water exchange between adjacent sea basins. In the land period, it primarily occurs through surface and groundwater flow.

Vertical advection

This process represents transport of radionuclides by vertical bulk movement of water and is the quantitatively most important mechanism for vertical transport of radionuclides between pore water in adjacent regolith layers, and between aquatic sediments and the above water column.

Groundwater uptake

During dry periods of the year, capillary rise can cause an upward flow of groundwater to unsaturated soil layers. In areas receiving deep groundwater discharge, water uptake thus has the potential to transport water that contains radionuclides from saturated soil layers to the overlying cultivated and biologically active layer, where it can be taken up by fodder and food crops.

Vertical diffusion

Diffusion refers to the transport of radionuclides due to Brownian movement of molecules in solution and/or gas. The rate of diffusion is strongly dependent on distance; diffusion is only considered to be a quantitatively important at scales of less than one metre. Consequently, this process is considered relevant for vertical transport of radionuclides between adjacent regolith layers, and between the sediment surface and water. Diffusion of radionuclides in gas is included in the process degassing, see below.

[20] Vegetation ingrowth is also referred to as rate of infill in older SKB literature (e.g. Brydsten and Strömgren 2010).

Solid liquid phase partition

In regolith layers, and in the water column, there is an exchange of elements (including radionuclides) between the solid state (the soil/sediment matrix and suspended particulate matter), and the liquid state (pore water or the water column). The exchange of radionuclides between the solid and liquid state is considered to be fast (occurring in days) as compared with the model resolution (years), and thus this process is described by an equilibrium sorption coefficient (K_d), rather than by dynamic fluxes (see Saetre et al. 2013a and Tröjbom et al. 2013).

Sedimentation

Particles suspended in the water column will be pulled downwards by gravity, and ultimately settle on the top of the uppermost sediment layer in aquatic ecosystems. Thus, the process sedimentation, refers to the flux of radionuclides associated with the surface structure of suspended particulate matter, or stored in suspended particulate organic matter, to the corresponding inventory in the upper aquatic sediments.

Burial

If the rate of sedimentation of particulate matter is larger than the rate of resuspension, or if the rate of production of litter is larger than the rate of mineralisation, there is a net accumulation of sediments, and the total thickness of the regolith layer will grow. As the depth of the upper biologically active zone is limited by oxygen supply from above, the deeper part of this zone will become anoxic because of burial. Radionuclides associated with buried sediments will consequently be translocated from the upper sediments to the oxygen-depleted sediment layers below.

Degassing

There will be an exchange of gas between the open-water and soil (soil pore water) surfaces and the overlying atmosphere. Degassing refers to the radionuclide flux caused by this exchange of dissolved gas from the water column (for aquatic ecosystems), or from the soil pore water (for terrestrial ecosystems), to the atmosphere. For saturated soils, degassing is limited by the phase transition, whereas for well-drained agricultural ecosystems it is limited by gas diffusion through air-filled soil pores.

Gas uptake

Gas uptake refers to the radionuclide flux caused by the gross exchange of gas from the atmosphere (source) to gas dissolved in the water column, or in the soil pore water of surface peat, for aquatic and mire ecosystems, respectively. This is the opposite flux to degassing (above).

Drainage/cultivation

Draining lakes and wetlands will lower the groundwater table, and organic regolith layers above the water table will subside due to compaction and decomposition. In the model, the process ‘drainage/cultivation’ refers to the corresponding transfer of radionuclides from wetland regolith layers to the unsaturated layer of cultivated soil in an agricultural ecosystem. This transfer of radionuclides controls initial radionuclide inventories in the cultivated soil, but it does not affect radionuclide inventories in natural ecosystems.

Fertilisation

The key principle behind the agrarian infield-outland system is to fertilise arable land with nutrients from meadows and pastures, using animal manure as organic fertiliser (Section 6.2.1). The process fertilisation thus represents the input of radionuclides originally stored in vegetation to cultivated soil. In the infield-outland land-use variant, the radionuclides are originally stored in wetland vegetation. This is also true for fertilisation with ash from combustion of wood in the garden-plot variant. In addition, the garden plot also considers peat ash (similarly to wood ash) and marine macroalgae (drawn from the primary producer compartments in the sea during the marine stage) as relevant sources for fertilisation.

Irrigation

Radionuclides in water can be transferred to soil and vegetation through irrigation of arable land. Under the current climatic conditions, only irrigation of soil for growing potatoes and vegetables in the open is plausible in the Forsmark area. Thus, irrigation refers to the input of radionuclides from irrigation water to cultivated soil on the scale of a household garden-plot. In a warmer climate, irrigation is also considered as an option to cover crop water deficit for large-scale cultivation of cereal, fodder and tubers.

Radionuclide decay/ingrowth

Radioactive decay is the process by which a nucleus of an unstable atom loses energy by emitting particles (e.g. alpha or beta) or gamma rays of ionising radiation. Radioactive decay is treated as a removal mechanism in all model compartments. For radioactive decay that results in radioactive decay products, a production term is included in all model compartments representing the corresponding ingrowth of the decay products. The contribution of the ingrowth of short-lived decay products is accounted for by assuming secular equilibrium.

Table 7-2. Overview of radionuclide flows (processes) included in the BioTEx model (see Figure 7-1). The processes have been categorised with respect to the underlying mechanism, namely mass-flow of solids (MS), water (MW) or gas (MG), diffusion in water (DW) or in gas (DG), or incorporation into or release from organic matter due to photosynthesis (PP) or mineralisation (Min). "Y" indicates that the process is included as a dynamic flow between compartments in the aquatic, mire or agricultural sub-model. * indicates that only the steady-state outcome of the process is taken into account. Superscripts indicate that flows can occur between ecosystems (BTW), that the initial inventory in agricultural soil is conditioned on environmental concentrations in natural ecosystems (INIT). Superscripts also specify the system(s) of cultivation; drained mire (DM), infield-outland agriculture (IO) or a garden plot (GP). ** Indicates that the process is restricted to warm climate for DM and IO.

Process	Related FEP in Chapter 6	Type	Radionuclide flux		
			Aqua	Mire	Agri
Biological					
Bioturbation	Bioturbation	MS	Y		Y^{DM}
Plant (root) uptake	Uptake, Primary production	PP	Y	Y	*
Leaf retention/translocation	Uptake, Primary production	PP			Y^{**}
Litter respiration/release	Primary production, Decomposition	Min	Y	Y	Y^{IO}
Litter production	Excretion, Particle release/trapping	PP	Y	Y	
Regolith Mineralisation	Decomposition	Min	Y	Y	Y
Vegetation ingrowth^{BTW}	Primary production, Covering, Terrestrialisation	MS	Y	Y	
Water bound					
Advective horizontal^{BTW}	Convection	MW	Y	Y	
Advective vertical	Convection	MW	Y	Y	Y
Diffusion (vertical)	Convection	DW	Y	Y	
Water uptake	Convection	MW			Y^{DM}
Solid liquid phase dissociation	Reactions, Sorption/desorption		*	*	*
Sediment dynamics					
Sedimentation	Deposition	MS	Y		
Resuspension	Resuspension	MS	Y		
Burial	Deposition, Resuspension, Decomposition	MS	Y	Y	
Gas transport/transition					
Degassing	Phase transition, Convection	MG/DG	Y	Y	Y
Gas uptake	Phase transition	MG	Y	Y	
Human behaviour					
Drainage/cultivation$^{BTW, INIT}$	Stage of succession	MS			Y^{DM}
Fertilisation^{BTW}	Anthropogenic release	MS			$Y^{GP,IO}$
Irrigation	Anthropogenic release	MW			Y^{**}
Radiological					
Radionuclide decay/ingrowth	Decay		Y	Y	Y

7.3.2 Hydrology and advective transport

Detailed hydrological flow modelling contributes to the modelling of transport and accumulation of radionuclides in the biosphere in several ways. The underpinning flow modelling comprises several components; the exchange of water between individual sea basins and the coastal zones (Chapter 5, and Werner et al. 2013), the identification of discharge areas for groundwater potentially carrying radionuclides from the repository (Chapters 5, 10 and 11), the network of present and future streams (Werner et al. 2013), and the modelling of ground- and surface-water flows at the level of individual biosphere objects (Chapters 5 and 9, and Werner et al. 2013). Here in the PSAR, the biosphere objects and flow modelling components developed earlier in SR-PSU are utilized.

7.4 Calculating future exposure of humans

The doses to humans resulting from a potential release of radionuclides from SFR are evaluated over 100 000 years. The evaluation is based on estimated activity concentrations of radionuclides in the environment (air, soil and water; see previous sections), and in plants and animals that may provide food for human inhabitants. Assumptions on properties and habits of the humans who will live in or utilise the biosphere objects are required to estimate external exposure and intakes of food and water that contain radionuclides. Earlier in SR-PSU, assumptions on human habits were derived from historically sustainable land-uses which would result in relatively high exposures. The land-uses were formalised into a number of potentially exposed groups (PEGs). These groups are also used here in the PSAR, ensuring that the most exposed group is evaluated in the calculations (see Section 6.2.1 for more details).

Radionuclides in the environment may lead to both external and internal exposure. As earlier in SR-PSU, the total dose from exposure to radionuclides in the environment is again the sum of exposure through ingestion, inhalation and from external irradiation. The internal exposure from ingestion is the product of the activity concentration in the food (or water) and the amount of that food (or water) consumed. The resulting dose is calculated by multiplication with the appropriate dose factor for ingestion which accounts for retention in the human body and exposure from decay products.

Both radionuclides in gaseous form and radionuclides adsorbed to small particles (aerosols) contribute to the activity concentration in air. This means that the internal exposure from inhalation of contaminated air depends on the activity concentration in air, the inhalation rate, and the time spent in contact with the air. The dose from inhalation is then calculated by multiplying exposure with an appropriate dose coefficient.

External exposure through the environment is calculated from the activity concentrations in environmental media and the time spent in contact with or close to the media. In this safety assessment, only exposure from the soil is considered, since this is the only medium expected to be associated with both high activity concentrations and long exposure times.

The exposure pathways considered here in the PSAR are summarised in Chapter 6. A more detailed description, including the mathematical models, is given in Saetre et al. (2013a, b).

7.5 Changes to the BioTEx model since SR-PSU

The model used here in the PSAR is largely the same as earlier in SR-PSU, but several minor modifications have been made. Most of them were introduced already in the safety evaluation of SFL (SKB TR-19-05). Some updates have been made in response to the SSM reviews of SR-Site and SR-PSU (e.g. SSM 2017, 2018, Walke et al. 2017). Other modifications are introduced to increase the consistency in the calculations, for example with respect to parameter interdependencies and the handling of stable and radioactive carbon. Such modifications are part of SKB's continuously ongoing work to improve the transparency, efficiency and comprehensiveness of the BioTEx model. The model updates are described in detail in the following and summarised in Table 7-4.

7.5.1 State variables in aquatic and mire ecosystems

Vertical discretisation of regolith compartments

The lower regolith layers, RegoLow and RegoGL, were treated as two single compartments in SR-PSU. In SE-SFL these compartments were divided into five sub-compartments each in order to give a better representation of physical dispersion on the scale of a biosphere object. This update is retained in the PSAR, and the increased discretisation of these compartments corresponding to the till and glacial clay layers has the potential to affect both the time to reach equilibrium and the equilibrium concentration of radionuclides.

Peat thickness

In SR-PSU, the development of peat thickness was described by a deterministic time-dependent parameter (Grolander 2013). In SE-SFL the differential equation used to calculate this parameter was incorporated into the BioTEx model (Equation 6-2 in Saetre et al. 2013a). This update is retained in the PSAR, and the amount of soil carbon in the peat layer is calculated with a separate compartment, as a function of carbon input (burial) and loss (mineralisation). The input of refractory organic matter to the deeper peat layer, $Burial_C$ (kgC m^{-2} a^{-1}), is in turn, a function of plant production less the mineralisation in the upper peat layer:

$$Burial_C = NPP_{ter} f_{refrac,ter} - z_{regoUp,ter} dens_{regoUp,ter} f_{C,peat} minRate_{regoUp,ter}$$

where

NPP_{ter}	area-specific net primary production of the mire vegetation (kgC m^{-2} a^{-1}),
$f_{refrac,ter}$	fraction of refractory organic matter [kgC kgC^{-1}],
$z_{regoUp,ter}$	thickness of surface peat (m),
$dens_{regoUp,ter}$	density of surface peat layer (kgdw m^{-3}),
$f_{C,peat}$	fraction of carbon in surface peat (kgC kgdw^{-1}), and
$minRate_{regoUp,ter}$	mineralisation rate of refractory organic surface peat (kgC kgC^{-1} a^{-1}).

The burial rate is by definition positive. To avoid negative carbon inputs, a lower limit is used to truncate the output of the function in the PSAR (see Section 8.2.2).

While this update has no effect for deterministic calculations, it will ensure consistency in the behaviour of stable carbon (i.e. peat) and radionuclides[21] and ensure reasonable burial rates in probabilistic calculations.

7.5.2 Updates affecting agricultural ecosystems

Retention of radionuclides in plants not accounted for with respect to leaching

In SR-PSU, the effect of plant storage on radionuclide transport was accounted for by a scaling factor (f_{crop}). That is, the plant fraction that was not available for leaching. However, with the parameter values (i.e. *CR* values) that are used for crops, the fraction of radionuclides immobilised in biomass is small (< 1 %), and the effect on radionuclide retention in the plant–soil system is marginal. Thus, the calculations of activity concentrations in the regolith in agricultural systems are simplified in the PSAR by not accounting for the fraction retained in plants.

Start of cultivation in drained mire

In SR-PSU, the threshold for drainage and cultivation of the mire in object 157_2 was set to the point in time when the lower-most point in the object is 1 m above the sea level (~4500 AD). In the PSAR, cultivation of a drained mire is instead evaluated from the point in time when the highest point in

[21] The importance of consistency in the calculations of stable and radioactive carbon in probabilistic calculations has been pointed out by SSM's external reviewer of SR-PSU (Walke et al. 2017).

the object is 1 m above sea level (~3200 AD). This is also the threshold for digging a well. This update increases the comprehensiveness of the assessment, as early drainage is now included in the assessment. However, dose consequences from early cultivation are limited by the small size of the wetland. Thus, when cultivation is first deemed feasible, approximately 1 ha land has emerged (with the capacity to support ~15 % of the potentially exposed group). Nevertheless, given the relative fast change in sea level postulated in the *base case* (Chapter 9), the emerged land area can fully support the DM farmers around 4000 AD.

Time for cultivation in infield-outland agriculture

In SR-PSU, a steady-state solution was used to evaluate the accumulation of radionuclides due to the use of animal manure as organic fertiliser. The radionuclides originate from wetland hay used as winter fodder for domestic animals. However, for strongly sorbing radionuclides with a long half-life (e.g. Cs-135), the time to reach steady-state is very long. Inorganic soils have the potential for sustainable cultivation for long periods of time. However, continuous hay-making will deplete wetlands of nutrients, and wetland hay-making is likely to be sustainable on a time-scale of decades (Kardell 2018). In the PSAR, it is cautiously assumed that a wetland may be used sustainably for hay-making for a period of 500 years.

In mathematical terms, the dynamic behaviour of the radionuclide inventory in agricultural soil due to fertilization (not taking into account chain decay) can be described by the following system of ordinary differential equations:

$$\frac{dRegoUp_{org,IO}}{dt} = Litter_{prod} - Decay_{regoUp,org} - Miner_{regoUp,org},$$

$$\frac{dRegoUp_{IO}^{14C}}{dt} = Miner_{regoUp,org}^{14C} - Decay_{regoUp}^{14C} - Leaching_{regoUp}^{14C} - Degassing_{regoUp}^{14C}$$

$$\frac{dRegoUp_{IO}^{RN}}{dt} = Litter_{release}^{RN} + Miner_{regoUp,org}^{RN} - Decay_{regoUp}^{RN} - Leaching_{regoUp}^{RN}$$

where

$RegoUp_{org,IO}$ is the activity of a radionuclide (including C-14) stored in soil organic matter (Bq),

$RegoUp_{IO}^{14C}$ is the total activity of inorganic C-14 in cultivated soil (Bq),

$RegoUp_{IO}^{RN}$ is the activity of radionuclide RN in inorganic form in cultivated soil (Bq),

$Litter_{prod}$ is the flow of radionuclides (including C-14) stored in refractory organic matter in fertilisers to soil organic matter in the cultivated soil (Bq a^{-1}),

$Litter_{release}^{RN}$ is the flow of radionuclide RN due to the release from organic fertilisers to the soil as consequence of fast decomposition of organic matter in animal manure (Bq a^{-1}),

$Decay_{regoUp,org}$ is the loss of radionuclides stored in soil organic matter due to radioactive decay (Bq a^{-1}),

$Decay_{regoUp}$ is the loss of radionuclides in inorganic form in cultivated soil due to radioactive decay (Bq a^{-1}),

$Miner_{regoUp,org}$ is the flow of radionuclides from an organic inventory to an inorganic inventory due to mineralization (Bq a^{-1}),

$Leaching_{regoUp}$ is the loss of radionuclides from an inorganic inventory due to percolation of groundwater (Bq a^{-1}), and

$Degassing_{regoUp}^{14C}$ is the loss of inorganic C-14 due to degassing (Bq a^{-1}).

Detailed descriptions of the activity flows used above is found in Saetre et al. (2013a).

Solving these systems of differential equations for the radionuclide inventories, and division by the soil mass, yields the following expressions for the activity concentration in cultivated soil at time *t*. In the PSAR these expressions are used to calculate the activity concentration in the soil after 500 years of haymaking (t = 500 year).

$$AC_{RegoUp,org,IO}(t) = Litter_{prod}\frac{1-e^{-(\lambda+minRate)t}}{\lambda+minRate}\Big/V\rho$$

$$AC^{14C}_{RegoUp,IO}(t)$$
$$= \frac{Litter^{14C}_{prod}minRate}{k^{14C}_{leach}+k^{14C}_{degass}-minRate}\left(\frac{1-e^{-(\lambda^{14C}+minRate)t}}{\lambda^{14C}+minRate}-\frac{1-e^{-(\lambda^{14C}+k^{14C}_{leach}+k^{14C}_{degass})t}}{\lambda^{14C}+k^{14C}_{leach}+k^{14C}_{degass}}\right)\Big/V\rho$$

$$AC^{RN}_{RegoUp,IO}(t) = Litter^{RN}_{release}\frac{1-e^{-(\lambda^{RN}+k^{RN}_{leach})t}}{\lambda^{RN}+k^{RN}_{leach}}\Big/V\rho$$
$$+\frac{Litter^{RN}_{prod}minRate}{k^{RN}_{leach}-minRate}\left(\frac{1-e^{-(\lambda^{RN}+minRate)t}}{\lambda^{RN}+minRate}-\frac{1-e^{-(\lambda^{RN}+k^{RN}_{leach})t}}{\lambda^{RN}+k^{RN}_{leach}}\right)\Big/V\rho$$

$$V\rho = z_{regoUp}area_{IO}N_{group}dens_{regoUp}$$

where

λ	is the radionuclide decay rate for all radionuclides (a^{-1}),
$minRate$	is the mineralisation rate (a^{-1}),
k_{leach}	is the leaching rate for all species (a^{-1}),
k^{14C}_{degass}	is the degassing rate for C-14 (a^{-1}),
z_{regoUp}	is the thickness of biologically active layer (m),
$area_{IO}$	is the surface area of the cultivated field supporting one individual in a group of infield-outland farmers (m^2),
N_{group}	is the number of individuals in the most exposed group of infield-outland farmers (-), and
$dens_{regoUp}$	is the soil density (kgdw m^{-3}).

Atmospheric concentrations

In SR-PSU, the atmosphere was treated as being in dynamic equilibrium in agricultural ecosystems, and the concentrations of volatile radionuclides in the canopy atmosphere (and layers above) were calculated using a steady-state solution (Saetre et al. 2013a, Section 8.1). In SE-SFL the efficiency of these calculations was increased for the garden plot, by first calculating the atmospheric concentration for a unit release rate, and then calculating the canopy atmosphere concentrations by multiplying the sum of source terms[22] with this scale factor.

This update is retained in the PSAR and applied to all atmospheric calculations for terrestrial ecosystems. In a probabilistic context, this means that the scaling factor is calculated once for every parameter realisation, and then applied to all points in time for this realisation. The calculations are done with the area of the fully emerged object. This is a cautious simplification in the period when the terrestrial area is expanding, as advective dilution in the atmosphere decreases with the size of the terrestrial area. Separate scaling factors are calculated for root crops and vegetables, as the crops differ with respect to canopy height and leaf morphology.

Radionuclide ingrowth

In SR-PSU, activity concentrations in drained agricultural and garden-plot soils were calculated using analytical solutions of the transport equations, and concentrations were averaged over an adult lifetime. This computationally efficient approach is retained in the PSAR. However, the transport equations cannot be solved for ingrowth of radioactive decay products, and therefore the contributions of longer-lived decay products were accounted for by scaling factors for the parent radionuclides, on the level of dose coefficients (Grolander 2013, Section 3.4.2).

[22] The source terms to the atmosphere include soil degassing, litter mineralisation and evaporation of irrigation water intercepted by leaves.

In the PSAR, a similar approach is taken, but to increase the transparency, the ingrowing activity is accounted for on the level of the decay products instead of their parent radionuclides. Moreover, the contribution of decay products is calculated in respect of soil concentrations instead of doses, which increases the consistency in probabilistic calculations (as variations in CR for the decay products are considered). The new scaling factors, or ingrowth matrices, are described in detail in Section 8.2.2 and their performance is evaluated in Section 7.6.3.

7.5.3 Processes

Plant uptake

In SR-PSU, plant root uptake of C-14 was regulated by the given concentration of stable carbon dissolved in the pore water (DIC). In SE-SFL, this parameter was replaced by model calculations. This update is retained in the PSAR. The calculations are based on soil respiration (a well-known and measured soil property) and the rate of degassing, and the calculations are based on the same principles as used for C-14. This model update makes transport calculations of stable carbon (C-12) and C-14 consistent and ensures that this consistency is maintained in probabilistic simulations. The function for calculating DIC in porewater was derived as a part of the complementary work of SR-PSU (Saetre and Ekström 2017b).

In SE-SFL, plant uptake of radionuclides intercepted on leaves, and subsequent translocation to edible parts, was included for agricultural land-use variants with irrigation. This update is retained in the PSAR, and the considered crops are potatoes (in the garden plot land-use variant), and cereals (agricultural land use variants in the cases for a warm climate). Interception of radionuclides is calculated from the activity concentration in the irrigation water, the leaf area index and the leaf storage capacity (Saetre et al. 2013a)[23]. The translocation of radionuclides is then represented by an empirical translocation factor that describes the fraction of an intercepted radionuclide that ends up in the edible part of the crop (IAEA 2010).

In SR-PSU, leaf retention was only accounted for with respect to vegetables grown in a garden plot. Now, large-scale irrigation is considered as an option to cover the water deficiency of crops in a warmer climate (see Irrigation below). Consequently, leaf retention is also accounted for with respect to fodder (consumed by cattle)[24].

In the PSAR, new site measurements of chlorine in plants and peat were used to update parameter values associated with plant uptake and release (Section 8.2.3). With the update of parameter values, an unrealistic accumulation of chlorine in peat is avoided. Thus, there is no need for the chlorine-specific limit on maximum uptake that was used in SR-PSU (Saetre et al. 2013a, Section 6.2.1). Thus, in the PSAR, this expression has been removed from the BioTEx model and plant uptake of radioactive chlorine in mire vegetation is modelled in the same way as for all other radionuclides except C-14.

Litter release

In SR-PSU, the fraction of radionuclides in litter that is released through mineralisation of labile organic matter (df_{decomp}) was specified as a parameter. In SE-SFL, this fraction was calculated within the model as a function of the refractory organic material in the litter and the inorganic fraction of the plant's element inventory[25]. This update is retained in the PSAR and is motivated as it preserves the dependence of release from the litter on the content of refractory litter in probabilistic simulations and makes sure that the parameter combinations are plausible[26].

[23] The amount of intercepted radionuclides correspond to the leaf retention at the time for irrigation ($t = 0$) in Equation 7-55 in Saetre et al. (2013a).

[24] Radionuclides intercepted (and retained) by cereal grain are considered to be included in the empirical factor that describes translocation.

[25] Function described in Section 9.6.3 in Grolander (2013).

[26] This issue was pointed out by Walke et al. (2017) with respect to the parametrisation of microalgae and plankton.

Groundwater uptake

In SR-PSU, it was cautiously assumed that the radionuclide concentration in the water from the saturated zone below the drained and cultivated soil was that of glacial clay (unless this layer was entirely incorporated into the cultivated layer). In SE-SFL, the concentration of the water in the saturated zone was taken to be that of the uppermost undisturbed regolith layer when the mire is drained (see Saetre et al. 2013a, Section 7.2.1). Mires formed in lake basins typically have a thick peat layer, and consequently the post-glacial gyttja (rather than the glacial clay deposited even deeper) tends to be the uppermost saturated layer that is undisturbed by ditching. This update is considered to be more realistic than the SR-PSU assumption and is therefore used in the PSAR. This model update does not have any effect on groundwater uptake in object 157_2, as this object has relatively thin regolith layers. However, it would affect the uptake in objects 157_1 and 116 if the geosphere release were to be discharged directly into these objects[27].

Degassing

In SR-PSU, the diffusivity of CO_2 in unsaturated soil (D_CO2_soil) was originally calculated for typical values of porosity and soil saturation for three soil types, and the uncertainties of these parameters were quantified by probabilistic simulations (Grolander 2013, Section 5.4.5). In complementary calculations, the diffusivity was incorporated as a function in the model (Saetre and Ekström 2017b). This update is retained in the PSAR, as it makes the interdependency of parameter values transparent in the model code and ensures that the dependency is maintained in probabilistic simulations.

Irrigation

In SR-PSU, irrigation was only considered relevant for the potentially exposed group associated with a garden plot. In SE-SFL, a warmer climate with an increased crop water demand was considered, and the effects of covering the water deficit with irrigation water was evaluated. According to the PSAR description of the warmer climate, the potential evapotranspiration will increase more than precipitation during the growing season, and summers may be relatively dry (Chapter 4). This means that the crop water demand is expected to increase (Section 8.3.1). Thus, in the PSAR, the possibility that an increased crop water demand is covered by irrigation also on a large scale (i.e. on the drained mire and for infield-outland agriculture) is evaluated in the *warm climate calculation case*.

7.5.4 Dose calculations

Dose from inhaling combustion gases and aerosols

In SR-PSU, aggregated dose coefficients were used to convert activity concentrations in combusted fuel directly to dose from inhalation of particles and gases outside a house (Saetre et al. 2013a, Section 9.5). To increase consistency with exposure calculations from inhalation of other sources (Saetre et al. 2013a, Section 9.2), these calculations were made in two steps in SE-SFL. This update is also included in the PSAR. In a first step, the concentration in air is calculated by multiplying the activity concentration in the combusted fuel with the fraction that ends up in fly ash and exhaust gas after the combustion (as described in Equation 7-66 in Saetre et al. 2013a), and then applying a conversion factor accounting for the fuel combustion rate and atmospheric dispersal (Stenberg and Rensfeldt 2015, Grolander and Jaeschke 2019). In the second step, the activity concentration in air is multiplied with the inhalation rate, the time for exposure and the dose coefficient for inhalation (as described in Equation 9.5 in Saetre et al. 2013a).

Dose from utilizing a drilled well in the well interaction area

In SR-PSU, the dose from a drilled well was evaluated both for a well placed within the biosphere object and for a well placed within the *well interaction area* (Section 5.5). The well interaction area is the area where deep groundwater is expected to have the highest concentrations of radionuclides; wells drilled there would be in the path of the contaminant plume originating from SFR (Section 5.5).

[27] A geosphere release reaching objects 157_1 and 116 is considered in a supporting calculation case with a subhorizontal fracture in the bedrock (Section 10.5).

The probability that a drilled well would be placed within the biosphere object, once the object was fully emerged and drilling of the well was feasible, was assumed to be 100 %. The probability that a well was drilled within the *well interaction area* was assumed to be a function of the current well density in the area multiplied by that part of the *well interaction area* that was at least 1 m above sea level. This probability therefore increased with time as the area emerged from the sea eventually reaching a maximum probability of 13 %.

Following the review of SR-PSU, it was decided to modify the method with which the dose is calculated to reflect the recommendations of SSM. In the PSAR, the probability that a well is drilled within the *well interaction area* is not accounted for, i.e. it is assumed to have a 100 % probability. Instead, the well is treated as an exposure pathway and the dose from the drilled well is assessed for a garden-plot household through ingestion of water and small-scale irrigation. However, the exposed group utilizing the drilled well is considered to be small, corresponding to a risk criterion of 10^{-5}. This is a full order of magnitude larger than the regular risk criterion of 10^{-6} considered for the PSAR (Section 2.3.5). In order to make results between exposed populations comparable, the resulting dose from a well drilled within the *well interaction area* is normalized by dividing by a factor of ten[28]. This is equivalent to the ratio (or log-difference) between the regular risk criterion (10^{-6}) and the risk criterion appropriate for a small group (10^{-5}).

The fraction of the radionuclides potentially reaching a well drilled in object 157_2 is expected to be significantly smaller than the fraction reaching a well in the *well interaction area* (Werner et al. 2013). This results in higher water concentrations for a well drilled in the *well interaction area* than that from a potential well drilled within object 157_2 (discussed in Appendix C). As exposure from the former is evaluated in the PSAR, doses from a potential well drilled within biosphere object 157_2 is considered to be of less relevance for the evaluation of safety, and it is not included in the PSAR.

7.5.5 Hydrology and advective transport

For the most part, the ground and surface water flow components in the BioTEx model used in the PSAR are the same as those implemented already in SR-PSU (Saetre et al. 2013a). However, the BioTEx modelling for the PSAR introduced a few modifications to these methods. They are briefly described below.

In the PSAR, the vertical discretisation for each the compartments representing the two deepest regolith layers (RegoLow and RegoGL) is increased from one to five vertical layers (sub-compartments), thus requiring a corresponding increase in the resolution with which the vertical groundwater flows are described. This was accomplished by first assuming that the magnitudes of the vertical groundwater flows changed linearly between the top and bottom boundaries of the regolith layer (cf Figure 5-9) and then using linear interpolation to calculate the flows at each of the vertical positions in the new discretization. This division of each compartment into five sub-compartments should result in a degree of numerical dispersion that is similar to that expected due to the physical macro dispersion. The more finely discretised model is also better suited to examine the depth-dependent change in transport dynamics within the bottom two regolith layers. This method for increasing the vertical discretization of the regolith compartments was first used in the modelling done during SE-SFL. A detailed description of the methodology used can be found in SKB (TR-19-05).

Minor adjustments are also made regarding how surface and subsurface water flows within biosphere object 157_2 are accounted for throughout the different phases of the object's development. For the PSAR, the runoff from object 157_2 is considered to reaches the downstream object 157_1 via a stream within the object (see Section 5.3.1 for details). In SR-PSU, it was assumed that no stream formed in object 157_2.[29]

[28] This scaling also maintains the gap between the calculated dose and the dose corresponding to the risk criterion for all groups, when the latter is represented by 14 μSv (as in most results figures).

[29] Potential consequences of this assumption are evaluated with the alternative assumption that the runoff from object 157_2 reaches object 157_1 through diffuse groundwater flows. This is evaluated in the *alternative landscape configuration calculation case*.

Steady-state vertical groundwater fluxes are used for the BioTEx modelling in the PSAR. To capture the transient nature of the fluxes caused by the development of the landscape, multiple snapshots in time are modelled throughout the different stages of an object's development. For the objects in the PSAR, these snapshots are associated with: the entire period for which an object is submerged; the terrestrial period following the full development of the mires within an object; and the transition period between these two states (Table 7-3). Results from the hydrological modelling (see Werner et al. 2013) are used to calculate the vertical fluxes for the submerged and fully terrestrial periods. For the transition periods, linear interpolation is used to estimate the vertical groundwater fluxes; the fluxes are assumed to vary proportional to time and the difference between the submerged and terrestrial fluxes (Appendix G in Saetre et al. 2013a). This approach was also used in SR-PSU with the exception of minor modifications for object 157_2.

For the PSAR, the transition between a sea ecosystem and a stream is added in order represent the projected landscape development of object 157_2. This transition is treated similarly to the transition from sea to lake with minor differences in the period over which the transition takes place; the start of the transition is the time when land within the object first emerges from the sea and the end is when all the land within the object has emerged from the sea.

Moreover, in the PSAR, the terrestrial groundwater fluxes used for the early terrestrial period (~5000 AD) are considered to be applicable for the entire terrestrial stage of the object and are applied to the mire as soon as the land within the object has emerged from the sea. This simplification was made since changes in vertical groundwater fluxes are projected to be relatively insignificant once the biosphere object is above water and the local watershed (Figure 5-1) has emerged from the sea.

In SE-SFL, a simplified water balance model for a mire was developed (Figure 7-3; see also Chapter 5 in Grolander and Jaeschke 2019). From this model, groundwater flows can be derived from net precipitation, discharge from the geosphere, and object and catchment characteristics. In SE-SFL, this system was implemented as a hydrological subroutine within a time-independent mire model (see SKB TR-19-05, Section 13.4). In the PSAR, this model is used for several supporting calculation cases (see Table 6-3) including a sensitivity analysis of the landscape and hydrological parameters for object 157_2 (Section 11.4). This simplified water balance model is also used to derive object parameters for periglacial conditions (Section 8.3.2).

Table 7-3. Transition periods during which vertical flux rates of groundwater are interpolated. During each transition period, the rates of a number of groundwater flows (column q_i) in the aquatic (aqu) and terrestrial (ter) part of the biosphere object change instantly or linearly between the values at the start (column Start) and end (column End) of the transition period. 1 = a biosphere object developing through a lake period. 2 = a biosphere object that does not go through a lake stage. The object-specific parameters describing the start and end of the transition periods are: 3 = threshold_start, 4 = threshold_isolation, and 5 = threshold_end (Grolander 2013).

		Time Period		Water flux q_i (m a^{-1})		
Ecosystem	Transition	Start	End	Start	End	q_i
Aquatic	Sea to Lake[1]	Lake isolation at low water[3]	Lake isolation[4]	$q_{i,sea}$	$q_{i,lake,iso}$	Bedrock_Low_aqu, Low_Bedrock_aqu, Low_GL_aqu, GL_Low_aqu, GL_PG_aqu, PG_GL_aqu, PG_Up_aqu, Up_PG_aqu, Up_Water_aqu, Water_Up_aqu
	Sea to Stream[2]	First land above water[3]	All land above water[4]	$q_{i,sea}$	$q_{i,lake,iso}$	
Mire	Sea to Mire[2]	First land above water[3]	All land above water[4]	$q_{i,ter,iso}$	$q_{i,ter,iso}$	Bedrock_Low_ter, Low_Bedrock_ter, Low_GL_ter, GL_Low_ter, GL_PG_ter, PG_GL_ter, PG_Up_ter, Up_PG_ter, Up_Water_ter, Water_Up_ter
	Mire expansion	Lake isolation/ All land above water[4]	Mire expansion completed[5]	$q_{i,ter,iso}$	$q_{i,ter,end}$	

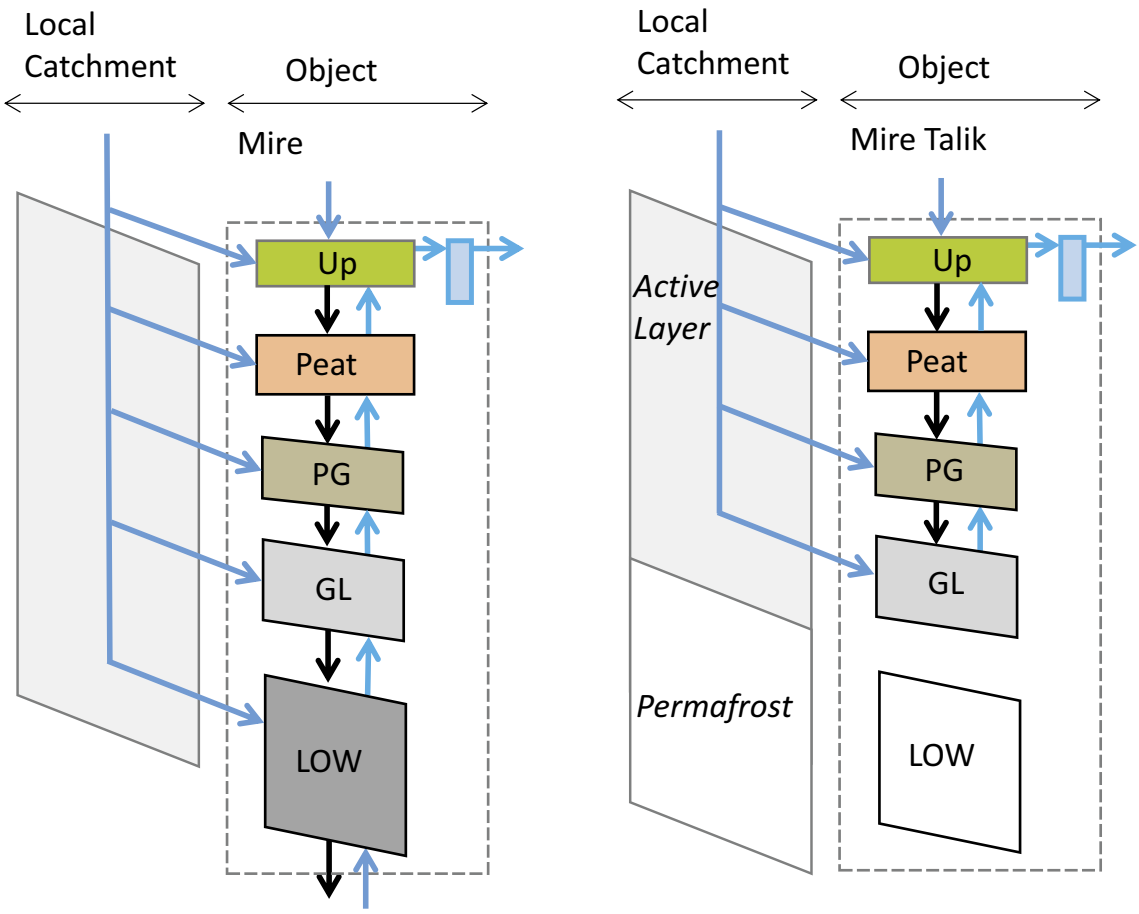

Figure 7-3. *Simplified water balance models for a mire object in temperate (left) and periglacial (right) conditions. The coloured boxes represent regolith layers or stream water. The light grey box represents regolith in the local catchment. The arrows represent flows of water. The dark blue arrows indicate water discharged into the object from the local catchment or from the bedrock. The black arrows indicate percolating water. Light blue arrows represent flows of water calculated from water balance. Note that the groundwater flow is blocked by permafrost below the active layer (white colour).*

Table 7-4. Overview of updates to the biosphere transport and exposure model (BioTEx). The first column indicates if the update affects state variables, processes or dose calculations, and which ecosystem models are affected by the modification.

Type/Sub-model	Update	Short description	Rationale
State variables			
Aqua, Mire	Vertical discretisation[1]	RegoLow and RegoGL, that in SR-PSU were represented by one compartment each, are divided into five sub-compartments each.	Numerical dispersion within these layers becomes more similar to physical dispersion.
Mire	Peat thickness[1]	Time-dependent parameter replaced with explicit modelling of the amount of organic carbon in the peat layer.	Increased consistency between stable carbon and C-14 calculations in probabilistic simulations.
Agriculture			
All	Plant retention	Adjustment for plant retention excluded by removing parameter *f_crop*.	Model simplification (plant retention not important for transport with present parameter values).
All	Ingrowth of radioactive decay products	Contribution of decay products is accounted for at the level of soil concentrations (instead of at the level of dose coefficients).	Improved transparency, and increased consistency in probabilistic calculations (differences in CR for decay products is now taken into account).
Drained-mire agriculture (DM)	Earlier start of cultivation[2]	Start of cultivation is allowed once the highest (rather than the lowest) point of a sloping object is 1 m above sea level.	Increased comprehensiveness, as early drainage of a small wetland areas is included in assessment.
Infield-outland agriculture (IO)	Time for continuous cultivation[2]	Previous steady-state assumption replaced with 500 years of continuous cultivation.	Reduced cautiousness with respect to long-term accumulation.
Garden-plot household (GP)	Atmospheric concentrations	Repeated calculations replaced with scaling factors.	Improved computational efficiency.
Processes			
Plant uptake	Uptake of C-14[1]	Parameter for DIC concentration (*Conc_DIC*) in terrestrial ecosystems replaced by a function.	Increased consistency between stable carbon and C-14 calculations, particularly in probabilistic simulations.
	Leaf uptake[1]	Plant uptake through translocation of intercepted irrigation water.	Completeness of transport pathways.
	Interception	Interception of radionuclides by fodder under irrigation included.	Follows from the PSAR description of *warm climate*.
	Root uptake of Cl[2]	Expression limiting maximum Cl uptake removed.	Model simplification (function redundant with updated parameters from new site data).
Litter release	Fraction released[1]	Parameter (*df_decomp* for Cl-36) replaced with a function.	Parameter inter-dependency explicitly expressed.
Groundwater uptake	Origin of water	Concentration of water taken from first undisturbed regolith layer below ditching depth[3].	Increased realism and consistency between ecosystem (Mire) and exposure sub-models (Drained-mire).
Degassing	Diffusion from unsaturated soil	Parameter for diffusivity (*D_CO2_soil*) replaced with a function.	Parameter inter-dependency explicitly expressed.
Irrigation	Large scale irrigation in warm climate	Irrigation is considered a potential source to cover water deficit of crops in summer.	This update ensures a more comprehensive evaluation of exposure pathways.
	Book-keeping of decay products for agricultural systems[1,2]	Contribution of decay products is accounted for at the level of soil concentrations (instead of at the level of dose coefficients).	Improved transparency, and increased consistency in probabilistic calculations (variation in CR for decay products is now taken into account).

Table 7-4. Continued.

Type/Sub-model	Update	Short description	Rationale
Dose calculations			
Inhalation [GP]	Dose from combustion	Aggregated dose coefficients replaced by explicit (two-step) calculations.	Improved consistency with dose calculations of inhalation from other sources (i.e. aerosols and $^{14}CO_2$).
Drilled well [GP]	Drilled well in bedrock[2]	Drilled well associated with future agricultural settlements replaced by a well in the well interaction area. Exposure to small group evaluated (GP). Fraction of the release described by a function.	Simpler handling. Potential for risk dilution reduced as the probability of drilling a well is set to 1.
Hydrology			
Aqua	Stream in object 157_2	Runoff from object 157_2 is considered to be discharged to a stream before reaching downstream areas.	Increased consistency within description of landscape. Allows evaluation of dose rates to non-human biota in limnic ecosystems.
Aqua, Mire	Vertical interpolation	The vertical flows between sub-compartments (in RegoLow and RegoGL) are calculated by linear interpolation from the flows across the regolith layer boundaries.	Increased vertical resolution. Can potentially capture flow changes within a regolith layer.
Aqua, Mire	Temporal interpolation[2]	Transition from sea to stream included. Terrestrial flows assigned at once when land has emerged.	Feature to support updated description of object 157_2. More realistic handling directly after shoreline passage.

[1] Indicates that the model updates address issues in SR-Site and SR-PSU raised by SSM, or their external experts.

[2] Indicates modifications incorporated after SE-SFL (SKB TR-14-06).

[3] This update has no effect on object 157_2.

7.6 Evaluation of model updates

7.6.1 Lessons learned from SE-SFL

Most model updates in the PSAR were introduced in SE-SFL, and their effects were readily evaluated there by model inter-comparisons (SKB TR-19-05, Chapter 9). The evaluation focused on natural systems since long-term accumulation in a mire (followed by drainage and cultivation) is expected to be the pathway leading to the highest exposure to future inhabitants. This is for example the case for the radionuclides that are most important for dose in SR-PSU (SKB TR-14-06, Section 10.5) and in SE-SFL (SKB TR-19-05, Section 11.2). Four relatively long-lived, but biogeochemically different radionuclides were selected to examine the model performance (C-14, Cl-36, Mo-93 and Ni-59). The model comparison was performed for two biosphere objects; a large lake-mire complex with a relatively low area-specific discharge from the bedrock, and a smaller mire object with a relatively high rate of area-specific discharge.

The increased vertical discretisation of the two deepest regolith layers clearly has the potential to affect environmental concentrations (and the time to reach equilibrium concentrations). This is because radionuclides are retarded in the more discretised model due to a reduced numerical dispersion, which also better corresponds to the expected actual physical dispersion. An increased vertical resolution can also capture a lower advective flow the lower sections of the regolith compartments. However, the effect of an increased discretisation strongly depends on the properties of the considered biosphere object and radionuclide, and the effects of the model update vary throughout the regolith profile. For example, the SE-SFL model comparison shows that in an area with a high groundwater discharge from the bedrock, the vertical discretisation will have little or no effect on steady-state groundwater concentration of the four examined radionuclides.

On the other hand, in areas with a limited discharge from the bedrock, the residence times of radionuclides like Mo-93 and Ni-59 may be similar to (or even exceed) the half-life for radioactive decay in the two lowermost regolith layers. Thus, a notable reduction of activity may occur, and consequently

significantly less activity will reach the layers above it. However, for mobile radionuclides (e.g. C-14) the effect of a more finely discretised model is less pronounced. That is, the finer discretisation can capture a lower advective flow (and a lower rate of dilution) in the lower sections of the regolith compartments. However, as the activity concentrations of mobile radionuclides are only marginally affected by radioactive decay due to the relatively short retention time in the system, concentration shifts in the lower regolith do not propagate to the upper layers.

7.6.2 Comparison with SR-PSU

To quantify how all the updates in the PSAR BioTEx model jointly affect model performance, the landscape dose conversion factors (LDF) are calculated for all radionuclides included in the assessment (Appendix C). The LDF reflects the time dependent radionuclide specific dose that result from a constant release to one or more biosphere objects in the landscape. Following the method in SR-PSU, the doses from a unit release rate for each of 51 radionuclides to biosphere object 157_2 are calculated with the *base case* model. The simulations are carried out deterministically with the updated parameter values for the PSAR fixed at the best estimates for a period of 18 000 years[30], and the contributions from decay products are not included in the dose calculations. The highest dose (for each radionuclide) over the assessment period is referred to as the maximum LDF. For simplicity, the comparison with the maximum LDFs from SR-PSU is restricted to the primary discharge area in the PSAR (i.e. biosphere object 157_2).

The LDF values calculated with the PSAR settings generally agree well with those calculated earlier in SR-PSU, and for 80 % of the radionuclides the difference in LDF values is within a factor of two (Figure C-1). The finer discretisation of the lower regolith layers increases the simulated transport time through these layers in the PSAR model. However, the effect of the discretisation is only significant for a few radionuclides. For example, Tc-99 and Zr-93 are retained more strongly in the lower regolith, which reduces the accumulation in the overlying regolith layers. As a consequence, the dominant exposure route shifts from the ingestion of food to the ingestion of water from a well drilled in the bedrock, and the resulting LDF is more than an order of magnitude lower than that in SR-PSU. Several other radionuclides are also affected by the discretisation, but for these radionuclides the effect is modest (Cs-135 and Sn-126) or small (Ni-59, Pd-107 and Nb-94).

For radionuclides with a physical half-life shorter than 1 000 years, the dominating exposure route is the ingestion of water, typically from the drilled well which is assessed in the garden-plot household exposure group. In the PSAR, the dose from short-lived radionuclides is typically a factor of two larger than in SR-PSU. This is due to the combined effect of a changed handling of the drilled well and the updates in the representation of small-scale irrigation (see Appendix C for a detailed discussion).

The LDFs of three other radionuclides differ between the PSAR and SR-PSU for partly other reasons than the increased discretisation or the handling of the drilled well. The LDF for C-14 is almost twice as large in the PSAR as in SR-PSU, whereas the LDFs for Cl-36 and H-3 are halved. For C-14, the increase is a combination of higher activity concentrations in the groundwater associated with the finer regolith-layer discretization and a higher rate of groundwater uptake during the vegetation season. For Cl-36, two plant-related parameters (concentration ratio and the fraction of plant Cl in inorganic form) are updated based on recent field studies in Forsmark (Section 8.2.3). These updated parameters that result in a lower accumulation of Cl-36 in peat are considered to give a better representation of Cl cycling in mire ecosystems. The LDF for H-3 is dominated by the drinking water from a dug well at the time when the highest point of biosphere object 157_2 has emerged 1 m above the sea. Earlier in SR-PSU, the area-specific groundwater flows in the object were assumed to be similar to those under sea-covered conditions as part of the object is still covered by the sea at this time. In the PSAR, the more reasonable assumption of high groundwater flow characteristic of the terrestrial conditions is applied also in an early, partially terrestrial stage, and this causes a reduction of the concentrations in the dug well.

[30] In addition, maximum LDFs from probabilistic simulations are calculated and compared with the results from the deterministic and probabilistic results within the PSAR (Section C2.2).

7.6.3 Handling of decay products in agricultural ecosystems

In the PSAR, the method to handle the contributions of longer-lived decay products is updated. Similarly to SR-PSU, the contribution from decay products is calculated analytically disregarding all other loss and transformation processes. However, in the PSAR the contribution of decay products is accounted for at the level of soil concentrations, in contrast to accounting for them as late as in the dose coefficient level in SR-PSU calculations. This new approach is applied separately to drained-mire farmers (DM), garden-plot households (GP) and infield-outland farmers (IO), as the source of the activity, and the considered period for in-growth differs between the groups (see Section 8.2.2 for details). For example, for each unit of activity concentration of Mo-93 in agricultural soil, ingrowth results in 52 % activity concentration of Nb-93m in DM soil. The corresponding numbers for GP and IO are 40 and 84 %, reflecting 50 and 500 years of continuous input of Mo-93, respectively (Table 8-2).

The performance of this new analytic method used to describe the activity concentration in agricultural ecosystems was evaluated by a model comparison. In the comparison, the results from the *base case* (Chapter 9) are contrasted with results from other numerical simulations. In this, simulations for the three agricultural ecosystems are carried out with initial conditions (DM) and/or activity concentrations of source terms (DM, GP and IO) taken from the time point for maximum soil concentrations for each radionuclide. There are several combinations of source terms for the GP variants. However, for this comparison the variant with irrigation only (from a drilled well) is selected, as the effects of organic fertilization (with macroalgae) is covered in the IO system, and the fertilization with radionuclides in inorganic form is mathematically equivalent to irrigation of soil.

For all radionuclides that are not generated by radioactive decay in the biosphere system (including C-14, Mo-93, Ca-41 and Ni-59) the analytic solution and the numerical simulations resulted in identical average activity concentrations for all agricultural systems. The approximation of the ingrowth turned out to be very good for all three systems at the time of maximum concentration, with an error within 2 % and a typical deviation of less 0.1 % (Table 7-5). The main reason why the approximation works so well is that the leaching rate associated with the modest runoff (0.15–0.2 m a^{-1}) is slow for most elements compared with the period of radionuclide ingrowth (50 or 500 years). This means that the radioactive decay and ingrowth are the rate-determining processes for the activity of long-lived decay products in the modelled systems.

It is concluded that the analytic approach describes the behaviour of ancestral radionuclides in a correct manner, and that the use of scaling factors yields a good approximation of the in-growth of longer-lived radionuclides. The approach reduces the simulation time by more than a factor of 10 compared with running numeric simulations, which is the rationale for its use. Given the updates in the PSAR, the ingrowth of longer-lived decay products can now be followed at the level of activity concentrations in the soil, and the doses resulting from ingrowth are consistent with the imposed variation of concentration ratios in probabilistic simulations.

Table 7-5. Error (δ) of average activity concentration in agricultural soil for longer-lived decay products as calculated with the analytic solutions combined with scaling factors (see text for details). The comparison is done for each longer-lived decay product and agricultural system at the time point for the maximum concentration (indicated in the column 'time'). For these time points the exact contribution of decay products is calculated by explicit numeric simulations. In the table, decay products with an absolute error larger than 0.1 % are displayed in bold. Decay products that deviated less than 0.1 % are shown in italic, however, as all members of decay chains Am-242m→*Pu-242* and Cm-244→*Pu-240*→*U-236* deviated less than 0.1 % they are excluded from the table for clarity.

		Drained-mire (DM)		Infield-outland (IO)		Garden-plot (GP)	
		δ (%)	time (AD)	δ (%)	time (AD)	δ (%)	time (AD)
Mo-93→, Zr-93→	**Nb-93m**	−0.1	7100	−1.5	8800	−0.8	3900
Am-242m→*Pu-238*→, U-238→	**U-234** ↓	0.0	20 000	0.1	18 000	0.0	10 200
	Th-230↓	0.0	102 000	−0.2	26 500	0.0	102 000
	Ra-226↓	0.0	102 000	0.0	102 000	0.0	102 000
	Pb-210↓	0.2	102 000	0.0	102 000	0.0	102 000
	Po-210	0.2	102 000	0.0	102 000	0.0	102 000
Am-243→*Pu-239*→*U-235*→	**Pa-231**↓	0.0	37 000	−0.2	19 000	0.4	94 500
	Ac-227	0.1	37 500	−0.1	19 200	2.0	96 000
Cm-245→	**Pu-241** ↓	0.1	44 500	0.0	49 500	0.0	12 000
Am-241→*Np-237*→*U-233* →	**Th-229**	0.0	102 000	−0.2	102 000	0.0	102 000

8 Data used in the biosphere assessment

In this chapter, all data used for calculating doses to humans and dose rates to non-human biota (NHB) are presented. The doses and dose rates are calculated using the BioTEx model presented in Chapter 7, with further details on the approach to calculate dose rates to NHB presented in Appendix D. The parameters are largely based on site investigations performed by SKB. These investigations have resulted a detailed description of the Forsmark site, its development (summarised in Chapters 3 to 5) and the NHB organisms (summarised in Section 6.3.1). The site description is an essential source of data in the PSAR, and since only a few updates of the site description have occurred since SR-PSU, most of the parameters related to the BioTEx model are directly taken from the quality assured SR-PSU datasets (Grolander 2013, Tröjbom et al. 2013). This set also includes parameters that do not strictly depend on the location of the repository (e.g. generic parameters and characteristics of potentially exposed groups). In the PSAR, the generic parameters for individual radionuclides (i.e. radionuclide half-lives, branching ratios and dose coefficients for human exposure) are presented in the **Radionuclide transport report**, Chapter 3.

Due to updates of the BioTEx model (Chapter 7), several new parameters are introduced in the PSAR. Where applicable, values for these parameters are taken from SE-SFL (Grolander and Jaeschke 2019). However, as SE-SFL was primarily based on deterministic calculations, probability density functions (PDFs) are derived for these parameters in the PSAR (see below). Availability of new site data (e.g. with respect to chloride) and revision of the calculations in SR-PSU also motivated updates of a limited number of parameter values. Finally, following the parameter nomenclature in SE-SFL, there are also a few updates related to the naming of parameters in the PSAR.

Most of the parameter values selected for the present-day climate conditions are considered to be applicable also for the warmer and colder climate conditions. However, some parameters and parameter values describing altered climate conditions are updated in the PSAR. For a comprehensive description of these updates, in the context of the postulated future climate evolution, see Sections 10.2 and 10.3.

For the NHB, all concentration ratio (CR) parameters are revised in the PSAR, as significant updates have been made to the literature database (Wildlife Transfer Database; WTD[31]). These data are used for parametrization when no site data is available, and therefore the update of the literature database affects a large number of parameter values. The new values are derived using the same methods as in SR-PSU (Tröjbom et al. 2013) and all values together with magnitude of change since SR-PSU are presented in Appendix E. As the ERICA methodology also has been updated since SR-PSU, new dose conversion coefficients (DCCs) and occupancy factors (OCC) for NHB are also derived in the PSAR (see Appendices D and E).

This chapter first describes the general principles of how the data have been selected for the BioTEx model used in the PSAR (Section 8.1). Next, detailed descriptions of the considerations and calculations underlying the new or updated BioTEx parameters are given in Section 8.2 and Section 8.3. In Section 8.4, data selection and changes in parameter values for NHB parameters are addressed. Finally, Section 8.5 briefly describes the quality assurance (QA) process that is applied in the PSAR to assure that data are complete, correct and traceable. All updates to parameters in the *base case* since SR-PSU are listed in Table 8-1 and updates to the *warm* and *cold climate calculation cases* can be found in Table 8-5.

[31] https://www.wildlifetransferdatabase.org/

8.1 Methods for selecting parameter values, analogues and probability density functions

As in previous safety assessments, SKB aims to make the description of transport and accumulation of radionuclides in natural ecosystems as comprehensive as possible. The mathematical approach used in the assessment assumes that a system can be adequately represented by a limited number of compartments, each of which is homogeneous and connected to other compartments (Chapter 7). Discharge of radionuclides into the biosphere system is evaluated over thousands of years, and the annual dose from exposure is calculated over an adult lifetime (Section 2.3.5) at the scale of a biosphere object (Chapter 5). At these spatiotemporal scales, it is assumed that most biogeochemical interactions can be approximated by equilibrium or steady-state conditions. Thus, ecosystems are represented by average conditions, and fluxes of water, solid matter and gas are described as functions of aggregated empirical parameters.

Parameters that describe ecosystem characteristics and primary transport pathways are preferably given realistic values (Section 2.3.8), reflecting average properties and natural variations in present conditions. That is, the parameter values are integrated over spatial variations within an area corresponding to the scale of a biosphere object, and over temporal variations in an annual scale. The general approach has been described in Grolander (2013) and Tröjbom et al. (2013). Thus, when the variation in a parameter value is quantified (e.g. in terms of standard deviation, or maximum and minimum values), the measures of variation should primarily reflect the random variation between biosphere objects. This is for example implicit in site investigation when the observational units of sampling designs are multiple lakes, mires or agricultural fields. However, it is hard to strictly apply this approach when site data have been collected in different schemes or when site data are unavailable, and parameter values need to be derived from literature data or are based on analogues. For further details, see Section 8.1.2 and the descriptions of the parameter value derivation in Sections 8.2 to 8.4.

The term data or parameter uncertainty is used in the context of assessing the precision of the estimated doses. This uncertainty refers to the sum of natural variations, comprising variations due to real and identifiable heterogeneity in nature and measurement uncertainties (i.e. errors in measurements).

8.1.1 Use of analogues

SKB strives to, as far as possible, utilise site-specific information for Forsmark for selecting parameter values and their probability density functions. However, in some cases site data are not available. In these cases, the parameter values are estimated from literature data, or by using analogues. At SKB, isotope, elemental and parameter analogues are used. Regardless of the type, analogues can be estimated using both site and literature data. The isotope analogues are commonly utilised assuming that in an environment, the behaviour of different isotopes of the same element is identical, however, acknowledging that for certain elements or conditions this is not fully true (Tröjbom et al. 2013). The second type of analogues, the elemental analogues (EA), is based on biogeochemical properties of the elements lacking data. The choice of EAs is explained in detail in Tröjbom et al. (2013). Typically, elements of the same group in the periodic table are used as they have the same number of outer electrons that can participate in chemical reactions and, thus, they have similar chemical properties. However, even if elements are chemically similar, their behaviour in natural environments can differ. As the speciation of some elements varies with for example redox conditions, it is not always possible to use a single analogue. In such conditions different analogues are used for, for example, oxidising and reducing environments (see Section 13.5.3 for further discussion of this issue). The third type of analogues is the parameter analogues (PA). When using PAs, data for similar species or soil types are utilised to fill data gaps, assuming that the element behaves similarly in both organisms, materials or conditions in the given environmental context. For example, for some parameter values reflecting warmer conditions, data from southern Sweden are used as parameter analogues.

8.1.2 Probability density function

Most of the parameters are described by best estimate (BE) values together with a probability density function (PDF). The PDF includes both natural variation and measurement uncertainties. Where sufficient data are available, the shape of the PDF for each parameter has been judged to be approximately

normal on either the original scale, a logarithmic scale or a probit[32] scale. The mean value on the assigned scale is used as the best estimate (e.g. the arithmetic mean and the geometric mean for a normal and log-normal distributions, respectively). For each parameter, maximum and minimum values are also identified to set limits on the possible range of the parameter value. These can reflect natural limitations (e.g. many properties cannot take negative values) or they can be based on expert judgement (e.g. with respect to expected future natural variation). However, in many cases this knowledge is insufficient and then the minimum and maximum values are pragmatically set to the 5th and 95th percentiles of the assigned PDFs. In the generation of parameter samples, only values within the assigned minimum–maximum range are drawn, this increases the probability of this range compared to the original PDF that is not truncated (Ecolego, **Model tools report**).

When data are insufficient to estimate the shape of the PDFs, e.g. for properties of future site conditions estimated from literature data, the parameters are typically represented by a uniform distribution (a range with all values having the equal probability to occur) and a best estimate. For most of the parameters that are assigned a uniform distribution, the best estimate corresponds to the arithmetic mean of the minimum and maximum values.

It is also important to remember that parameter variation should reflect natural variation within the context of the calculation case. In the PSAR, the *base case* postulates present-day conditions for the full assessment period. Consequently, typical values and natural variation are as far as possible determined from data collected in Forsmark (under present-day conditions). Thus, large-scale variation in response to considerable change in the climate or in the chemical environment are not factored into the estimates of natural variation. Relevant aspects of large-scale systematic variations are instead considered by postulating separate calculation cases that are constructed to directly address expected changes in environmental conditions. For example, these might relate to a warmer climate, a colder climate or a shift in soil conditions caused by calcite leaching (Sections 10.2, 10.3 and 11.5). For parameters that are considered to be significantly affected by such changes, separate sets of probability density functions are specified.

In the PSAR, as in previous safety assessments, the projected development of regolith layers and the associated ecosystem succession have been described with the regolith-lake development model (Chapter 4 and 5). In the BioTEx calculations, the landscape development is represented by time series of parameters describing the biosphere object, and by utilising flow conditions for three separate successional stages (submerged, early and late terrestrial periods). This representation is reasonable, as it captures process understanding, and it is internally consistent, as the groundwater flows are conditioned on the postulated topography and regolith stratigraphy. However, as these correlated properties are the output from a single deterministic realisation, no uncertainties have been assigned to these parameters. Instead, uncertainties in landscape geometries, regolith depths and hydrological flows are considered to be covered by the parameter ranges in alternative outlines of object 157_2 (Section 11.3). In addition, following the practise introduced in SE-SFL, the effects of uncertainties in object properties are examined in a separate sensitivity analysis (Section 11.4).

In order to assess the potential annual dose to a representative person in a potentially exposed group, assumptions on the habits and characteristics of future humans inhabiting the area are needed. Due to the long timescales, SKB deems it impossible to assign characteristics and habits that are likely to provide realistic estimates of the actual features and behaviour of humans in the far future. Four potentially exposed groups are used in this assessment (described in Section 6.2.1), which are to be interpreted as credible bounding cases with respect to the identified exposure pathways (Section 2.3.5). Consequently, no uncertainties are assigned to parameters used to calculate the exposure arising from environmental concentrations. These parameters include characteristics assigned to the reference man (e.g. annual intakes of air, water and carbon) and the dose coefficients (for ingestion, inhalation and external exposure). In addition, there are a limited number of parameters that are considered not to vary (e.g. radioactive half-life, radionuclide branching ratios, the density of water and the diffusivity of an element in water) or that are postulated as fixed values corresponding to a specific climate evolution (i.e. CO_2 concentration) (Section 8.2.1).

[32] Probit is the inverse to the cumulative distribution function of the standard normal distribution Φ^{-1}. Parameters expressed on the probit-scale are thus constrained between 0 and 1 after back-transformation.

In the PSAR, most of the BioTEx calculations are based on probabilistic simulations with a time-dependent geosphere release, and, thus, the calculations rely on parameter values from the full PDFs. However, best estimates are used for deterministic benchmark calculations that are used to evaluate the impact of the parameter uncertainties. In addition, best estimates are used in combination with a unit release rate to calculate the landscape dose conversion factors (LDFs). These allow a direct comparison with the results from SR-PSU.

8.2 Description of updated BioTEx parameters in the *base case*

There are nearly 360 parameters used in the BioTEx model, of which one third represents element- or radionuclide-specific properties with unique values for each element/radionuclide. Parameters that reflect processes related to transport and accumulation of, and exposure to, radionuclides can be divided into nine categories: Landscape geometries, Regolith properties, Hydrological parameters, Terrestrial ecosystem properties, Aquatic ecosystem properties, Element-specific properties (e.g. sorption coefficients (K_d) and concentration ratios (CR)), Human characteristics, Radionuclide-specific properties and Non-human biota parameters. For each category except for the non-human biota parameters, the changes since SR-PSU are provided in Table 8-1 for the *base case* and in Table 8-5 for the *warm* and *cold climate calculation cases*. The major changes are discussed in Sections 8.2.1 to 8.2.4. and the changes to the parametrisation are described in Section 7.5. Updates with respect to non-human biota parameters are described in Section 8.4.

Table 8-1. Overview of parameter changes since SR-PSU (Grolander 2013). Parameters that are new in the PSAR are highlighted in bold and the definitions of these parameters as well as their values are presented in Sections 8.2.1 to 8.2.4. The table also lists parameters that have updates to their values since SR-PSU or for which the parameter name has changed. Also, the parameters that have been excluded since SR-PSU are listed. GP = garden-plot household, DM = drained-mire farmers, IO = infield-outland farmers, Cl = chlorine.

Parameter	Category	Change since SR-PSU	Comment
New and updated parameters			
area (GP)	Human	See 8.2.2 for an updated value	
Beta_posWell (Release)	Hydrological	See 8.2.4 for definition and value	Replaces f_well_interaction_Area and p_well_interaction_Area
Beta_wellfrac (Release)	Hydrological	See 8.2.4 for definition and value	Replaces f_well_interaction_Area and p_well_interaction_Area
burial_C_min	Terrestrial	See 8.2.2 for definition and value	
conc_air_combPeat	Terrestrial	See 8.2.1 for definition and value	Replaces doseCoef_combPeat
conc_air_combWood	Terrestrial	See 8.2.1 for definition and value	Replaces doseCoef_combWood
Conc_C_atmos	Terrestrial/Aquatic	See 8.2.1 for an updated value	
cR_agri_fodder [Cl]	Element-specific	See 8.2.3 for an updated value	
cR_ter_mush [Cl]	Element-specific	See 8.2.3 for an updated value	
cR_ter_pp [Cl]	Element-specific	See 8.2.3 for an updated value	Replaces conc_Cl_PP_ter and conc_Cl_regoUp_ter_D
D_CO2_air	Terrestrial	See 8.2.1 for definition and value	Replaces D_CO2_peat, D_CO2_clay, D_CO2_soil (GP/IO)
dens_regoUp_gyttja (DM)	Regolith	Name change	Replaces dens_regoUp_clay (DM)
doseCoef_ext	Radionuclide-specific	See Appendix A.5 in the **Radionuclide transport report** for updated values	
doseCoef_ing	Radionuclide-specific	See Appendix A.5 in the **Radionuclide transport report** for updated values	
doseCoef_inh	Radionuclide-specific	See Appendix A.5 in the **Radionuclide transport report** for updated values	

Table 8-1. Continued.

Parameter	Category	Change since SR-PSU	Comment
f_area_tuber (GP)	Human	See 8.2.2 for an updated value	
f_area_veg (GP)	Human	See 8.2.2 for an updated value	
f_C_wood (GP)	Terrestrial	See 8.2.2 for updated PDF	
f_inorg_Cl_PP_aqu	Aquatic	See 8.2.3 for definition and value	Replaces df_decomp_aqu
f_trans_tuber	Terrestrial	See 8.2.2 for definition and value	Used for process Translocation
halfLife	Radionuclide-specific	See Section 3.3.3 or Appendix A.5 in the **Radionuclide transport report** for updated values	
Ingrowth500ReleaseMatrix	Radionuclide-specific	See 8.2.2 for definition and value	Replaces dose_ingrowth_agri_**ext/ing/inh**
Ingrowth50ReleaseMatrix	Radionuclide-specific	See 8.2.2 for definition and value	Replaces dose_ingrowth_agri_**ext/ing/inh**
Ingrowth50Matrix	Radionuclide-specific	See 8.2.2 for definition and value	Replaces dose_ingrowth_agri_**ext/ing/inh**
LeafStoreCapacy	Terrestrial	Name change and merging of two parameters	LeafStoreCapacy_tuber (GP) LeafStoreCapacy_veg (GP)
NPP_veg (GP)	Terrestrial	See 8.2.2 for an updated value	
percolation_agri (DM/GP/IO)	Terrestrial	See 8.2.4 for an updated value	
poro_regoUp_gyttja (DM)	Regolith	Name change	Replaces poro_regoUp_clay (DM)
probit_f_inorg_Cl_PP_ter	Terrestrial	See 8.2.3 for definition and value	Replaces df_decomp_ter
probit f_refrac_ter	Terrestrial	See 8.2.2 for definition and value	Replaces f_refrac_ter
q_bedrock_low_eco_i	Hydrological	See 8.2.4 for definition and value	eco_i = sea, lake, ter_iso, ter_end
q_low_bedrock_eco_i	Hydrological	See 8.2.4 for definition and value	
q_downstream (object 157_2)	Hydrological	See Appendix F for updated values	
q_rego_k_rego_j_eco_i (object 157_2)	Hydrological	See Appendix F for updated values	k, j are adjacent regolith layers {Low, GL, PG, Up, Water} eco_i = sea, stream
q_rego_k_rego_j_eco_i (object 157_2)	Hydrological	See Appendix F for updated values	k, j are adjacent regolith layers {Low, GL, PG, Peat, Up, Water} eco_i[33] = ter_iso/ter_end
q_sat_unsat_agri (DM)	Terrestrial	Name change, see also 8.2.2 for updated values	Replaces Flux_water_satSoil_agri (DM)
S_w_regoUp_gyttja (DM)	Regolith	Name change	Replaces S_w_regoUp_clay (DM)
SoilResp (GP/IO)	Terrestrial	See 8.2.2 for definition and value	Replaces conc_DIC_regoUp (GP/IO)
SoilResp_gyttja (DM)	Terrestrial	See 8.2.2 for definition and value	Replaces conc_DIC_regoUp (DM)
SoilResp_peat (DM)	Terrestrial	See 8.2.2 for definition and value	Replaces conc_DIC_regoUp (DM)
SoilResp_ter	Terrestrial	See 8.2.2 for definition and value	Replaces conc_DIC_regoUp_ter
time_exposure_comb (GP)	Human	See 8.2.1 for definition and value	Replaces doseCoef_combPeat and doseCoef_combWood
time_irrigationPeriod (GP)	Terrestrial	See 8.2.2 for definition and value	Replaces time_vegPeriod (GP)
washoffCoef_veg (GP)	Terrestrial	Name change	Replaces washoffCoef (GP)

[33] For object 157_2 parameter values with suffix iso and end are identical (derived from 5000 AD water balance).

Table 8-1. Continued.

Parameter	Category	Change since SR-PSU	Comment
yield_tuber (GP)	Terrestrial	Name change	Replaces biom_tuber (GP)
yield_veg (GP)	Terrestrial	Name change, see also 8.2.2 for new values	Replaces biom_veg (GP)
z_regoPeat_equlib	Landscape	See 8.2.2 for definition and value	Replaces minRate_regoPeat
Excluded parameters			
biom_cereal (DM)	Terrestrial	Removed and not replaced	Activity fraction in crop is not important for leaching
biom_fodder (DM)	Terrestrial	Removed and not replaced	Activity fraction in crop is not important for leaching
biom_tuber (DM)	Terrestrial	Removed and not replaced	Activity fraction in crop is not important for leaching
f_well_agri	Hydrological	Removed and not replaced	Updated handling of drilled wells in the PSAR see 8.2.4.
threshold_land	Regolith	Removed and not replaced	Parameter used to define time to initiate calculations for mire, now initiated when area of mire is greater than 10 m^2

8.2.1 Atmosphere-related parameters

Diffusivity of CO_2 in air

In SR-PSU, the parameter related to the diffusivity of CO_2 in regolith was calculated from the porosity, degree of water saturation and the diffusivity of CO_2 in air using the Millington-Quirk model (Millington and Quirk 1961, Grolander 2013). Following the development in SE-SFL, these calculations are now done within the BioTEx model (Chapter 7) Consequently, the diffusivity of CO_2 in air (*D_CO2_air*) is a required parameter. The best estimate of this parameter was reported to be 446 $m^2\ a^{-1}$, corresponding to an average soil temperature of 10 °C for the ground-frost-free period in Forsmark (see Section 8.5.10 in Grolander and Jaeschke 2019 for calculation of the parameter value). In the PSAR, the upper and lower limits for this parameter are calculated from a postulated temperature span between 6.4 and 16 °C. The lower limit, 436 $m^2\ a^{-1}$, corresponds to average yearly air temperature given the present climate, whereas the upper limit, 463 $m^2\ a^{-1}$, corresponds to the present-day summer air temperature (June – August) in Forsmark. This parameter is only used for agricultural ecosystems and a uniform distribution is considered to be appropriate.

Concentration of carbon in the atmosphere

The total carbon concentration in the atmosphere (*conc_C_atmos*) is calculated from the fractional content of CO_2 (ppm) in the atmosphere. As in SR-PSU, this is done by applying the ideal gas law for the vegetation period (i.e. the part of the year when the temperature is above +5 °C), and then converting the molar content of CO_2 in the atmosphere to units of carbon. As the climate developments evaluated in this safety assessment are considered to bracket the uncertainty in probable climate conditions (Section 4.1), no additional uncertainties are imposed on the selected values (see Section 8.3). The calculated concentrations are applicable to aquatic, mire and cultivated ecosystems. In the *base case* the atmospheric CO_2 fraction is 377 ppm, the average air temperature for the vegetation period (April to November) is 12.1 °C and the carbon concentration is 0.00019 $kgC\ m^{-3}$.

Concentration in air after combustion of peat and wood and time of exposure

In the PSAR the calculations used to convert activity concentrations in combusted fuel to dose from inhalation of particles and gases outside a house have been updated in accordance with updates introduced in SE-SFL (Section 7.5.2). The first step of the calculations requires parameters describing the ground-level activity concentration in air per unit activity concentration in peat or wood, *conc_air_combPeat* and *conc_air_combWood* (Section 8.5.11 in Grolander and Jaeschke 2019)

given a postulated values for the consumption rate of biomass fuel, the height and wall areas of the house, and the distance from the house where the exposure occurs (Stenberg and Rensfeldt 2015). The SE-SFL parameter values are directly applicable in the PSAR, and the values used are 2.49×10^{-7} and 2.16×10^{-7} (Bq m^{-3} per Bq $kgdw^{-1}$) for combustion of wood and peat, respectively. The second step requires the exposure time outdoors. As in SR-PSU, a cautious upper bound is used for this parameter (Stenberg and Rensfeldt 2015). That is, the outdoor combustion time, *time_exposure_comb,* is set to all hours of the day, which corresponds to 8 760 hours per year.

8.2.2 Terrestrial ecosystem parameters

Refractory organic carbon of mire vegetation

Refractory organic carbon is the part of the net primary production that is not decomposed or exported, but contributes to peat accumulation of organic carbon (i.e. the refractory organic matter remaining after initial mineralisation). In SR-PSU, this parameter was determined from literature data based on litter decay experiments (Grolander 2013, Section 9.9.1). In the PSAR, this approach is also used to derive the PDF of the parameter.

The wetlands that are influenced by discharge of deep groundwater are considered to be in the fen stage. In this stage, grasses and sedges dominate the primary production. Thus, to derive a PDF for the parameter *f_refrac_ter* (unitless), data from three fens in North America were re-examined (Moore et al. 2002). The analysis showed that the between site variation for the first-order rate for decomposition (k) of the field layer is negligibly small compared with the variation between litter types. Moreover, the variation in decomposition rate between litter types is approximately normally distributed. Thus, the stochastic variation (i.e. the mean and the standard deviation) in decomposition rate k is estimated from individual field-layer litter types (e.g. *Carex* and *Typha* species, n = 12).

In the PSAR 1 000 randomly drawn decomposition rates k are drawn from a normal distribution and used to calculate the fraction of litter remaining after 5 years[34] of decomposition (*f_refrac_ter*). To determine a PDF for these fractions, they are probit-transformed. This transformation ensures that the PDF is naturally constrained between 0 and 1. Based on this approach, the mean and standard deviation for the parameter *probit_f_refrac_ter* are −0.52 and 0.28 (unitless), respectively. The minimum and maximum values are set to the 5 % and 95 % confidence limits of the normal distribution (on the probit scale), yielding minimum and maximum and values of −0.98 and −0.07, respectively. This corresponds to a mean fraction of refractory organic carbon of 30 % with a confidence interval between 16 and 47 %.

The carbon burial rate in mire ecosystems

In the PSAR the input of refractory organic matter to the deeper peat layer, *Burial_C* (kgC m^{-2} a^{-1}), is a function in the BioTEx model (Section 7.5.1) rather than a parameter as was the case in SR-PSU (Grolander 2013). The burial rate is calculated from six parameters and equals plant production less the mineralisation in the upper peat layer (Section 7.5.1). The rate is by definition positive. To avoid that the function returns negative carbon inputs, it is deemed appropriate to use a lower limit for the output of the burial function in the PSAR (*burial_C_min)*.

The input rate of carbon to deep peat is not easily observable. However, Clymo et al. (1998) combined field data and mass-balance modelling and derived a plausible range of carbon inputs to the mesotelm between 20 and 40 gC m^{-2} a^{-1}, where the input increased with warmer climate. Moreover, it was suggested that the input rate was approximately 20 % higher than the average long-term rate for carbon accumulation.

There are extensive reviews characterising the long-term carbon accumulation in boreal mires, and an average value of 20 gC m^{-2} a^{-1} was presented in Sohlenius et al. (2013c). However, the variation between studies and locations is considerable, partly due to different responses to climate, mire type and age of the mire. The authors also presented data from the Forsmark area, and calculated a mean peat accumulation rate of 0.9 mm for fens (Sohlenius et al. 2013c). Applying a typical density and

[34] 5 years correspond to the length of the field experiment in Moore et al. 2002.

carbon content of peat collected in Forsmark (100 kgdw m^{-3}, and 0.4 kgC $kgdw^{-1}$, Grolander 2013) this equals 36 gC m^{-2} a^{-1}, which is a rate that is consistent with estimates from C-14 dated peat from 1 000 to 2 000 years old fens in the area (Schoning 2014).

Yu (2006) reported that the long-term carbon accumulation for fens in Canada ranged between 7.8–113 gC m^{-2} a^{-1}. As peat formation and degradation are happening simultaneously at the mire, the carbon input rate must be larger than the peat accumulation rate. Thus, it is reasonable to upscale these values by 20 % (cited from paragraph above). Such an upscaling results in an expected input rate of 48 gC m^{-2} a^{-1} in Forsmark, with upper and lower limits, from Canadian fens, of 9 and 136 gC m^{-2} a^{-1}, respectively.

To evaluate whether random combinations of values for the six parameters[35] used to calculate the carbon burial rate yields a plausible range of carbon input, 1 000 Monte-Carlo samples were drawn. For each parameter combination the carbon input rate was calculated (Figure 8-1). The median burial rate was 0.067 kgC m^{-2} a^{-1}, with c 3 and 8 % of probabilistic realisations falling below and above the plausible limits mentioned above. Thus, rates calculated within the BioTEx model will be somewhat higher than expected[36] but still within a reasonable range. However, to avoid unrealistically low burial rates (that will underestimate accumulation of radionuclides in organic form), value of 0.009 kgC m^{-2} a^{-1} is selected as a lower limit for the function (i.e. as *burial_C_min*). This value is used for the burial rate in the few simulations where the mass balance returns a rate below this limit.

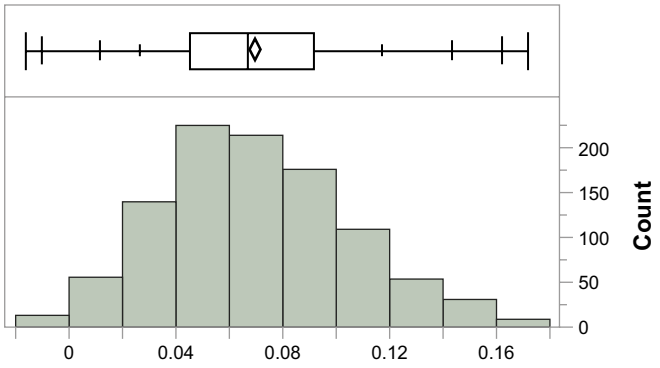

Figure 8-1. *Histogram showing the distribution of Burial_C, calculated from probabilistic samples of five underlying parameters (see equation in Section 7.5.1). The box-plot displays the range (minimum to maximum value) with quantiles interspersed (left to right): 0.5 %, 2.5 %, 10 %, 25 %, 50 %, 75 %, 90 %, 97.5 % and 99.5 %. The diamond represents the arithmetic mean.*

[35] The six parameters are NPP_ter, f_refrac_ter, z_regoUp_ter, dens_regoUp_ter, f_C_peat and minRate_ regoUp_ter (see Section 7.5.1 for details).

[36] High burial rates lead to higher accumulation of radionuclides in organic matter. Thus, rates calculated in the BioTEx model will be somewhat cautious with respect to soil concentrations, plant uptake and subsequent exposure by humans.

The thickness of peat at equilibrium

The final peat thickness in the mature mire of each biosphere object is calculated deterministically by the RLDM (Chapter 4). In SR-PSU, the mineralisation rate in the deep peat (*minRate_regoPeat*) was calculated from the peat thickness and several other biosphere parameters that are varied in probabilistic calculations (Grolander 2013, Section 9.9.2). In SE-SFL, the calculation of the mineralization rate was incorporated as a function in the BioTEx model (SKB TR-19-05). As this modification allows for a consistent handling of dependencies and the propagation of uncertainties, it is kept in the BioTEx model also for the PSAR (Chapter 7). Consequently, the final peat thickness in the mature mire (*z_regoPeat_equlib*) is an explicit model parameter in the PSAR. To ensure consistency with other landscape parameters (Section 8.1.2), it is treated deterministically. Thus, the parameter is treated as an object specific constant with the values of 0.2 m for object 157_2, 1.4 m for object 157_1 and 1.1 m for object 116 (as illustrated in Figure 5-5).

Soil respiration in different types of regolith

In SR-PSU, the concentration of dissolved inorganic stable carbon (DIC) in the upper regolith layers was a parameter on its own. However, in supplementary calculations of soil degassing, the DIC concentration is derived as a function of soil respiration (Saetre and Ekström 2017b). In SE-SFL, the BioTEx model was updated accordingly, and in the PSAR this update is retained. Thus, a parameter for soil respiration is required.

The parameter values that were used in SE-SFL were based on literature data on soil respiration that are considered to be applicable also to Forsmark conditions. That is, the value for respiration in the upper peat layer was derived from data for four Nordic boreal mires (Lindroth et al. 2007). The best estimate for mire ecosystems, *SoilResp_ter*, is taken to be the mid-range value 0.33 kgC m^{-2} a^{-1}. The minimum value 0.21 kgC m^{-2} a^{-1} corresponds to the northern subarctic regions of Northern Finland, and the maximum value 0.46 kgC m^{-2} a^{-1} corresponds to a mire in the southern part of Sweden.

The respiration rates for organic and inorganic agricultural soils were derived from a broad review, where estimates reflecting Nordic arable conditions were selected (Oertel et al. 2016 and references within). The parameter values for cultivated soils are collected from southern Finland and expressed for a soil temperature of 10 °C, which corresponds to the average soil temperature in Forsmark during the ground-frost-free period. The range in these data reflects the range associated with different types of vegetation cover, including bare soil, barley, potato and grass (in order of increasing respiration). The best estimate for organic soils, *SoilResp_peat/gyttja* (corresponding to drained-mire farming), and inorganic soils, *SoilResp* (corresponding to infield-outland farming and garden-plot horticulture), are taken to be the mid-range values of 2.0 and 0.82 kgC m^{-2} a^{-1}, respectively. The minimum values, 0.95 and 0.17 kgC m^{-2} a^{-1}, correspond to bare soil, whereas the maximum values 3.1 and 1.5 kgC m^{-2} a^{-1}, correspond to grass covered soils. For all three parameters a uniform distribution is used as probability density function.

The carbon content in the stem wood

The carbon content in the stem wood is estimated from data for Norway spruce. In SR-PSU, the parameter *f_C_wood* was given a constant value of 0.48 kgC $kgdw^{-1}$ based on measurements from the site (Löfgren 2010, Table 6-5). In the PSAR a normal distribution is used to describe the probability density function, and based on the same data, a standard deviation of 0.07 kgC $kgdw^{-1}$ is assigned to the parameter. The minimum and maximum values are set to the 5 % and 95 % confidence limits of the normal distribution, yielding minimum and maximum values of 0.36 kgC $kgdw^{-1}$ and 0.60 kgC $kgdw^{-1}$, respectively.

Yields of vegetables and tubers in the garden plot

The parameters that describe the production of vegetables are based on national statistics for the production of cabbage between 1971 and 2008, made available from the Swedish Board of Agriculture. Based on the content of protein (1.1 %), carbohydrates (4.7 %) and lipids (0.1 %) of cabbage (National

Food Agency, Sweden), a conversion factor of 27 gC $kgfw^{-1}$ is used to convert the production into carbon content[37]. In SR-PSU, this conversion was done incorrectly, but the mistake was corrected in SE-SFL (Grolander and Jaeschke 2019).

In the PSAR, the corrected values are used. In addition, the minimum and maximum values have been adjusted to correspond the 5 % and 95 % confidence limits of the corresponding normal distributions for the statistical cabbage yields. Thus, in the PSAR, the parameter representing the production or harvest of vegetables, *yield_veg* (kgC m^{-2} a^{-1}), has the arithmetic mean value of 0.11 and the standard deviation 0.014. The minimum and maximum values are set to 0.09 and 0.14. Note that the name of the parameter was changed from *NPP_ag_veg* to *yield_veg* in SE-SFL to be more informative, and also *biom_tuber* was changed to *yield_tuber*. These name changes are kept in the PSAR. As in SR-PSU, the total net primary production is calculated by assuming that the roots contribute to 25 % of the total production (Grolander 2013, Section 9.11). The corresponding values for the net primary production of vegetables, *NPP_veg* (kgC m^{-2} a^{-1}), are: 0.15 (arithmetic mean), 0.02 (standard deviation), 0.12 (minimum), and 0.19 (maximum).

The productivity of vegetables also affects the area of the garden-plot needed to support a family group with vegetables and root crops, and the fraction of that plot used for cultivation of tubers. Following SE-SFL (Grolander and Jaeschke 2019, Section 9.3), the parameter *area* is thus updated to the value 54 m^2 (per individual), and the parameter *f_area_tuber* is updated to 0.46 (unitless). As the vegetables are cultivated on the rest of the garden plot, it follows that *f_area_veg* is updated to 0.54 (unitless).

Crop water demand

In the summer when evapotranspiration exceeds precipitation, plants need additional water to cover the water demand required for growth and development. This additional water is referred to as the crop water demand (CWD) and it can be covered by groundwater uptake or by irrigation.

In SR-PSU, the water demand for temperate conditions was estimated for barley based on a study by Johansson and Klingspor (1977). They calculated the daily balance between precipitation and evapotranspiration during the vegetation period for a number of crops and regions in Sweden during a normal year and a dry year (detailed description of methods in Johansson 1973). The estimated range was considered to also cover a warmer climate than at present.

In the PSAR, present-day climate is handled in the *base case* (Chapter 9), whereas a warmer climate (with possibly dry summers) is handled in the *warm climate calculation case* (Section 10.2). Following the SE-SFL methodology, the present-day estimate of CWD is now based on water demand for a normal year, averaging over the three crops grown in the drained mire land-use, i.e. barley (0.56), hay (0.37) and potatoes (0.07) (area weights). The Southcentral coastal area of Sweden is the most representative region for Forsmark, and the future water demand is assumed to be normally distributed. Thus, the range between Northern Sweden (low demand) and the very south of Sweden (high demand) is considered to cover a reasonable range of variation within present-day conditions. This range can be described with a mean water demand for cereals of 0.050 m a^{-1}, and a standard deviation of 0.009. The minimum and maximum values of 0.035 (north) and 0.065 (south) are assumed to corresponds to the 5 % and 95 % confidence limits of the normal distribution. In the *base case* this water demand is assumed to be fully covered by groundwater uptake from the saturated soil *q_sat_unsat_agri.*

Irrigation of a garden plot

For a well-drained garden plot, the water demand during the growing season is considered to be fully covered by irrigation. The parameter *amount_irrig* describes the amount of water (per unit area) used to irrigate a garden plot. As for large-scale cultivation, the water demand is estimated from the study by Johansson and Klingspor (1977) and as in SR-PSU the water demand of the most sensitive of the examined crops (i.e. potatoes) is considered representative for garden plot cultivation.

[37] The carbon content in proteins, carbohydrates and fats are: 0.53, 0.44 and 0.66 kgC kg^{-1} (references within Avila and Bergström 2006).

In SE-SFL the period of irrigation of the garden plot was updated from the total length of the growing season, Grolander 2013) to the period most sensitive to water shortage (Grolander and Jaeschke 2019, Section 8.5.2), and the parameter name was changed accordingly (from *time_vegPeriod* to *time_irrigationPeriod).* With reference to cabbage, the length of the drought sensitive period was set to 40 days. In the PSAR this value is considered to be applicable also to Forsmark, and the minimum and maximum values are set to 30 and 50 days, reflecting a 10-day shortened or prolonged span of the drought-sensitive period.

Translocation of radionuclides for tubers

The transfer of radionuclides from leaves to edible parts is referred to as translocation. As this process is now included in the BioTEx model in the PSAR for situations with irrigation, a parameter describing the fraction of radionuclides deposited on the leaves of crops that ends up in the edible parts of the plant is required. In SE-SFL the parameter *f_trans* was introduced for tubers following one of the IAEA (2010) definitions[38]. In the PSAR, a probability density function is introduced for this parameter.

In the PSAR, the IAEA data compilation of translocation factors for tubers is used as source data (IAEA 2010, Table 10). Cs is selected to represent mobile elements, and the translocation factor for Cs (n = 23) is cautiously applied to all radionuclides. Thus, the geometric mean for *f_trans_tuber* is assigned the value 11.6 %. The span between the listed minimum and maximum values (1.3 and 46 %) is used to calculate a geometric standard deviation of 3.0. The minimum and maximum values are set to the 5 % and 95 % confidence limits, respectively, of the corresponding log-normal distribution, yielding values of 1.9 and 69 % (which are systematically higher than the reported range).

Exposure to radioactive decay products in agricultural lands

Activity concentrations in agricultural soils are calculated using analytical solutions (Saetre et al. 2013a, Chapter 7). The concentrations used to calculate exposure are average concentrations over 50 years (GP and DM land-use variants) of cultivation, or after 500 years of continuous fertilization (IO variant). The activity concentrations calculated with the algebraic expressions do not consider the exposure due to longer-lived radioactive decay products that may build up during this 50- or 500-year period.

The system of differential equations governing the decay and ingrowth of radionuclides in a decay chain $A_1 \rightarrow A_2 \rightarrow \ldots A_n$ can be written as:

$$\frac{dA_1}{dt} = S_1 - \lambda_1 A_1$$
$$\frac{dA_2}{dt} = S_2 - \lambda_2 A_2 + BR_{1,2}\lambda_2 A_1$$
$$\ldots$$
$$\frac{dA_n}{dt} = S_n - \lambda_n A_n + BR_{n-1,n}\lambda_n A_{n-1}$$

where

A_i is the activity of radionuclide *i* at time t (Bq),

S_i is a source term of radionuclide *i* at time t (Bq a^{-1}),

λ_i is the decay constant for radionuclide *i* (a^{-1}),

$BR_{i,j}$ is the branching ratio between radionuclide *i* and *j* (unitless).

[38] The translocation factor (%) is defined as the ratio of the activity, on a ground area basis, of the edible part of a crop at harvest time (Bq m^{-2}) to the foliage activity of the crop at the time of deposition (Bq m^{-2}).

The solution to the system of equations with source terms can be written as (Bateman 1910):

$$A_n(t) = \lambda_n \sum_{i=1}^{n} \left[\prod_{j=1}^{n-1} BR_{j,j+1}\lambda_j \times \frac{1}{\lambda_i} \sum_{j=i}^{n} \left(\frac{A_i(0)e^{-\lambda_j t}}{\prod_{\substack{p=i \\ p\neq j}}^{n}(\lambda_p - \lambda_j)} + \frac{S_i\left(1 - e^{-\lambda_j t}\right)}{\lambda_j \prod_{\substack{p=i \\ p\neq j}}^{n}(\lambda_p - \lambda_j)} \right) \right]$$

To handle the contribution from longer-lived radioactive decay products, the dose coefficients of parent radionuclides were upscaled in SR-PSU (Saetre et al. 2013a, Section 9.1). In the PSAR, a similar approach is used, but to increase the transparency, the ingrowing activity is summed over each decay product. Moreover, the contribution of decay products is calculated on the level of soil concentrations as it increases the consistency in probabilistic calculations. Thus, in the PSAR, the ingrowing activity of decay products is calculated from the soil activity of the parent radionuclide. The scaling factors represent the fraction of the parent radionuclide activity that should be added to the activity of the decay product due to ingrowth. The factors for the calculations are presented pair-wise in Table 8-2, and the parameter names for the three sets of factors in matrix form are: *Ingrowth50Matrix* (DM), *Ingrowth50ReleaseMatrix* (GP) and *Ingrowth500ReleaseMatrix* (IO).

The calculations of the scaling factors are done separately for DM, GP and IO agriculture, as the source of the activity and the considered period for in-growth differ between the groups. The factors are calculated by first solving the differential equations for the parent – decay product pairs, considering the initial condition (DM) or the input of the ancestral radionuclides (GP, IO), and the loss/ingrowth through radioactive decay. For DM and GP, the fraction between decay product and parent is calculated from the average concentration over a 50-year period, whereas for IO the fraction is calculated from the activity of parent and decay product after 500 years of ingrowth. Thus, for DM, the scaling factors are calculated by setting the initial activity of the parent radionuclide to unity and disregarding the input from groundwater uptake. As radionuclide ingrowth occurring over a longer time, by definition, produces more radioactive decay products than over a shorter time, it is a cautious simplification to disregard the ingrowth originating from groundwater uptake. For GP and IO, the initial concentrations of the parent (and decay product) are set to zero, and a unit release of the parent is added each year, representing a constant input through irrigation or fertilisation.

As an example, the calculation steps for DM scaling factors for Nb-93m due to ingrowth from Mo-93 are shown. Mo-93 has a half-life of 4 000 years and a branching ratio of 88 % to Nb-93m, which has a half-life of 16 years. Thus, by applying the Bateman equation without sources we have for DM the following equation for the scaling factor:

$$DM_{93Mo}^{93mNb} = \int_0^{50} 88\%\lambda_{93mNb}\left(\frac{e^{-\lambda_{93Mo}t}}{\lambda_{93mNb} - \lambda_{93Mo}} + \frac{e^{-\lambda_{93mNb}t}}{\lambda_{93Mo} - \lambda_{93mNb}}\right)dt \Bigg/ \int_0^{50} e^{-\lambda_{93Mo}t}\,dt$$

$$= BR_{93Mo,93mNb}\lambda_{93mNb}\left(\frac{1 - e^{-\lambda_{93Mo}50}}{\lambda_{93Mo}(\lambda_{93mNb} - \lambda_{93Mo})} + \frac{1 - e^{-\lambda_{93mNb}50}}{\lambda_{93mNb}(\lambda_{93Mo} - \lambda_{93mNb})}\right) \Bigg/ \frac{1 - e^{-\lambda_{93Mo}50}}{\lambda_{93Mo}}$$

$$= \left\langle BR_{93Mo,93mNb} = 88\,\%, \lambda_{93mNb} = \frac{LN(2)}{16.13}, \lambda_{93Mo} = \frac{LN(2)}{4000} \right\rangle = 52\,\%$$

The calculation is similar for GP, but a constant source term is used for Mo-93 (and no initial activity is considered). This is also true for the calculations of IO, but the ingrowth represents the results after 500 years of constant input, so there is no need to integrate the Bateman equation.

Table 8-2. Scaling factor pairs for DM (drained-mire farmers), GP (garden-plot household) and IO (infield-outland farmers) considering the ratio of activity of parent radionuclides to be added to long-lived radioactive decay products in agricultural lands. For example, for each unit of activity concentration of Mo-93 in agricultural soil, ingrowth results in 52 % activity concentration of Nb-93m in DM soil. The corresponding numbers for GP and IO are 40 and 84 %, reflecting 50 and 500 years of continuous input of Mo-93, respectively.

Decay product	Parent	DM	GP	IO	Decay product	Parent	DM	GP	IO
Ac-227	Pa-231	5.0×10^{-1}	3.7×10^{-1}	9.4×10^{-1}	Pu-240	Cm-244	3.4×10^{-3}	2.0×10^{-3}	4.9×10^{-2}
	U-235	2.0×10^{-4}	1.1×10^{-4}	4.7×10^{-3}	Pu-241	Cm-245	6.2×10^{-1}	4.8×10^{-1}	9.6×10^{-1}
	Pu-239	2.6×10^{-12}	1.1×10^{-12}	7.2×10^{-10}	Pu-242	Am-242m	8.3×10^{-6}	5.4×10^{-6}	1.1×10^{-4}
	Am-243	7.8×10^{-16}	2.7×10^{-16}	2.5×10^{-12}	Ra-226	Th-230	1.1×10^{-2}	7.2×10^{-3}	1.0×10^{-1}
Am-241	Pu-241	5.3×10^{-2}	3.0×10^{-2}	5.4×10^{-1}		U-234	1.7×10^{-6}	8.3×10^{-7}	1.6×10^{-4}
	Cm-245	1.9×10^{-2}	1.0×10^{-2}	2.9×10^{-1}		Pu-238	6.5×10^{-11}	2.5×10^{-11}	1.2×10^{-7}
Nb-93m	Mo-93	5.2×10^{-1}	4.0×10^{-1}	8.4×10^{-1}		U-238	5.8×10^{-11}	2.3×10^{-11}	5.6×10^{-8}
	Zr-93	5.7×10^{-1}	4.4×10^{-1}	9.3×10^{-1}		Am-242m	3.9×10^{-12}	1.3×10^{-12}	4.0×10^{-8}
Np-237	Am-241	8.2×10^{-6}	5.4×10^{-6}	9.2×10^{-5}	Th-229	U-233	2.4×10^{-3}	1.6×10^{-3}	2.3×10^{-2}
	Pu-241	3.4×10^{-7}	1.4×10^{-7}	4.7×10^{-5}		Np-237	1.7×10^{-7}	8.6×10^{-8}	1.7×10^{-5}
	Cm-245	8.5×10^{-8}	3.6×10^{-8}	1.6×10^{-5}		Am-241	7.1×10^{-13}	2.8×10^{-13}	8.6×10^{-10}
Pa-231	U-235	5.3×10^{-4}	3.5×10^{-4}	5.3×10^{-3}		Pu-241	2.0×10^{-14}	5.2×10^{-15}	4.1×10^{-10}
	Pu-239	8.7×10^{-12}	4.3×10^{-12}	8.7×10^{-10}		Cm-245	3.3×10^{-15}	9.7×10^{-16}	8.1×10^{-11}
	Am-243	3.1×10^{-15}	1.3×10^{-15}	3.1×10^{-12}	Th-230	U-234	2.3×10^{-4}	1.5×10^{-4}	2.3×10^{-3}
Pb-210	Ra-226	5.0×10^{-1}	3.7×10^{-1}	9.4×10^{-1}		Pu-238	1.2×10^{-8}	5.7×10^{-9}	2.0×10^{-6}
	Th-230	4.0×10^{-3}	2.1×10^{-3}	8.9×10^{-2}		U-238	1.1×10^{-8}	5.4×10^{-9}	1.1×10^{-6}
	U-234	4.9×10^{-7}	2.0×10^{-7}	1.3×10^{-4}		Am-242m	8.8×10^{-10}	3.5×10^{-10}	8.0×10^{-7}
	Pu-238	1.6×10^{-11}	5.3×10^{-12}	9.8×10^{-8}	U-233	Np-237	1.1×10^{-4}	7.3×10^{-5}	1.1×10^{-3}
	U-238	1.4×10^{-11}	5.0×10^{-12}	4.4×10^{-8}		Am-241	6.0×10^{-10}	3.0×10^{-10}	7.1×10^{-8}
	Am-242m	8.3×10^{-13}	2.4×10^{-13}	3.1×10^{-8}		Pu-241	2.0×10^{-11}	6.3×10^{-12}	3.5×10^{-8}
Po-210	Pb-210	1.0×10^{-0}	9.8×10^{-1}	1.0×10^{-0}		Cm-245	4.0×10^{-12}	1.4×10^{-12}	8.8×10^{-9}
	Ra-226	4.9×10^{-1}	3.6×10^{-1}	9.4×10^{-1}	U-234	Pu-238	7.5×10^{-5}	4.9×10^{-5}	1.1×10^{-3}
	Th-230	3.8×10^{-3}	2.0×10^{-3}	8.9×10^{-2}		U-238	7.1×10^{-5}	4.7×10^{-5}	7.1×10^{-4}
	U-234	4.7×10^{-7}	1.9×10^{-7}	1.3×10^{-4}		Am-242m	7.4×10^{-6}	3.7×10^{-6}	5.4×10^{-4}
	Pu-238	1.5×10^{-11}	5.0×10^{-12}	9.7×10^{-8}	U-235	Pu-239	2.5×10^{-8}	1.6×10^{-8}	2.5×10^{-7}
	U-238	1.4×10^{-11}	4.7×10^{-12}	4.4×10^{-8}		Am-243	1.2×10^{-11}	5.9×10^{-12}	1.2×10^{-9}
	Am-242m	7.8×10^{-13}	2.2×10^{-13}	3.1×10^{-8}	U-236	Pu-240	7.4×10^{-7}	5.0×10^{-7}	7.5×10^{-6}
Pu-238	Am-242m	1.5×10^{-1}	1.0×10^{-1}	7.3×10^{-1}		Cm-244	1.9×10^{-9}	8.0×10^{-10}	3.5×10^{-7}
Pu-239	Am-243	7.2×10^{-4}	4.8×10^{-4}	7.2×10^{-3}					

8.2.3 Chlorine-specific parameters

Concentration ratio for mire vegetation

Since SR-PSU, the chlorine (Cl) content in terrestrial vegetation and organic soils have been determined for two mire and four wetland forest ecosystems in Forsmark (Svensson et al. 2021). In accordance with previous SKB methodology, green vegetation samples are subdivided into four functional groups (Table 8-3). The Cl content in dry weight was converted to carbon units using a generic factor of 0.42 gC gdw^{-1} (Grolander 2013). In the PSAR, these new site data are combined with previously collected samples from six forest ecosystems (Hannu and Karlsson 2006, Engdahl et al. 2006, both used in Grolander 2013) to determine the concentration ratios (CR) for mire vegetation: *CR_ter_pp* [Cl] (kgdw kgC^{-1}).

For each location, the mean concentration for a functional group, or for the top soil layer, is calculated from all available samples (Table 8-3). The two mire ecosystems were both sampled at two locations within a mire, and samples from these locations are considered as independent in the calculations of CR. This is a reasonable assumption as the locations were more than 100 m apart, and it can be viewed as giving twice as much weight to samples from the most representative habitats (i.e. fens as opposed to different types of forests).

Table 8-3. Cl concentrations for vegetation and soil samples. The values represent the geometric means of all relevant samples collected at each location. 1 = Svensson et al. (2021), 2 = Hannu and Karlsson (2006), 3 = Engdahl et al. (2006). FM = Forsmark, LX = Laxemar.

Ecosystem	Site	Location	Upper regolith (mg kgC^{-1})	Bottom layer (mg kgC^{-1})	Field layer (mg kgC^{-1})	Shrub layer (mg kgC^{-1})	Tree layer (mg kgC^{-1})
Moderately rich fen[1]	FM	AFM001389 N	1.1×10^{3}	3.5×10^{3}	9.9×10^{3}		
Moderately rich fen[1]	FM	AFM001389 S	7.4×10^{2}	3.5×10^{3}	8.1×10^{3}		
Poor fen[1]	FM	AFM001385 W	4.0×10^{2}	1.6×10^{3}	3.2×10^{3}	1.5×10^{3}	
Poor fen[1]	FM	AFM001385 E	3.0×10^{2}	1.9×10^{3}	1.3×10^{3}	1.5×10^{3}	
Alder spruce swamp forest[1,2]	FM	AFM001076	1.4×10^{2}	3.7×10^{3}	4.7×10^{4}	3.5×10^{4}	4.0×10^{3}
Norway spruce forest[2]	FM	AFM001068	8.6×10^{1}	8.6×10^{3}	8.5×10^{4}	9.8×10^{3}	1.1×10^{4}
Norway spruce forest[2]	FM	AFM001247	2.2×10^{2}	1.8×10^{3}	6.9×10^{4}	2.4×10^{4}	1.9×10^{4}
Oak forest[3]	LX	ASM001426	9.1×10^{1}	3.2×10^{2}	5.6×10^{3}	4.7×10^{2}	2.9×10^{2}
Alder shore forest[3]	LX	ASM001434	4.3×10^{3}	4.7×10^{3}	7.8×10^{3}		9.1×10^{2}
Norway spruce forest[1]	LX	ASM001440	1.2×10^{2}	5.2×10^{2}	4.5×10^{3}		7.7×10^{2}

To examine to what extent the site and the plant functional group affect the chloride concentrations, and to estimate an appropriate CR-value for mire vegetation in Forsmark, the collected data was analysed with the following mixed model:

$$y = Site + Type + Group(Type) + Site \times Type + Site \times Group(Type) + Location$$

In the model, Cl concentration is the dependent variable (y), and *Site* [Forsmark, Laxemar], *Type* [Regolith, Plant], and *Group*[Bottom, Field, Shrub, Tree] are fixed categorical factors. *Location* [AFM001389 N, …, ASM001440] links together all the samples from a location, and it is treated as a random factor. The analysis was carried out on a logarithmic scale, which resulted in approximately normally distributed residuals.

The results show that the Cl concentrations are significantly different between functional groups ($p_{Group} = 0.015$, Figure 8-2). That is, the Cl concentration in the field layer is approximately twice as high as in the shrub and tree layers, and considerably (i.e. a factor of five) higher than in the bottom layer. Moreover, these differences are consistent across the two examined sites ($p_{Site\times Group} = 0.45$), even though there is a clear difference in the CR values between the sites, as indicated by a significant interaction between site and type ($p_{Site\times Type} = 0.037$) (Figure 8-2).

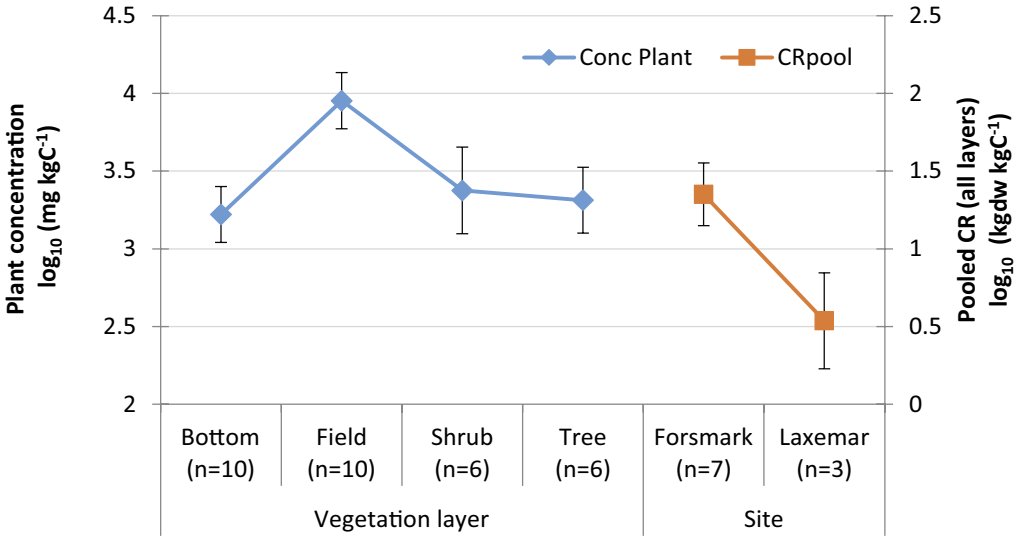

Figure 8-2. *Plant chlorine concentrations and pooled CR-values derived from 42 plant and soil samples collected at a total of 10 locations in Forsmark and Laxemar. Blue diamonds represent least square means across both sites. Red squares represent the difference in the ratio of plant and regolith concentrations at each site. Error bars represent the standard error.*

The wetlands that are influenced by discharge of deep groundwater are considered to be in the fen stage. In this stage, grasses and sedges dominate the primary production, and thus, samples from the field vegetation are considered to be the most appropriate for representing terrestrial primary producers on future mires. As this group also has the highest concentrations of Cl (and consequently the highest CR) this choice is also considered to be cautious with respect to consumption of food collected on the mire (including mushrooms), and for the pathway where wetland hay is used as fodder for domestic animals.

Thus, the CR-value is estimated on a logarithmic scale, and as the average difference in Cl concentration between the field-layer and soil in Forsmark locations (which equals ~1.6). The random stochastic variation is estimated from the residual variation for the full data set (n = 42.). The variation for CR equals the variation of a difference (between the field-layer and soil), which is two times the stochastic variation (σ^2_{error} = 0.2). Note that the variation caused by the location $\sigma^2_{Location}$ cancels out when CR is calculated from paired samples. (In the mixed model this is evident, as the Location term is shared by all plant and soil samples in a location.) After back-transformation, the geometric mean for *cR_ter pp* [Cl] equals 45 kgdw kgC^{-1}, and the geometric standard deviation equals 4.4. The minimum and maximum values correspond to the 5 % and 95 % confidence limits of the log-normal distribution, which equals to 4 and 508 kgdw kgC^{-1}, respectively. As in SR-PSU, these values are also used for fodder production on a drained mire (*cR_agri_fodder*) and for Cl uptake by mushrooms (*cR_ter_mush*) (Grolander 2013).

The fraction of inorganic chlorine in mire vegetation

In SR-PSU, the rate of radionuclide release through fast mineralisation of litter was described by the rate of carbon loss and an element-specific discrimination factor (*df_decomp_ter*). For Cl, this factor was treated as a parameter and calculated from the partitioning of radionuclides between organic and inorganic forms in the plants[39]. Following the development in SE-SFL, this calculation has been incorporated as a function in the BioTEx model, and consequently a parameter describing the inorganic content in mire vegetation (*f_inorg_Cl_PP_ter*, unitless) is needed in the PSAR.

As with the CR chlorine parameters, the new field layer data from mire and wetland ecosystems from Forsmark (Svensson et al. 2021) were used. For each location, the mean concentration for the field layer was calculated from all available samples. As with the CR values, the two mire ecosystems are represented by two sampling locations each, which resulted in a total of nine independent samples. As the parameter represents a fraction, which is constrained to be between 0 and 1, a probit distribution is an appropriate representation. Thus, the data were probit-transformed, and the characteristics of the PDF are expressed on the probit-scale. That is, the mean and standard deviation for the parameter *probit_f_inorg_Cl_PP_ter* are 2.45 and 0.25 (unitless), respectively. The minimum and maximum values are set to the 5 % and 95 % confidence limits of the normal distribution (on the probit scale), yielding minimum and maximum and values of 2.0 and 2.9, respectively. This corresponds to a mean fraction of inorganic Cl of 99.3 % with a confidence interval between 97.9 % and 99.8 %.

No specific data have been collected from aquatic primary producers in Forsmark. Instead, the range from terrestrial vegetation (Svensson et al. 2021) is used to set a range of possible fractions of inorganic chlorine in aquatic primary producers (*f_inorg_Cl_PP_aqu*). Thus, the minimum value is taken to be 76 %, corresponding to bryophytes in the bottom layer (mean from eight locations), and the maximum value is taken to be 99 %, corresponding to vascular plants in the field vegetation (taken from above). In accordance with the lack of data, the PDF was set to be uniform, and the central ('best estimate') value was set to the mid-range value of 87 %.

[39] df_decomp = f_org + f_inorg/(1-f_refrac), where f_org and f_inorg are the fractions of a radionuclide in organic matter and inorganic form respectively, and f_refrac is the fraction of refractory organic matter in litter (which is left after initial mineralisation) (Section 9.6.3 in Grolander 2013). Note that by definition f_org + f_inorg = 1, and thus, only one of the fractions needs to be included as a parameter.

8.2.4 Hydrological parameters

Surface and groundwater flow under temperate conditions

The parameterization of regolith flux parameters for the PSAR uses the same methodology as in SR-PSU with a few minor changes. Area-specific fluxes through the regolith were calculated using MIKE SHE water balance components (Section 7.6 in Werner et al. 2013). Vertical upward and downward fluxes across the bedrock–regolith boundary (*q_bedrock_low* and *q_low_bedrock*) were calculated using linear interpolation between the water balance flux components from above and below the boundary. This was done for each stage/ecosystem (see Figure 5-8 for an illustration and Appendix F for the derived parameter values).

The MIKE SHE water balances were also used to parameterize the fluxes between the different regolith layers. For the PSAR, the discretisation of the two lowest regolith layers has been increased from one compartment, as was used for SR-PSU, to five sub-compartments (Chapter 7). Linear interpolation between the modelled fluxes at the upper and lower boundaries of the regolith layers was used within the BioTEx model to parameterize the fluxes of these compartments.

In the *base case* of the PSAR, a stream drains the mire ecosystem in object 157_2 (Figure 9-3). Consequently, hydrological parameters for object 157_2 were derived from the 5000 AD water balance for object 157_2 that has a stream (Figure A1-56 in Werner et al. 2013). As the differences in flow components between 5000 AD and 11 000 AD were marginal in the original water balances (Werner et al. 2013, Figures A1-42, 49), the conditions for 5000 AD with a stream are considered to be a reasonable approximation also for the later points in time.

Object 157_2 lacks a pronounced lake stage, and thus, the area-specific flows below the stream are assumed to be similar to those under the mire. In the BioTEx model, the geosphere release is distributed in proportion to the area of the terrestrial and aquatic ecosystems, respectively. As the stream makes up only a tiny part of the object (< 1 %), the release of radionuclides to the stream from below is marginal in the modelling. This implies that the groundwater flow parameters beneath the stream have little or no bearing on the calculated stream water concentrations. Thus, approximating the flows under the stream with those under the mire is an adequate handling. Consequences of radically different assumptions, namely, that all of the geosphere release reaches the stream water directly, without passing through any regolith layers (minimising retention and degassing), are examined in the alternative landscape configuration calculation case (Section 10.6).

Percolation from unsaturated soils

Percolation is the net downward flux from unsaturated cultivated soil to the saturated zone. In SR-PSU, percolation was derived from hydrological modelling using the runoff term at landscape scale from SR-Site MIKE-SHE simulations (Bosson et al. 2010). In the PSAR, the best estimate for *percolation_agri*, 0.174 m a^{-1}, corresponds to the runoff from similar simulations carried out in SR-PSU (Werner et al. 2013, Table 5-1). The estimate reflects runoff from the landscape above the repository for present climate conditions at 5000 AD, when all biosphere objects have emerged from the sea (referred to as the local model area in Werner et al. 2013). The minimum value, 0.15 m a^{-1}, corresponds to the site description of Forsmark, and is based on the meteorological and hydrological monitoring programme (Johansson 2008, Section 3.3.3). The maximum value, 0.20 m a^{-1}, corresponds to simulated runoff for a later development stage without lakes (11 000 AD, Table 5-1 in Werner et al. 2013) and is similar to the best estimate used in SR-PSU. The probability density function is selected to be uniform between the minimum and the maximum values.

The fraction of a potential release reaching a drilled well

The parameter *f_well* describes the fraction of a potential release from the repository that may reach a water-supply well drilled into the bedrock in the *well interaction area* (see Section 5.6).

In SR-PSU, a number of theoretical wells were placed within this area and modelled using DarcyTools. Particle tracing studies were used to estimate how the wells would affect radionuclide transport. Starting positions for the particles were placed within the individual vaults of both SFR1 and SFR3 (Figure 1-2 in Chapter 1). For each hypothetical well position, modelling results were examined as a ratio of the total number of vault-specific particles captured normalized by the total number of particles

released for that specific vault (*f_well*) or the "well fraction". For all wells capturing particles released from SFR1, the average particle-capture ratio per facility part is 5.61 % (the average ratio per well is 6.75 %), whereas the corresponding ratio for SFR3 is 3.56 % (the average ratio per well is 3.43 %) (Werner et al. 2013). For SR-PSU, a well fraction of 10 % was used for the analyses as a cautious high estimate. For the PSAR, the results of these particle tracing studies are still used, but the data have been reanalysed in order to allow for a probabilistic handling of the uncertainty surrounding the potential position of the well.

According to the modelled results, the well fraction does not vary independent of the well position, i.e. different wells receive more or fewer particles from multiple waste vaults depending on the position of the well (Werner et al. 2013, Appendix 3). To capture this co-variation structure, the data are described with a mixed linear model. In the statistical model, the well fraction is treated as an independent variable, the waste vault (i.e. particle starting position) is treated as a fixed categorical factor and the hypothetical well position is treated as a random variable. As fractions are constrained between 0 and 1, the data are probit-transformed prior to the analysis, and zeros are cautiously treated as missing values.

The analysis shows that the difference in well fraction between waste vaults is limited (column "Mean" in Table 8-4). However, to account for the relatively large fraction from the silo, which could potentially affect the future dose, β_{wellfrac} is estimated individually for each vault. Thus, the typical well fraction is estimated for each waste vault by its least square mean (on the probit scale). Approximately 25 % of the variation in well fraction can be explained by the well position which is shared by all waste vaults ($\sigma^2_{wellpos}$).

In the probabilistic simulations with BioTeX, this structure is captured by drawing random numbers for each of the waste vaults (with separate means and variation σ^2_{res}), and then adding the random effects of the well position (with mean 0 and variation $\sigma^2_{wellpos}$):

$$Probit\left(f_{well_i}\right) = \beta_{wellfrac_i} + \beta_{posWell},$$

$$f_{well_i} = \Phi\left(\beta_{wellfrac_i} + \beta_{posWell}\right),$$

$$i = \{1BTF, 2BTF, \ldots, 1BRT\},$$

where the parameters associated with β are described in Table 8-4, and Φ stands for the cumulative normal distribution function. The uncertainty is modelled on the probit-scale and thus the function needs to be back-transformed. The expected values from such simulations tend to yield higher values than the arithmetic means of the original raw data. This is expected as fractions of zero are cautiously disregarded when the structure of the data is modelled.

Table 8-4. Parameters (β_{wellfrac}, $\beta_{posWell}$) used to calculate the fraction of a potential release that reaches a well drilled in the well interaction area in probabilistic simulations. The expected well fraction (see the text) for each waste vault, as determined from simulations (n = 1 000), is shown for reference (right-most column).

Name	Repository	Mean	Std dev	Exp($f_{\text{well\_int}}$)
β_{wellfrac}	1BTF	−2.01	0.83	7.3 %
	2BTF	−2.43	0.83	4.0 %
	1BLA	−2.21	0.83	5.3 %
	1BMA	−2.26	0.83	4.9 %
	Silo	−1.81	0.83	9.6 %
	2BLA	−2.17	0.83	5.3 %
	3BLA	−2.26	0.83	5.1 %
	4BLA	−2.35	0.83	4.7 %
	5BLA	−2.33	0.83	4.5 %
	2BMA	−2.32	0.83	4.9 %
	1BRT	−2.49	0.83	3.4 %
	All	−2.24	0.83	5.4 %
$\beta_{posWell}$		0	0.49	NA

8.3 Description of updated BioTEx parameters in warm and cold calculation cases

While most parameters in the *base case* (Section 8.2) are applicable also to the calculation cases describing and warmer and colder climates (Sections 10.2 and 10.3, respectively), some of the parameters are specific to these cases. As compared with SR-PSU, a few new parameters are introduced in the PSAR, and the values of a few parameters in the warm and cold calculation cases are updated (Table 8-5). These changes in are explained in detail in Sections 8.3.1 and 8.3.2.

Table 8-5. Overview of parameter changes in the warm and cold climate calculation cases since SR-PSU. Parameters that are new in the PSAR are highlighted in bold. Updates in parameter values and parameter names are also listed in the table. GP = garden plot, DM = dried mire, IO = infield-outland, Cl = chlorine.

Parameter	Category	Change since SR-PSU	Comment
Warm climate calculation case			
amount_irrig (GP, **DM**, **IO**)	Terrestrial	See 8.3.1 for updated value for GP, and definition for DM and IO.	
biom_pp_ter	Terrestrial	See 8.3.1 for updated value	
conc_C_atmos	Terrestrial/Aquatic	See 8.3.1 for updated value	
f_trans_cereal (DM, IO)	Terrestrial	See 8.3.1 for definition	
N_irrig (GP, **DM**, **IO**)	Terrestrial	See 8.3.1 for updated value for GP, and definition for DM and IO.	
NPP_cereal, fodder, tuber, veg (GP, DM, IO)	Terrestrial	See 8.3.1 for updated value	
percolation_agri (GP, DM, IO)	Terrestrial	See 8.3.1 for updated value for GP, and definition for DM and IO.	
q_bedrock_low, q_low_bedrock (objects 157_1, 157_2, 116)	Hydrological	See 8.2.5 for definition and Appendix F for values	
q_downstream (objects 157_1, 157_2, 116)	Hydrological	See Appendix F for updated values	
q_rego_k_rego_j_eco_i (objects 157_1, 157_2, 116)	Hydrological	See Appendix F for updated values	k, j are adjacent regolith layers {Low, GL, PG, Up, Water} eco_i = lake/stream
q_rego_k_rego_j_eco_i (objects 157_1, 157_2, 116)	Hydrological	See Appendix F for updated values	k, j are adjacent regolith layers {Low, GL, PG, Peat, Up, Water} eco_i[40] = ter_iso/ter_end
q_sat_unsat_agri (DM)	Terrestrial	Name change, see 8.3.1 for updated values	Replaces Flux_water_sat-Soil_agri (DM)
time_irrigationPeriod (GP, **DM**, **IO**)	Terrestrial	See 8.3.1 for updated value for GP, and definition for DM	
washoffCoef_fodder (DM)	Terrestrial	See 8.3.1 for definition	
yield_cereal, fodder, tuber, veg (GP, DN, IO)	Terrestrial	Name change, see 8.3.1 for updated value	Replaces biom_cereal, fodder, tuber, veg
Cold climate calculation case			
conc_C_atmos	Terrestrial/Aquatic	See 8.3.1 for updated value	
q_bedrock_low, q_low_bedrock (objects 157_1, 114)	Hydrological	See 8.2.4 for definition and Appendix F for values	
q_downstream (object 157_2)	Hydrological	See 8.3.2 for definition and Appendix F for updated values	
q_rego_k_rego_j_eco_i (objects 157_1, 157_2)	Hydrological	See 8.3.2 for definition (157_2) and Appendix F for updated values	k, j are adjacent regolith layers {Low, GL, PG, Up, Water} eco_i = lake/stream_perm
q_rego_k_rego_j_eco_i (objects 157_2)	Hydrological	See 8.3.2 for definition and Appendix F for updated values	k, j are adjacent regolith layers {Low, GL, PG, Peat, Up, Water} eco_i = ter_end_perm

[40] For object 157_2 parameter values with suffix iso and end are identical (derived from 5000 AD water balance).

8.3.1 New and updated parameters in the warm climate calculation case

Crop water demand

The increased water demand for vegetables and potatoes in the garden-plot household under a warmer climate is calculated with the same response used for large-scale cultivation (see above). This results in a mean amount of irrigation of 0.115 m a^{-1} in the *warm climate calculation case*, with a standard deviation of 0.040. Given the size of the garden-plot (270 m^2), and a 90-day irrigation period, this corresponds to an irrigation water demand of 350 litre per day. The minimum and maximum values are set to the 5 % and 95 % confidence limits of the corresponding normal distribution of the random variable CWD, resulting in values of 0.049 and 0.180 m a^{-1}, respectively. The corresponding values, i.e. mean, standard deviation, minimum and maximum CWD, for the variant with the dry summers are 0.154, 0.040, 0.088 and 0.220 m a^{-1}, respectively. This corresponds to an average daily water demand of 465 litre during the irrigation period.

In the *warm climate calculation case*, the concentration of stable CO_2 in the atmosphere is adjusted to an elevated level and values for ecosystem parameters, such as biomass, net primary production and crop yield are adjusted to reflect a warmer climate. Ground and surface water flows for the mire state of biosphere object 157_2 in a warmer climate have been simulated with the MIKE SHE tool. Adding large-scale irrigation as an exposure pathway to DM farming requires the definition of new parameters describing this practice. Moreover, the processes for accumulation on edible parts of crops (cereals), element translocation to edible parts (potatoes) and leaf weathering (fodder) are added to the models describing irrigated agriculture. The amount and frequency of irrigation of a garden plot are also adjusted to reflect warmer conditions. All these updates are described in this section. In SR-PSU, the values assigned to the piston velocity (*piston_vel_ter*) and leaf area index (*LAI_ter* and *LAI_cereal*) were also adjusted in a warm climate (Tables 9-8 and 9-12 in Grolander 2013). These adjustments are considered to be applicable also in the PSAR.

Concentration of carbon in the atmosphere

The total carbon concentration in the atmosphere (*conc_C_atmos*) for the *warm climate calculation case* is calculated similar to the *base case* (Section 8.2.1). However, the atmospheric CO_2 concentration is derived from the maximum concentration of the RCP4.5 greenhouse-gas emissions scenario (IPCC 2013). The average air temperature during the vegetation period is calculated taking the sum of the maximum air temperature increase, as estimated for the next 10 000 years under RCP4.5 (Section 4.2 and the **Climate report**, Section 3.4.4), with the air temperature of the normal year (Section 4.2). For the cold climate a value of 200 ppm is used. This is typical of a glacial episode during the Quaternary as determined from ice-core records spanning the last 800 000 years (**Climate report**, Section 3.1).

As the climates assumed in the warm and cold calculation cases are considered to envelope the uncertainty in the probable future climate evolution (Section 4.2), no additional uncertainties are imposed on the selected values (i.e. the parameters are treated as constants in the PSAR). The calculated concentrations are applicable to aquatic, mire and cultivated ecosystems (Table 8-6).

Table 8-6. Carbon content in the atmosphere in different calculation cases.

Calculation case	Atmos. CO_2 fraction (ppm)	Average air temperature (°C) [Vegetation period]	Carbon conc. (kgC m^{-3})
Base case	377	12.1 [April–Nov]	0.00019
Warm climate	540	13.7 [March–Dec]	0.00028
Cold climate	200	7 [June–Sept]	0.00010

Crop water demand

For the PSAR, the crop water demand (CWD) under the changed climatic conditions is calculated using global hydrological models. A multi-model approach is used for these calculations wherein three different hydrological models are used to calculate CWD with hydrometeorological data from four different climate models. All combinations of hydrological models and hydrometeorological data

are used to generate an array of outputs resulting in 12 CWD datasets. Linear models are then used to examine the variance of the outputs and generate a function for CWD (Appendix G) and estimate the change of CWD due to variations in summer temperatures and precipitation according to the two variants of the warm climate case relevant to the PSAR (Table 4-1).

Results indicate a mean water demand of 0.064 m a^{-1} for large-scale cultivation in the *warm climate calculation case*, with a standard deviation of 0.022. The minimum and maximum values are set to the 5 % and 95 % confidence limits of the corresponding normal distribution around the random variable CWD, resulting in values of 0.028 and 0.100 m a^{-1}. The corresponding values, i.e. mean, standard deviation, minimum and maximum CWD, for the variant with low summer precipitation are 0.086, 0.022, 0.050 and 0.120 m a^{-1}, respectively. In the *warm climate calculation case*, the water demand of large-scale cultivation is considered to either be fully covered by groundwater uptake from the saturated soil, *q_sat_unsat_agri,* or fully by irrigation*, amount_irrig* (Section 10.2).

The increased water demand for vegetables and potatoes in the garden-plot household under a warmer climate is calculated with the same response used for large-scale cultivation (see above). This results in a mean amount of irrigation of 0.115 m a^{-1} in the *warm climate calculation case*, with a standard deviation of 0.040. Given the size of the garden-plot (270 m^2), and a 90-day irrigation period, this corresponds to an irrigation water demand of 350 litre per day. The minimum and maximum values are set to the 5 % and 95 % confidence limits of the corresponding normal distribution of the random variable CWD, resulting in values of 0.049 and 0.180 m a^{-1}, respectively. The corresponding values, i.e. mean, standard deviation, minimum and maximum CWD, for the variant with the dry summers are 0.154, 0.040, 0.088 and 0.220 m a^{-1}, respectively. This corresponds to an average daily water demand of 465 litre during the irrigation period.

Timing of irrigation events

Large-scale irrigation was not considered in SR-PSU. However, in a warmer climate, the water demand may exceed the precipitation, and irrigation can be used to cover this deficit (see Section Crop water demand). As large-scale irrigation is considered in the two variants of the *warm climate calculation case* in the PSAR (Section 10.2), parameters describing the timing of this irrigation are required. In addition, a warm climate is considered to affect the irrigation regime of a garden plot (Grolander and Jaeschke 2019). Note that while the crop water demand is expected to be higher in the variant of the calculation case with *low summer precipitation* than in the variant with *high summer precipitation*, the timing of the irrigation is considered to be similar in both variants.

Cereals are sensitive to drought during three different life stages; germination, spike development and early seed development (Wesström and Joel 2014). In SE-SFL, it was assumed that the total crop water demand is covered by irrigation during the latter two periods of the growing season (*N_irrig* = 2) and this parameter value is considered to be applicable also in the PSAR. This is a cautious assumption, as translocation to the grain after irrigation is higher later in the growing season (see Translocation of radionuclides for cereal below). The minimum and maximum values for *N_irrig* are set to 1 and 3, reflecting irrigation in one or all of the drought-sensitive life stages (uniform distribution).

In Sweden, barley is ready for harvest approximately 49–56 days after the start of the spike development (Pedersen 2004). Accordingly, in SE-SFL the irrigation period (*time_irrigationPeriod*) was set to 60 days, and this parameter value is considered to be applicable also in the PSAR. The minimum and maximum values are set to 50 and 70 days, respectively, reflecting a 10-day shortened or prolonged span of the drought-sensitive period (uniform distribution).

In SE-SFL, a warmer climate was considered to require watering throughout the growing season for vegetables and tubers, maintaining a similar time interval between irrigation events as in the *base case*. Due to the prolonged season requiring irrigation from 40 to 90 days, the number of irrigation events was increased from four to ten. In the PSAR these assumptions originally made for the Laxemar are considered to be applicable also to Forsmark. The uncertainties in these estimates are considered to be covered by increasing or decreasing the length of the period and the number of events by 20 %. Thus, the minimum and maximum values for *time_irrigationPeriod* in the garden plot is 70 and 110 days, and the corresponding values for *N_irrig* are 8 and 12 times (uniform distributions).

Translocation of radionuclides for cereal

The translocation for tubers, which are irrigated in the present-day climate, is described above in Section 8.2.2 (Translocation of radionuclides for tubers). In a warmer climate, cereals are also considered to be irrigated, and consequently an additional parameter is needed. Colle et al. (2009) recommended separate translocation factors to cereal grain for mobile, medium mobile and non-mobile elements. However, the elemental coverage in literature data is limited. Thus, as a cautious simplification, the translocation factor for mobile elements is adopted for all elements.

For cereals the late grain growth stage (15–45 days before harvest) is selected as the most relevant life-stage (see Grolander and Jaeschke 2019 for a discussion). For this stage Colle et al. (2009) list a geometric mean for translocation factor to the grain for mobile elements being 5.2 %, with a range between 0.28 and 32 % (n = 16). Assuming that this skewed distribution can be captured by a log-normal distribution, the range between the minimum and maximum values, from a sample of 16 observations, is expected to approximately overlap with the width of a 90 % confidence interval (i.e. ± 1.65 standard deviations on a logarithmic scale). Thus, the geometric mean and the geometric standard deviation for *f_trans_cereal* used in the PSAR are 5.2 (%) and 4.2, respectively. The minimum and maximum values are set to the 5 % and 95 % confidence limits of the log-normal distribution, yielding minimum and maximum values of 0.5 and 56 %, respectively (which are systematically higher than the reported range). It can be noted that the arithmetic mean from this distribution is 6.3 %. This is similar to the empirical estimate of 6 % that was derived for Sr and Cs under Swedish conditions in the SE-SFL assessment (Grolander and Jaeschke 2019).

Wash-off coefficient for fodder

The activity of radionuclides deposited on a crop with irrigation water will decrease with time as a result of rain, wind and growth. The rate of decrease is described by a weathering half-life or a first-order rate constant that is referred to as the wash-off coefficient. This is applicable only in the *warm climate calculation case* since in the *base case* no irrigation of fodder crops is assumed. In SE-SFL, large-scale irrigation was introduced in a warm climate, and the wash-off coefficient was used to describe the fate of radionuclides intercepted by fodder (parameter *washoffCoef_fodder*; Grolander and Jaeschke 2019). In SE-SFL, the wash-off coefficient for fodder was based on studies on grass only (n = 3, IAEA 2010). However, for a more robust estimate of the potential variation, all samples available in IAEA (2010) are used (n = 8). Moreover, the probability density function is determined on the rates (rather than the weathering half-lives). This results in an arithmetic mean value of 18 a^{-1}, and a standard deviation of 6.6 a^{-1}, assuming a normal distribution. The minimum and maximum values are set to the 5 % and 95 % confidence limits of the distribution, yielding values of 7 a^{-1} and 29 a^{-1}, respectively.

Surface and groundwater flow

To derive hydrological parameters for a warmer climate, additional MIKE SHE simulations have been performed for a suite of climate conditions for the local MIKE SHE Model at 5000 AD (Sassner et al. 2022). Two of the simulations used similar external conditions as postulated in the *warm climate variant* (Section 4.1). That is, compared with the *base case* (i.e. the normal year in Werner et al. 2013), the annual average temperature increases by 5 °C (4 °C), and the potential evapotranspiration increases by 34 % (18 %) (summer response in parentheses). Moreover, in the first (warm) scenario the yearly rainfall increases by 19 % (11 %). In the second scenario (warm with dry summer) the yearly rainfall also increases (by 10 %), but the summer rainfall (June–August) decreases by 13 %.

For these MIKE SHE simulations, water balances were constructed for three biosphere objects, namely 157_2, 157_1 and 116 (Appendix F), and the water-balance components were translated to flux parameters for the BioTEx model (Werner et al. 2013, Section 7.6). A summary of the responses in hydrological parameters is presented in the *warm climate calculation case* (Chapter 10). All the individual parameters, *q_rego_k_rego_j*, for the lake/stream and the mire parts, and their values are presented in Appendix F.

The percolation from unsaturated cultivated soil is also adjusted in the two variants of *warm climate calculation case*. Thus, the best estimate for *percolation_agri* in the warm climate is set to 0.15 m a^{-1} which equals the runoff at the landscape scale (Figure A6-4). The uncertainty range is set to the same span as in the *base case*, yielding a minimum value of 0.125 m a^{-1} and maximum value of 0.175 m a^{-1} (with a uniform PDF). The corresponding values for the variant with dry summers are: 0.100 (best estimate), 0.075 (minimum), and 0.125 (maximum) m a^{-1}.

Net primary production, biomass and crop yield

In SR-PSU net primary production (NPP) and biomass in mires were considered to increase by 50 % in a considerably warmer climate compared with the present-day conditions (Section 9.3 in Grolander 2013 and references within). As the temperature increase postulated in the *warm climate calculation case* is similar to that in SR-PSU, it is considered appropriate also in the PSAR. Thus, for warm conditions the mean, minimum and maximum values for *biom_pp_ter* and *NPP_ter* are calculated by upscaling the corresponding values from the *base case* by 50 %.

In SR-PSU the net primary production of all crops was increased in a warm climate to rates presently observed in central Europe (Section 9.11 in Grolander 2013 and references within). The same approach is used in the PSAR. That is, the mean, the standard deviation, the minimum and the maximum values for *NPP* of all crops in all land-use variants are upscaled by 70 % in the *warm climate calculation case*. This is also done for the yield of vegetables and tubers produced in a garden plot (Table 8-7).

In the PSAR irrigation and translocation are considered in all agricultural systems in the *warm climate calculation case*. Thus, the yield is required to calculate the activity concentration of irrigated crops and fodder. Following the SR-PSU method, the *yield* is calculated from net primary production, accounting for threshing loss and straw yield for cereals (5 % and 40 %, respectively) and below-ground production for cereal/fodder and tubers (33 % and 150 % of above ground production, respectively) (see Section 9.11 in Grolander 2013 and references within). That is, the mean, the standard deviation, the minimum and the maximum values for the *yield* of all crops in the drained mire and infield–outland systems are calculated by down-scaling the corresponding NPP values (Table 8-7).

Table 8-7. Net primary production, biomass (*biom*) and crop yield (*yield*) values used in the warm climate calculation case. Note that the central value (best estimate) corresponds to the arithmetic mean for parameters with a normal distribution.

Ecosystem/land-use	Name	Unit	Central Value	Std. Dev.	Minimum	Maximum	Distribution
Mire	NPP_ter	kgC m^{-2} a^{-1}	0.48		0.38	0.65	uniform
	biom_pp_ter	kgC m^{-2} a^{-1}	3.45		2.25	9.00	uniform
Drained-mire	NPP_cereal	kgC m^{-2} a^{-1}	0.20	0.04	0.16	0.32	normal
	NPP_fodder	kgC m^{-2} a^{-1}	0.36	0.07	0.18	0.49	normal
	NPP_tuber	kgC m^{-2} a^{-1}	0.27	0.04	0.16	0.38	normal
	yield_cereal	kgC m^{-2} a^{-1}	0.10	0.02	0.08	0.17	normal
	yield_fodder	kgC m^{-2} a^{-1}	0.27	0.05	0.14	0.37	normal
	yield_tuber	kgC m^{-2} a^{-1}	0.16	0.03	0.09	0.23	normal
Infield–outland	NPP_cereal	kgC m^{-2} a^{-1}	0.17	0.03	0.10	0.24	normal
	yield_cereal	kgC m^{-2} a^{-1}	0.09	0.02	0.05	0.12	normal
Garden-plot	NPP_tuber	kgC m^{-2} a^{-1}	0.61	0.10	0.38	0.83	normal
	yield_tuber	kgC m^{-2} a^{-1}	0.37	0.06	0.23	0.50	normal
	NPP_veg	kgC m^{-2} a^{-1}	0.26	0.03	0.20	0.32	normal
	yield_veg	kgC m^{-2} a^{-1}	0.19	0.02	0.15	0.24	normal

8.3.2 Updated parameters in the cold climate calculation case

In SR-PSU ecosystem parameters were adjusted for periglacial conditions. For lakes these include the resuspension (*res_rate_perm*) and sedimentation rates (*sed_rate_perm*) and the production of edible fish (*prod_edib_fish_lake_perm*) and crayfish (*prod_edib_cray_lake_perm*) (Sections 4.5.1, 4.5.2, 8.10.1 and 8.10.2 in Grolander 2013). For mires the values of biomass (*biom_pp_ter_perm*) and net primary production (*NPP_ter_perm*) of vegetation, the mineralisation rate in surface peat (*minRate_*

regoUp_ter_perm), the piston velocity for gas exchange (*piston_vel_ter_perm*) and the solubility of CO_2 in porewater (*solubilityCoef_ter_perm*) were adjusted (see Table 9-2 and Sections 9.9.1, 9.4.5 and 9.4.6 in Grolander 2013). Moreover, parameters describing hydrological flows were derived for a lake and a mire above through taliks (Grolander 2013, Tables D-2 and D-3). These adjustments are considered to be applicable to the cold climate calculation case also in the PSAR. In addition, parameters describing groundwater flows across the bedrock regolith boundary, and the flow conditions in object 157_2 in periglacial conditions are derived in the PSAR, as described below.

Surface and groundwater flow under cold and glacial conditions

In SR-PSU, water-flow components were derived for two potential taliks (see Sections 4.3 and 4.5.3) in a future permafrost landscape. These two taliks represent a lake (object 114) and a mire (object 157_1) (see Section 5.4). The hydrological modelling of the taliks is described in Werner et al. (2013) and hydrological parameters for the two taliks in the BioTEx model are presented in Grolander (2013). The flows across the bedrock-till boundary for the two taliks are calculated in the PSAR.

Biosphere object 157_2 is assumed to be frozen during the periglacial periods. In SR-PSU, the upper peat layer (RegoUp) was used to represent the active layer (~0.3 m). In the PSAR, the active layer is expanded to also include the layers of deep peat (RegoPeat), post glacial clay-gyttja (RegoPG) and glacial clay (RegoPG). Together these three layers have an average thickness of 0.65 m, and the profile thus agrees well with the assumptions used in detailed hydrological modelling (an active layer of 1 m, Section 5.8 in Werner et al. 2013). A conceptual water balance model is used to compute hydrological flows in the regolith profile of the active layer in object 157_2 (Section 7.5.5) as described below. As in temperate conditions, the area flows below the stream are assumed to be similar to those under the mire[41].

First, the parameters describing percolation ($\beta_{percol,ter}$, δ_{percol}) are derived from the temperate water balance of object 157_2 (for details and the resulting parameter values, see Chapter 5 in Grolander and Jaeschke 2019, and Table 11-2, respectively). Next, the net precipitation in the object and runoff in the local catchment are increased to 0.217 m a^{-1} to reflect a colder climate (Table 5-3 in Werner et al. 2013) and the groundwater discharge from the bedrock is considered to be blocked (i.e. set to 0) by permafrost in object 157_2. Then, features from the water balance of the mire talik (157_1) are used to adjust the pathways of runoff and percolation in object 157_2 as follows: The fraction of surface runoff ($f_{disch,surf}$) is set to 0.9, reflecting that 90 % of runoff from the local catchment is in the form of surface runoff. The parameter describing the vertical distribution of below-ground runoff ($\delta_{discharge}$) is set to 25 (m^{-1}), reflecting that more than 98 % of the sub-surface runoff reaches object 157_2 in the upper 0.2 m[42]. Surface runoff is not considered to contribute to the percolation, but 10 % of the net precipitation falling on the object is set to contribute to it ($f_{surfperc,obj}$). With these settings, the upward flows in each regolith layer are then calculated from the water balance in each regolith compartment. All the resulting parameter values for *q_rego_k_rego_j* are presented in Appendix F, Table F-2.

8.4 Description of data selection and changes in concentration ratio values for non-human biota

Concentration ratio (CR) values for the non-human biota (NHB) are needed for calculating the exposures of non-human biota to ionising radiation from radionuclide releases originating from SFR (for the calculations, see Chapter 12). These parameter values are calculated using site data when available, and literature data when the site data are lacking. This has been the practice since the SR-Site assessment (Jaeschke et al. 2013). All NHB CR values have been thoroughly revised since SR-PSU due to significant increases in the Wildlife Transfer Database (WTD) that is used as literature data for these parameters. The reference organisms defined in the ERICA tool are used to represent the species at the Forsmark site (Section 6.3.1), and the selection of representative organisms is described in

[41] This also includes the groundwater flows under the stream in the mire talik 157_1.

[42] The discharge in the upper 0.2 m horizon is derived by integration of the function describing how the discharge decreases with depth from 0 to 0.2 m (Grolander and Jaeschke 2019, Section 5.5.2). After normalising with the total discharge, the expression of the fractional discharge in the upper 0.2 m becomes $(1-e^{0.2\ \delta discharge})$.

more detail in Chapter 12. Limnic reptiles have been added as a representative organism in the PSAR assessment. The site-specific CR values are the same as used in SR-PSU and are presented in Tröjbom et al. (2013), Section 3.1. In connection with the updating of the values for NHB CR parameters, also dose conversion coefficients (DCC) and occupancy factors (OCC) of the reference and representative organisms were updated due to the additions mentioned above and the updates of the ERICA tool (see Chapter 12, Appendices D and E). For NHB CR values, geometric mean (GM) and geometric standard deviation (GSD) are used in the PSAR.

8.4.1 Availability and selection of literature data for parameterisation

Since SR-PSU, an extensive update of the CR data in the WTD has been made available. The WTD is a joint effort by the International Commission on Radiological Protection (ICRP) and the International Atomic Energy Agency (IAEA) to create a database where CR values for wildlife are collected for assessments of radiological safety of the environment. The WTD consists of two data tables; one table where CR values are derived for the reference animals and plants defined by ICRP, and a second table by IAEA, where data for several generic wildlife types are reported. Both of these tables are derived using data from the same underlying sources. The database tables are updated continually when new data are made available. During the parameterisation of CR values for SR-PSU both of the tables were available at the WTD website (Tröjbom et al. 2013). However, only the ICRP Summary table was officially reported (ICRP 2009) and for this reason only ICRP data were included in the SR-PSU assessment.

The updates to WTD since SR-PSU include an addition of 17 000 new CR values (samples) (Brown et al. 2016), which translates into an addition of 239 and over 300 CR cases (organisms) to the ICRP and IAEA Summary tables, respectively. Updated versions of these two databases are available at wildlifetransfer.org and are also uploaded to SVN (see Section 8.5). As neither of these tables are reported in any publication, they are here referred to as WTD ICRP 2015 (ICRP 2015) and WTD IAEA 2015 (IAEA 2015). The CR data for general wildlife groups from the IAEA Summary table were also used to update the database within ERICA Tool, version 1.2. The ERICA Tool 1.2 update includes a simplified and revised method for extrapolating CR values when empirical data are lacking. The previous methods for deriving CR values for the ERICA Tool has been proven to lead to both underestimated and overestimated CR and also environmental media screening concentration levels (EMCLs) (Brown et al. 2013). The recommendation therefor is now to use CR values for “similar reference organisms” instead of similar taxonomy was also added and it is advised against the use of CR values for freshwater organisms as parameter analogues for marine organisms and vice versa (Brown et al. 2013).

For most organisms, data are available only for a limited number of elements. For limnic biota updated data are reported in the WTD for several of the organisms of interest; birds, crustaceans, fish, insects, macroalgae, mammals, molluscs, phytoplankton, zooplankton and vascular plants. For several of these biota types, data were previously available only for a few of the elements of interest, and literature data are still missing for many organism/element pairs. For marine biota updated data are available for fish, molluscs, birds, crustaceans, mammals, polychaete worms, macroalgae, plankton and zooplankton. For terrestrial organisms, updated data include values for birds, detritus and soil invertebrates, reptiles, flying insects, mammals, grasses, shrubs, trees and bryophytes. No new data were available for limnic or terrestrial amphibians and data for gastropods for both environments are missing.

In the PSAR, the WTD IAEA 2015 (IAEA 2015) data were selected for sense checks of the site-specific values and, in the case of missing site data, for selecting the parameter values, with the exception of two cases; for the flying insects no appropriate data were listed in the WTD IAEA 2015 (IAEA 2015) table and for the limnic gastropods there are no appropriate literature data in either of the tables. For flying insects, arachnid data were used in SR-PSU, but for the PSAR this is now substituted by data for adult bees which are included in the WTD ICRP 2015 (ICRP 2015) table as a new organism. For limnic gastropods, the ERICA version 1.2 approach is used, and mussels were selected as a parameter analogue. For the organism-element pairs missing information, element or parameter (organism) analogues, or a combination of these, are used according to the methods and assumptions described in Tröjbom et al. (2013).

8.4.2 Selection of data source per parameter

For each parameter/element case the available data sources were compared, or sense checked, to determine if there is an overlap between data from different data sources. The results from these sense checks were used when selecting data and to assess the quality of the selected data. The methods used for these sense checks are described in Section 4.5 in Tröjbom et al. (2013). In more than half (55 %) of the parameter/element cases either an element analogue (EA), a parameter analogue (PA) or a combination of both (EP) is used. For certain elements and organisms most of the parameter values are based on analogues. For elements this is the case, for example, for lanthanides and trivalent actinides that are considered to be suitable analogues for each other (Ac, Am, Cm, Eu, Ho, Nd, and Sm). For a detailed description on the selection of EAs see Section 2.7 in Tröjbom et al. (2013). For organisms, analogues were mostly used for organisms in aquatic ecosystems, such as limnic amphibians and marine birds. The selected data source for each parameter/element case, parameter and element analogues and the outcome of the sense check are summarised in Appendix E, Table E-1.

8.4.3 Changes in parameter values since SR-PSU

For all the NHB CR parameters, the values for at least some of the elements were changed. Also, one completely new parameter is included, as freshwater reptiles are now included as a representative species. All the GM and GSD values used in the PSAR are available in Table W-2 in Appendix E. After the updates, 27.6 % of GM values for NHB parameters deviate from SR-PSU values (Appendix E, Table E-2). Most of the updated values are within one order of magnitude of the old value, and the changes are concentrated to a few elements and parameters. The elements with most changes include Ag, Po, Pu and Tc and the parameters with most updates are for zooplankton in limnic environments, and terrestrial detritivorous arthropods, flying insects, mollusc gastropods and annelids. The changes for the individual parameters and elements are described in more detail in Appendix E. However, it should be noted that most of the CR values used for NHB in the PSAR are the same as used in SR-PSU, as these values are based on site-specific data that have not been updated. For a small percentage (~3 %) the change is larger than two orders of magnitude, and for a few CRs the values have changed even more. Large changes in reported CR values typically affect a limited number of elements (Po, Pu, Tc and Ag) and/or representative organisms (e.g. zooplankton, terrestrial arthropods, flying insects, molluscs and annelids). These changes are typically due to data discarded by the WTD or that previous gaps have been filled in with new data.

8.5 Quality assurance procedure

Controlled handling of data and workflow is crucial to guarantee the quality of data and model results. All data used in the PSAR have gone through a factual review by experts and a quality review step. The data used in the PSAR are stored together with relevant metadata (authorship, date of change, revision number and references) in Excel spreadsheets to facilitate input, review and quality management by modelers as well as the data suppliers (subject experts). These Excel spreadsheets are automatically read by the modelling software. To ensure that the data in supporting documents are interpreted and handled correctly, the subject experts review the excel files before the calculations are finalised. Intermediate and final versions of the Excel spreadsheets are stored in a revision control system with a central server-based data repository (SVN) using the software “Subversion” (https://subversion.apache.org/).

Each dataset has a specified delivery file on SVN. In SVN, files are version controlled which increases the traceability of data. Documentation and background material used in the parameterisation process can be stored in SVN adjacent to the delivery files. This handling simplifies data access and quality management including tracing of data.

The modeler has the responsibility for the model development and specifies the parameters, the descriptions and units. The modeler helps to create the structure of the delivery files so that the use of dependencies, categories and parameter names and units will be compatible with the model implemented in the modelling software.

A subject expert is responsible for and delivers data according to the specifications given by the modeler. The data delivery consists of three items:

1. Parameter data in the specified delivery files.
2. Text describing the data, how the data has been derived and references.
3. References and background files where calculations have been done (when applicable).

A second (independent) subject expert reviews the data in the delivery files, making sure references are correct and that the calculations are consistent with the description. The reviewer documents the review directly in the delivery file, both as a review statement and per parameter in the dedicated column of the delivery file. For the calculations in the biosphere assessment, all quality assured data files are stored in the same SVN location, and the parameter descriptions are reported in this chapter (Sections 8.2 to 8.4). Information on references and background files are also provided in the delivery files. The general format of the delivery files is described in Appendix A in Åstrand et al. (2022), and a brief description of the data files for the *base case* is given in Appendix H.

9 The *base case*

9.1 Introduction

The *base case* constitutes the basis for the radionuclide transport and dose calculations in the PSAR (**Post-closure safety report**, Section 7.4). External conditions follow from the *present-day climate variant* of the reference evolution, and thus it is assumed that present-day climate conditions prevail for the entire assessment period of 100 000 years (Section 4.1.1). Although this assumption is not realistic, per se, this case is considered to give a reasonable description of the evolution of the repository, the geosphere and the biosphere. This is due to the assessment that the Forsmark climate will likely remain temperate for the next 100 000 years if current, or higher, levels of anthropogenic greenhouse-gas emissions continue for the next few decades (Section 4.1). Hence, despite its simplicity and lack of climate evolution, the anticipated small changes of the Forsmark climate over the next 100 000 years are adequately captured by the *base case*. Physical and biological properties of the ecosystems are thus assumed to be constant throughout the assessment period, for example, no change in the average air temperatures is assumed when selecting values for ecosystem parameters.

The *base case* provides a benchmark for the post-closure safety assessment and, thus, enables straightforward evaluation of differences with respect to other calculation cases. To this end, models built for the other calculation cases typically are only described if they deviate from the *base case*, and results are compared with those for the *base case*. In addition, when analysed with a unit geosphere activity release rate, it allows for comparisons with results from the previous safety assessment SR-PSU (Appendix C). This calculation case also fulfils the regulatory requirement that an assessment of a repository's protective capability should include a case where the biosphere conditions prevailing at the time for the application will not change[43].

The potential doses to human inhabitants and the environment are evaluated by performing transport and exposure calculations for the full assessment period from 2000 to 102 000 AD. For this assessment, a probabilistic time-dependent activity release from the geosphere is used (Section 9.2).

This chapter presents the description of the *base case* from a biosphere assessment perspective (Section 9.2), including aspects such as the radionuclide releases from the geosphere, the evolution of surface conditions and potentially exposed groups and populations. In the *base case*, present-day conditions are used to characterise ecosystems (Section 3.5), including the chemical conditions of the surface environment (Section 3.4). This is also true for the surface hydrology and the bedrock hydrogeology in the initial submerged period (Section 3.3). The climate conditions and shoreline displacement of the *base case* are described under the *present-day climate variant* in Section 4.1.1. Future conditions with respect to the development of topography and regolith, of surface hydrology and ecosystem succession are broadly described in Sections 4.2, 4.3 and 4.5, respectively. In particular, the development of the landscape, including the surface geology, stratigraphy, and thickness of regolith strata and infilling of lakes, follows a deterministic description (Section 4.7). The representation of future human inhabitants reflects potential behaviour that would result in relatively high exposure (Section 6.2) and the selected potentially exposed groups are consistent with present and historical land-use in the region (Sections 3.6 and 4.6). Descriptions of the *base case* in the near-field and geosphere are presented in the **Radionuclide transport report**, Sections 5.3 to 5.5.

The outcome from analysing the *base case* with the biosphere transport and exposure model (BioTEx) is presented in this chapter (Section 9.3), together with a discussion of the results. Annual doses to different potentially exposed groups, contributions of exposure pathways, and the dynamics of radionuclide transport and accumulation throughout the regolith profile are discussed. A main objective in this section is to explore how the key patterns in environmental activity concentrations and annual doses arise from the geosphere release, radionuclide properties and mechanisms such as transport (including dilution, retention, retardation, degassing), plant uptake, radioactive decay and radiotoxicity. The discussion mainly focuses on differences in behaviour and resulting doses among selected key radionuclides for the total annual dose, with the aim to provide a general understanding

[43] SSMFS 2008:37 §10 (SSM 2008a).

to facilitate the analysis and interpretation of other calculation cases (Chapters 10 and 11). Note that this chapter addresses dose to humans and that dose rates to non-human biota, for the *base case* and other relevant calculation cases, are addressed in Chapter 12.

Furthermore, this chapter addresses the effect of uncertainties in input parameters on the probabilistically simulated annual doses (Section 9.4). At the end of the chapter, the biosphere part of the *base case* is summarised and discussed (Section 9.5).

9.2 Description of the *base case*

Geosphere activity release

In the *base case*, a time-dependent probabilistic activity release from the geosphere is used to evaluate the transport, accumulation and subsequent exposure in the biosphere (**Radionuclide transport report**, Section 5.7).

As described in Chapter 5, most of the geosphere release is likely to be discharged into biosphere object 157_2, given the reference bedrock case (BC1, Öhman and Odén 2018). Moreover, hydrogeological modelling of release locations in the landscape in 22 statistical bedrock realisations showed that more than 80 % (and in most cases more than 90 %) of the particles released from SFR would end up in the basin of biosphere object 157_2 (Figure 9-1). Moreover, less than 3 % of the released particles typically reach any other biosphere object after the submerged period (that ends at 3000 AD in this case, see below).

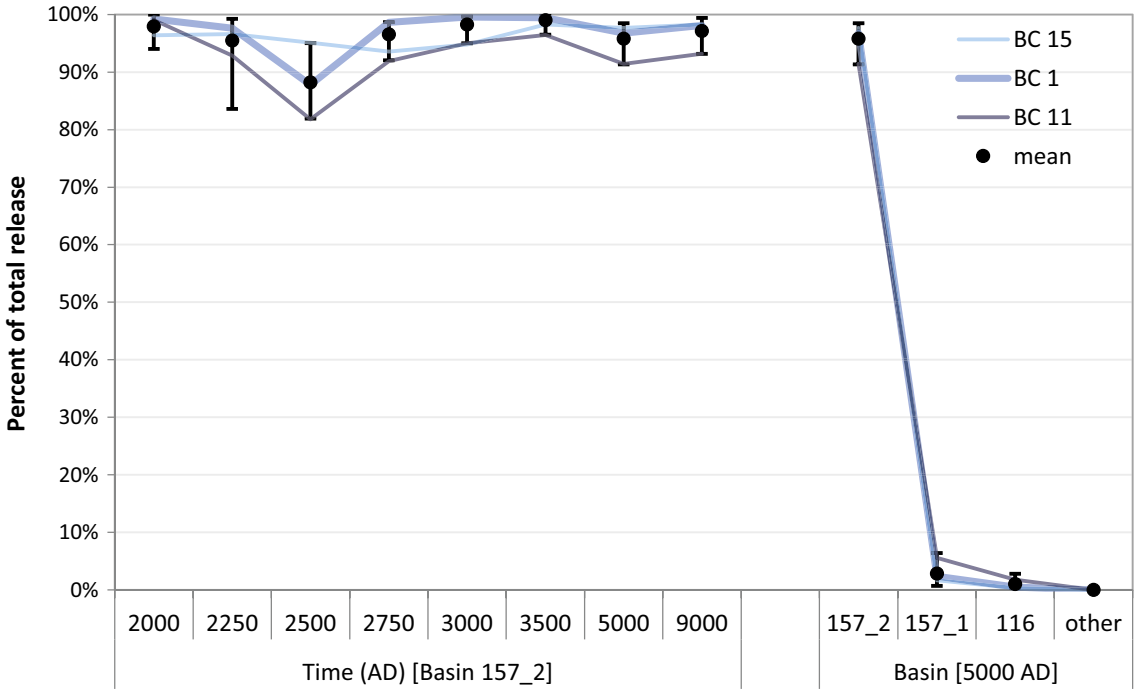

Figure 9-1. *Fractions (%) of total potential release from SFR that are discharged into the basin of biosphere object 157_2 over time (left panel) or at 5000 AD (right panel, also including other basins). The thick blue line represents the reference bedrock case (BC1), whereas the thin lines represent the other two representative bedrock cases (BC11 and BC15) according to Öhman et al. (2014). Surface positions for discharging particles are taken from Öhman and Odén (2018). Mean (black circles) and 90 % confidence interval (vertical bars) are given for the 22 bedrock cases (excluding eight cases with an assumed subhorizontal fracture in the bedrock, these are handled separately in Section 10.5).*

In the *base case*, the entire geosphere release is cautiously assumed to be discharged to biosphere object 157_2. Subsequently radionuclides are transported to other objects through water exchange or stream water (see below). The effects of a geosphere release distributed to several biosphere objects are evaluated in the *subhorizontal fracture calculation case* (Section 10.5).

Extraction of radionuclides in groundwater from wells drilled into the geosphere downstream of the repository is evaluated in the area where groundwater is expected to have the highest concentrations of radionuclides, i.e. the *well interaction area* (Section 5.5). The average fraction of the release that reaches such a well is expected to be between 3.4 % (1BRT waste vault) and 9.6 % (silo), accounting for variability due to the position of the well. This fraction is handled probabilistically, accounting for differences between waste vaults and co-variation caused by the spatial position of the well (Section 8.2.4). The concentration in the extracted well water is simply calculated by dividing this fraction of the release by the postulated water extraction rate (700 litres per day, Grolander 2013, Section 12.1.1).

Landscape description

As described in Section 4.1.1, the initial shoreline regression of the *base case* is assumed to be dominated by the isostatic rebound since the last glaciation. The gradual rise of biosphere object 157_2 and the *well interaction area* above sea level resulting from this shoreline displacement is summarised in Table 9-1. Object 157_2 is located north of SFR, currently on a gentle underwater hillslope. The deepest parts of the object are presently approximately 6 m below the sea and the shallowest (southern) parts of the object will emerge first from the sea. During the submerged period, radionuclides are expected to reach all basins in direct or indirect contact with basin 157_2, through lateral exchange of water between basins (Figure 9-2). However, during periods of fully terrestrial conditions (after ~4500 AD for object 157_2), radionuclides will only reach objects that are connected with the primary discharge area via surface runoff (Figure 9-3).

In the *base case*, the biosphere description is focused on the primary discharge area. Transport and accumulation of radionuclides in regolith layers and water bodies are described for both the marine and terrestrial periods of biosphere object 157_2. Exposure from downstream objects is also evaluated, but for these recipients, water is the only environmental transport medium considered. This simplification is reasonable under marine conditions, as aquatic pathways are the only relevant pathways for human exposure during this period. This approach is also reasonable in the terrestrial period when the transport mode between objects is flowing stream water (Saetre and Ekström 2016). The effects of assuming diffuse overland-water transport, rather than stream transport, are examined in the *alternative landscape configuration calculation case* (Section 10.6). In that case, regolith accumulation in the downstream object is explicitly represented and evaluated, as was the case in SR-PSU (SKB TR-14-06).

Table 9-1. Overview of the evolution of biosphere object 157_2 and the *well interaction area*, resulting from the initial shoreline displacement assumed in the *base case* (Section 4.1.1).

Year AD	Surface above SFR	Biosphere object 157_2	Well interaction area (WIA)
2000	Submerged	Submerged	Submerged
2500	Shoreline located directly above SFR	Submerged	Submerged
3000	> 75 % terrestrial	Highest point (southern part) above sea level*	Highest area > 1 m above sea level
3500	Terrestrial	20 % of the object above sea level, and highest point > 1 m above sea level	25 % of area > 1 m above sea level
4000	Terrestrial	90 % of the object above sea level	67 % of area > 1 m above sea level
4500	Terrestrial	Whole object > 1 m above sea level, mire fully developed.	Whole area > 1 m above sea level
5000	Terrestrial	Whole object > 1 m above sea level, mire fully developed	Whole area > 1 m above sea level

* Dug well and draining possible.

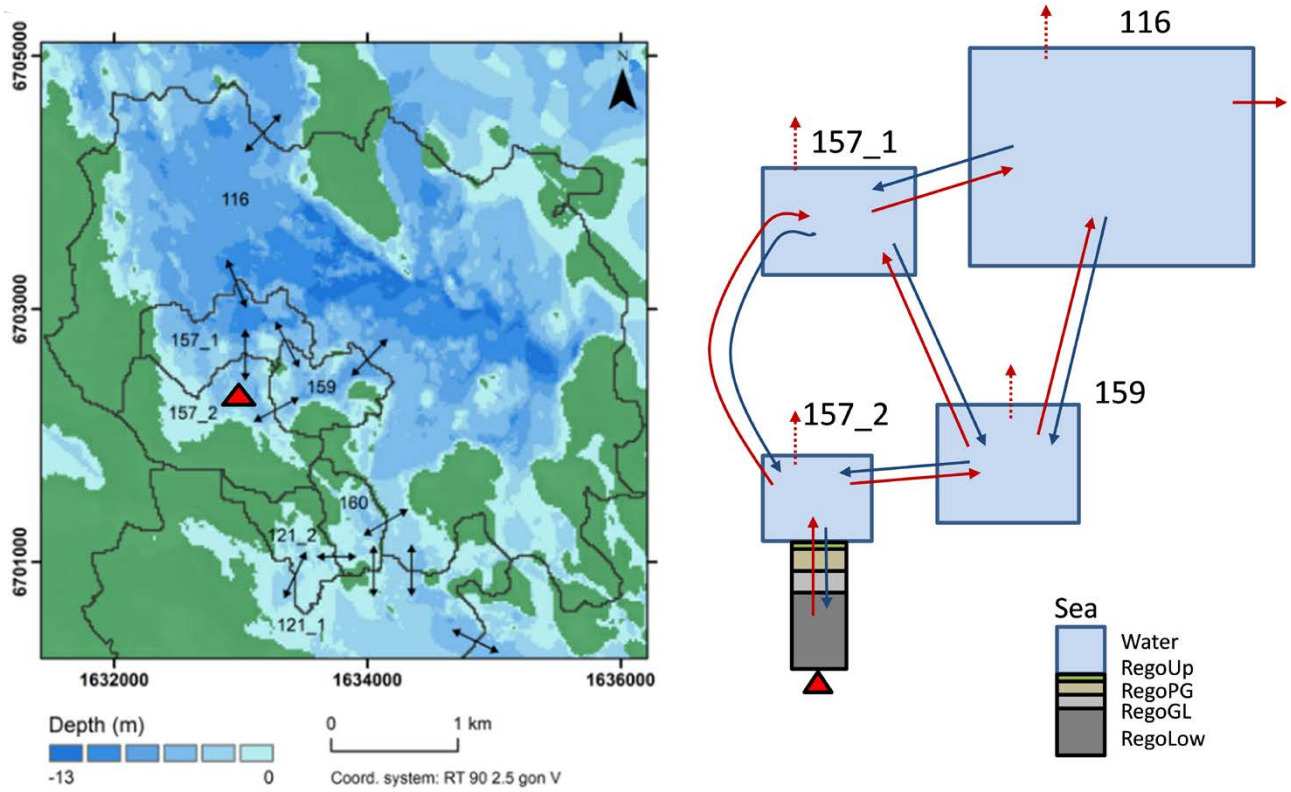

Figure 9-2. *Conceptual model of discharge and dispersion of radionuclides that reach the biosphere via groundwater from the geosphere during the marine stage. Left: water depth and dispersion routes of radionuclides between basins at 3000 AD. Biosphere object 157_2 receives radionuclide-containing groundwater from below. All biosphere objects receive radionuclides via lateral seawater flow during the marine stage. The red triangle represents the location of the geosphere release (object 157_2).* [44] *Right: schematic sketch over the dispersion of radionuclides between regolith layers and surface seawater volumes within and between biosphere objects. Red arrows show transport of radionuclides along a declining solute concentration gradient. Blue arrows show transport of radionuclides in the opposite direction. The regolith layers included are (from below); till (RegoLow), glacial clay (RegoGL), post-glacial clay-gyttja (RegoPG), biologically active surface sediments (RegoUp). The light blue boxes represent seawater. Dashed arrows represent loss of C-14 to the atmosphere. Note that the figure represents a snapshot in time and that exchange with basins south of 116 has been excluded for clarity.*

The transport and accumulation of radionuclides is simulated in a landscape that is undisturbed by humans. However, after the biosphere object has emerged sufficiently above the sea level to prevent intrusion of saline water, consequences of draining and cultivating the mire complex, and extraction of water from a dug well, are evaluated in parallel with the undisturbed development. Similarly, the effects of water extraction from a well drilled into the geosphere are evaluated when the *well interaction area* is sufficiently elevated above the sea. The threshold for cultivation and extraction of well water has been set to one metre above the prevailing sea level, approximately corresponding to the highest storm-surge levels in the area (**Climate report,** Section 3.5 and Grolander 2013, Werner et al. 2013). Given the assumed shoreline displacement in the *base case*, the upland parts of object 157_2 and the *well interaction area* will have emerged one meter above the sea level around 3200 and 3000 AD, respectively. Other land-uses that are affected by the shoreline displacement are harvesting of hay for cattle and collection of biofuels for warming (and ash fertilization). These activities are assessed as soon as the highest point of the biosphere object is elevated above the sea (~3000 AD).

[44] Detail from Figure 5-5

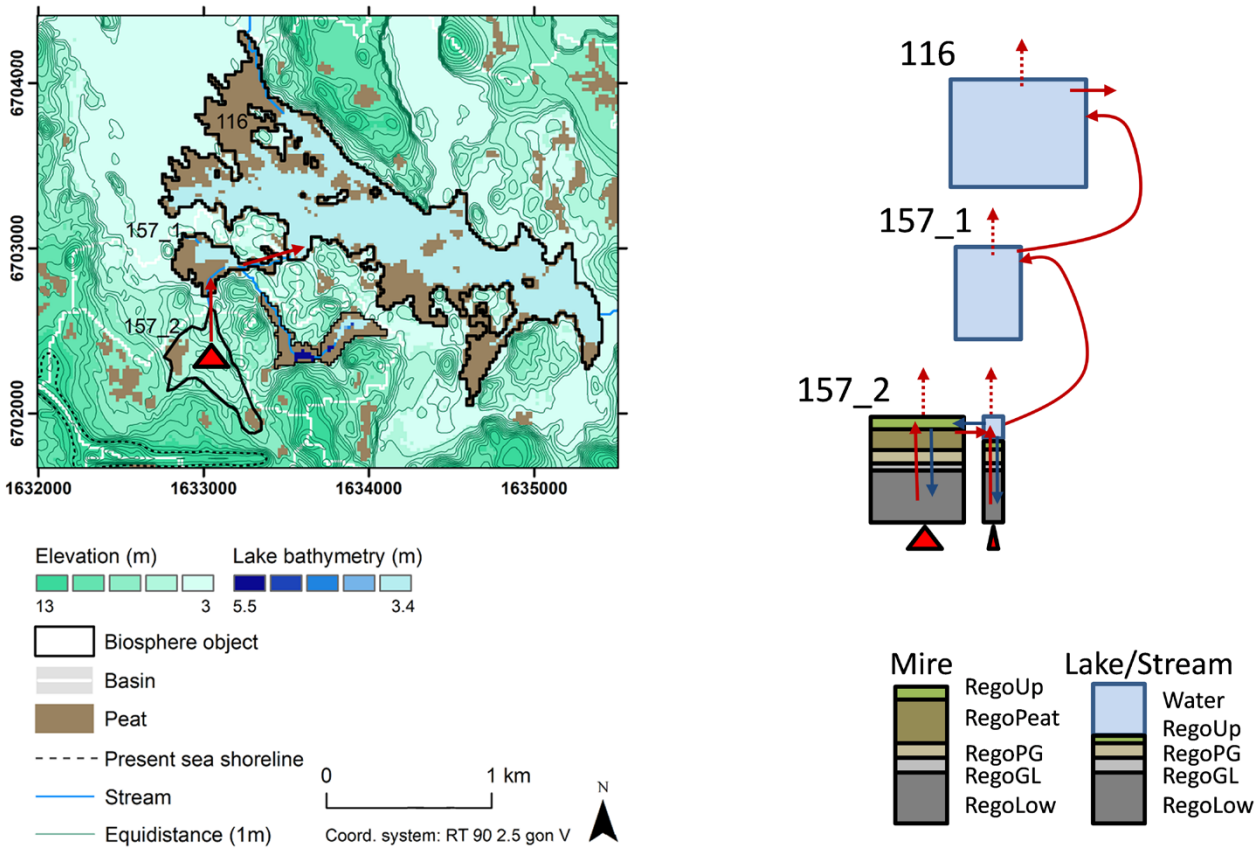

Figure 9-3. *Conceptual model of discharge and dispersion of radionuclides that reach the biosphere via groundwater from the geosphere during the terrestrial stage. Left: ground-surface elevation and water depths in lakes at 5000 AD. The red triangle represents the location of the geosphere release (object 157_2). Downstream objects 157_1 and 116 receive radionuclides via surface water during the terrestrial stage. Right: schematic sketch of the transport of radionuclides between regolith layers and surface waters within and between biosphere objects. In both the panels, red arrows show transport of radionuclides along a declining solute concentration gradient. Blue arrows show transport of radionuclides in the opposite direction. The regolith layers for aquatic ecosystems are labelled as in Figure 9-2. In terrestrial parts deep peat (RegoPeat) and surface peat (RegoUp) are stratified on top of clay-gyttja. The light blue boxes represent lake and stream water. Dashed arrows represent loss of C-14 to the atmosphere. Note that the figure represents a snapshot in time and that the lake basins in 157_1 and 116 will ultimately be filled with peat so that only a stream remains.*

Surface hydrology

In SR-PSU, the MIKE SHE hydrological modelling tool was used to model the water balances of the future biosphere objects (areas potentially affected by releases) at three points in time: 3000 AD (end of submerged period), 5000 AD (terrestrial period, when objects are either lake-mire complexes or mires) and 11 000 AD (terrestrial period, all objects are mires) (Werner et al. 2013). Temperature, precipitation and potential evapotranspiration time-series from locally measured meteorological data during a standardized one-year period (see "normal" year in Section 4.1.1) were used as input data to the simulations. Hydrological modelling and parameter values are further described in Sections 4.3 and 8.2.4.

In the PSAR, the same modelling is utilised, but now it is assumed that the runoff from object 157_2 reaches the downstream object 157_1 via a stream (Section 7.5.2 in Werner et al. 2013). Potential consequences of this assumption are evaluated with the alternative assumption that the runoff from object 157_2 reaches object 157_1 through diffuse overland-water flows. This is evaluated separately in the *alternative landscape configuration calculation case* (Section 10.6).

Ecosystem parameters

Ecosystem parameters are primarily based on site data from lakes, wetlands and marine basins in the area, and they are applied to future ecosystems by assuming present-day climate (i.e. temperature and precipitation) and current chemical conditions of the surface environment. The parameters updated since SR-PSU include those used to describe the accumulation of organic carbon and those describing the crop and water regime of the garden-plot household. In addition, new parameters for chlorine are derived from recent field measurements in Forsmark. These updates and additions are described in Section 8.2.3.

Potentially exposed groups and populations

The annual dose to a representative individual is calculated, as the mean annual dose of 1 000 simulations, for four different exposed populations, representing bounding cases to cover the highest exposure from different radionuclides: 1) hunter-gatherers (HG), 2) infield-outland farmers (IO), 3) drained-mire farmers (DM), and 4) garden-plot households (GP). These different populations are described in Section 6.2 and in SKB (TR-14-06). Exposure pathways included are the ingestion of food and drinking water, inhalation of air, and direct external irradiation (see Section 6.2 for details). These potentially exposed groups are often referred to as "land-use variants" in the discussion of the results.

The exposure from a well drilled in the area where groundwater is expected to have the highest concentrations of radionuclides originating from SFR (i.e. the *well interaction area*, Section 5.5) is only considered to be relevant for a small group. The pathways considered for this group are the ingestion of water and small-scale irrigation (GP). As the group is small, a risk criterion of 10^{-5} is considered appropriate[45].

9.3 Analysis of the *base case*

Annual doses to the potentially exposed groups

The resulting annual doses to the potentially exposed groups, arising from the geosphere release, are presented in Figure 9-4. During the initial submerged period when agriculture in object 157_2 is not possible, hunters and gatherers (HG) in the area is the most exposed group and the resulting dose is low. Ingestion of fish is the primary exposure pathway during this period. The relatively low doses are due to low groundwater flows causing a limited geosphere release in combination with a relatively high exchange of water between sea basins. Note that during this period, also the garden-plot household (GP) group receives doses, albeit at very low levels, as they collect seaweed from object 157_2 and use it to fertilise a kitchen garden. Beginning from 3000 AD, when drilling of wells becomes possible (Table 9-1), the GP group utilizing water from a drilled well has the highest dose and this situation persists for 200 years. At 3200 AD, when the most elevated areas of object 157_2 has emerged 1 m above sea level, it is considered feasible to drain and cultivate the peatland in object 157_2 and to extract water from a dug well in the object. At this time, less than 1 ha of land has emerged and the area can only support 15 % of the DM group. However, due to the relatively fast shoreline regression in the *base case*, the emerged land area can fully support the whole group of DM farmers already around 4000 AD. Thus, the DM farmers receive the highest dose of all groups and it is the most exposed group for most of the assessment period. The following presentation and discussion of the results therefore focus mainly on this group. For this group, released radionuclides are considered to accumulate in the undisturbed mire ecosystem up to the point of drainage. The average annual dose from early cultivation (first 50 years following drainage, approximately corresponding to a human lifetime of the most exposed generation) is evaluated for each point in time, cautiously assuming that the mire has not been disturbed prior to the point of drainage. Infield-outland farmers (IO) are exposed through hay from

[45] To make the dose comparable to that of other exposed populations, it is divided by a factor of ten (Section 7.5.4) to compensate for the different criteria applied to large and small exposed groups.

the mire in object 157_2 (outland) that is consumed by cattle and thus produces organic fertilizers for cultivation of cereals (infields). Though it is cautiously assumed that this transfer of radionuclides can be maintained for 500 years, accumulation in the infield is always considerably lower than in regolith layers exposed by cultivation in the drained mire. However, for radionuclides where exposure primarily occurs through ingestion of meat and milk, exposure can be equally high from using mire hay as fodder. This occurs in particular when radionuclides accumulate in organic matter (e.g. Ca-41), as is the case around 30 000 AD when the doses to IO and DM farmers are similar (Figure 9-4).

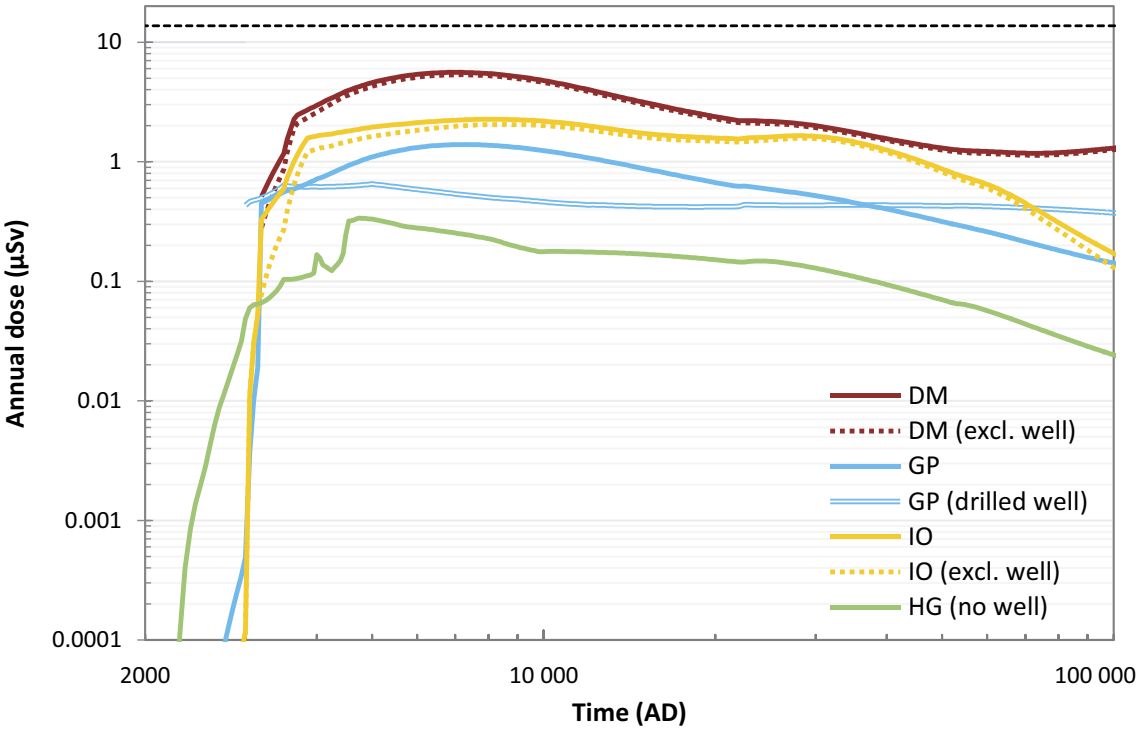

Figure 9-4. *Total annual doses to different exposed groups in the base case, that is to hunter-gatherers (HG), infield-outland farmers (IO), drained-mire farmers (DM) and garden-plot households (GP). The doses are the arithmetic mean of 1 000 probabilistic simulations. The dose contribution from well water is highlighted by including results where exposure to DM and IO from dug wells are replaced with exposure from stream water (dashed coloured lines). The doses to GP from a dug and from a drilled well are shown separately (blue lines). The dashed black line shows the annual dose (14 µSv) corresponding to the regulatory risk criterion for a large group.*

Radionuclide-specific annual doses and exposure pathways

As mentioned above, hunter-gatherers (HG) is the most exposed group during the initial 1 000 years, when the area is submerged. The group forage in multiple sea basins in this period, and the dose is dominated by C-14. It can be noted that most of the exposure originates from basins 116 and 157_2 (Figure 9-6). In the short period after 3000 AD, when the drilled well to garden plot farmers (GP) yields highest dose, C-14 also contributes significantly to dose (40 %). Other radionuclides that contribute to dose during this period are Ag-108m (15 %), and U-238, Ac-227 and I-129 (~ 10 %).

The dose is considerably higher when it is possible to draining and cultivate the mire in object 157_2. Mo-93 and C-14, contribute most to the total annual dose during the first 20 000 years after closure, with some contributions from U-238, I-129 and Ca-41 (Figure 9-5). The dose maximum, ca 5.6 μSv, occurs 5 000 years after closure of the repository (around 7000 AD), where Mo-93 and C-14 contribute with 60 % and 15 % to the total annual dose, respectively.

Ca-41 is the radionuclide contributing most to the total annual dose during the period between 20 000 and 60 000 AD. The total annual dose decreases during this period (with an initial dose of approximately 2.4 μSv) as contributions from Mo-93, I-129 and uranium isotopes gradually decrease with time. The decline in total annual dose is partly compensated by increased contributions from Ca-41 and decay products of U-235 (Ac-227 and Pa-231) in the middle of the period.

Ni-59 becomes increasingly important towards the end of the assessment period, and becomes the radionuclide contributing most to the total annual dose after 60 000 AD. At this time, the total annual dose is ca 1 μSv, but increases slightly by the end of the assessment period. Ni-59 contributes a third of the total annual dose at the end of the assessment period, with contributions of about 30 % and 15 % from Cs-135 and Ac-227, respectively.

Indeed, Ni-59 and Cs-135 show an increasing dose trend at the end of the assessment period. As they both are long-lived, are released during long periods of time and move slowly in the biosphere regolith layers, they are relevant to dose in a very long-time perspective. Thus, to investigate the behaviour of these radionuclides, simulations were performed for an additional 900 000 years for the *base case*. These simulations show that while the doses of Ni-59 and Cs-135 continue to increase for some time after 102 000 AD, their contributions remain well below the dose corresponding to the risk criterion. Specifically, Ni-59 reaches a maximum of about 0.5 μSv at 120 000 AD and decreases continuously after that, and Cs-135 reaches a maximum of about 1.5 μSv at 450 000 AD, after which it gradually decreases.

The temporal variation of the radionuclide-specific annual doses is strongly influenced by the geosphere releases, presented as the radiotoxicity (see Section 2.3.7) of the annual geosphere releases in the upper panel of Figure 9-5. However, there are also other factors affecting the temporal patterns and relations between the magnitudes of geosphere releases and doses for the different radionuclides. These include radionuclide- and element-specific properties that influence their transport and accumulation in the biosphere, transfer to plants and foodstuffs, and the potential radiological consequences arising from the radionuclides that humans are exposed to, either by intake or as external irradiation.

Exposure from drinking water from the dug well is related to the radionuclide concentrations in the pore water in the till (the lowest regolith layer). This pathway is important early in the assessment period when the size of the emergent land area may be limiting exposure or at times before the radionuclides have had time to accumulate in the upper regolith layers from which the plant uptake occurs. Consistently with this, the *base case* results show that the drinking water from the dug well is the most contributing exposure pathway for Mo-93, Ca-41 and Ni-59 early in the assessment period, ranging from a few hundreds of years (for Mo-93 and Ca-41) to a few thousands of years for Ni-59. However, the annual dose from C-14 from all sources of drinking water is relatively low. This is because the dose coefficient for ingestion of C-14 in water is 20 times smaller than that for ingestion of food, as C-14 in water is in inorganic form that is lost as CO_2 through the respiratory system rather than being assimilated in the human body. Note that exposure to radionuclides in the deep groundwater also is considered as a relevant exposure pathway (GP drilled well in Figure 9-4). However, factoring in that this pathway is only relevant for a small group, the maximum dose from a drilled well is relatively low compared to other exposure pathways (e.g. the dose from ingestion of crops from the drained mire is more than a factor of seven higher, Figure 9-7).

The further presentation of the results is focused on the four radionuclides that contribute most to dose in the drained mire, namely C-14, Mo-93, Ca-41 and Ni-59 (see below), followed by a shorter overview of a few less dose-contributing radionuclides with varying behaviour, including decay chains. Note that there is a considerable release of radiotoxicity of radionuclides that are of minor importance for dose. These radionuclides are grouped together in the "other" category in Figure 9-5. The radiotoxicity of the release is dominated by Ag-108m, plutonium isotopes and shorter-lived decay products of the U-238 decay chain (Ra-226, Pb-210 and Po-210). The fact that these radionuclides combined have a higher radiotoxic release from the geosphere than the most dose-dominating radionuclides implies that their activity is substantially reduced during transport through the till (long residence times in the till in relation to the physical half-life) before being available for exposure in the above regolith layers exposed by cultivation.

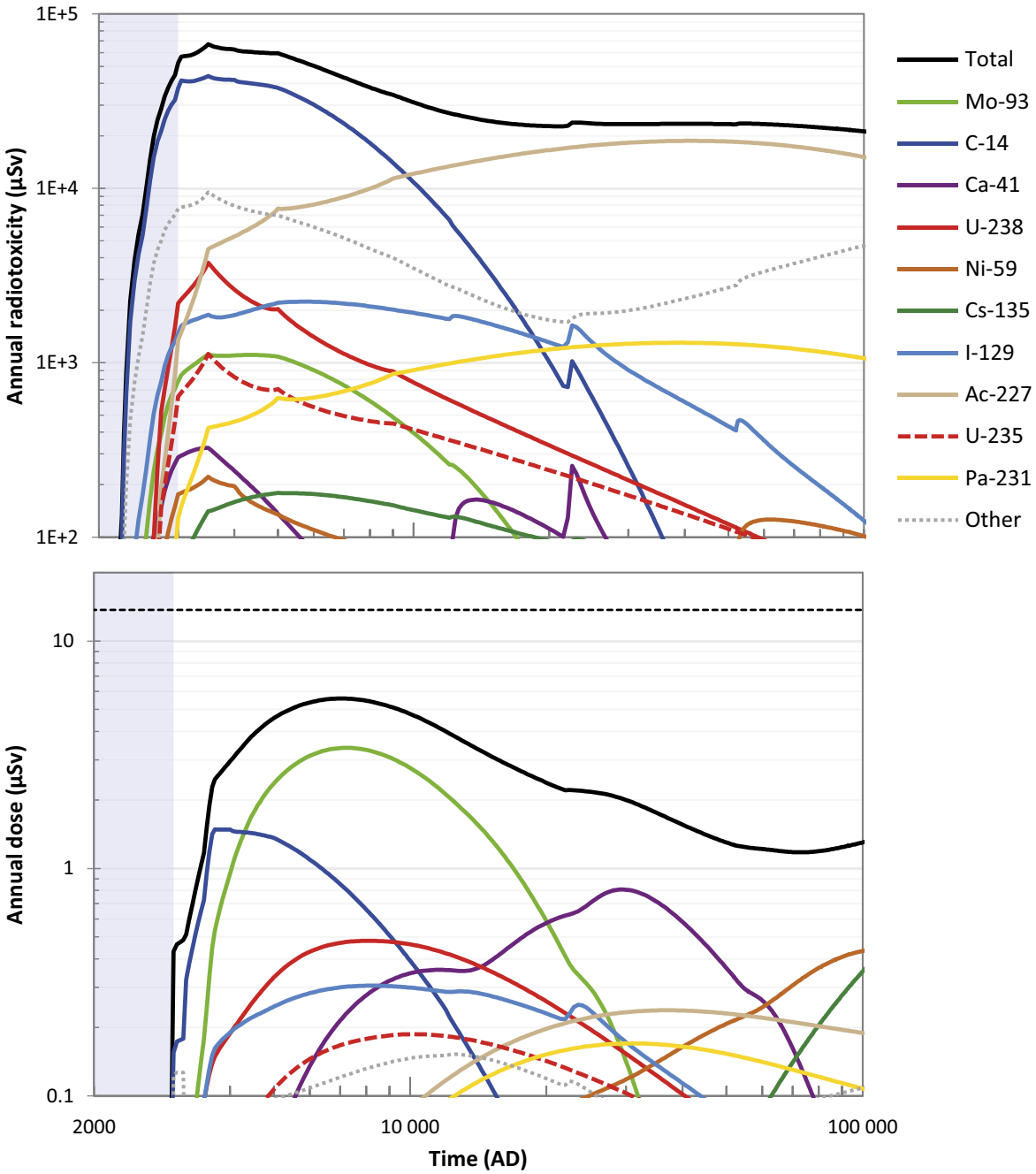

Figure 9-5. *Annual radiotoxicity of the geosphere release of some radionuclides (upper panel), and annual doses to the most exposed group in the base case for the radionuclides contributing most to the total annual dose (lower panel). Note that the vertical scale differs in the two panels. The annual dose (14 µSv) corresponding to the regulatory risk criterion is indicated by the black dashed line in the lower chart.*

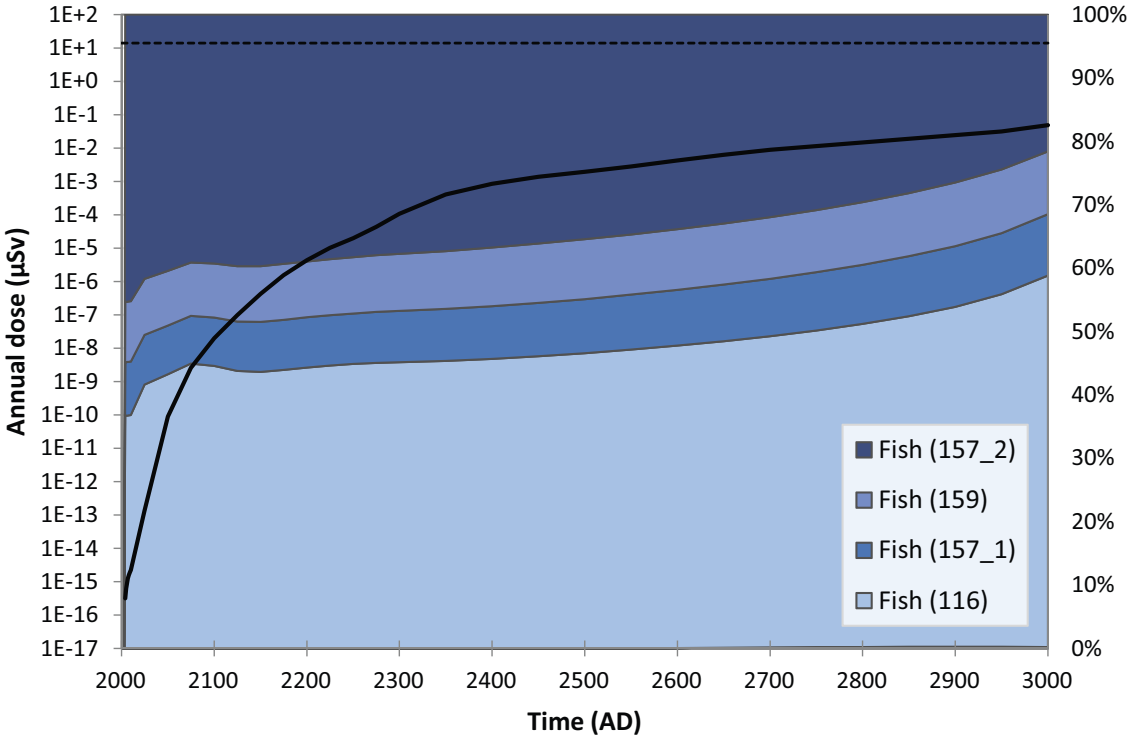

Figure 9-6. *Total annual dose to hunter-gatherers (HG) (black line) and relative contributions to the annual dose from different objects providing fish for the HG group during the submerged period in the base case. There are no other exposure pathways during this period affecting the HG group. The annual dose (14 µSv) corresponding to the regulatory risk criterion is indicated by the black dashed line.*

During the first 10 000 years, ingestion of crops is the most important exposure pathway from the drained mire. At this time C-14 and Mo-93 contributes most to the dose. Cereals, which account for 60 % of the intake of dietary carbon (Grolander 2013, Section 10.4) explain between 30 to 70 % of the total dose during the assessment period (Figure 9-7). However, after 20 000 AD the relative importance of the dose contributing radionuclides shifts towards Ca-41 and Ni-59. As these radionuclides have high transfer rates from fodder to meat and milk products, the relative importance of these exposure pathway increase, accounting for approximately 50 % of the dose most the assessment period.

Mo-93 is a key radionuclide for total dose in the period up to 20 000 AD (Figure 9-5). It has a relatively high transfer to crops, especially to cereals, and a low transfer to animal products (Table 9-2). At the total dose maximum, the other exposure pathways related to the ingestion contributes approximately 10 % (tubers, milk) or less (water, meat). The doses due to external irradiation and inhalation are insignificant.

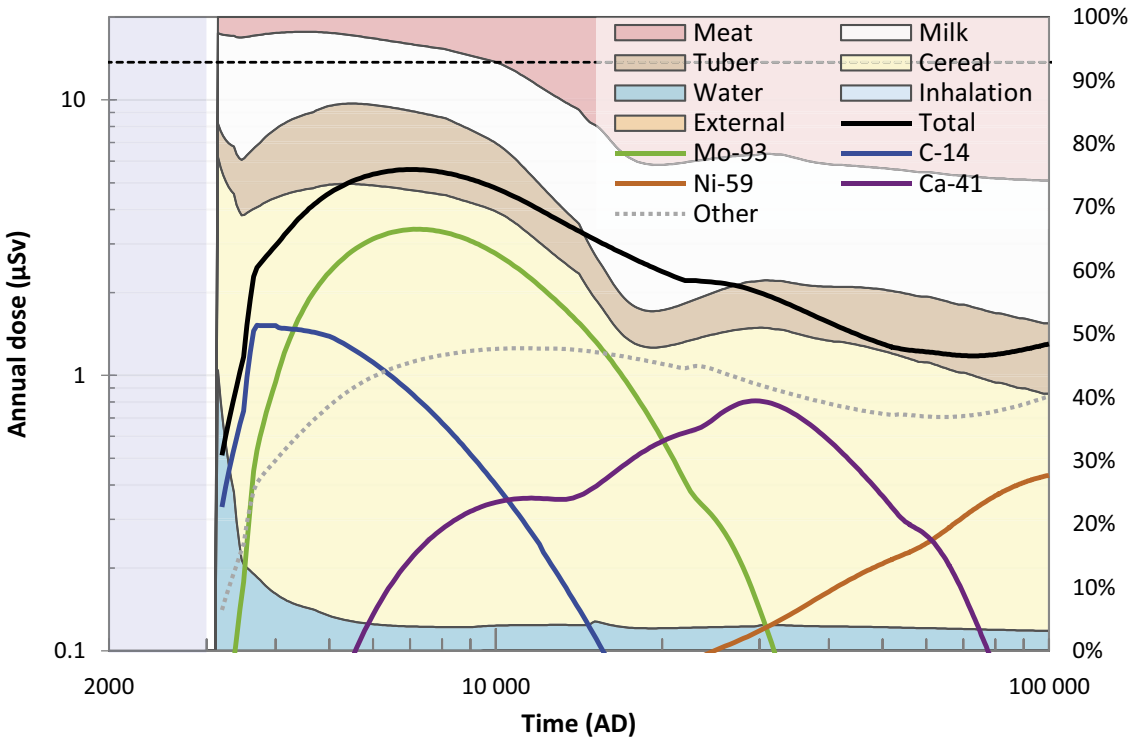

Figure 9-7. *Relative contribution of the different exposure pathways to the annual dose to DM farmers during terrestrial conditions (coloured areas linked to the vertical axis to the right), and corresponding total annual dose as well as radionuclide-specific annual doses for C-14, Mo-93, Ca-41 and Ni-59 (lines linked to the vertical axis to the left) in the base case. Note that the doses due to inhalation and external irradiation are too small to be visible in the figure. The annual dose (14 µSv) corresponding to the regulatory risk criterion is indicated by the black dashed line.*

Properties of key radionuclides

To illustrate and understand how radionuclide properties influence the assessment results in terms of doses and environmental activity concentrations, the following discussion focuses specifically on the four radionuclides that contribute most to the annual dose, i.e. C-14, Mo-93, Ca-41 and Ni-59. These four radionuclides also cover a wide range of radionuclide- and element-specific properties (Table 9-2). As the highest dose results from draining the mire in object 157_2, note that radionuclides in surface and deep peat, in clay-gyttja and in glacial clay all are exposed by cultivation. However, the till layer is considered to be buried below the ditching depth, and radionuclides from this layer only reach the cultivated soil through uptake of groundwater.

C-14 differs from the other three radionuclides in several ways; it does not adsorb to soil particles or suspended material, it is highly volatile and will degas when in contact with the atmosphere, and its long-term accumulation occurs through plant fixation and subsequent storage of organic matter in deep peat. Mo-93, in turn, has highly variable sorption properties. While molybdenum is relatively mobile in inorganic regolith layers, it adsorbs much more strongly onto sediments that are rich in organic matter, including peat and post-glacial clay gyttja. Molybdenum has a relatively high transfer to plants. Ca-41 is moderately sorbing in most regolith layers. Calcium has a relatively high transfer to plants and accumulates in organic matter. Ni-59 is a long-lived radionuclide that adsorbs strongly on till and especially on glacial clay. Thus, while Ni-59 is unlikely to cause exposure to organisms in surface ecosystems in time spans of thousands of years, it has great potential for accumulation in glacial clay that can result in doses after drainage and cultivation.

The potential radiological consequences due to the ingestion of individual radionuclides depends on the physical properties of the emitted radiation (type of radiation, the yield and energy of their emissions) and the degree to which they are taken up and accumulated in various tissues and organs of humans (ICRP 2012). Ingestion dose coefficients are used to estimate the committed effective dose due to intake by ingestion of different radionuclides, which usually is the exposure mode dominating the doses. Mo-93 is the most radiotoxic of the four radionuclides addressed here, with approximately a one to two order of magnitude higher ingestion dose coefficient than the other three radionuclides (Table 9-2).

Table 9-2. Selected properties of radionuclides contributing significantly to the dose. K_d is the sorption coefficient in the regolith layers, *CR* the soil-to-plant concentration ratio, *TC* the transfer coefficient to animal products, and *DC* the ingestion dose coefficient. The colours and their intensities reflect the magnitude of each parameter, where blue shades symbolise lower values and yellow larger values. The dashed line indicates that the soil cultivated after the mire is drained, RegoUp (DM), is not part of the mire regolith horizon (above the line).

Parameter	Unit	Specification	C-14	Mo-93	Ca-41	Ni-59
Half-life	years		5 700	4 000	102 000	101 000
K_d [(a)]	m^3 $kgdw^{-1}$	RegoUp_ter	0	4.3	0.31	1.9
		RegoPeat	0	3.9	0.38	2.6
		RegoPG	0	3.4	0.037	1.1
		RegoGL	0	0.22	0.95	17
		RegoLow	0	0.021	0.29	0.79
		RegoUp (DM)	0	0.74	0.11	0.83
CR [(a)]	m^3 $kgdw^{-1}$	cereals	- [(b)]	1.2	0.23	0.016
		tubers	- [(b)]	0.90	0.39	0.14
		fodder	- [(b)]	0.26	1.5	0.14
TC [(a)]	day $kgfw^{-1}$	meat	- [(b)]	0.001	0.013	0.16
	day L^{-1}	milk	- [(b)]	0.0011	0.02	0.00095
DC [(c)]	Sv Bq^{-1}	ingestion	5.8×10^{-10} [(d)]	3.1×10^{-9}	1.9×10^{-10}	6.3×10^{-11}

a) Geometric mean.

b) Parameter not relevant since a specific activity approach is used for C-14.

c) Constant value.

d) The dose coefficient for C-14 due to ingestion of water is 2.9×10^{-11} Sv Bq^{-1}.

In the following, the doses arising from the exposure to these four radionuclides in the *base case* are analysed and discussed further.

Results for C-14

Carbon is a volatile element that is the primary component of all known organisms. The modelling of C-14 differs from that of other radionuclides in the BioTEx model, as it is affected by gas transfer. Moreover, the primary exposure pathways of C-14 involve fixation of C-14 in plants through primary production. In the BioTEx model this is described by a specific activity approach (Section 7.5.3, Saetre et al. 2013a), and it is cautiously assumed that all the C-14 reaching the surface ecosystems will be in a form that is available for uptake by primary producers (i.e. as CO_2 or HCO_3^-). Dissolved organic (radio) carbon (DOC) originating from the repository is expected to be in the form of low molecular weight carbon, which will be mineralised when it reaches biologically active regolith layers. Under anaerobic conditions microbial mineralisation may result in the formation of methane. However, it is cautiously assumed that this methane will be oxidised to carbon dioxide once it reaches aerobic environments (e.g., surface peat and lake water).

C-14 is highly mobile in the geosphere. Its near-field release is only retarded by the advective travel time of the water through the geosphere (**Radionuclide transport report**, Section 5.5). Thus, the dynamics of the release from the geosphere is almost identical with that from the near-field (black lines in Figure 9-8). The total release rate of C-14 from the geosphere increases shortly after closure of the repository and reaches a maximum just after the submerged period ends, around 3000 AD, the maximum level lasting for about 1 000 years. The geosphere release then decreases for the rest of the assessment period.

C-14 is highly mobile also in the biosphere and does not significantly adsorb to soil particles or suspended material (a zero K_d is applied in the modelling). Thus, most of the released C-14 is exported from the system, mainly by water exchange with surrounding basins during the submerged stage or by degassing during the terrestrial stage (Figure 9-8). Only a minor fraction is retained within the regolith layers. The residence time of C-14 in the terrestrial state is only 10 years, though the time to reach equilibrium with respect to organic carbon is considerably longer (i.e. hundreds of years). This is an insignificant time in relation to its half-life of 5 700 years, and consequently the radioactive decay in the biosphere system is negligible.

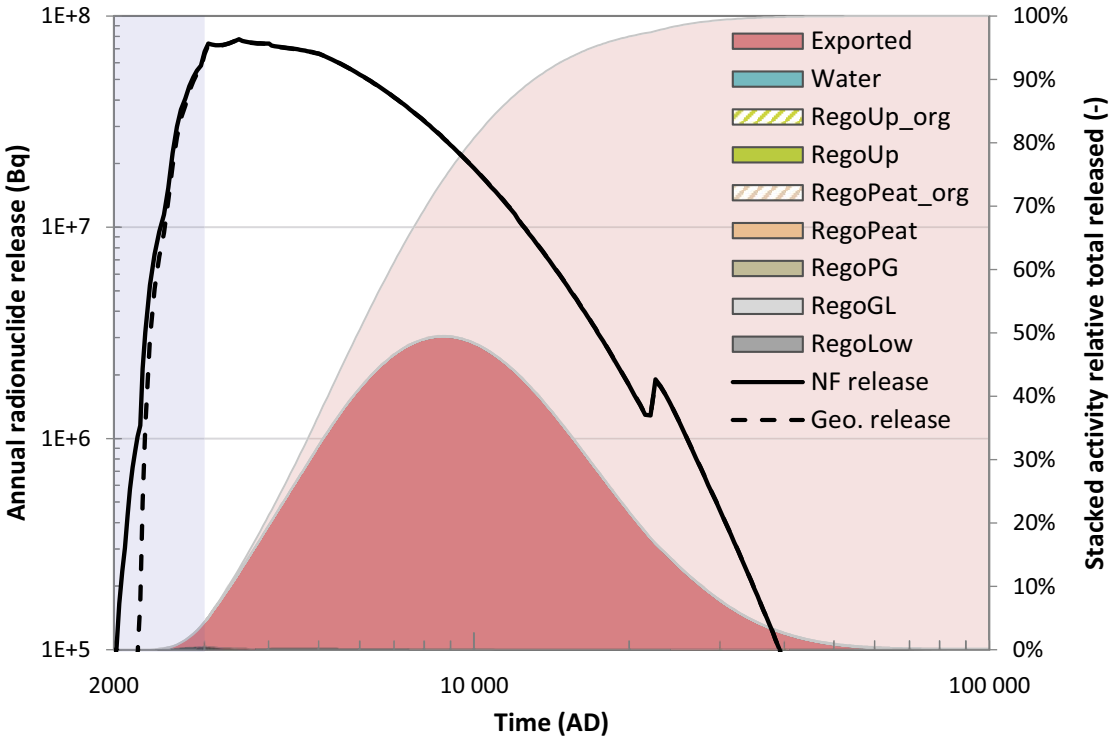

Figure 9-8. *The release of C-14 from the near-field to geosphere and from geosphere to the regolith (the black lines, left vertical axis) plotted together with the distribution of the activity inventory of released C-14 (non-transparent coloured areas, right vertical axis). The release peak at 22 000 AD is related to cement degradation in the repository (Radionuclide transport report, Section 5.3). Semi-transparent colours, except the blue area indicating submerged conditions, represent the amount decayed within the regolith layers or after export from the object. The activity inventories in the regolith layers are insignificant in relation to the amount exported (red) and the amount decayed after export (semi-transparent red). The inventory in the regolith layers is shown on a different scale in Figure 9-9.*

The top panel in Figure 9-9 shows the activity concentrations in the pore water in the regolith layers and in the water body. Since the radionuclide releases from the repository are diluted by the groundwater flows, the pore water activity concentration will decrease towards the surface. This is because the contribution of sub-surface runoff and precipitation (that bear no released radioactivity) on groundwater flows increases towards the surface. The distribution of the activity inventory of C-14 within the regolith layers (bottom panel of Figure 9-9) is mainly controlled by the groundwater flow, the thicknesses and porosities of the regolith layers, and the accumulation in the organic matter in the regolith.

During the submerged period, a higher fraction of the released activity is retained in the regolith layers, and most of the activity is found in the lower regolith layer. The reason for this is the relatively low upward fluxes of deep groundwater during this period. In addition, the overlaying regolith layers are still relatively thin during this period. At the end of the submerged period, more than 90 % of the retained activity is found in RegoLow.

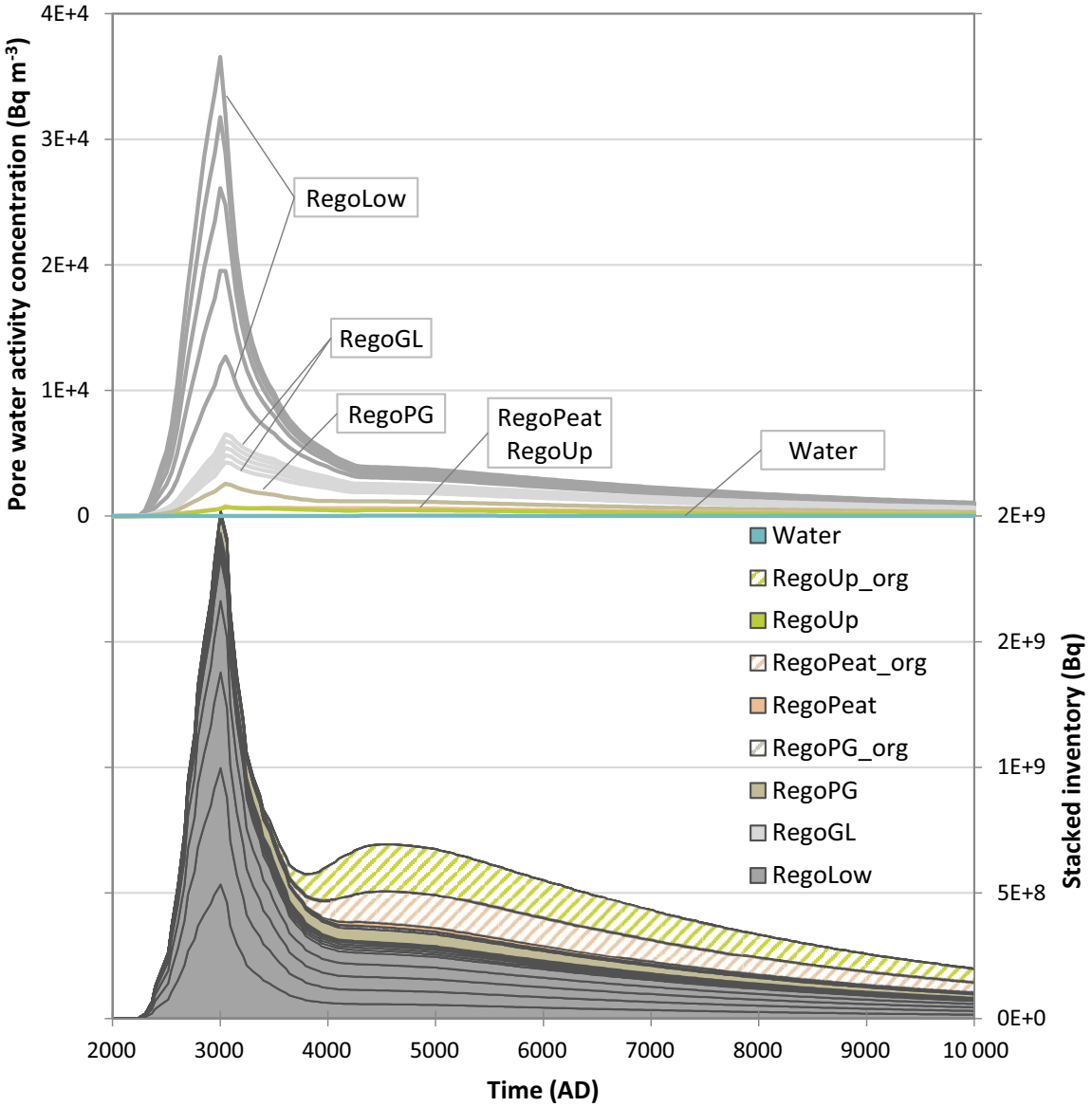

Figure 9-9. *Activity concentration in the pore water (top) and activity inventory (bottom) of C-14 in the regolith layers in the mire. The areas with diagonal stripes for RegoPeat, RegoUp and Rego_PG in the bottom figure indicate the inventory in the organic fraction. Note the linear and zoomed in time-axis compared with the logarithmic time-axes in other similar figures.*

When the biosphere object emerges above sea level, the upward fluxes of deep groundwater increase. Simultaneously, subsurface runoff from the local watershed contributes to generate additional groundwater flow in the object. Even though there is a rise in activity release from the geosphere, the porewater concentration and the amount of activity in the biosphere object decreases. The largest fraction of the total retained activity is still found in the lower regolith layer, but the storage of C-14 in the organic matter in the upper layers becomes more important than during the submerged period. When the discharge object is fully terrestrial, almost 50 % of the retained activity is found in the organic matter in the two peat layers (Figure 9-9). Although the peat contributes substantially to the initial inventory of the agricultural soil, the primary source of radionuclides during 50 years of cultivation originates from groundwater uptake (Figure 9-10, left panel).

The annual dose maximum for C-14 (1.5 µSv) occurs around 3700 AD when the emerged area of object 157_2 is sufficient to fully support the dietary needs of the most exposed group. Due to the high mobility of carbon in the regolith, and fast transfer to plants, the doses are proportional to the geosphere releases of C-14 after this time point (Figure 9-8).

Groundwater uptake is the primary source for C-14 in the drained and cultivated mire and accumulation in organic matter is a minor source for exposure during cultivation (Figure 9-10, left panel). The annual dose from C-14 is dominated by ingestion of food, contributing more than 90 % of the total dose (Figure 9-10). Cereals contribute with 60 %, and milk and tubers contribute with an additional 25 % and 10 % respectively. The activity concentration in crops is the result of plant uptake from soil pore water (root uptake) and from the atmosphere (foliar uptake). The specific activity in fodder is assumed to be conserved in animal products. Although the contribution of root uptake to carbon fixation is limited to a few percent of the whole amount of fixation (Grolander 2013), this uptake mechanism is about as important as atmospheric uptake with respect to uptake of C-14. This is due to the specific activity of C-14 in the soil pore water being two orders of magnitude higher than in the atmosphere. The ingestion of drinking water contributes less than 10 % to the total dose, and the doses due to the inhalation and external irradiation are insignificant.

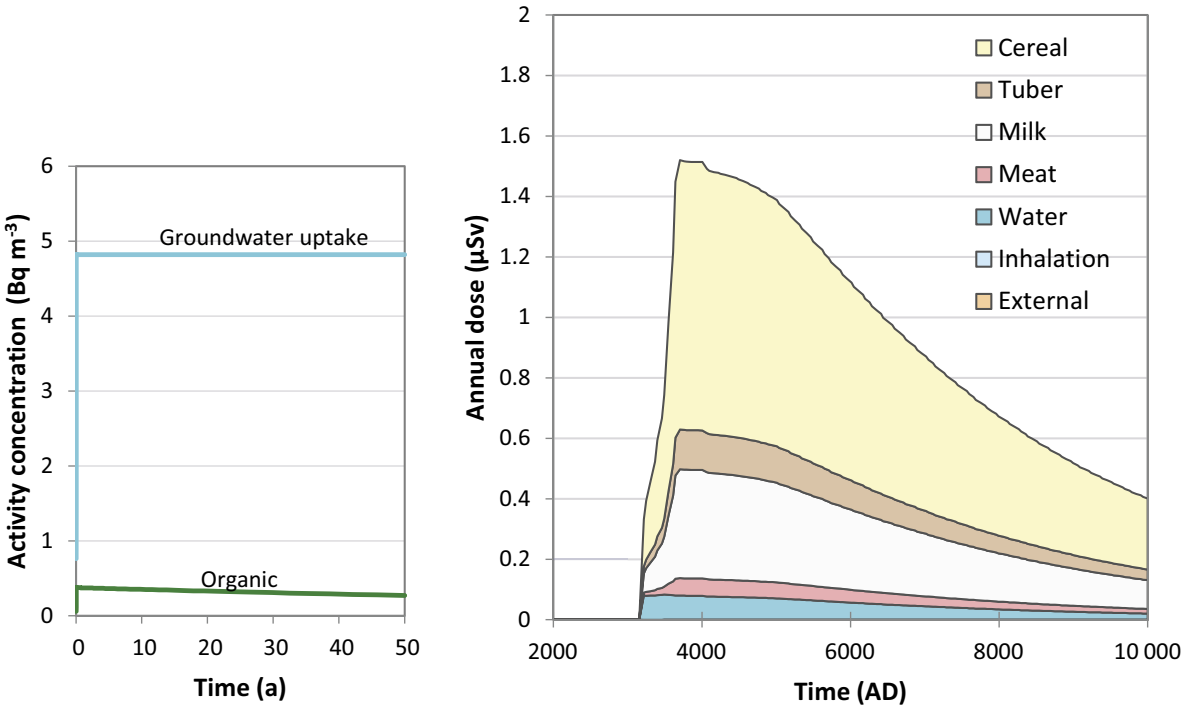

Figure 9-10. *The contribution from different sources to the activity concentration of C-14 in the pore water during the first 50 years of cultivation of the drained mire, at the time of maximum activity in the soil (left), and the annual dose for C-14 from the different exposure pathways for drained mire farmers (DM) (right) in the base case. The dose from drinking water originates from a dug well.*

The ratio between C-14 and stable carbon, which is referred to as the specific activity of C-14, is much higher in water bodies than in the atmosphere. As this ratio is conserved in the food chain, aquatic foodstuffs were a major exposure pathway in earlier safety assessments of the existing SFR (Bergström et al. 2008, Avila and Pröhl 2008). However, this exposure pathway was less important in SR-PSU. This was partly because a significant fraction of the C-14 released to the mire in 157_2 was degassed before it reached any water body, and partly due to the inclusion of groundwater uptake and plant fixation of C-14 from root uptake in the productive agricultural ecosystems.

Nevertheless, as C-14 is by far the most important radionuclide when it comes to exposure from aquatic ecosystems, and as a benchmark for other calculation cases, Figure 9-11 shows the activity concentration of C-14 in water and the annual dose for different exposure pathways for the hunter-gatherers (HG) group. The figure shows the results up to 10 000 AD; this is the period when most of the development related to aquatic ecosystems occurs (i.e. the biosphere objects emerge from the sea and lakes are formed), and it includes the initial submerged period during which HG is the most exposed group (Figure 9-4). The dose resulting from consuming food items from natural ecosystems (by HG) is dominated by fish, especially from the large lake in biosphere object 116, up to ca 9500 AD (Figure 9-11). After that, ingestion of forest food (game, berry and mushrooms) contributes the most to the dose, as the open lake area is successively colonized by mire vegetation.

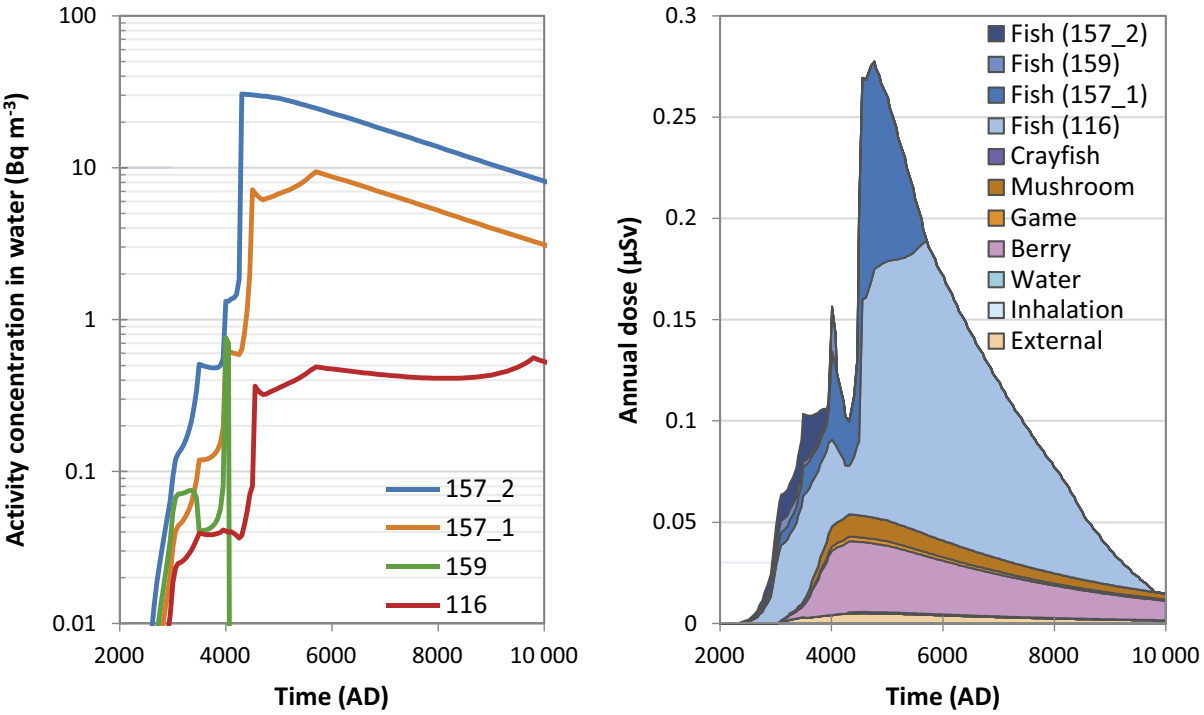

Figure 9-11. *Activity concentration of C-14 in the water of the biosphere objects (left) and the annual dose from C-14 for different exposure pathways for hunter-gatherers (HG) (right) in the base case. Note the linear and zoomed in time-axis compared with the logarithmic time-axis in similar figures.*

Results for Mo-93

Mo-93 is similarly to C-14 mobile in the geosphere and is primarily delayed by the advective travel time of the water flowing in the fracture system connecting the repository and the surface system (**Radionuclide transport report**, Section 5.5), resulting in the shape of the activity releases from geosphere being almost identical with the corresponding near-field releases (black lines in Figure 9-12). The total release of Mo-93 from the geosphere increases shortly after repository closure and its maximum occurs around 3400–4400 AD (Figure 9-12). The geosphere release then generally decreases for the rest of the assessment period.

Mo-93 sorbs rather strongly in the organic-rich upper regolith layers (Table 9-2), resulting in considerable retention and accumulation in the postglacial clay-gyttja layer (RegoPG) and in the peat (RegoPeat and RegoUp). The transport through the biosphere object (residence time) would take on average about 7 700 years for stable molybdenum. The inventory maximum of Mo-93 in the upper, dose contributing regolith layers (RegoGL to RegoUp) occurs about 2 500–3 000 years after the maximum release from the geosphere, before a steady-state condition has been reached (Figure 9-12). Since the physical half-life of Mo-93 and its residence time in the biosphere object are in the same order of magnitude, both radioactive decay within the object and export out from the system with water are important removal mechanisms, with the radioactive decay responsible for about 40 % and the export about 60 % of the removal of Mo-93 at the time of the dose maximum.

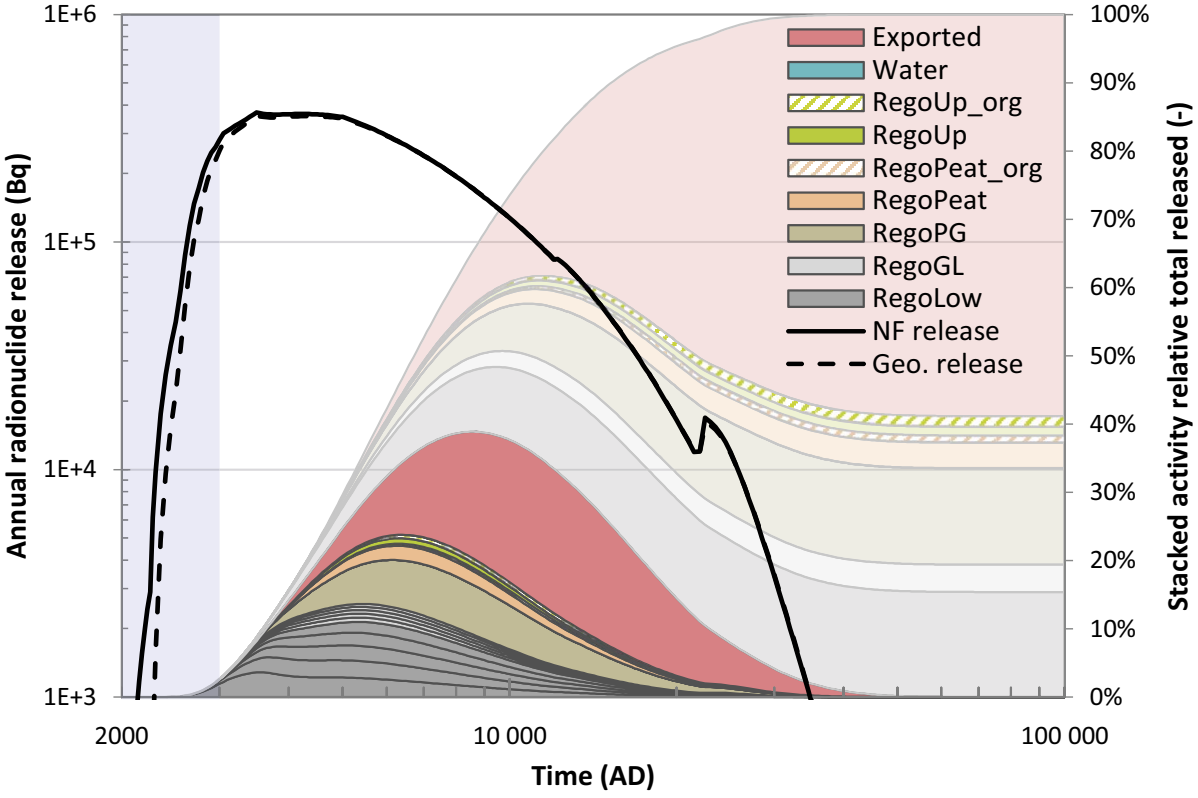

Figure 9-12. *The release of Mo-93 from the near-field to geosphere and from geosphere to the regolith (the black lines, left vertical axis) plotted together with the activity inventory of Mo-93 in regolith layers (non-transparent coloured areas, right-hand vertical axis). The late release peak around 22 000 AD is related to cement degradation in the repository (Radionuclide transport report, Section 5.3). Semi-transparent colours, except the blue area indicating submerged conditions, represent the amount decayed within each layer or after export from the object.*

During the submerged period, the activity in the regolith is small and almost all is found in the lower regolith layer (Figure 9-13). This is due to the very low upward fluxes of deep groundwater (see the corresponding discussion for C-14 above). When the biosphere object has emerged above sea level, the upward fluxes of deep groundwater increase and the thicknesses of overlaying regolith layers with higher sorption capacity for Mo-93 grow, which affects the radionuclide distribution within the regolith layers. There is still a substantial fraction of the total activity in the lower regolith layer, but the overlaying layers become more important. Around the time for maximum activity inventory in the biosphere object, at 6300 AD, about 45 % of the activity inventory is found in RegoLow, and 45 % is found in organic-rich regolith layers (RegoPG, RegoPeat and RegoUp). A small but notable fraction of the activity in these layers is stored in the organic matter (areas marked with diagonal stripes in Figure 9-12 and Figure 9-13).

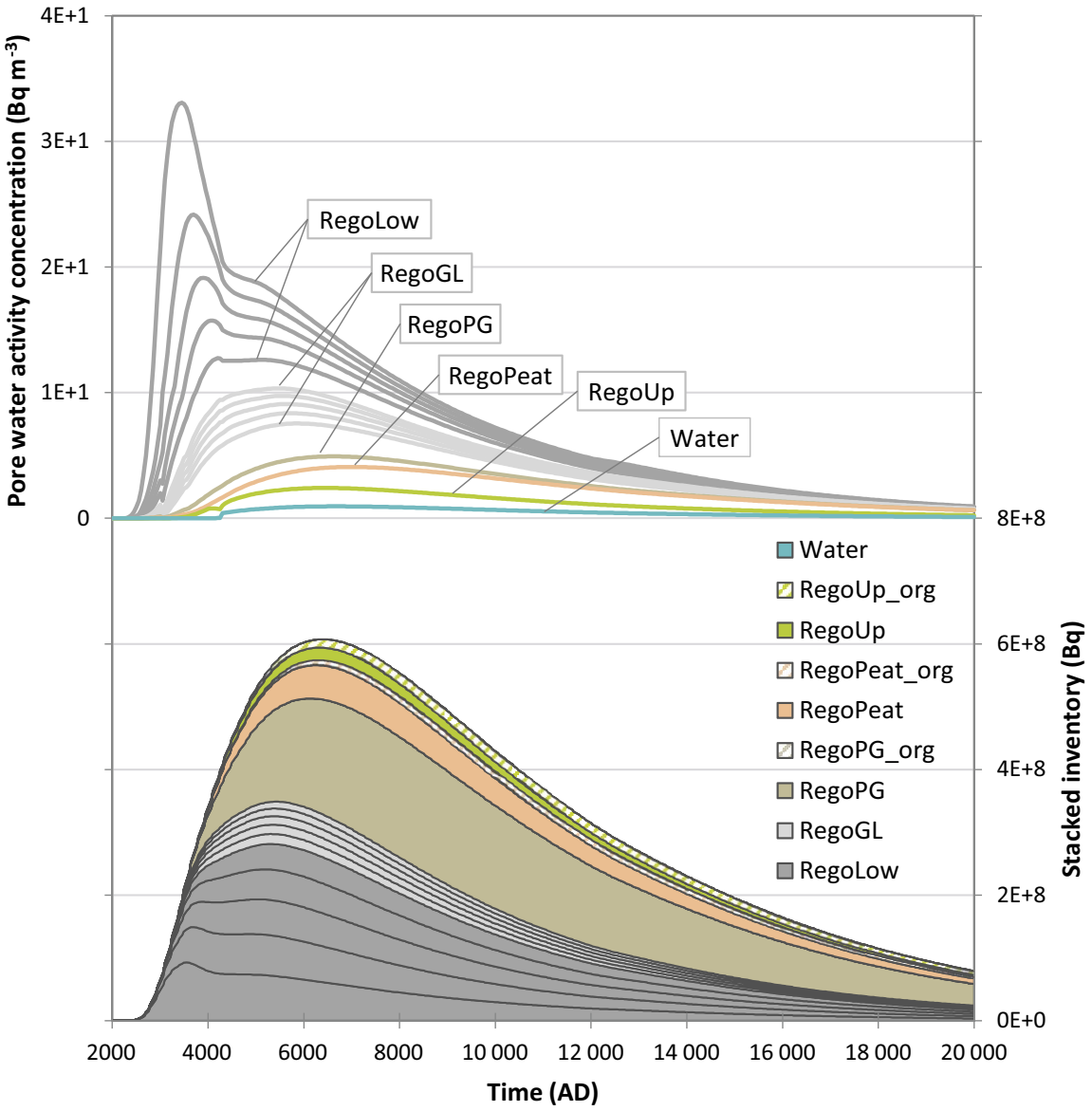

Figure 9-13. *Activity concentration in the pore water (top) and activity inventory (bottom) of Mo-93 in regolith layers in the mire. The areas with diagonal stripes for RegoUp and RegoPeat in the bottom figure indicate the inventory in the organic fraction. Note the linear and zoomed in time-axis compared with the logarithmic time-axis in similar figures.*

All of the regolith layers above RegoLow contribute to activity in the cultivated soil when the mire is drained. However, adsorbed (inorganic) Mo-93 is the most important source, and the contributions from Mo-93 that have accumulated in the organic matter and from plant uptake of groundwater play a minor role in comparison (left panel in Figure 9-14).

The dose maximum (3.4 µSv) occurs around 7200 AD (Figure 9-14). The dose from Mo-93 is almost entirely dominated by the ingestion of cultivated crops. Cereals contribute about 80 % and tubers about 17 % of this. This is as expected, because molybdenum is an essential element and Mo-93 is thus readily taken up by plants. The importance of Mo-93 in crops for the total maximum doses is a combined effect of high accumulation of Mo-93 in the upper regolith layers, relatively high transfer to cereals and tubers, and the dietary assumptions (70 % of the energy demand is covered by consumption of cereals and tubers) (Table 9-2). It can also be noted that Mo-93 has a low transfer from the fodder to animal products. Ingestion of water, meat and milk contribute all together only with a few percent, and the doses due to inhalation and external irradiation are insignificant for Mo-93.

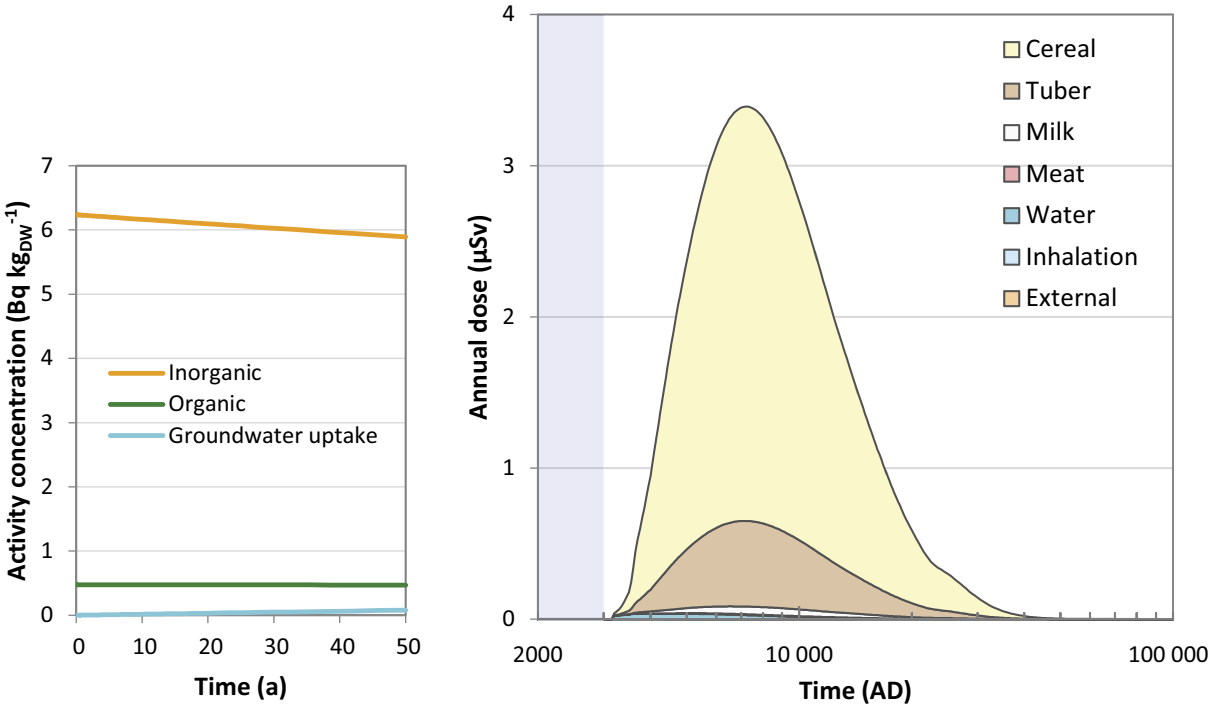

Figure 9-14. *The contribution from different sources to the activity concentration in cultivated soil during the first 50 years of cultivation of the drained mire, at the time of maximum activity in the soil (left), and annual dose for Mo-93 for different exposure pathways for drained mire farmers (DM) (right) in the base case. The dose from drinking water originates from a dug well. Note that most of the exposure pathways have so small contributions that they are not discernible in the figure.*

Results for Ca-41

As for C-14 and Mo-93, also Ca-41 is highly mobile in the geosphere, resulting in similar activity releases from the geosphere as from the near-field (black lines in Figure 9-15). The shape of the release is due to sequential contributions of both the initial release from two sets of waste vaults (two first peaks, 2–5BLA and 2BMA) and the development of the cement material properties in the waste vaults (two last peaks) (**Radionuclide transport report**, Section 5.3).

In the biosphere, Ca-41 sorbs rather strongly in the inorganic regolith layers (Table 9-2), resulting in considerable retention in the two bottom-most layers (RegoLow and RegoGL; Figure 9-15). The transport through the biosphere object (residence time) is long, and it would take on average 15 000 years for stable calcium to reach the surface under terrestrial conditions. The physical half-life of Ca-41 is about an order of magnitude longer than its residence time in the biosphere object and, hence, export from the system with water is the dominating removal mechanism (over 90 %). The slow transport and the marginal effects of radioactive decay imply that the Ca-41 inventory in the biosphere is the result of a more or less continuous accumulation until the time of the maximum.

During the submerged period, virtually all activity is found in the lower regolith layer (Figure 9-16); this is due to the very low upward fluxes of deep groundwater (see the corresponding discussion for C-14 above). When the biosphere object has emerged above sea level, the upward fluxes of deep groundwater increase and the accumulation in the upper regolith layers above the till becomes notable. However, most of the total activity is still retained within the lowest regolith layer, and around the time for maximum activity inventory (ca 26 000 AD), almost 90 % of the retained activity inventory is still found in RegoLow.

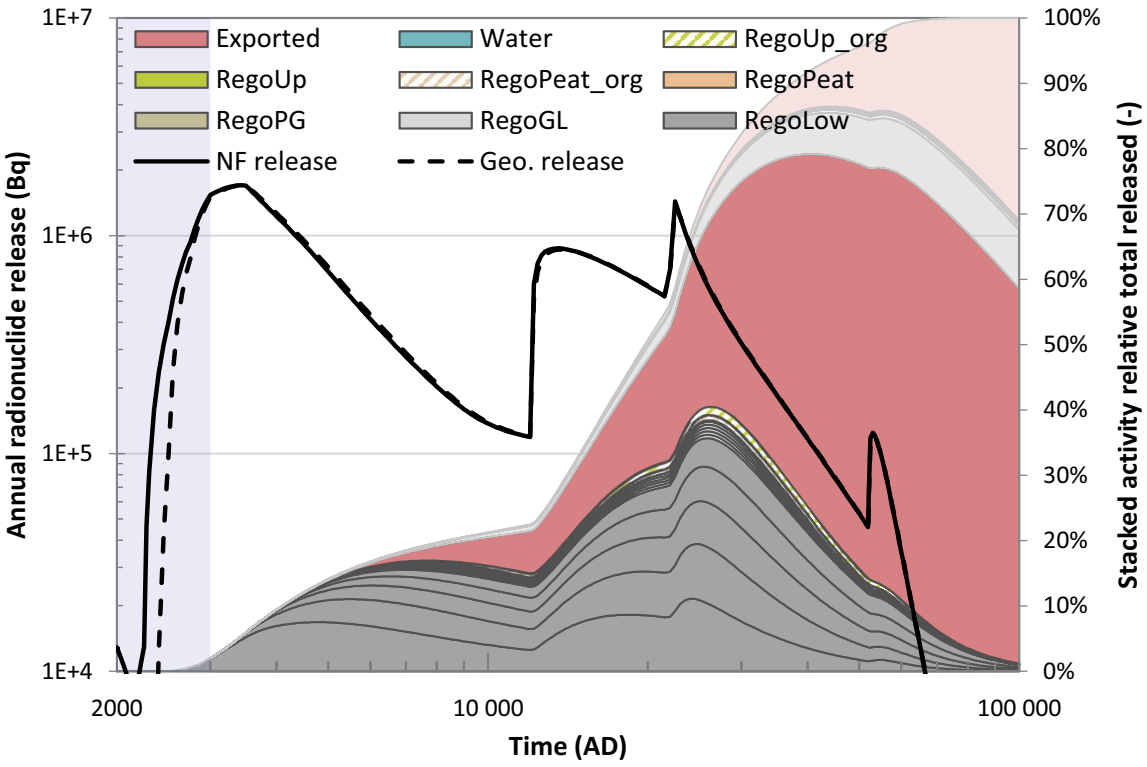

Figure 9-15. *The release of Ca-41 from the near-field to geosphere and from geosphere to the regolith (the black lines, left vertical axis) plotted together with the activity inventory of released Ca-41 (non-transparent coloured areas, right hand vertical axis). Sudden release changes around 12 000, 22 000 and 52 000 AD are related to physical and chemical cement degradation in the 2BMA waste vault (Radionuclide transport report, Section 5.3). Semi-transparent colours, except the blue area indicating submerged conditions, represent the amount decayed within each layer or after export from the object.*

There is a shift in the direction of the gradient of pore water activity concentration in RegoLow after the geosphere release maxima, which is most visible after the third peak (Figure 9-15 and Figure 9-16). About 1 000 years after this peak release, there is a distinct peak in the pore water activity concentration in the first layer of till (RegoLow) and the concentration decreases upwards and is lowest in the fifth, and uppermost, till layer (top panel of Figure 9-16). At ca 31 000 AD the situation has become reversed, the pore water activity concentration in the RegoLow sub-compartments now increases upwards. This shift is the combined effect of a relatively steep decrease in the geosphere release after the peak and of the slow upward migration of the relatively large radionuclide inventory (due to sorption) in shallower layers, causing a faster depletion of the deeper compartments compared with the shallower ones.

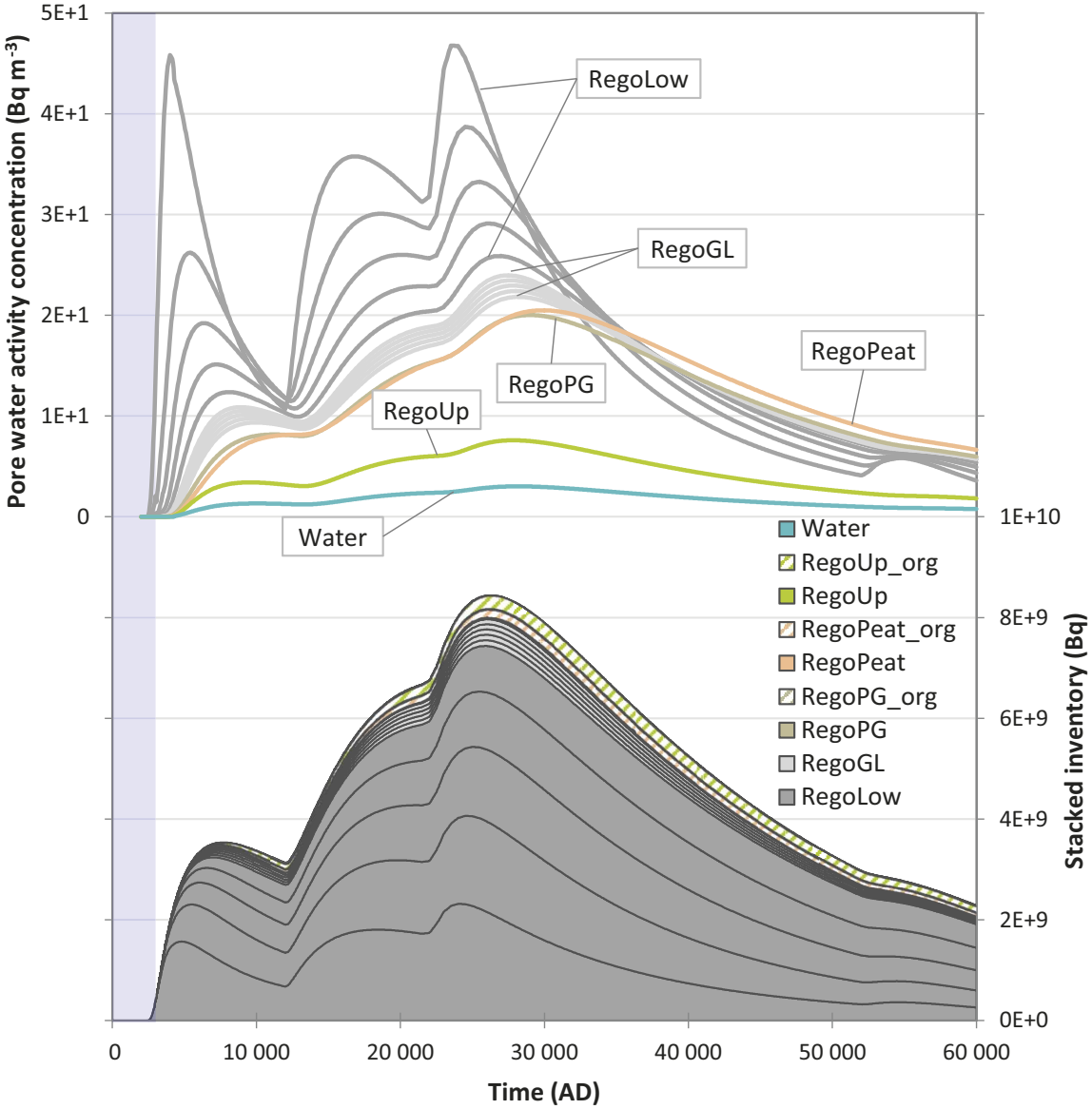

Figure 9-16. *Activity concentration in the pore water (top) and activity inventory (bottom) of Ca-41 in regolith layers in the mire. The areas with diagonal stripes for RegoUp and RegoPeat in the bottom figure indicate the inventory in the organic fraction. Note the linear and zoomed in time-axis compared with the logarithmic time-axis in similar figures.*

When the mire is drained at the time of maximum activity in the soil, it is the glacial clay (RegoGL) that accounts for approximately 50 % of the initial radionuclide inventory in the cultivated soil, with additional contributions from the organic layers of RegoPeat and RegoUp, together contributing 45 %. Thus, initially the primary source for the activity in cultivated soil comprises of the radionuclides sorbed on the inorganic soil particles. However, as this activity is slowly leached from the soil during the cultivation period, the contribution from Ca-41 stored in the organic matter becomes equally and eventually slightly more important (left panel in Figure 9-17).

The dose maximum from Ca-41 (0.8 µSv) occurs around 30 000 AD (Figure 9-17). The annual dose from Ca-41 is highly dominated by the ingestion of food, especially animal products. At the dose maximum, the ingestion of meat and milk together contribute about 80 % to the total dose. That the ingestion of animal products is the most important pathway, is a combined effect of the relatively high plant uptake of Ca-41 by fodder (as compared to the uptake by cereals and tubers) followed by a relatively high transfer from consumed fodder to animals (as compared with Mo-93) (Table 9-2). The ingestion of water contributes less than one percent, and the doses due to inhalation and external irradiation are insignificant also for Ca-41.

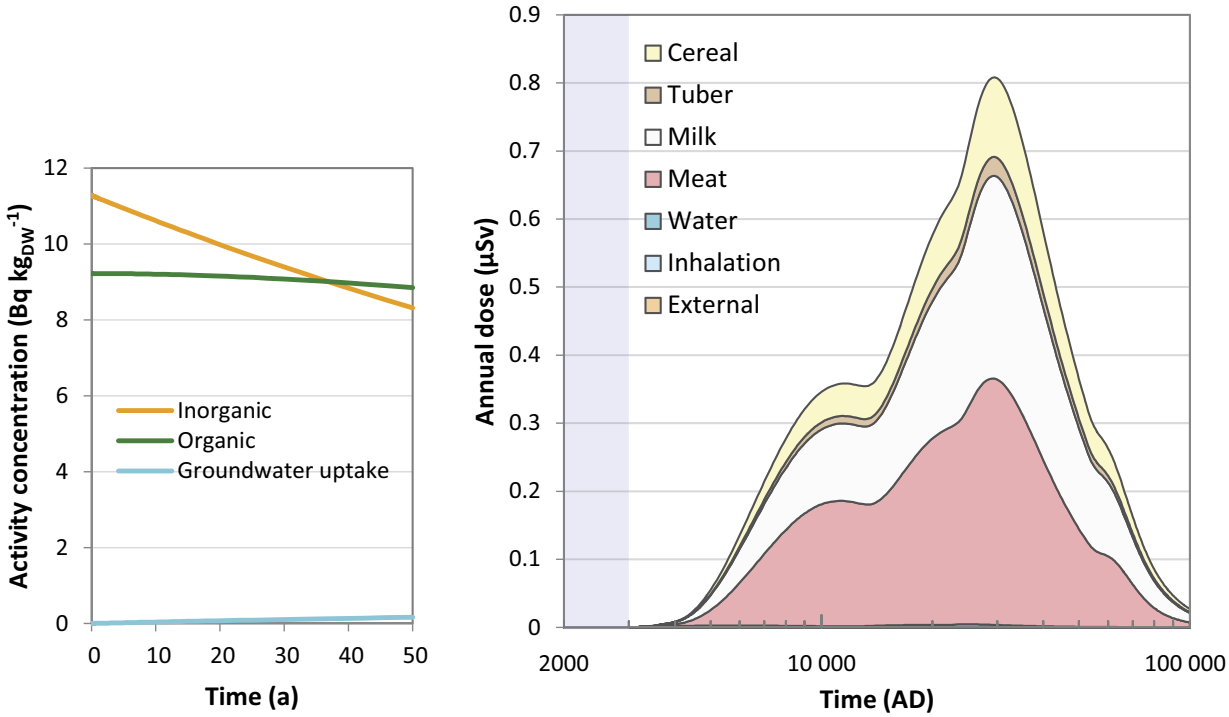

Figure 9-17. *The contribution from different sources to the activity concentration in cultivated soil during the first 50 years of cultivation of the drained mire (at the time of maximum activity in the soil) (left), and annual dose for Ca-41 for different exposure pathways for drained mire farmers (DM) in the base case (right). The contributions of water, inhalation and external exposure are too small to be discernible in the figure.*

Results for Ni-59

Unlike the three radionuclides discussed above, Ni-59 is a rather immobile radionuclide that sorbs in the near-field. This, results in a relatively late near-field and geosphere release (black lines in Figure 9-18). The geosphere release for Ni-59 is initially dominated by release from waste vaults 1–5BLA. Later in the assessment period there are two distinct rises in the releases. These correspond to an increased corrosion rate (1BRT), and an increased diffusivity (1–2BMA) in the near-field (**Radionuclide transport report**, Section 5.3).

Ni-59 reaching the biosphere primarily sorbs in inorganic regolith layers, resulting in considerable retention in the two bottom-most layers, RegoLow and especially RegoGL (Figure 9-18). The transport through the biosphere object (residence time) is long, it would take on average about 50 000 years for stable nickel to reach the surface under terrestrial conditions. The effect of the slow transport can be seen in the timing of the maximum porewater concentration; the peak in RegoUp has not been reached 25 000 years after the peak in the layer where the release enters, i.e. RegoLow (Figure 9-19). Since the physical half-life of Ni-59 and its residence time in the biosphere object are of the same order of magnitude, both the radioactive decay within the object and the export from the system with water are important removal mechanisms. At the end of the simulation, half of the released activity from the geosphere is still stored within the regolith layers.

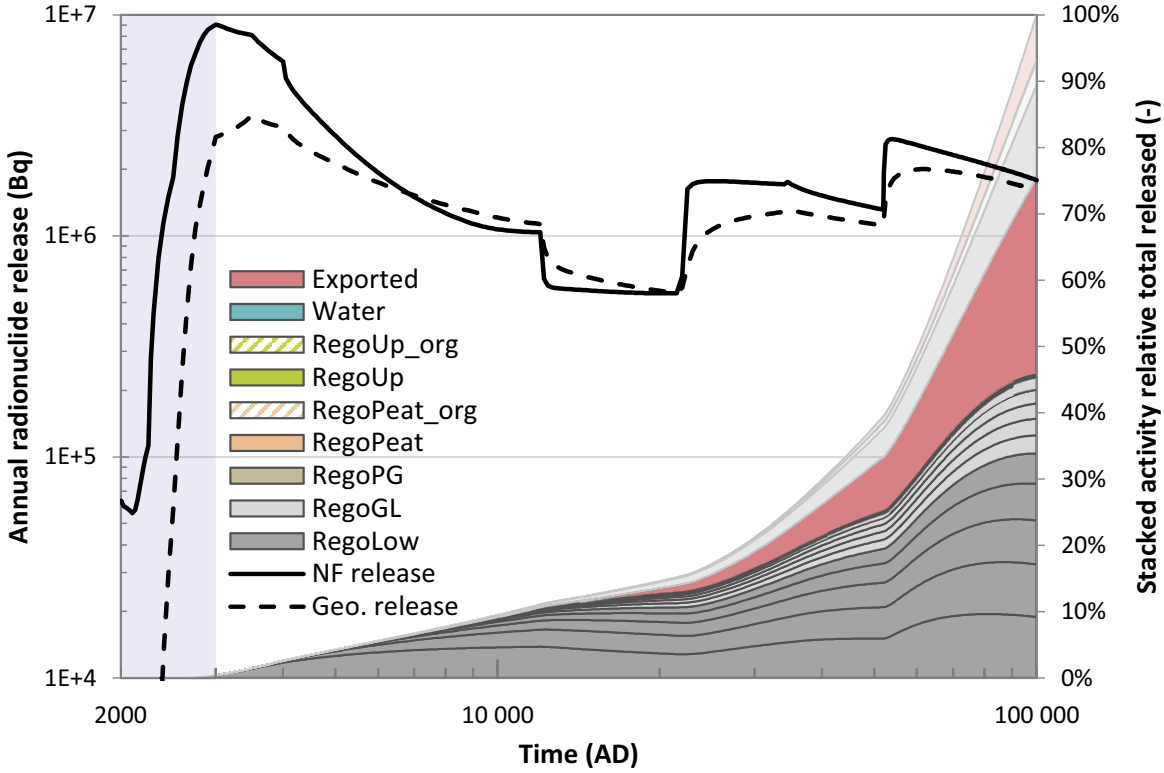

Figure 9-18. *The release of Ni-59 from the near-field to geosphere and from geosphere to the regolith (the black lines, left vertical axis) plotted together with the activity inventory of released Ni-59 (non-transparent coloured areas, right hand vertical axis). Sudden release changes around 12 000, 22 000 and 52 000 AD are mainly related to physical and chemical cement degradation in 1–2BMA (Radionuclide transport report, Section 5.3). Semi-transparent colours, except the blue area indicating submerged conditions, represent the amount decayed within each layer or after export from the object.*

Since the major part of the geosphere releases occur in the second half of the assessment period, and the transport is slow through the biosphere object, the activity inventory increases in all regolith layers towards the end of the assessment period (Figure 9-19). The exception is the inventory in RegoLow, for which all sub-compartments reach their maximum concentrations before the end of the assessment period.

During the submerged period, virtually all activity in the biosphere is found in the lower regolith layer (Figure 9-18); this is due to the very low upward fluxes of deep groundwater. When the biosphere object has emerged above sea level, the upward flux of deep groundwater increases and accumulation in regolith layers above the till becomes notable. However, most of the released activity is retained within the lowest regolith layers for the entire assessment period. The activity inventory reaches its maximum at the end of the assessment period. At this point in time, 75 % of the activity inventory is found in RegoLow (till) and 25 % in RegoGL (glacial clay). Consequently, the activity sorbed in the glacial clay is the primary source of activity in the cultivated soil once the mire is drained (left panel in Figure 9-20).

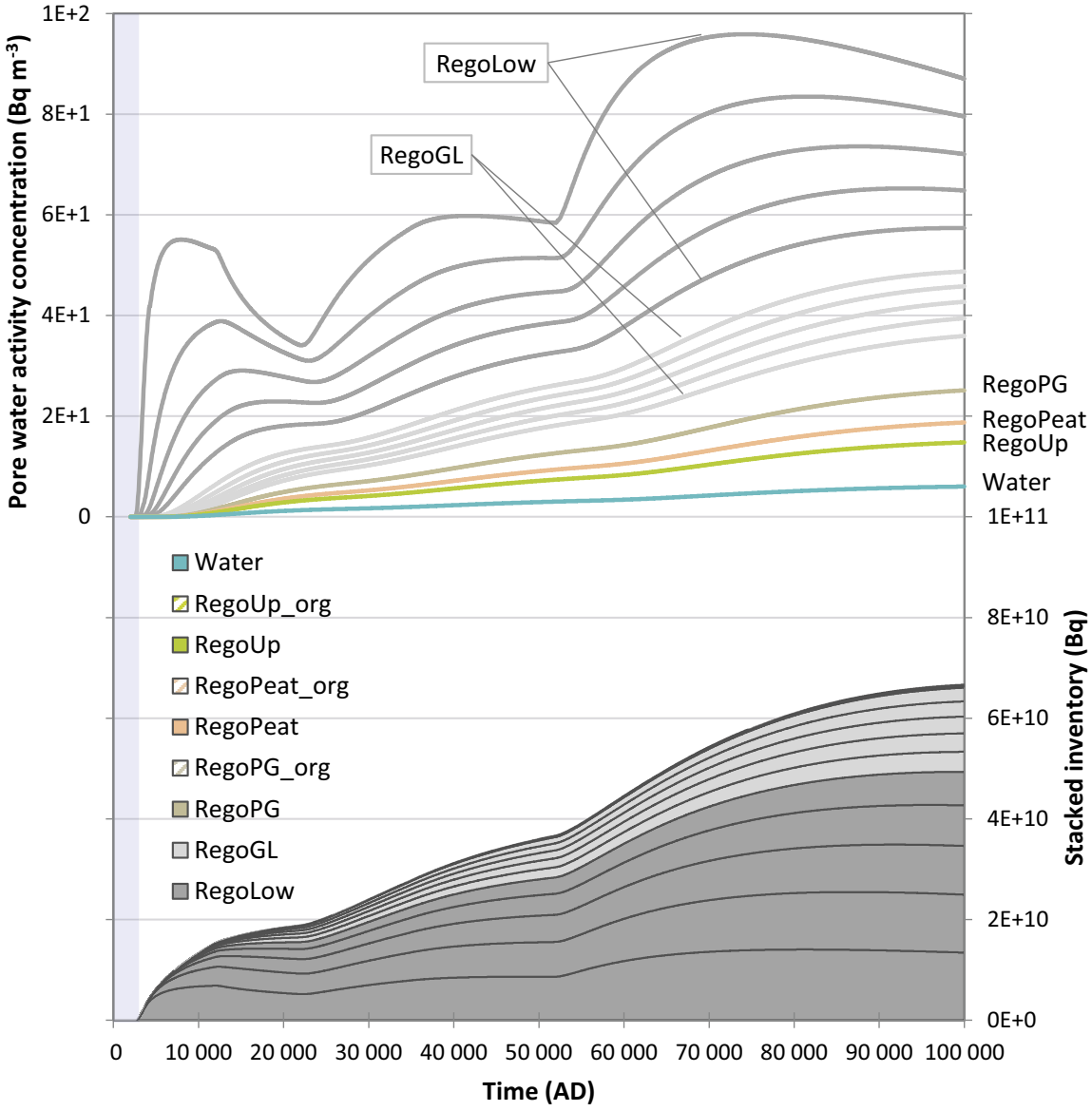

Figure 9-19. *Activity concentration in the pore water (top) and activity inventory (bottom) of Ni-59 in regolith layers in the mire. Note the linear time-axis compared with the logarithmic time-axis in similar figures.*

The highest dose from Ni-59 (0.44 µSv) occurs at the end of the assessment period (right panel of Figure 9-20). Simulations have also been performed beyond 100 000 AD, indicating that Ni-59 reaches a dose maximum that is marginally higher (0.46 µSv) 15 000 years after the end of the assessment period.

The slow transport of Ni-59 results in the annual dose being dominated by the ingestion of water from the well for the first 3 000 years. However, the dose is very low in this period, in the order of nSv, and is not visible in Figure 9-20. After a few thousands of years, the dose from the ingestion of food exceeds the dose from ingestion of water and then dominates the total dose for the rest of the assessment period. Due to high transfer from fodder to meat (Table 9-2, one and two orders of magnitude higher than for Ca-41 and Mo-93, respectively), the consumption of meat contributes most to the annual dose from Ni-59. The contribution of this pathway is typically about 60 %. Ingestion of tubers is the second-most contributing pathway with about 20 % to the total dose. Contributions from inhalation and external irradiation are insignificant.

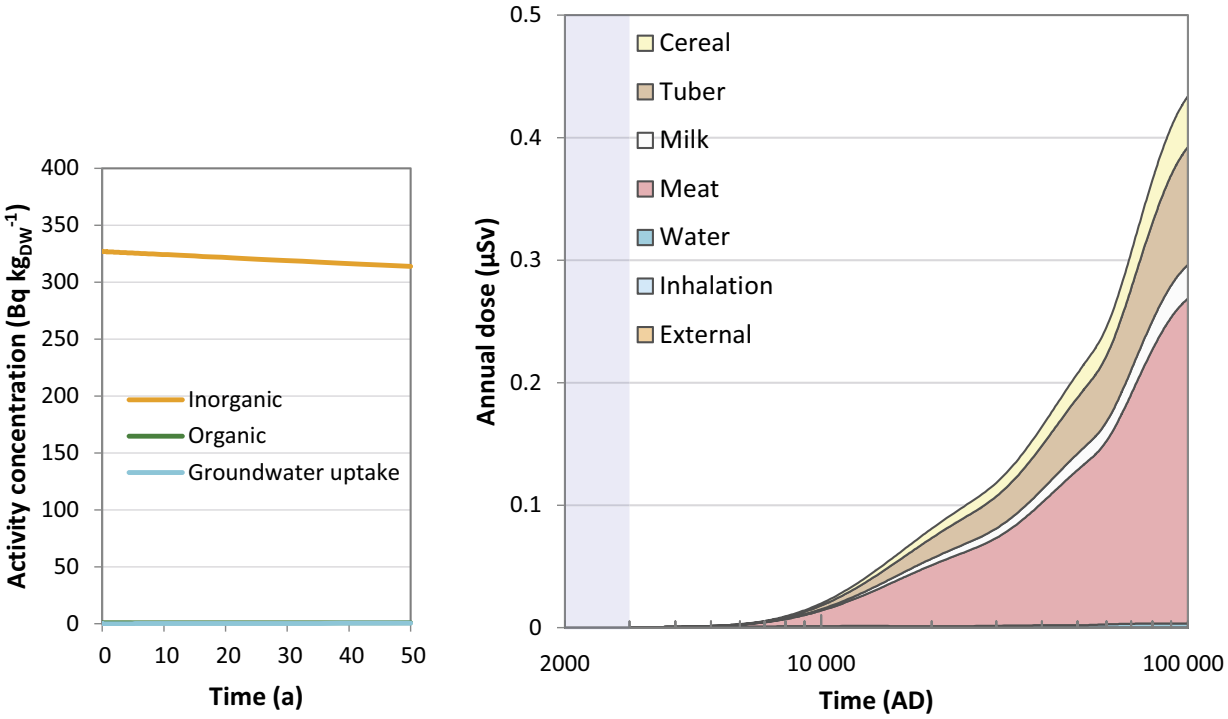

Figure 9-20. *The contribution from different sources to the activity concentration in cultivated soil during the first 50 years of cultivation of the drained mire (at the time of maximum activity in the soil) (left), and annual dose for Ni-59 for different exposure pathways for drained mire farmers (DM) in the base case (right). The contributions of water, inhalation and external exposure are too small to be discernible in the figure.*

Other radionuclides and decay chains

The analysis above focuses on the four radionuclides that dominate the dose to the most exposed group during different periods of the simulation and gives an overview of radionuclides with different properties and behaviours in the biosphere. Below, this detailed radionuclide specific analysis is complemented by a synoptic approach. In this analysis the dose from additional radionuclides, with an even broader range of properties and behaviours, are compared to that of the original set.

The maximum dose of Mo-93, Ca-41 and Ni-59 relative the maximum annual geosphere release is ~1:400 (i.e. the blue circles are above the 1:1 000 isocline in Figure 9-21). This ratio is about two orders of magnitude lower for C-14; it is ~1:30 000 (i.e. the blue circle for C-14 is below the 1:10 000 isocline in Figure 9-21). One reason for this is the high mobility and marginal accumulation of C-14 in regolith layers that are drained and cultivated (Figure 9-21). As mentioned earlier, losses due to decay in the regolith are small for C-14 and Ca-41, but Mo-93 and Ni-59 doses would be 50 % and 30 % higher if the decay in the regolith was not accounted for. These hypothetical doses correspond to the grey circles in Figure 9-21 (as these radionuclides are not affected by ingrowth).

Cs-135, U-238 and I-129 are three radionuclides that also contribute significantly to the total annual doses (Figure 9-5, lower panel). The maximum dose of Cs-135 (0.4 μSv) and its ratio of dose to geosphere radiotoxicity (1:500) are similar to those of Ni-59 (Figure 9-21). Likewise, the maximum dose of Cs-135 occur at the end of the analysis period. Cs-135 sorbs strongly in regolith, especially in the glacial clay (325 m^3 $kgdw^{-1}$). This makes accumulation in the regolith even more important to the dose of Cs-135 than for Ni-59. Cs-135 is more long-lived than Ni-59 and losses due to decay in the biosphere are insignificant (no grey circle shown for Cs-135 in Figure 9-21). The primary exposure pathway is through accumulation in glacial clay, followed by plant uptake. As plant uptake (i.e. the CR) for fodder is an order of magnitude higher than for other crops, consumption of milk and meat is the main pathway for exposure.

Doses from U-238 and I-129 both contribute to the maximum total dose (Figure 9-5, lower panel). Their maximum radiotoxicity releases are larger than for Mo-93, Ca-41 and Ni-59, but their dose to release ratios are lower (~1:7 500). For U-238, this is explained by the relatively short period with high releases around 3000 AD. Radionuclides in this release are dispersed by the moderate retention in the regolith and results in a maximum dose of 0.5 μSv about 5 000 years later (Figure 9-5). Despite limited plant uptake the dose is dominated by consumption of cereal. Since U-238 is extremely long-lived (half-life 4.5 billion years) decay is negligible (Figure 9-21) and losses from the biosphere system are due to export alone. I-129 is more mobile. This results in a marginal accumulation in the regolith and substantial losses from the biosphere through export, and almost no losses through decay (no grey circle shown for I-129 in Figure 9-21). This results in a dose curve that closely follow the geosphere releases (Figure 9-5). The low accumulation in combination with a relatively low plant uptake explains the limited maximum doses (0.3 μSv) dominated by exposure from drinking well water and milk.

Ag-108m, Pu-239, Pu-240 and Ra-226 all have larger maximum geosphere releases than Mo-93, Ca-41 and Ni-59, but their maximum doses are considerably lower (i.e. below 0.03 μSv) and the maximum dose to release ratio is below 1:40 000. A major explanation for the low ratios is that these radionuclides have short physical half-lives in relation to their residence times in the biosphere. Thus, most of the released activity is lost in the till and never reaches the shallower regolith layers that are exposed by cultivation (grey circles are considerably larger than blue circles in Figure 9-21). As a consequence, Ag-108 and Pu-240 primarily expose through extraction of well water from the till. This implies that sorption in this layer also directly reduces the radionuclide concentration of the major exposure pathway (i.e. the concentration in the well water). Pu-239 has a longer half-life (in relation to its residence time), and although only a small fraction of the released Pu-239 escapes the till, the primary exposure pathway is accumulation in glacial clay, and the subsequent plant uptake and consumption of harvested crops (primarily cereal).

Most of the Ra-226 that is released from the geosphere is also lost through decay in the lowest regolith layer. However, the primary source of Ra-226 is not direct release from the geosphere, but ingrowth due to radioactive decay within the biosphere. This is reflected in the ratio between the annual dose (blue circle) and the hypothetical dose without ingrowth (orange circle in Figure 9-22). This ratio is 4.5, indicating that ingrowth from Th-230 is almost four times as important as direct release from the geosphere. The primary exposure pathway for Ra-226 is similar to that of Pu-239. In addition, consumption of well water also contributes somewhat to the maximum dose (20 %).

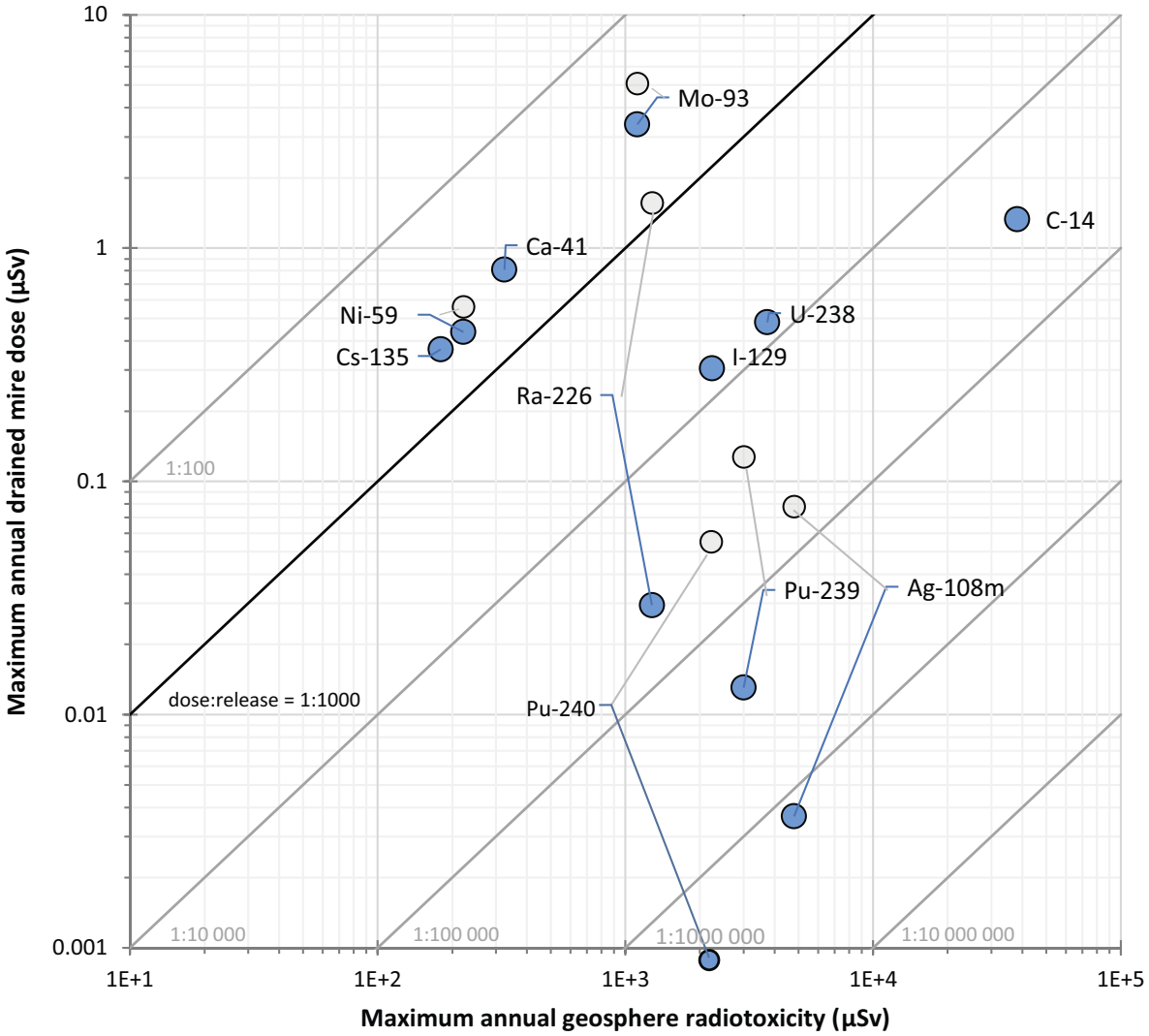

Figure 9-21. *Maximum annual doses from the drained mire as a function of the maximum annual geosphere release of radiotoxicity (blue circles). The grey circles show how large the maximum doses would have been if the activity of radionuclides did not decrease with decay or increase with ingrowth (for decay products) in the biosphere (< 10 % from maximum annual doses are not shown). The black isoline (black diagonal line) show where maximum doses are one part per mille (or 1:1 000) of the maximum geosphere release and the grey isolines show other linear relationships between maximum doses and maximum releases. The figure contains all radionuclides with a maximum annual dose > 0.1 µSv or a maximum annual geosphere release > 1 000 µSv, except for the decay products Pa-231 and Ac-227 in the U-235 decay chain (see Figure 9-22).*

The maximum doses from U-235 and its decay products Pa-231 and Ac-227 are about 0.2 µSv each (Figure 9-22) and in particularly the two latter contribute to the total annual doses from 20 000 AD and onwards (Figure 9-5). Similarly to U-238, U-235 has a half-life that is orders of magnitude longer than its residence time in the biosphere, and the behaviour of U-235 in the biosphere is practically identical to that of U-238 (see above). Thus, the differences in the maximum doses and the dose curves of the two uranium isotopes are primarily due to differences in the geosphere release (Figure 9-5).

The activity of U-235 in regolith layers results in ingrowth of Pa-231 activity, with a rate of 2×10^{-5} y^{-1}, corresponding to the half-life of Pa-231 (33 000 years). The ingrowth of Pa-231 is five times more important for the maximum doses from Pa-231 than the direct release from the geosphere (see span between blue and orange circles in Figure 9-22). The strong sorption of Pa-231 in the glacial clay (K_d = 100 m^3 $kgdw^{-1}$) inhibits a net upward transport from this layer. Although ingrowth of Pa-231 occurs throughout the regolith profile, the accumulation is largest in the two lowermost regolith layers. Decay of Pa-231 in the regolith is significant and doses would have been three times larger without

losses from decay (see span between grey and orange circles in Figure 9-22), while losses through exported from the biosphere are marginal. The primary exposure pathway is through accumulation in glacial clay and the subsequent plant uptake and consumption of cereals.

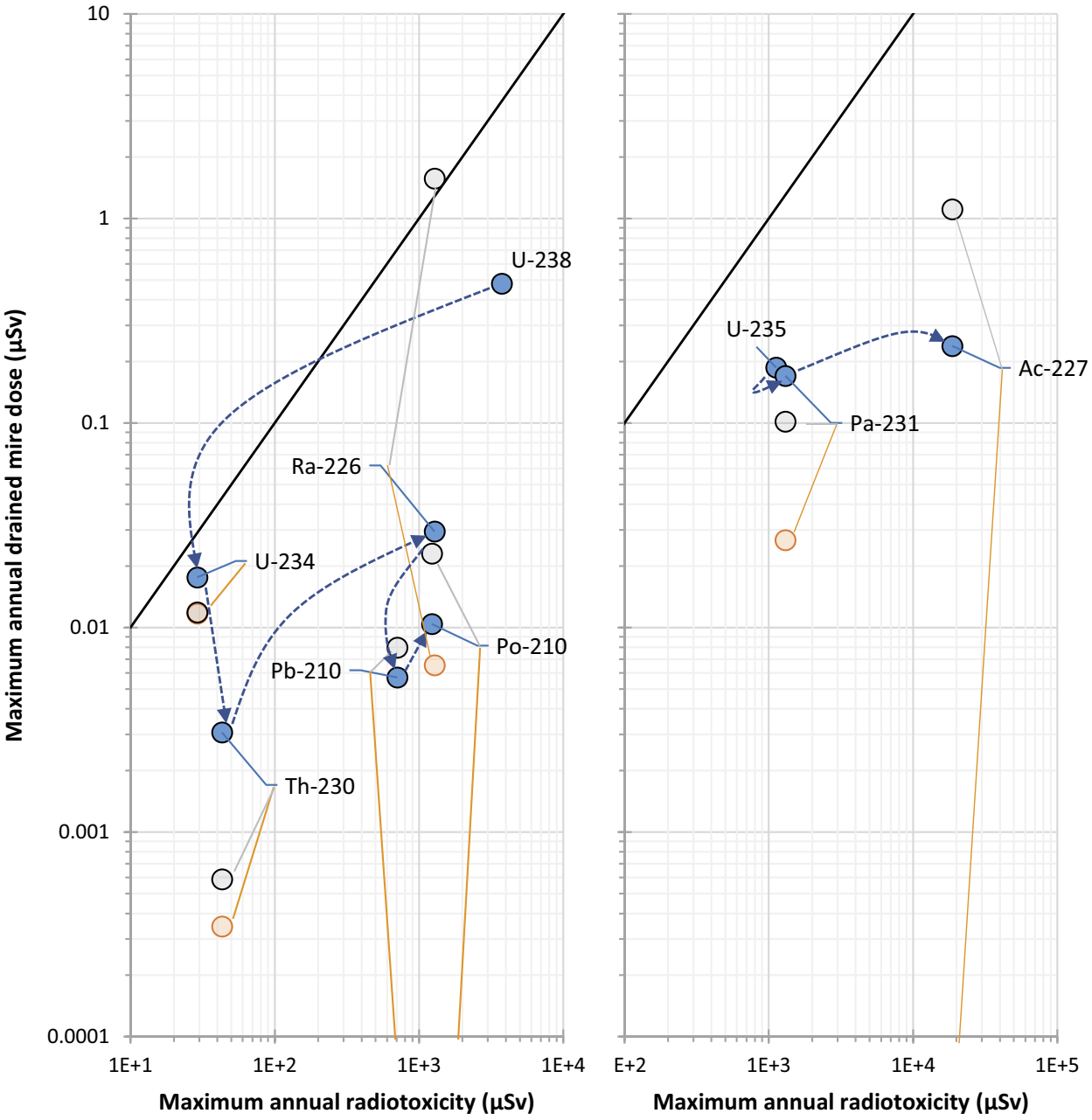

Figure 9-22. *Maximum annual doses from the drained mire versus the maximum annual geosphere release of radiotoxicity (blue circles) for the U-238 decay chain (left panel) and the U-235 decay chain (right panel). The dark blue dashed arrows indicate links between parental radionuclides and their decay product (disregarding short-lived radionuclides). The orange circles show how large the maximum doses would be without ingrowth from parental radionuclides in the biosphere. The grey circles show how large the maximum doses would be if the activity of radionuclides did not decrease with decay or increase with ingrowth within the biosphere. The black isoline show where maximum doses correspond to 1:1 000 of the maximum geosphere release of radiotoxicity.*

The activity of Pa-231 results in ingrowth of Ac-227. This decay product has a relatively short half-life (22 years), and consequently the rates of ingrowth and decay are several orders of magnitude larger than transport rates within the biosphere. Thus, ingrowth and decay are the only processes of importance for the activity of Ac-227, and the activity will in practice be identical to that of Pa-231 (they are in secular equilibrium). Thus, it is not surprising that dose resulting from the geosphere release of Ac-227 is several orders of magnitude lower than that from ingrowth (orange versus grey circles in Figure 9-22). As plant uptake and transfer coefficients for meat and milk for Ac-227 are assigned to have the same distribution as for Pa-231, the primary exposure pathway of Ac-227 is near identical to that of Pa-231.

In the U-238 decay chain, the long-lived U-234 and Th-230 display similar behaviour in terms of ingrowth, accumulation and decay as U-238 and Pa-231 respectively, while the more short-lived Ra-226, Pb-210, Po-210 behave more like Ac-227 (Figure 9-22). However, except for U-238, the maximum doses from the radionuclides in this decay chain are substantially lower than for the U-235 decay chain.

9.4 The effects of parameter uncertainties

The annual dose for each point in time is calculated probabilistically, running 1 000 realisations with different randomly drawn sets of ecosystem parameters. The uncertainty in input parameters, that is data uncertainties, causes a significant variation in the calculated dose between these realisations that underlie the expectation value (mean) of the annual dose (Figure 9-23, grey lines). The difference between the 5th and the 95th percentiles of the dose typically spans an order of magnitude, and this span tends to widen with time. Although uncertainties will inevitably increase far into the future, the pattern in the simulations primarily reflects the differences in uncertainties associated with the individual radionuclides that contribute to the dose in the sequence. That is, the uncertainties in the dose from C-14 and Mo-93, that contribute early, are relatively small compared with the uncertainties of dose from Ca-41 and Ni-59, that contribute later in the simulations (for further details on uncertainties of individual radionuclides see the *ecosystem properties calculation case, Section 11.2*).

In Figure 9-23, the mean dose is consistently above the median dose (blue and orange lines in Figure 9-23). This is expected, because the total dose (at each point in time) is approximately log-normally distributed, in turn reflecting that most of the important input parameters are positively related to the dose and have a positively skewed distribution. Based on the central limit theorem (see Ekström 2017 for details), the confidence intervals of the mean value can be estimated with good precision assuming that it is normally distributed (thin blue lines in Figure 9-23). The confidence interval of the mean exhibits small variability (less than 10 % of the mean dose), clearly indicating that the number of realisations (1 000) is sufficient for an acceptable level of convergence.

The deterministic simulation with the best estimate for each input parameter yields systematically lower dose than the mean dose from probabilistic calculations. This indicates that parameter uncertainty does not lead to an underestimation of the dose.

In the geosphere model the main features of transport and retention are captured by factors acting in a multiplicative manner and the key parameters are log-normally distributed. In such circumstances, the median output from probabilistic simulations will be similar to a single run using median values as the best estimate for parameters. However, in the surface system, there are parallel pathways for accumulation and for exposure. That is, several regolith layers contribute to activity in the drained and cultivated soil and the pathways for ingestion include cereals, potatoes, meat, milk and water. When parallel pathways have similar importance, and the underlying parameters are positively skewed in a direction that increases exposure, the dose from probabilistic simulations has a strong tendency to be higher than that of the deterministic simulation, which uses the best-estimate values. This is because only a few parameters with high values are needed to get a sum that is higher than that resulting from the best estimates[46]. Moreover, for a few biosphere parameters, the probability distribution functions (PDF) have been biased towards increased exposure, by selecting the PDF's central value above the best estimate.

[46] This is in analogy with the arithmetic mean being systematically higher than the geometric mean (here, equalling the best estimate) of a log-normal distribution.

The effects of parallel pathways and biased PDFs on dose can most clearly be seen in the period between 20 000 to 60 000 AD when Ca-41 contributes most to the dose (Figure 9-5). For Ca-41, glacial clay (RegoGL), and the organic matter in peat layers (RegoUp_org, RegoPeat_org) all contribute to the accumulation of Ca-41 in agricultural soil, and three partly separate ingestion pathways (cereals, meat and milk) contribute to dose involving four different parameters for radionuclide transfer (*ecosystem properties calculation case*). In addition, PDFs for plant uptake in mire vegetation (that drives accumulation in peat) and in fodder that drives the exposure via meat and milk) both have (geometric means (i.e. central values) above the corresponding best estimates used in the deterministic calculations. Taken together, this results in a somewhat counter-intuitive distribution of probabilistic results, where less than 5 % of the simulations result in doses that are smaller than the deterministic calculations (i.e. the 5th percentile curve is above that for the deterministic results in Figure 9-23).

Another source of uncertainty in the probabilistic simulations is related to the potential for temporal dilution of radionuclides. This occurs when the timing of the maximum (or peak) dose differs between simulations, e.g. due to uncertainties in parameters affecting the retardation of radionuclides, and leads to an underestimation of dose when the average is calculated for a fixed point in time. This is because even for the time point that yields the highest mean dose, there will be simulations where the dose maximum occurred earlier or later in time. The temporal dilution that occurs from such averaging is expected to be larger for short-term dose peaks than for dose peaks lasting longer.

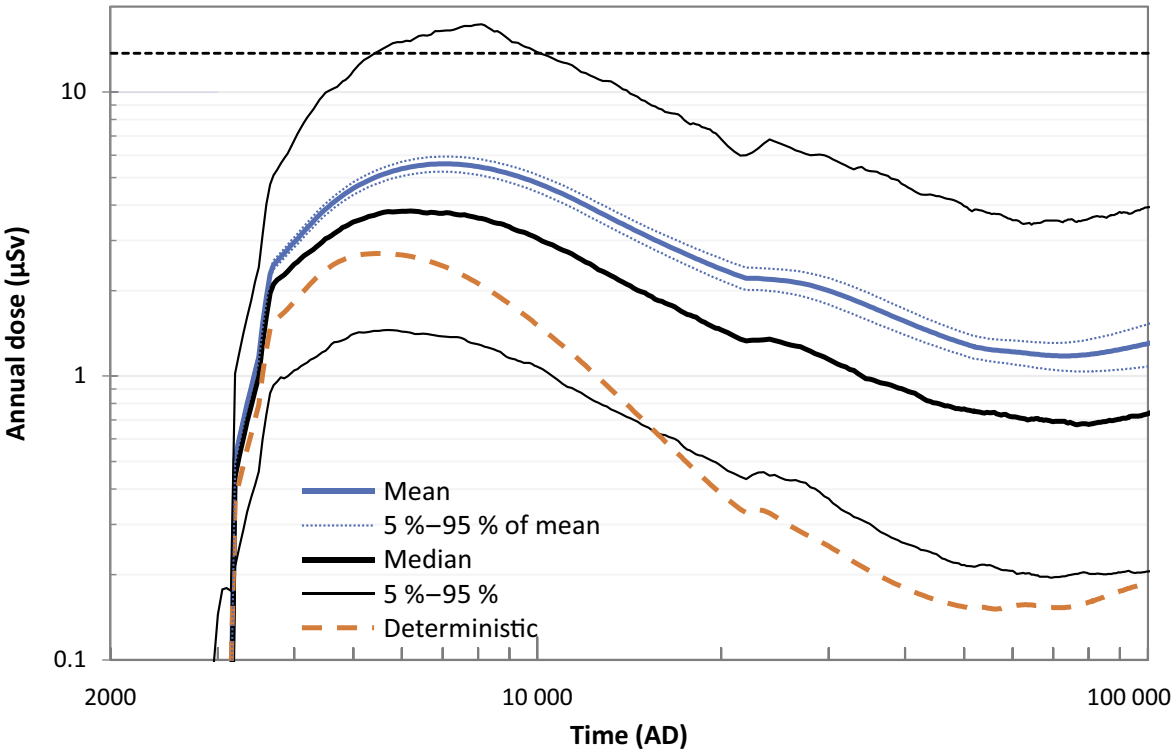

Figure 9-23. *Distribution and characteristics of the total annual dose in the base case. Blue colour represents the mean (expectation) value of the dose from probabilistic simulations, with the 90-percent confidence interval of the mean (thin blue dotted lines). The span of the 1 000 realisations is shown as the 5th and the 95th percentile of the simulations (thin black lines) and the 'typical dose' (i.e. the median) from the realisations is shown in black. The dose calculated from one deterministic simulation using best estimates for all input parameters is shown for comparison (dashed orange line). The annual dose (14 µSv) corresponding to the regulatory risk criterion is indicated by the black dashed line. The blue shading indicates the submerged period.*

The potential for temporal dilution can be assessed by considering the maximum dose from each of the probabilistic simulations, irrespective of the time of the peak. The mean of such maximum dose is referred to as the *mean-of-peaks*, and it can be contrasted against the dose from each simulation at the time of maximum for the average dose (~7000 AD in the *base case*), referred to as the *peak-of-means*. The mean-of-peaks is by definition greater than (or equal to) the peak-of-means. The ratio between the two is referred to as the *risk dilution ratio* (e.g. Wilmot and Robinson 2004). Note that also in a deterministic calculation the peak dose from different radionuclides may be separated by thousands of years, due to the properties of the radionuclides, of the repository and of its environment. Thus, some caution must be applied when interpreting mean-of-peak doses, so that the appropriate temporal spread of dose and risk is not unduly disregarded. In the *base case*, the ratio between the mean-of-peaks and the peak-of-means (vertical axis position of grey and orange cross-hairs, respectively, in Figure 9-24) is 1.26, indicating that temporal dilution is not likely to have any significant effect on the results.

Approximately 80 % of the peak dose values in the probabilistic simulations occur before 10 000 AD, reflecting dominance of the dose by C-14 and Mo-93 (upper histogram in Figure 9-24). However, in about 20 % of the calculations, the maximum dose occurs after 10 000 AD. This results in a bimodal distribution of the maximum dose after 10 000 AD, reflecting the separate, differently timing contributions from Ca-41 and Ni-59 to the total dose (the second and third peaks, respectively, in the upper histogram of Figure 9-24). Thus, the mean-of-peaks calculation combines doses from peaks that are separated in time partly due to systematic differences in parameter values between radionuclides in combination with the assumed evolution of the repository. Inclusion of the second and third peaks in the mean-of-peak calculations will overestimate the potential for temporal dilution, as the separation of peaks reflects expected effects of retention and dispersion in relation to the degradation of the engineered barriers. Because of this, the risk dilution ratio of individual radionuclides is a more appropriate metrics. These ratios amount to 1.05, 1.10, 1.20 and 1.02 for C-14, Mo-93, Ca-41 and Ni-59, respectively. Consequently, the potential for temporal dilution appears to be 10 % or less for the first 10 000 years when the dose maximum occurs. This strengthens the conclusion that temporal dilution introduced by the probabilistic simulations is unlikely to have any significant effect on the results.

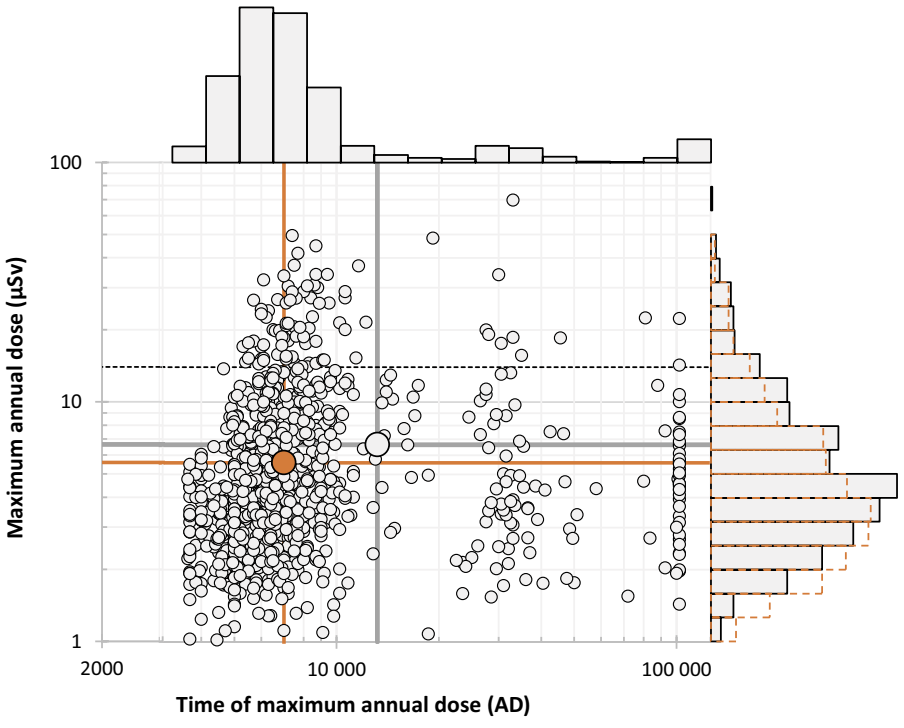

Figure 9-24. *Distribution of peak characteristics for the total dose from the 1 000 realisations used in the probabilistic calculations in the base case. The histogram to the right shows the distribution of the peak doses, and the histogram on the top shows the distribution of the corresponding peak times. The scatter plot in the centre shows these two characteristics for each of the 1 000 realisations. The distribution of the dose from each of the simulations at the time of maximum for the mean dose (7000 AD) is indicated by the orange line in the right-hand histogram for reference. The mean-of-peaks is 26 % higher than the peak-of-means, as indicated by the horizontal grey line being above the horizontal orange line. The annual dose (14 µSv) corresponding to the regulatory risk criterion is indicated by the black dashed line.*

9.5 Summary and discussion

The *base case* constitutes the basis for the radionuclide transport and dose calculations in the PSAR. In the *base case*, present-day climate conditions prevail for the entire assessment period, and physical and biological properties of the ecosystems are constant throughout the period, for example, no change in the average air temperatures is assumed when selecting values for ecosystem parameters. The geosphere release is assumed to be discharged to biosphere object 157_2, and radionuclides are transported to other objects through water exchange or by stream water.

The total annual dose throughout the entire 100 000-year assessment period is below the dose (14 μSv) that corresponds to the regulatory risk criterion. The maximum total annual dose of 5.6 μSv occurs around 7000 AD. Draining and cultivation of a mire (DM) is the land use variant resulting in the highest doses. This is primarily because radionuclides can accumulate in the upper regolith (e.g. peat) of the mire over long periods of time prior to the drainage and subsequent exposure, and because the cultivated ecosystems are highly productive.

In the biosphere, properties related to transport, sorption, accumulation and radioactive decay determine environmental activity concentrations in the regolith profile, in relation to the geosphere releases. Uptake in plants and transfer to animal products and radiotoxicity are other key properties affecting the radionuclide-specific doses. Four radionuclides are of specific interest in the PSAR, namely Mo-93 and C-14 that contribute the most to the total dose from the time of repository closure up until the time of dose maximum, Ca-41 that contributes the most in the middle of the assessment period, and Ni-59 that contributes the most at the end of the assessment period.

In the biosphere, the non-sorbing radionuclide C-14 mainly follow the groundwater flow. C-14 is quickly transported through the regolith layers (~ 10 years) and is only marginally affected by radioactive decay. Instead, it is to a large degree exported from the system by water exchange with the surrounding marine basins during the submerged stage, or by degassing to the air during the terrestrial stage (right-hand panel in Figure 9-25). Accumulation in the organic matter of the relatively thin peat layers is associated with slightly longer time scales (~ 100 years), but overall environmental concentrations closely follow the geosphere release rate. This means that the level of the geosphere release is almost directly correlated to the potential dose consequences in the drained mire (after the cultivated area has become sufficiently large to fully support the dietary needs of the most exposed group).

The sorbing radionuclides, on the other hand, are retained in the regolith, and the accumulation of activity and the average transport (or residence) times are positively correlated to the strength of the sorption. For Mo-93 and Ni-59 this is the case; the average transport time in the biosphere is in the same order as their physical half-lives, and thus a noticeable amount of the released activity decays within the biosphere. However, for Ca-41, the half-life is almost an order of magnitude larger than the average transport time, so, export from the system with water is a dominant removal mechanism despite the retention in the regolith.

At the times for the maximum doses specific to each of these radionuclides (Mo-93, Ca-41 and Ni-59), approximately 40 % of the accumulated releases are stored in the regolith profile of the biosphere object (Figure 9-25). This activity inventory corresponds to an accumulation of release over several thousands and tens of thousands of years for Mo-93 and Ca-41, respectively. For Ni-59, accumulation over the entire assessment period (100 000 years) contributes to the activity maximum at the end of the simulation. However, the distribution of the accumulated activity differs between radionuclides (Figure 9-25). Ca-41 and Ni-59 are strongly sorbing in the inorganic regolith layers, and so are retained within the lowest regolith layer (till), which is not exposed by draining and cultivation. Mo-93, on the other hand, sorbs more strongly in the organic-rich upper regolith layers. This means that most of the accumulated Mo-93 activity will become accessible for exposure when the object is cultivated. For C-14, a noticeable portion of accumulated activity is attributed to the organic components in the peat (left panel Figure 9-25). However, this C-14 accumulation is of minor importance for the exposure during cultivation. Instead, groundwater uptake is the primary source for C-14 in the pore water of the drained and cultivated mire (Figure 9-25, left panel).

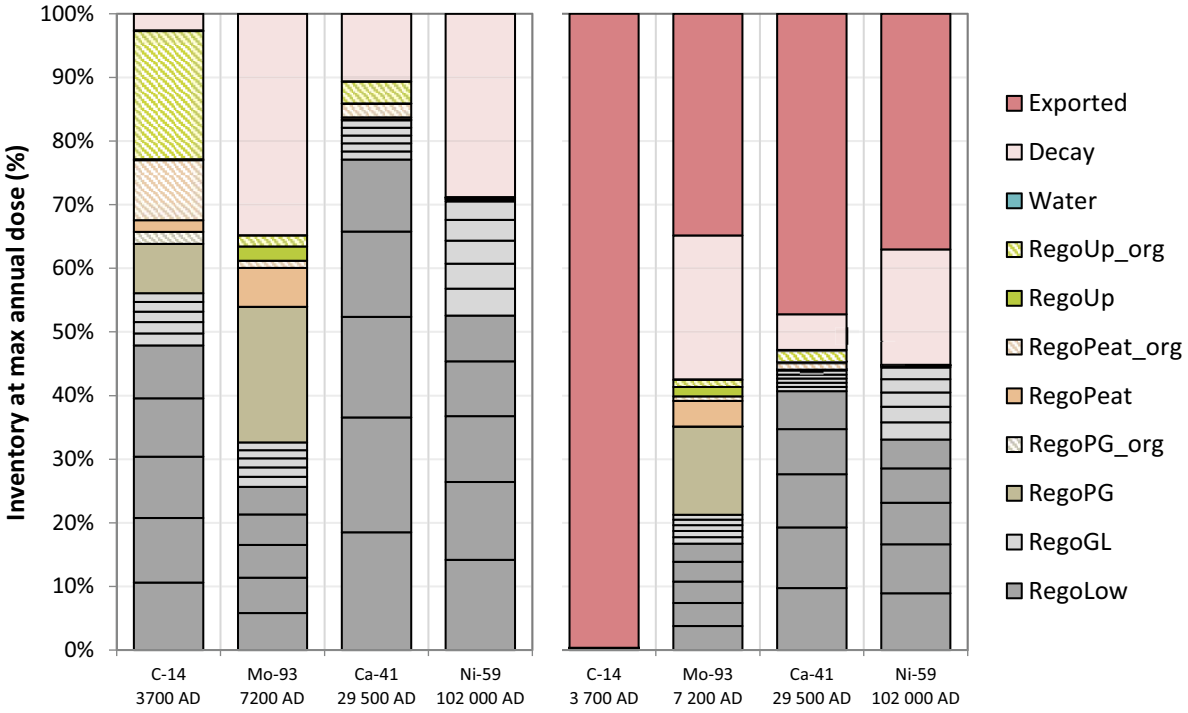

Figure 9-25. *Relative distribution of the radionuclide inventories, plotted for the time of the radionuclide-specific dose maxima in the different regolith compartments and the amounts that have decayed within the regolith (left), presented also as modified to include the amounts exported out of the system (right). Radionuclides exported from the system are degassed to the atmosphere (C-14) or are exported downstream, finally reaching the Baltic Sea. Potential consequences of regional and global exposure are evaluated as collective doses (Radionuclide transport report, Chapter 9).*

The most important exposure pathways from the drained mire are the ingestion of cultivated crops and the ingestion of animal products. These pathways are linked to the uptake of radionuclides by plants, either directly in the edible crops or indirectly via the fodder consumed by livestock. Carbon is the main structural component of life, and therefore the bioavailability of C-14 is particularly high. Both Mo-93 and Ca-41 are essential plant nutrients, and plant uptake of these two radionuclides is also high (in cereal for Mo-93 and in fodder for Ca-41) as compared with the uptake of Ni-59 (Table 9-2). The radionuclide-specific annual doses also depend on the ingestion radiotoxicities of the radionuclides (i.e. the product of the activity of a radionuclide and its corresponding ingestion dose coefficient). Of the four radionuclides discussed here, Mo-93 is the most radiotoxic, having an ingestion dose coefficient about one order of magnitude higher than C-14 and Ca-41 and two orders of magnitude higher than Ni-59 (Table 9-2).

Exposure from drinking water from the dug well is important early in the assessment period when the size of the emergent land area may be limiting the other exposure pathways or at times before the radionuclides have had time to accumulate in the upper regolith layers where the plant uptake occurs. Exposure to radionuclides in the deep groundwater is also considered in this *base case*. However, this pathway is only relevant for a small group, so the dose from a drilled well, when reduced by a factor of ten to account for the different regulatory standard adopted, becomes lower than from the dug well. Irrespective of source, the contribution of the exposure via drinking water to the total dose maximum is marginal.

In summary, the annual dose in the *base case* directly depends on the geosphere release. However, radionuclide- and element-specific properties influence transport and accumulation in the biosphere, and for sorbing radionuclides (e.g. Mo-93, Ca-41 and Ni-59) it is the accumulated long-term release, rather than maximum annual release, that is of relevance for doses. As contrast, the dose from C-14 follow rather closely the dynamics of the release. The vertical patterns of accumulation in the regolith profile, transfer to plants and foodstuff, and the ingestion radiotoxicity are other factors that modulate

the dose in relation to the geosphere release. Thus, for example, it is the combined effects of relatively undispersed geosphere release, high sorption in the organic-rich regolith layers, high plant uptake and high radiotoxicity that lead to dose from Mo-93 that is large in relation to the annual release of Mo-93.

The analysis in this chapter confirms that the behaviour of the BioTEx model is reasonable and conforms to SKB's general understanding of the surface systems at Forsmark. Differences in transport and accumulation patterns of individual radionuclides are also explainable in terms of radionuclide-specific properties as presented above. Moreover, it is shown that temporal dilution, due to the probabilistic approach used for the geosphere release and ecosystem parameters, is unlikely to introduce any significant bias on the calculated doses. Taken together, the analysis helps to build confidence that the model results from the *base case* are reliable and credible.

10 Other calculation cases in the main scenario

10.1 Introduction

The *base case* of the main scenario is presented in Chapter 9. This chapter describes the two other calculation cases analysed within the main scenario, representing a range of probable future climate developments, and the three other calculation cases in support of the main scenario. The outcome of analysing the cases with the BioTex model is presented and discussed. As for the *base case*, the calculation cases in this chapter are described from a biosphere perspective (the near-field and geosphere are addressed in the **Radionuclide transport report)**. Furthermore, this chapter focuses on doses to humans, dose rates to non-human biota are addressed in Chapter 12.

In addition to the *base case*, the main scenario includes two calculation cases representing the range of probable evolution of external conditions:

- The *warm climate calculation case* is defined based on the *warm climate variant* of the reference evolution, representing warmer-than-present conditions in the repository environs including the effect of a delayed shoreline regression (Section 10.2).
- The *cold climate calculation case* is defined based on the *cold climate variant* of the reference evolution, representing a development towards colder conditions in the repository environs including the effect of periglacial conditions during the last 50 000 years of the assessment period (Section 10.3).

The resulting doses from analysing these cases as well as the *base case* are propagated to the radiological risk assessment (**Post-closure safety report**, Chapter 10). The calculation cases for the main scenario are complemented with three supporting calculation cases, to cover the potential effects of uncertainties in landscape development and the properties of the discharge area. These supporting calculations are used as input for the selection of assumptions in the *base case* and, thereby, ensures that the evaluated uncertainties do not contribute to underestimate the maximum dose in the main scenario (**Post-closure safety report**, Section 7.2). Thus, results from these supporting calculation cases are not necessary to propagate to the radiological risk assessment. The supporting calculation cases are:

- The *timing of shoreline regression calculation case* that assesses uncertainties in the timing of the transition of the area above SFR from submerged to terrestrial conditions (Section 10.4).
- The *subhorizontal fracture calculation case*, in which the distribution of the geosphere release over a greater area than in the *base case*, caused by a large subhorizontal fracture in the bedrock, is assumed (Section 10.5).
- The *alternative landscape configuration calculation case* that assesses uncertainties with respect to the transport pathways and development of the future Forsmark landscape (Section 10.6).

The first of these supporting calculation cases is identified in the overall safety assessment (**Post-closure safety report**, Chapter 7). The other two, which were identified in SR-PSU (Saetre and Ekström 2016, 2017a) are considered to be relevant and appropriate for evaluating potential effects of uncertainties associated with the future discharge area. However, uncertainties with respect to the properties of the biosphere object, which is closely linked to the description of the landscape, are addressed in the *alternative delineation calculation case* (Section 11.3). The sensitivity of the calculated dose to landscape and object properties, including surface and groundwater flows, is further addressed in a separate supporting calculation case (*mire object properties calculation case,* Section 11.4).

10.2 Warm climate calculation case

This calculation case is developed to evaluate doses to humans (and dose rates to non-human biota, presented in Chapter 12) for the *warm climate variant* of the reference evolution (Section 4.1.1). This variant describes a considerable climate warming during the initial thousands of years after closure, prolonged submerged conditions in the Forsmark area and, identical to the *base case*, temperate climate conditions at Forsmark for the entire assessment period (Figure 4-1).

As compared with the *base case*, both the surface water availability and the shoreline displacement are affected by a warmer climate, and hydrology and ecosystem parameters are adjusted accordingly. In the light of the uncertainty in the seasonal precipitation change in a warmer climate (Section 4.1.1), the effects of a warmer climate are examined in two variants with, respectively, higher and lower summer precipitation compared with present: the *high summer precipitation* variant and the *low summer precipitation* variant.

In the *base case*, it is assumed that drained-mire (DM) farmers cultivate crops that satisfy their water demand via groundwater uptake. However, as the climate becomes warmer, the potential evapotranspiration is projected to increase at a faster rate than the precipitation (Table 4-1), resulting in an increased water demand for crops and a potential usage of irrigation water to satisfy this demand. In the *warm climate calculation case*, it is therefore assumed that the increased water demand is satisfied either by groundwater uptake or sprinkler irrigation. To this end, an additional exposed group is considered in the calculations: DM farmers practicing large-scale irrigation.

10.2.1 Description of the calculation case

Climate conditions

The climate conditions follow from the *warm climate variant*, corresponding to temperate climate conditions at Forsmark for the complete assessment period of 100 000 years after closure (Section 4.1.1). The maximum changes in air temperature, precipitation and potential evapotranspiration, described in Table 4-1, are for simplicity assumed to persist for the entire assessment period. This simplification is considered to be pessimistic as it overestimates the average difference between potential evapotranspiration and precipitation, i.e. the water demand at the surface, during the summer season compared with that arising if a more realistic temporal climate evolution would be used. However, the maximum dose typically occurs during the early stages of the assessment period when the warming is expected to be relatively similar to its maximum value. Thus, the impact on maximum dose of a constant-in-time climate evolution is expected to be small compared with a more realistic temporal evolution.

Geosphere release

The transport pathways in the near-field and in the geosphere are not expected to be affected by a warmer climate (**Post-closure safety report**, Section 6.4). However, as the shoreline regression occurs later in time compared with the *base case* (see below), the radionuclide transport will also be delayed. Thus, the geosphere release is affected by the delayed shoreline regression in this calculation case, but it is still assumed to be discharged to biosphere object 157_2.

Landscape description

The initial shoreline displacement follows from the *warm climate variant*, corresponding to 4 500 years of initial submerged conditions (Section 4.1.2). The prolonged submerged conditions, relative to the *base case*, are handled by assuming that the present shoreline position will prevail until 5500 AD, after which the initial shoreline displacement of the *base case* will follow. Thus, the shoreline displacement of the *base case* is assumed to be shifted 3 500 years forwards in time, implying that biosphere object 157_2 begins to emerge above sea level around 6500 AD, instead of around 3000 AD in the *base case* (Figure 10-1). This simplified representation is considered to adequately capture the main features of a delayed shoreline regression (**Data report**, Chapter 12). The approach is also arguably cautious, as it does not account for the expected increase in water exchange between the assessed basins (Figure 5-4) and Öregrundsgrepen (which is in contact with the Baltic Sea). In addition, it does not account for the expected slow-down of the isostatic rebound with time that could reduce the rate of shoreline regression and influence the area of the biosphere object during emergence. Alternative shoreline displacements, resulting in both shorter and longer initial periods of submerged conditions than assumed here, are analysed in the *timing of shoreline regression calculation case* (Section 10.4).

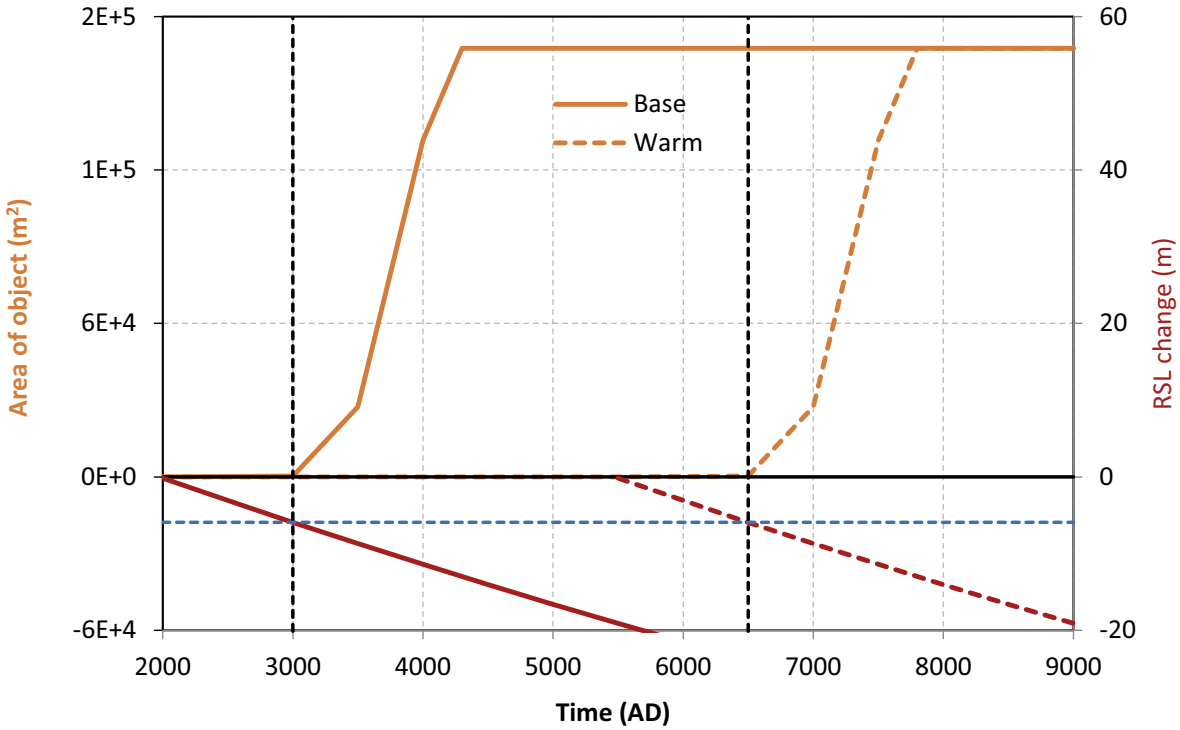

Figure 10-1. *Evolution of relative sea level (RSL) in the base case and warm climate calculation case (red lines), and the resulting area of object 157_2 that has emerged above sea level (orange lines). The vertical black dashed lines indicate the time when the object starts to emerge above the sea.*

Surface hydrology and irrigation

Ground and surface water flows for the mire state of biosphere object 157_2 in a warmer climate have been simulated with the MIKE SHE tool (Appendix F). The simulations are based on the climate description for the two variants given above, and hydrological parameter values are derived from MIKE SHE water balances (see Surface and groundwater flow in Section 8.3.1). In addition to object-specific flows, the net precipitation from the new MIKE SHE simulations (Figures F-1, F-5) was used to characterise percolation in the unsaturated agricultural soils (left panel in Figure 10-2). The simulations also show that the groundwater table in object 157_2 will be above or close to the surface, even for the *low summer precipitation* variant (Sassner et al. 2022, Figure 4-11). These results indicate that the area will be a wetland also under warmer conditions.

In a warmer climate, the projected increased evapotranspiration is greater than the projected increase in precipitation leading to an expected increase of the plant water deficit during the vegetation period. This is true for both variants of the calculation case. An increased demand for water could either fully or partly be supplied by an increased groundwater uptake through capillary rise, and/or it could be satisfied by irrigation. A multi-model approach is used to forecast the response of crop water demand in agricultural systems (See Crop water demand in Section 8.3.1, and the panel on the right in Figure 10-2)[47]. Moreover, it is cautiously assumed that the crop water demand is fully compensated by water containing radionuclides originating from the repository, either from capillary rise of groundwater or from irrigation with surface water.

The opportunities to cover irrigation with groundwater abstraction may be very limited in a future with longer dry periods during the growing season due to competition for water from other sectors of society (Mattson et al. 2018). Therefore, it is expected that irrigation demands will to a large extent have to rely on surface water. If existing surface water reservoirs are insufficient, construction of wetland or irrigation dams are likely options to secure the supply of water. In line with the expectations of the

[47] For this purpose, output data for sixteen combinations of global climate and hydrological models were utilised (Gosling et al. 2019). The data were provided by the second phase of the Inter-Sectoral Impact Model Intercomparison Project (ISIMIP2, available at https://www.isimip.org/).

Swedish Board of Agriculture (Mattson et al. 2018), surface water is considered appropriate to use for large scale irrigation in warmer climate. Therefore, this assumption is also adopted for the *warm climate calculation case*.

Ecosystem parameters

Values for ecosystem parameters, such as biomass, net primary production and crop yield are adjusted to increased air temperature based on literature data from warmer locations (Grolander 2013). The concentration of stable CO_2 in the atmosphere is adjusted to elevated levels in accordance with the RCP4.5 emissions scenario (540 ppm).

Large-scale irrigation of cereal and fodder production is not practiced in Forsmark under present conditions. Adding large-scale irrigation as an exposure pathway to DM farming thus requires the definition of new parameters describing this practice (Section 8.3.1). Moreover, the processes for accumulation on edible parts of crop (cereals), element translocation to edible parts (potatoes) and weathering of intercepted radionuclides (fodder) are added to the models describing agriculture in warmer conditions. The amount and frequency of irrigation of a garden plot are also adjusted to reflect warmer conditions.

Owing to their different representations of the summer climate, the crop water deficit during the vegetation season, and thus the irrigation and plant groundwater uptake, is higher in the *low summer precipitation* variant than in the *high summer precipitation* variant.

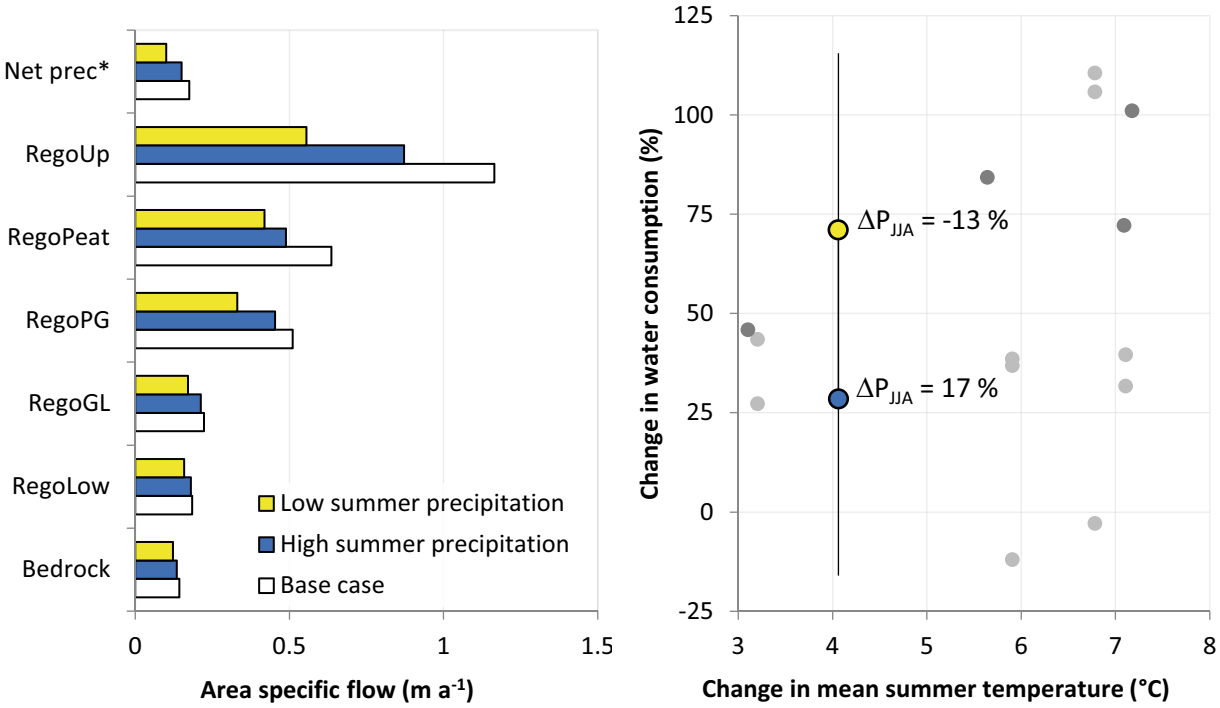

Figure 10-2. *Response in the surface hydrology and the water demand for arable land for the two variants of the warm climate calculation case. Left: area specific upward groundwater flows for the mire in object 157_2 and net precipitation (*) at the landscape level, as predicted with the MIKE SHE modelling tool (Appendix F). Yellow represents flows in the variant with low summer precipitation, blue flows in the variant with high summer precipitation, and white the flows given present day climate used in the base case. Right: changes in crop water demand due to changes in summer temperature and precipitation as estimated from a global multi-model approach (Gosling et al. 2019). Coloured symbols represent the mean changes as compared to the demand in the base case. Error bars represents the standard deviation corresponding to the uncertainty in projections between hydrological models (Appendix G). Dark grey circles correspond to results for the grid point closest to Forsmark, whereas light grey circles represent the average response for entire Scandinavia.*

Potentially exposed groups

In addition to the potentially exposed groups of humans defined in the *base case*, a variant of drained-mire farmers practicing large-scale irrigation at a relatively low intensity is added (two irrigation events per season at a scale of several hectares, evaluated over 50 year of cultivation). Long-term large-scale irrigation (500 consecutive years) is assessed by the infield-outland (IO) farming group (two irrigation events per season). The effects of short-term irrigation at higher intensities (ten irrigation events per season) with well water, either from a dug or a drilled well, are assessed for the garden-plot (GP) household group.

10.2.2 Annual doses

A warmer climate leads to a reduction of the maximum dose with respect to the *base case* as assessed for the exposed group receiving the highest dose (Figure 10-3). This response is primarily an effect of the prolonged period of submerged conditions as this serves to delay and reduce the geosphere release of C-14 and Mo-93. Moreover, elevated CO_2 levels in the atmosphere (540 ppm vs 380 ppm in the *base case*) serve to increase the atmospheric dilution of C-14 (i.e. by lowering the atmospheric C-14 to C-12 ratio). However, this reduction is off-set by an increased groundwater uptake of C-14 (for farming without irrigation) to compensate for the decreased net precipitation in a warmer climate, and by an increased accumulation of sorbing radionuclides in regolith layers due to a decreased groundwater flow in the mire ecosystem.

The dose from C-14 is nearly proportional to the rate of groundwater uptake and its activity concentration, as this is the primary source for C-14 in the drained mire (see the *base case*, Section 9.3, and the *ecosystem properties calculation case*, Section 11.2.2). In the *low summer precipitation variant*, the groundwater uptake increases by 70 % (right panel in Figure 10-2) and the dilution of groundwater decreases by ~15 % (RegoLow in Figure 10-2). Thus, almost twice as much of a radionuclide released from the geosphere reach the cultivated soil, which affects both root and foliar uptake of C-14 proportionally. This results in higher C-14 doses in the *low summer precipitation variant* than in the *base case* despite a delayed release and an increased concentration of C-12 in the atmosphere (upper panel in Figure 10-4).

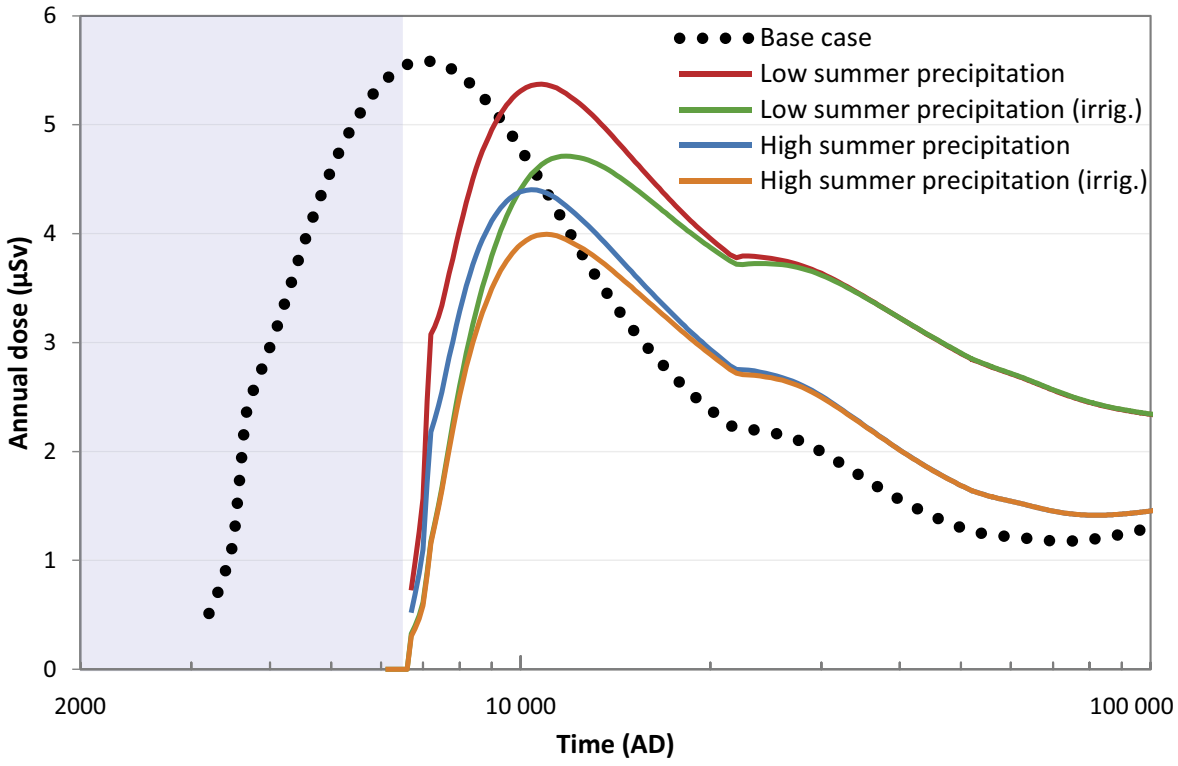

Figure 10-3. *Annual dose to DM farmers, without and with large-scale irrigation, in the two variants of the warm climate calculation case. The annual dose in the base case is shown for comparison (black dotted line). The blue shading indicates the submerged period.*

The accumulation of radionuclides in the regolith layers is greatest in the *low summer precipitation variant*, where the upward groundwater flow is reduced by between ~20 % (glacial clay) and 35 % (deep peat) in layers that are exposed when the mire is drained (left panel of Figure 10-2). The increased accumulation leads to a noticeable increase in the dose from for example Ca-41, Ni-59 and Ac-227, and the dose is consistently higher than in the *base case* for the period after 20 000 AD (upper panel of Figure 10-4). The annual dose after 20 000 AD varies between 2 to 4 μSv in the *low summer precipitation variant*, as compared with doses of 2 μSv or lower in the *base case*. It can be noted that the relative increase is most pronounced for Ac-227 and Pa-231. This is because accumulation of U-235 is the primary source of Pa-231 and its decay product Ac-227. A decrease in the groundwater flow thus affects both the source and the dilution of Ac-227 and Pa-231.

The effect of irrigation is evaluated using stream water to compensate for the crop water deficit. This is reasonable because stream water is generated locally and is readily available in the discharge area. As stream water is diluted with the runoff generated in the catchment, the dilution is more than a factor four larger than in groundwater used to meet the crop water demand assuming capillary rise from the saturated lower regolith layer. The effect of surface water dilution is only noticeable in the early stage when C-14 contributes to the dose (Figure 10-3), and in this stage the annual dose is consistently lower in variants with irrigation. However, after ~20 000 AD there is no difference in doses with respect to the source of water satisfying the crop water deficit. This is because accumulation in mire regolith layers is the dominating source for activity for the other dose-contributing radionuclides (e.g. Mo-93, Ca-41, Ni-59 and Ac-227). Thus, accumulation of activity that ends up in the cultivated soil occurs prior to drainage, and the activity in the cultivated soil is only marginally affected by groundwater uptake and irrigation.

A comparison of the dose between the exposed groups confirms the conclusions from the *base case*; long-term accumulation in natural ecosystems is the most important exposure pathway also in a warmer climate (Figure 10-4, lower panel). Thus, although the dose to IO farmers increases in the warm climate as compared with the *base case* (~40 %), the potential dose contribution from long-term irrigation with surface water is marginal compared with accumulation in mire ecosystems or long-term addition of organic fertilizers (as seen by comparing IO-irrig with IO and DM in Figure 10-4). Moreover, high-intensity irrigation with well-water in a warm climate results in marginally higher dose than in the *base case*, and doses from production of vegetables result in a lower dose than agriculture on the field scale (as seen by comparing GP with DM and IO in Figure 10-4). The reason for the weak response to increased irrigation of the garden plot is primarily due to the limited importance of irrigation compared with the fertilization pathway. The fertilization regime is not altered in the warm climate, and all ash produced by a household is used for fertilization.

In the PSAR, leaf interception is introduced as an additional transport pathway that contributes to the radionuclide concentration of irrigated crops. Approximately 5 and 15 % of radionuclides intercepted on cereal and potato leaves are translocated to edible parts, and about half of the radionuclides intercepted on fodder remains at harvest. However, the storage capacity of leaves is limited to 0.2–0.4 mm of irrigation water per event (Grolander 2013). Thus, the contribution of intercepted radionuclides to plant concentrations is typically below 1 % for most dose contributing radionuclides (i.e. Mo-93, Ca-41, Ni-59 and Ac-227). For C-14 the contribution from interception is considered to be negligible, as CO_2 in a thin water film will equilibrate with the atmosphere within minutes (see Section 7.3.5 in Saetre et al. 2013a). Thus, intercepted C-14 will be lost to the atmosphere before the crops are harvested.

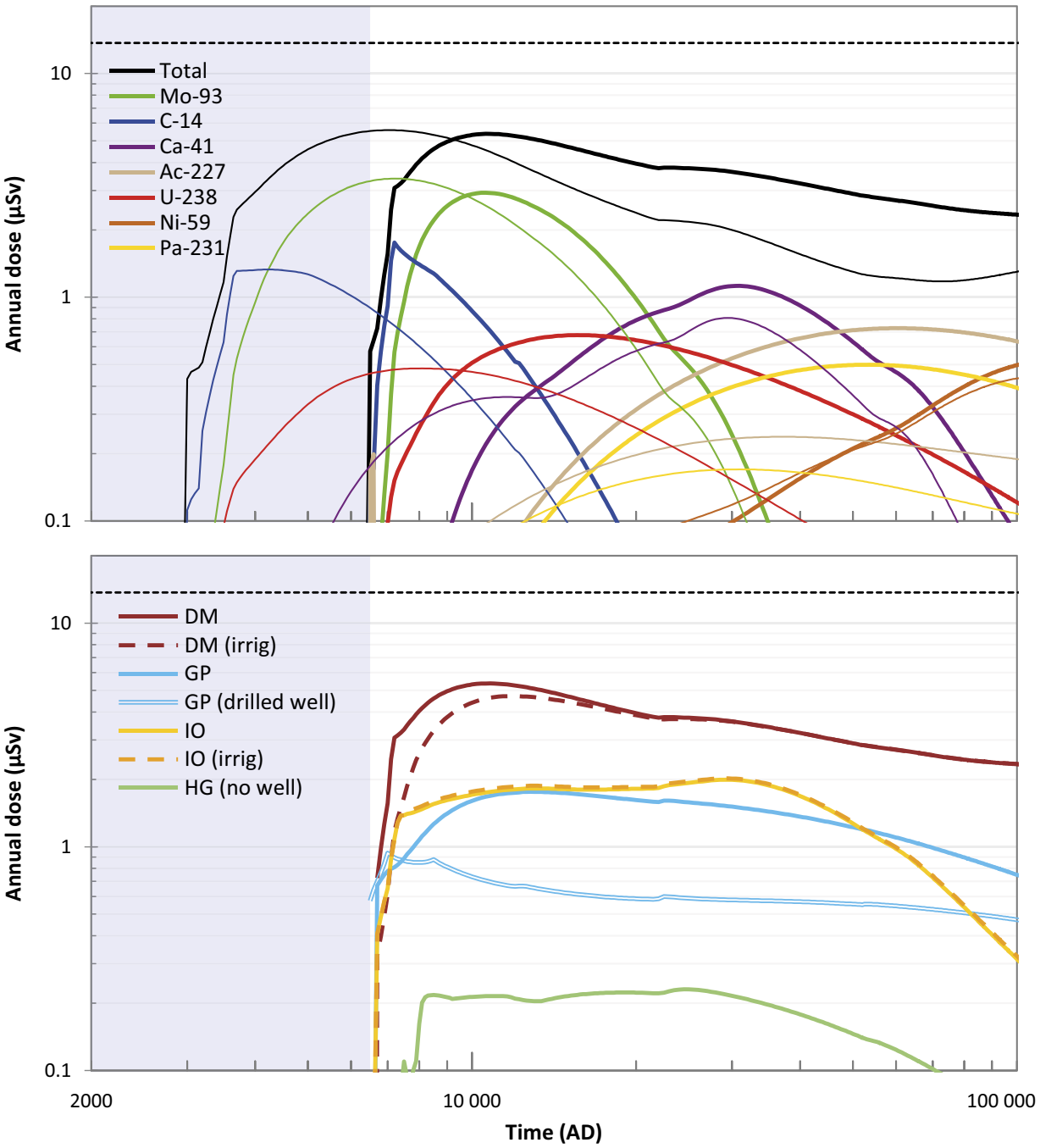

Figure 10-4. *Annual doses from different radionuclides (upper panel) and to the potentially exposed groups (lower panel) in the low summer precipitation variant of the warm climate calculation case. The radionuclide-specific doses are only shown for the most exposed group DM (with groundwater uptake). For clarity, only the radionuclides contributing most to the total dose are shown. The annual dose in the base case is shown for comparison (thin lines). Dashed black horizontal line shows the annual dose corresponding to the regulatory risk criterion (14 µSv).*

10.3 Cold climate calculation case

This calculation case is developed to evaluate doses to humans (and dose rates to non-human biota, presented in Chapter 12) for the *cold climate variant* of the reference evolution (Section 4.1.1). External conditions at Forsmark are characterised by two periods of periglacial conditions during the latter half of the assessment period (Figure 4-1). Doses are evaluated both during and between the periglacial periods.

The periods of periglacial conditions are characterised by considerably lower air temperatures than at present, resulting in the development of permafrost and frozen bedrock conditions at Forsmark. There is however a wide range of potential air temperatures, approximately between −11 °C and −1 °C, that could influence the post-closure development of frozen bedrock conditions (**Post-closure safety report**, Section 6.5.3). Motivated by this uncertainty, two simplified bounding variants are evaluated in this calculation case; the *continuous permafrost* variant without talik and the *permafrost with talik* variant (more details in the **Radionuclide transport report**, Section 6.3.1).

Continuous permafrost describes a situation where the climate becomes sufficiently cold to induce frozen bedrock conditions at repository depth. Frozen conditions are assumed to hinder all release to the surface during periglacial conditions, and doses are evaluated in the active layer of the biosphere objects that directly (object 157_2) or indirectly (down-stream objects 157_1 and 116) receive radionuclide releases from the geosphere during the preceding temperate conditions.

In the *permafrost with talik* variant, the climate is assumed to be sufficiently cold to induce freezing of the ground close to the surface, but still warm enough to maintain unfrozen conditions at repository depth. In this variant, the geosphere release is assumed to reach the surface ecosystem via a discharge talik, i.e. locally unfrozen ground connecting the deep groundwater with the surface. Therefore, doses in the *permafrost with talik* variant are evaluated both for geosphere releases to a lake talik in biosphere object 114 in Öregrundsgrepen and to a mire talik in object 157_1 (Section 5.5). For both variants, ecosystem and hydrological parameters are adjusted to reflect periglacial conditions and in the *permafrost with talik* variant the properties of the biosphere objects are adjusted to represent the assumed talik.

10.3.1 Description of the calculation case

Climate conditions

The climate and climate-related conditions correspond to the *cold climate variant* of the reference evolution, described in Section 4.1.1. In summary, the evolution of climate domains is identical to the *base case* except for the occurrence of two periglacial periods, one between 61 000 AD and 69 000 AD and another between 81 000 AD and 102 000 AD. Periods of permafrost growth and decay are for simplicity neglected in the calculations. Thus, transitions to and from the periglacial landscapes described by the variants are assumed to be instantaneous.

Geosphere release

In a permafrost landscape, discharge of deep groundwater may be restricted to areas on top of unfrozen land, so-called discharge taliks, or it may be blocked by continuous permafrost. In *continuous permafrost*, the near-field and geosphere releases are halted by the frozen bedrock conditions during periglacial periods. Once the water flow again increases during the subsequent temperate period, releases of radionuclides that do not decay significantly are similar to those immediately prior the onset of the preceding periglacial period. This means that releases during the subsequent temperate period could be marginally higher than the releases during the corresponding time in the *base case* (**Radionuclide transport report**, Section 6.3.5).

For decay products, the frozen conditions may lead to accumulation of radionuclides from their parents trapped in the frozen barriers and bedrock, and the accumulated activity could result in a subsequent period with elevated geosphere release of these radionuclides (**Radionuclide transport report**, Figure 6-7). However, none of the radionuclides contributing substantially to the dose after the first periglacial period have significantly higher geosphere releases than in the *base case*. As geosphere release only occurs in temperate periods in the *continuous permafrost* variant, all release is directed to the one single discharge area, namely object 157_2, as in the *base case*.

In the *permafrost with talik* variant, the geosphere release reaches the biosphere system through a discharge talik. The distribution of unfrozen conditions in permafrost landscapes is influenced by a number of factors, including air temperature, topography, snow cover, availability of water bodies and vegetation (Johansson et al. 2006, Hartikainen et al. 2010). Unfrozen conditions and discharge taliks are typically formed below lakes. Results from bedrock hydrogeology modelling show that groundwater from the extended repository could be discharged to large future lakes in Öregrundsgrepen (Odén et al. 2014). Furthermore, mire vegetation might inhibit permafrost development and discharge taliks below mires cannot be excluded (Cohen-Corticchiato and Zwinger 2021). Thus, in the *permafrost with talik* variant, the entire geosphere release during periglacial conditions is either directed to a future lake in object 114 or to a mire in object 157_1 (Section 5.4).

When discharge taliks are present, the geosphere release is assumed to be equally large as in the *base case* (**Radionuclide transport report**, Section 6.3). During temperate periods, the release is assumed to reach the same discharge area as in the *base case* (object 157_2) in both variants.

Landscape description

The initial shoreline displacement is taken from the *cold climate variant* (Section 4.1.2). This means that the landscape development in the *cold climate calculation case* is identical to the *base case* up until the onset of the first period of periglacial climate domain at 61 000 AD.

All lake-mire systems in the area above the repository are considered to have reached a mature state before 50 000 AD and a stationary representation of the mire in object 157_1 at its mature state is used to evaluate doses. Lake infilling is considered to be slow in periglacial conditions (Brydsten and Strömgren 2010) and thus a stationary representation of a hypothetical deep lake (i.e. a permanent lake without ingrowth and ecosystem succession) in object 114 farther out in Öregrundsgrepen is also used to evaluate doses.

Surface hydrology

Permafrost has a major influence on bedrock hydrology and near-surface hydrogeology. The hydrologically active period in the course of a year is short and groundwater flows are restricted to a relatively thin active layer. Moreover, taliks may connect the unfrozen groundwater flow system in the bedrock with the surface system. In SR-PSU, near-surface water-flow components were derived for the same potential future taliks as considered in this calculation case (Sections 4.3 and 5.4, and Odén et al. 2014). The hydrological modelling of taliks was described in Werner et al. (2013) and the hydrological parameters for the two taliks (biosphere objects 157_1 and 114) modelled in SR-PSU (Grolander 2013) are used also in the PSAR.

Biosphere object 157_2 is assumed to have a continuous permafrost layer during periglacial periods. Thus, in the biosphere modelling all solute transport (advection and diffusion) in object 157_2 is halted in the till layer that is considered to be permanently frozen. However, as the active layer thaws in summer, transport processes are assumed to be maintained to some extent in the regolith layers above the till.

A conceptual water-balance model was used to compute hydrological flows in the regolith profile of the active layer in object 157_2 (Section 7.5.5). The water balance is driven by the input of groundwater from the local catchment and net precipitation falling on the object, whereas the discharge from the bedrock is assumed to be zero due to the permafrost. The net precipitation and runoff are assumed to increase by ~25 % in a future permafrost landscape (Werner et al. 2013, Table 5-3). Other hydrological parameters were set to reflect a high proportion of surface runoff and a limited contribution of discharge from the catchment below a depth of 0.2 m, as indicated by the hydrological modelling of permafrost conditions (Section 8.3.2). Based on these assumptions, the upward flows are calculated from the water balance in each compartment (see Figure 10-5).

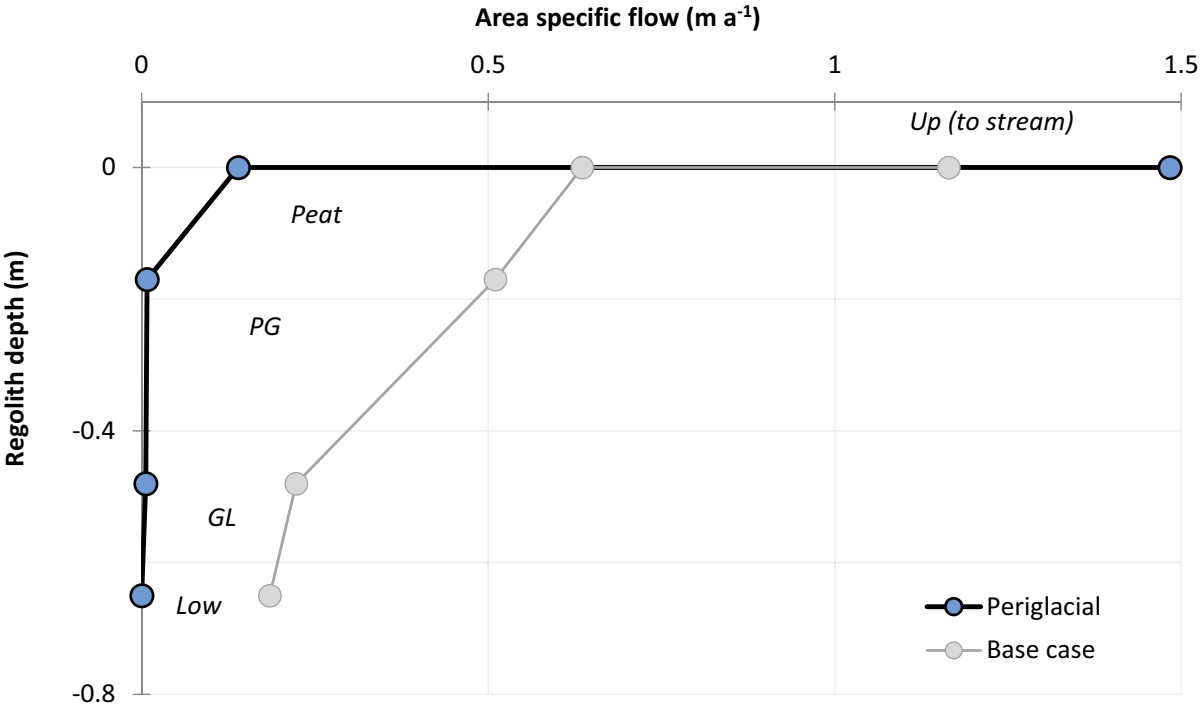

Figure 10-5. *Upward groundwater flows for object 157_2, and discharge to the stream during periglacial and temperate (base case) conditions. During periglacial conditions, the till (Low) is assumed to be permanently frozen and the active layer (GL, PG, Peat, Up) is non-frozen for a short summer period. Groundwater flows are calculated based on the conceptual water-balance model for a mire. The discharge from the bedrock is set to zero, and the runoff is increased by ~25 % in relation to the base case. Following the flow patterns in the mire talik 157_1, the runoff from the local catchment is forced towards the surface and the percolation is lowered (see Section 8.3.2 for details).*

Ecosystem parameters

The solubility of CO_2 is adjusted to reflect levels typical of a lower temperature, and primary production, mineralisation, production of edible fish and crayfish are altered to better reflect permafrost conditions (Section 8.3).

Potentially exposed groups

During periglacial conditions, permafrost will impose strong limitations on agriculture, and wells will not yield any water from the frozen ground. Thus, in the periglacial periods the potentially exposed group is hunters and gatherers (HG) foraging in the Forsmark landscape. HGs are assumed to collect food from a large area and can thereby utilise food from several biosphere objects at the same time (i.e. objects 157_2, object 157_1 and object 116). In the variant where the geosphere release is directed to the lake talik (object 114), no additional downstream objects are considered.

During temperate conditions, the potentially exposed groups are identical to those assessed in the *base case* (Section 9.2).

10.3.2 Annual doses

Before the first onset of periglacial conditions at 61 000 AD, the modelled conditions and the resulting doses in the *cold climate calculation case* are identical with the *base case*. The main result in the *cold climate calculation case*, both with *continuous permafrost* and *permafrost with talik*, is that doses during periglacial periods are at least one order of magnitude lower than in the *base case* at the corresponding time (Figure 10-6). The main reason is that the only possible exposure pathway during periglacial conditions is considered to be related to hunting and gathering, which generally results in lower doses than cultivation and well water usage (see Section 9.3 and Figure 9-4). Whereas doses to

drained-mire (DM) farmers after 50 000 AD are dominated by radionuclides like Ca-41 and Ni-59 that sorb and accumulate in regolith layers that become cultivated, I-129 dominates the dose to hunters and gatherers. This radionuclide is transported relatively quickly through the regolith. The main exposure pathway is ingestion (of wildlife and berries), but also drinking surface water contributes to the dose.

Doses to hunters and gatherers are similar in the *continuous permafrost* and the *permafrost with talik* variants, both during temperate as well as periglacial periods. The reason is that the doses are generally dominated by exposure from radionuclides that have accumulated in object 157_2 during the preceding temperate periods (i.e. I-129). In both the *continuous permafrost* and *permafrost with talik* variants, the geosphere release to biosphere object 157_2 ceases during periglacial periods. In combination with continued leaching of radionuclides from the hydrologically active regolith layers in object 157_2, this results in a total dose to hunters and gatherers that is lower during periglacial periods than in the *base case* (Figure 10-6).

In the *permafrost with talik* variant, the exposure from releases to a lake talik in object 114 is marginal in relation to the exposure hunters and gatherers get from foraging in the vicinity of biosphere object 157_2 and the mire talik (object 157_1). Therefore, only results from the variant with a talik in 157_1 are reported here. As radionuclides leach from the regolith layers in biosphere object 157_2, doses initially decrease during the periglacial periods (Figure 10-6). The geosphere release to the talik eventually reaches the upper regolith in object 157_1 and starts to contribute to the dose. This counteracts the decrease and doses become slightly higher than in the *continuous permafrost* variant (Figure 10-6). At the end of the second and somewhat longer permafrost period, the dose contribution from object 157_1 is similar to the dose contribution from object 157_2.

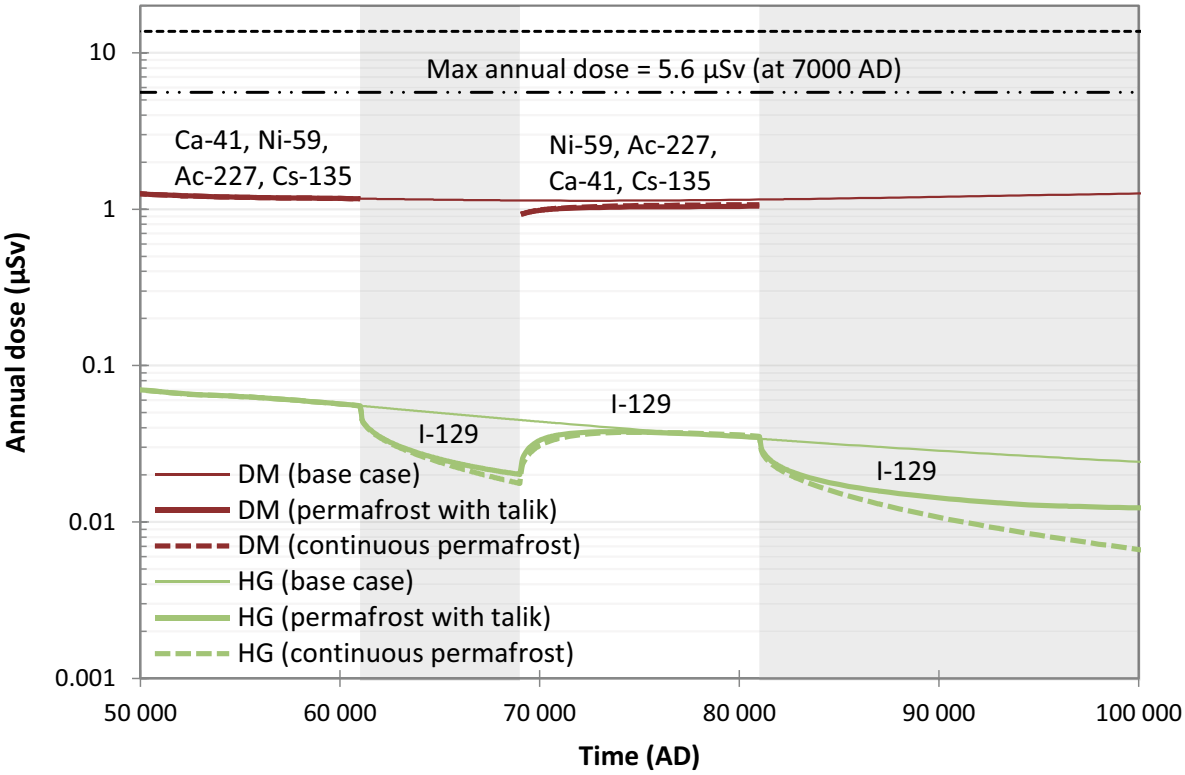

Figure 10-6. *Total annual doses to drained mire farmers (DM) and hunters and gatherers (HG) in the cold climate calculation case in the continuous permafrost variant (dashed line) and permafrost with talik variant (solid line) with a talik in biosphere object 157_1 (but with exposure also from 157_2). Doses from a release through a talik into a lake in biosphere object 114 are below 0.001 µSv and are therefore not shown. Base case doses are plotted for comparison as thin lines. During periglacial conditions (grey background shading), when only hunting and gathering is possible (HG green line), doses drop by more than one order of magnitude compared with the base case doses (DM red line). The radionuclides contributing most to the doses to DM farmers and HG are indicated in the plot. The maximum annual dose during the assessment period (same as the base case) is indicated by the dashed-dotted line. The annual dose (14 µSv) corresponding to the regulatory risk criterion is indicated by the black dashed line.*

As soon as farming is possible again during temperate conditions after the first periglacial period, doses to drained-mire farmers in object 157_2 exceed doses to hunters and gatherers by more than one order of magnitude. Those doses to DM farmers are initially somewhat lower than in the *base case* due to the lack of releases to object 157_2 and the depletion of accumulated inventory in the regolith due to leaching during the preceding periglacial period, but eventually approach the levels of the *base case* doses. The marginally higher geosphere releases of radionuclides, including decay products, trapped in the near-field and geosphere by the permafrost in the *continuous permafrost* variant, does not affect doses significantly. Note that the maximum annual dose occurring at 7000 AD is a factor 5 higher than doses occurring after the onset of the periglacial conditions (Figure 10-6).

10.4 Timing of shoreline regression calculation case

During the transition from submerged to terrestrial conditions in the area above SFR, the continuous shoreline regression will result in a gradual increase of the hydraulic gradient in the parts emerging from the sea and, consequently, in gradually higher groundwater flow rates. Thus, the timing of the shoreline regression will affect the transport of radionuclides in the near-field, geosphere, and biosphere system as well as the timing of ecosystem succession and the potential for exposure in the biosphere.

In the *base case*, the initial period of submerged conditions is set to 1 000 years based on the assumption that the global sea-level rise until repository closure and post closure is negligible (Section 4.1.2). Although this simplification facilitates comparisons with the results in SR-PSU, where the same duration of the submerged period was used, it is arguably not fully realistic since it does not account for the ongoing and anticipated future sea-level rise.

At present, sea-level rise due to melting of Earth's ice sheets and glaciers, and thermal expansion of sea water offsets about 40 % of the post-glacial isostatic rebound at Forsmark (**Climate report**, Section 3.5.1). The influence of sea-level rise on the shoreline displacement at Forsmark is expected to continue for several thousands of years after repository closure (**Climate report**, Sections 3.5.3 and 3.5.4). The uncertainty in projected global sea-level rise over the coming millennia is large, ranging from a couple of metres to more than 50 m depending on the amount of global warming and how Earth's ice-sheets and glaciers will respond to that warming (**Climate report**, Section 3.5.3).

At Forsmark, this uncertainty translates to between 1 300 and 18 300 years of initial submerged conditions above the repository (**Climate report**, Section 3.5). One case of shoreline displacement within this interval, corresponding to 4 500 years of initial submerged conditions, is evaluated in the *warm climate calculation case* (Section 10.2). The *timing of shoreline regression calculation case* discussed in this section covers the remaining uncertainty by postulating a delay of 5 000, 10 000, 15 000 and 20 000 years in shoreline regression relative to the *base case*. Aside from altering the timing of the initial shoreline displacement and the corresponding groundwater flows, transport and associated radionuclide decay, the handling in the near-field, geosphere and biosphere in this calculation case is identical to the *base case*.

10.4.1 Description of the calculation case

Climate conditions

Uncertainty in global sea-level rise and the corresponding shoreline regression at Forsmark is the motivation for this calculation case. Apart from that, the *base case* climate conditions are applied in this calculation case, namely present-day temperate conditions persist for the entire assessment period.

Geosphere release

The low groundwater flows during the extended submerged periods clearly influence the geosphere releases in relation to the *base case* (left panel in Figure 10-7). The changes in the radionuclide-specific releases are described in detail in the **Radionuclide transport report**, Section 5.8.2.

Landscape description

The methodology for handling the delayed shoreline regression and the resulting ecosystem succession of biosphere object 157_2 follows that of the *warm climate calculation case* (Section 10.2). That is, the present (2000 AD) shoreline position is assumed to prevail for the duration of the delay, after which the initial shoreline displacement of the *base case* is assumed to follow. Dose consequences are evaluated in four additional calculation variants with a delayed shoreline regression of 5 000, 10 000, 15 000 and 20 000 years relative to the *base case*. In addition, the corresponding results from the *warm climate calculation case*, with a delay of 3 500 years, are included for reference (Figure 10-7 and Figure 10-8).

Surface hydrology

The relationship between the shoreline regression, relative sea levels and the resulting near-surface groundwater flows in object 157_2 used in the *base case*, is used also in this calculation case. Thus, the delays in the temporal development of the near-surface groundwater flows follow the delays in the shoreline regression and correspond to the changes in bedrock groundwater flows.

Ecosystem parameters and potentially exposed groups

The ecosystem parameters from the *base case* are used in this calculation case. The potentially exposed groups are identical to the *base case*, but only doses to drained-mire (DM) farmers are reported and discussed since they always comprise the highest total maximum doses.

10.4.2 Annual doses

The main effect of the longer submerged periods is to lower the maximum total annual doses compared with the *base case*. The lower groundwater flows during submerged conditions delay the radionuclide transport from the near-field and geosphere to the biosphere system (Figure 10-7, upper panel). This results in more decay of the radionuclides that dominate the maximum annual dose in the *base case*, namely Mo-93 and C-14, before they reach the surface system and are available for determining exposure. Consequently, maximum doses from those two radionuclides occur later and decrease with increasing duration of the delay (Figure 10-7 and Figure 10-8).

As a result of the lower doses from Mo-93 and C-14, longer-lived radionuclides become more important for the total dose for the longest submerged periods. For shoreline regression delays of 15 000 and 20 000 years, Ca-41 dominates the total dose maximum (Figure 10-7, lower panel and Figure 10-8). This radionuclide has a half-life of 102 000 years and therefore does not decrease substantially due to decay in the near-field or geosphere with a longer submerged period. Furthermore, due to the conditions in the repository, Ca-41 and other radionuclides with long half-lives may accumulate and be flushed out at a higher rate from the near-field when groundwater flow increases after the extended submerged period (**Radionuclide transport report**, Section 5.8.2). This results in a higher maximum release from the near-field and the geosphere (~200 % higher with 20 000 years delay). However, Ca-41 is sorbed effectively in the regolith layers that contribute to exposure, and thus accumulated geosphere releases are also important for exposure to this radionuclide in the biosphere. In contrast to the maximum geosphere release, the accumulated geosphere release of Ca-41 does not change substantially compared with the *base case*. The increase in maximum dose from Ca-41 is therefore limited (~50 % higher with 20 000 years delay, Figure 10-7) in relation to the maximum release, and the maximum total dose with a delayed shoreline regression never exceeds the maximum total dose in the *base case*.

Maximum releases of I-129 increase, similarly to Ca-41, by up to about 200 % for the longest submerged period. Because iodine is more mobile in the regolith than calcium, the release maximum of I-129 is more effectively propagated to increased doses (100 % higher with 20 000 years delay, Figure 10-7). However, this has only a small effect on maximum total doses, since the dose contribution of I-129 is limited (Figure 10-8).

Decay products can accumulate in the near-field also due to ingrowth from parental radionuclides retained in the repository during submerged periods, resulting in higher maximum releases after longer submerged periods. For example, maximum near-field releases of Pa-231 and Ac-227 (decay

products of U-235), increase by an order of magnitude with a 20 000 year longer submerged period (**Radionuclide transport report**, Section 5.8.2). However, those releases never reach the regolith layers cultivated by farmers, because they are effectively retained, and decay, in the geosphere and especially in the till. Instead, the exposure from Pa-231 and Ac-227 is primarily caused by ingrowth from U-235 within the regolith.

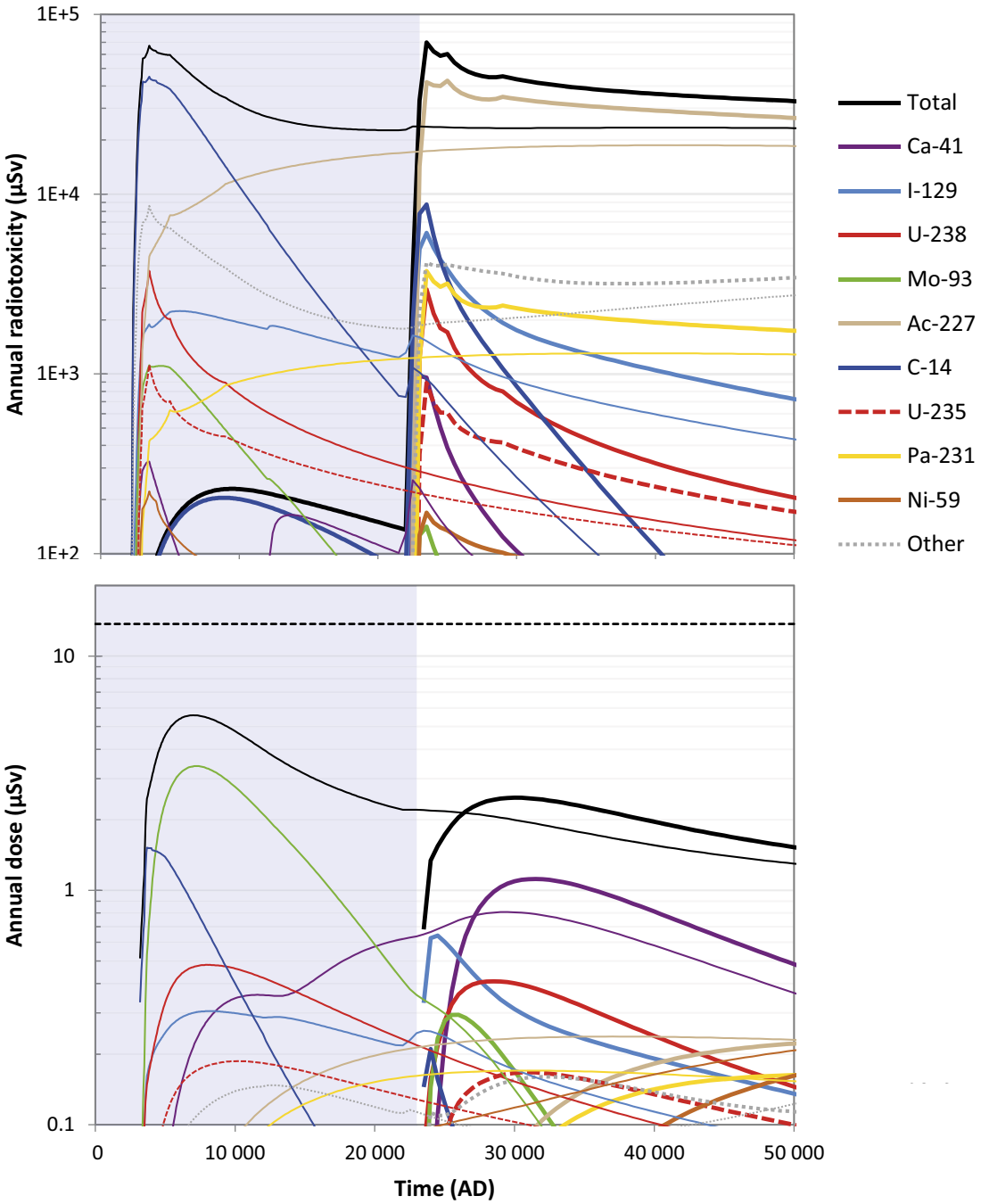

Figure 10-7. *Radiotoxicity releases from the geosphere (upper panel) and annual dose (lower panel) to drained mire farmers with a delayed shoreline regression of 20 000 years. Coloured lines represent the contribution from individual radionuclides and black lines the total radiotoxicity and total annual doses respectively. Thick lines illustrate results from the delayed shoreline regression and corresponding thin lines are results from the base case for comparison. The light blue background colour indicates the prolonged submerged period. The annual dose (14 µSv) corresponding to the regulatory risk criterion is indicated by the horizontal black dashed line. Note that the time is presented on a linear scale unlike in most of the graphs.*

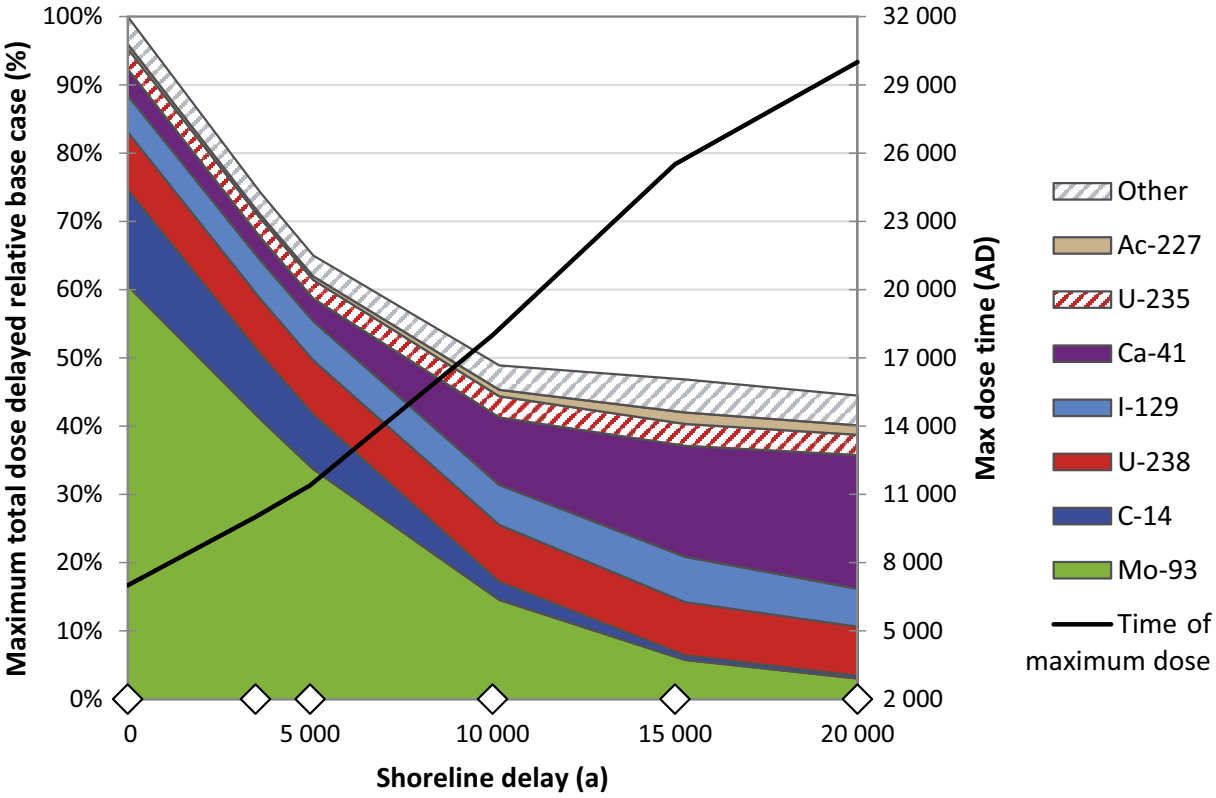

Figure 10-8. *Percentage of total maximum and radionuclide specific annual doses relative to the base case (left y-axis) and timing of total maximum annual doses (right y-axis) as a function of the delay in shoreline regression relative to the base case (x-axis). A shoreline delay of 0 years corresponds to the base case; this case and the calculations with delayed shoreline regression are indicated by white diamonds on the x-axis. The total height of the stacked areas shows the maximum dose relative to the base case and the height of the individually coloured areas show the radionuclide-specific dose contribution to the maximum dose. Note that the time is presented on a linear scale unlike in most of the graphs.*

10.5 Subhorizontal fracture calculation case

This supporting calculation case is developed to evaluate doses to humans assuming distribution of the geosphere release over a greater area than in the *base case*, caused by a large subhorizontal fracture in the bedrock. In this case, the geosphere release is not restricted to object 157_2, but radionuclides are also discharged to the regolith of the two downstream objects designated 157_1 and 116. Although based on model realisations, this kind of subhorizontal structure in the bedrock is considered to be unlikely, the calculation case is used to give a credible illustration of the effects of a distributed geosphere release.

There are two variants of this calculation case. In the first variant, *distributed release*, the geosphere release is dispersed to the three discharge areas, and the groundwater flow is assumed to be the same as in the *base case*. In the second variant, *distributed release and modified bedrock discharge*, the upward groundwater flow rates from the bedrock in the three discharge areas are also modified, so that the postulated shift in discharge pattern is matched with changes in groundwater flow.

The two variants build on complementary studies carried out within SR-PSU to address uncertainties with respect to the future landscape (Saetre and Ekström 2016, 2017a). The selected variants, together with the *alternative landscape configurations calculation case* (Section 10.6), are considered to be the most relevant and informative cases from a broader suit of calculations covered by Saetre and Ekström (2016, 2017a).

10.5.1 Description of the calculation case

Climate conditions

The *base case* climate conditions are applied in this calculation case, namely present-day temperate conditions persist for the entire assessment period.

Bedrock hydrogeology

The hydrogeological description of the bedrock in the SFR-area consists of two components: 1) the deterministically modelled, known deformation zones (so-called Hydraulic Conductor Domains, HCDs) and 2) the stochastically modelled, less fractured rock mass between these deformation zones (the so-called Hydraulic Rock Domain, HRD). The first component includes both deformation zones and shallow bedrock aquifer structures. The second component includes stochastically generated fractures, some of which are deterministically linked to boreholes. In the original SR-PSU, the stochastic fracture network outside the regional model domain was represented by a single realisation. Therefore, the effects of uncertainties in the hydraulic rock domain on the location and properties of discharge areas were not examined.

In a complementary study, Öhman and Odén (2017) examined how the heterogeneity caused by the fracture network outside the SFR regional model domain affected flow paths and the groundwater outflow from the rock to the surface system. The results showed that fracture network outside the SFR regional domain typically had little or no effect on the location of the discharge from the repository. However, in one of the cases (R02), a substantial fraction of the particles from SFR1 (i.e. the existing part of SFR), ended up outside object 157_2. In this realisation, a relatively shallow subhorizontal fracture led water from the bedrock below object 157_2 in the direction of object 116, and groundwater was discharged to low points in the terrain where the fracture was intersected by steep vertical structures. In spite of the partial shift of discharge locations (and extended path lengths), key performance measures in the geosphere (i.e. advective travel time and F-quotient) were shown to be practically unaffected by the subhorizontal fracture. The stochastic methods used in the generation of the fracture networks indicate that a fracture structure of this type (i.e. like that of scenario R02) is unlikely (Öhman and Odén 2017).

Geosphere release

A total of 30 “bedrock cases” (i.e. variations in the parameterisation of the bedrock hydrological model) were used to study the sensitivity of repository performance to uncertainties in the bedrock geohydrology in Öhman and Odén (2018). In eight of these bedrock cases, the R02 realisation was implemented as a part of the HRD outside the SFR regional domain. Particle tracking studies were performed with 10 000 particles released from each waste vault under nine fixed positions of the shoreline displacement in the *base case*. During submerged conditions > 80 % of the particles released in the model reached the basin of object 157_2 in all R02-realisations (Figure 10-9). However, in the terrestrial stage, ~40 % of the particles released from SFR1 and SFR3 reached the basins of either of the two downstream objects (157_1 and 116). This pattern was most pronounced with the 5000 AD shoreline position. For some of the individual waste vaults (e.g. 1BTF, 2BTF, 1BRT and 2BLA) more than 50 % of released particles were discharged outside 157_2 at 5000 AD (Figure 10-10). Also, none (SFR1) or less than 10 % (SFR3) of simulated particles ended up in biosphere objects other than 116, 157_1 and 157_2 during the terrestrial stage. Correspondingly, in this calculation case, the geosphere release from each waste vault is partitioned to the three biosphere objects 157_2, 157_1 and 116 according to the average fractions reaching each basin across the eight bedrock cases (Figure 10-10). For simplicity, the fractions of the release are held constant over the simulation period, and the pattern from 5000 AD is applied in the calculations. This simplification is considered appropriate as the geosphere release, and the resulting doses, are largest in the terrestrial stage. The chosen shoreline position also has the largest spread of the geosphere release, which should give the largest difference as compared with the *base case*, in which all radionuclides are released to object 157_2.

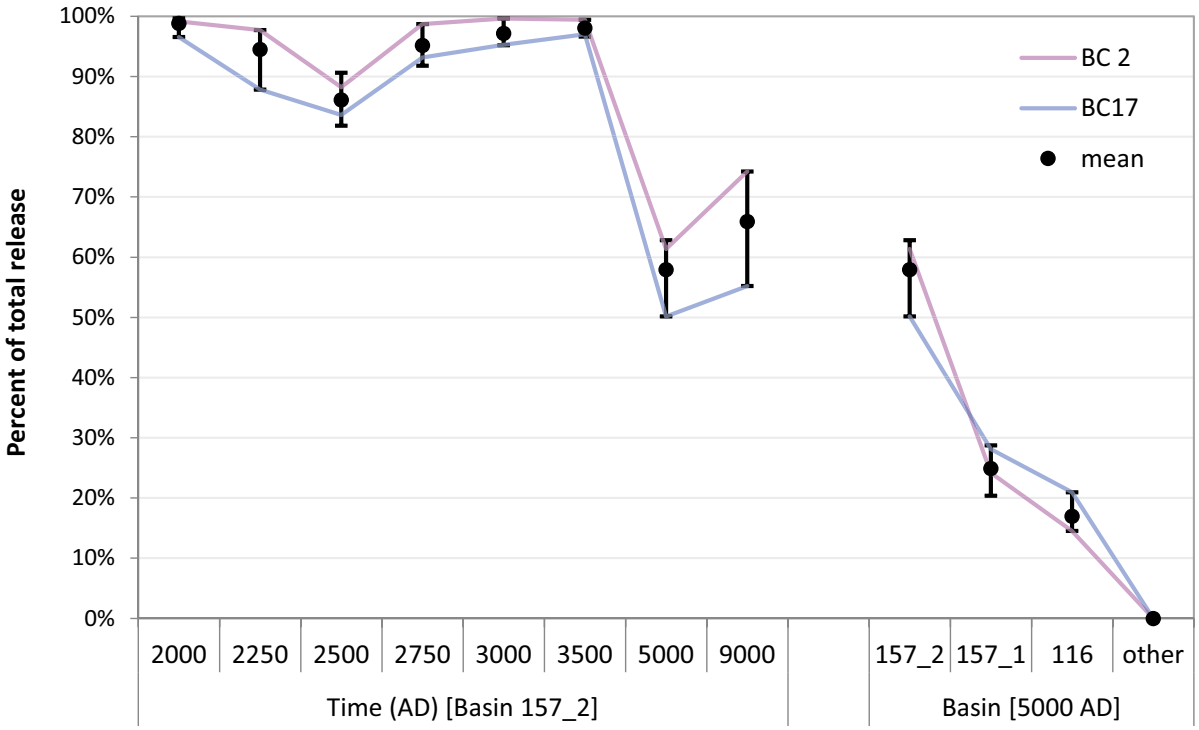

Figure 10-9. *Fractions (%) of total potential release from the SFR repository that are discharged into the basin of biosphere object 157_2 over time (left part of the graph) or into other biosphere objects at 5000 AD (right part of the graph). The mean of the eight bedrock cases (BC) with a subhorizontal fracture are shown (black circle) together with the minimum and maximum values (error bars). The two BCs with the smallest (purple, 39 %) and largest (blue, 50 %) releases outside basin 157_2 at 5000 AD shoreline position are shown with lines for reference. Surface positions for discharging particles are taken from Öhman and Odén (2018).*

		Biosphere object		
	Vault	157_2	157_1	116
SFR1	1BLA	59 %	29 %	12 %
	1BMA	73 %	20 %	8 %
	1BTF	47 %	38 %	15 %
	2BTF	45 %	39 %	16 %
	Silo	57 %	30 %	13 %
SFR3	1BRT	45 %	34 %	21 %
	2BMA*	62 %	13 %	25 %
	2BLA	56 %	25 %	19 %
	3BLA	55 %	21 %	24 %
	4BLA	69 %	14 %	18 %
	5BLA	72 %	11 %	17 %

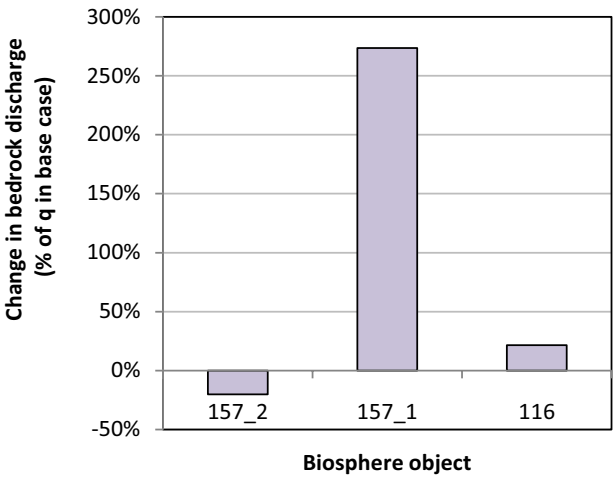

Figure 10-10. *Characteristics of deep groundwater discharge to the biosphere system in the subhorizontal fracture calculation case. Left panel shows the distribution of particles released to the basins of three biosphere objects under the 5000 AD shoreline position (data from Öhman and Odén 2018). These percentages are used to distribute the geosphere release between the three biosphere objects at all times of this calculation case. The asterisk indicates that all the release is assumed to reach the three objects, although 3 % of particles were originally mapped outside the three basins. Right panel shows the change in area specific bedrock discharge in the subhorizontal fracture calculation case relative the discharge given base case conditions (data from Öhman and Odén 2017). The change is used to adjust the discharge of groundwater from the bedrock to the till in the variant with distributed release and modified bedrock discharge (see text for details).*

Landscape description

The properties and development of the landscape from the *base case* are used in this calculation case. However, as the release is distributed between three biosphere objects, the BioTEx model (Chapter 7) includes a full implementation of the aquatic and terrestrial parts for all three biosphere objects. Therefore, radionuclide accumulation in regolith layers is also accounted for in objects 157_1 and 116 (Figure 10-11).

Surface hydrology

A subhorizontal fracture is not expected to alter runoff or surface water flows significantly. Thus, the hydrological flows of the *base case* are considered to be appropriate also for this calculation case. However, hydrogeological simulations suggest that the bedrock discharge to object 157_1 may increase considerably (270 %) (right panel in Figure 10-10, Öhman and Odén 2017). The fracture may also modify the bedrock discharge in object 157_2 (decrease) and 116 (increase), but these changes are expected to be more modest (~20 %). To evaluate if such changes in bedrock discharge would affect transport and dose calculations, groundwater flows are also modified in the second variant of this calculation case (*distributed release and modified bedrock discharge*). In this variant, the flow from the bedrock to the till is either up- or down-scaled in the terrestrial period (i.e. when land has emerged) with respect to the first variant (*distributed release*). To maintain water-balance in the regolith profile, the change in flow is also added (or subtracted) to the upward flow component of all stacked regolith compartments. This adjustment is done individually for each of the three biosphere objects.

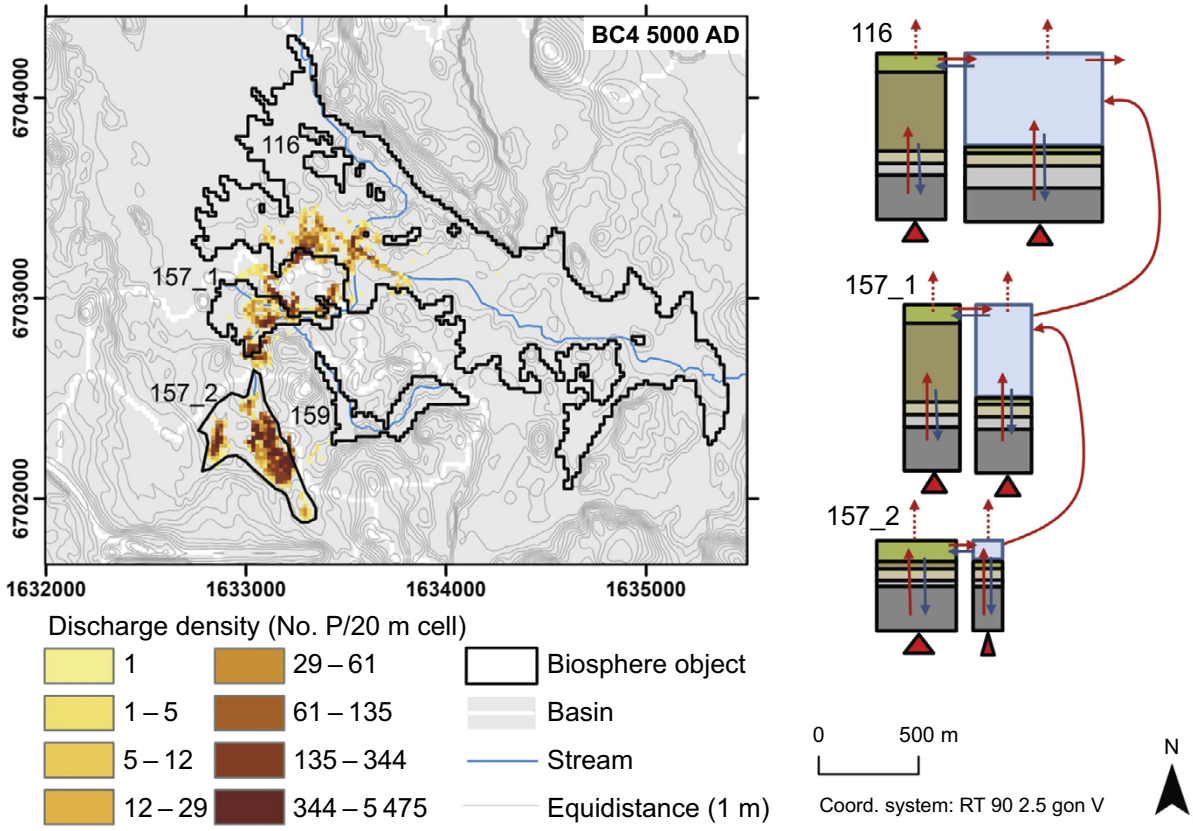

Figure 10-11. *Spatial pattern of geosphere release and BioTEx model structure used in the subhorizontal fracture calculation case. Left: pattern of particles released from the SFR repository at the bedrock surface (number of particles per surface cell). Bedrock case four (BC4) is used for the illustration, as the particle distribution in this case is similar to the average of the eight R02 bedrock cases. The areal extension of lakes in the biosphere objects 157_1 and 116 at 5000 AD is shown in Figure 9-3. Right: schematic sketch of the transport of radionuclides (red triangles and arrows) between regolith layers and surface waters within and between biosphere objects. The figure represents a snapshot in time when all three objects have emerged above sea-level and lakes are still open in objects 157_1 and 116 (represented by relatively wide stacks of aquatic compartments). Symbols and colours are as explained in Figure 9-3.*

Ecosystem parameters and potentially exposed groups

Ecosystem properties are not considered to be affected by the large sloping fracture, and consequently the parameters from the *base case* are used in this calculation case. The same potentially exposed groups of humans are used as in the *base case*.

10.5.2 Annual doses

Distributed release variant

The subhorizontal fracture is projected to redistribute the release from SFR, so that approximately 45 % of the release from SFR1 directly reaches the two downstream objects, and most of this release reaches the smaller object 157_1. The effects of the fracture on the release from SFR3 are similar. However, a somewhat smaller fraction of the release is redirected to the two downstream objects (~40 %) and this release is distributed more evenly between them. It can also be noted that the effect of the fracture on the release from individual waste vaults varies somewhat from this general pattern (Figure 10-10).

In the *base case* all geosphere release reaches object 157_2. The two primary effects of a redistribution of the geosphere release are reduction of the activity that reaches object 157_2, and a change in the pathways by which radionuclides reach and accumulate in the two downstream objects. A change in the pathway is important because radionuclides reaching the downstream objects via groundwater discharge potentially accumulate more in the regolith layers than if those radionuclides reach the object via stream water (as postulated in the *base case*). Moreover, for C-14, which is degassed to the atmosphere at a rate far exceeding that of export via surface water, a subhorizontal fracture pathway also implies that a larger amount of its activity will reach the downstream objects.

As expected, the distributed release associated with the subhorizontal fracture results in a dose in object 157_2 that is approximately 60 % of that in the *base case* (Figure 10-12, upper panel). The dose reduction varies somewhat over time, as the radionuclides that contribute most to dose originate from different waste vaults, and the fracture affects the release from individual waste vaults differently. Nevertheless, the reduction in total dose is typically around 40 % (including the total dose maximum). This corresponds well with the reduction of the geosphere release to 157_2 from the silo, 2BMA and the five BLA vaults, which are the waste vaults contributing most to the dose (**Radionuclide transport report**, Section 5.9.2).

Directing part of the geosphere release directly to object 157_1 (~30 % from SFR1) results in a higher dose in this object than in object 157_2 for a period of ~1 300 years after emergence and in the period after 25 000 AD (Figure 10-12, upper panel). During the latter part of the assessment period (after ~40 000 AD) the dose in object 157_1 even exceeds that of the *base case* by up to approximately 50 %, though the maximum dose never exceeds the maximum dose in the *base case* (Figure 10-12, upper panel). The initial dose peak reflects C-14 exposure from draining and cultivating the mire in the object (Figure 10-12, lower panel). The relatively high dose is caused by a low dilution of C-14 in the saturated layer of object 157_1 (relative to the dilution occurring in object 157_2), as groundwater uptake is the primary source for C-14 in the cultivated soil. With time, the whole lake basin in object 157_1 is assumed to be succeeded by a mire, resulting in the formation of a peat layer that is substantially thicker than projected in object 157_2 (Figure 5-5). In the period beyond 25 000 AD, accumulation of I-129, uranium isotopes and associated decay products (e.g. Pa-231 and Ac-227) in this peat layer results in a dose that exceeds that in object 157_2 (Figure 10-12, lower panel).

The assumed geosphere release to object 116 is limited (typically < 20 %) and the object and its watershed are relatively large (e.g. Figure 5-5). Thus, the dose that results from a direct release to this object is clearly below that of the other two objects given a distributed release, and typically an order of magnitude below the dose in the *base case*. An exception to this is the submerged period. In this period the release into object 116 contributes significantly to the total dose (data not shown). However, the distribution of the geosphere release has a marginal effect on the total dose at this time, as compared to the *base case*, and the limited exposure from foraging the sea ecosystem results in a very low dose (see *base case*, Figure 9-4).

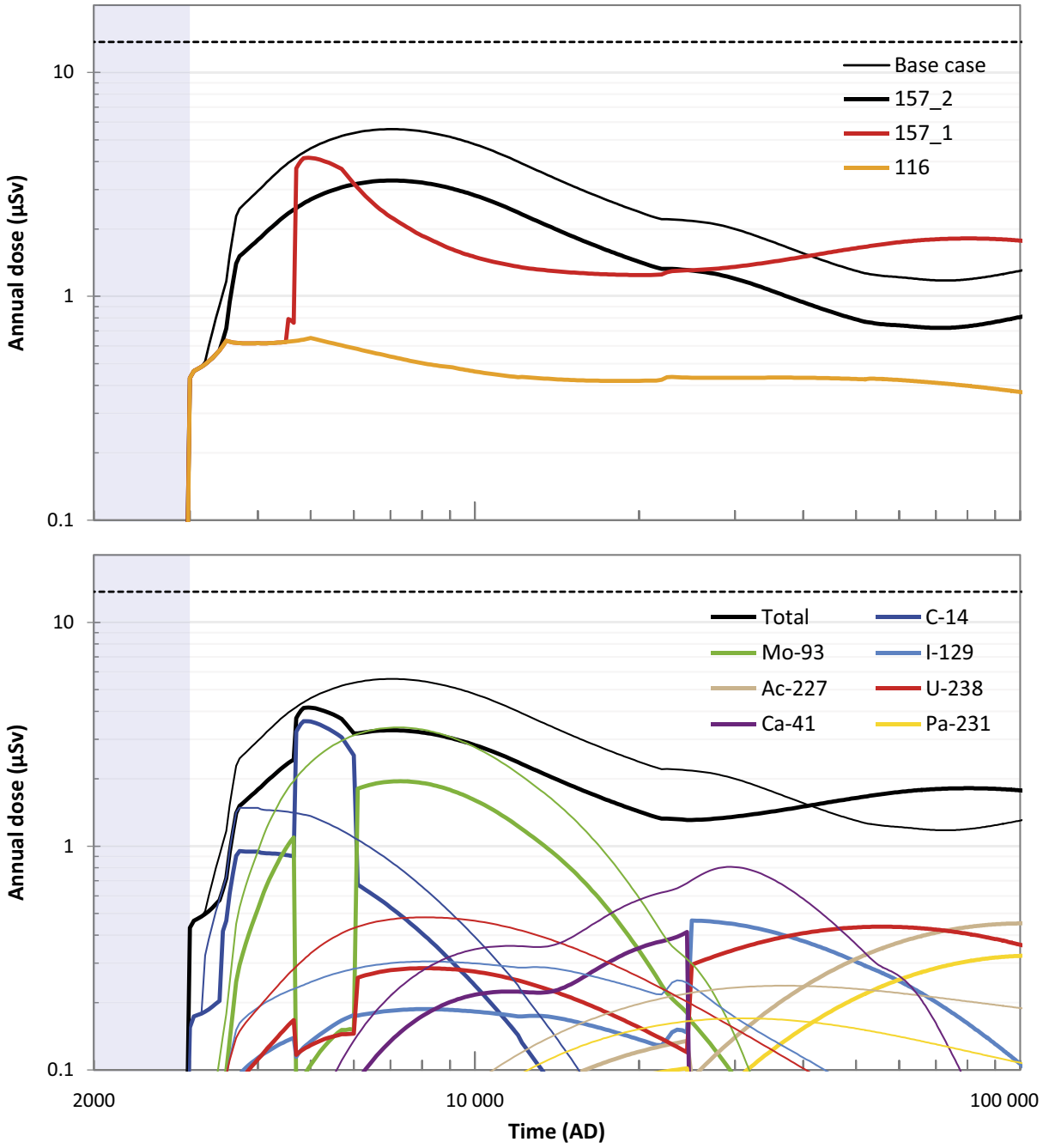

Figure 10-12. *Annual dose in the distributed release variant of the subhorizontal fracture calculation case. Top: total annual doses in the three objects receiving fractions of the distributed release. Bottom: doses from different radionuclides. For clarity only the seven radionuclides that contribute most to the total dose curve are shown. Note that the object yielding the highest dose shifts over time and this causes abrupt changes in the doses from individual radionuclides. Doses in the base case are shown for reference with thin lines. The annual dose (14 µSv) corresponding to the regulatory risk criterion is indicated by the horizontal black dashed line.*

Distributed release and modified bedrock discharge variant

In addition to distributing the geosphere release across multiple biosphere objects, a subhorizontal fracture is also considered to alter the discharge of groundwater from the bedrock. An increased discharge from the bedrock will decrease the transport time and increase the degree of groundwater dilution. Its effects are likely to be more pronounced in the lower section of the regolith profile.

The projected changes in the discharge from the bedrock to object 157_2 and 116 are small and have a marginal effect on the calculated transport of radionuclides in the biosphere system and annual doses (Figure 10-13). However, for object 157_1 the discharge from the bedrock increases by 270 % (Figure 10-10, right panel). This shift results in a reduction of the dose peak in the early terrestrial period to approximately half of that with unmodified bedrock discharge, and the maximum dose in object 157_1 becomes lower than the dose in object 157_2. It can also be noted that the dose in the period between 10 000 and 78 000 AD increase somewhat in object 157_1 (up to 30 %).

As noted above, the early dose peak is due to C-14. This radionuclide has a short residence time in regolith layers (Section 9.3). The reduction in dose corresponds to an increased dilution of C-14 in the layers feeding groundwater to the cultivated soil, that is in glacial clay or post-glacial clay gyttja depending on the thickness of the developing peat at the time. Subsurface runoff from the local catchment also contributes to the groundwater flow in these layers. Thus, the effect of bedrock discharge on groundwater flow and dilution is dampened. The increased dose and the earlier shift of the dose dominating object (now occurring at 18 000 AD) is due to the shortened transport time through the lower regolith profile. This leads to a reduced time for released activity to reach the peat, e.g. for U-238 and U-235 (which decays into Pa-231 and Ac-227). In addition, an increased flow rate increases the activity of radionuclides that are reduced by radioactive decay along the pathway towards the surface (e.g. of Ca-41). However, the maximum dose after 18 000 AD in object 157_1 is still well below the maximum dose of the *base case* (Figure 10-13).

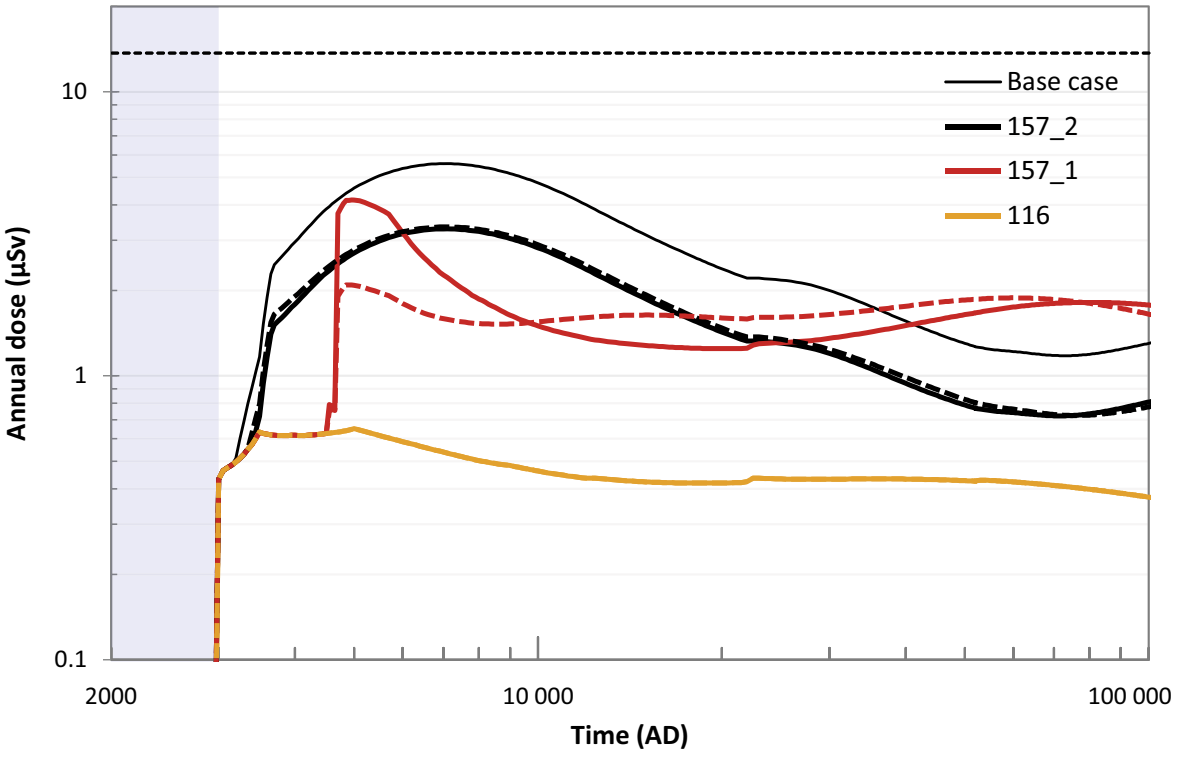

Figure 10-13. *Effects of bedrock discharge associated with a subhorizontal fracture on the total annual dose in three biosphere objects. The graph is identical with left panel in Figure 10-12, but doses from the variant with a distributed release and a modified discharge have been added with dashed lines. Note that a modified bedrock discharge has no effect on the dose in object 116 (i.e. the two lines appear as one). The annual dose in the base case is shown for comparison (thin black line). The annual dose (14 µSv) corresponding to the regulatory risk criterion is indicated by the horizontal black dashed line.*

10.6 Alternative landscape configuration calculation case

This calculation case is developed to evaluate potential effects on doses to humans of uncertainties with respect to the transport pathways and development of the future Forsmark landscape. Alternative descriptions of the ground- and surface-water pathways are used, and potential effects of accumulation in the downstream object, or of a direct release of radionuclides to surface water, are evaluated. In addition, the effects of an alternative development of the small lake downstream the primary object are evaluated.

In the *base case*, radionuclides from the primary biosphere object (157_2) are discharged to a stream and reach the surface water of the downstream object (157_1). This choice is motivated by the modelling results in Werner et al. (2013), who found that the overland water flow in the area between the objects is of the same order of magnitude as the calculated stream discharges in the other small streams included in the future stream network. The flow of surface water from the aquatic to the terrestrial ecosystem in the downstream object is limited (Werner et al. 2013, Figure A1-41), and consequently radionuclide accumulation in mire peat is not considered in the *base case*. Moreover, large fractions of volatile radionuclides that are released from the geosphere to the mire in 157_2 in the *base case* are lost to the atmosphere before being discharged to stream water.

Three variants of this calculation case are selected to evaluate these uncertainties in the landscape configuration: 1) *no stream* – a landscape where there is no stream connecting objects 157_2 and 157_1, 2) *release to surface water* – a landscape in which the geosphere release reaches surface water directly, and 3) *open lake* – a landscape in which the geosphere release reaches surface water directly and the lake 157_1 is always open (as opposed to being replaced by a mire).

The *no stream* variant largely corresponds to the biosphere *base case* in SR-PSU, and thus, besides illustrating potential effects of extensive accumulation in the downstream object, facilitates a comparison with the previous assessment. However, as consequences of a direct release to surface water are evaluated in the *release to surface water* variant (below), the distribution of runoff between aquatic and terrestrial parts of the recipient has also been modified to be more informative (and perhaps also more realistic, see Landscape description below).

The *release to surface water* variant also addresses uncertainties with respect to transport pathways to the downstream lake. It builds on complementary studies carried out within SR-PSU to address uncertainties with respect to transport pathways in the future landscape (Saetre and Ekström 2016). This variant, together with the *horizontally sloping bedrock fracture calculation case* (Section 10.5), are considered to be the most relevant and informative cases from a broader suit of calculations (Saetre and Ekström 2017a). The starting point for this variant is the view that aquatic food can be an important exposure pathway for C-14. Thus, this variant is more hypothetical, as retention in regolith, and release to the atmosphere in the primary biosphere object are practically unaccounted for in the terrestrial stage. This variant can also be seen as an upper bounding case for extensive sub-surface transport from the primary discharge area or for a localised upwelling in the stream due to e.g. hyporheic flow.

The *open lake* variant is near identical to the *release to surface water* variant. However, to ensure that exposure from the aquatic food chain is not overlooked, doses from an open lake in 157_1 are also evaluated (at all times) in this variant.

10.6.1 Description of the calculation case

Climate conditions

The *base case* climate conditions are assumed also in this calculation case, namely that present-day temperate conditions persist during the entire simulation period.

Geosphere release

The transport pathways in the near-field and the geosphere are not expected to be significantly affected by surface runoff pathways or ditching activities in the overburden. Thus, the *base case* geosphere release is used also in this calculation case, and all radionuclides from the repository are discharged to biosphere object 157_2. However, in the *release to surface water* variant, the release is directed directly to the stream water in object 157_2.

Landscape description

The properties and development of the landscape in the *base case* are used also in this calculation case. However, the *no stream* variant assumes that no stream will develop in object 157_2. Instead, the flow of shallow groundwater from the wetland in 157_2 to the downstream lake-mire complex in 157_1 is conceptualised as a diffuse outflow of near-surface water (Figure 10-14, see also Werner et al. 2013, Section 6.2.3). In SR-PSU, it was cautiously assumed (with respect to exposure from C-14) that this water will reach the mire and the lake parts of the downstream object in proportion to the surface area of each ecosystem (see Section 4.3.2 in Saetre et al. 2013a for details). However, the wetland vegetation expands from the shores of the lake, the water body is most likely to be surrounded by a zone of wetland vegetation. In accordance, the *no stream* variant assumes that all radionuclides will reach the mire part of the recipient. This model setup also ensures that accumulation of radionuclides in the peat of the downstream object is not underestimated due to the assumed transport pathways in the future landscape.

In the *release to surface water* variant, the groundwater flow pathway in object 157_2, as described in the *base case*, is postulated to be disrupted. Such a disturbance could for example be caused by a large-scale draining for forestry purposes. The variant is not designed to give a realistic description of such an enterprise. Instead, an upper boundary of the consequences is examined by making the simplifying assumption that *all* geosphere release is discharged into water filled man-made ditches. Thus, from the time point when the whole object is above the sea level (i.e. at 4300 AD), the geosphere release is directed directly to the running water in object 157_2 (Figure 10-14). The properties of the stream (in terms of length and surface area) are for simplicity set to be those of the undisturbed stream in the *base case*. With these assumptions all the activity of non-volatile long-lived radionuclides in the geosphere release will reach the aquatic ecosystem in the downstream object, and only negligible amounts of C-14 (< 1 %) will be lost to the atmosphere before the stream water enters the lake in object 157_1.

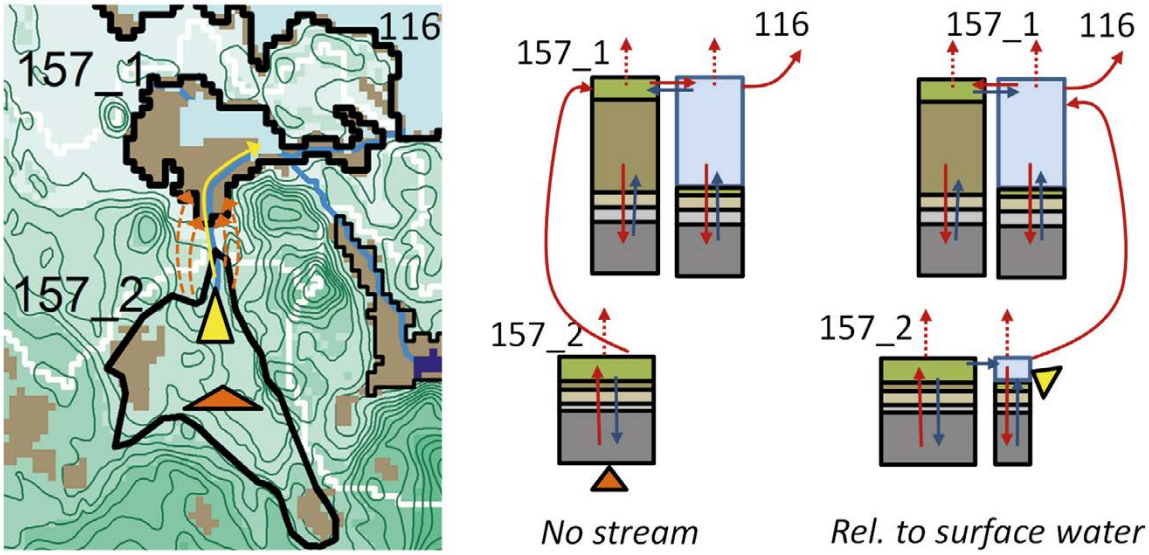

Figure 10-14. *Transport pathways and the model structures used in the alternative landscape configurations calculation case. Left: conceptual sketch of the transport of radionuclides with runoff water from biosphere object 157_2 to biosphere object 157_1 (orange and yellow arrows). The underlying map is from Figure 9-3. Right: schematic sketch over radionuclide transport within and between biosphere objects as represented in the BioTEx model. Triangles represent geosphere release (orange = no stream, yellow = release to surface water). The figure represents a snapshot in time when all three objects have emerged above sea-level. Symbols and colours are as explained in Figure 9-3.*

There are uncertainties as to where lakes will be formed in the future Forsmark landscape, and for how long they will persist (Gunia et al. 2021). Thus, restricting the description of the landscape development to that of the reference evolution (Chapter 4) may overlook possible alternative developments. Moreover, human activities such as damming and lake restoration could result in a water reservoir long after the time point when natural succession would have resulted in a complete infilling of the original lake basin. Uncertainties with respect to the presence of a relatively small water reservoir located near the primary discharge area, are addressed in the *open lake* variant. This simulation postulates that a water reservoir will always be in the downstream object 157_1, and the properties of the water body, for simplicity, are taken to be those of the open lake 157_1 at the point of isolation. Thus, in this variant, exposure from the lake is evaluated in two variants, one considering, and the other disregarding a likely (or normal) lake succession (as described in Chapter 4).

Surface hydrology

In the *no stream* variant, hydrological parameters for object 157_2 are derived from MIKE SHE water balances for the object lacking a stream, as was done in the *base case* calculations in SR-PSU (Werner et al. 2013, Grolander 2013). However, it can be noted that water-balances for two terrestrial time-points were derived for the no stream case (5000 and 11 000 AD), whereas only one time-point was used for the base case with a stream (5000 AD, *base case*) (Werner et al. 2013). The runoff from object 157_2, for both time-points, is identical with that in the *base case*, but the surface water pathways to the downstream object are changed (see above). In the *release to surface water* and *open lake* variants, all runoff and groundwater discharge are assumed to be collected in a system of ditches, which in water-balance terms is equivalent to assumptions made for the stream in the *base case*.

Ecosystem parameters

In all three variants of this calculation case, ecosystem properties are not considered to be affected by the imposed changes in landscape configuration. This is a reasonable simplification with respect to the downstream object 157_1. Large-scale draining would most likely lower the groundwater level and change the characteristics of the mire in object 157_2. However, as this ecosystem will receive little or no geosphere release, the accumulation of radionuclides will be significantly less than in the undrained mire assessed with the hunter gatherer exposure group in the *base case*. Moreover, the fate of radionuclides and the doses from a drained mire are already evaluated in the *base case*. In the *base case*, the mire is converted into an agricultural ecosystem, where soil compaction and high production is likely to result in much higher exposure than would be the case from a drained natural ecosystem used for. e.g. forest production.

Potentially exposed groups

The potentially exposed groups of humans are identical to the *base case*, and as in the *base case*, the doses are evaluated in biosphere objects 157_2, 157_1 and 116. In the *no stream* variant, there is no surface water available in object 157_2. Nevertheless, as in SR-PSU, it is cautiously assumed that runoff-water from the mire will be available to collect as drinking water for humans and livestock (Saetre et al. 2013a, Sections 9.3 and 9.4).

10.6.2 Annual doses

No stream

Export of radionuclides with diffuse overland-water flow from object 157_2 has practically no effect on the maximum dose from draining and cultivating the object as compared with the *base case* (where radionuclides are exported via a stream). This is expected, as the conditions in the primary object are changed only marginally in this variant and the accumulation of Mo-93 is near identical. However, as the groundwater flow increases slightly in the lower regolith (~20 %) after mire completion at 4500 AD, the dose from C-14 decreases correspondingly (Figure 10-15). The last successional stage of object 157_2 was not described for the variant with a stream, and thus the difference is considered to be driven by lack of data (in the *base case*) rather than by a shift in hydrology caused by the absence of a stream. Nevertheless, the effect is limited to C-14, for which the doses rather depend on groundwater uptake (Section 9.3).

Radionuclides accumulate in the downstream mire in object 157_1 throughout the simulation. After approximately 10 000 years, the doses from the two objects are similar, and for the rest of the simulation period, draining and cultivation of object 157_1 results in higher doses (Figure 10-15). However, the maximum dose in object 157_1 never exceeds the maximum in object 157_2 (which is similar to that of the *base case*). The dose in the downstream object 116 is considerably lower than that in object 157_1 (data not shown).

These results are similar to those reported in the supplementary study of SR-PSU (Saetre and Ekström 2016). It is the contribution of accumulation in the ~1.4 m thick peat layer, filling the lake basin in object 157_1, that accounts for the increased activity in drained and cultivated soil after 10 000 AD.

Apart from Ca-41, it is primarily radionuclides with high K_d values in peat (~10 m^3 $kgdw^{-1}$) that contribute to the comparatively high dose, namely U-238, U-235 and its decay products Pa-231 and Ac-227 (Figure 10-15). These radionuclides are so tightly sorbed to the upper peat that the burial rate, on average, is greater than the down-stream advective transport. The strong sorption in peat, and the relatively long half-lives, result in a substantial accumulation in the deeper peat, and accumulated U-235 acts as an additional source for Pa-231 through radioactive decay. Ac-227 also sorbs strongly in peat, but this is of little significance because it has a short half-life (22 years). The origin of the Ac-227 activity in deep peat is almost exclusively the ingrowth from decay of Pa-231. The accumulation of Ca-41 is also comparatively high in object 157_1. For Ca-41, which has modest K_d values in deep and upper peat, it is plant uptake, followed by burial and storage of Ca in organic form, that drive the accumulation (cf *base case*).

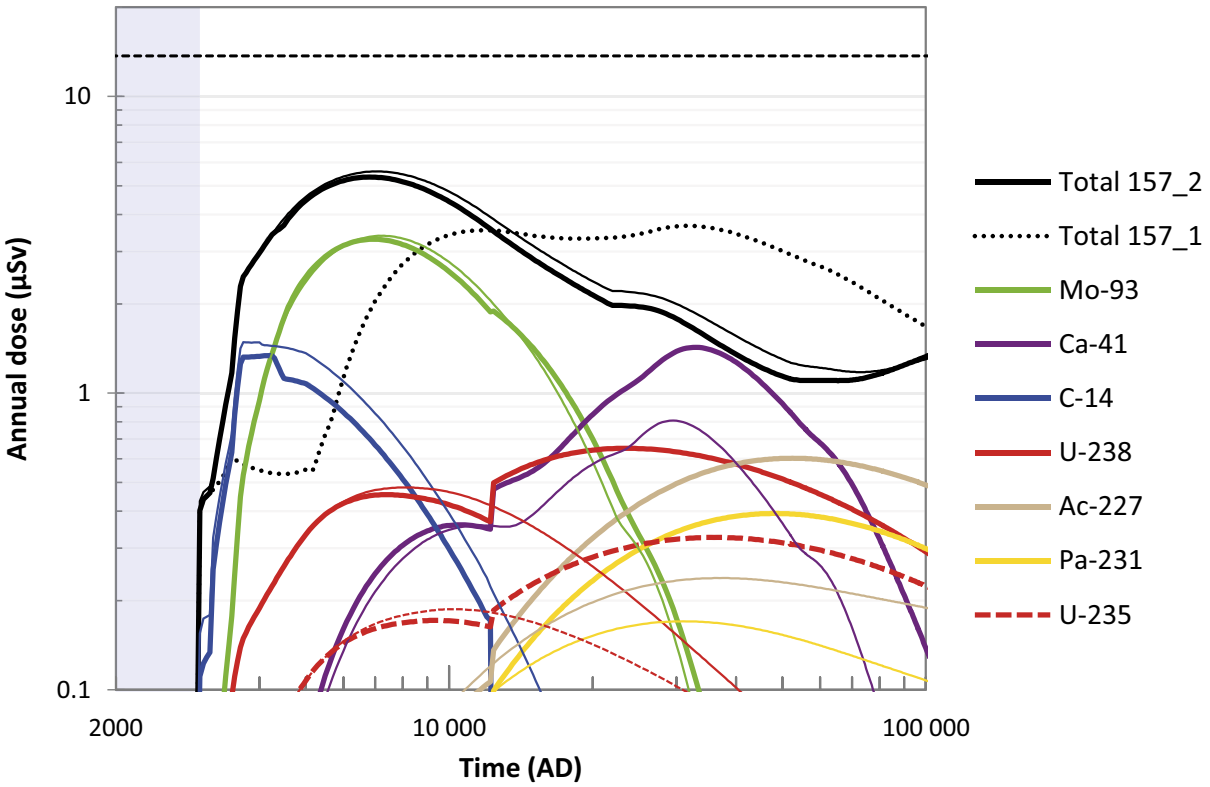

Figure 10-15. *Annual dose in two objects from different radionuclides in the no stream variant of the alternative landscape configuration calculation case. For clarity only the seven radionuclides that contribute most to the total dose curve are shown. Note that during the first 10 000 years after closure the highest dose results from object 157_2 (thicker solid black line), but later in the simulation the dose is higher in object 157_1 (dotted black line). The shift in maximum dose from object 157_2 to object 157_1 is the cause of the abrupt change in the dose from Ca-41, U-238 and U-235. Doses in the base case are shown for reference with thin lines. The annual dose (14 µSv) corresponding to the regulatory risk criterion is indicated by the horizontal black dashed line.*

Release to surface water

A change in the vertical location of the geosphere release, from the deep regolith to stream water, clearly shifts the relative importance of exposure pathways as compared with the *base case*. The shift is expected, since a key process for the major pathway in the *base case*, namely long-term accumulation in mire ecosystem, is lacking in this variant. Moreover, when the transport pathway through regolith is short-circuited, radionuclides that normally are retained in deeper regolith layers can reach the surface and cause exposure via aquatic ecosystems. This is the case for Pu-239 and Pu-240 which have a very high bioavailability in lake water (i.e. high concentration ratio for fish) and are highly radiotoxic when ingested. As a result, exposure from C-14, Pu-239 and Pu-240 results in a dose that exceeds the dose in the *base case* for a brief period between ~4500 AD and ~5000 AD (Figure 10-16). However, the dose maximum does not exceed the dose maximum in the *base case*.

It is hunting and gathering in aquatic ecosystems that result in the highest dose in this variant. The dose maximum occurs a few hundred years after isolation of the two lakes down-stream object 157_2 (~4500 AD), and consumption of fish from object 116 is the dominating exposure pathway. This is primarily due to the large production capacity for fish in this lake (at isolation the production capacity is 20 times larger than in object 157_1) in combination with a modest increase in diluting surface water flows (the catchment of object 116 is six times greater than that of 157_1). For C-14, exposure from lake 157_1 is initially almost as important as from the larger lake. This is because degassing in lake 157_1 reduces the export of radionuclides to lake 116, and because degassing of C-14 in the lake is relatively large (as compared to advective transport). However, the dose contribution from lake 157_1 decreases as the lake production capacity declines when it is filled with mire vegetation, and within 1 000 years the contribution from this lake is negligible for all radionuclides (Figure 10-16). The large lake in object 116 is also gradually replaced by a mire, but the succession is considerably slower. This succession, in combination with a reduced geosphere release, explains the declining doses from C-14, Pu-240 and Pu-239. When the lake is infilled (~10 000 AD), hunters and gatherers are no longer the most exposed group (Figure 10-16).

In the period before the object is drained (4300 AD), and the geosphere release is directed directly to the running water, the dose is identical to that of the *base case*. In the period after mire ingrowth is completed (~10 000 AD) cultivating the mire in object 157_2 results in the highest dose (Figure 10-16). This may at first seem counterintuitive as there is no release to the area when cultivation is feasible. However, radionuclides have accumulated in sea sediments prior to emergence. Thus, early farmers are exposed to Mo-93 that has accumulated in glacial clay and clay-gyttja during the submerged period. Thereafter, radionuclides successively migrate from the till, causing increasing exposure from draining, until the inventory of Mo-93 has been washed-out. The relatively strong sorption of Ca-41 in the lower regolith slows down the release of this radionuclide from till to the upper regolith layers. This delayed release (and subsequent accumulation) of Ca-41 contributes to the dose around 10 000 AD and prolongs the period when draining the mire in object 157_2 causes the highest exposure. In the last period it is exposure to Ac-227 in water extracted from a well drilled in the bedrock that results in the highest dose (a pathway that is identical with that in the *base case*).

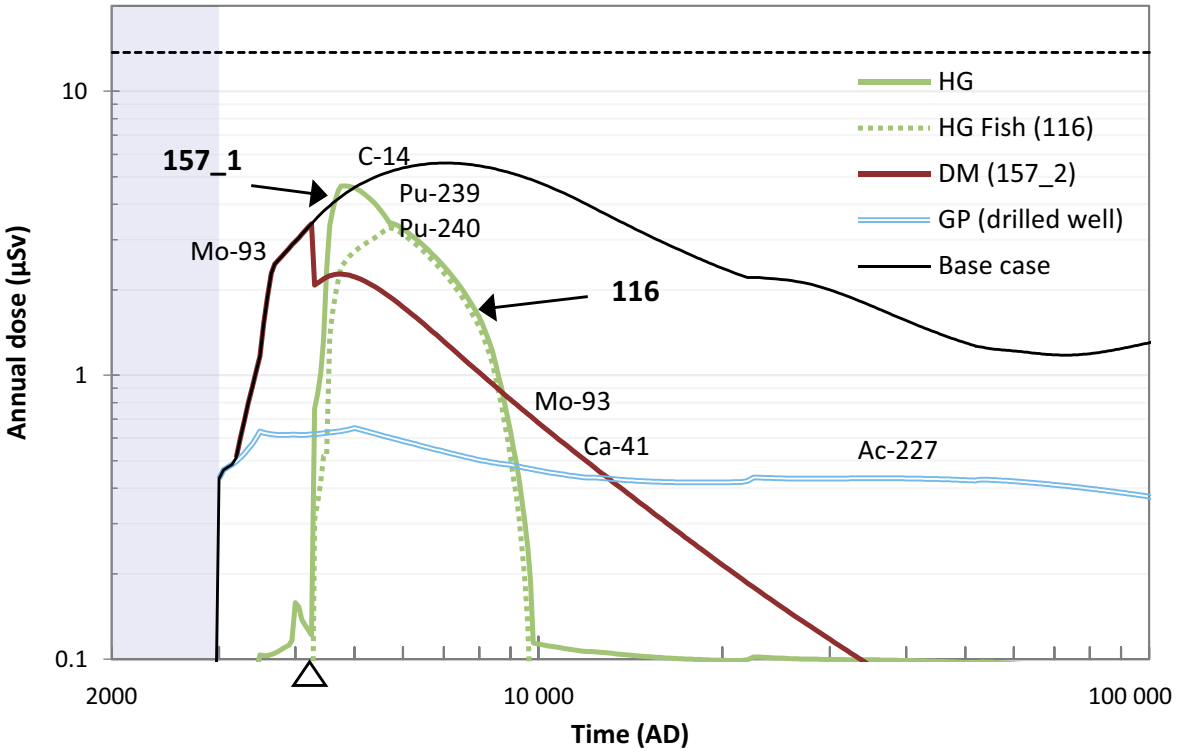

Figure 10-16. *Annual dose to different potentially exposed groups in the release to surface water variant of the alternative landscape configuration calculation case. In this case the geosphere release is directed directly to the running water in object 157_2 at 4300 AD (white triangle), Radionuclides that contribute most to the shape of the dose are indicated above the curves (for details on some radionuclide-specific doses see Figure 10-17). Hunters and gatherers (HG, green line) forage in all objects affected by the geosphere release (157_2, 157_1, 159 and 116). However, consumption of fish from object 157_1 and in particular from object 116 (dotted green line) is the dominating exposure pathway. Drained-mire farmers receive the highest dose for a few thousand years after 10 000 AD (red line). The exposed group utilising water from a drilled well in the bedrock (double blue line) is the same as in the base case. The doses to the most exposed group in the base case (DM in object 157_2) is shown for reference (thin black line), and the annual dose (14 µSv) corresponding to the regulatory risk criterion is indicated by the black dashed line.*

Open lake

Postulating that an open water body will be maintained in object 157_1 for the full simulation period has a marginal effect on the maximum dose (it increases by ~10 %, see Figure 10-17). However, an open lake in 157_1 prolongs the period with relatively high dose by approximately 1 000 years and extends the period when hunters and gatherers are the most exposed group by another 10 000 years. These results are explained by the exposure to Pu-239 and Pu-240 via fish from lake 157_1 (Figure 10-17). The increase in the dose from these radionuclides reflects the maintained production capacity of fish in the open lake 157_1, which given a normal lake succession is considered to be gradually converted into a mire within 1 200 years.

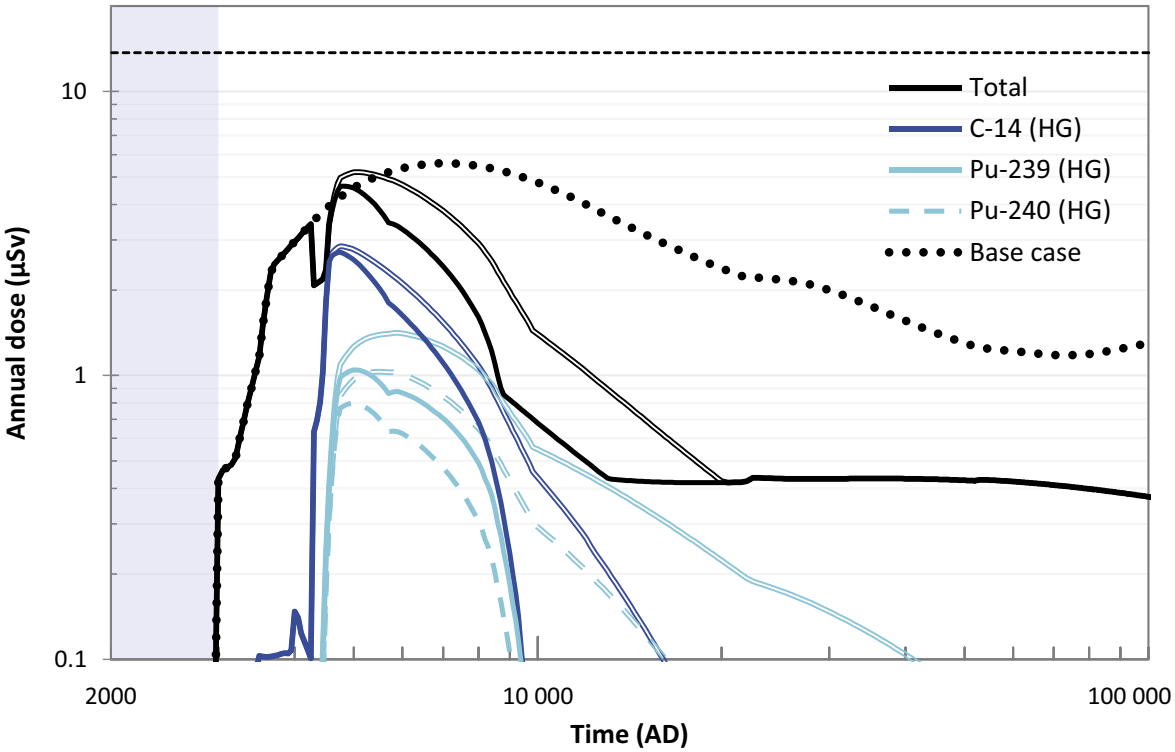

Figure 10-17. *Radionuclide-specific doses to hunter and gatherers from C-14, Pu-240 and Pu-239 (blue lines) and total doses to the most exposed group (black lines) for the release to surface water (thick lines) and open lake (double lines) variants. The annual dose (14 µSv) corresponding to the regulatory risk criterion is indicated by the black dashed line.*

11 Supporting calculation cases for the biosphere

11.1 Introduction

The main scenario includes three calculation cases, the *base case* (Chapter 9), and the *warm climate calculation case* and the *cold climate calculation case,* representing a range of probable future climate evolutions (Sections 10.2 and 10.3). To support the selection of assumptions for the main scenario, and to improve the confidence in the reported doses, a set of supporting calculation cases are defined in the **Radionuclide transport report**, Chapter 5. Three of the supporting calculation cases primarily concern uncertainties affecting the biosphere calculations, and these are described in more detail in Sections 10.4 to 10.6. In addition, four supporting calculation cases have been formulated to evaluate the sensitivity of calculated doses to uncertainties in the description of the biosphere system. These four cases, which are only presented in this report, are

- The *ecosystem properties calculation case*, evaluating the sensitivity of radionuclide-specific annual doses to variations in ecosystem parameters (Section 11.2).
- The *alternative delineation calculation case*, evaluating the impact on doses from variations in the outline of the biosphere object 157_2 (Section 11.3).
- The *mire object properties calculation case*, evaluating the sensitivity of activity concentrations and annual doses to variations in object properties. These properties include object geometries, regolith thickness, and parameters that drive or modify groundwater flows (Section 11.4).
- The *calcite depletion calculation case*, evaluating potential effects of a change in the mobility of radionuclides due to calcite depletion (Section 11.5).

The *ecosystem properties calculation case* and the *mire object properties calculation case* aim to evaluate the sensitivity of annual doses and activity concentrations, to variations in ecosystem and object properties. Because the maximum doses occur during the terrestrial period in the *base case* (Chapter 9), a simplified representation of the key biosphere object is used in the analysis. That is, the transition from an aquatic to a terrestrial ecosystem is not explicitly described here; instead, the biosphere object is described as a mature mire ecosystem during the entire simulation.

The simplification of using a time-independent ecosystem model allows probabilistic calculations to be made that capture uncertainties with respect to ground and surface water flows. This is achieved by applying the hydrological subroutine developed in SE-SFL (SKB TR-19-05, Section 7.5.5) in the mire model. In the subroutine, groundwater flows are derived from net precipitation, discharge from the geosphere, and object and catchment characteristics (Section 7.5.5). Applying the subroutine ensures that the water balance is preserved in all compartments during probabilistic calculations, and that flows are consistent with the thickness of regolith layers and the area of the object and its catchment.

Although the probabilistic treatment of the surface hydrology is only utilized in the *mire object properties calculation case,* the common model setup is used also with the *ecosystem properties* and *alternative delineation calculation cases*, facilitating direct comparison between them. The last supporting calculation case, the *calcite depletion calculation case,* is designed to addresses uncertainties with respect to the evolution of the chemical environment. To make it comparable with other cases illustrating the effects of scenario uncertainty (i.e. the *warm* the *cold* and *timing of shoreline regression* cases) the model setup is similar to that of the *base case*.

11.2 Ecosystem properties calculation case

In this supporting calculation case, the sensitivity of radionuclide-specific doses to variations in ecosystem parameter values is examined. The aims of the analysis are to 1) show which parameter uncertainties (including natural variation) have the largest influence on the variation of doses, and 2) illustrate how parameters with significant effects on the results affect the calculated doses. Ecosystem parameters are used in the broadest sense, including regolith properties (e.g. porosity, density and saturation),

characteristics of aquatic and terrestrial ecosystems (e.g. biomass, and rates of primary production and mineralisation) and element-specific properties for regolith layers, suspended particles and organisms (including K_d and *CR* values). The parameters examined are those that vary randomly in the *base case*.

11.2.1 Description of the calculation cases

General conditions, parameters and exposed groups

The *base case* assumptions are used in this supporting calculation case, except for the geosphere release and the landscape description (see below). That is, present-day temperate conditions persist during the entire simulation period and the geosphere release is discharged into biosphere object 157_2. Thus, apart from the model setup, this case sis identical with the *base case* (including the variation of ecosystem parameters)[48]. As land-use associated with draining the mire results in the highest total dose in the *base case*, the sensitivity analysis only evaluates doses to the corresponding potentially exposed group (DM).

Geosphere release

As the aim of this analysis is to examine the relative importance of biosphere parameters, the average geosphere release is used for all 1 000 simulations. That is, the geosphere release is time dependent, but it is averaged over the 1 000 realisations at each time. Moreover, by excluding variation in the geosphere release, the total variation explained from the multiple regression (i.e. R^2 value) gives a direct indication as to how well the dose can be approximated from a linear combination of the effects of selected individual ecosystem parameters on a logarithmic scale.

Landscape description

The landscape description is simplified in this calculation case and is represented by a mire in its mature stage. At this stage, the object has emerged fully out of the sea and depressions in the terrain have been filled with peat (this occurs ~4500 AD in the *base case*). However, although the description of the mire is time independent, the time point for when the mire can first be drained is taken from the *base case*. Using a time independent representation is motivated by the fact that the maximum radionuclide-specific dose from all the examined radionuclides in the *base case* results from draining the mire in its mature stage.

Selection of radionuclides

As in the *base case*, 1 000 Monte Carlo simulations are performed. The results from these are used in the sensitivity analysis. The analysis is limited to the four radionuclides that contribute most to the annual dose, i.e. C-14, Mo-93, Ca-41 and Ni-59 (Section 9.3). These four radionuclides cover a wide range of radionuclide- and element-specific properties (Table 9-2).

Sensitivity analysis

The primary endpoints of the analysis are radionuclide-specific annual doses. For each time point in the simulation of the assessment period, the doses are analysed with a multiple regression approach (Figure 11-1 to Figure 11-4). To quantify the overall importance of each parameter, the fraction of the total response variation explained by each parameter is determined. To illustrate how key parameters affect the calculated doses, the regression (or beta) coefficients are also reported.

[48] As in the *base case*, correlations between ecosystem parameters are not accounted for in this calculation case. This simplifies the sensitivity analysis and interpretation of β coefficients.

As most of the underlying relationships are multiplicative, the analysis is carried out on logarithms of the data. For small disturbances, the beta coefficients from an analysis on logarithms indicate the percentage of response (in dose) expected for a percentage of change in the parameter values. A beta coefficient of 1, thus indicates that the dose increases by approximately 10 % if the parameter value increases by 10 %[49]. This is referred to as a proportional response.

As the number of parameters is large, the multivariate analysis is preceded by a univariate screening step, in which the radionuclide-specific dose is analysed with each parameter individually in a linear correlation analysis. Parameters that explain at least 0.5 % of dose variation at any time point are carried forward to the next step. In this step, a multiple regression with the selected parameters is carried out for the time point of maximum dose, and parameters that explain at least 0.5 % of the dose variation (in the presence of the other parameters) are presented in Table 11-1. The regression coefficients, and the corresponding variation explained[50], are the endpoints of interest in the analysis of the results.

Table 11-1. Effects of parameter variation on radionuclide-specific dose variation at the time for the maximum dose. For each of four radionuclides, the percent variation explained by selected parameters (%Var) are presented together with the beta coefficients (β). The total variation explained by the linear combination of selected parameters is presented at the bottom (R^2). The beta coefficient expresses the sensitivity of the dose to a disturbance in parameter value. The strength of the response is colour coded from negative (blue) to positive (yellow), and for small disturbances β can be interpreted as the percent change in radionuclide specific dose per percent change in parameter value.

	C-14		Mo-93		Ca-41		Ni-59	
Parameter	%Var	β	%Var	β	%Var	β	%Var	β
LAI_{cereal}	2 %	0.4						
$f_{rootUptake}$	62 %	0.5						
$SoilResp_{gyttja}$	18 %	−0.5						
$q_{sat,unsat,agri}$	13 %	0.9						
$z_{regoUp,ter}$					0.7 %	0.3		
$ingRate_{C,cattle}$					0.5 %	0.7		
TC_{meat}					6 %	0.1	18 %	0.5
TC_{milk}					8 %	0.4		
$CR_{agri,fodder}$					15 %	0.5	9 %	0.4
$CR_{agri,cereal}$			53 %	0.7	5 %	0.4	2 %	0.2
$CR_{agri,tuber}$			8 %	0.2	0.6 %	0.1	9 %	0.2
$CR_{ter,pp}$			1.2 %	0.1	12 %	0.4		
$Kd_{regoUp,ter}$			2 %	0.2	2 %	0.2		
$Kd_{regoPeat}$			0.9 %	0.1				
Kd_{regoPG}			15 %	0.3				
Kd_{regoGL}			2 %	0.1	9 %	0.5	32 %	0.8
$Kd_{regoLow}$			1.0 %	−0.1	10 %	−0.5	10 %	−0.4
R^2	95 %		82 %		68 %		80 %	

[49] In natural logarithms, the linear multiple regression describing the dose (y) is:
$\ln(y) = \beta_0 + \beta_1 \times \ln(x_1) + \beta_2 \times \ln(x_2) + \ldots \beta_n \times \ln(x_n)$.

Taking the exponential of each side:
$y = \exp(\beta_0) \times x_1^{\beta_1} \times x_2^{\beta_2} \times \ldots x_n^{\beta_n}$

Thus, the linear, additive relationship is transformed into a multiplicative relationship. However, it is worth also noting that, for small perturbations, the system again becomes additive. Consider:
$y = F x_1^{\,a} \times x_2^{\,b}$

Make small perturbations $\delta_1 x_1$ and $\delta_2 x_2$ in x_1 and x_2. Then the perturbed value of y' is given by:
$y' = F x_1^{\,a}(1 + \delta_1)^a \times x_2^{\,b}(1 + \delta_2)^b$

To first order in each of the terms:
$y' = F x_1^{\,a}(1 + a\delta_1) x_2^{\,b}(1 + b\delta_2)$

and to first order in the product:
$y' = y(1 + a\delta_1 + b\delta_2)$

[50] The amounts of explained variation for individual parameters are estimated from the square of the standardised regression coefficients, SRC (Schroeder et al. 1986).

11.2.2 Results

For each of the radionuclides, parameters explaining at least 1 % of the dose variation for an individual radionuclide (at any point in time) are displayed in overview figures (Figure 11-1 to Figure 11-4). Results from more detailed analysis at the times of maximum dose are presented in Table 11-1. This analysis includes all parameters explaining at least 0.5 % of variation in radionuclide-specific dose at those times. To ease the interpretation of the analysis, results are presented and discussed for each selected radionuclide individually.

Results for C-14

Carbon is a non-sorbing element that is volatile in inorganic and organic and forms (CO_2 and CH_4). Carbon is also the primary component of all known organisms. C-14 has a half-life of 5 700 years. Since only a fraction of the released C-14 is taken up by mire vegetation and subsequently stored in peat (with a residence time of hundreds of years), the overall residence time of C-14 is very short in the mire ecosystem (< 10 years, Section 9.3). Thus, C-14 accumulation has no significant effect on the temporal pattern of the C-14 dose, and the effects and relative importance of individual parameters do not change over time (Figure 11-1).

The primary source of C-14 in agricultural ecosystems on a drained mire is groundwater uptake from the undisturbed and saturated till layer (RegoLow). Thus, the C-14 dose increases in proportion to the rate of groundwater uptake, and this is seen as a positive beta coefficient (β) close to unity for $q_{sat,unsat,agri}$ in the sensitivity analysis (Table 11-1). The primary exposure pathway for C-14 is ingestion of cereals (Section 9.3), and carbon fixation in cereals from the rhizosphere and from the plant canopy both are processes contributing quantitatively. The specific activity of C-14 in soil pore water is much higher than in the atmosphere, and therefore the plant concentrations (and C-14 dose) increase with the fraction of root uptake (seen as a positive β-coefficient for $f_{rootUptake}$,in Table 11-1). Dilution with stable carbon in the soil, due to respiration, decreases the C-14 dose (negative β for $SoilResp_{gyttja}$, Table 11-1). On the other hand, an increased leaf area decreases dilution with stable carbon in the canopy atmosphere by slowing down the gas exchange with the ambient atmosphere. Thus, a higher specific activity in the canopy atmosphere leads to an increased activity and in the crop, and consequently a higher dose (positive β for LAI_{cereal}, Table 11-1).

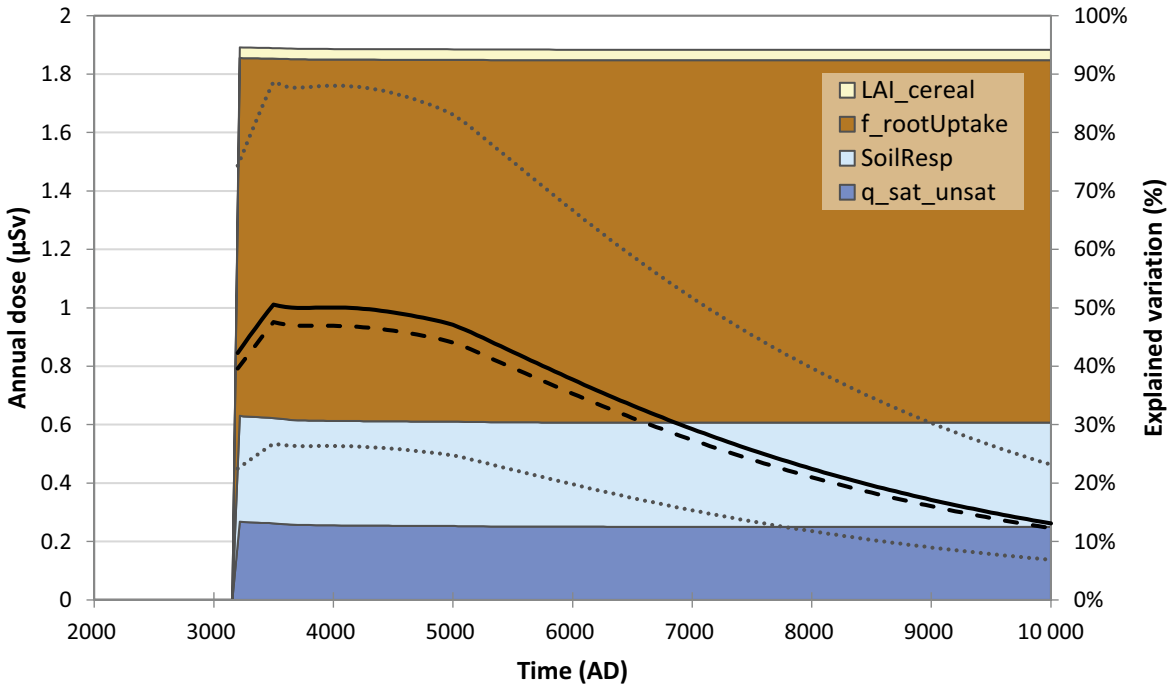

Figure 11-1. *Radionuclide-specific dose variation as a function of time for C-14. The mean (solid line) and median (dashed line) dose are shown together with the empirical 90 percent confidence interval (dotted lines represent the 5th and 95th percentiles, respectively) (left axis). Stacked fields represent the dose variation explained by individual parameters (% of total variation, right axis).*

The main driver of variation in C-14 dose is the uncertainty in the fraction of carbon that is fixed from roots. In the analysis, the value of this parameter varies over an order of magnitude (1 to 10 %, Grolander 2013) and it explains more than 60 % of the C-14 dose variation. Uncertainties with respect to soil respiration and the groundwater uptake also have a noticeable effect on the variation in C-14 dose (~20 and 10 % explained variation, respectively). However, the effects of these parameters on the variation are less pronounced as they are less uncertain than the fraction of root uptake (they vary by a factor of three or less, Grolander 2013).

The variation in C-14 doses is relatively low. This is indicated by the width of the 90 percent confidence interval, where the ratio between the upper (95th) and lower (5th) percentiles is limited to a factor of three (dotted lines Figure 11-1). Moreover, the distribution of C-14 dose is approximately normal, as indicated by nearly equal arithmetic and geometric mean. Thus, a reduction in dose variation is not expected to have any noticeable effect on the mean value from probabilistic calculations.

Results for Mo-93

Molybdenum is an essential element for plants and has variable sorption properties in regolith (Section 9.3). Mo-93 has a half-life of 4 000 years, which is in the same order of magnitude as the residence time of stable molybdenum in the mire ecosystem (~2 000 years). In the simulations, it takes approximately one half-life to approach steady-state activity in the full regolith profile. Thus, a substantial part of the released Mo-93 activity decays on its passage through the regolith profile (~40 %). Although sorption in the lower regolith is relatively weak, it explains most of the dose variation in an early stage[51]. However, at the time interval corresponding to the highest average dose (> 2 µSv, ~5000–11 000 AD), the sorption in multiple regolith layers and the plant uptake, in particular, drives the variation in the Mo-93 dose (Figure 11-2, Table 11-1).

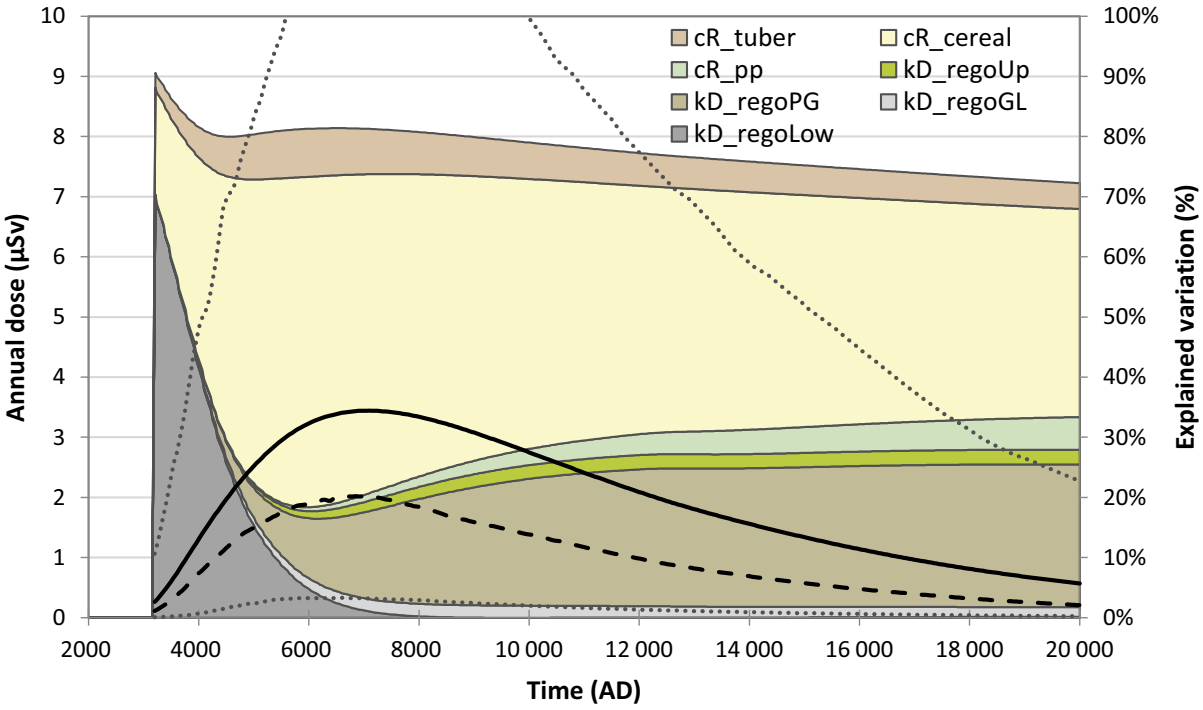

Figure 11-2. *Radionuclide-specific dose variation as a function of time for Mo-93. The mean (solid line) and median (dashed line) dose are shown together with the empirical 90 percent confidence interval (dotted lines, represent the 5th and 95th percentiles, respectively) (left axis). Stacked fields represent the dose variation explained by individual parameters (% of total variation, right axis).*

[51] High K_d-values leads to a lower dose in the early stage primarily due to retention delaying the transport to upper regolith layers that are exposed by cultivation. With K_d-values in the upper range of the probability distribution, the activity in geosphere release will also be notably reduced (to ~50 %) by radioactive decay before leaving the till.

The primary source of Mo-93 in agricultural ecosystems is accumulation in mire organic rich regolith layers (primarily post-glacial clay gyttja) with some contribution from the glacial clay (Section 9.3). Thus, the Mo-93 dose increases with the K_d of all contributing regolith layers (positive β for K_d of regoPG, regoPeat, regoUp$_{ter}$, and regoGL, Table 11-1). Moreover, an increased uptake in mire vegetation leads to increased accumulation of Mo-93 in organic matter of peat layers (positive β for $CR_{ter,PP}$). The variation explained by $CR_{ter,PP}$ increases with time, indicating that the importance of organic storage increases as inorganic Mo-93 is leached out of from the regolith. However, the response to parameters contributing to accumulation is comparatively weak. This is partly because multiple layers contribute to the accumulation and the influence of each individual layer is typically modest. Moreover, for post-glacial clay gyttja, which on average contributes with approximately half of the activity in agricultural soils, the positive effect of increased accumulation is offset by a negative effect due to radioactive decay. That is, increased sorption in RegoPG, increases the decay in this layer, which in turn reduces the transport of Mo-93 to the above peat layers and subsequent uptake and storage in an organic form.

Mo-93 is readily taken up by plants, and increased plant uptake results in an increased dose (seen as positive β for $CR_{agri,cereal}$ and $CR_{agri,tuber}$, Table 11-1). As cereal is the dominant food source, the dose response to an increase in plant uptake is near proportional. The contribution from ingestion of tubers to the dose is typically a quarter of that from cereal, and consequently the dose response is correspondingly weaker.

The main driver of variation in Mo-93 dose is the uncertainty in the plant to soil concentration ratio for cereal. In the analysis the value of $CR_{agri,cereal}$ varies over two orders of magnitude (with a geometric standard deviation, GSD, of 3) and this variation explains approximately half of the variation in the maximum Mo-93 dose (Table 11-1). Uncertainties with respect to sorption in post-glacial clay gyttja and plant uptake by tubers also have a noticeable effect on the variation in Mo-93 dose (~15 and 10 % of the variation explained, respectively, Table 11-1). It can be noted that the variation explained by these parameters is large in relation to the modest β coefficients (ranging ~0.2–0.3), which is due to a high variability in the controlling parameters (the GSDs for the two parameters are 5 and 7, respectively, Grolander 2013).

The variation in Mo-93 doses is modest, with the width of the 90 percent confidence interval spanning a 30-fold difference (dotted lines in Figure 11-2). Moreover, the distribution of Mo-93 dose is approximately log-normally distributed, and the arithmetic mean is approximately a factor of two greater than the geometric mean. The dose variation could potentially be lowered by reducing the uncertainty in the concentration ratio for cereal. However, the effect of a reduction in parameter variation on the mean value of the Mo-93 dose is expected to be limited (as indicated by the difference between the median and the mean dose).

Results for Ca-41

Calcium is an essential element for plants, and sorbs relatively strongly in inorganic regolith layers (Section 9.3). Ca-41 has a long half-life (102 000 years). The residence time of stable calcium in the mire ecosystem is an order of magnitude shorter than the half-life of Ca-41. Thus, most of the radionuclides discharged from the bedrock will reach the surface with a marginal loss due to radioactive decay (typically less than 10 %). It takes more than 10 000 years to approach steady-state activity concentrations in all regolith layers. Thus, sorption in the lower regolith explains most of the dose variation during the first 10 000 years[52]. However, at the time corresponding to the highest average dose (> 0.3 μSv, from ~17 000 to 63 000 AD) additional factors such as sorption in the glacial clay layer, plant uptake and biological transfer rates drive the variation in the Ca-41 dose (Figure 11-3, Table 11-1).

[52] High K_d-values leads to a lower dose due to retention delaying the transport to glacial clay, which is exposed by cultivation.

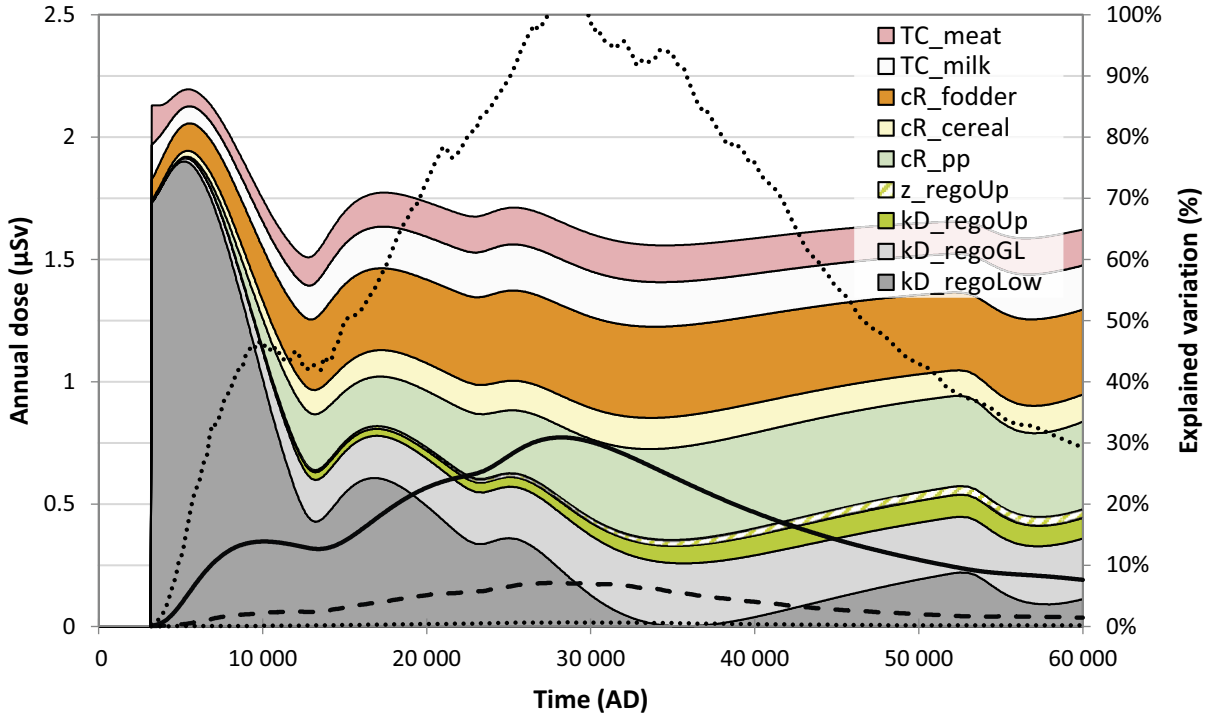

Figure 11-3. *Radionuclide-specific dose variation as a function of time for Ca-41. The mean (solid line) and median (dashed line) dose are shown together with the empirical 90 percent confidence interval (dotted lines, represent the 5th and 95th percentiles, respectively) (left axis). Stacked fields represent the dose variation explained by individual parameters (% of total variation, right axis).*

The primary source of Ca-41 in the agricultural ecosystem is accumulation in glacial clay and in peat (Section 9.3). Thus, the Ca-41 dose increases strongly with the K_d of glacial clay in the mire ecosystem (positive β for Kd_{regoGL} Table 11-1). Activity taken up by mire plants accumulates in organic matter, and surface and deep peat contribute significantly to the activity in agricultural soil. Thus, an increase in mire plant uptake and organic storage leads to increased activity in drained soil, and higher Ca-41 doses (positive β for $CR_{ter,PP}$, $Kd_{regoUp,ter}$ and $z_{regoUp,ter}$). The main exposure pathway for Ca-41 involves cultivation of fodder plants for meat and dairy production (Section 9.3). Thus, the Ca-41 dose increases with increased uptake by fodder plants ($CR_{agri,fodder}$), with increased ingestion rate ($ingRate_{C,cattle}$) and with increased transfer from fodder to meat and milk (TC_{meat}, TC_{milk})[53] (positive β for the three parameters in Table 11-1). The sorption in the till ($Kd_{regoLow}$) also has a negative effect on the Ca-41 dose at the time of the maximum dose (Table 11-1, at about 30 000 AD). This is primarily because the sorption in the lower regolith causes temporal dilution of the peak transport rates to upper layers at the time of the maximum dose.

No single parameter dominates the variation of the maximum Ca-41 dose, instead several parameters have a moderate influence, and 30 % of the dose variation is unexplained by first-order multiplicative effects. The results reflect the diversity in factors affecting accumulation of and exposure to Ca-41, and the fact that pathways contribute partly in parallel (i.e. in a non-multiplicative manner). Nevertheless, a multiplicative model explains almost 70 % of the dose variation. Reflecting transport and accumulation in inorganic regolith layers; the uncertainty in the K_d for till and glacial clay explains 10 % and 9 % of dose variation, respectively. With respect to accumulation in peat, the *CR* for mire vegetation, and the K_d and the thickness of the upper peat together explain 15 % of variation. With respect to exposure

[53] Transfer coefficients are used to quantifying radionuclide transfer to both milk (d L^{-1}) and meat (d $kgfw^{-1}$) as the equilibrium ratio of the radionuclide activity concentration in milk/meat (Bq kg^{-1} or Bq L^{-1}) to the daily dietary radionuclide intake of livestock (Bq d^{-1}).

from cultivation, the *CR* for fodder explains 15 % of variation and ingestion rate and the transfer coefficients for meat and milk together explain 15 % of variation. Most of these parameters are associated with uncertainties spanning two orders of magnitude (GSD between 3 and 4, Grolander 2013)[54].

The variation in Ca-41 doses is large, with a width of the 90 percent confidence interval covering more than two orders of magnitude (dotted lines in Figure 11-3). Moreover, the Ca-41 dose is approximately log-normally distributed, and the arithmetic mean is about a factor four greater than the geometric mean. The mean dose could potentially be lowered by reducing the uncertainty in the dose variation, but this would require that uncertainties in a number of parameter values are reduced. To address single parameters with a high variability (e.g. TCs) is expected to have a limited effect on the dose variation.

Results for Ni-59

Nickle sorbs relatively strongly in inorganic regolith layers. Ni-59 has a half-life (101 000 years) that is somewhat longer than the residence time of stable nickel in the mire ecosystem. Most of the radionuclides released to the biosphere system are retained in the lower regolith layers and approximately 20 % of activity in the geosphere release decays before it reaches the surface. Moreover, the activity in the biosphere keeps accumulating throughout the assessment period (Section 9.3).

As sorption in the till delays transport to upper layers, and therefore increases the loss due to radioactive decay, variation in K_d for this layer (RegoLow) explains most of the dose variation during the first half of the assessment period. However, the dose maximum occurs in the second half of the simulation (after the last geosphere peak release ~ 50 000 AD). At this stage steady-state conditions are approached in all regolith layers and sorption in the glacial clay layer, plant uptake and biological transfer also have clear effects on the variation of the Ni-59 dose (Figure 11-4, Table 11-1).

The primary source of Ni-59 in the agricultural ecosystem is accumulation in glacial clay (Section 9.3), and thus the Ni-59 dose increases clearly with the K_d value of glacial clay (positive β for Kd_{regoGL} Table 11-1). The main exposure pathway for Ni-59 is ingestion of meat (Section 9.3), which is related to cultivation of fodder plants used for meat production. Thus, the Ni-59 dose increases with uptake of fodder plants ($CR_{agri,fodder}$), and by increased biological uptake and transfer from fodder to meat (TC_{meat},) (positive β for the two parameters in Table 11-1).

Moreover, ingestion of other crops also contributes to the Ni-59 dose, and the dose increases with increased uptake of Ni-59 by tubers and cereal (positive β for $CR_{agri,tuber}$ and $CR_{agri,cereal}$, Table 11-1). As mentioned above, the negative effect of sorption in the till is also noticeable at the time of the maximum dose (negative β for $Kd_{regoLow}$, Table 11-1).

No single parameter dominates the variation of Ni-59 dose. Instead, the two sorption coefficients that affect transport and accumulation explain ~ 40 %, the two parameters associated with the fodder-meat pathway explain 30 %, and the two parameters associated with uptake in crops explain 6 % of variation. Most of these parameters have values that vary over two orders of magnitude (GSD between 3 and 4). The value of the concentration ratio for tuber varies even more (GSD ~ 7), inflating the explained variation as compared to its relatively weak effect on dose response.

Variation in Ni-59 doses is relatively modest, with the width of the 90 percent confidence interval almost spanning a 50-fold difference at the time for maximum dose (dotted lines in Figure 11-4). However, the distribution of Ni-59 is relatively balanced, with the arithmetic mean being just a factor of two greater than the geometric mean. To lower the variation of the Ni-59 dose will require a reduction of the uncertainty of multiple parameters, and even so, the joint effect on the average dose is expected to be limited (as indicated by the difference between the mean and the median doses).

[54] The transfer coefficient for meat (*TC*meat) is an exception. This parameter is based on data from IAEA (2010), and accordingly is assigned a very high variation (GSD = 30, n = 3). Thus, the weak dose response of this parameter (β ~ 0.1) is clearly inflated by a high degree of uncertainty.

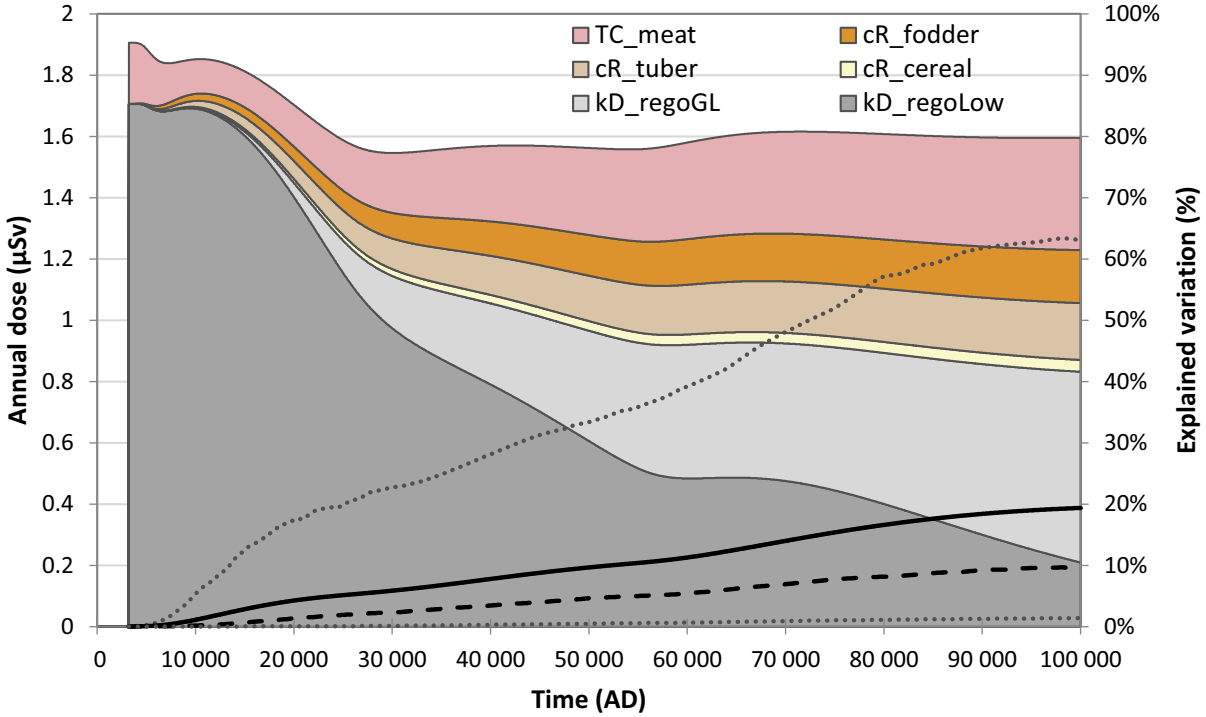

Figure 11-4. *Radionuclide-specific dose variation as a function of time for Ni-59. The mean (solid line) and median (dashed line) dose are shown together with the empirical 90 percent confidence interval (dotted lines, represent the 5th and 95th percentiles, respectively) (left axis). Stacked fields represent the dose variation explained by individual parameters (% of total variation, right axis).*

11.3 Alternative delineation calculation case

In this supporting calculation case, the sensitivity of total and radionuclide-specific doses to variation in the outline of the biosphere object 157_2 is examined. Several characteristics of the biosphere objects have significant influence on the transport and accumulation of radionuclides, and some of these are directly related to the size of the object and its catchment (SKB TR-19-05, Section 13.4). Thus, to illustrate how the size, position and properties of the biosphere object may affect environmental concentrations and resulting doses and dose rates to NHB, four alternative delineations of biosphere object 157_2 were considered in SR-PSU (SKB TR-14-06, Section 6.4).

The original outline of object 157_2 was identified based on hydrogeological particle tracking from the repository to the bedrock-regolith interface, in combination with the characteristics of the terrain given by the digital elevation map (Chapter 5). Though the outline of this gentle hill-slope area appears to be reasonable and robust from several perspectives (Sections 5.1 and 5.2), there are inevitable uncertainties with respect to both the description of the future landscape (as described by the regolith-lake development model and the surface hydrological model) as well as to properties of the area with the highest concentration of radionuclides. Thus, each of the previously outlined areas provided the basis for a separate simulation. To allow for an unbiased evaluation, the original object 157_2 is treated in the same way as the alternative delineations (referred to as the *reference* in the results section). This makes the total number of variant calculations five in the *alternative delineation* calculation case.

11.3.1 Description of the calculation cases

Outlined areas

To illustrate how the size, position and properties of the biosphere object may affect environmental concentrations and resulting doses, biosphere object 157_2 is delineated in four ways in addition to the outline used in the *base case* (Section 5.1.2). Object 157_2 was originally delineated by enveloping most of the discharge points that were modelled during the terrestrial period, following the general

outline of the local basin. Special attention was paid to ensure that the drainage outlet of the object matched that of the larger basin (Section 5.1.2). These strict criteria were not imposed on the alternative delineations, which are made to illustrate different assessment perspectives:

a) *Areas with upward hydraulic gradients (UpwGrad)*. For this delineation, the areas with a steady upward flow of groundwater from the deep bedrock to the surface are collectively defined as the object area. The area was identified based on flow modelling results from MIKE SHE and calculated using hydraulic head differences between adjacent calculation layers. That is, head differences were calculated for the two layers in the regolith, in the bedrock located just below the regolith, and in the bedrock at a depth of approximately 60 m. Areas defined as discharge areas at all three levels (i.e. at the surface, between the two regolith calculation layer and at the regolith bedrock boundary) were selected as an alternative delineation of biosphere object 157_2 (Figure 11-5, panel a). It can be noted that the outlined area shows striking similarities with the discharge pattern at the bedrock-surface interface in the terrestrial period (lower panels in Figure 5-4).

b) *Wetland areas (Wetl)*. For this delineation, the area of the object that has wetland properties is considered. Moreover, it was assumed that these areas are connected through the flow of surface water and groundwater, at least for parts of the year when they are flooded. In Sweden, wetlands are defined as areas which for most of the year are below or just above the local groundwater level, and where hydrophilic (i.e. moisture-loving) species make up at least 50 % of the vegetation (Löfroth 1991). Considering the yearly groundwater fluctuations in the object (Figures A1-15, 21 in Werner et al. 2013), the areas where the yearly average of the groundwater level was no more than 25 cm below ground level were selected as an alternative delineation of biosphere object 157_2 (Figure 11-5, panel b).

c) *Uphill area with a high density of discharged particles (Uphill)*. In this delineation a relatively small area uphill from the stream outlet in the original object is considered (Figure 11-5, panel c). The delineation broadly corresponds to an area of the bedrock-surface interface with a high density of discharged particles during the terrestrial period (lower panels in Figure 5-4). The area is approximately one third of the original object and the watershed is about half of that in the original object, and consequently the effects of ground- and surface-water dilution should be considerably lower than postulated in the original object. Thus, this delineation can be seen to quantify the upper end of environmental concentrations in parts of the object which are likely to receive most of the geosphere release.

d) *Most suitable arable land (Agri)*. In this delineation, the area most suitable for cultivation is considered (Figure 11-5, panel d). The layers of glacial clay, post-glacial gyttja and peat will be thickest and thus most suitable for agriculture, in the northern parts of the object, close to the outflow. Following the description of the landscape in Chapter 4, the most suitable arable land is outlined as the area where the combined thickness of glacial clay, post-glacial clay-gyttja and peat is at least 0.5 m after drainage (see yellow areas in Figure 4-6). The outlined area is only a fifth of the original object (Figure 11-5, panel d), and results from this area exemplify hypothetical consequences from a release to a small area with relatively thick post-glacial deposits. Observe that there is a mismatch between the cultivated area in this case and of the locations of most radionuclide release points. Thus, postulating that the full geosphere release is discharged into this area is clearly pessimistic.

Each of the alternative representation of object 157_2 reflects a stylised approach to outlining the area of interest. However, the alternative outlined areas should not be seen as equally likely representations of areas affected by groundwater from the repository. On the one hand, it is plausible to assume that the geosphere release will affect most of the area with a steady upward flow from the bedrock to the surface (a, *UpwGrad*) and the open wetland areas (b, *Wetl*) (Figure 5-4). The uphill area (c, *Uphill*) is also likely to receive a substantial fraction of the geosphere release, but to postulate that all radionuclides are released to this area is considered a pessimistic assumption.

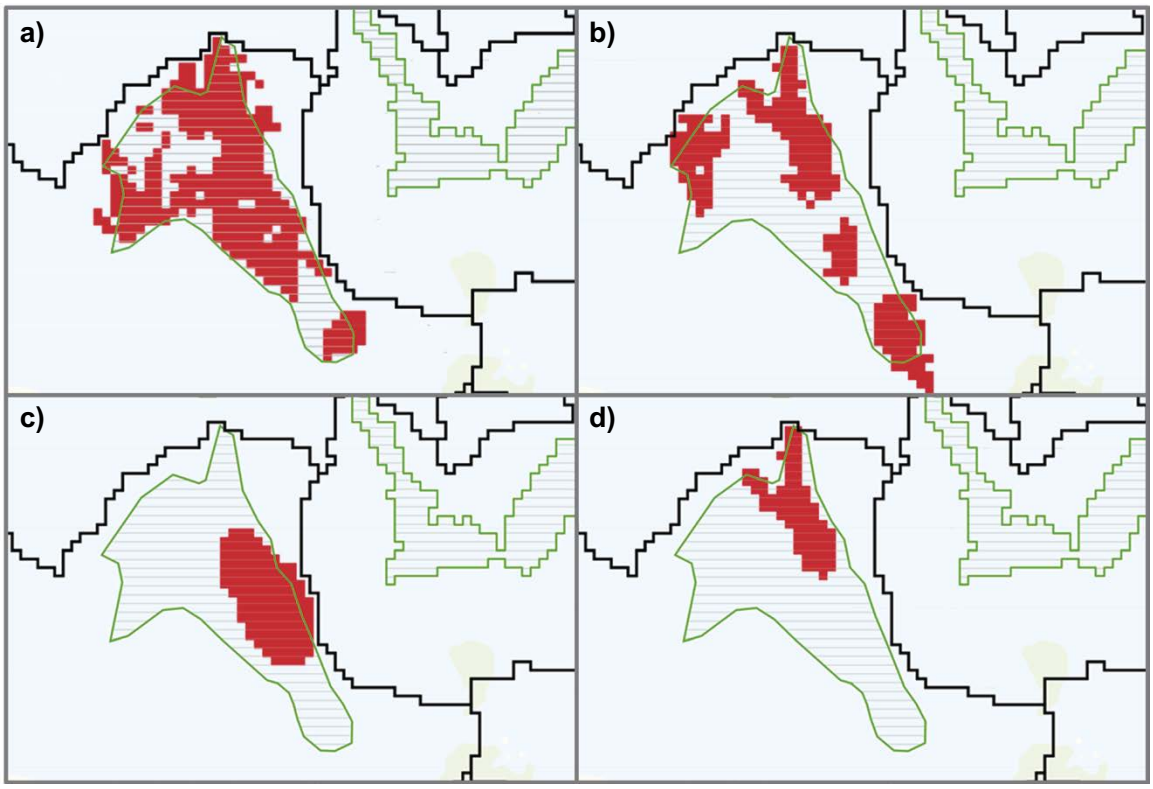

Figure 11-5. *Alternative delineations of biosphere object 157_2. The green line indicates the original object and the red areas the alternative outlines of the biosphere object. a) Areas with a continuous upward hydraulic gradients from bedrock to surface (UpwGrad). b) Wetland areas with an average water table at the surface or not deeper than 0.25 m below the surface (Wetl). c) Uphill area with a high density of discharged particles at the bedrock-regolith interface (Uphill). d) Most suitable area for cultivation, after drainage of mire (Agri). Reproduced from Figure 6-14 in SKB (TR-14-06).*

The most downhill area (d, *Agri*), is the smallest area. Although radionuclides that reach the surface water can be expected to pass through the upper layers of this object, only a smaller fraction of the total geosphere release is expected to be discharged into this area from the bedrock. Moreover, the area is only sufficient to support one family with food, and thus the exposed group utilizing this area is small. To make results between exposed populations comparable, the resulting dose from the *Agri* area could arguably be normalized by dividing by a factor of ten (see Section 7.5.4). This has not been done. Thus, although the results from this variant illustrates the potential effects of slow transport in a small discharge area with a thick layer of glacial clay, it is unreasonable to evaluate the repository safety by a direct comparison of doses calculated for this variant with the dose corresponding to the regulatory risk criterion (14 μSv).

General conditions, parameters and exposed groups

The *base case* conditions are used in this supporting calculation case, except for the location of the geosphere release, the landscape description and the surface hydrology (see below). That is, present-day temperate conditions persist during the entire simulation period and terrestrial ecosystem parameters vary as in the *base case*. As land-use associated with draining the mire results in the highest total dose in the *base case*, only doses to drained-mire (DM) farmers are evaluated. The results from these simulations are also used to assess dose rates to non-human biota (Chapter 12).

Geosphere release

The full *base case* geosphere release from the probabilistic simulations is discharged to each of the alternatively outlined areas and to the original object.

Landscape description

The general properties of the terrestrial landscape from the *base case* are used in this calculation case. However, for simplicity, the landscape description is simplified in this case and object 157_2 is represented by a mire in its mature stage (Section 11.1). Average regolith thicknesses are extracted from the 3D version of the landscape at 5000 AD that was implemented in the MIKE SHE model (Werner et al. 2013). This snapshot is considered to reflect a mire in a mature fen-stage.

The four alternative delineations are smaller than the original object of ~ 150 000 m^2, and they span in sizes from 30 000 m^2 to 130 000 m^2 (Figure 11-6, left panel). As expected, there are systematic differences in the average thickness of regolith layers that are related to the position in the landscape. The thickest regolith layers are found in the area closest to the stream outlet (i.e. the *Agri* variant). In relative terms, the largest variation in thicknesses between the alternative delineations is found in glacial clay (RegoGL) and peat (RegoPeat), thicknesses of which vary by factors of 10 and 3, respectively (Figure 11-6, left panel).

Surface hydrology

In these calculation cases, the simplified water-balance model developed in SE-SFL was used to extract independent parameters that describe the input of water from the bedrock, from the local catchment and from the atmosphere, respectively (Section 11.1, Section 7.5.5, Figure 7-3). This was done separately for each outlined area, the original object 157_2 included. Each input term is expressed as the product of an area-specific input and the area of the object or the local catchment. The distribution of the groundwater discharge from the local catchment (i.e. the runoff) is partitioned into a surface and a sub-surface flow, and the below-ground flow decreases with depth. Percolation is constrained by the net atmospheric input, and the penetration of the percolating water decreases with depth. The parameters describing discharge from the local catchment and percolation are listed in Table 11-2 and described in detail in Chapter 5 in Grolander and Jaeschke (2019).

Radionuclides are expected to enter the biosphere object from the geosphere. Thus, upward water flows are important for dilution in sub-surface layers and for the fate of radionuclides affected by radioactive decay (e.g. Section 4 in Saetre and Ekström 2017a, and Section 13.4.2 in SKB TR-19-05). Upward flows ($m^3\ a^{-1}$) are calculated from the water mass balance for each layer by the hydrological subroutine. The regolith layers of object 157_2 (including its alternative delineations) are relatively thin (typically < 0.5 m) compared with the resolution of the uppermost calculation layer of the hydrological model (2.5 m). This means that there are uncertainties with respect to the vertical flow across layers within the first 2.5 m of the soil profile. Since an alternative method of interpolation is used in the new hydrological subroutine[55], individual flows may be either higher or lower than the flows used in the corresponding sensitivity calculations in SR-PSU.

Nevertheless, area-specific and volumetric flows are similar to those used in SR-PSU. That is, the area specific flows typically vary by a factor of three between the outlined areas, whereas volumetric flows vary by an order of magnitude (Figure 11-6, right panel). The volumetric horizontal flow of water from surface peat to the stream is similar in all outlined objects, except for the uphill area, where the flow is approximately halved, due to a smaller local catchment.

[55] In SR-PSU the flows within this layer were calculated by splitting the layer into two layers, 0.5 m and 2.0 m thick, respectively. The subsurface drainage was allocated to the uppermost layer. Vertical flows at planes between boundaries were calculated by linear interpolation (Section 7.2 and 7.6 in Werner et al. 2013). In the hydrological subroutine of the BioTEx model, discharge from the local catchment and percolation are both assumed to decrease exponentially with depth, and upward flows are calculated by water balance (Chapter 5 in Grolander and Jaeschke 2019).

Ecosystem parameters

All ecosystem parameters for the mire and stream ecosystems are identical to the *base case*. The marine ecosystem is excluded from the model.

Table 11-2. Parameters used in the hydrological sub-model to describe the flow of ground- and surface-water in the five outlined areas. The parameters are derived from the flow components of MIKE SHE water balances (Figures A1-52 to A1-56 in Werner et al. 2013). The resulting upward groundwater flows are displayed in Figure 11-6.

	Catchment discharge			Object boundaries		Percolation			
	runoff	$f_{disch,surf}$	$delta_{discharge}$	NetPrec	$q_{Bedrock}$	$f_{surfperc,LC}$	$f_{surfperc,obj}$	$b_{percol,ter}$	$delta_{percol}$
Bio obj	(m a^{-1})	(-)	(m^{-1})	(m a^{-1})	(m a^{-1})	(-)	(-)	(-)	(m^{-1})
Ref	0.16	0.88	0.76	0.17	0.14	0.32	1	8.3	0.26
Disch	0.16	0.89	0.67	0.18	0.18	0.18	1	10	0.53
Wetl	0.17	0.62	2.30	0.16	0.12	0.31	1	1.1	0.76
Exit	0.17	0.67	0.99	0.17	0.19	0.30	1	7.3	0.17
Agri	0.18	0.97	0.70	0.14	0.07	0.01	1	5.1	1.00

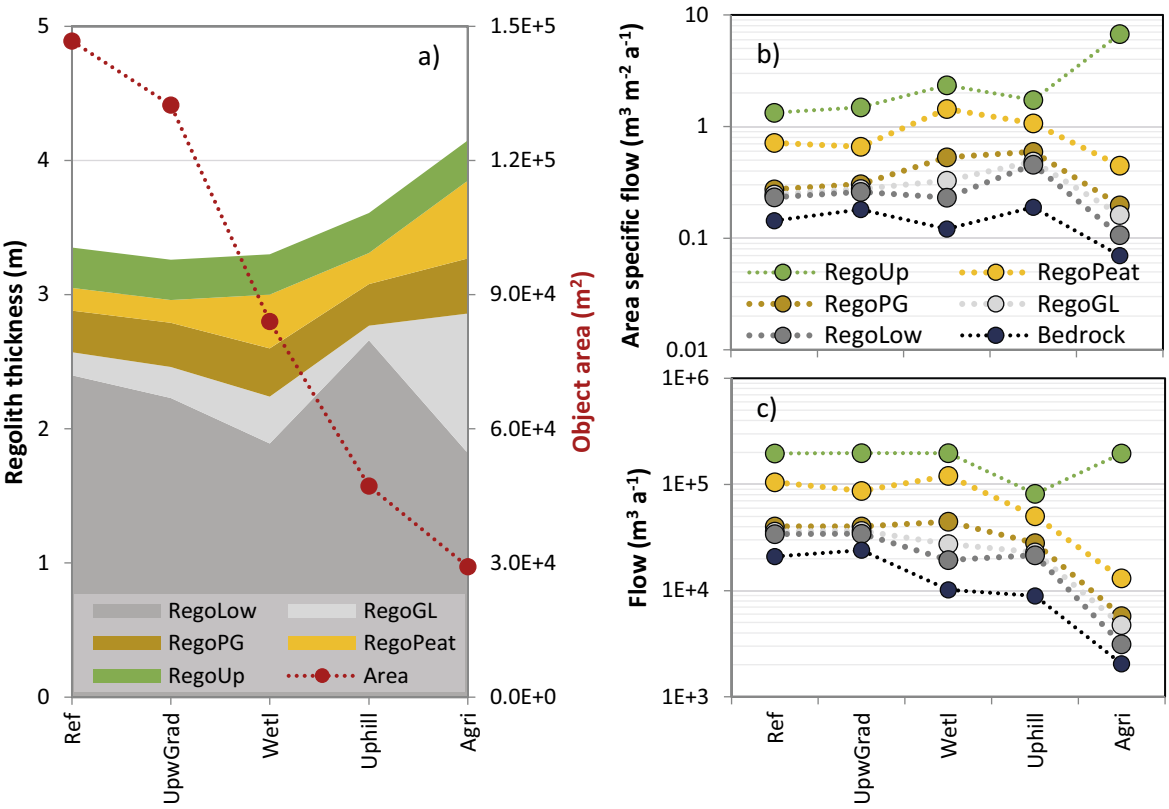

Figure 11-6. *Properties of biosphere object 157_2 (Ref) and alternative delineations (UpwGrad, Wetl, Uphill and Agri). The panels show regolith thickness and object areas (a), upward area specific groundwater flows (b) and volumetric flows (c). Green symbols (RegoUp) represent horizontal flow of surface water, from surface peat to the stream. Object delineations are ordered from largest (UpwGrad, left) to smallest (Agri, right) area.*

11.3.2 Results

The results in this sensitivity analysis are based on a simplified representation of biosphere object 157_2, which excludes the marine ecosystem succeeding the fen stage. Moreover, parameters describing groundwater flows are derived using a different methodology from that in the *base case*. This results in a reduced maximum dose in the *reference* by 10 % as compared with the *base case*. The response for most dose contributing radionuclides is similar and the difference rarely exceeds 20 % (Figure 11-7). Moreover, the time to reach the maximum dose is somewhat shortened for many radionuclides as compared with the *base case* (e.g. Ca-41 and Ni-59). These differences, that are primarily caused by changes in the hydrological descriptions, are limited. Thus, the simplified representation of the biosphere object, in combination with the alternative description of the surface hydrology, is considered to be adequate. Nevertheless, for an unbiased evaluation, the doses in the four alternative sub-areas are evaluated by comparisons with dose in the *reference*, and not with the *base case*.

Geosphere release to each of the alternatively outlined areas results in a higher maximum dose than in the *reference* area (Figure 11-7 and Figure 11-8). Total doses are generally higher than in the *reference* throughout the simulation, and results from higher radionuclide-specific doses of C-14 (in the initial period), Mo-93 (during the dose maximum), Ca-41 (in the period following the dose maximum) and Ni-59, Cs-135, and decay products from U-235 (at the end of the simulation period). The properties of the smallest sub-areas also affect the timing of the dose peaks. In the *Uphill* sub-area, which has a relatively thin layer of glacial clay, peaks of sorbing radionuclides tend to occur earlier than in the *reference* (red line in lower panel of Figure 11-7). The opposite is true for the *Agri* sub-area, where transport is slow due to a thick layer of glacial clay (blue line in lower panel of Figure 11-7). At the end of the simulation, the dose from Ni-59 is noticeable in all alternative sub-areas. However, in the *Uphill* sub-area the accumulation of Cs-135 contributes more to dose than that of Ni-59. In the *Agri* sub-area where the transport of Ni-59 (and Cs-135) is slow, decay products from U-235 (i.e. Pa-231 and Ac-227) are instead the main contributing radionuclides with respect to the total dose in the second half of the simulation (data not shown).

The Upward, Wetland and Uphill sub-areas

In spite of the variation in object specific properties, the increase in total radionuclide-specific doses is typically limited to a factor of two in the sub-areas (Figure 11-7 and Figure 11-8). The sub-area with an *Upward hydraulic gradient* largely overlaps with that of the original object (reference), and the properties of the reference area and the delineated sub-area are similar. Thus, it is not surprising that the total and radionuclide-specific doses are similar in the two areas. Nevertheless, the results indicate that the original outline of the biosphere object gives a good representation also of the parts where conditions for vertical transport from repository depth are favourable and where radionuclides from the geosphere are likely to be discharged.

The *Wetland* sub-area is about half of the size of the reference area, and the groundwater flow from the bedrock is reduced to a similar degree. This results in till pore water concentrations that are approximately twice as large as in the *reference*. However, the contribution of subsurface runoff increases towards the surface, and flow in upper soil profile is like that in the *reference*. Moreover, layers of glacial clay and deep peat are notably thicker than in the reference area. Taken together, this results in an enhanced area-specific accumulation in the glacial clay, and to a lesser extent also in peat. The effects on radionuclide-specific doses depend on processes related to the dominant exposure pathway (e.g. plant uptake from till for C-14), and the relative importance of accumulation in different regolith layers (e.g. high contribution from glacial clay for Ca-41 and Ni-59) (see Section 9.3). Thus, release to the wetland results in doses for C-14, Ca-41 and Ni-59 that are at least a factor two larger than in the reference area, whereas the differences for Mo-93 and total dose are somewhat smaller.

The *Uphill* sub-area has a size that is approximately a third of the *reference* area and a catchment that is approximately half of that for the other sub-areas. However, the location of this area is associated with an elevated discharge from the bedrock, and therefore the reduction of the upward groundwater flow (m^3 $year^{-1}$), as compared to the *reference* area, is modest. The relatively thin layer of glacial clay clearly limits the accumulation of sorbing radionuclides, but this effect is partly counterbalanced by the fast transport that decrease the loss of Mo-93 and Ni-59 activity through radioactive decay. Finally, the size

of the object is not considered to be sufficient to support the needs of the most exposed group[56]. Thus, the *Uphill* sub-area can provide three quarters of the food required by the group, (and the remaining quarter is considered to be provided from outside the object unaffected by the geosphere release). Taken together, this results in doses that are similar to those of the *Wetland* sub-area (i.e. a factor two larger than in the *reference* area). However, it can be noted that the radionuclide specific dose from Ni-59 is similar to that in the *reference* area.

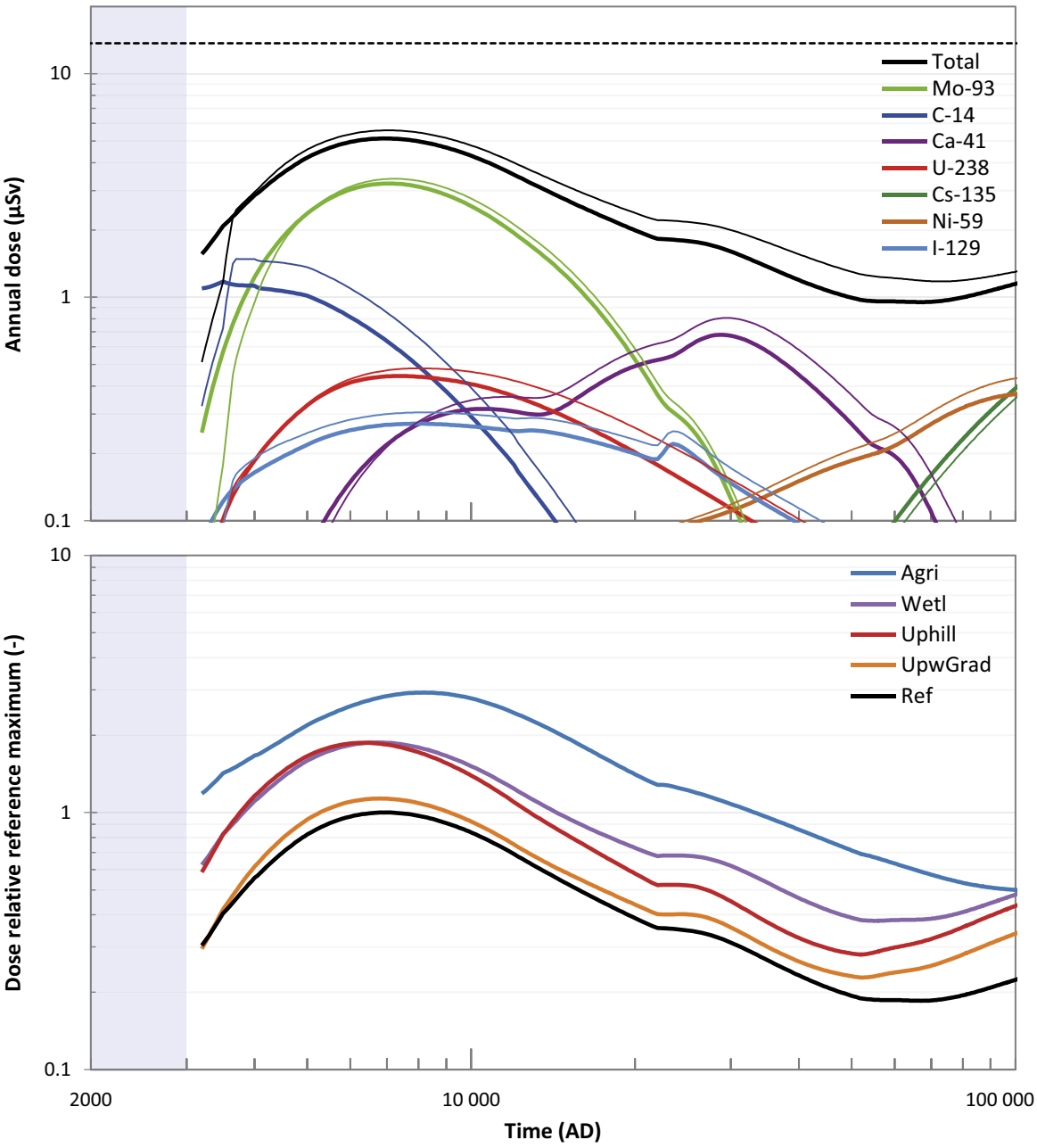

Figure 11-7. *Dose from object 157_2 and alternatively outlined areas calculated with a version of the BioTEx model in which the biosphere object is represented by a constant mire and surface hydrology from a simplified hydrological model (see text for details). Upper panel: total and radionuclide-specific doses for object 157_2 (reference) as compared with the corresponding doses in the base case (thin lines). Lower panel: total doses in the four alternatively outlined areas relative to the maximum dose in the original outline (reference, black). Dashed black lines show the annual dose corresponding to the regulatory risk criterion (14 µSv).*

[56] According to the description of potentially exposed groups, six hectares are considered to be needed for the production of cereal, fodder and tubers required to sustainably support two families of self-sufficient farmers (Section 6.2).

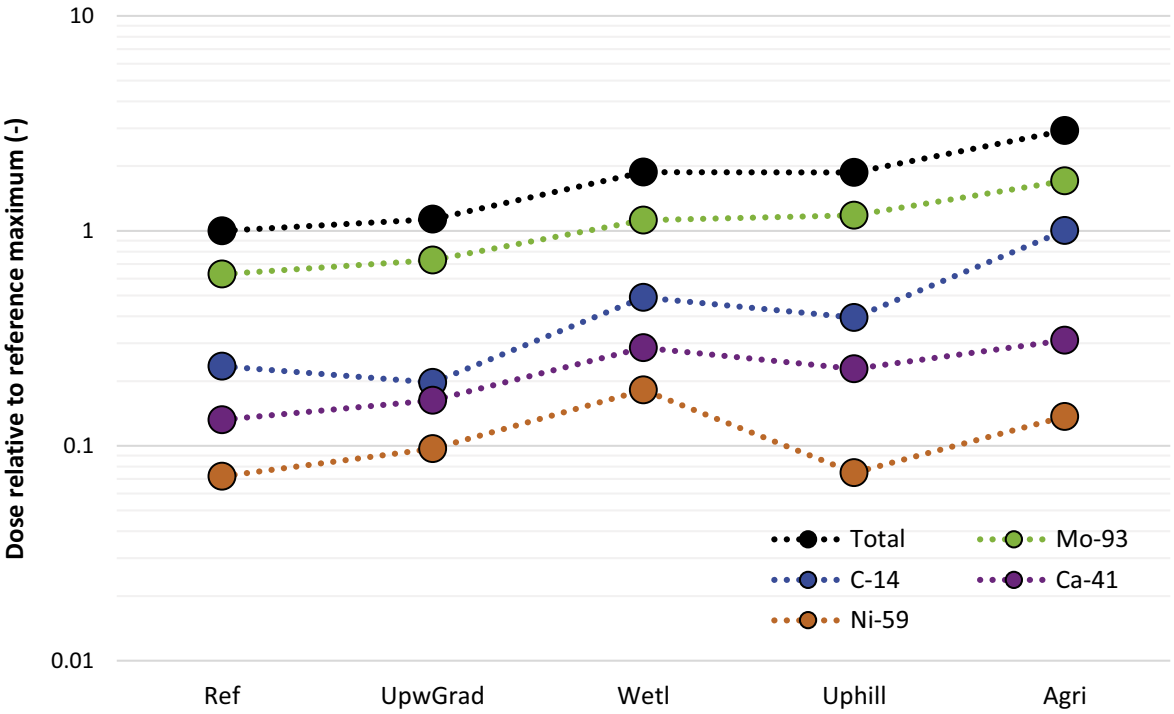

Figure 11-8. *Total and radionuclide-specific maximum doses for biosphere object 157_2 (reference) and the four alternatively outlined areas. The maximum doses are expressed relative the total dose in the original object (reference). The lines have been added as a visual guide.*

The Agri sub-area

In the *Agri* sub-area, the smallest of the alternative object areas, the maximum dose is a factor of three above that in the *reference* area. The *Agri* sub-area is located in the lowermost part of object 157_2 and it has been outlined based on its suitability for cultivation. There are no indications that radionuclides from the geosphere release would be selectively released in this area. Nevertheless, it overlaps with the area of continuous upward hydrological gradient and thus it is expected to receive part of the geosphere release (Figure 11-5). As the *Agri* sub-area is substantially smaller than the original outlined object, and the area-specific ground waterflows also are notably lower, the upward groundwater flow is almost an order of magnitude lower than in the *reference* (Figure 11-6). However, the relatively slow transport in this sub-area results in a noticeable reduction of activity due to radioactive decay along the transport pathway. Thus, for Mo-93 the difference in porewater concentration between this sub-area and the *reference* area declines along the transport pathway, and at the surface the concentration is a factor two lower than in the *reference* (left panel in Figure 11-9), despite a similar degree of dilution in the uppermost layer to that in the reference area.

It is interesting to note that although the size of the *Agri* sub-area is only a fifth of the original object, the accumulated activity of the radionuclides examined exceeds that in the original object (data for Mo-93 are shown in right panel in Figure 11-9). This is primarily due to accumulation in the thicker layer of glacial clay. However, as exposure is determined by the uppermost regolith layers (i.e. 0.5 m after soil subsidence) not all of the activity of glacial clay is exposed by cultivation. Instead, the activity exposed in cultivated soil is similar to that in the *reference* area. This makes the area-specific activity, and the concentration in the agricultural soil, five times larger in the *Agri* sub-area. As with the other small objects, the size of the *Agri* sub-area is not sufficient to support the needs of the most exposed group. Thus, the sub-area can only provide half of the food required by the group cultivating the area. Taken together this results in a dose from Mo-93 that is almost three times as large as in the *reference*. The dose from C-14 (primarily reflecting the porewater concentration in till) increases somewhat more, whereas the increase in doses of Ca-41 and Ni-59, (primarily reflecting accumulation in glacial clay) is restricted to a factor of two. The relatively weak response is due to retention that increases the loss by radioactive decay and delays the transport to layers above the till.

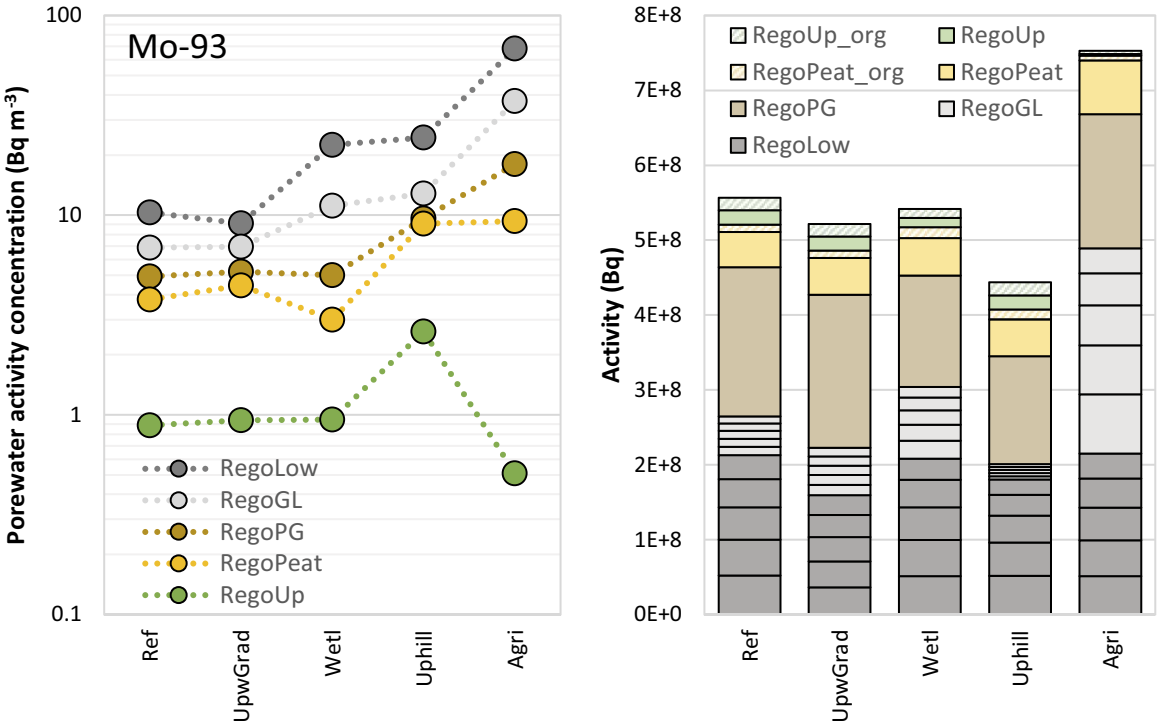

Figure 11-9. *Porewater activity concentrations (Bq m^{-3}, left) and accumulated activity (Bq, right) of Mo-93 in biosphere object 157_2 (reference) and the four alternatively outlined areas. Values are presented for five regolith layers, and they represent the time points of the maximum radionuclide-specific dose for each area. Lines have been added as a visual guide only.*

11.4 Mire object properties calculation case

In this supporting calculation case, the sensitivity of activity concentrations and doses to variations in object properties is examined. These properties include object geometries, regolith thicknesses, and parameters that drive or modify groundwater flows and those parameters that were not varied in the probabilistic simulations of the *base case*. Together with the *alternative delineation supporting calculation case* above, this case illustrates potential effects of uncertainties in the description of the landscape, and the associated surface hydrology.

By varying object properties independently, this case can disentangle effects of individual properties that are intertwined in the landscape (e.g. regolith thickness and vertical distribution of groundwater flow) or happened to be confounded in the *alternative delineation case* (e.g. the smallest object has the thickest layer of glacial clay). The case is similar to the sensitivity analysis previously carried out in SE-SFL (SKB TR-19-05, Section 13.4), but this analysis is focused on the effects of variations *within* the gentle hillslope where object 157_2 is located (rather than on variation between discharge areas located in different basins). Also, the analysis is carried out with a time-dependent geosphere release, and it uses annual dose as its primary endpoint.

11.4.1 Description of the calculation cases

General conditions, parameters and exposed groups

The *base case* assumptions are used in this supporting calculation case, except for the geosphere release and the landscape description (see below). That is, present-day temperate conditions persist during the entire simulation period. To simplify interpretation of results with respect to object properties, all terrestrial ecosystem parameters are fixed at typical values (i.e. best estimates from the probability distributions used in the *base case*). As land-use associated with draining the mire results in the highest total dose in the *base case*, the sensitivity analysis only evaluates doses to the corresponding potentially exposed group (DM).

Geosphere release

The *base case* geosphere release is used, and all radionuclides from the repository are discharged to the biosphere object. To facilitate interpretation of results, the average geosphere release is used for all simulations (Section 11.2.1).

Landscape description

The landscape description is simplified in this calculation case and the discharge area is represented by a mire in its mature stage (Section 11.1). In each simulation, fixed parameter values for the area of the object, the area of the local catchment (i.e. the watershed less the area of the object) and the thickness of each regolith layer are used. The parameters are constrained to reflect a reasonable range for an area within the basin of object 157_2. In practice, this is achieved by randomly drawing parameter values from uniform distributions, where the upper and lower limits of the distributions are taken from the alternative delineations of object 157_2 (including the original object) in the *alternative delineation calculation case*. Thus, the size of the object and the size of the local catchment vary by approximately a factor three, whereas the thicknesses of peat and glacial clay vary by factors of ten and three, respectively (Table 11-3, Figure 11-6).

Surface hydrology

The simplified water balance model developed in SE-SFL (Section 11.1, Section 7.5.5, Figure 7-3) is used in this calculation case. The surface hydrology is described in terms of independent parameters describing the input of groundwater from the bedrock and the local catchment, and input from the net precipitation falling on the object. As with the landscape parameters, the hydrological parameters are fixed over time in each simulation, but randomly varied between simulations. Upper and lower values for parameters are constrained by the range in the alternative delineations of object 157_2 (Table 11-2).

The runoff from the catchment and that from the object are considered to be strongly correlated. In the simulations this dependence is handled by first drawing a random value for the net precipitation in each simulation, and then calculating the runoff from the catchment as a product of this precipitation (*NetPrec*) and a scaling factor ($sf_{specDisch,catch}$). The scaling factor simply represents the ratio of the specific runoff in the catchment and in the object, and, in the text, it is referred to as the relative net precipitation. In the *alternative delineation calculation case*, the fraction of the runoff from the catchment that is discharged directly into the stream ($f_{disch,stream}$) and the fraction of net precipitation that infiltrates from the surface ($f_{surfperc,obj}$) were fixed at values of zero and one, respectively. To allow an evaluation of also these parameters, a hypothetical value of 0.5 is used as an upper and lower limit of these two fractions (Table 11-3).

The prescribed variation in hydrological parameters is typically within a factor of two, but the bedrock discharge varies by almost a factor of three between alternative delineations. Parameters describing the percolation profile (b_{percol} and $delta_{percol}$) show an even larger variation. This is because the underlying MIKE SHE water balances have a relatively coarse vertical resolution compared with the stratification in the upper part of the regolith profile, leading to relatively large uncertainties in the estimated parameters.

Selection of radionuclides, endpoints and analysis

As in the *base case*, 1 000 Monte Carlo simulations were performed, each with a unique set of parameters that were kept constant throughout the simulation, and the output was used in a sensitivity analysis. The analysis is limited to the total annual dose and results for the four radionuclides, i.e. C-14, Mo-93, Ca-41 and Ni-59 (Section 9.3). These four radionuclides contribute significantly to the annual dose at different times and cover a wide range of radionuclide- and element-specific properties (Table 9-2).

The primary endpoints of the analysis are the total and radionuclide-specific doses, typically at the time for the maximum dose. In addition, results for pore water activity concentrations are presented to illustrate how the mechanisms of dilution, retention and radioactive decay affect transport and accumulation throughout the regolith profile. As with the *ecosystem properties calculation case*, the results are analysed with a multiple regression analysis approach on a logarithmic scale (Section 11.2).

Table 11-3. Parameters describing object properties that are varied in the sensitivity analysis. All parameter values between the listed min and max values are considered equally likely in the analysis (i.e. they are assigned a uniform distribution).

Parameter	Unit	Range Min	Range Max	Description
Boundary flux				
NetPrec	m a^{-1}	0.14	0.18	Area-specific precipitation less evapotranspiration.
$q_{bedrock}$	m a^{-1}	0.07	0.19	Area-specific discharge from bedrock.
Surface extension				
$area_{obj}$	10^4 m^2	5	17	Size of biosphere object.
$area_{catch}$	10^4 m^2	40	110	Size of catchment excluding the biosphere object.
Regolith thickness				
$z_{regoPeat}$	m	0.2	0.6	Thickness of deep peat at equilibrium.
z_{regoPG}	m	0.3	0.4	Thickness of post glacial sediments.
z_{regoGL}	m	0.1	1.0	Thickness of glacial clay.
$z_{regoLow}$	m	1.8	2.7	Thickness of till.
Catchment discharge				
$sf_{specDisch,catch}$	-	0.8	1.1	Scale factor which is multiplied with NetPrec to calculate area-specific discharge from the catchment. Referred to as relative net precipitation in text.
$f_{disch,stream}$	-	0	0.5	The fraction of the runoff from the catchment that is discharged directly into the stream. Upper limit hypothetical.
$f_{disch,surf}$	-	0.5	1	The fraction of the discharge from the local catchment that reaches the object as surface (or overland) water.
$delta_{disch}$	m^{-1}	0.7	1.4	The rate of decrease with depth for groundwater discharge from the local catchment.
Percolation				
$f_{surfperc,LC}$	-	0.01	0.3	Part of surface runoff that contribute to percolation.
$f_{surfperc,obj}$	-	0.5	1	Fraction of net precipitation that infiltrates from the surface. Lower limit hypothetical.
$b_{percol,ter}$	m^{-1}	1	10	The rate of decrease of percolation at reference depth with thickness of the glacial clay layer.
$delta_{percol}$	m^{-1}	0.2	1	The rate of decrease of percolation with depth below the reference level.

11.4.2 Results

In general, the dose at each time point can be well described as being determined by a multiplicative combination of the input parameters. The regression (on a logarithmic scale) typically explained more than 80 % of the variation in dose (coloured area in lower panel of Figure 11-10). This means that the regression, or beta (β), coefficients give a good indication of how sensitive the dose is to changes in parameter values, and the interpretation of these coefficients is the focus of the analysis below.

The results from the Monte Carlo simulations can also be used to show how uncertainty in parameters describing object properties affects dose estimates. In this calculation case. the specified variation in the parameter values is limited to *within object heterogeneity* with respect to forecast properties, and uncertainties with respect to ecosystem properties are not considered. Thus, the 90th percentile confidence interval in the mean dose in these simulations is much narrower than in the *base case*. In this case, the interval typically spans a factor of three, as compared with a factor of twenty in the *base case* (lower panel of Figure 11-10 and Figure 9-25). Most of this variation is driven by the uncertainty assigned to the area of the biosphere object (green area in lower panel of Figure 11-10).

As ecosystem parameters are fixed, the shape of the dose curve is like that of the deterministic simulations in the *base case* (Figure 9-25). However, due to systematic shifts in parameter values as compared with the properties of the original outline of object 157_2 (e.g. object area and thicknesses of several regolith layers), the maximum dose is approximately a factor of two higher than in the deterministic *base case*. Since all the parameters are assigned uniform distributions (Table 11-3), the distribution of the calculated dose is less skewed than when ecosystem parameters are varied. This is because most

of the ecosystem parameters that influence dose variation were assigned log-normal distributions (e.g. all K_d, *CR* and *TF* parameters). Thus, in this calculation case, the upper and lower confidence intervals (p95 and p05) for the total dose are at similar distances from the mean value, which in turn is marginally higher than the median (Figure 11-10, lower panel). Moreover, the postulated variation in object properties yields a considerably lower variation of the maximum dose than in the *ecosystem parameter calculation case*; the confidence interval spans less than a factor of three in this case as compared with an order of magnitude when ecosystem parameters are varied (Figure 13-5).

A decreased area of the object is always associated with an increase in the dose during the simulations; β typically varies between −0.5 and −0.8, with a value of −0.7 at the dose maximum (Figure 11-10). This translates into an increase in dose of between 30 % and 40 % when the area of the object is halved. The thickness of the peat layer and net precipitation also affect the maximum dose, and a doubling of the parameter value results in 20 % higher (peat thickness) or lower (net precipitation) maximum dose. There are several additional properties that have a limited effect at the time of maximum dose, namely; the area-specific discharge from the bedrock, the area of the catchment, and the relative net precipitation in the catchment. A doubling of the value of any of these parameters results in a reduction of the maximum dose by ~15 % (or less) at the time for the maximum dose.[57] The responses of the maximum total dose can be explained by the sensitivities of the dose-dominating radionuclides, i.e. Mo-93 and C-14. Furthermore, the sensitivity of the total dose to individual parameters clearly changes over time (upper panel in Figure 11-10). The primary reason for this is the shifts in the relative importance of radionuclides contributing to the dose. The responses in doses and pore water concentrations of the four radionuclides that dominate the annual dose during different periods are described below, and the mechanisms behind the responses are briefly explained.

Results for C-14

In the initial period of the simulation, C-14 contributes most to dose. The primary transport pathway is groundwater uptake, and in an object with thin soil layers the source of the uptake is the porewater in till (Section 9.3). The concentration of C-14 in the porewater decreases in proportion to the upward groundwater flow through this layer due to increased dilution. Thus, in this period, the dose decreases relatively strongly with the area of the object and the area-specific discharge from the bedrock (β near 1 for the two parameters in Table 11-3). That is, a doubling of either of these two factors corresponds to an almost halved dose from C-14. The effects of these two factors on the concentration of porewater are displayed in Figure 11-11, and it is mainly the response concentration in the till (RegoLow) that is impacting on the dose from C-14.

Results for Mo-93

Mo-93 is the main contributing radionuclide at the time of the maximum total dose (Figure 11-10, right panel). Thus, in addition to the area of the object and the discharge from the bedrock, which also influence C-14 doses, the properties influencing the total maximum dose primarily reflect the Mo-93 specific dose response. For Mo-93, accumulation in clay gyttja (RegoPG) and deep peat (RegoPeat) is a key process affecting the dose due to ingestion of cultivated crops, which is the primary exposure pathway (Section 9.3). Thus, thicker layers of clay-gyttja and peat increase the inventory of Mo-93 that is exposed when the mire is cultivated. A doubling of the thickness of these layers increases the dose by between 20 % and 30 % (β of 0.3 and 0.4, Table 11-3). In addition, the dose from Mo-93 decreases with groundwater dilution in these layers. This dilution increases with object area and net precipitation. However, the dose response for object area is weaker than for C-14 (β is −0.6, Table 11-3). This is because runoff from the catchment also contributes substantially to groundwater flows in clay gyttja and peat. The flow from the catchment is the product of the area of the catchment and net precipitation in the catchment. The net precipitation in the catchment, in turn, is expressed as the product of the net precipitation in the object (*NetPrec*) and the relative net precipitation in the catchment ($sf_{specDisch,catch}$). Thus, a doubling of any of these factors leads to a reduction of ~20 % to 30 % in Mo-93 dose (β's for the three parameters range from −0.5 to −0.3, Table 11-3). As the net precipitation affects both the percolation in the object and the runoff from the catchment, it has a stronger effect than the other two parameters (because these influence only the catchment runoff).

[57] The size of the disturbance takes the parameter value out of bounds for area-specific net precipitation and relative net precipitation. The listed response is primarily for comparison with other parameters.

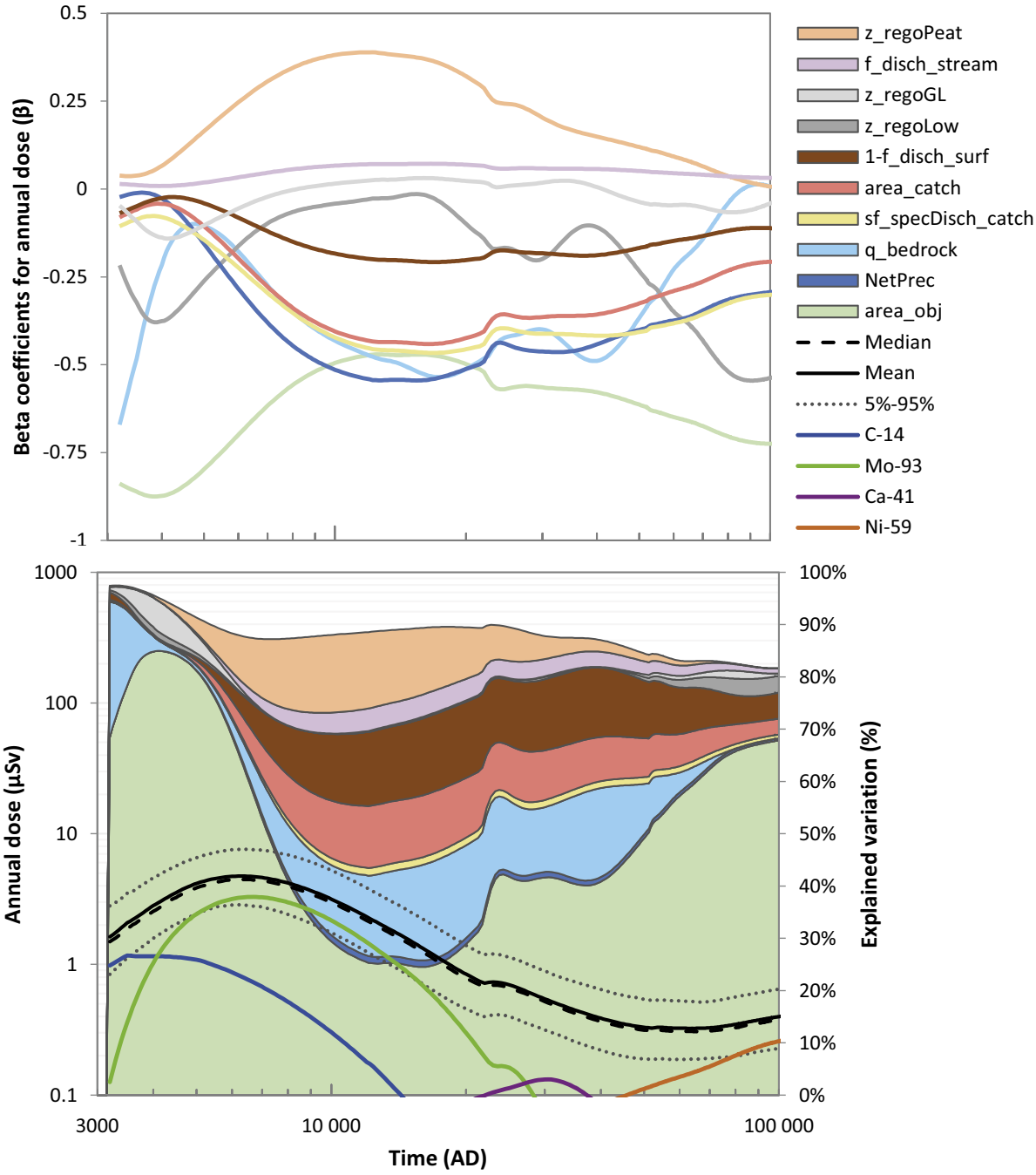

Figure 11-10. *Sensitivity of the total dose to a change in parameter values of object properties. Upper panel: beta coefficients (β) as a function of time in the simulation. The coefficient represents the change in dose per unit change in parameter value on a logarithmic scale. For a small disturbance the coefficient corresponds to the percent change in response for a unit percent disturbance. Lower panel: variation in total dose as a function of time. Stacked fields represent the dose variation explained by individual parameters (right axis). Note that the colour of β and that of the variation match. The mean and median total doses (black solid line and black dashed line, respectively) are shown together with the empirical 90 percent confidence interval (dotted lines, representing the 5th and 95th percentiles, respectively) (left axis). The mean radionuclide-specific doses from four radionuclides are shown for reference (coloured solid lines). Parameters explaining less than 1 % of the variation throughout the simulation period have been excluded from the figure for clarity.*

Mo-93 is also notably affected by radioactive decay (Section 9.3). In this analysis, this is evident from the effect of the bedrock discharge on porewater concentration along the regolith profile (Figure 11-11). In the lower layers, dilution is the predominant mechanism affecting porewater concentration (and β for $q_{bedrock}$ is negative). However, an increased discharge shortens the transport time, which reduces the effects of radioactive decay along the transport pathway. Thus, in the upper regolith layers the effects of bedrock discharge is positive. Altogether, there is no net effect from the bedrock discharge on the Mo-93 dose (Table 11-3). The thickness of regolith layers also increases transport time and the effects of radioactive decay. For Mo-93 this effect partly counteracts the positive effect of regolith thickness on accumulation, especially in the clay-gyttja layer.

Results for Ca-41

In the *base case*, Ca-41 contributes substantially to the dose for a long period of time after the dose maximum (Section 9.3). The dose contribution is less pronounced when ecosystem parameters are kept at fixed values, as in this analysis (see also discussion Section 9.4), but the response is still of interest. For Ca-41, sorption in glacial clay (RegoGL) is the primary process for accumulation and subsequent exposure (Section 9.3). Thus, an increase in the thickness of glacial clay increases the inventory of Ca-41 that is exposed when the mire is cultivated. However, this effect is reduced if only the upper parts of the glacial clay are exposed by cultivation, for example when the glacial clay layer is considerably thicker than the cultivated soil (see also *alternative delineation calculation case* above). Thus, the response to an increased thickness of this layer is relatively modest (β is 0.3 Table 11-3); a doubling of the glacial clay layer increases the dose by approximately 20 %. The dose from Ca-41 also decreases with groundwater dilution in this layer. This dilution is driven by both bedrock discharge and runoff from the catchment area, and the effects are reflected in negative βs for the parameters associated with these flows as discussed above (Table 11-3). In addition, an increase of the thickness of the till layer reduces the activity concentration in all layers above the till, including the glacial clay (Figure 11-11). This effect reflects that increased retention in till smooths temporal peaks in the geosphere release and increases the loss of activity through radioactive decay.

Results for Ni-59

In the last period of the simulations, Ni-59 gives a substantial contribution to the dose (Figure 11-10 right panel). As with Ca-41, accumulation in glacial clay (RegoGL) is a key process affecting doses due to ingestion of cultivated crops and animal products, which are the primary exposure pathways for this radionuclide (Section 9.3). As this radionuclide is released relatively late, retention in the till layer will delay and decrease the accumulation in glacial clay within the assessment period. That is, if the till layer is thick and/or if the area-specific discharge from the bedrock is low, maximum concentrations in glacial clay will not be reached within the time frame of the assessment. Thus, a doubling of the thickness of the till layer leads to a 25 % reduction of the dose from Ni-59. As with Ca-41, an increased thickness of glacial clay increases the inventory of activity that is exposed when the mire is cultivated. However, a thicker glacial clay layer also delays the dose maximum and increases the loss through radioactive decay, and therefore the net effect on Ni-59 dose is marginal (β is close to 0). This effect is clearly seen in the activity concentration in all layers above the glacial clay, which are reduced by a thicker layer of glacial clay (Figure 11-11). Moreover, although an increased area-specific discharge leads to a larger dilution of Ni-59 in glacial clay, overall a change in this parameter has no effect on dose. This response is because an increased discharge also reduces the transport time, which allows for a faster transport through the till layer, so that the maximum dose is reached within the assessment period and less activity is lost through radioactive decay.

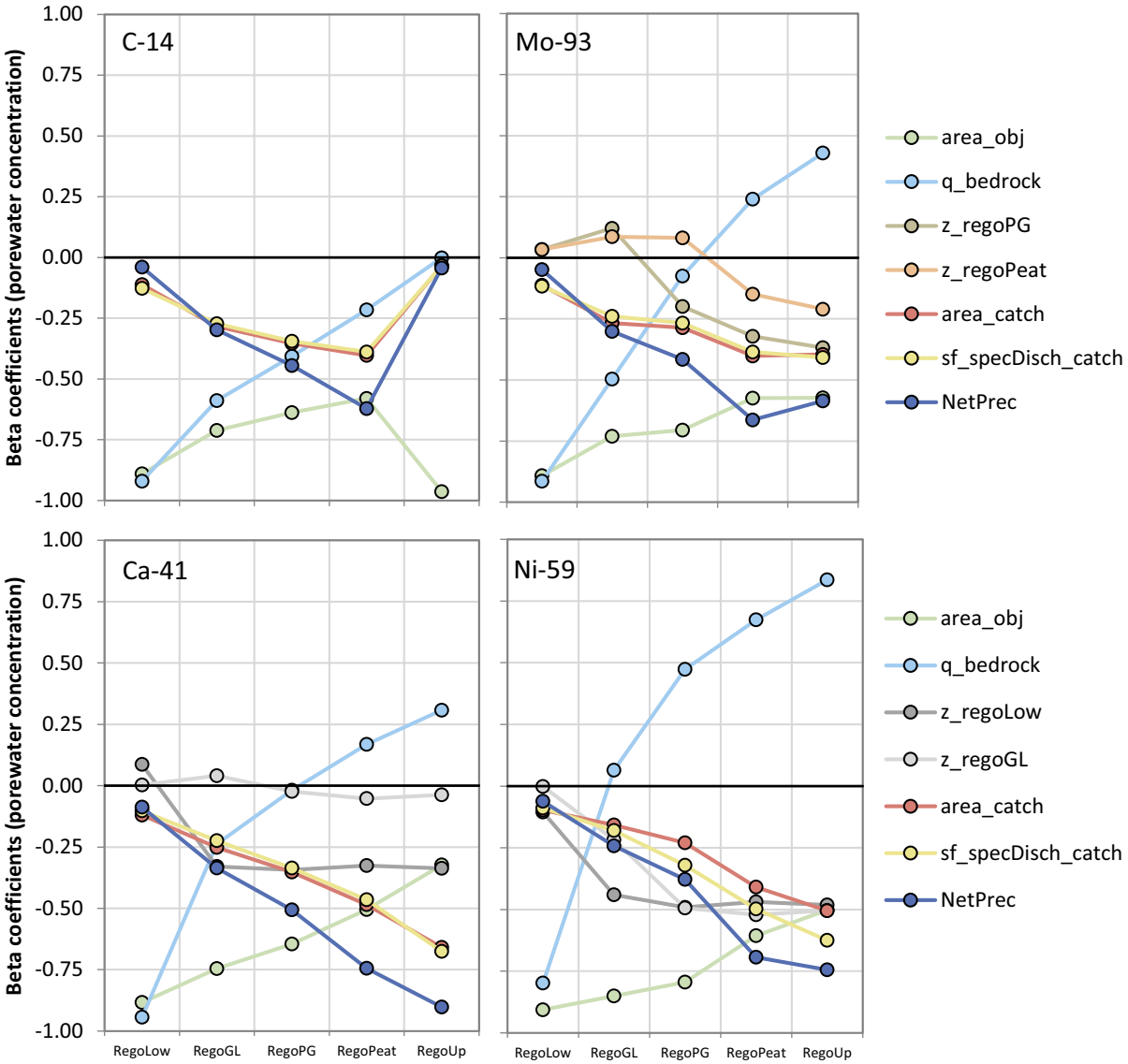

Figure 11-11. *Sensitivity of response in pore water concentrations of C-14, Mo-93, Ca-41 and Ni-59 along a regolith profile to changes in parameter values. The beta coefficient (β) expresses the sensitivity of the dose to a disturbance in parameter value. Parameters with small β coefficients have been excluded from the figure for clarity unless they are discussed in the text. The effect of dilution alone can be seen in the four lowermost layers for C-14. However, in RegoUp degassing is the process controlling C-14 concentrations. For all other radionuclides, the vertical patterns are the result of the combined effects of dilution, radioactive decay and retardation (see text for details).*

Effects of additional hydrological parameters

Parameters describing the vertical distribution of the runoff from the catchment affect doses and pore-water concentrations as expected. That is, when runoff is channelled to the surface, or to the near-surface zone, then the groundwater flow (and the dilution of radionuclides) in deeper layers is reduced. However, the effect on dose is limited; a doubling of the infiltrating fraction of runoff ($1-f_{disch,surf}$) typically reduces the accumulation in glacial clay and clay-gyttja, and the corresponding doses, by only 10 % ($\beta \sim -0.1$, Table 11-4). The effect of a change in the depth distribution of runoff ($delta_{disch}$) is similarly weak. For this parameter, larger values are associated with shallow groundwater flows and less dilution in deep regolith layers (e.g. regoLow and regoGL as evident in positive β for C-14 and Ca-41). As previously noted (SKB TR-19-05, Section 13.4), variation in parameters controlling percolation ($delta_{percol}$, $f_{surfperc,LC}$, b_{percol}) has a marginal effect on environmental concentrations. The results in

this study confirm that doses are also insensitive to variations in these parameters (Table 11-4). This is not surprising as the amount of water that percolates to the deep peat and below (where radionuclide accumulation has a significant influence on dose) is small, as compared with the amounts of discharge from the bedrock and the catchment.

Table 11-4. Effects of parameter variation on radionuclide-specific dose variation at the time for the radionuclide-specific maximum dose. For each of four radionuclides, the percent variation explained by each selected parameter (%Var) is presented together with the beta coefficient (β). The total variation explained by the linear combination of selected parameters is presented at the bottom (R^2). The beta coefficient expresses the sensitivity of the dose to a disturbance in parameter value. The strength of the response is colour coded from negative (blue) to positive (yellow). The relative dose response to a doubling of a parameter value equals 2^{β}.

	C-14		Mo-93		Ca-41		Ni-59	
Parameter	%Var	β	%Var	β	%Var	β	%Var	β
$area_{obj}$	54 %	−0.8	46 %	−0.6	43 %	−0.6	62 %	−0.8
$q_{bedrock}$	39 %	−0.9	0.1 %	−0.0	3.9 %	−0.3	0.2 %	0.1
NetPrec			1.2 %	−0.5	0.6 %	−0.4	0.4 %	−0.3
$sf_{specDisch,catch}$			0.9 %	−0.3	0.6 %	−0.3	0.5 %	−0.3
$area_{catch}$	0.5 %	−0.1	7.4 %	−0.3	4.1 %	−0.3	1.7 %	−0.2
$z_{regoLow}$			0.2 %	−0.1	0.6 %	−0.3	1.4 %	−0.4
$1\text{-}f_{disch,surf}$	2.1 %	−0.1	5.7 %	−0.1	11 %	−0.2	3.6 %	−0.1
$delta_{percol}$	0.7 %	−0.1						
b_{percol}	0.9 %	−0.1						
z_{regoPG}			0.5 %	0.3			0.3 %	−0.2
$f_{disch,stream}$	0.2 %	0.0	2.7 %	0.1	1.3 %	0.0	0.5 %	0.0
z_{regoGL}			0.5 %	−0.0	18 %	0.3	0.2 %	0.0
$delt_{disch}$	1.0 %	0.2			0.6 %	0.1		
$z_{regoPeat}$	0.2 %	0.1	16 %	0.4			0.2 %	−0.0
R^2	98 %		82 %		84 %		71 %	

11.5 Calcite depletion calculation case

The geochemistry of the young landscape of the Forsmark area is characterised by the large amount of calcite deposits in the till and glacial clay. As the landscape matures, the geochemical conditions will be gradually altered: the easily weathered calcite will be depleted from the local soils, more organic matter will accumulate, and the weathering of the more resistant silicate minerals will continue. Since the solubility of calcite is limited under alkaline conditions, the weathering of calcite is driven by the addition of protons to the system:

$$CaCO_3(s) + H^+(aq) \leftrightarrow Ca^{2+}(aq) + HCO_3^-(aq)$$

Hence, calcite weathering will initially consume protons until saturation is reached. The increase in pH will depend on the buffering capacity of the system, but calcite-bearing soils are typically associated with high pH (see below). Once saturation is reached, calcite will buffer against acidifying processes in the soils, thereby maintaining pH at high levels. It will also lead to high concentrations of Ca and carbonate species, typically hydrogen carbonate, in the local soil water and groundwater. Typically, the protons are taken from carbonic acid, which is formed upon dissolution of CO_2 in the water. The resulting overall reaction will therefore be:

$$CaCO_3(s) + CO_2(aq) + H_2O \leftrightarrow Ca^{2+}(aq) + 2HCO_3^-(aq)$$

Here, calcite dissolution buffers against the increasing concentrations of carbonic acid as CO_2 is dissolved in the water. The overall effect will therefore be an increase in Ca and a doubled increase in hydrogen carbonate, since one hydrogen carbonate ion is formed from the dissolution of calcite and one from the dissolution of CO_2. Hence, there will be a substantial increase of the alkalinity as the result of calcite weathering.

In a future landscape, where calcite has been depleted, the water chemistry will be more affected by weathering of silicates, which typically are more weathering-resistant than calcite. Hence, lower concentrations of Ca and hydrogen carbonate can be expected in the future. Furthermore, calcite can no longer buffer pH at such high levels, which should lead to lower pH in a future landscape. For comparison, the O horizon in Forsmark currently has an average pH of 6.2, while the average for Swedish soils (which mostly do not contain calcite) is 4.2 (Lundin et al. 2004). These differences in pH persist throughout the soil profiles to the C horizon, where soils in Forsmark exhibit an average pH of 7.2, while the national average is 5.3. Hence, a decline in pH by as much as 2 pH units is not an unrealistic expectation for the future landscape in Forsmark.

The decreasing pH and carbonate concentrations can be expected to affect the mobility of several elements, although the quantitative effects of calcite leaching on element transport and accumulation are uncertain. In this supporting calculation case, potential effects of a change in the mobility of radionuclides due to calcite depletion are examined. This is done by systematically shifting the K_d-values in the regolith layers expected to be significantly affected by calcite depletion.

The effects of calcite on element mobility are approximated through a postulated change in pH, and the depletion is assumed to cause a gradual change in the sorption properties of affected soil layers. This will indirectly also capture the effect of changes in the carbonate concentration, since more carbonate is transformed into hydrogen carbonate and carbonic acid as pH declines, thereby altering the effects of carbonate complexation on certain elements (Figure 11-12). Two levels for pH shifts and two rates of change are combined into four variant calculations, which are carried out for nine key elements: Cs, Mo, Ni, U, and elements Th, Ra, Pb, Pa and Ac, which represent the most long-lived radionuclides from the decay chains of U-235 and U-238, respectively.

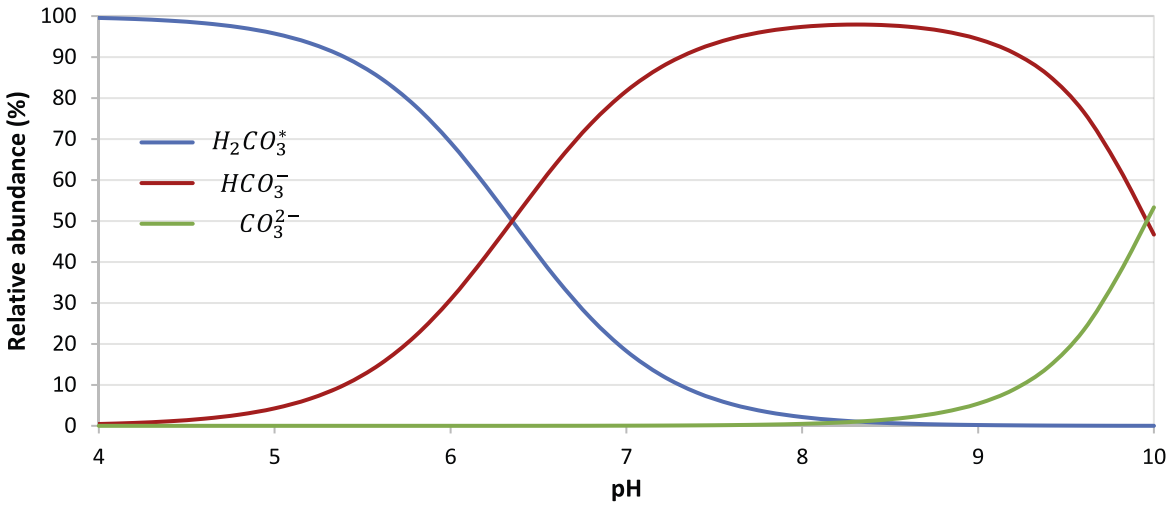

Figure 11-12. *Speciation of the carbonate system as a function of pH. $H_2CO_3^*$ includes both dissolved carbon dioxide in the water and carbonic acid and will dominate at pH < 6.3. In the Forsmark area pH is normally higher, occasionally reaching > 9 in lake water, so the dominating species is typically hydrogen carbonate, HCO_3^-. Carbonate, CO_3^{2-}, which is present mainly at higher pH, is the species controlling the solubility of calcite and is also a strong ligand for certain metal ions. One example of groundwater from calcite-bearing till in the Forsmark area is the well SFM0009, which has a total carbonate concentration of 320 mg L^{-1} and is saturated with respect to calcite, although the pH is only 7.1 and < 0.1 % of the total carbonate concentration is present as carbonate ions.*

11.5.1 Description of the calculation case

Effects of pH on element mobility

The concentration of hydrogen ions (H^+) is of particular importance for the processes that control sorption. Higher H^+ concentrations, i.e. lower pH, will increase the protonation of functional groups, resulting in more neutral or positively charged sorption sites and, consequently, fewer negatively charged sites and surfaces. Thus, the cation sorption capacity of organic matter, clay minerals and mineral oxides is expected to decrease at lower pH. Conversely, the sorption capacity of anionic radionuclides can generally be expected to increase as sorption surfaces become more positively charged at lower pH. Moreover, pH can also affect the mobility of elements through its influence on their speciation and the precipitation of, for example, calcite (Lidman 2022).

Thus, the lowering of pH can be expected to generally result in increased mobility for elements that exist as cations. For example, the sorption of the monovalent Cs^+ ion in soils is often strongly dependent on clay minerals, and it has been observed that the sorption of Cs decreases as a result of increased competition from other alkali metals and hydrogen ions (i.e. lower pH) (e.g. Fuller et al. 2014, Söderlund et al. 2016). Nickel tends to sorb to organic matter and, especially at higher pH, to (hydr)oxides of Al, Fe and Mn (e.g. Martino et al. 2003, Arai 2008, Vasyukova et al. 2010). This sorption decreases at lower pH, causing higher mobility of Ni (e.g. Barrow and Whelan 1998, Soares et al. 2011). Pb has many similarities with Ni, but it tends to sorb more strongly and can remain sorbed at lower pH than Ni. This is illustrated in Figure 11-13 by the modelled sorption of Ni and Pb onto a hypothetical ferrihydrite surface in Forsmark.

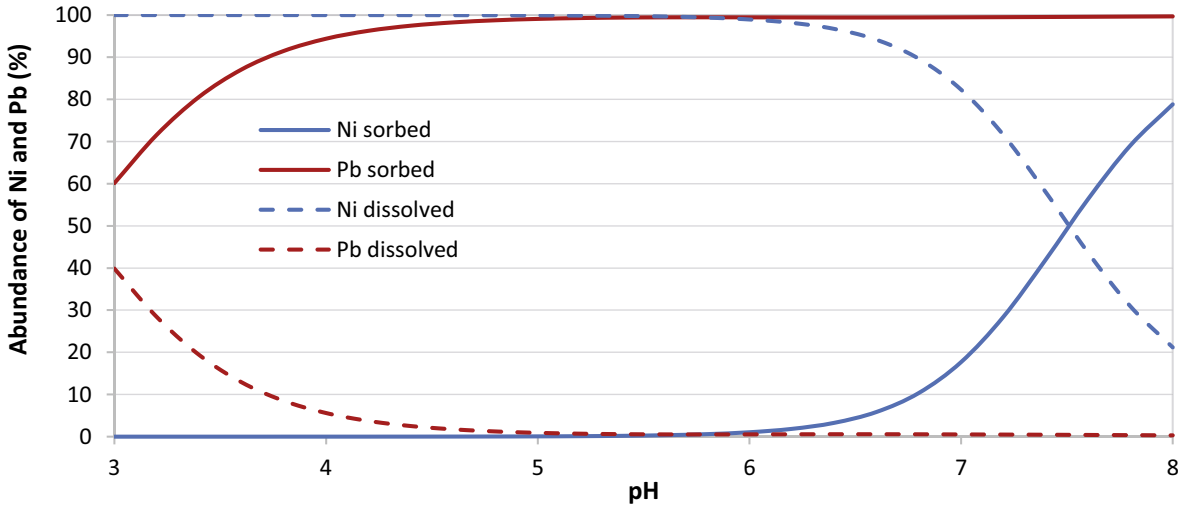

Figure 11-13. *Modelled pH dependence of the sorption of Ni and Pb onto a hypothetical ferrihydrite surface. The model is based on Visual MINTEQ (Gustafsson 2012), water chemistry from Forsmark (SFM0009) and the ferrihydrite model of Tiberg et al. (2013). In this example Ni is gradually desorbed as pH falls below 7, while the sorption of Pb remains high even at low pH.*

Radium has clear biogeochemical similarities to Ca and, above all, to Ba. The mobility of Ra in the Forsmark area is believed to be partly dependent on the presence of barite ($BaSO_4$) in the soils because Ra can co-precipitate with barite (Jaremalm et al. 2013). The solubility of barite is, however, not strongly dependent on pH so the effects of co-precipitation with barite on the mobility of Ra are likely to remain regardless of the future pH in the Forsmark area. The amount and origin of barite in the soils of the Forsmark area is currently not known so there is a possibility that there also will be a depletion of barite in the future, which then would lower the sorption of Ra. However, not all soils in the area are believed to contain barite and, even when barite is present, Ra may sorb also onto other surfaces, e.g. Fe (hydr)oxides and clay minerals. The sorption of Ra has in such cases been observed to decrease at lower pH (e.g. Sajih et al. 2014, Chen and Kocar 2018). Hence, both effects would favour an increased mobility of Ra in a future landscape. Thorium, occurring as Th^{4+}, is a strongly sorbing element with generally low solubility, although higher solubility is expected at low pH (Langmuir and Herman 1980). Low pH has also been observed to decrease the sorption of Th onto, for example, gibbsite (an Al hydroxide) (Hongxia et al. 2006). Due to the low solubility of Th its transport is expected to occur mainly in colloidal form (Dahlqvist et al. 2007). Since the density of sorption sites on, for example, dissolved organic matter is strongly dependent on pH, this could to some extent counteract the decreasing sorption onto the solid phase. However, observations from a range of soils in the United Kingdom demonstrate that higher Th concentrations can be expected in acidic soils (Ahmed et al. 2012). This is also consistent with the observed trend in the site-specific K_d measurements from Forsmark (see below).

The decay products of the U-235 chain include Ac-227 and Pa-231, which also constitute the most abundant isotopes of these two elements in the environment. Due the comparatively low abundance of U-235 in the environment and the relative difficulty to measure Ac-227 and Pa-231 in environmental samples, data on these elements are comparatively scarce. This is true also for the safety assessment, where both radionuclides are modelled using element analogues (Tröjbom et al. 2013). Actinium, occurring as trivalent Ac^{3+}, is believed to have considerable similarities to the lanthanides, in particular La, and based on that analogy carbonate complexes are not expected to play a major role for the mobility of Ac in the Forsmark area (Rönnback et al. 2008, Deblonde et al. 2021). Protactinium occurs predominately in the pentavalent state, but it is not known to form any actinyl ion similar to, for example, the uranyl ion, UO_2^{2+}, of U^{6+} (Toraishi et al. 2006, Naour et al. 2019). Hence, Pa is not expected to form the same type of mobile carbonate complexes as U, which should make it much less sensitive to changes in pH (see the discussion on U below). Due to the lack of data in both the scientific literature and the site investigation areas the K_d-values for Ac and Pa, respectively, were assumed to remain constant throughout the *calcite depletion calculation case*. Nevertheless, it is important to include Ac-227 and Pa-231 in the dose calculations, since the distribution of these radionuclides in the surface environment, and consequently the associated radiation doses, will be affected by the fate of their common parent radionuclide, U-235.

The effect of a decreasing pH on the mobility of anions is expected to be in the opposite direction to that for cations. That is, a decreased competition with hydroxide (OH^-) ions and an increased protonation of mineral surfaces (more positive charge) is expected to decrease the mobility of anions in general. Molybdenum, for example, which primarily occurs as the oxyanion molybdate (MoO_4^{2-}), is expected to become less mobile at lower pH. Molybdate sorbs, for instance, onto Al and Fe (hydr) oxides, particularly at low pH (Mikkonen and Tummavuori 1993, Xu et al. 2013). Molybdate can also sorb onto organic matter, and this appears to be especially important at pH below ca 5–6 (Wichard et al. 2009, Gustafsson and Tiberg 2015). Lower pH could also potentially increase the reduction of Mo(VI) to insoluble Mo(IV) in more reducing environments or the association of Mo with insoluble sulphides. In the groundwater of the Forsmark area higher pH is typically associated with higher Mo concentrations (Lidman 2022).

In Forsmark, the mobility of U is strongly dependent on the presence of anionic or neutral carbonate complexes (Figure 11-14, Krall et al. 2019). This means that the mobility of U will decrease drastically if pH and, consequently, the carbonate concentration drop due to calcite depletion. pH can also decrease as a result of increasing CO_2 pressure in the groundwater, but as long as the groundwater is in equilibrium with calcite the carbonate concentration will be high enough to keep U as mobile carbonate complexes (Figure 11-15). Hence, the major shift in U mobility is expected to occur as the influence of calcite disappears. The impact of carbonate on the sorption of U has been confirmed in laboratory experiments (Wazne et al. 2003, Zheng et al. 2003), and areas in boreal Europe with carbonate-rich waters also tend to have higher U concentrations, which most likely is related to the higher mobility of uranyl-carbonate complexes (Åström et al. 2009).

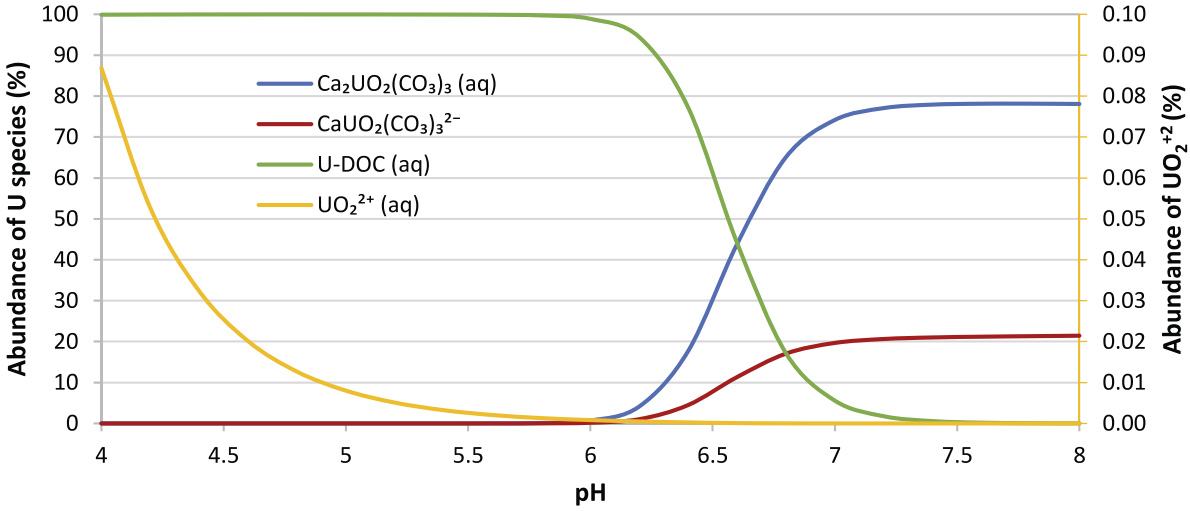

Figure 11-14. *Example of modelled speciation of U in groundwater from calcite-bearing till in Forsmark (SFM0009) using Visual MINTEQ (Gustafsson 2012). If the pH remains above 6.5–7 the U speciation is dominated by neutral or anionic carbonate complexes, but at pH < 6 these complexes disappear and the U speciation is instead dominated by complexes with dissolved organic carbon (DOC), which indicates a shift to a cationic form. The concentration of free uranyl ions (UO_2^{2+}), which probably is the most bioavailable form, remains low throughout the entire pH range in this example (< 0.1 %). Note that the abundance of free uranyl ions is displayed on the righthand axis.*

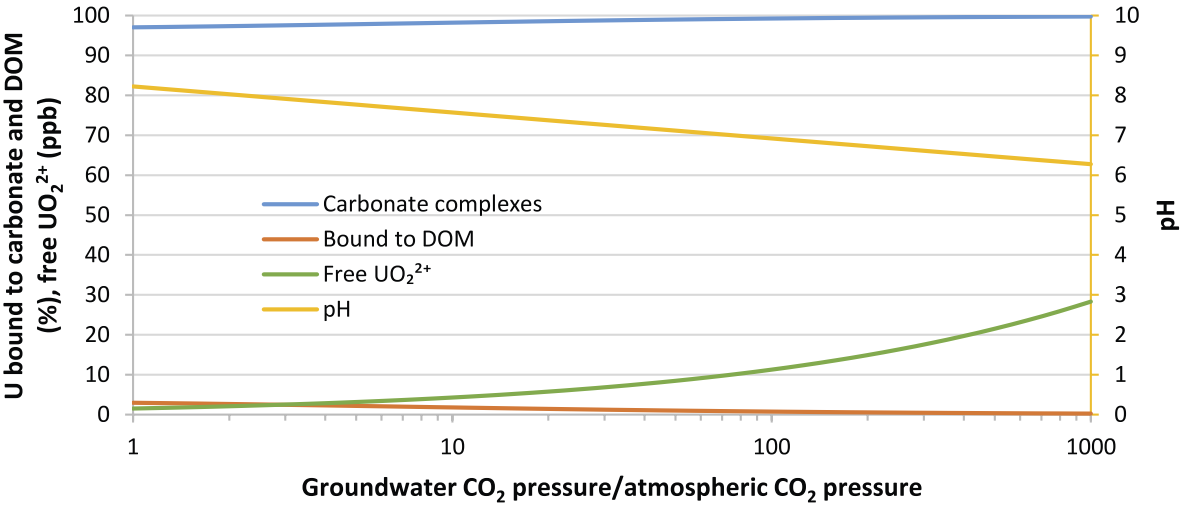

Figure 11-15. *Modelled speciation of U(VI) and pH in a groundwater at equilibrium with calcite and containing 10 mg L^{-1} DOC, where increasing CO_2 pressure (from 1–1 000 times the atmospheric CO_2 pressure) drives the calcite weathering. The decrease in pH is caused by the increasing concentrations of carbonic acid in the groundwater. There is a marginal change in the U speciation, but nearly all U remains associated with carbonates even at pH 6.3. Note that the fraction of free uranyl ions is shown on the ppb scale.*

Postulated shifts in pH for regolith layers

The groundwater in Forsmark is currently circumneutral or slightly alkaline and, in most cases, saturated with respect to calcite (Data for glacial clay and sandy till in Figure 11-16, Jaremalm et al. 2013). By contrasting the soil chemistry of Forsmark with that of inland Sweden, which lacks the influence from calcite, the effects of calcite outwash can be estimated. Such a comparison suggests that the pH of both surface and deeper regolith layers may change by as much as 2 pH units (Lundin et al. 2004, Löfgren 2011). However, the pH response is expected to be dependent on the initial state of the regolith layer, and some regolith layers are unlikely to be significantly affected by calcite depletion at all (see below).

The till and glacial clay layers are the primary calcite-containing regolith layers in Forsmark, which is indicated by pH values typically well above 7 in the area (Figure 11-16, Sheppard et al. 2011). The pH of these layers is also highly variable. If calcite is depleted, the pH is likely to drop. Weathering of other minerals than calcite, mainly silicates, will still be able to keep pH at moderate levels, but since silicates generally are more weathering-resistant than calcite, substantially lower pH can be expected. As discussed above, the pH of soils in the Forsmark area are on average ca 2 pH units higher than the national average of Swedish soils, which mostly do not contain calcite. Thus, a drop in pH by one or two pH units is considered to give a reasonable coverage of the uncertainty in the pH response.

The peat of the sampled wetlands also has relatively high pH (~5, Sheppard et al. 2011), reflecting that the wetlands are moderately rich fens influenced by minerogenic groundwater or surface water. Again, depending on the initial pH, a decreased influence of alkaline calcite-influenced groundwater could well lead to a drop of one or even two pH units as indicated by the pH typical of nutritionally poor and extremely poor fens. The decrease can be compared with the decline in pH by about 1 pH unit that has been observed over a 50-year period in a Swedish mire because of acid deposition (Sjörs and Gunnarsson 2002). In some cases, the decreasing pH was accompanied by increasing Ca concentrations in the mire water, which illustrates that the sorption of Ca – and most likely other cations in general – decreases when pH declines.

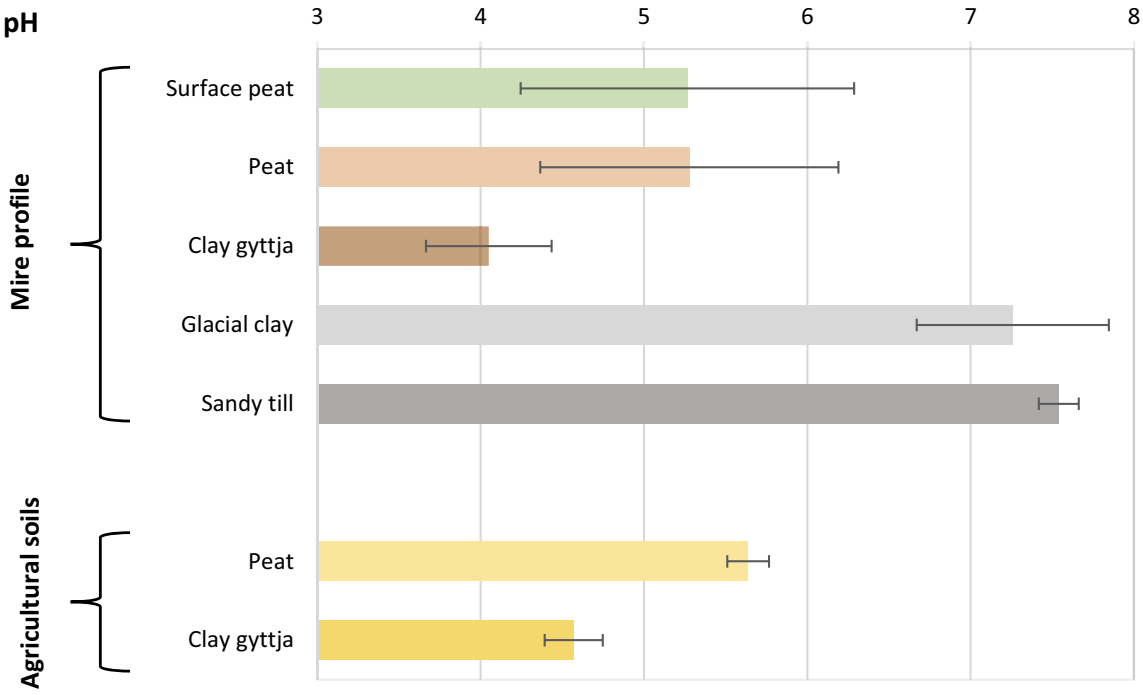

Figure 11-16. *Soil pH from $CaCl_2$ extractions in the Forsmark area. Mean and standard deviations (whiskers) from 4 to 6 locations are given. Surface peat and cultivated soils were sampled at a soil depth of 20 cm. All other regolith layers were sampled at 50 cm below the surface. Data from Sheppard et al. (2011). Calcite is found primarily in glacial clay and sandy till.*

The post glacial clay-gyttja (RegoPG) and cultivated soils are less likely to be affected by calcite leaching. This is because the clay-gyttja samples that have been used to determine K_d are poor in calcium and already have a low pH (~4, Sheppard et al. 2011). Agricultural soils are managed, and therefore any significant losses in calcite, if at all present, are likely to be balanced by the active management of these soils. This reasoning is supported by historical and present agricultural practice on organic soils (Berglund 2008) and by the observation that the pH range in cultivated peat and clay-gyttja and soils is remarkably narrow as compared with the corresponding uncultivated soils (Figure 11-16, whiskers on yellow vs orange/brown bars). Hence, it is deemed that the pH of post glacial clay-gyttja and agricultural organic soils is not affected by the depletion of calcite in this calculation case.

Postulated shifts in K_d for selected radionuclides

K_d-values under calcite-depleted conditions were calculated as a function of the postulated change in pH (Δ) and empirical regression coefficients (β) for the seven selected elements:

$$K_d(\Delta pH) = K_{d,0} 10^{\beta \cdot \Delta pH}$$

where $K_{d,0}$ is the regolith-specific K_d value used in the *base case*.

The regression coefficients are taken as the average values from two independent studies, Sheppard (2011) and Sohlenius et al. (2013b). The meta-analysis by Sheppard (2011) is based on various studies where K_d-values were determined for multiple elements by extracting pore water from soil at field moisture conditions. The number of samples is typically above 100 for the selected elements. The study of Sohlenius et al. (2013b) was based on a field campaign near the Forsmark area. In this study, the K_d-values of five different soil types were determined at two depth levels from incubations at field capacity (n = 50).

The seven selected elements showed a similar and expected response in the two studies (Figure 11-17). That is, the K_d-value increased with pH for elements expected as cation species, namely Ni and Cs and three elements in the U-238 decay chain (Th, Ra and Pb), whereas it decreased for Mo (anionic) and U (complexation with carbonate). Note that for U the response is only valid for pH above 5.5, which includes mineral rich regolith layers like till (RegoLow) and glacial clay (RegoGL). This is consistent with the modelled U speciation, which indicates that the mobile neutral or anionic uranyl-carbonate complexes are only important at pH > 6 (Figure 11-14). The underlying reason is that even with a constant total carbonate concentration, the fraction of free carbonate ions will decrease with decreasing pH. This decrease will accelerate as the first pK_a value of carbonic acid is reached at pH 6.3. Even if the total concentration of the carbonate system remains high, only about 10 ppm will be present as carbonate ions at pH 6, and consequently the importance of the mobile uranyl-carbonate complexes will gradually decline (Figure 11-14). In the literature data, the relationship for U increased weakly with clay content, and a slope for 25 % clay content is selected. However, for organic soils with a pH close to or below 5.5 the mobility of U is already very limited (K_d > 3.8 $m^3\ kg_{DW}^{-1}$, Tröjbom et al. 2013) and appears to be insensitive to changes in pH (data from Sohlenius et al. 2013b).

It can be noted that the K_d-values of Cl and I do not respond to pH in either of the studies. In for example Japanese andosols increased sorption of chloride and iodide has been observed at lower pH, but this pH effect might not be observable given the generally low anion exchange capacity of Swedish soils and the weak sorption capacity of these ions (Yoshida et al. 1992). Also, the K_d-value of Ca is not reported in Sheppard et al. (2011) and does not respond to pH in Sohlenius et al. (2013b).

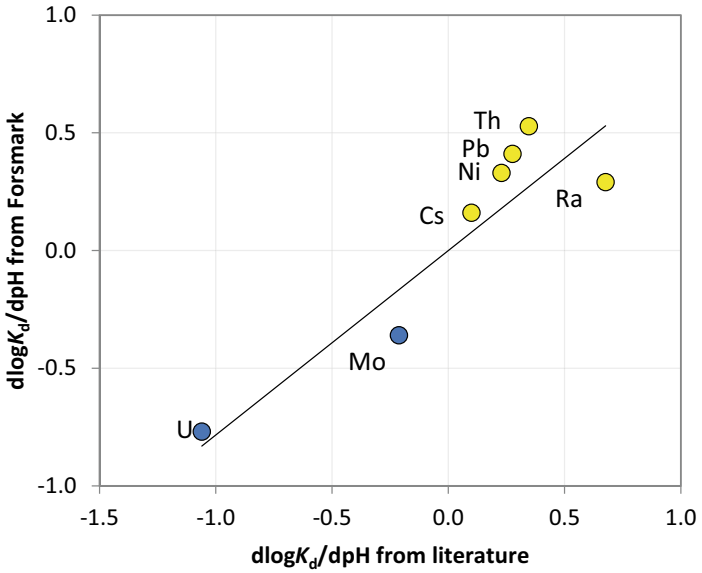

Element	dlogK_d/dpH
Ra	0.5
Th	0.4
Pb	0.3
Ni	0.3
Cs	0.1
Mo	-0.3
U (pH>5.5)*	-0.9

Figure 11-17. *Postulated change in log10 K_d-values to shifts in pH. The figure shows the concordance in pH response between a literature study (Sheppard 2011) and response measured in the latest large field campaign in Forsmark (Sohlenius et al. 2013b). Colour indicates whether the mobility of the element is expected to increase when calcite is depleted (yellow) or if the mobility is expected to decrease (blue). The table lists the response used in the sensitivity case, which corresponds to the average of the two studies. *Note that the mobility of U is only expected to respond to a decrease in pH in minerogenic soils (RegoLow and RegoGL) with a relatively high pH (see the text).*

Time for calcite depletion

The time required for calcite depletion in Forsmark is uncertain and estimates range from a few thousand years of leaching (Tröjbom and Grolander 2010) to more than 50 000 years (Section 4.4). The span in the estimated time primarily reflects uncertainties with respect to the calcite concentrations in deeper soil horizons and the amount of calcite-rich till in the landscape. Furthermore, the dissolution of calcite is dependent on the addition of protons and the leaching of Ca and carbonate from the soils with the groundwater, which also make the weathering of calcite dependent on, for example, future changes in the hydrology, the transport of acids such as carbonic acid to deeper soil layers and the future levels of acidification. For parts of the landscape with a thick (~4 m) layer of calcite-rich till, the upper range is considered the more plausible estimate.

In this sensitivity calculation, the K_d-values are assumed to be stable until the biosphere is isolated from the sea (i.e. T_{iso} equals 4300 AD for object 157_2). Thereafter, the K_d-values of selected elements change linearly to reach their alternative value (corresponding to a decline of 1 or 2 pH units after 3 000 or 50 000 years (T_{depl}), respectively:

$$K_d(\Delta pH, t) = \begin{cases} K_{d,0}, & t \le T_{iso} \\ K_{d,0} + \left(K_{d,0}10^{\beta \cdot \Delta pH} - K_{d,0}\right)\dfrac{t - T_{iso}}{T_{depl}}, & T_{iso} < t < T_{iso} + T_{depl} \\ K_{d,0}10^{\beta \cdot \Delta pH}, & t \ge T_{iso} + T_{depl} \end{cases}$$

Hence, the sensitivity calculations comprised four different variants: rapid depletion of calcite (3 000 years) with a large drop in pH (2 pH units); slow depletion of calcite (50 000 years) with a large drop in pH; rapid depletion of calcite with a modest drop in pH (1 pH unit); and slow depletion of calcite and a modest drop in pH.

General conditions, parameters and exposed groups

The *base case* assumptions are used for all other aspects of the simulations. That is, present-day temperate conditions persist during the entire simulation period and that the geosphere release is discharged into biosphere object 157_2. The properties and development of the landscape and parameters describing surface hydrology also follow those in the *base case*. As land-use associated with draining the mire results in the highest dose from Ca-41 in the *base case*, the sensitivity analysis only evaluates dose to this potentially exposed group (DM).

Several aspects of natural ecosystems (i.e. lakes and mires) are likely to be affected by changes in pH caused by calcite leaching (see Section 4.4). However, with the exception of sorption coefficients, most parameters that are identified as important for dose variation (see the sensitivity analysis in the *ecosystem properties calculation case* above) are not expected to be sensitive to calcite depletion, given the assumption that agricultural soils are actively managed. Thus, limiting this calculation case to illustrating the responses of doses to changes in K_d-values is considered a reasonable simplification for capturing potential effects of calcite depletion.

11.5.2 Results

Calcite depletion is expected to modify transport so that radionuclides in inorganic regolith layers are either immobilised (Mo and U) or mobilised (Ni, Cs, Ra, Th, Pb) to a larger extent than under present conditions (Figure 11-17). A similar response is expected in surface and deep peat. In general, an increased immobilisation will lead to increased accumulation and higher doses when the regolith layers are used for cultivation. In addition, an increased immobilisation in the till (RegoLow) will delay transport to the above layers. Thus, when the residence time is sufficiently long in relation to the half-life, less activity will reach the layers that are used for cultivation. Thus, the response to calcite depletion depends on radionuclide properties, their sensitivity to changes in pH, and to the timing of the geosphere release. The simulations suggest that calcite depletion may have significant effect on the radionuclide-specific doses towards the end of the assessment period (Figure 11-18 to Figure 11-21). Depending on radionuclide, the dose may either increase or decrease as compared with the *base case*. However, the total doses at this time are still expected to be clearly below the maximum dose of the *base case*.

In the *base case*, Mo-93 contributes most to the maximum dose occurring around 7000 AD, and Ni-59 dominates doses towards the end of the assessment period (Figure 9-5). The sorption response of these elements to calcite depletion is modest. A pH decrease by two units leads to an increased (Mo) or decreased (Ni) sorption coefficient by a factor of four, as compared with the *base case*. For Mo-93, the increased sorption delays the timing of the maximum dose by a few thousand years or less, and the maximum dose is marginally affected (< 5 % difference as compared with the *base case*) (Figure 11-18). The weak response is partly because the stronger sorption and higher accumulation in shallower peat layers, which subsequently are cultivated, are off-set by an increased loss of activity through radioactive decay due to stronger sorption also in the lowest regolith layers. The effects of calcite depletion are also dampened because the geosphere release of Mo-93 occurs relatively early as compared with the postulated progression of calcite leaching.

The effects of calcite depletion are more pronounced for Ni-59, and a decrease of two pH units leads to a reduction of dose to approximately half of that in the *base case*, irrespective of the rate of calcite depletion (Figure 11-19). This response is primarily due to a reduction of the accumulation in glacial clay. It can also be noted that a relatively fast calcite depletion (i.e. in 3 000 years) results in an earlier rise of Ni-59 doses than in the *base case*. Ni-59 releases in this variant capture the dynamics of the geosphere release and the Ni-59 doses are relatively high at the dose maximum for Mo-93. However, the contribution of Ni-59 doses at this time is limited (~0.1 μSv, i.e. ca 2 % of the total dose), and Ni-59 is therefore not expected to affect the total dose significantly.

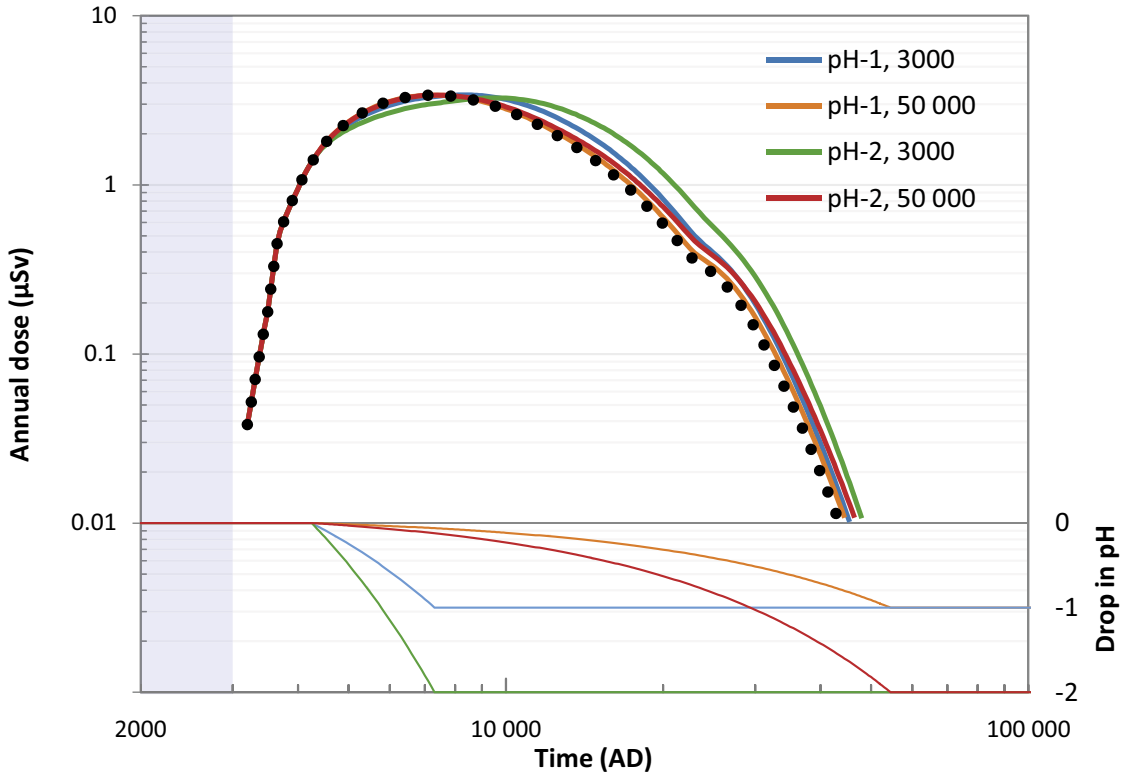

Figure 11-18. *Radionuclide-specific annual dose for Mo-93 in the calcite depletion calculation case in the upper panel. The four variants are indicated by coloured lines and the corresponding change in pH is shown in the lower panel. For example, the dose response to a two unit decrease in pH in 3 000 years is indicated by the green line. The corresponding doses in the base case are shown for reference (black dotted line).*

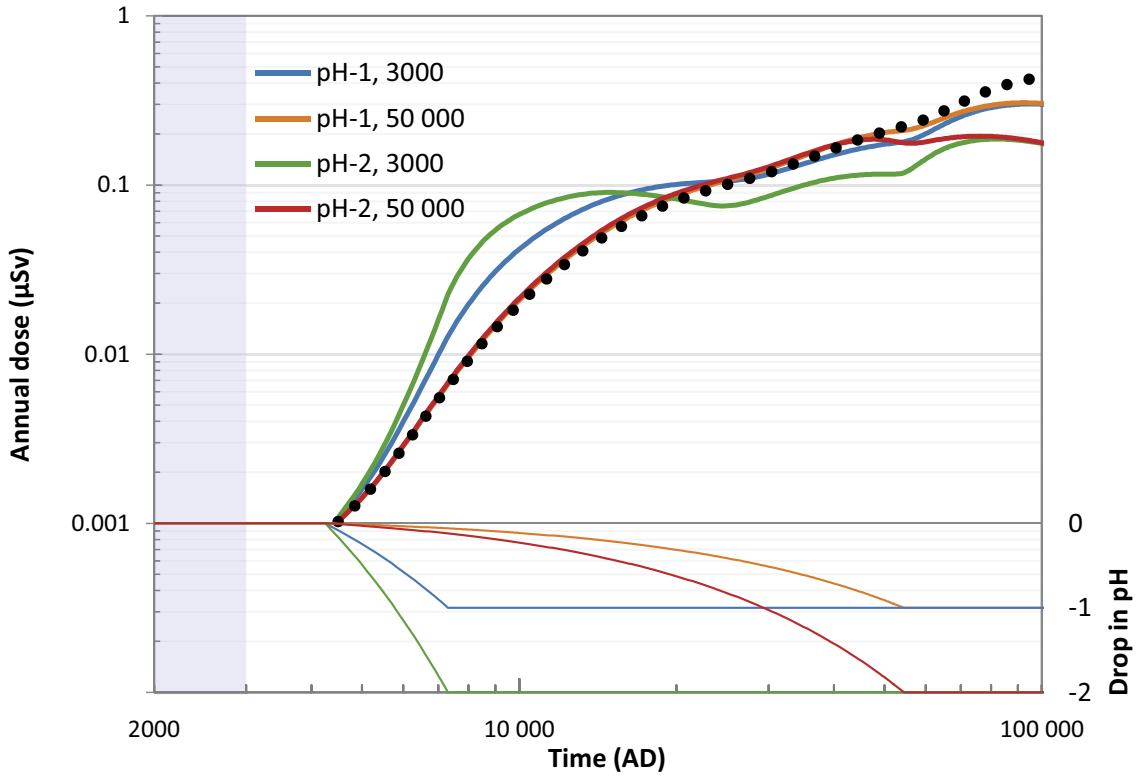

Figure 11-19. *Radionuclide specific annual dose in the calcite depletion calculation case for Ni-59 in the upper panel. The four variants are indicated by coloured lines and the corresponding change in pH is shown in the lower panel. For example, the dose response to a two unit decrease in pH in 3 000 years is indicated by the green line. The corresponding doses in the base case are shown for reference (black dotted line).*

The response of U-238 to calcite depletion is much stronger (Figure 11-20). Overall, stronger sorption of U in the regolith keeps more U in the system, allowing for increased ingrowth of decay products and, eventually, higher doses. A pH decrease of one or two units results in increased sorption coefficients in the inorganic layers, RegoLow (till) and RegoGL (glacial clay), by a factor of eight and sixty-four, respectively. Depletion of calcite thus tends to delay the transport of U from the till. The activity stored in the two inorganic layers also increased significantly, and less activity reached the regolith layers above (RegoPG, RegoPeat and RegoUp), as compared with the *base case*. Although the depth profile of the activity is inverted, as compared with the *base case*, the net effect on the maximum total concentration in regolith layers exposed by cultivation is marginal for U-238. That is, with calcite depletion, the accumulation in glacial clay is similar to that in the combined layers of clay-gyttja and peat in the *base case*. However, for U-234 considerably more activity builds up in the glacial clay when calcite is depleted as compared with the layers exposed by cultivation in the *base case*. This is primarily due to long-term ingrowth from U-238. For U-234 a pH decrease of two units results in five to six times higher maximum dose from cultivation than in the *base case*, and accumulation is still increasing at the end of the assessment period. The activity of U-234 is not considered to contribute significantly to the total dose at any time, but it is the primary source for the decay products Th-230, Ra-226, Pb-210 and Po-210.

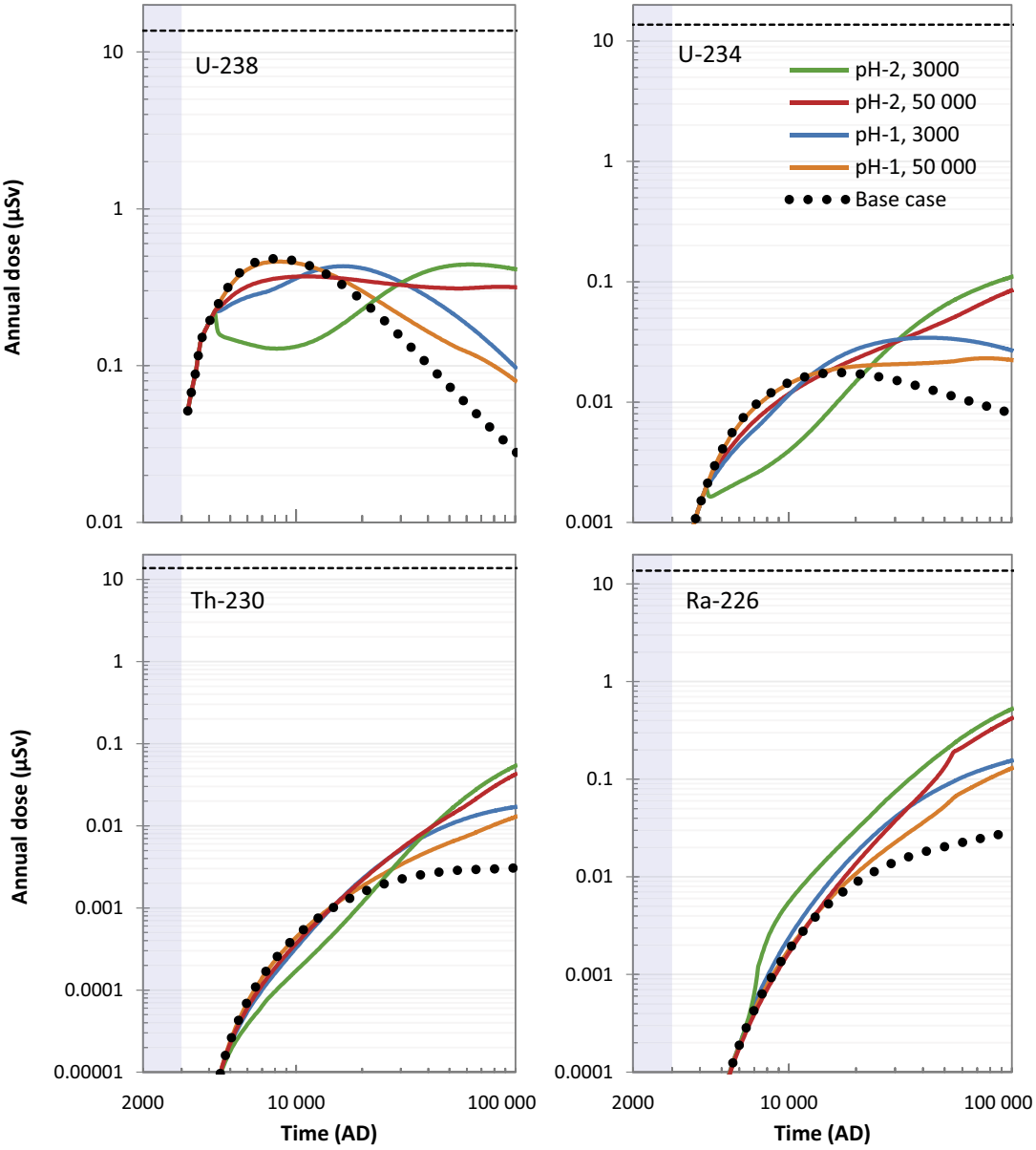

Figure 11-20. *Annual dose in the calcite depletion calculation case for the most long-lived radionuclides in the U-238 decay chain. Results from the four variants are indicated by coloured lines (as described in Figure 11-17). The corresponding doses in the base case are shown for reference (black dotted line).*

The decay products from U-234 are all expected to be in the form of cation species, and consequently their mobility increases when the pH decreases. However, the response in the sorption coefficient to a change of pH varies (Figure 11-17). A decrease of pH by two units decreases K_d for Ra by an order of magnitude, whereas the response is weaker for Th and Pb (a factor of six and four, respectively). The response in radionuclide accumulation and doses also depends on the behaviour of the internal source term, i.e. the accumulation of the parent radionuclide. Thus, for Th-230 a fast calcite depletion initially results in a lower dose. This is due to the increased retardation of U in the till, and that sorption of Th in the till is still strong ($K_d > 3.7$ m^3 kg$_{DW}^{-1}$) in spite of the six-fold decrease of the sorption coefficient.

In the *base case*, almost all Ra-226 activity that is released to the till from the bedrock decays, and less than 0.1 % is exported to the above layers. However, a ten-fold lowering of K_d increases the importance of advection, and the rate of upward export from till increases more than a hundred-fold as compared with the *base case*. Thus, fast calcite depletion may increase the dose of Ra-226, independently of the inventory of Th-230 in the glacial clay. The doses from Pb-210 and Po-210 follows the dose from Ra-226 (data not shown). This is because the retention times of Pb and Po in regolith tends to be long compared with the half-lives of Pb-210 and Po-210 (22 and 0.4 years, respectively) within the examined range of K_d-values (data not shown). At the end of the simulation the doses from Pb-210 and Po-210 amounts to approximately half of the dose from Ra-226.

The long-term response to the postulated regimes of calcite depletion is more relevant, as the dose from Th-230 and its decay products increases throughout the simulations, reaching maximum values at the end of the assessment period. At that time, the overall pattern is like that of U-234. The bottom line therefore is that calcite depletion causes higher doses than in the *base case* for radionuclides in the U series. The response is clearly larger for a pH decrease of two units than for a decrease of one unit, while the rate of calcite depletion is of less importance for the maximum doses. In addition, it can be noted that the quantitative response of Th-230, Ra-226, Pb-210 and Po-210 is stronger than that of U-234. When the dose contribution from all the examined decay products in the U-238 series are summed up, a change of one or two pH units leads to an increase in the annual dose by approximately a factor of four and fourteen, respectively, as compared with the *base case*. In addition, it can be noted that the total dose from the U-238 series, ~ 1 μSv for a pH decrease of two units, is more than a factor two above the dose from Ni-59 in the *base case*. Thus, long-term changes in the environment that are driven by calcite leaching have the potential to change the relative importance of the dose contributing radionuclides. However, although the importance of U-238 and its decay products increases when the pH drops in the regolith layers, the total dose from the chain at the end of the assessment is still below the maximum levels associated with the release of Mo-93 in the *base case* (~ 3.4 μSv).

The conclusions from the U-238 decay chain largely apply also for the U-235 decay chain (Figure 11-21). Due the shorter half-life of U-235 as compared to U-238 the dynamics of the calcite depletion will influence the dose from U-235 somewhat differently, but the general trend that the timing of the maximum dose is delayed remains. The period up to 10 000–20 000 AD tends to display a lower dose than the *base case*, while the opposite is true after that. Particularly in the most extreme case with a rapid calcite depletion and a sharp decline in pH (Tdep3000 dPh2) leads to a significantly lower dose from U-235 during the first 20 000 years, but instead the dose is significantly higher than the *base case* towards the end of the modelling period. As discussed with respect to U-238, these results seem reasonable given that it will take longer time for U-235 to reach the surface environment when there is a stronger sorption, but eventually this will lead to higher doses than the *base case* as less U-235 is lost from the system.

While the annual dose from U-235 is predicted to peak at ca 0.2–0.3 μSv, the most significant contribution from the U-235 decay chain is expected from its decay products, Pa-231 and Ac-227, which in some scenarios reach levels > 1 μSv towards the end of the calculation period (Figure 11-21). In the *base case*, the maximum dose from Pa-231 was 0.17 μSv, but in the calcite depletion case it increased to between 0.48 μSv and 1.1 μSv, depending on the model assumptions. Likewise, the maximum annual dose from Ac-227 increased from 0.24 μSv in the *base case* to between 0.67 μSv and 1.7 μSv in the calcite depletion case. Hence, the dose from the U-235 decay chain is expected to exceed the dose from both Ni-59 and the U-238 decay chain during the later stages of the calculation period.

Looking at the temporal dynamics of most long-lived decay products of U-235, i.e. Pa-231 and Ac-227, the patterns are fairly similar to the decay products in the U-238 decay chain, although the difference in half-life and the invariant K_d-values for Pa and Ac lead to slight differences (Figure 11-21). The relatively short half-life of Ac-227 ($T_{½}$ = 21.8 a), comparable to that of Pb-210, implies that it cannot develop a

profoundly different pattern than its immediate parent, Pa-231. The calculation case with rapid calcite leaching and a large drop in the pH leads to markedly lower doses from Pa-231 and Ac-227 up to ca 20 000 AD as compared to the *base case*. Again, this is related to a higher sorption of U-235 in the soils, which means that it takes a longer time for U-235 and its decay products to reach the surface environment. The other three scenarios, however, fall relatively close to the *base case* during this initial period. All scenarios, however, predict higher doses than the *base case* from Pa-231 and Ac-227 towards the end of the calculation period, particularly in the two scenarios where the pH declines by 2 pH units (Figure 11-21). As discussed for the U-238 decay chain elements, the reason is the higher accumulation of U-235 in the soils, which over time allows a build-up of Pa-231, Ac-227 and other more short-lived radionuclides near the surface. Evidently, this is entirely caused by the lower mobility of U, because the K_d-values for both Pa and Ac were kept constant in the modelling. Nevertheless, Pa-231 and Ac-227 will both contribute with a significant dose under the calcite depletion calculation case, in some scenarios exceeding 1 μSv per year towards the end of the modelling period. This implies that the U-235 decay chain has the potential to be the dominating contributor to the annual dose during the later stages of the evaluation period and increases the importance of properly understanding the fate of Pa and Ac in the surface environment.

In the *base case,* Cs-135 accumulates in regolith throughout the assessment period. A strong retention of Cs-135 in the till delays the transport to layers that can be cultivated. As a monovalent cation, it is not surprising that calcite depletion would increase the mobility of Cs. A higher mobility implies a faster transport to layers affected by draining and cultivation and, thus, an increased dose at the end of the assessment period. However, the pH response is relatively weak (Figure 11-17). A decrease of two pH units leads to a limited increase in dose (less than a factor of two) and the rate of depletion has a marginal effect on the results (data not shown). Nevertheless, the dose contribution from Cs-135 is noticeable at the end of the assessment (0.7 μSv) at which time it exceeds the dose from Ni-59 in the *base case.*

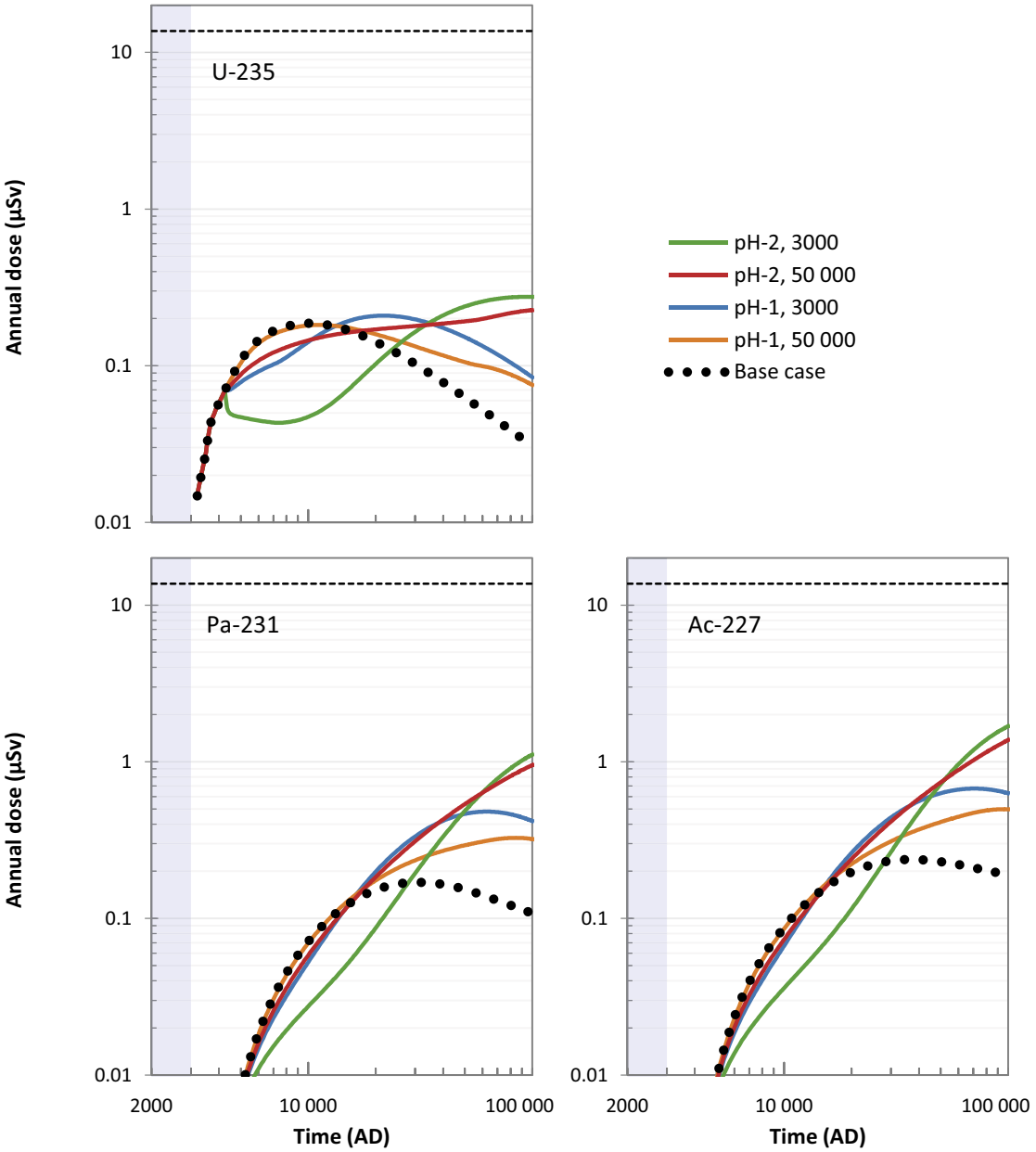

Figure 11-21. *Annual dose in the calcite depletion calculation case for the most long-lived radionuclides in the U-235 decay chain. Results from the four variants are indicated by coloured lines (as described in Figure 11-17). The corresponding doses in the base case are shown for reference (black dotted line).*

12 Exposure of non-human biota

12.1 Introduction

Exposures of non-human biota (NHB) to ionising radiation from radionuclides originating from SFR is estimated by calculating absorbed dose rates. Calculations for NHB are performed for three calculation cases of the main scenario, including the *base case*, the *warm climate calculation case* (high and low summer precipitation variants) and the *cold climate calculation case* (variants with continuous permafrost and permafrost with a talik). In addition, calculations for NHB are performed for the supporting calculation case addressing alternative delineations of biosphere object 157_2. This is done to illustrate potential effects of a release restricted to a habitat relevant for a protected species and/or to areas smaller than the original outline of object 157_2. The descriptions of the calculation cases addressed in this chapter are found in Section 9.2 (the *base case*), Chapter 10 (the *warm climate calculation case* and the *cold climate calculation case*) and Chapter 11 (the *alternative delineation calculation case*).

This chapter briefly summarises the method used to derive the dose rates to NHB (Section 12.3) and then presents an analysis of dose rates under the *base case* (Section 12.4). Key points from the calculation cases of the main scenario with alternative climate development are presented in Sections 12.5 and 12.6, followed by the *alternative delineation calculation case* (Section 12.7). Finally, the results from all calculations are summarised and conclusions with respect to radiological impacts on NHB are drawn (Section 12.8).

12.2 Background

Radiation exposures of plants and animals living in the biosphere objects are the result of external exposure (i.e. radiation from radionuclides in water, sediment or soil) and internal exposure (i.e. from radionuclide uptake or intake). Both external and internal exposure directly depend on the activity concentrations in the environmental media, and thus temporal and spatial variations in dose rates for any organism group are expected to follow those of the environmental media. For mobile organisms, the assessed activity concentration in media is cautiously considered to be the average activity concentration with which the organism would come in contact. The radioactivity released from the repository contains different radionuclides, and their impacts on biota differ, depending on their half-lives, decay modes (reflected in the *dose conversion coefficients*, DCC; see Section 8.4), and their availability for uptake, physiological/metabolic processes and trophic transfer in biota and their food webs (described by *concentration ratios*, CR; see Section 8.4). The radionuclide with the highest environmental activity concentration does not always dominate the exposure, as is evident in the following sections.

Consistent with previous assessments (Jaeschke et al. 2013, SKB TR-14-09), the dose assessment results have been interpreted with respect to the ERICA screening dose rate (see Section 2.3.5). Consideration is also given to relevant ICRP Derived Consideration Reference Levels (DCRLs), where these are more restrictive than the generic ERICA screening value. The ERICA Integrated Approach utilises a single screening dose rate of 10 μGy h^{-1} across all organism types, which is, in general, more cautious than similar screening benchmarks recommended by UNSCEAR (UNSCEAR 2011; 100–400 μGy h^{-1}) and ICRP (ICRP 2008; 4–4 000 μGy h^{-1}). The ICRP employs bands of dose rates (named Derived Consideration Reference Levels; DCRLs), for a range of reference organism types (corresponding to ICRP's own Reference Animals and Plants), within which further consideration is recommended. For some vertebrates and coniferous trees (e.g., pine), a DCRL band of 4–40 μGy h^{-1} is applied, the lower level of which can be considered a more restrictive benchmark than the ERICA screening dose rate. The ICRP DCRLs are recommended as benchmarks against which acceptability, in terms of environmental impacts of planned activities, should be gauged (ICRP 2014). DCRLs for fish, grasses and macroalgae are 40–400 μGy h^{-1} and for invertebrates are as high as 400–4 000 μGy h^{-1}; for these organisms, application of the ERICA screening dose rate is much more cautious. There is no ICRP DCRL available for either Phytoplankton (simple plants and bacteria) or Zooplankton (typically made up of microscopic crustaceans and insect larvae) and direct comparison is therefore not possible; however, these organisms are acknowledged to be less radiosensitive than the likes of mammals and pine trees (Harrison and Anderson 1996, Whicker and Schultz 1982) and therefore the use of the ERICA screening value for dose rate evaluation is considered to be cautious.

The ecosystems are separated into aquatic and terrestrial. During the initial submerged period, the aquatic portion of the biosphere object is considered to be marine (sea); whereas the site is in fact brackish. Thus, the ecosystem has been assumed to be equivalent to marine conditions. However, as the land rises and lake basins and wetlands are isolated, the aquatic ecosystem is considered to transition to freshwater. Agricultural ecosystems were not considered relevant in the analysis, as discussed in SKB (TR-14-09). Some organism types (e.g. Annelid) were included in the terrestrial ecosystem, where un-drained wetland ecosystems are clearly an inappropriate choice as a habitat; however, the use of such organism types in a wetland has been maintained in this assessment to give a cautious assessment for such organism types that may exist in surrounding non-wetland terrestrial ecosystems, including marginal areas in transition from wetland to terrestrial. The possibility of organisms interacting with more than one ecosystem (e.g. living on land but eating from aquatic environments) has been investigated in SKB (TR-14-09), and while it was deemed feasible for dose rates to occur in certain occupancy combinations higher than those from occupancy in a single ecosystem, the difference was very small, less than from most other sources of uncertainty. No species/organism types (potentially) living in the water but eating from land were identified (Jaeschke and Grolander 2017).

12.3 Method to derive dose rates

The method used to calculate adsorbed dose rates to NHB is described in detail in Appendix D and is summarised in this section. In short, dose rates to non-human biota are calculated in BioTEx, using the recently updated ERICA code (ERICA tool v2.0), adapted and implemented into the Ecolego modelling platform. Previous iterations of the ERICA tool/code have been used in previous safety assessments for geological repositories for radioactive waste, including the previous assessment for SFR (Jaeschke et al. 2013, SKB TR-14-09).

Species at the site are represented by several reference organisms included in ERICA, in terrestrial, freshwater and marine ecosystems. Reference organisms mirror the reference man concept employed in human dose calculations. The ERICA reference organisms are designed to represent the range of organisms typically found throughout Europe and have been deemed suitably representative of species in Sweden (Jaeschke et al. 2013). In previous assessments, the differences in parameters (geometry, occupancy and concentration ratios) between site-specific species and the ERICA reference organisms led to minimal differences in dose rates (Jaeschke et al. 2013, SKB TR-14-09) and reflect the similar findings that generically parameterised reference organisms are sufficient to represent site-specific organisms (Charrasse et al. 2019). Of the ERICA reference organisms, ‘Marine Reptile’ and ‘Sea anemones & True corals’ are deemed not relevant to the site, now or in the future, and have been removed from consideration. It was determined that one organism category, microphytobenthos (a community of small photosynthesising organisms that occupy the bottom of the shallow lakes) was not represented, and so was user-defined.

Dose rates from each radionuclide to non-human biota were calculated from the activity concentrations in environmental media (ACs) and within the body of the organism. Concentrations of radionuclides within the body were estimated using transfer factors (concentration ratios, CRs) from those in the environmental media inhabited by the types of organism under consideration (Saetre et al. 2013a, Section 10.2.2).

Dose conversion coefficients (DCCs) were then used to estimate external and internal dose rates for each radionuclide, which were adjusted using weighting factors for each relevant type of radiation (alpha, high- and low-energy beta and gamma) and based on the organism’s occupancy (OCC) of each environmental medium of relevance. The occupancies of organism types used in this assessment follow those of the ERICA reference organisms, which have in some cases become more biased towards occupancy in or on soil/sediment than earlier versions of ERICA such as those used in Jaeschke et al. (2013) and SKB (TR-14-09). A previous study, following SR-PSU, tested the effect of soil/sediment bias, using amphibians. The study indicated that changing Terrestrial Amphibians occupancy from “on soil” to “in soil” increased the dose rate by just 64 %, whereas the increase in dose rate in Freshwater Amphibian from changing “on sediment” to “in sediment” was less than 1 %.

Internal and external dose rates were summed to give a total dose rate for each radionuclide. The total dose rates from each radionuclide were summed to give a final total dose rate to each organism type, which was then compared with a screening dose rate to assess the radiological impacts on populations of non-human biota. Dose rates below the screening dose rate are considered to be of no significant radiological consequence to populations of non-human biota and require no further investigation.

12.4 The *base case*

12.4.1 Results for the aquatic ecosystem

The aquatic ecosystem that receives release of radionuclides from SFR can be divided into two stages, the marine stage prior to the full emergence of biosphere object 157_2 (2000 AD to 4300 AD), and the freshwater stage, which occurs once the biosphere object is fully emerged (4300 AD to 102 000 AD). Release of radionuclides and subsequent exposures of organisms are considered to begin shortly after closure (Figure 12-1). Dose rates to marine organisms increase steadily until emergence, due to the combined effect of increasing concentrations of C-14 reaching the biosphere system and decreasing water exchange in the basin of the biosphere object. After emergence, the dose rates to organisms increase sharply when the radionuclides are released to a relatively small stream. This is due to a marked decrease in the amount of flowing water that dilutes the radionuclide release. About half of organisms experience their dose rate maximum at the transition (4300 AD), followed by a steady decline, reflecting the ambient concentrations of C-14. The remaining half of organism types maintain a higher dose rate, with a maximum occurring later (~ 16 000 AD), attributable to dose rates from Ac-227.

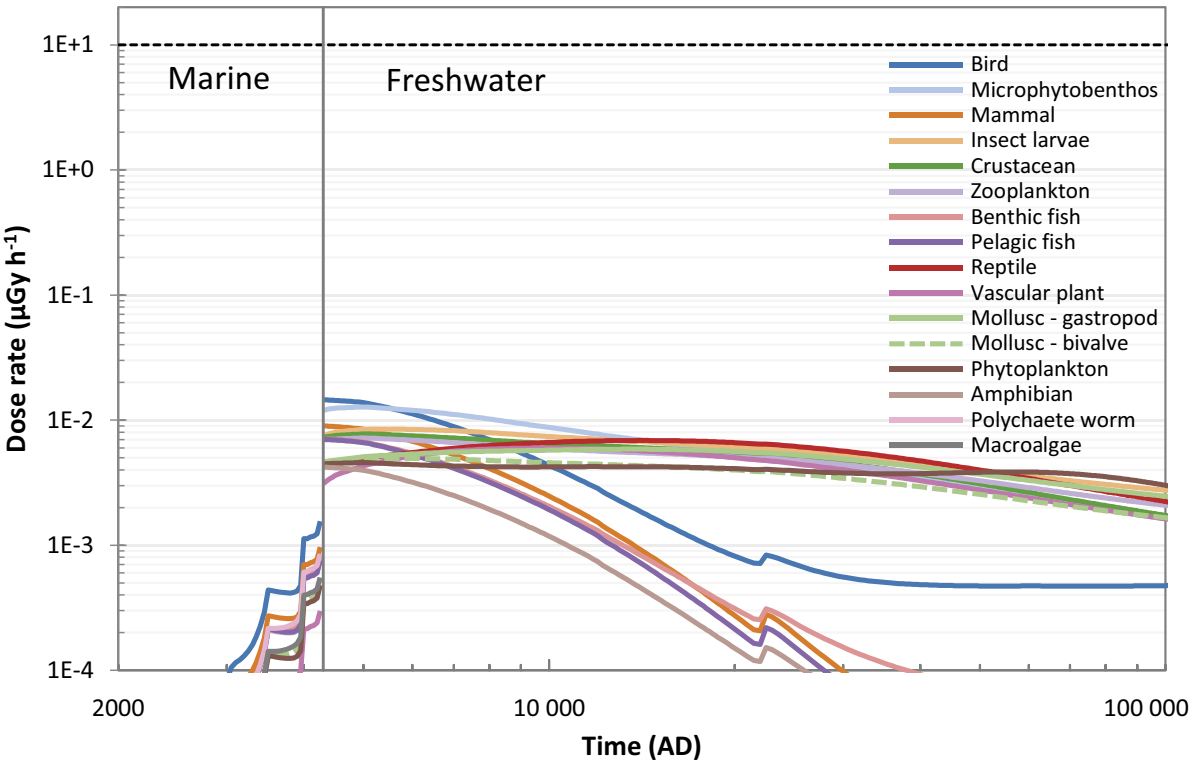

Figure 12-1. *Dose rates to aquatic organisms before emergence in the marine era (to the left of the vertical line) and after emergence (to the right of the vertical line) of the biosphere object, under the base case. The horizontal dashed line indicates the screening dose rate (10 µGy h^{-1}).*

The highest dose rates are found in (freshwater) Bird (1.4×10^{-2} µGy h^{-1}, 4300 AD), followed by Microphytobenthos, with dose rates of around 1×10^{-2} µGy h^{-1}, approximately three orders of magnitude lower than the screening dose rate. These two organism types correspond to the earlier peak of exposures (4300 AD), with dose rates dominated by C-14 (freshwater Bird: 99 %). Details of the dose rates from specific radionuclides over time in the freshwater Bird are depicted in Figure 12-2.

The most exposed organism types of the second dose rate maximum (~16 000 AD) are Reptile, Insect Larvae and Zooplankton, with peak dose rates of about $6–7 \times 10^{-3}$ µGy h^{-1}, dominated by Ac-227 (freshwater Reptile: ~80 %). Details of the dose rates from specific radionuclides over time in the freshwater Reptile are depicted in Figure 12-2. Radionuclides such as Ac-227 become dominant as U-235 and its decay products accumulate in peat. An important factor for variation in exposures in the later period is the concentration ratios of radionuclides (particularly, Ac-227) in freshwater organisms. The CRs of Ac-227 in organisms exhibiting lower total dose rates in the later stage (i.e. Bird, Benthic and Pelagic fish, Mammal, and Amphibian) are approximately three orders of magnitude lower than those applicable to the organism types that exhibit higher dose rates throughout this period.

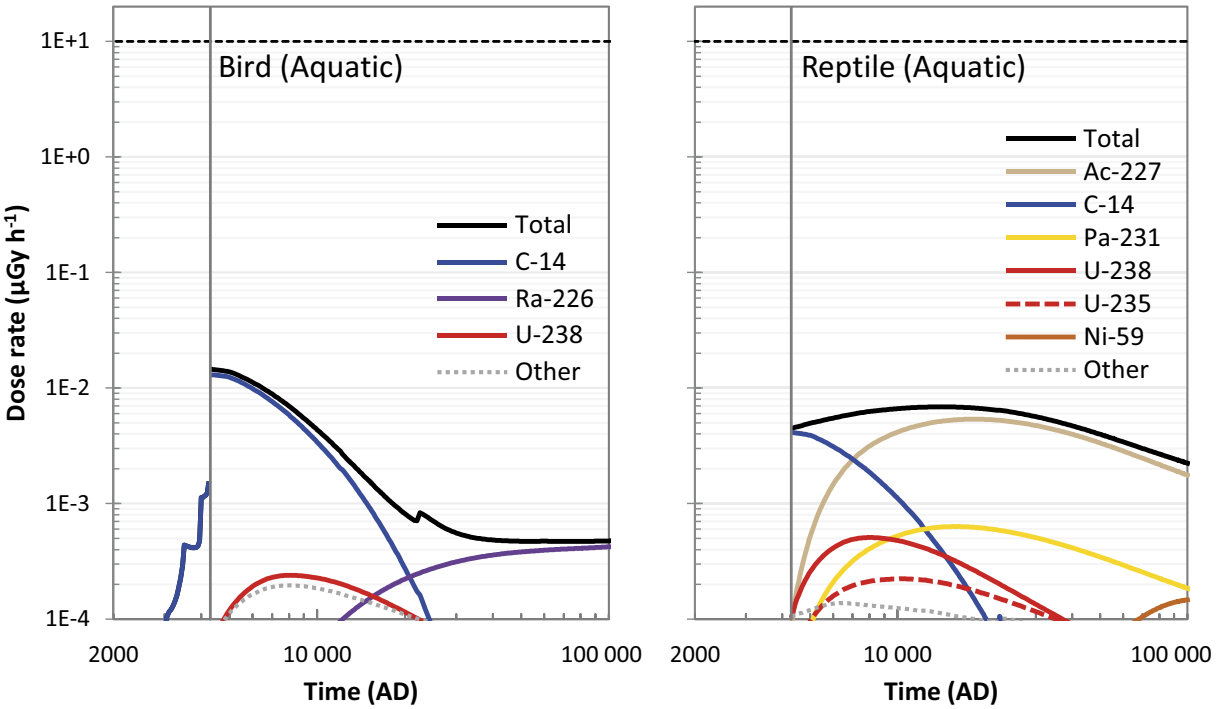

Figure 12-2. *Radionuclide-specific dose rates to Bird (left) and Reptile (right), the aquatic organisms with highest dose rate maxima in the first and second peak, under the base case. The horizontal dashed line indicates the screening dose rate (10 µGy h^{-1}). The vertical line indicates the emergence of freshwater and terrestrial systems replacing the marine one.*

12.4.2 Results for the terrestrial ecosystem

Exposures in the terrestrial ecosystem begin at 3000 AD, when the first parts of object 157_2 start to emerge from the sea (Figure 12-3). The exposure increases as land continues to emerge out of the sea, levelling-off (in most organism types) at the point of complete emergence (~4300 AD).

Organisms show two patterns of exposure (Figure 12-3, left figure). Most of the species get their maximum dose rates about 10 000 AD, but a few organisms receive maximum dose rates earlier, at the point of complete emergence. The organisms at 10 000 AD are more exposed, and the dose rates are dominated by uranium isotopes. The maximum dose rates experienced are 1.1×10^{-2} µGy h^{-1} (Lichen & Bryophytes), with the next most exposed organisms in the range of $4–7 \times 10^{-3}$ µGy h^{-1} (Annelid, Mollusc-gastropod, Arthropod-detritivorous and Reptile). These values are about one third of the highest dose rates to aquatic organisms. In Lichen & Bryophytes, U-238 and U-235 together contribute to approximately 95 % of the total dose rate.

Bird, Tree, and Grasses & Herbs are most exposed at emergence, with dose rates of just below 1×10^{-3} µGy h^{-1}. Dose rates to the Bird are dominated by C-14 (70 %). However, as in previous assessments, Cl-36 contributed significantly to the dose rate to terrestrial plants (Tree, Grasses & Herbs and Shrub), due to the high concentration ratio of chlorine. In all three organism types of plants, the dose rates from Cl-36 exceed those from C-14. However, the dose rate from Cl-36 in these organisms may be somewhat exaggerated, as suggested by the most recent analysis of soil and vegetation samples from Forsmark (Section 8.2.3)[58].

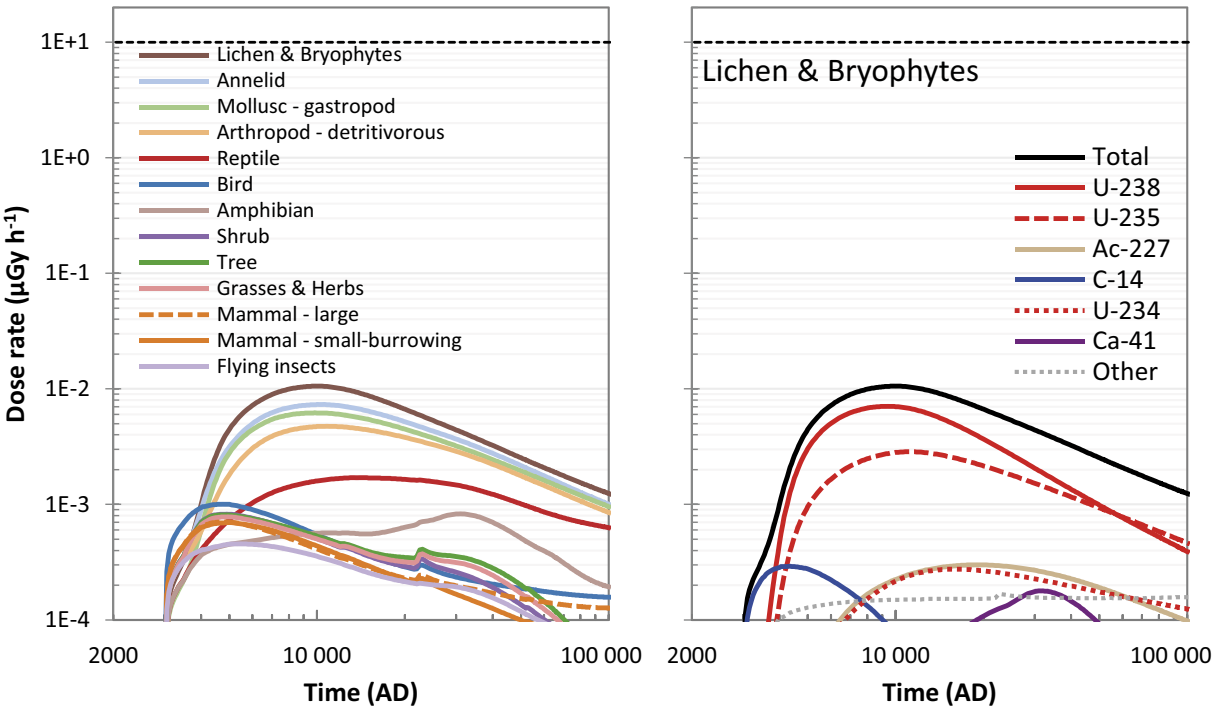

Figure 12-3. *Total dose rates to terrestrial organisms, under the base case (left). Radionuclide-specific dose rates to Lichen & Bryophytes, the terrestrial organism with highest dose rate maximum, under the base case (right). The horizontal dashed line indicates the screening dose rate (10 µGy h^{-1}).*

[58] Following a simplified approach for NHB, the CR-values are not updated with site data in PSAR. The typical CR-value used for Cl, expressed per unit carbon, is 390 kgdw kgC^{-1}. In the PSAR new data from the site is used to update the CR-values used to calculate uptake and accumulation of Cl in the mire (Section 8.2.3). The field layer is selected to represent the peat forming vegetation in fens (CR = 45 kgdw kgC^{-1}). The Cl concentration in green leaves of trees and shrubs are considerably lower than in the field layer (which includes herbs and grasses, Figure 8-2). Thus, the calculated dose from Cl to these organisms in the NHB calculations are likely to be cautious.

12.5 Warm climate calculation case

Under warm climate conditions, surface water availability and shoreline regression will be affected relative to the *base case*, with the possibility of higher and lower precipitation (*high summer precipitation* variant and *low summer precipitation* variant, respectively). The *warm climate calculation case* is characterised by an increased sea level that delays land emergence; object 157_2 starts to emerge at 6500 AD and is fully isolated at 7800 AD (see Section 10.2.1 for further details). The delayed evolution of the terrestrial and freshwater ecosystems means that the radionuclides from SFR have decayed for longer (about 3 500 years) before reaching these ecosystems, which reduces dose rates from radionuclides with shorter half-lives (such as C-14). Sea-level rise will also delay the transition from marine to freshwater ecosystems, as compared with the *base case*. As the largest dose rates are seen at, or a short period after, the time of emergence, the result is that the maximum dose rates occur later in both variants of the calculation cases.

12.5.1 High summer precipitation variant

The effect of warming of the environment alone (*high summer precipitation* variant) has little impact on the magnitude of dose rates to organisms. However, the later emergence of the biosphere object from the sea leads to a delayed release of radionuclides to freshwater and terrestrial ecosystems.

As the highest dose rates to freshwater organisms in the *base case* occurred immediately after emergence, the delay in emergence under the *high summer precipitation* variant leads to a lower maximum dose rate to freshwater organisms in this case. The highest dose rate overall occurred in the aquatic (freshwater) Bird being 9.9×10^{-3} μGy h^{-1} at the transition from marine to freshwater ecosystems, approximately half of the value of the highest dose rate of the *base case*. At this time, C-14 remains the dominant radionuclide for the most exposed organisms (Bird, ~90 %). However, due to a narrower release peak of C-14 and a later emergence of the freshwater ecosystem, the highest geosphere release of C-14 occurs while the basin is a marine ecosystem. At the time for the transition from marine to freshwater conditions, the release of C-14 has decreased to less than half of the peak value. In general, the dose rates to aquatic organisms in the *high summer precipitation* variant broadly reflect those of the *base case* but are truncated, cutting-short the earlier dose rates, by the delayed emergence.

Lichen & Bryophytes is the most exposed organism in the terrestrial ecosystem throughout the assessment, with a dose rate of 1.2×10^{-2} μGy h^{-1} around 15 000 AD. Again, like with the aquatic system, dose rates to organisms occur later, but when land is fully emerged, they are similar to the corresponding terrestrial values of the *base case*. The maximum dose rates to terrestrial organisms occur thousands of years after the emergence of land in both the *high summer precipitation* variant and the *base case*. At that time, uranium isotopes dominate the dose. The release peaks of these radionuclides are relatively flat and as they have long half-lives the activity of the release is marginally affected by a delay of a few thousand years. Thus, the later emergence has minimal impact and the maximum dose rates are approximately the same in these two cases.

12.5.2 Low summer precipitation variant

The *low summer precipitation* variant also exhibits a delayed exposure of the freshwater and terrestrial organisms, relative to the *base case*. However, the maximum dose rates are greater than in the *high summer precipitation* variant, in particular from radionuclides that are important in the later stages of the assessment period (i.e. isotopes of uranium, and decay products from U-235). The response is the result of the decreased ground and surface water flows associated with a drier climate, which reduces the dilution of radionuclides. Consequently, the activity in environmental media reaches higher concentrations in the *low summer precipitation* variant.

For aquatic organisms, the dose rates are similar to those of the *high summer precipitation* variant until emergence. After emergence, the two variants diverge, with dose rates from the *low summer precipitation* variant trending slightly higher. This is due to a slower transport that eventually results in a higher accumulation of uranium. Thus, maximum dose rates from U-238 and from the decay products of U-235 occur much later in the assessment, at around 25 000 to 30 000 AD (Figure 12-4). Freshwater Reptile experiences the largest dose rate, 1.5×10^{-2} μGy h^{-1}, which is dominated by Ac-227 (~80 % of the total dose rate).

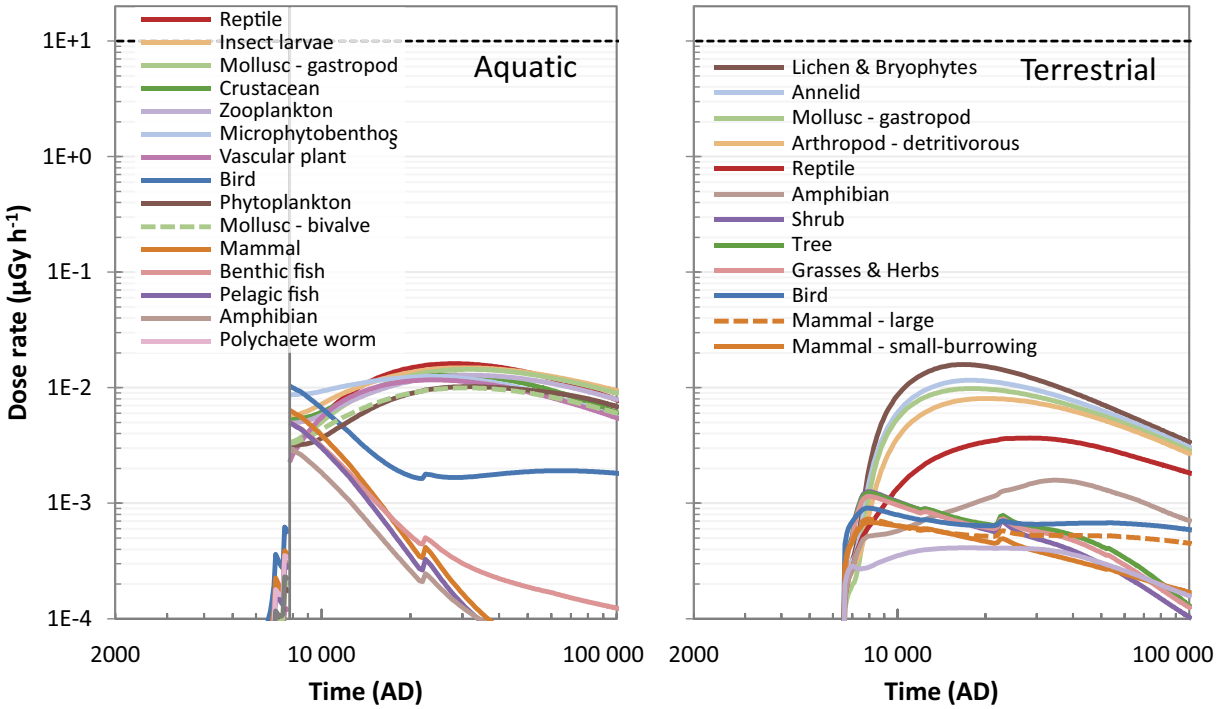

Figure 12-4. *Dose rates to aquatic organisms (left) and terrestrial organisms (right), under the low summer precipitation variant of the warm climate calculation case. The horizontal dashed line indicates the screening dose rate (10 µGy h^{-1}). Organisms are colour-labelled as in Figure 12-1 (aquatic) and Figure 12-3 (terrestrial). The vertical line indicates the emergence of freshwater system replacing the marine one.*

In terrestrial organisms, the dose rates in the *low summer precipitation* variant diverged from those of the *high summer precipitation* variant from the beginning, trending higher. Similarly to the freshwater organisms, it is the accumulation of uranium isotopes that leads to higher maximum dose rates at about 16 000 AD (Figure 12-4). The highest of these, 1.8×10^{-2} µGy h^{-1} at 16 000 AD in Lichen & Bryophytes, is the highest across all organisms, ecosystems and variants of the *warm climate calculation case* and the *base case* combined. For this organism the dose rate is dominated by U-238 (~70 %).

12.6 Cold climate calculation case

Under the *cold climate calculation case*, two periglacial periods are anticipated following the end of the current interglacial period at about 61 000 AD (see Section 10.3.1 for further details). Periglacial conditions are characterised by lower air temperatures and the development of permafrost and frozen bedrock. Effects of the presence/absence of a discharge talik are examined via two separate variants of the *cold climate calculation case*, namely the *continuous permafrost* variant without talik and the *permafrost with talik* variant. The same organisms as in the *base case* are assessed in the cold climate. However, limnic amphibians and mammals, and terrestrial trees, gastropods, amphibians, reptiles, and annelids may not be viable, and might no longer be present at the site in a cold climate (Jaeschke et al. 2013).

In both variants of the *cold climate calculation case* dose rates are identical to those in the *base case* in the first temperate period (before 61 000 AD), and the maximum dose rates (in object 157_2) are similar also in the second temperate period. However, during the periglacial periods (61 000 to 69 000 AD and 81 000 AD to 102 000 AD), the dose rates drop, because of lower activity concentrations in environmental media in a cold climate.

12.6.1 Continuous permafrost variant

During the two periglacial periods, the dose rates to all organisms (aquatic and terrestrial) decrease. The dose rates to the most exposed organisms decrease by up to a factor of five at the end of the first periglacial period, and the corresponding decrease is almost an order of a magnitude at the end of the second periglacial period (blue lines in Figure 12-5). However, by this stage, the dose rates are significantly lower than the maximum rates (solid black line in Figure 12-5), thus the decreases have no impact on the radiological consequences to non-human biota. Between the periglacial periods, the dose rates return to the corresponding rate in the *base case*. The pattern is very similar in the terrestrial ecosystem, though the dose rates are somewhat lower to these organisms.

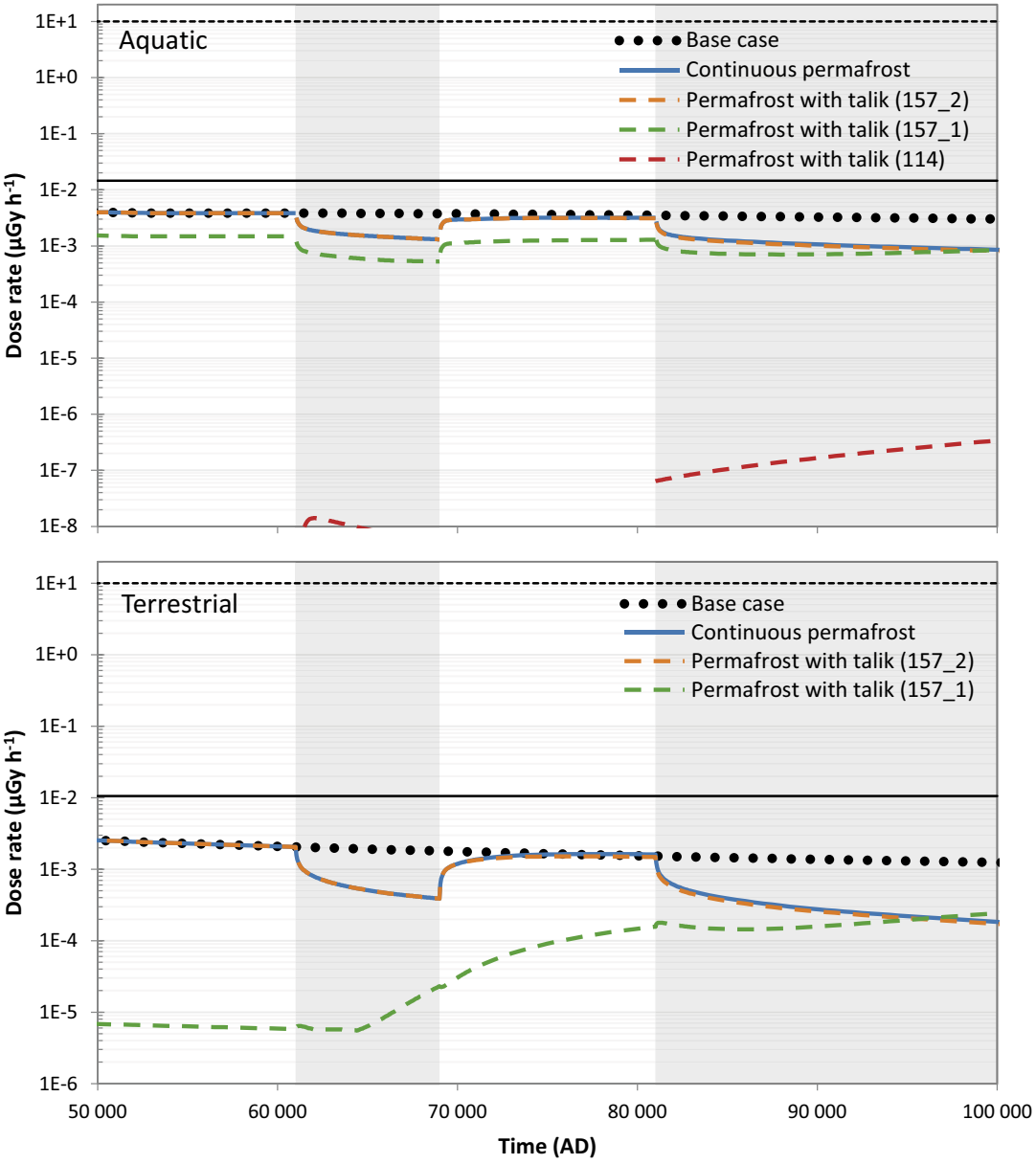

Figure 12-5. *Dose rates to aquatic organisms (top) and terrestrial organisms (bottom) in the cold climate calculation case. Colours and line styles are used to differentiate between the two variants (continuous permafrost and permafrost with talik) and between biosphere objects within the permafrost with talik variant (i.e. objects 157_2, 157_1 and 114). Periglacial periods are indicated by the light grey shaded areas. The maximum dose rate from the temperate period (solid black line) and the dose rate from the base case (dotted black line) are shown for reference. The upmost, fully horizontal dashed line indicates the screening dose rate (10 µGy h^{-1}). Note that the time scale is linear (unlike in most of the other figures in this report) and that the dose rates are shown on different scales for aquatic and terrestrial organisms respectively.*

The dynamics of the dose rates are similar in the aquatic and terrestrial ecosystems. The decreased rates in the periglacial period reflect the consideration that biosphere object 157_2 is isolated from the geosphere release by permafrost, and thus the environmental concentrations decrease as accumulated radionuclides leach out from the object. In the subsequent temperate period, environmental concentrations return to steady-state conditions as the geosphere release is re-established, and the pattern is repeated in the second periglacial period.

12.6.2 Permafrost with talik variant

In the *permafrost with talik variant*, object 157_2 is again isolated from the geosphere release by permafrost. Instead, groundwater from the repository is assumed to reach the surface system via a discharge talik under a large lake (object 114) or a mire formed in a small lake basin (object 157_1).

For aquatic organisms the dose rate from the stream in object 157_2 is always higher than the dose rates from the aquatic ecosystems above a discharge talik. Thus, the highest dose rates from this variant are near identical with that from the *continuous permafrost variant* (orange dashed line on top of blue solid line in left panel of Figure 12-5).

It can be noted that dose rates to aquatic organisms in the stream in object 157_1 are consistently lower than in the running water of the up-stream object 157_2. This is because it takes time for radionuclides released to the bottom of a talik to reach the surface of object 157_1, which has a thick regolith layer as compared with object 157_2 (Figure 5-6). For most of the time, the dose rates in 157_1 simply reflect the radionuclides received with streaming water from object 157_2, diluted with the additional runoff from the sub-catchment of object 157_1. The exception to this is at the end of the second periglacial period when radionuclides released to the talik contribute significantly to the dose rates; at this time the dose rates in the stream in object 157_1 are similar to those in the up-stream water.

Geosphere release to a large future lake during periglacial periods yields dose rates that are many orders of magnitude below those in the other aquatic ecosystems (Figure 12-5, upper panel). This is expected as object 114 is projected to be among the last lakes in the main river valley of Forsmark, and consequently its catchment is much larger than those of biosphere objects 157_1 and 157_2 (see Section 5.5).

For terrestrial organisms, the dose rates from the mire in object 157_2 are higher than the dose rates from the mire talik in object 157_1 (Figure 12-5, lower panel). However, radionuclides released during the first periglacial period are transported up through the regolith layers in the mires of object 157_1 during the temperate period. Activity concentrations keep building up in surface peat during the second periglacial period, and at the end of the assessment, dose rates in the mire talik exceeds those in up-stream object (green dashed line in lower panel of Figure 12-5).

12.7 Alternative delineation calculation case

In this supporting calculation case, the sensitivity of dose to variations in the outline of the biosphere object 157_2 is examined. Several characteristics of the biosphere objects have significant influence on the transport and accumulation of radionuclides. Thus, to illustrate how the size, position and properties of the biosphere object may affect environmental concentrations and resulting dose rates, four alternative delineations of biosphere object 157_2 are used in the PSAR (Section 11.2). In the calculations, a simplified version of the BioTEx model was used, and marine ecosystems are not included in the assessment. The maximum dose rates from this simplified model (labelled *reference* in Table 12-1) are similar to those from the *base case* (Ter in Tables 12-1) (See also Section 11.3.2). Nevertheless, for consistency with the analysis of doses to humans, results from the alternative delineations are expressed relative to those in the *reference* variant.

The *reference* variant, which is delineated to resemble the original biosphere object 157_2, results in a similar maximum terrestrial dose rate (1.13×10^{-2} μGy h^{-1}, Lichen & Bryophytes, 7900 AD), but a somewhat higher maximum aquatic dose rate (2.72×10^{-2} μGy h^{-1}, marine Bird, 3500 AD) when compared with the corresponding maximum values in the *base case*.

Despite higher dose rates, compared with the calculation cases in the main scenario, none of the dose rates to organisms exceed the screening dose rate (10 μGy h^{-1}); the highest dose rate remained over two orders of magnitude lower than this level. Therefore, no significant radiological impact to NHB is anticipated under any of the alternate delineation variants.

Of the four alternatively delineations of object 157_2, the *Wetland areas (Wetl)* is considered of particular interest, as it reflects the habitat of protected species in Forsmark, namely the pool frog and the fen orchid. The lowest lying area *(Agri)* is also the smallest area (~3 ha) and covers approximately one fifth of the original object. This part of the original object also has relatively thick post-glacial deposits (Figure 11-4). The highest altitude area *(Uphill)*, is also relatively small (i.e. approximately one third of the original object) and has catchment that is about half of that in the original object (and in all other delineations). Consequently, the effects of water dilution in surface peat and stream water are notably lower in this variant.

In the aquatic system, the two variants with the smallest areas have the largest dose rates. That is, the *Agri* and the *Uphill* variants have dose rates that are approximately three times higher than in the *reference* variant (Figure 12-6, left panel). Bird and Microphytobenthos are the most exposed organisms, and maximum dose rates (mostly from C-14) occur when the object has just emerged (Table 12-1). The elevated dose rates are due to a decreased degassing of C-14 in the mire, prior to transport into the stream. In the *Uphill variant* less runoff from a smaller catchment also contributes to elevate the dose rates. Dose rates to Phytoplankton (mostly from Pu-239) in the *Uphill* variant are somewhat elevated also around 50 000 AD; at this time, the dose rates are about 50 % above the corresponding rates in the *reference* variant. Moreover, it can be noted that the maximum dose rates (which are predominantly from C-14) in the *Wetland areas* variant are 50 % larger than those in the *reference* variant (Figure 12-6, Table 12-1).

In all variants, the highest dose rates in the terrestrial ecosystem occur a few thousand years after emergence (~7000 AD), or later, in Lichen & Bryophytes (Figure 12-6, right panel). In each variant, U-238 contributes most to the maximum dose rates (Table 12-1), with additional contribution from U-235 (data not shown). Differences in dose rates between the variants primarily reflect differences in the catchment area, which generates most of the water that dilutes radionuclides in surface peat. Thus, the dose rates in the *Uphill* variant are approximately three times higher than in the *reference* variant, which in turn is similar to those in the *Wetland* and *Upward gradient* variants. In addition, transport rates affect environmental concentrations and dose rates. Thus, in the *Uphill* variant with the fastest transport, the increase in the maximum dose rate is somewhat higher than expected from the differences in the catchment area (i.e. a factor of two). In the *Agri* variant, with the slowest transport rates, elevated dose rates appear significantly later than in the *reference* variant. The *Agri* variant has the same catchment area as the *reference*, and it is instead the retention in the regolith profile that lowers the maximum dose rates by ~30 %, as compared with the *reference* variant. That is, the prolonged transport time extends the release and flattens out the geosphere release peak.

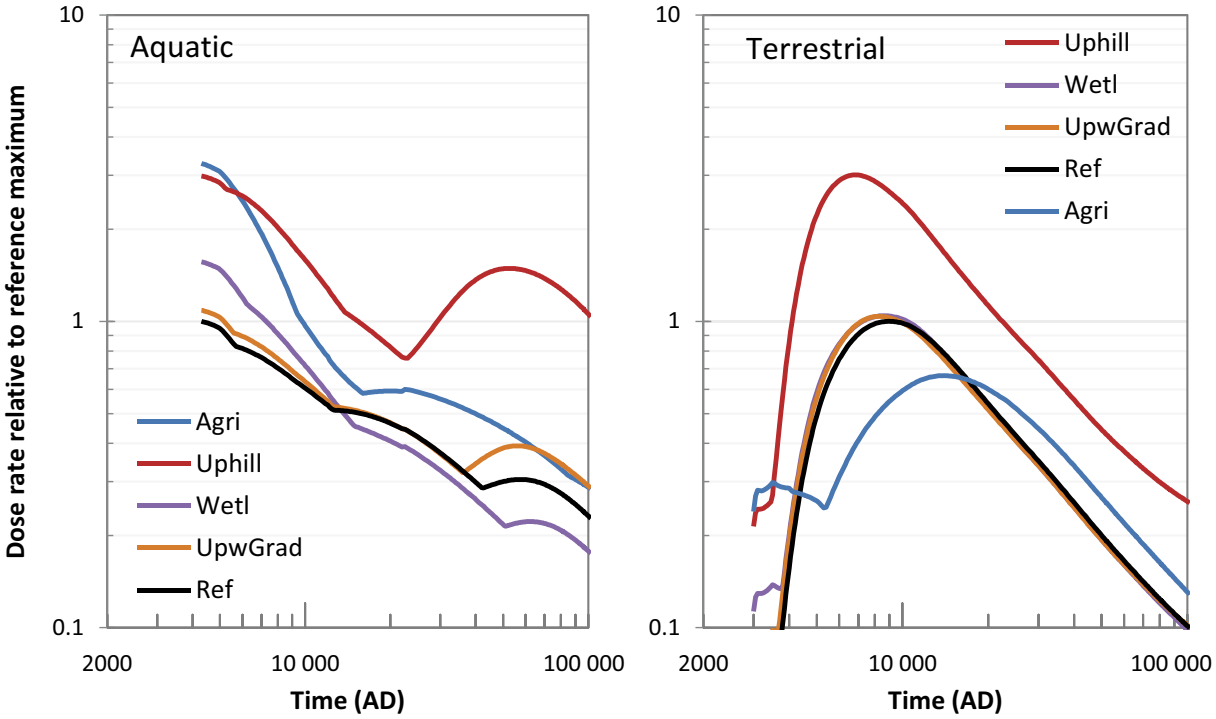

Figure 12-6. *Dose rates to the most exposed organisms (varying over time) (aquatic on the left, terrestrial on the right) relative to the maximum dose rate in the original outline ("Ref") after the emergence of the biosphere object, under different alternate delineation variants. Aquatic organisms are shown on the left, terrestrial organisms on the right. "Agri" = most suitable arable land variant; "Uphill" = uphill area with a high density of discharged particles variant; "Wetl" = wetland areas variant; "UpwGrad" = areas with upward hydraulic gradients variant; "Ref" = reference variance corresponding to the original outline of object 157_2.*

Table 12-1. The maximum dose rates to non-human biota found in the five variants in the *alternative delineation calculation case*. For each variant, data for the relevant aquatic and terrestrial ecosystems are given.

Calculation case variant	Ecosystem	Time of maximum (year AD)	Organism type	Maximum dose rate (μGy h^{-1})	Key radionuclide (contribution to dose rate)
Most suitable arable land (*Agri*)	Aqu	4300	Bird	4.7×10^{-2}	C-14 (100 %)
	Ter	14 000	Lichen & Bryophytes	6.9×10^{-3}	U-238 (61 %)
Uphill area with a high density of discharged particles (*Uphill*)	Aqu	4300	Bird	4.2×10^{-2}	C-14 (98 %)
	Ter	6800	Lichen & Bryophytes	3.1×10^{-2}	U-238 (70 %)
Wetland areas (*Wetl*)	Aqu	4300	Bird	2.2×10^{-2}	C-14 (99 %)
	Ter	8600	Lichen & Bryophytes	1.1×10^{-2}	U-238 (67 %)
Areas with upward hydraulic gradients (*UpwGrad*)	Aqu	4300	Bird	1.5×10^{-2}	C-14 (99 %)
	Ter	8300	Lichen & Bryophytes	1.1×10^{-2}	U-238 (68 %)
Reference (*Ref*)	Aqu	4300	Bird	1.4×10^{-2}	C-14 (99 %)
	Ter	9000	Lichen & Bryophytes	1.0×10^{-2}	U-238 (67 %)

12.8 Summary and conclusions

In all calculation cases, the maximum dose rates are three orders of magnitude below the ERICA screening dose rate (10 μGy h^{-1}) and occur relatively early in the assessment period (Table 12-1 and Table 12-2). Furthermore, all dose rates are considerably below the lower boundary of the most restrictive ICRP DCRL (4 μGy h^{-1}; which only applies to certain vertebrate animals and coniferous trees). Therefore, it is not anticipated that populations of non-human biota will be significantly negatively impacted by radionuclides released from the repository, under any of the assessed scenarios.

In the aquatic system, C-14 dominates the maximum dose rate, and it arises at the time when the biosphere object is first fully emerged from the sea. In the terrestrial system, uranium isotopes (or their decay products) contribute most to the dose rates, and the maximum rates typically occur several thousands of years after the emergence. Freshwater Bird and Lichen & Bryophytes are the most exposed organisms in aquatic and terrestrial ecosystems, respectively, except for the aquatic environment under the *low summer precipitation* variant of the *warm climate calculation case* where Reptile was slightly more exposed than the Bird.

The variants of the *warm climate calculation case* result in later maximum dose rates relative to those in the *base case* because of the delayed emergence of the biosphere object. The dose rates to organisms in the *high summer precipitation* variant are lower than those of the *base case*. The dry conditions in the *low summer precipitation* variant lead to somewhat larger dose rates, but the increase is limited to ~10 % for aquatic organisms and ~60 % for terrestrial organisms.

The dose rates during periglacial conditions in both variants of the *cold climate calculation case* are significantly lower than the dose rates in the *base case* for corresponding periods. These drops in dose rate occur for all organisms in both ecosystem, and are most pronounced in the lake talik of the *permafrost with talik variant*. However, as they occur late in the assessment period, when dose rates already have decreased, they have no significance for the maximum dose rates over the assessment period.

The *alternate delineation calculation case*, which is a supporting calculation case in the *base case* of the main scenario, shows that dose rates to aquatic organisms may increase by a factor of three if radionuclides from SFR are released to an area that is a factor of five smaller than the original biosphere object. The dose rates to terrestrial organisms are less sensitive to the size of the discharge area. However, in the *Uphill* variant, which has a smaller catchment, dose rates may increase by a factor of two. The difference in sensitivity to a change in object properties between aquatic and terrestrial ecosystems is due to the transport behaviour of the dose rate contributing radionuclides (i.e. C-14 and uranium isotopes, respectively). Regardless of sensitivities, the resultant dose rates remain well below the screening value.

An internal study following SR-PSU (Jaeschke and Grolander 2017) explored the modulation of dose rates with affected area. The study indicated that in order for dose rates to reach a level of concern, the radionuclide releases from the geosphere would have to be limited to a surface area of 40 × 40 m, which would have extremely limited relevance for most if not all populations of non-human biota at the site. For wider context, the IAEA proposed a reference area of 100 – 400 km^2 around nuclear facilities for general assessments of impact to non-human biota, based on typical annual distributions of wind direction, and the direction of water flows in rivers, lakes and oceans (IAEA 2018). The justification of the scale of the reference area was that it was "*sufficiently large to ensure that mixing of the effluents with the environmental media occurs and that the number of individuals of the species considered in the assessment is suitably large.*". The delineations included in the present assessment are of the range 0.03–0.15 km^2, significantly smaller than the IAEA reference area. While issues of mixing are not a concern in this context, the number of individuals of each relevant population that may be affected, within the very small delineations of the assessment area, can be expected to be very limited. This means that the proportion of the population impacted by radiation within the assessment area will be equally limited, and thus the radiological impact to the overall population could be significantly less than indicated by the present assessment, which cautiously assumes the whole population is present within the assessment area.

Compared with the margin between the calculated dose rates and the levels of potential concern, the dose rates are relatively insensitive to the postulated span in climate conditions and object properties. Overall, the conclusion of an insignificant negative impact on the non-human biota is considered to be robust with respect to uncertainties in the future climate and the development of the landscape.

Table 12-2. Summary of information relating to the maximum dose rates to non-human biota found in the *base case*, the *warm climate calculation case*, and the *cold climate calculation case*. For each calculation case, data for the most exposed aquatic (always freshwater) and terrestrial organism are listed. Note that for the *cold climate calculation case* only dose rates during periglacial conditions are considered here.

Calculation cases	Ecosystem	Time of maximum (year AD)	Organism type	Maximum dose rate (μGy h^{-1})	Key radionuclide (contribution to dose rate)
Base case	Aqu	4300[a]	Bird	1.5×10^{-2}	C-14 (99 %)
	Ter	10 000	Lichen & Bryophytes	1.1×10^{-2}	U-238 (66 %)
Warm climate (high summer precipitation)	Aqu	7800[a]	Bird	9.9×10^{-3}	C-14 (99 %)
	Ter	14 600	Lichen & Bryophytes	1.2×10^{-2}	U-238 (65 %)
Warm climate (low summer precipitation)	Aqu	28 000	Reptile	1.6×10^{-2}	Ac-227 (84 %)
	Ter	16 800	Lichen & Bryophytes	1.6×10^{-2}	U-238 (63 %)
Cold climate (continuous permafrost)	Aqu	61 000[b]	Insect larvae	3.2×10^{-3}	Ac-227 (63 %)
	Ter	61 000[b]	Lichen & Bryophytes	1.6×10^{-3}	U-238 (37 %), U-235 (37 %)
Cold climate (permafrost with talik)	Aqu (Talik[e])	102 000[c]	Insect larvae	3.9×10^{-7}	Ac-227 (59 %), U-238 (23 %)
	Ter (Talik[f])	102 000[c]	Annelid[d]	2.6×10^{-4}	Ac-227 (52 %), U-235 (17 %), U-238 (15 %)

a) Year of emergence.

b) Start of first assessed periglacial period.

c) Last year of assessed periglacial period.

d) The corresponding values for Lichens and Bryophytes which persist in cold conditions are 2.4×10^{-4} with 33 % and 32 % contribution from U-235 and U-238, respectively.

e) Lake in biosphere object 114.

f) Mire in biosphere object 157_1.

13 Summary, discussion of uncertainties and conclusions

13.1 Introduction

The main role of the post-closure safety assessment, documented in the **Post-closure safety report**, is to demonstrate that SFR is radiologically safe for humans and the environment after closure. This is done by evaluating compliance with respect to the Swedish Radiation Safety Authority's regulations concerning post-closure safety and the protection of human health and the environment (Section 1.2). Such an evaluation depends on calculations describing dispersion of radionuclides in the environment, and the purpose of the biosphere assessment of the PSAR is thus to allow a quantitative evaluation of potential radiological impacts from projected releases from SFR. The intention is not to simulate conditions that will necessarily be present in the future, but to capture the main features of transport, accumulation and exposure for a suite of possible future conditions. The level of detail and most assumptions underlying the biosphere model used in the PSAR are based on the SR-PSU biosphere assessment (SKB TR-14-06).

The BioTEx model has proven to be useful through experience (SKB TR-14-06) and the data used for the parametrisation are, as far as possible, derived from the site investigation programme. The model setup used in SR-PSU has been considered to give a good description of the biosphere system and to yield reasonable results (e.g. SSM 2019). In Chapter 9 the outcome from the BioTEx model in the *base case* is analysed in detail. Differences in transport and accumulation patterns of individual radionuclides are highlighted and explained in terms of radionuclide-specific properties. The analysis confirms that the model behaviour is reasonable and conforms with SKB's general understanding of the surface systems at Forsmark.

An evaluation of potential radiological consequences far into the future is inevitably associated with large uncertainties. Handling of uncertainties is thus an integral part of a safety assessment (Section 2.3.9), and this chapter therefore discusses uncertainties and their potential impact on the results of the performed calculations. Following the overall methodology applied for the post-closure safety assessment in the PSAR, uncertainties are categorised into four broad classes (**Post-closure safety report**, Section 2.5). This chapter is structured accordingly, and *System uncertainty*, *Scenario uncertainty*, *Modelling uncertainty* and *Data uncertainty* are discussed in the first four sections below. All four categories of uncertainty contain elements of epistemic (i.e. knowledge-based and reducible) and aleatory (i.e. random in nature and irreducible) uncertainties, and a particular aspect of uncertainty could fall within more than one of the categories. In addition, assumptions and reliability with respects to the two radionuclides that contribute substantially to dose relatively early in the assessment (C-14 and Mo-93) are discussed in some detail. Finally, the uncertainties from all calculation cases are brought together and discussed. In the light of the examined uncertainties, it is concluded that the *base case* representation of the surface system is appropriate and that the results from this calculation case are robust with respect to the examined uncertainties.

13.2 System uncertainty

System uncertainty concerns comprehensiveness issues, i.e. if all relevant features, events and processes (FEPs) have been identified and included in a satisfactory manner in the analysis. The handling of uncertainties with respect to potentially exposed groups (PEGs) are also discussed in this section.

13.2.1 Handling of potentially safety-relevant biosphere FEPs

Handling of FEPs is an integrated part of SKBs ongoing work to improve the biosphere assessment methodology. Many relevant FEPs are included as components and/or processes in the BioTEx model (Saetre et al. 2013a, Appendix E). Other FEPs are accounted for in the derivation of parameter values for the model or by making cautious assumptions. The mapping of FEPs to different modelling activities in the safety assessment and the check against internationally identified FEPs (Chapter 6) demonstrate that relevant FEPs are included and represented in the PSAR assessment.

13.2.2 Land use and exposure of future human inhabitants

The uncertainties with respect to the degree to which future humans will inhabit and/or utilise natural resources in the biosphere object have been handled according to Swedish regulations (SSM 2008a) and in line with U.S. and international standards and guidance (e.g. ATSDR 2005, ICRP 2006) That is, the assigned characteristics and habits of the PEGs are reasonable and sustainable with respect to physical constraints of the landscape, to human needs for nutrients and energy, and to present and/or historical land use.

The PEGs used in the evaluation are based on a comprehensive review of exposure pathways (Chapter 6). Land-use variants that resulted in relatively high exposure, and the associated PEGs, have primarily been identified from historical self-sustainable communities (Saetre et al. 2013b). By evaluating a variety of PEGs, all with habits that lead to relatively large exposures, uncertainties in the extent of the use of natural resources by humans are considered to be adequately covered.

The PEGs used in the PSAR are described in SKB (R-14-02, Section 3.4), and all parameters for food intake and exposure times are justified in Chapter 10 of Grolander (2013). Below is a short summary of the assumptions underlying the characteristics of these groups. This partly builds on a more detailed discussion provided as supplementary material in SR-PSU (Saetre and Lindgren 2017).

Drained mire farmer

Draining and cultivation of a mire in the discharge area is the land use that causes the highest dose. This is primarily because radionuclides can accumulate in peat over a long period prior to exposure, and because the dose-contributing radionuclides primarily yield dose through ingestion of food. The handling of this land use in the biosphere evaluation is cautious, as the effect of cultivation is evaluated at all possible times without accounting for the probability that the mire has already been drained (which would decrease the potential for long-term accumulation)[59]. Assessing long-term accumulation in mires is also cautious with respect to mire succession. That is, fens are expected to be succeeded by ombrotrophic bogs, where the raised bog plain is expected to decrease the influence of discharging groundwater (Charman 2002).

Also, given the geosphere release and the time to reach equilibrium for C-14 and Mo-93, these simplifying assumptions are considered to be reasonable for the maximum dose. That is, the residence time for C-14 is very short, and the same results would have been achieved by assuming that a fen is present at the time for the maximum dose. For Mo-93, maximum environmental concentrations are reached within the first 4 000 years after emergence, and this time is similar to the residence time for Mo-93. Undisturbed fens of age up to 3 000 years are presently observed in the region (North Uppland; Schoning 2014), and the average age of fens (as indicated by Carex/Sedge/Bryales peat) that have been drained and cultivated in the area is similar (3 100 years, Sohlenius et al. 2013c). Thus, the cautious simplifications of undisturbed accumulation are fit for purpose.

In the PSAR, cultivation of a drained mire is evaluated from the time when the highest point in the object is 1 m above sea level (~3200 AD). In the transitional period, saltwater intrusion is not considered to limit cultivation. Given the relative fast change in sea level postulated in the *base case* (Chapter 9), the emerged land area can fully support the DM farmers around 4000 AD, which is approximately 500 years earlier than when cultivation of a drained mire was first considered to occur in SR-PSU. The adjusted start of cultivation considered in the PSAR allows for a more robust assessment of C-14, as this pathway is not ruled out early in the assessment when the geosphere release is expected to be relatively high.

[59] Doses from the drained mire can only persist over a few generations as the drained peat soils subside and conditions for cultivation deteriorate (Sohlenius et al. 2013c, Chapter 3). Thus, the expectation value of dose to an individual living in the vicinity of the mire at a predefined time in the future is less than the expectation value of dose to an individual living at the unknown time at which the mire has just been drained.

Infield–outland agriculture

The key principle behind the agrarian infield-outland system is to fertilise arable land with nutrients from outlands (nearby pastures and forests), using animal manure as organic fertiliser. For this land-use variant, radionuclides in wetland hay reach the cultivated soil through fertilisation with manure, and thus accumulate over time in arable infields. In SR-PSU, a steady-state solution was used to evaluate the accumulation of radionuclides due to the use of animal manure as organic fertiliser. For strongly sorbing radionuclides with a long half-life (e.g. Cs-135), this approach is pessimistic, as the times required to reach steady-state is very long.

Inorganic soils have the potential for sustainable cultivation for long periods of time, and in the PSAR, it is assumed that radionuclides from wetland hay will accumulate for a period of 500 years (Section 7.5.2). This is still a cautious assumption, as continuous haymaking will deplete wetlands of nutrients, and wetland haymaking is likely to be sustainable on a timescale of decades rather than centuries (Kardell 2018). As the annual dose from infield-outland farming never exceeds that from a drained mire, this cautious assumption does not affect the evaluation of the repository safety. If this exposure pathway were to result in a dose similar to (or higher than) that of drained mire farming, a more thorough substantiation of the assumptions with respect to the sustainable use of wetland hay would be warranted.

Garden plot household

The potentially exposed group that uses a kitchen garden was introduced by SKB to evaluate doses that may result from a number of exposure routes that are not covered by the other groups. These include small-scale irrigation and fertilization with algae or ash from biofuel. Large-scale irrigation is rare in Sweden today and it is mainly areas cultivated with potatoes and horticultural products that are irrigated, whereas irrigation of serials is rare, algal and ash production originating from object 157_2 is considered to be insufficient for fertilization on the scale of self-sufficient agriculture (~5 hectare) (see Sections 3.4 and 5.1 in SKB R-14-02 for a quantitative discussion).

The postulated small-scale utilisation of the environment and natural resources is considered to be compatible with present-day practice in Sweden. Thus, parameters describing combustion, fertilization and irrigation reflect small-scale energy utilisation and cultivation under current conditions. For consistency, the intake of potatoes and vegetables reflects a typical contemporary Swedish diet (Wikberger and Johansson 2006). If this group consumed more vegetables and tubers, the potential exposure could be higher than with the postulated consumption. SKB has chosen to avoid undue cautiousness by not combining extreme patterns of consumption with the requirement that the most exposed group has a high degree of utilisation of natural resources from the area with the highest concentration of radionuclides. This is in accordance with the BIOMASS methodology (IAEA 2003, Lindborg 2018, Lindborg et al. 2022).

In the *base case*, the exposure pathway resulting in the highest dose for the garden plot is related to fertilization with peat ash. For this group, it is assumed that all ash from the combustion of peat (which corresponds to a household's energy needs for heating) is used to fertilize the kitchen garden. The size of the kitchen garden corresponds to the area needed to support the group with the postulated fraction of potatoes and vegetables. If consumption rates are assumed to be two times higher this would require a two times larger kitchen garden. The rate of fertilization (per square metre), and the concentration in soil and plants, would then be reduced by a factor of two. Thus, for the dominant pathway the dose calculations are insensitive to the assumptions of the intake of crops from the garden plot.

Hunter-gatherers

For hunter-gatherers no explicit assumptions about the composition of the diet are made. As the productivity of fish, game, berries and mushrooms is low, it is instead assumed that the group eats all food produced in the areas affected by the release from the repository; that is, objects 157_1, 157_2, 159, and object 116 when the landscape is below sea level, and objects 157_2, 157_1 and 116 when the landscape has emerged above sea level (see Section 9.3 in Saetre et al. 2013a).

In the terrestrial period, the dietary fraction for a food item is proportional to the size and productivity of the area, and inversely proportional to the selected group size (Equation 9-22 in Saetre et al. 2013b). Accounting for the productivity of the landscape when characterizing the most exposed group follows SKB's previous methodology (in SR-Site) and is supported by IAEA's advice for analysis of radiation safety (IAEA 2012).

The productivity in natural ecosystems have been estimated from data collected in Forsmark (Grolander 2013). The group size of hunter-gatherers has been selected as 30 individuals, based on an extensive compilation of historical ethnological data (Marlow 2005). This number corresponds to a typical (median) size for a family group of hunter-gatherers, and is also the expected size of such a group given the area-specific standing biomass in the terrestrial ecosystems of Forsmark (Grolander 2013, Section 10.10). Thus, the assumptions made are reasonable and well founded in ethnological observations and the characteristics of ecosystems in Forsmark.

Exposure from a drilled well

The method to evaluate exposure from a drilled well has been updated in the PSAR. The well is now considered to be located in the bedrock of the area where groundwater has the highest concentrations of radionuclides from SFR (Section 5.6). The probability of drilling a well in this area is set to unity, and the exposed group utilizing the drilled well is considered to be small (Section 7.5.4). This means that the applicable risk criterion is 10 times larger than the regular risk criterion. Uncertainties in the fraction of the release that reaches the well are accounted for in probabilistic calculations (Section 8.2.4). As in SR-PSU, well water is used to irrigate a kitchen garden. In the PSAR, the process of translocation of radionuclides intercepted on leaves to edible parts is now accounted for (Section 7.5.3), and the interval between irrigation events is shortened (Section 8.2.2)[60]. The overall effect of these updates is a systematic, but limited, increase in the dose from the drilled well as compared with SR-PSU (Appendix C)[61].

The methodological updates, with respect to the exclusion of the probability of drilling a well and the handling of the uncertainties in the release reaching the well, make the calculations more consistent with the handling of exposure pathways within the biosphere object (e.g. a dug well). The updates relating to irrigation are considered to make the exposure calculations more comprehensive and robust. All these changes are intended to be in line with comments and recommendations given by SSM in the review of SR-PSU and SAR-08 with respect to exposure from a drilled well.

13.3 Scenario uncertainty

Scenario uncertainty typically refers to uncertainties associated with significant changes over time with respect to external and internal biosphere conditions. This includes uncertainties in the response to large-scale climate change, landscape development and long-term changes in the chemical environment. In general, scenario uncertainties contain a larger element of aleatory (i.e. irreducible) uncertainty than the other uncertainty classes.

13.3.1 Large-scale climate changes

In the PSAR, the uncertainty of future climate is handled by using three variants of reference external conditions, namely: the *present-day climate variant*, the *warm climate variant* and the *cold climate variant*. Collectively, these variants define the range of probable climate evolutions at Forsmark over the next 100 000 years (Section 4.1). These three variants are then used as basis for three calculation cases: the *base case*, the *warm climate calculation case* and the *cold climate calculation case*, where

[60] Translocation is accounted for irrespective of the source of irrigation.

[61] This statement refers to margin between the calculated dose and the dose criterion corresponding to a small group. In absolute terms the annual dose and the risk criterion has increased by an order of magnitude as compared with SR-PSU.

the *base case* is the reference point for all calculations. In this case, temperate climatic conditions (similar to those at the present day) are assumed to prevail for the full assessment period, and ecosystems gradually transform from submerged to terrestrial conditions (see Section 9.2).

The warm climate calculation case

In the *warm climate calculation case* anthropogenic greenhouse gas emissions comparable to present levels are assumed to continue for the next few decades, followed by a gradual decline towards net-zero emissions by the beginning of the 22nd century (Section 10.2). The local mean annual air temperature is assumed to increase by a maximum of 5 °C above the present value within the current millennium, and the annual potential evapotranspiration is expected to increase by more than 30 %. Moreover, annual precipitation is projected to increase by ~10–20 % relative to present day but the precipitation during the summer months (June to August) may either increase or decrease. Taken together, these changes are expected to reduce runoff and groundwater discharge and to increase the water deficit for cultivated crops. For simplicity, the maximum changes in air temperature, precipitation and potential evapotranspiration are assumed to persist for the entire assessment period.

The effects of a decrease in groundwater discharge in combination with an increased crop water demand are expected to increase the dose from mobile radionuclides. This response is partly evident in the doses from C-14. However, the maximum dose in the *warm climate calculation case* is lower than that in the *base case*. In a warmer climate, increased melting of land-based ice sheets and thermal expansion of sea-water are expected to result in a prolonged submerged period with limited groundwater flows. As a result, the releases of C-14 and Mo-93 from the geosphere are delayed with respect to the *base case*, and thus their activities are reduced by radioactive decay.

The postulated changes in the biosphere associated with a warmer climate increase doses from Ca-41 and Ni-59 during the period subsequent to the dose maximum (i.e. after 20 000 AD). However, this increase is modest (approximately a factor of two) and the dose during this period does not exceed the maximum dose in the *base case*.

The calculated doses are insensitive to assumptions of irrigation, as radionuclide accumulation prior to drainage and cultivation is found to be a more important source of activity in crops than import with water during cultivation. The dose from C-14 is an exception to this pattern. However, in this case, irrigation with surface water results in a lower dose than if the plant water deficit is satisfied by plant uptake of groundwater. Finally, it is noted that the effects of translocation of activity intercepted on leaves to edible parts of crops is insignificant for the radionuclides that contributes most to dose.

The *warm climate calculation case* is considered to adequately address relevant effects of a warmer climate, considering changes in the sea level, atmospheric CO_2 concentrations, plant and crop production, surface hydrology and the additional effects of large-scale irrigation and plant translocation. The results are reasonable given the delayed emergence and in line with the response in the sensitivity analyses of temperate conditions (e.g. effects of groundwater uptake on C-14 dose and of net precipitation on Ca-41 in Sections 11.2 and 11.4).

If emissions of greenhouse gases were to accelerate in the future, more extreme changes in the climate are to be expected, with potential implications for sea levels, the groundwater system and the feasibility of specific agricultural practices.

The cold climate calculation case

In the *cold climate calculation case*, external conditions at Forsmark are characterised by two periods of periglacial conditions during the second half of the assessment period (Section 10.3). In these periods the air temperatures are considerably lower than at present, resulting in the development of permafrost and frozen bedrock conditions. Given the uncertainty in the air temperatures in these periods, two variants with different permafrost coverage are considered. In the *continuous permafrost* variant, the geosphere releases to the biosphere system cease during periglacial periods and in the *permafrost with talik* variant they are routed through a discharge talik to either a mire (object 157_1) or a lake (object 114) ecosystem.

The main result, for both variants, is that doses are at least an order of magnitude lower during periglacial periods than in the *base case* at the corresponding time. The main reason is that the only possible exposure pathway during this time is related to hunting and gathering and this generally results in lower doses than cultivation and well water usage. Consequently, the highest annual doses during periglacial periods after 60 000 AD are at least two orders of magnitude below the maximum doses in the *base case* that occur around 7000 AD (see Section 9.3). Despite the different transport pathways between the *continuous permafrost* and the *permafrost with talik* variants during periglacial periods, the doses are relatively similar. The reason is that the doses in both variants are dominated by radionuclides accumulated in object 157_2 during the temperate periods *before* periglacial periods. The dose contribution from radionuclides released through the talik in object 157_1 is limited until near the end of the second periglacial period. Furthermore, accumulation due to ingrowth in the near-field and geosphere during *continuous permafrost* conditions did not result in doses that exceeded the dose in the *base case* during the temperate period after the periglacial period.

The *cold climate calculation case* is considered to adequately address relevant effects of a colder climate, considering changes in atmospheric CO_2 concentrations and surface hydrology, reduced production of lake and mire ecosystems and exclusion of cultivation and well water extraction. The results are reasonable given doses from similar exposure pathways in temperate conditions and the transport times required for accumulation at the surface. The results are also consistent with SKB's general understanding about how the conditions in the bedrock and surface systems will change in a periglacial climate and influence annual doses.

13.3.2 Landscape development

The future landscape in Forsmark will develop in response to the regression of the shoreline, the erosion and deposition of regolith layers and the succession of ecosystems. The potential effects of uncertainties in the shoreline regression are discussed below, and references are given to sections where the potential effects of uncertainties in other aspects of the landscape development are discussed.

Timing of shoreline regression

When the area above SFR emerges out of the sea, groundwater flow rates in the near-field, geosphere, and biosphere system will increase. Thus, if the shoreline regression is delayed, the transport of radionuclides to the surface ecosystems will also be delayed and modified as compared with the *base case*. The uncertainty in projected global sea-level rise over the coming millennia is large, ranging from a couple of metres to more than 50 m. At Forsmark, this uncertainty translates to between 1 300 and 18 300 years of initial submerged conditions above the repository. The *base case* and the *warm climate calculation case* cover the lower region of this range. The *timing of shoreline regression calculation case* covers the remaining uncertainty by postulating a delay of 3 500, 5 000, 10 000, 15 000 and 20 000 years in the shoreline regression relative to the *base case* (Section 10.4).

A longer submerged period than in the *base case* results in lower maximum total annual doses, and those doses will occur at later times. The decrease is mainly a consequence of more radioactive decay in the near-field of the radionuclides that contribute most to the maximum dose in the *base case* (Mo-93 and C-14), as they are retained in the near-field due to slower transport during the prolonged submerged period. Maximum near-field and geosphere releases of radionuclides with longer half-lives, like Ca-41, can increase with a longer submerged period and result in higher maximum radionuclide-specific doses. However, such increases of radionuclide-specific doses are limited and maximum total doses do not exceed the maximum dose in the *base case*. In conclusion, the assumption of a relatively short submerged period in the *base case* is somewhat cautious, as using longer and more realistic submerged periods results in lower maximum annual doses.

Other aspects of landscape development

The main features of the Forsmark landscape are determined by the bedrock topography, which is expected to change only marginally over the next 100 000 years. However, wave erosion, sedimentation, and mire formation will affect the regolith stratigraphy overlying the bedrock, as well as the related dynamics. In the PSAR, as in previous safety assessments, the expected development of regolith layers

and the associated ecosystem succession have been described deterministically with the regolith-lake development model (Section 4.7.1). Despite the persistence of the large-scale topography, the outcomes from landscape development models are intrinsically uncertain. This is true, for example, with respect to the presence and development of lakes and streams and the projected regolith stratigraphy.

Uncertainties with respect to the presence of streams and lakes in the landscape are discussed in Section 13.4.2 (*alternative landscape configuration*). This section also considers potential effects of alternative transport pathways to the surface. Potential effects of uncertainties in object geometry, regolith stratigraphy, and the local hydrology are discussed in Sections 13.4.2 (*alternative object delineation)* and 13.5.4 (*mire object properties)*. In Section 13.8.2, the dose response to postulated disturbances in regolith depths is discussed. To get a balanced interpretation of results, the size of the discharge area and the likelihood of the geosphere release reaching an area are also factored into the discussion.

13.3.3 Development of the chemical environment

Calcite leaching

The geochemistry of the young landscape of the Forsmark area is expected to be altered gradually. As calcite is depleted, the pH and the carbonate and Ca concentrations of the groundwater are expected to be reduced, potentially affecting the mobility of several elements. The *calcite depletion calculation case* illustrates how the uncertainties associated with the changes in the future geochemistry may affect future transport of radionuclides and doses (Section 11.5). This is done by systematically shifting the K_d-values in regolith layers, as expected to be significantly affected by the pH shifts associated with calcite depletion. The shift starts when object 157_2 is fully emerged and is completed 3 000 or 50 000 years later, representing rapid or slow depletion of calcite, respectively (Section 11.5.1). This time span for the calcite leaching was estimated based both on mass-balance calculations using hydrological and chemical data from the site-investigations (Section 4.4).

The mobility of elements that exist as anions (e.g. Mo) and those that form strong mobile complexes with carbonate (e.g. U) is expected to decrease, whereas the mobility of elements in cationic form is likely to increase (e.g. Ni, Th, Ra, Pb and Cs). However, how these changes may affect doses depends on several factors, such as the timing of the geosphere release, the initial element mobility, the strength and direction of the sorption response to a pH shift, in which regolith layers the pH is considered to be affected by calcite depletion, and to what extent ingrowth and radioactive decay affect the activity concentrations of individual radionuclides.

The pH also affects the amount of dissolved inorganic carbon (DIC) in water, and the DIC concentration is expected to decrease with a lower pH. This is because HCO_3^- and CO_3^{2-} are the dominant species of the carbonate system at high pH (Figure 11-10)[62], and these species are not in direct equilibrium with gaseous CO_2. (Hence, the water can hold higher DIC concentrations at higher pH.) However, the uptake and concentration of C-14 in primary producers is modelled as being proportional to the ratio of C-14 to stable carbon. In the BioTEx model, DIC concentrations in the biologically active soil layer are a direct function of the CO_2 production from soil respiration (Saetre and Ekström 2017b). A change in pH will affect the speciation of C-14 and stable carbon in water in the same way, and thus the ratio of the two in soil pore water is only marginally affected by parameter changes in response to pH. The exposure to C-14 from drinking surface water will decrease with a lower pH because C-14 is more readily degassed. However, this is an insignificant source of C-14 exposure as compared with drinking water from a dug well, and thus carbon specific parameters were not changed in the calcite depletion calculations.

For Ca, K_d showed no significant relationship with pH in the Forsmark area (Sohlenius et al. 2013b). However, it is plausible to postulate that the K_d for till and glacial clay will decrease if the solid phase is depleted of calcite. To examine the sensitivity of the calculated dose to a decline in the K_d of Ca with time, the sorption coefficients for till and glacial clay were decreased by one or two orders of magnitude over a period of 3 000 or 50 000 years. When the K_d decreases by one or two orders of magnitude in the layers where Ca-41 primarily is retained, so does the residence time of Ca-41 in the regolith system. When the change in K_d occurs over 50 000 years, this shift has a limited

[62] In the BioTEx model the speciation of C-14 is described by the parameter f_H2CO3 (Grolander 2013).

effect on the accumulation of Ca-41, as compared to the *base case*. However, when the K_d change has been completed within 3 000 years of emergence, the dynamic of Ca-41 accumulation and the resulting dose is much faster and trails the four geosphere release peaks (green and blue lines in Figure 13-1). In spite of the changed dynamics, the maximum dose is similar to, or lower than, that in the simulations with an unadjusted sorption coefficient (~0.8 µSv). Thus, it is concluded that the maximum doses calculated in the *calcite depletion case* are insensitive to the adsorption properties of Ca, and that the use of unadjusted values is reasonable.

In the simulations, the decreased mobility delays the dose maxima of Mo-93 and U-238 but has limited effect on the magnitude of the maximum dose for these two radionuclides. However, the pH-induced accumulation of U-238 and U-235 in till and glacial clay becomes an important source of activity for decay products (U-234, Th-230. Ra-226, Pb-210, Pa-231, Ac-227). The maximum doses from all decay products in the U-238 and U-235 series increase, irrespective of whether the mobility of the decay products changes or not. This is due to the stronger retention of U in the soils, allowing for more ingrowth of decay products in the surface environment. An increased mobility results in an earlier maximum dose and a noticeable reduction of the dose from Ni-59. For Cs-135 faster transport has a different effect, as it increases the maximum dose at the end of the simulations.

The results suggest that both the magnitude and the rate of the change for a shift in pH may be important for the transport and dose dynamics of the examined radionuclides. However, maximum radionuclide specific doses are relatively insensitive to the rate of calcite depletion. The overall conclusion is that uncertainties that arise from future calcite depletion are not likely to affect the interpretation of the maximum annual dose from the *base case*. This is because the dose from Mo-93 dominates the maximum dose in both calculation cases. Calcite depletion is expected to increase the annual dose at the end of the assessment period. However, the dose at this time is still expected to be lower than the Mo-93 dose and clearly lower than the maximum annual dose of the *base case*. In conclusion, uncertainties with respect to changes in the chemical environment due to depletion of calcite are not expected to significantly affect the maximum dose or the conclusions from the *base case*.

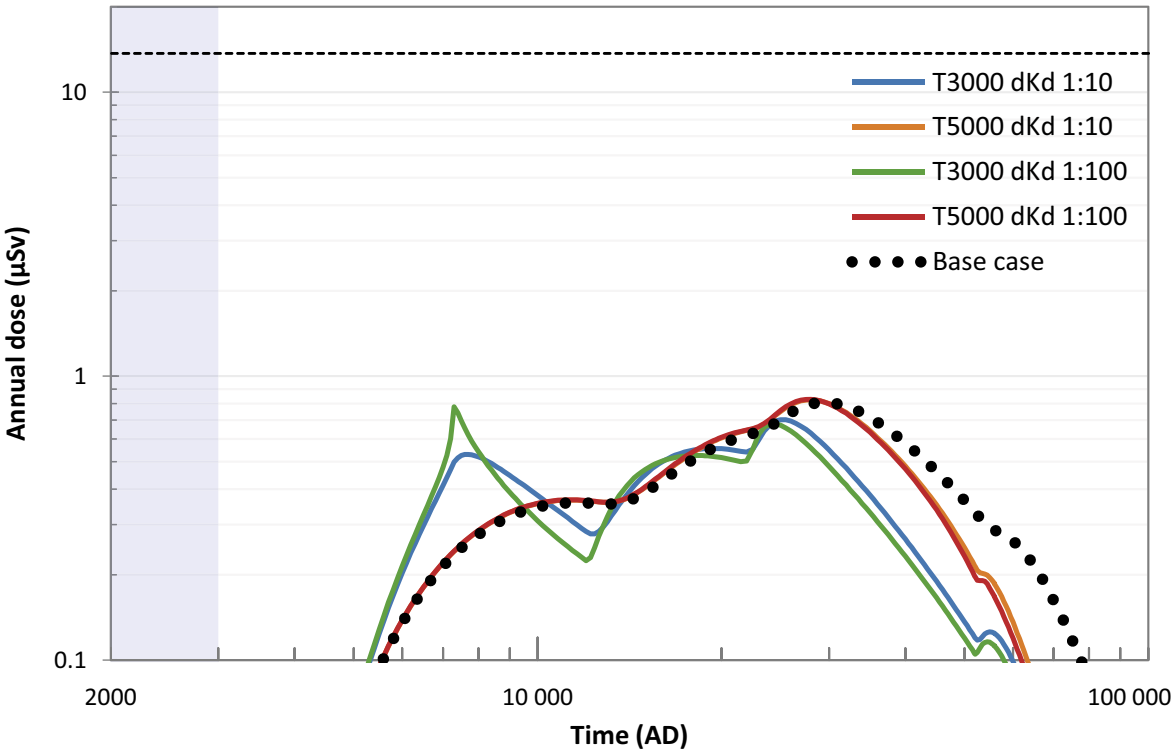

Figure 13-1. *Annual dose from Ca-41 given a decrease in the K_d for till and glacial clay by one (blue and orange) or two (green and red) orders of magnitude. As in the calcite depletion calculation case, the shift occurs over 3 000 years (blue and green) or 50 000 years (orange and red). The corresponding doses with unaltered K_d-values are shown for reference (black dotted line). The horizontal dashed black line shows the annual dose corresponding to the regulatory risk criterion (14 µSv).*

Long term cultivation

In SE-SFL, it was examined to what extent the dose to future farmers is affected by long-term cultivation of soils that originate from draining a lake or a mire (SKB TR-19-06, Section 13.2). If such soils are cultivated for long periods, the organic content is expected to decrease due to oxidation until most of the organic carbon content is lost (Sohlenius et al. 2013c). In the calculations, a module of the BioTEx model describing continuous cultivation was utilized, and parameters describing soil with a low organic content were selected. The quantitative effects of using parameter values associated with another chemical environment were limited and the response in terms of plant concentrations of individual radionuclides went in different directions (e.g. the dose from C-14 increased whereas that from Mo-93 decreased). Moreover, doses from continuously cultivated soils, irrespective of the parametrization, were clearly below those associated with cultivating the area directly after draining the mire. Thus, it was concluded that the development of the chemical environment associated with long-term cultivation of organic soils has no significant influence on the evaluation of the safety. As the most dose-contributing radionuclides overlap between the two assessments (with Mo-93 contributing most to the maximum dose), and as accumulation in peat prior to cultivation is a key process for exposure (Chapter 9), the conclusion is considered valid also for the PSAR.

13.4 Modelling uncertainty

Modelling uncertainties refer to uncertainties arising from an incomplete knowledge or lack of understanding of ecosystems and the processes important for transport and accumulation at the site, and their representation in simplified models. This includes uncertainties in the location and properties of the area where radionuclides are discharged, and uncertainties in transport pathways within the landscape. This section also includes a brief discussion on an ecosystem succession in object 157_2, building on supplementary material provided in SR-PSU.

13.4.1 Dispersion of geosphere release by a subhorizontal fracture

The *subhorizontal fracture calculation case* examines the effects of uncertainties associated with the location of the geosphere release (Section 10.5). In the *base case*, all the geosphere release is considered to be discharged into biosphere object 157_2. In this calculation case, the geosphere release is not restricted to object 157_2, but radionuclides are also discharged to the regolith of the two downstream objects 157_1 and 116.

In summary, the results from the *subhorizontal fracture calculation case* show that the uncertainties in the distribution of the release to different biosphere objects are unlikely to have any significant effects on the maximum dose used to evaluate post-closure safety of the SFR repository. Thus, the relatively simplistic representation of the interface between the geosphere and the biosphere system in the *base case*, where all geosphere release is discharged into object 157_2, is considered to be adequate for assessing maximum doses.

The analysis of the *subhorizontal fracture calculation case* indicates that accumulation of activity after 40 000 AD could result in doses that are higher than in the *base case*. This happens if a substantial fraction of the geosphere release is discharged into biosphere object 157_1, and causes an accumulation of U-238, U-235 and its decay products in the relatively thick peat layer. However, the effect on the dose is modest (less than a factor of two), and the dose resulting from a distributed release never exceeds the maximum dose in the *base case*. Running the simulations with a modified bedrock discharge (that better reflects conditions given a subhorizontal fracture) suggests that the distributed release is likely to yield higher maximum doses in object 157_2 than in downstream objects, strengthening the picture that it is sound to use object 157_2 for the evaluation of maximum doses.

The large subhorizontal fracture that is postulated to occur in this calculation case is considered to be unlikely. Nevertheless, the case is considered to give a credible illustration of the effects of a more dispersed geosphere release, and the case demonstrates that the calculation of doses is insensitive to plausible alternative assumptions with respect to the distribution of the geosphere releases in the biosphere system.

13.4.2 Configuration of the landscape and transport pathways

The analysis of the *no stream* variant indicates that accumulation of Ca-41, U-238, U-235 and its decay products could result in an elevated dose if the release reaches a relatively thick layer of peat, as considered in the downstream lake basin 157_1. However, the effect on the dose is modest and the dose resulting from downstream peat accumulation never exceeds the maximum dose in object 157_2.

Postulating that the entire geosphere release reaches surface water directly, as in the *release to surface water* variant, is not considered to be a plausible assumption. Nevertheless, the variant serves as a bounding case for potential consequences due short transport pathways from the geosphere to surface water, that would lead to minimal losses of activity due to degassing (C-14) and/or radioactive decay[63]. As the maximum dose from this variant is similar to that of the *base case*, it is concluded that uncertainties with respect to these aspects of transport pathways do not have any significant effect on the maximum dose. The variant also demonstrates that inclusion of the large lake 116 ensures that exposure to C-14 in aquatic ecosystems is adequately assessed.

It is concluded that the potential effects of uncertainties with respect to transport pathways within the landscape are unlikely to have any significant effects on the maximum dose used to evaluate post-closure safety of the SFR repository. Thus, the relatively simplistic representation of the landscape downstream of object 157_2 in the *base case*, including a small lake fed by runoff from 157_2 through a small stream and a larger lake further downstream, is considered to be adequate.

13.4.3 Alternative delineation of object 157_2

The *alternative delineation calculation case* examines the effects of uncertainties associated with the outline of the biosphere object 157_2 (Section 11.3). The case also illustrates how the size, position and properties of the biosphere object may affect environmental concentrations and resulting doses and dose rates to non-human biota (NHB; discussed in Section 13.6). The outlined sub-areas, together with the original object, represents different sets of object properties with values that typically span a factor of two to three.

All of the outlined sub-areas are smaller than the original object. A reduction in area together with low groundwater flow and thick regolith layers results in elevated radionuclide concentrations in drained and cultivated soil (see also the *mire object properties calculation case* below). However, areas that are more likely to receive discharge of groundwater from repository depth are characterised by an elevated area specific flow rate (e.g. *UpwGrad* and *Uphill*). Moreover, subsurface runoff from the catchment may contribute substantially to the groundwater flow in the upper regolith profile (e.g. in *Wetl*). Both of these factors tend to reduce the effects of a small discharge areas on the upward groundwater flow, and the maximum dose in the alternatively outlined areas is typically within a factor of two of that in the original object.

In the hypothetical case of a release to the lowermost part of the original object (i.e. *Agri*), there are multiple factors that elevate radionuclide accumulation (small area, thick glacial clay and a reduced area specific discharge from the bedrock). However, despite relatively large differences in object properties (~ factor of five) the total dose is only elevated by a factor of three. This is due to a number of reasons that work in the opposite direction; slow transport increases the loss of activity due to radioactive decay, a small area cannot fully support a reasonably sized group of farmers, and exposure through drainage is limited to the upper part of the regolith profile. If only a fraction of the groundwater release were to occur in this small area, then the resulting dose is unlikely to exceed that of the other sub-areas (see Section 13.8.2).

It is concluded that uncertainties with respect to the outline of biosphere object 157_2 are only expected to have a small effect (within a factor of two) on calculated doses. The case also demonstrates that the calculated dose is relatively insensitive to variation of object properties even when correlations due to the position in the landscape are taken into account.

[63] Shorter transport pathways can be hypothesised due to extensive and deep ditching, horizontal transport in conductive regolith layers and/or by localised upwelling in stream water.

13.4.4 Ecosystem succession in object 157_2

In a supplementary study to SR-PSU, potential consequences of conceptual uncertainties in the landscape were examined by describing a future lake stage in object 157_2 (Saetre and Ekström 2017a). In one case, a 500-year transitional period with aquatic ecosystems gradually being converted to a mire was explicitly modelled. As compared with the *base case*, where the shallow pools are instantly filled with peat, this description had no significant effect on the calculated maximum dose. In addition, an excavated lake was postulated as a bounding case for the existence of future water bodies in object 157_2. It was shown that the exposure resulting from an artificial lake can give rise to a somewhat higher doses than in the *base case*. However, this was not due to direct exposure from consumption of aquatic food, but through ditching and cultivation of the biosphere object at a later stage. In this case, it was accumulation in a peat layer thicker than in the *base case*, and a lower bulk density of the cultivated soil that caused elevated concentrations. It was concluded that including a natural lake stage in the description of object 157_2 does not have any considerable effect on the calculated maximum dose. As the landscape description and the performance of the BioTEx model are very similar in SR-PSU and the PSAR (Chapter 4 and Appendix C), the conclusion is considered to still be valid. Consequently, the relatively simplistic representation of the development of object 157_2 in the *base case*, excluding the stage with shallow pools, is considered to be adequate. Potential effects of uncertainties with respect to the thickness of regolith layers are examined in Section 13.5.4 and further discussed in Section 13.8.2.

13.5 Data uncertainty and sensitivity analyses

Uncertainties associated with the values of the parameters that are used in the implemented models are termed data uncertainties. These uncertainties partly arise because the biosphere model uses single spatially averaged values for parameters (derived from measurements at discrete locations), whereas in reality properties vary continuously in space. Parameter uncertainty may also stem from difficulties in obtaining precise measurements, lack of measurements from relevant conditions, or because aggregated parameters represent the net outcome of multiple processes.

In the PSAR, site-specific data, generic data, and expert judgement are used to assign reasonable values to model parameters (Chapter 8). In this section, the effects of data uncertainty on the calculated doses in the *base case*, and the sensitivity of the biosphere calculations to variations in parameters describing ecosystem properties and mire object properties are discussed. The section also includes a note on the use of element analogues when data from Forsmark are sparse or lacking.

13.5.1 The effects of parameter uncertainties on total dose

The uncertainty in ecosystem parameters causes a substantial variation in the calculated dose in the *base case*. The difference between the 5th and the 95th percentiles of the dose typically spans an order of magnitude (Figure 9-21). This span tends to widen with time, reflecting the differences in uncertainties associated with the individual radionuclides that contribute to the dose in sequence. However, the confidence interval of the mean exhibits small variability (below 10 % of the mean dose) clearly indicating that the number of realisations (1 000) is sufficient for an acceptable level of convergence (Figure 9-21).

The mean dose is consistently above the median dose, reflecting that many of the important parameters in the *base case* are positively correlated with the annual dose and have positively skewed distributions. Moreover, deterministic simulations with best estimates, typically corresponding to the median values of individual parameters, yield a lower dose than the median dose from probabilistic calculations. This is due to parallel processes or pathways contributing with similar importance in the dose calculations (Section 9.4). The fact that the mean dose is always higher than the deterministically calculated dose indicates that parameter uncertainty does not lead to an underestimation of the dose (see further discussion of this issue below).

Another source of uncertainty in the probabilistic simulations is related to the potential for temporal dilution of radionuclides. This occurs when the timing of the maximum (or peak) dose differs between simulations, e.g. due to uncertainties in parameters affecting the retardation of radionuclides, and leads

to an underestimation of dose when the average is calculated for a fixed point in time. The potential for temporal dilution is assessed by the *risk dilution ratio* (Section 9.4). In the *base case* this ratio is 1.26 over the whole assessment period. The risk dilution ratios for C-14 and Mo-93 amount to 1.05 and 1.10, respectively, indicating that the potential for temporal dilution is 10 % or less for the first 10 000 years when the dose maximum occurs. This strengthens the conclusion that temporal dilution introduced by the probabilistic simulations is unlikely to have any significant effect on the results.

13.5.2 The effects of ecosystem properties on radionuclide-specific doses

The sensitivity of radionuclide-specific doses to variations in parameters that vary in the *base case* is examined in the *ecosystem properties calculation case* (Section 11.2). Ecosystem parameters are used in the broadest sense, including regolith properties (e.g. porosity, density and saturation), characteristics of ecosystems (e.g. biomass density, and rates of primary production and mineralisation) and element-specific properties for regolith layers and organisms (including K_d and *CR* values).

The *ecosystem properties calculation case* examines the sensitivity of radionuclide-specific doses to changes in parameter values and identifies key drivers of uncertainty. Parameter values are varied as in the *base case*, and the responses of key radionuclides are examined, namely C-14, Mo-93, Ca-41 and Ni-59.

The C-14 dose is sensitive to changes in the rate of groundwater movement from saturated to the unsaturated layer in cultivated soil. As groundwater from the saturated layer is the primary source of C-14 activity in agricultural soil, the C-14 dose increases almost proportionally to an increase in the uptake rate. However, most of the C-14 dose variation (~60 %) is due to uncertainties in the fraction of root uptake. The doses from the other three radionuclides tend to increase with regolith sorption coefficient (K_d) and with increasing rates of biological uptake, i.e. with the values of concentration ratios and transfer factors (*CR* and *TC*). The exception is the K_d in till, which has a negative effect on dose. This is because retardation in till delays and disperses the release to the layers above, which are exposed by cultivation, and increases the loss of activity due to radioactive decay. The dose from Mo-93 is sensitive to changes in the *CR* for cereal, and uncertainty in this parameter explain approximately half of the dose variation. The dose from Ca-41 is sensitive to changes in the K_d for glacial clay and the *CR* for fodder, reflecting the primary exposure pathways for accumulation and exposure through consumption of meat and dairy products. Similarly, the dose from Ni-59 is sensitive to changes in the K_d for glacial clay and the *TC* for meat. For Ca-41 and Ni-59 the uncertainties in many parameters contributes notably to the dose variation.

The potential to reduce significant amounts of dose variation depends on the width of the dose distribution, and the proportion of the variation explained by the parameter uncertainty. Few dominating parameters with reducible uncertainties increase the possibilities to decrease the dose variation. The dose variation is relatively low for C-14. Moreover, the distribution of C-14 dose is balanced around the mean, and thus a reduction in dose variation is not likely to have any noticeable effect on the mean value from probabilistic calculations[64].

The variation in Mo-93 doses is modest. The dose variation could potentially be lowered by reducing the uncertainty in the concentration ratio for cereal. However, the effect of a reduction on the mean value of the Mo-93 dose is expected to be limited to less than a factor of two. No single parameter dominates the variation of Ca-41 and Ni-59. To lower the variation of the Ca-41 and Ni-59 doses would require a reduction of the uncertainty of multiple parameters. For Ca-41 this could lead to a reduction of the mean dose. However, for Ni-59, which has a relatively modest and balanced dose variation, the potential to affect the mean dose is limited.

Taken together, it is concluded that the identified parameters give a good picture of the BioTEx mechanisms for transport, accumulation, and uptake of, and exposure to, key radionuclides. Thus, the analysis supports the understanding of the model that is demonstrated in the *base case*. In addition, the

[64] For a log-normally distributed variable the mean is greater than the median. The difference is a function of the variation, and if the variation is sufficiently reduced the mean value will approaches the median value. For a variable with a balanced or normal distribution the mean and median values are similar, and the mean value is not systematically affected by the variation.

analysis identifies the parameters for which a reduction of uncertainties would reduce most the dose uncertainties. However, the potential to reduce the mean dose in probabilistic calculations in future assessments by reducing parameter uncertainties alone is limited. Still, it is important to make sure that the central values of key parameters are representative of the conditions postulated in a calculation case, rather than being biased by cautious assumptions. This is particularly important for parameters with high sensitivity indexes, as the dose may be near proportional to the central parameter values.

13.5.3 A note on element analogues

SKB strives to, as far as possible, utilise site-specific information for Forsmark for selecting parameter values and their probability density functions. However, in some cases site data are not available. In these cases, the parameter values are estimated from literature data, or by using analogues. Elemental analogues (EAs) are based on biogeochemical properties of the elements lacking data. Typically, an element of the same group in the periodic table is used as an analogue for the element that lacks data. However, even if elements are chemically similar, their behaviour in natural environments can differ. Furthermore, if the properties of an element change with the chemical environment, different analogues may be needed to reflect the behaviour in, for example, oxidising and reducing environments.

An example of an element with complex chemical behaviour and no site data is Tc, which only occurs naturally in ultra-trace concentrations. In nature, Tc is commonly found in two different oxidation states; in oxidising conditions Tc(VII) mainly as pertechnetate (TcO_4^-) and in reducing conditions Tc(IV) mainly as TcO_2. These two forms have very different solubility and sorption properties so for reliable parameter values, and eventually dose calculations, the EA needs to have a similar solubility pattern. One potential candidate as an AE for Tc is Mo, which may form ions closely resembling those formed for Tc. The most common forms of Mo in nature are Mo(VI) and Mo(IV), of which Mo(VI) is typically found as molybdate (MoO_4^{2-}) (Section 13.7.2). Despite their similar chemical form as oxy-anions, divalent molybdate is generally more reactive than monovalent pertechtanate. Thus, using Mo as an EA for Tc under oxidizing conditions is likely to underestimate the mobility of Tc. On the other hand, in reducing conditions the use of Mo(IV) as an EA has the potential to overestimate the mobility of Tc, as molybdate is stable under a wider range of redox conditions than Tc. For example, Tc(VII) can, unlike Mo(VI), be reduced by Fe(II) (Icenhower et al. 2010, Mayordomo et al. 2020), which is abundant in groundwater, and this could lead to considerable differences in the sorption properties of Tc and Mo, respectively.

Thus, SKB instead uses two other elements as EAs for Tc (Tröjbom et al. 2013). For oxidising conditions (e.g. upper regolith layers and agricultural soils), the EA is Re, which belongs to the same periodic group as Tc and has been proposed as an EA for Tc (Brookins 1986). A main reason why Re has not been more widely used as an analogue for Tc is probably that Re is a very rare element, which has not been analysed nearly as much as, for example, Mo. In oxidising environments Re occurs as perrhenate, ReO_4^-, which consequently is a direct parallel to pertechnetate, TcO_4^-. However, the behaviour of Re differs from Tc under reducing conditions, limiting the relevance of Re in reducing environments (Reinoso Maset et al. 2006). The ionic form of Tc has been shown to have a close correlation with the K_d of Fe (see 2.7.12 in SKB Tröjbom et al. 2013). That is, at sites with high K_d for Fe, Tc is assumed to be present as Tc(VII) and the EA is Re, while when the K_d-values for Fe are low, Fe(II) is assumed to be present and Tc(VII) is assumed to have been reduced to Tc(IV). Thus, under reducing conditions (e.g. till, glacial clay, clay-gyttja and deep peat layers), SKB uses Zr as an EA for Tc. The reason for this is that Zr is always in the form of Zr^{4+} in reducing conditions, and this species is expected to have a similar reactivity as Tc^{4+}. Thus, the use of Zr minimises the risk of parameter values being based on an ion with a different valency than Tc. Hence, SKB´s method to select EAs acknowledges the behaviour of the elements under different redox conditions, and this approach accounts for differences in environmental conditions along the transport pathway in a potential discharge area.

To examine the sensitivity of the model results to the choice of EA for Tc, the *base case* model was run with the alternative choice of Mo as element analogue for Tc. As compared with the *base case*, the sorption of Tc decreased significantly in inorganic layers with reducing conditions (i.e. in till and glacial clay), whereas it increased considerably in oxidizing conditions (i.e. upper peat and agricultural soil originating from draining a mire). The transport through the till and glacial clay is greatly enhanced, and activity accumulates throughout the regolith profile. This is in strong contrast with the *base case*, where most of the Tc-99 from the geosphere release never leaves the till layer, and exposure results from

accumulation in glacial clay only. However, although the timing and accumulation patterns are significantly altered, the accumulation in layers exposed by cultivation and the resulting dose is similar in the two simulations (Figure 13-2). Moreover, the dose from Tc-99 is too small to affect the maximum dose peak in the *base case* (~5.6 µSv). This is also true if plant uptake was to be increased with an order of magnitude, accounting for the difference in CR of cereals between Mo and Re (Tröjbom et al. 2013).Thus, it is concluded that the uncertainties associated with the adsorption properties of Tc-99 are highly unlikely to have any influence on the conclusions drawn from the *base case*.

13.5.4 Mire object properties

The sensitivity of doses and environmental activity to variations in parameters that describes the biosphere properties is examined in the *mire object properties calculation case*. The properties include object geometries, regolith thickness, and parameters that drive, or modify, groundwater flows. These parameters were not varied in the probabilistic simulations of the *base case*. By varying object properties independently, this case can disentangle effects of individual properties that are intertwined in the landscape (e.g. regolith thickness and vertical distribution of groundwater flow) or happen to be confounded in the *alternative delineation calculation case* (e.g. the smallest object has thickest layer of glacial clay).

The analysis shows that doses are most sensitive to the size of the biosphere object, and this property affects the doses from all examined radionuclides in a similar way. The primary reason for this is that in the simulations the discharge of groundwater from the bedrock scales with the area of the object, and this flow dilutes the radionuclides released from the geosphere especially in the lower section of the regolith profile. The response to size is strongest in the beginning and ending periods of the simulation, and a reduction of the object area by a factor of two typically results in a dose increase of between 30 and 40 %.

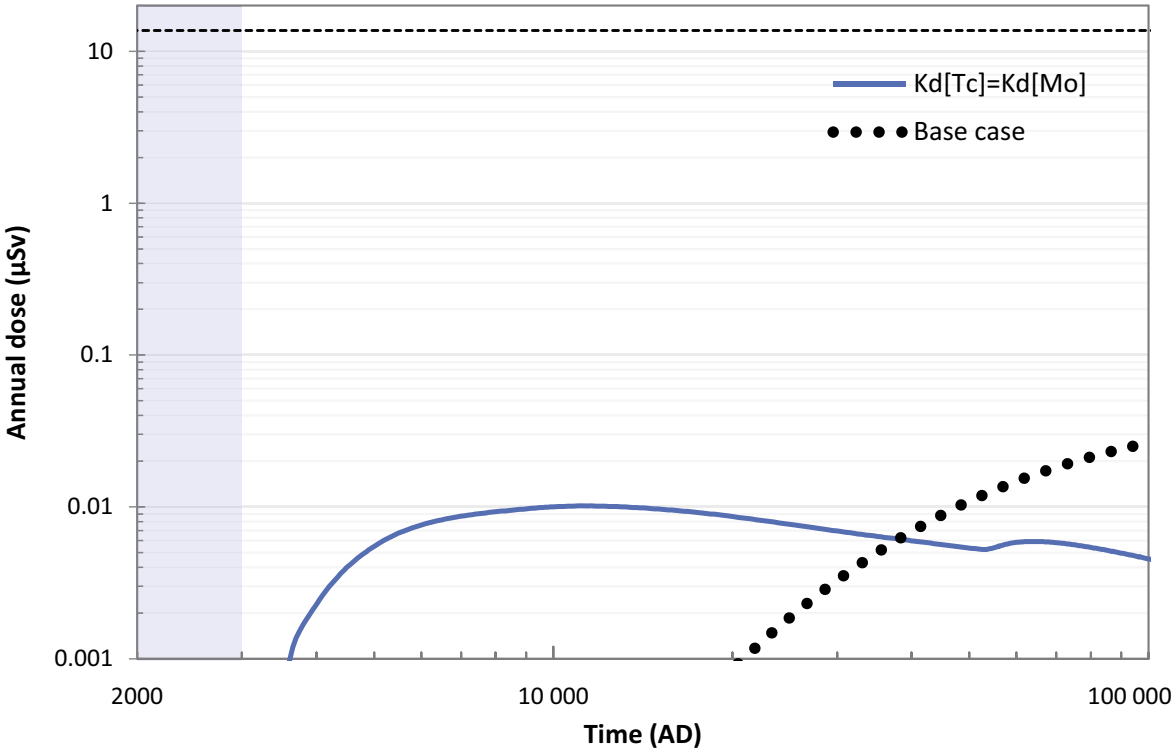

Figure 13-2. *Radionuclide specific dose from Tc-99 as a function of element analogue (EA) for sorption. The dotted line represents the base case, where Zr is used as analogue for reducing conditions and Re is used for oxidizing conditions. The blue line corresponds to the dose when Mo is used as an analogue for all regolith layers. The horizontal dashed black line shows the annual dose corresponding to the regulatory risk criterion (14 µSv).*

A change of the properties that control the discharge from the catchment and its vertical distribution also affects all radionuclides (though effects on C-14 are weak). The mechanism for this response is dilution of radionuclides by groundwater from the catchment. Moreover, a thicker till layer tends to decrease the dose from sorbing radionuclides, through the mechanisms of retardation and radioactive decay. However, the quantitative effects of individual parameters are weaker than that of the object size; a doubling of the value of these parameters typically results in a change of dose of below 20 %. In addition, there are a few object properties that have a substantial effect on individual radionuclides only. For example, the area-specific discharge from the bedrock has a near proportional effect on C-14 dose (through dilution) and the thickness of clay-gyttja and peat layers have a clear effect on Mo-93 dose (through increased accumulation).

In a landscape context, several object properties may be affected simultaneously by the topography of the basin and/or the position of an object. This means that a low-lying area may well have thick regolith layers of both clay-gyttja and peat. For Mo-93, the effect of a correlated change in these two layers would lead to a dose response as strong as that to a change in object area. While this analysis disentangles the effect of individual object properties it may not give a realistic picture of the response of properties that are intertwined in the landscape. Thus, the results from this sensitivity analysis should be seen as complementary to those from the *alternative delineation calculation case*. Potential effects of uncertainties in object properties on the maximum dose calculated in the *base case* is further discussed in Section 13.8.2.

13.6 Exposure of non-human biota

The modelling of dose rates to non-human biota utilises a number of assumptions and simplifications necessary to represent the diversity of environments and species, and the processes within.

The species of plants and animals present at the site (and by extension, anticipated to be present at the site in the future) are not modelled explicitly, but rather are represented by generically parameterised ‘reference organisms’ included in the ERICA tool. Further, the range of reference organism types were designed to span a range of shapes, sizes, habitat occupancies, biokinetics and radiosensitivities, as found in nature. The ERICA reference organisms are designed to represent the range of organisms typically found throughout Europe and have been deemed suitably representative of species in Sweden (Jaeschke et al. 2013). This includes ecologically and economically important species and vulnerable or protected species presently found in Forsmark.

In previous assessments, the differences in parameters (geometry, occupancy and concentration ratios) between site-specific species and the ERICA reference organisms led to minimal differences in dose rates (Torudd 2010, Jaeschke et al. 2013, SKB TR-14-09). The impacts of variation in size/geometry, occupancy and CRs have been investigated and discussed in detail in these previous assessments, with the CRs identified as the most significant factor in determining the dose rates. Where available, CRs from the Forsmark site have been used. Where data were not available, the next best elemental or organism analogues were used, and then values from literature and the CR database in ERICA were used. ERICA itself uses a tiered range of approaches to fill gaps in CRs to provide values using the best available data. Since the previous assessments, the CR values in ERICA (version 1.2 and later) were updated to reflect new and updated data in the Wildlife Transfer Database. While some of the updated CRs increased by more than two orders of magnitude, the impact on the total dose was found to be minor (Jaeschke and Grolander 2017).

The ERICA methodology represents organisms as simple ellipsoids with a uniform internal structure – organs or other specific structures of the body are not modelled explicitly. Consequently, subterranean components of plants (e.g. roots) are not explicitly described. While DCCs implicitly include internal incorporation of radionuclides into the plant, the model ignores a significant proportion of the biomass of such organisms that exists in soil where higher dose rates can be expected; the dose rates from external exposure to, and any internal incorporation specifically into, these parts of the plant may therefore be underestimated (Jaeschke et al. 2013). There is no model or data known for specifically calculating dose rate or impact to plant roots (Jaeschke and Grolander 2017). Calculations including exposure to roots, indicated that dose rates could be effectively doubled (Jaeschke and Grolander 2017). However, considering that the total dose rates in plants remain several orders of magnitude below the screening dose rate, this will not impact the overall conclusion that plant populations are not at significant risk.

The ERICA calculations assume that radionuclides are in secular equilibrium and thus dose rates from decay products with short half-lives (physical half-life < 10 days) are calculated implicitly. Radionuclides within the organisms are assumed to be distributed homogeneously. Heterogeneous distributions, such as those occurring in specific organs or from point sources, and relative radiosensitivities of various organs are not modelled. The ERICA tool documentation indicates that variation in DCCs due to source distribution geometry is expected to be low (less than a factor of ten) and homogeneous distribution is a reasonable approximation.

Exposures of non-human biota (NHB) to ionising radiation from radionuclides originating from SFR are estimated by calculating absorbed dose rates resulting from external exposure to radionuclides in environmental media, and internal exposure to internal radionuclides estimated from environmental media concentration via concentration ratios. Calculations for NHB, in marine, freshwater (lake) and terrestrial ecosystems, are performed for three calculation cases of the main scenario, including the *base case*, the *warm climate calculation case* (high and low summer precipitation variants) and the *cold climate calculation case* (deep and shallow freezing variants). In addition, calculations for NHB are performed for the supporting calculation case addressing alternative delineations of biosphere object 157_2. This is done to illustrate potential effects of a release restricted to a habitat relevant for a protected species and/or to areas smaller than the original outline of object 157_2.

In all calculation cases, the maximum dose rates are at least three orders of magnitude below the ERICA screening dose rate (10 μGy h^{-1}) and occur relatively early in the assessment period (Table 12-1 and Table 12-2). Furthermore, all dose rates are considerably below the lower boundary of even the most restrictive ICRP derived consideration reference level (DCRL) (4 μGy h^{-1}; which only applies to certain vertebrate animals and coniferous trees). Therefore, it is not anticipated that populations of non-human biota will be significantly negatively impacted by radionuclides released from the repository, under any of the assessed scenarios. This conclusion encompasses endangered species, species that are of economic or biological importance, as well as species that are important for ecosystem function.

The variants of the *warm climate calculation case* result in later maximum dose rates relative to those in the *base case* because of the delayed emergence of the biosphere object. The dose rates to organisms in the *high summer precipitation* variant are lower than those of the *base case*. The dry conditions in the *low summer precipitation* variant lead to somewhat larger dose rates, but the increase is limited to ~10 % for aquatic organisms and ~60 % for terrestrial organisms. The dose rates during periglacial conditions in both variants of the *cold climate calculation case* are significantly lower than the dose rates in the *base case* for corresponding periods.

The *alternate delineation calculation case* shows that dose rates to aquatic organisms may increase by a factor of three if radionuclides from SFR are released to an area that is a factor of five smaller than the original biosphere object. The dose rates to terrestrial organisms are less sensitive to the size of the discharge area than aquatic organisms. Further, although the present assessment cautiously assumes that the entire target population of each species is contained within the assessment area, it is presumed that the actual extent of populations would be larger, reducing the potential radiological impact on those populations. Thus, further reducing the assessment area through alternate delineations would further reduce the impact of such dose rates on all but the most localised populations of non-human biota.

Compared with the margin between the calculated dose rates and the levels of potential concern, the dose rates are relatively insensitive to the postulated span in climate conditions and object properties. Thus, the conclusion of an insignificant negative impact on the environment is considered to be robust with respect to uncertainties in the future climate and the development of the landscape.

13.7 Key radionuclides during the first 10 000 years

In this section the assumptions and reliability of models and parameters used for the two radionuclides that contribute most to the maximum dose relatively early in the assessment (C-14 and Mo-93) are discussed in detail. The discussion primarily builds on supplementary material provided as a part of the review process of the SR-PSU (Saetre and Lindgren 2017), and on recent literature reviews, covering the behaviour of methane and molybdenum in surface ecosystems (Ikonen 2022, Lidman et al. 2017, 2022).

13.7.1 Handling of C-14

In SR-PSU, the representation of C-14 in the BioTEx model was updated as compared with previous safety assessments (Saetre et al. 2013a). The updates enhanced the ability of the model to capture the main pools for carbon accumulation and provide an improved representation of processes controlling accumulation and transport of C-14 in the environment. The update also improved the consistency in the description of transport processes between sub-models as compared with the previous safety assessments (see Section 7 in Saetre and Lindgren 2017 for an overview of model development between SAR-08 and SR-PSU).

As in SR-PSU, the specific activity of C-14 in environmental media is used to calculate biological uptake of C-14 in the PSAR. For the calculations, C-14 in inorganic form (carbon dioxide and/or carbonate) is assumed to be mixed (physically and chemically) with the corresponding forms of stable carbon in the atmosphere and in ground and surface waters, resulting in a specific activity. To avoid bias, the transport and accumulation of stable elements and radioisotopes should be treated consistently. Consequently, model updates with respect to root uptake of C-14 and peat growth were introduced in the PSAR (Section 7.5). This means that dose calculations become insensitive to the burial and degassing rates of carbon. The latter case was illustrated for agricultural soils in a supplementary study to SR-PSU (Saetre and Ekström 2017b). In that study variation in soil saturation caused the degassing rate to vary over an order of magnitude, but this had marginal effect on the activity concentration in crops (Figure 13-3).

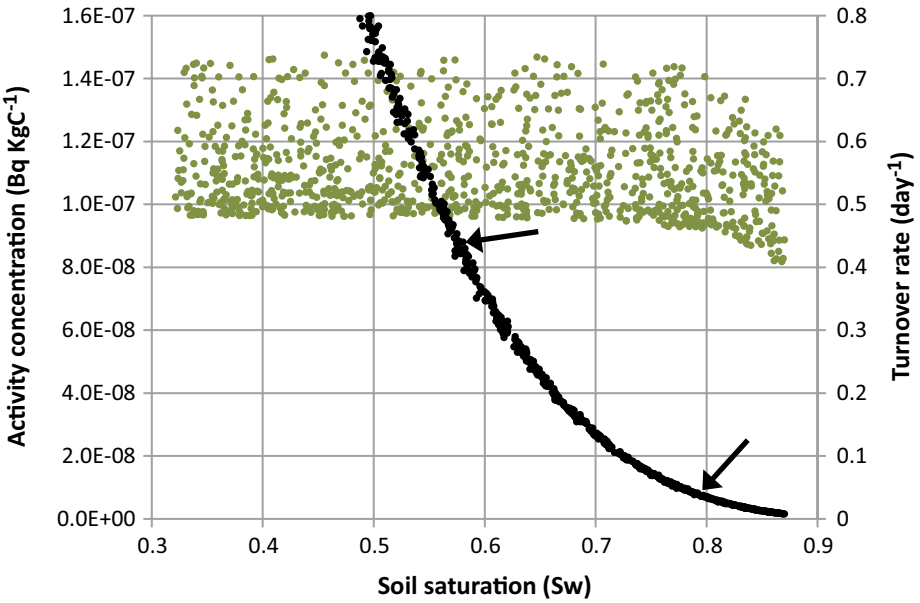

Figure 13-3. *Activity concentration in cereals and turnover rate of C-14 in groundwater (with respect to gas emission) as a function of degree of water saturation in agricultural soil. The results are based on 1 000 simulations where porosity, water saturation and soil respiration have been varied. Dark green dots indicate the total concentration of C-14 in the crop. Black dots represent the turnover rate of the DIC-14 storage in the pore water with respect to gas escape. The upper arrow indicates the turnover rate for typical ground conditions (Sw_regoUp = 0.57) in the simulations, while the lower arrow indicates a slow turnover rate of 0.04 per day. Figure modified from Saetre and Ekström 2017b.*

In the specific activity approach, an organism that takes up a stable element from the environment is assumed to take up the radioisotope in proportion to its relative concentration, and the organism achieves the same specific activity as in the environment at equilibrium. Using specific activity to calculate the uptake and concentration of C-14 in plants is common in models used to assess radiological safety (see, e.g., literature review by Limer et al. 2013). Heterotrophs (i.e. herbivores, predators, detritivores and omnivores) cannot fix inorganic carbon, and carbon in organic molecules therefore always originates from carbon fixed by primary producers. As discrimination of C-14 during carbon metabolism (and synthesis) is small, and the decay of radioactive carbon is slow compared to the life span of an organism, the specific activity of primary producers will be preserved throughout the food chain. Consequently, the specific activity in for example fish has been set to the same value as that in aquatic plants (macroalgae, microalgae and plankton) in the BioTEx model (Saetre et al. 2013a). This reasoning is also behind the IAEA's recommendations for the use of specific activity in the calculation of consequences from C-14 emissions to humans (IAEA 2009). The caveats on applying the same approach to modelling uptake of C-14 as for other radionuclides (i.e. based on *CR* values) has been pointed out by SKB and others (e.g. Avila et al. 2006), and is discussed in Section 7 in Saetre and Lindgren (2017).

Models for calculating radiological impacts from methane ($^{14}CH_4$) emissions from a geological repository have been developed for more than 20 years (Mobbs et al. 2014). These models have clearly shown that the uptake by plants, and the subsequent transfer of organic carbon to other organisms in the food chain, is by far the most important processes related to exposure of humans. Therefore, it is very common to make the simplifying (and potentially cautious) assumption that *all* C-14 activity reaching the biosphere is available for plant uptake (Shaw and Thorne 2016). This assumption is also maintained in the PSAR. For agricultural ecosystems, this assumption is highly realistic, as transport distances of a few decimetres in soil will ensure that practically all methane released from below is oxidized (Hoch 2014).

SKB has recently published a literature review with regard to the production and losses of methane in boreal wetlands, lakes and streams (Ikonen 2022). In anaerobic environments, methanogenic bacteria can convert both CO_2 and low molecular weight organic carbon compounds to methane. Methane can in turn be transported to the atmosphere (e.g. via bubble formation, diffusion, or transport in plant structures) or oxidized to CO_2 in oxygenated environments. It is well known that methane is formed and released from discharge areas for deep groundwater, i.e. lakes, streams and wetlands. Regional estimates of methane emissions during the vegetation period for treeless marshes are in the order of 30–50 mg CH_4 m^{-2} day^{-1} (see[65]). The corresponding figure for smaller lakes is lower (~ 1.5–15 mg CH_4 m^{-2} day^{-1}), whereas methane release in reed belts surrounding lakes has been estimated at around 200–300 mg CH_4 m^{-2} day^{-1}. However, there are no site-specific estimates of methane emissions for natural ecosystems in Forsmark, and even at a regional level, the relative importance of the underlying processes (production, consumption and transport) is unclear. To improve the site description of Forsmark, SKB has initiated a field investigations of methane production and consumption in streams and lakes (SKB 2016).

Based on the literature review (Ikonen 2022), it is reasonable to assume that parts of a discharge of C-14 that reach a water-saturated environment (i.e. wetlands or aquatic sediments), via outflow of deep groundwater, will be in the form of, or converted into methane. However, it is presently difficult to make relevant estimates of how much of a C-14 emission can reach the atmosphere as methane (and thus will not be available for plant uptake). Although the simplifying assumption that all C-14 is available for biological fixation is cautious, it is not an unreasonable simplification. For example, when the groundwater level is low, or when the water depth in a lake is large, in principle all methane formed in these environments is oxidized.

[65] The lower number refers to low sedge fens (*Eriophorum vaginatum*), whereas the higher number refers to high sedge fens (*Carex rostrata*).

13.7.2 Mo-93 in the surface environment of Forsmark

Molybdenum (Mo) is a transition metal (Z = 42) that can occur in different oxidation states in nature. The dominating oxidation state in surface water and groundwater is Mo(VI), which occurs as the oxyanion molybdate, MoO_4^{2-}. The tendency of high-valence states to form an oxyanion is a property that Mo shares with many of its closest neighbours in the periodic table of the elements, e.g. V, Cr, Tc, Re and W. Molybdate is stable over a wide range of chemical conditions, and, as an anion, Mo tends to be more mobile at high pH. Important retention processes for molybdate includes sorption onto Al and Fe oxyhydroxides, especially at low pH. It has also been demonstrated that molybdate can bind strongly to organic matter (Gustafsson and Tiberg 2015).

Under strongly reducing (approximately sulfidic) conditions Mo(VI) can be reduced, predominately to Mo(IV) (Crusius et al. 1996, Smedley and Kinniburgh 2017). This has far-reaching consequences for the mobility of Mo, since it implies that Mo is transformed from a relatively mobile oxyanion to a high-valence cation with low solubility. As a consequence, there can be appreciable accumulation of Mo in strongly reducing environments such as organic sediments (Crusius and Thomson 2000, Dahl et al. 2013, Wirth et al. 2013, Chappaz et al. 2014).

In the Forsmark area, Mo concentrations in till range between 0.060 µg g^{-1} and 1.4 µg g^{-1}, and weathering of albite is a possible source. In near-surface groundwater, Mo concentrations range between 0.063 µg l^{-1} and 31 µg l^{-1}. The Mo concentration tended to be higher in groundwater with high pH, which can be explained by a generally weaker sorption and higher mobility of anions in more alkaline waters. Particularly low Mo concentrations have been encountered in a groundwater well with high concentrations of sulfide. This is consistent with the expected reduction and immobilisation of Mo in sulfate-reducing environments. Surface waters tend to have lower Mo concentrations than near-surface groundwaters, ranging from 0.19–1.1 µg l^{-1} in lake water and from 0.082–1.9 µg l^{-1} in stream water. Mo concentrations display seasonal covariation with pH and V, suggesting that Mo is in the form of an oxyanion (i.e. molybdate). Thermodynamic modelling of groundwater and surface water also suggests that the speciation of Mo is dominated by molybdate and its complexes with Mg and Ca (Gustafsson 2012, Figure 13-4).

It is well-established that reduction of molybdate can cause significant accumulation of Mo in both marine and freshwater sediments (Dahl et al. 2010, Helz et al. 2011, Chappaz et al. 2014). In Stocksjön in Forsmark, Mo concentrations of up to 73 µg g^{-1} have been recorded. This is more than 50 times higher than the highest observations from the local till. In addition, the Mo/Ti ratios indicate that there has been a substantial accumulation of Mo. The enrichment of Mo coincides with high concentrations of S (up to 3.5 %), suggesting that these sediments are sulfidic. High Mo concentrations have also been observed in sediment cores from other sites in the Forsmark area, e.g. 14 µg g^{-1} in gyttja from a wetland near Bolundsfjärden, 8.0 µg g^{-1} in gyttja sediments from Eckarfjärden and up to 18 µg g^{-1} in marine sediments (Hannu and Karlsson 2006). This accumulation of Mo in strongly reducing environments is likely to be a major retention mechanism for Mo in the surface environment.

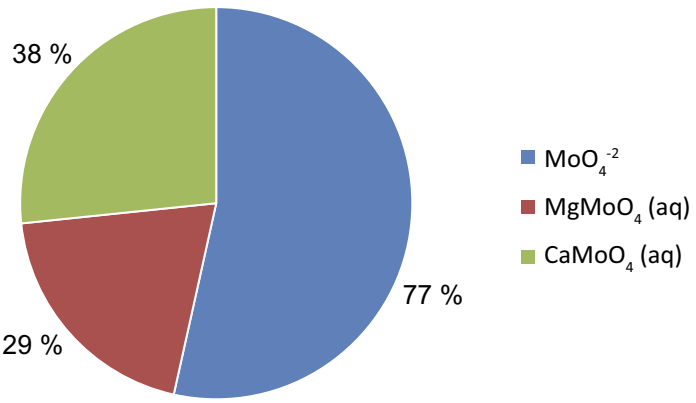

Figure 13-4. *Example of modelled Mo speciation in Bolundsfjärden during a period of high pH (pH = 9.1) 17 July 2006. The speciation does not appear to vary appreciably throughout the year (data not shown). Reproduced from Figure 14-14 in SKB (TR-19-05).*

Mo was included in the site-specific K_d measurements reported by Sheppard et al. (2011). The frequency distribution of Mo K_d-values displayed a clearly bimodal tendency, most likely reflecting the redox properties of Mo. The general pattern is that Mo exhibited low K_d-values in inorganic soils such as clay till and glacial clay, mostly in the range 0.06–0.26 $m^3\ kg^{-1}$, whereas higher K_d-values were found in more organic soil matrices such as clay gyttja and peat (up to 26 $m^3\ kg^{-1}$). The accumulation of organic matter in these soil types is related to lower redox potential so these differences are consistent with the general understanding of the biogeochemistry of Mo and the accumulation of Mo that has been observed in the site investigations, e.g. in sulfide-rich sediments. The low K_d-values in the till and glacial clay would support the view that Mo mainly is present as molybdate in these soils, whereas there is a preferential accumulation – and quite possibly reduction – of Mo in organic lake sediments and peat. The measured K_d-values therefore seem to reflect the redox behaviour of Mo, which is central to predicting the fate of Mo in the surface environment. Thus, it can be concluded that the K_d-values used in PSAR capture a significant part of environmental variation in the mobility of Mo, and that this variation is consistent with the understanding of underlying biogeochemical processes.

13.8 Final discussion

In this section, the results from all calculation cases are compared and discussed. The potential effects of uncertainties in properties of the biosphere object and the size of the discharge area are given specific attention. It is concluded that the maximum dose from the *base case* is robust, and the simplified representation is appropriate.

13.8.1 Comparison of data and scenario uncertainties

The variation of the maximum dose in the *base case* is driven by data uncertainties in the near-field, the geosphere and the biosphere system. A comparison with the *ecosystem parameters calculation case* clearly shows that uncertainties in biosphere parameters are the dominating source of data uncertainty in the *base case*. That is, the width of 90 % confidence interval in the ecosystem parameter calculation case covers approximately 75 % of the confidence interval of the *base case* (Figure 13-5). The remaining 25 % of the variation in the *base case* is driven by uncertainties in the release from the geosphere. Data uncertainties with respect to *object properties* are not included in the *base case* and is discussed separately in Section 13.8.2 below.

Mo-93 is the radionuclide that contributes most to the maximum dose, and thus K_d and *CR* values for Mo-93 explain much of the data uncertainty (Table 11-1). The relatively large contribution of biosphere parameters to the dose variation is reasonable, as they affect the dose from the total release from SFR, whereas parameters in the near-field typically affect the release from one or a few waste vaults. Moreover, data uncertainties associated with the geosphere have a minimal effect. This is expected as geosphere processes hardly influence the release of dose contributing radionuclides[66]. It can also be noted that land-use by the most exposed group is associated with substantial differences in the maximum dose. However, this has no effect on dose variation between calculation cases, as only the group with the highest mean dose is used to evaluate the calculation cases (the drained mire farmer, DM, group in most cases).

Large scale changes in the development of the future climate, or of the surface chemistry, are not assessed to affect the maximum dose significantly (see scenario uncertainties in Figure 13-5). In a warmer climate with dry summers, the maximum doses are slightly higher than in the *base case*, but do not increase if the plant water deficit is covered by irrigation with surface water. In a cold climate, the maximum dose occurs prior to the first periglacial period, and is thus identical with that in the *base case*. In periods with permafrost the dose is significantly lower than in the *base case*. This is primarily due to the climate restrictions on land use and causes a shift in dose-contributing radionuclides. However, sea level rise may have noticeable effects on the maximum dose, and a delay in the shoreline regression by 20 000 years may reduce the maximum doses by a factor of two.

[66] The effects of retention and radioactive decay in the geosphere is insignificant for C-14, Mo-93 and Ca-41 (Section 5.5.2 in Radionuclide transport report).

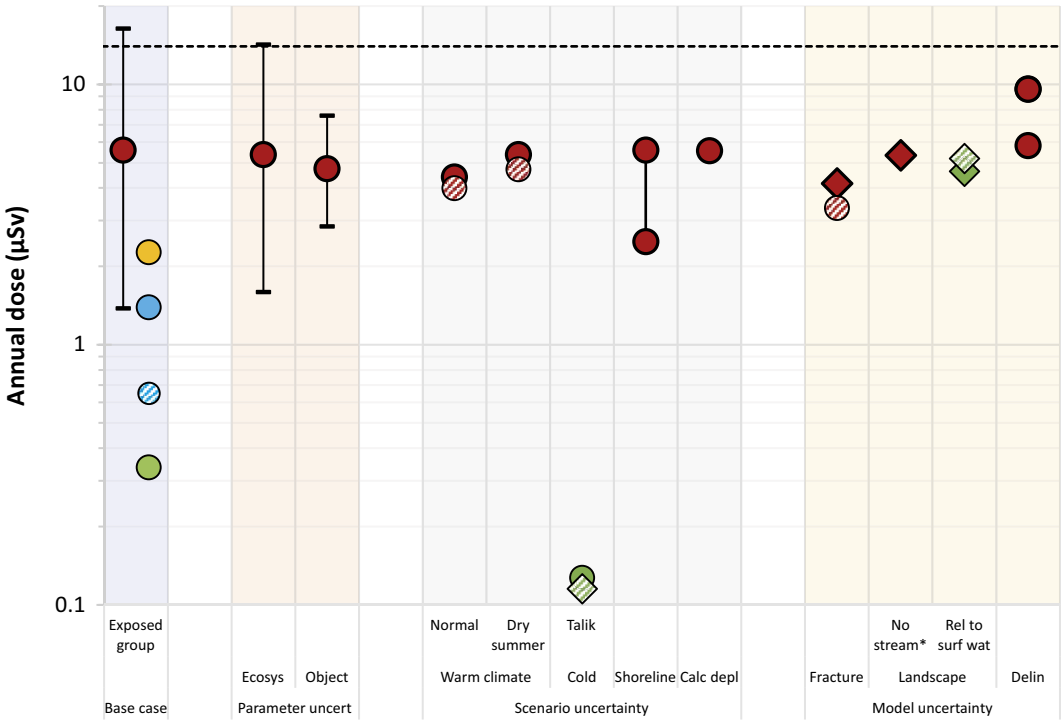

Figure 13-5. *Effects of data, scenario and modelling uncertainties on the maximum annual dose. Symbols show the mean dose and whiskers indicate the 90 % confidence interval. Doses to all exposed groups are shown for the base case whereas only doses to the most exposed group are shown for all other calculation cases (colour coding as in Figure 9-4, e.g. red indicates DM and green HG). Circles represent biosphere object 157_2, whereas diamonds represent the down-stream object 157_1. Stripes indicate irrigation (warm climate), considerably changed groundwater discharge from the bedrock (fracture) or halted mire ingrowth (release to surface). For the cold climate calculation case, the dose represents the periglacial periods and stripes indicate that hydrological parameters are modified. Note that only the variants with the highest and lowest doses are shown for the shoreline regression case. For the object delineation case doses overlap between sub-areas, and the dose from the Agri area is not shown.*

In the *base case*, and in most other calculation cases, the maximum dose occurs during the first 10 000 years. C-14 is the radionuclide that contributes most to the dose in the beginning of this period. However, for most of the period, including the dose maximum, Mo-93 is the radionuclide that contributes most to the dose. The radionuclide-specific dose from Mo-93 declines with time and is insignificant after 30 000 AD (Section 9.3). Thus, to get a more complete picture of how uncertainties affect the annual dose, the response of the highest dose after 30 000 AD is examined.

The uncertainty in dose increases with time (Section 9.4). The 90 % confidence interval of the highest dose after 30 000 years is approximately 30 % wider than at dose maximum. This is mainly due to the influence of Ca-41. As for the maximum dose, variation in ecosystem parameters is the primary source for the uncertainty in dose beyond 30 000 AD. However, for this part of the assessment period, scenario uncertainties tend to yield a higher dose than in the *base case* (Figure 13-6). For example, both in the *warm climate calculation case* and in the *calcite depletion calculation case* doses are approximately a factor of two higher than in the *base case*. In the latter case, the increase is due to accumulation of decay products from the U-238 and U-235 series at the end of the assessment. The dose also tends to increase with a rise in sea level, but the dose response is limited (~50 % increase). The responses to modelling uncertainties after 30 000 AD are mixed. That is, diffusive transport to the down-stream mire increases the dose by a factor of two, whereas the dose from a direct release to the surface water is more than an order of magnitude lower than in the *base case*. These results suggest that the *base case* scenario is not always cautious with respect to modelling and scenario uncertainties after 30 000 AD. Still, the effects are limited to a factor of two, and doses in this period never exceed the maximum in the *base case*.

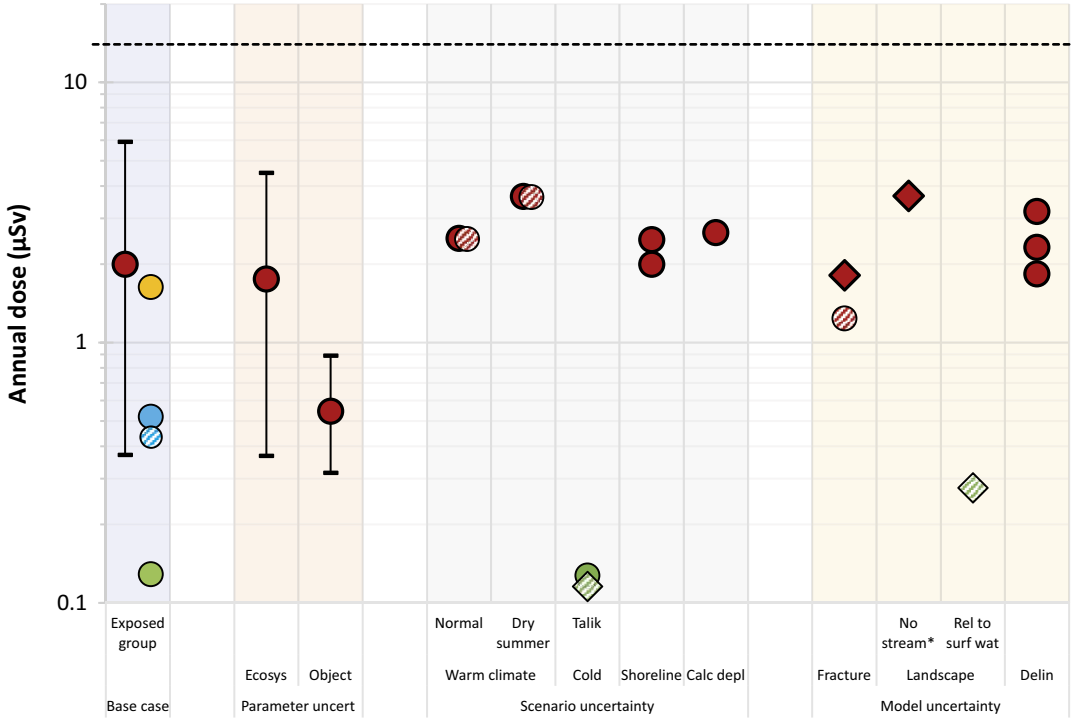

Figure 13-6. *Effects of data, scenario and modelling uncertainties on the highest annual dose after 30 000 AD. Symbols show the mean dose and whiskers indicate the 90 % confidence interval. The shape and colour coding of symbols are explained in Figure 13-5. Note that irrigation has no effect on long-term maximum doses (the striped symbols are imposed on top of the filled symbols in Warm climate).*

13.8.2 Uncertainty in landscape development and object properties

The *base case* calculations are based on a deterministic description of the development of the landscape in Forsmark that builds on the *reference evolution* (**Post-closure safety report**, Chapter 6). In the PSAR, this description is complemented by several other calculation cases that together cover a range of outcomes, that reflect reasonable future landscape developments.

The calculation cases that examine modelling uncertainties show that the maximum dose is insensitive to alternative representations of transport pathways and landscape configurations; the effects of alternative assumptions are typically limited to less than a factor of two as compared with the *base case* (see *modelling uncertainty* in Figure 13-5). This is true for the transport pathway down-stream of the primary discharge area (*no stream*), and for direct transport of the geosphere release to surface water (*rel to surf wat*). Maximum doses are also insensitive to the rate of lake infilling, as shown by an explicit description of this stage in object 157_2 (Section 13.4.4) and by a small persistent lake in the down-stream object (*rel to surf wat*, striped symbol). Similarly, distributing the release between three discharge areas, in accordance with a subhorizontal fracture (*fracture*) in the bedrock, has a limited effect on the maximum dose.

Uncertainties in the thickness of regolith layers and in associated groundwater flows are not accounted for in the *base case*. Instead, the heterogeneity within object 157_2 is used to illustrate the importance of *mire object properties* in a sensitivity analysis (Section 13.5.4). The dose variation due to uncertainties in object properties is notable, but clearly less important than variation caused by ecosystem parameters. That is, the width of the 90 % confidence interval associated with object properties is 30 % of that for *ecosystem parameters*, whereas the corresponding number is 20 % for the highest dose after 30 000 AD (Figure 13-5 and Figure 13-6). The sensitivity indices (i.e. β coefficients) for individual object properties also give an indication of the dose response to specified changes in for example regolith thicknesses and/or input of groundwater and surface water.

Though far from comprehensive, modelling uncertainties in the regolith thickness and surface hydrology have been reported in previous SKB studies. For example, a comparison of results from two different landscape models suggests the uncertainty in the thickness of post-glacial regolith layers in object 157_2 may span a factor of two (Gunia et al. 2021, Appendix A). Moreover, uncertainties associated with the MIKE SHE tool suggests that the area specific flow from the bedrock may vary by 20 % (Johansson and Sassner 2019). Further, the lower estimates for the yearly runoff (or net precipitation) in this assessment is approximately 30 % less than the typical value of 175 mm a^{-1} (Section 8.2.4). If these uncertainties are coupled with derived sensitivity indices (β in Table 11-4), changes in radionuclide specific doses can be calculated. For C-14, a decrease of groundwater flow from the bedrock by 20 %, in combination with an increase in the thickness of peat by a factor of two, increases the radionuclide specific dose by 25 %. The dose responses of the other three key radionuclides (Mo-93, Ca-41 and Ni-59) are more sensitive to combined changes in the thickness of regolith layers and in hydrological parameters. However, even for these radionuclides, hypothetical cautious changes in multiple properties increase the doses with no more than a factor of two[67].

The results from the *alternative delineations* within object 157_2 also illustrate the effects of uncertainties in properties that are affected by the landscape development. The combinations of parameter values that are used in this calculation case reflects natural co-variation due to the positions of the sub-areas in the landscape. The results suggest that coordinated changes in object properties have an effect on the calculated maximum dose that is limited to a factor of two (Delin in Figure 13-5). However, the size of the biosphere object is a main driver of the dose variation in this calculation case (Table 11-4). If the sensitivity indexes are used to adjust the doses in sub-areas to correspond to an object of the size used in the *base case*, then the increase in the maximum dose caused by regolith stratigraphy and surface hydrology is less than 50 % of that in the *base case*.

The fraction of a geosphere release that reaches a discharge area is dependent on the size and properties of the biosphere object. In the *alternative object delineation calculation case* this is not accounted for. Instead, the full geosphere release is cautiously assumed to be discharged into each of the outlined areas[68]. A quantitative mapping of the discharge from SFR using bedrock case BC1 for 5000 AD (Figure 5-3) shows that 80 % of the release is discharged in the area with an upward gradient, 60 % is discharged in the uphill area, 45 % is discharged in the wetland area, whereas only 15 % ends up in the small area with best potential for cultivation. Accounting for this reduction in the geosphere release, the doses from the alternative delineations are similar to, or less than, those calculated in the *base case*.

Moreover, the fraction of the release that reaches a sub-area of object 157_2 can fully be explained by the object area and the area specific discharge from the bedrock[69]. As expected, the fraction of the release decreases with a reduction in size or bedrock discharge. The *mire object property* analysis showed that doses from C-14 increase almost in proportion to the decrease of these two parameters. However, if the response of the geosphere release reaching the area was also to be accounted for, then doses from C-14 would be considerably less sensitive to changes in these two object properties.

[67] Systematic and cautious changes in parameters values causes the doses to increase between 70 % (Ca-41 and Ni-59) and 100 % (Mo-93). The postulated changes are that the net precipitation decreases by 30 % and the thickness is halved (all radionuclides). In addition, the flow from the bedrock changes by 20 % (increase for Ca-41, decrease for Ni-59), the thicknesses of peat (Mo-93) and glacial clay (Ca-41) layers is doubled, and the thickness of clay-gyttja either increases (Mo-93) or decreases (Ni-59) by a factor of two.

[68] It is recognized that this assumption is not applicable to the smallest area (Section 11.4.3), and the results are not carried forward to the comparative analysis.

[69] A linear function on log transformed data describes 99 % of the variation of the fraction released to the alternative delineated areas. The beta coefficients for the area of the object and for the area specific discharge of groundwater from the bedrock are both positive.

13.9 Conclusions

The main scenario consists of three calculation cases; the *base case*, the *warm climate calculation case* and the *cold climate calculation case*. In this report, the potential effects of additional scenario, modelling and data uncertainties are examined in eight additional calculation cases. Results from previous SKB assessments are also relevant for the discussion of uncertainties and supports the handling of two key radionuclides in this assessment.

The *base case* provides a benchmark for the post-closure safety assessment and, thus, enables straightforward evaluation of differences with respect to other calculation cases. It also fulfils the regulatory requirement that an assessment of a repository's protective capability should include a case where the biosphere conditions prevailing at the time for the application will not change. The case includes exposed groups that together reflect a broad set of relevant exposure pathways, and where the selected characteristics and habits of the groups are reasonable and sustainable. To facilitate efficient computations the representation of the biosphere is simplified in several ways, and the landscape description is deterministic. Supporting calculations demonstrate that the maximum dose is robust with respect to assumptions made. Probabilistic simulations may lead to temporal dilution of radionuclides. However, the mean doses from probabilistic simulations are always above the dose from deterministic simulations, and the mean-of-peaks is only 26 % above the peak-of-means for the dose maximum. This indicates that temporal dilution is not likely to have any significant effect on the results. Taken together, the surface system representation in the *base case* is considered to be appropriate and fit for purpose with respect to the demonstration of safety.

The *warm climate calculation case* accounts for a delayed shoreline regression, as well as increases in atmospheric CO_2 concentration and in plant and crop production. The case also includes expected changes in surface hydrology, and effects of large-scale irrigation and plant translocation. The *cold climate calculation case* accounts for a decrease in atmospheric CO_2 concentrations and a reduced production of lake and mire ecosystems. The case also includes alternative transport pathways, additional surface recipients and expected changes in the surface hydrology. The results from the two calculation cases are reasonable and consistent with SKB's general understanding of how climate affects the surface system. Thus, it is concluded that the two cases, together with the *base case*, adequately address relevant effects of future large-scale climate change that are part of the main scenario.

Uncertainties with respect to landscape development and object properties are examined in several calculation cases, including earlier supplementary material for SR-PSU. Results from these cases together show that the maximum dose is relatively insensitive to transport pathways in the landscape, the rate of shoreline regression and the succession of ecosystems, and alternative assumptions do not increase the maximum dose significantly as compared with the *base case*. Uncertainties in object properties clearly influence dose variation. However, the combined response to variation conditioned on the position in the landscape, or on model uncertainties in regolith thickness and surface hydrology, is limited. Finally, trends of increasing doses for areas of small size and/or in areas with low discharge of deep groundwater are likely to be counteracted by a reduced geosphere release. Taken together it is concluded that uncertainties in landscape development and object properties are unlikely to have any significant influence on the calculated dose and the evaluation of the repository safety.

References

SKB's (Svensk Kärnbränslehantering AB) publications can be found at www.skb.com/publications. SKBdoc documents will be submitted upon request to document@skb.se.

References with abbreviated names

Post-closure safety report, 2023. Post-closure safety for SFR, the final repository for short-lived radioactive waste at Forsmark. Main report, PSAR version. SKB TR-23-01, Svensk Kärnbränslehantering AB.

Barrier process report, 2023. Post-closure safety for SFR, the final repository for short-lived radioactive waste at Forsmark. Engineered barrier process report, PSAR version. SKB TR-23-04, Svensk Kärnbränslehantering AB.

Climate report, 2023. Post-closure safety for SFR, the final repository for short-lived radioactive waste at Forsmark. Climate and climate-related issues, PSAR version. SKB TR-23-05, Svensk Kärnbränslehantering AB.

Data report, 2023. Post-closure safety for SFR, the final repository for short-lived radioactive waste at Forsmark. Data report, PSAR version. SKB TR-23-10, Svensk Kärnbränslehantering AB.

FEP report, 2014. FEP report for the safety assessment SR-PSU. SKB TR-14-07, Svensk Kärnbränslehantering AB.

FHA report, 2023. Post-closure safety for SFR, the final repository for short-lived radioactive waste at Forsmark. Handling of future human actions, PSAR version. SKB TR-23-08, Svensk Kärnbränslehantering AB.

Geosphere process report, 2014. Geosphere process report for the safety assessment SR-PSU. SKB TR-14-05, Svensk Kärnbränslehantering AB.

Initial state report, 2023. Post-closure safety for SFR, the final repository for short-lived radioactive waste at Forsmark. Initial state of the repository, PSAR version. SKB TR-23-02, Svensk Kärnbränslehantering AB.

Model tools report, 2023. Post-closure safety for SFR, the final repository for short-lived radioactive waste at Forsmark. Model tools summary report, PSAR version. SKB TR-23-11, Svensk Kärnbränslehantering AB.

Radionuclide transport report, 2023. Post-closure safety for SFR, the final repository for short-lived radioactive waste at Forsmark. Radionuclide transport and dose calculations, PSAR version. SKB TR-23-09, Svensk Kärnbränslehantering AB.

Waste process report, 2023. Post-closure safety for SFR, the final repository for short-lived radioactive waste at Forsmark. Waste form and packaging process report, PSAR version. SKB TR-23-03, Svensk Kärnbränslehantering AB.

Regular references

Adill A, Holliland P B, Åkerlund C, 2021. Biologisk recipientkontroll vid Forsmarks kärnkraftverk: årsrapport för 2020. Lysekil: Swedish University of Agricultural Sciences. (Aqua reports 2021:6) (In Swedish.)

Adrian R, O'Reilly C M, Zagarese H, Baines S B, Hessen D O, Keller W, Livingstone D M, Sommaruga R, Straile D, van Donk E, Weyhenmeyer G A, Winder M, 2009. Lakes as sentinels of climate change. Limnology and Oceanography 54, 2283–2297.

Ahmed H, Young S, Shaw G, 2012. Solubility and mobility of thorium and uranium in soils: the effect of soil properties on Th and U concentrations in soil solution. Geophysical Research Abstracts 14, EGU2012-2994.

Aliyu A S, Ramli A T, Saleh M A, 2015a. Assessment of potential human health and environmental impacts of a nuclear power plant (NPP) based on atmospheric dispersion modelling. Atmósfera 28, 13–26.

Aliyu A S, Ramli A T, Garba N N, Saleh M A, Gabdo H T, Liman M S, 2015b. Fukushima nuclear accident: preliminary assessment of the risks to non-human biota. Radiation Protection Dosimetry 163, 238–250.

Andersen J H, Carstensen J, Conley D J, Dromph K, Fleming-Lehtinen V, Gustafsson B G, Josefson A B, Norkko A, Villnäs A, Murray C, 2017. Long-term temporal and spatial trends in eutrophication status of the Baltic Sea. Biological Reviews 92, 135–149.

Andersson E, 2010. The limnic ecosystems at Forsmark and Laxemar-Simpevarp. SKB TR-10-02, Svensk Kärnbränslehantering AB.

Andersson E, Aquilonius K, Sivars Becker L, Borgiel M, 2011. Site investigation SFR. Vegetation in streams in the Forsmark area. SKB P-11-18, Svensk Kärnbränslehantering AB.

Andersson P, Garnier-Laplace J, Beresford N A, Copplestone D, Howard B J, Howe P, Oughton D, Whitehouse P, 2009. Protection of the environment from ionising radiation in a regulatory context (PROTECT): proposed numerical benchmark values. Journal of Environmental Radioactivity 100, 1100–1108.

ANSTO, 2017. Screening assessment of dose rates to wildlife related to the Nuclear Medicine Mo99 Facility, ANSTO, March 2017. ANSTO-E-785, Australian Nuclear Science and Technology Organisation.

Aquilonius K (ed), 2010. The marine ecosystems at Forsmark and Laxemar-Simpevarp. SR-Site Biosphere. SKB TR-10-03, Svensk Kärnbränslehantering AB.

Aquilonius K, Qvarfordt S, Borgiel M, 2011. Validation of the marine vegetation model in Forsmark. SFR-Site Forsmark. SKB P-11-10, Svensk Kärnbränslehantering AB.

Arai Y, 2008. Spectroscopic evidence for Ni(II) surface speciation at the iron oxyhydroxides–water interface. Environmental Science & Technology 42, 1151–1156.

ATSDR, 2005. Public health assessment guidance manual (Update). U.S. Department of Health and Human Services, Public Health Service Agency for Toxic Substances and Disease Registry (ATSDR), Atlanta, Georgia.

Avila R, Bergström U, 2006. Methodology for calculation of doses to man and implementation in Pandora. SKB R-06-68, Svensk Kärnbränslehantering AB.

Avila R, Moberg L, 1999. A systematic approach to the migration of ^{137}Cs in forest ecosystems using interaction matrices. Journal of Environmental Radioactivity 45, 271–282.

Avila R, Pröhl G, 2008. Models used in the SFR 1 SAR-08 and KBS-3H safety assessments for calculation of ^{14}C doses. SKB R-08-16, Svensk Kärnbränslehantering AB.

Avila R, Thiry Y, Gilbin R, Agüero A, Thorne M, Sheppard M, Tamponnet C, Ikonen A, Xu S, 2006. Recommendations for improving predictions of the long-term environmental behaviour of ^{14}C, ^{36}Cl, ^{99}Tc, ^{237}Np and ^{238}U. Findings of the IUR "Radioecology and Waste" Task Force. IUR Report 6, International Union of Radioecology.

Avila R, Ekström P-A, Åstrand P-G, 2010. Landscape dose conversion factors used in the safety assessment SR-Site. SKB TR-10-06, Svensk Kärnbränslehantering AB.

BACC, 2008. Assessment of climate change for the Baltic Sea basin. The BACC (BALTEX Assessment of Climate Change for the Baltic Sea basins) author team. Berlin: Springer.

Barrow N J, Whelan B R, 1998. Comparing the effects of pH on the sorption of metals by soil and by goethite, and on uptake by plants. European Journal of Soil Science 49, 683–692.

Bateman H, 1910. The solution of a system of differential equations occurring in the theory of radio-active transformations. Proceedings of the Cambridge Philosophical Society 15, 423–427.

Beresford N A, Brown J, Copplestone D, Garnier-Laplace J, Howard B, Larsson C-M, Oughton O, Pröhl G, Zinger I (eds), 2007. D-ERICA: An integrated approach to the assessment and management of environmental risks from ionising radiation. Description of purpose, methodology and application. A deliverable of the ERICA project (FI6RCT-2004-508847). Available at: https://wiki.ceh.ac.uk/download/attachments/115017395/D-Erica.pdf

Berglund K, 1996. Agricultural improvement of cultivated organic soils II. Effects of liming and deep cultivation on soil properties and root development. Soil Use and Management 12, 169–175.

Berglund K, 2008. Torvmarker en resurs i jordbruket igår, idag och även imorgon? In Runefelt L (ed). Svensk mosskultur: odling, torvanvändning och landskapets förändring 1750–2000. Stockholm: Kungliga Skogs- och Lantbruksakademien, 483–498. (In Swedish.)

Berglund S, Lindborg T (eds), 2017. Monitoring Forsmark – evaluation and recommendations for programme update. SKB TR-15-01, Svensk Kärnbränslehantering AB.

Berglund Ö, Berglund K, Sohlenius G, 2009. Organogen jordbruksmark i Sverige 1999–2008. Uppsala: Swedish University of Agricultural Sciences, Department of Soil Sciences. (Rapport 12) (In Swedish.)

Bergström U, Barkefors C, 2004. Irrigation in dose assessments models. SKB R-04-26, Svensk Kärnbränslehantering AB.

Bergström U, Avila R, Ekström P-A, de la Cruz I, 2008. Dose assessments for SFR 1. SKB R-08-15, Svensk Kärnbränslehantering AB.

Bosson E, Gustafsson L-G, Sassner M, 2008. Numerical modelling of surface hydrology and near-surface hydrogeology at Forsmark. Site descriptive modelling, SDM-Site Forsmark. SKB R-08-09, Svensk Kärnbränslehantering AB.

Bosson E, Sassner M, Sabel U, Gustafsson L-G, 2010. Modelling of present and future hydrology and solute transport at Forsmark. SR-Site Biosphere. SKB R-10-02, Svensk Kärnbränslehantering AB.

Bosson E, Selroos J-O, Stigsson M, Gustafsson L-G, Destouni G, 2013. Exchange and pathways of deep and shallow groundwater in different climate and permafrost conditions using the Forsmark site, Sweden, as an example catchment. Hydrogeology Journal 21, 225–237.

Brookins D G, 1986. Rhenium as analog for fissiogenic technetium: Eh-pH diagram (25 °C, 1 bar) constraints. Applied Geochemistry 1, 513–517.

Brown J E, Alfonso B, Avila R, Beresford N A, Copplestone D, Pröhl G, Ulanovsky A, 2008. The ERICA Tool. Journal of Environmental Radioactivity 99, 1371–1383.

Brown J E, Beresford N A, Hosseini A, 2013. Approaches to providing missing transfer parameters values in the ERICA Tool – How well do they work? Journal of Environmental Radioactivity 126, 399–411.

Brown J E, Alfonso B, Avila R, Beresford N A, Copplestone D, Hosseini A, 2016. A new version of the ERICA tool to facilitate impact assessments of radioactivity on wild plants and animals. Journal of Environmental Radioactivity 153, 141–148.

Brunberg A-K, Nilsson E, Blomqvist P, 2002. Characteristics of oligotrophic hardwater lakes in a postglacial land-rise area in mid-Sweden. Freshwater Biology 47, 1451–1462.

Brunberg A-K, Carlsson T, Blomqvist P, Brydsten L, Strömgren M, 2004. Forsmark site investigation. Identification of catchments, lake-related drainage parameters and lake habitats. SKB P-04-25, Svensk Kärnbränslehantering AB.

Brundell P, Kanlén F, Westö A-K, 2008. Water use for irrigation. Report on Grant Agreement No 71301.2006.002–2006.470, Statistiska centralbyrån (Statistics Sweden).

Brydsten L, 1999. Shore line displacement in Öresundsgrepen. SKB TR-99-16, Svensk Kärnbränslehantering AB.

Brydsten L, 2009. Sediment dynamics in the coastal areas of Forsmark and Laxemar during an interglacial. SKB TR-09-07, Svensk Kärnbränslehantering AB.

Brydsten L, Strömgren M, 2010. A coupled regolith-lake development model applied to the Forsmark site. SKB TR-10-56, Svensk Kärnbränslehantering AB.

Brydsten L, Strömgren M, 2013. Landscape development in the Forsmark area from the past into the future (8500 BC–40 000 AD). SKB R-13-27, Svensk Kärnbränslehantering AB.

Cerdan O, Govers G, Le Bissonnais Y, Van Oost K, Poesen J, Saby N, Gobin A, Vacca A, Quinton J, Auerswald K, Klik A, Kwaad F J P M, Raclot D, Ionita I, Rejman J, Rousseva S, Muxart T, Roxo M J, Dostal T, 2010. Rates and spatial variations of soil erosion in Europe: A study based on erosion plot data. Geomorphology 122, 167–177.

Chapin F S, Matson P A, Mooney H A, 2002. Principles of terrestrial ecosystem ecology. New York: Springer.

Chappaz A, Lyons T W, Gregory D D, Reinhard C T, Gill B C, Li C, Large R R, 2014. Does pyrite act as an important host for molybdenum in modern and ancient euxinic sediments? Geochimica et Cosmochimica Acta 126, 112–122.

Charman D, 2002. Peatland and environmental change. Chichester: Wiley.

Charrasse B, Anderson A, Mora J C, Smith J, Cohenny E, Ikonen A T K, Kangasniemi V, Zorko B, Bonchuk Y, Beaumelle L, Gunawardena N, Amado V, Liptak L, Leclerc E, Telleria D, 2019. Does the use of reference organisms in radiological impact assessments provide adequate protection of all the species within an environment? Science of The Total Environment 658, 189–198.

Chen M A, Kocar B D, 2018. Radium sorption to iron (hydr)oxides, pyrite, and montmorillonite: implications for mobility. Environmental Science & Technology 52, 4023–4030.

Clymo R S, Turunen J, Tolonen K, 1998. Carbon accumulation in peatland. OIKOS 81, 368–388.

Cohen-Corticchiato D, Zwinger T, 2021. Modeling permafrost evolution at Olkiluoto for the next 120 000 years. Posiva Working Report 2021-14, Posiva Oy, Finland.

Colle C, Madoz-Escande C, Leclerc E, 2009. Foliar transfer into the biosphere: review of translocation factors to cereal grains. Journal of Environmental Radioactivity 100, 683–689.

Crusius J, Calvert S, Pedersen T, Sage D, 1996. Rhenium and molybdenum enrichments in sediments as indicators of oxic, suboxic and sulfidic conditions of deposition. Earth and Planetary Science Letters 145, 65–78.

Crusius J, Thomson J, 2000. Comparative behavior of authigenic Re, U, and Mo during reoxidation and subsequent long-term burial in marine sediments. Geochimica et Cosmochimica Acta 64, 2233–2242.

Dahl T W, Anbar A D, Gordon G W, Rosing M T, Frei R, Canfield D E, 2010. The behavior of molybdenum and its isotopes across the chemocline and in the sediments of sulfidic Lake Cadagno, Switzerland. Geochimica et Cosmochimica Acta 74, 144–163.

Dahl T W, Ruhl M, Hammarlund E U, Canfield D E, Rosing M T, Bjerrum C J, 2013. Tracing euxinia by molybdenum concentrations in sediments using handheld X-ray fluorescence spectroscopy (HHXRF). Chemical Geology 360–361, 241–251.

Dahlqvist R, Andersson K, Ingri J, Larsson T, Stolpe B, Turner D, 2007. Temporal variations of colloidal carrier phases and associated trace elements in a boreal river. Geochimica et Cosmochimica Acta 71, 5339–5354.

Deblonde G J-P, Zavarin M, Kersting A B, 2021. The coordination properties and ionic radius of actinium: A 120-year-old enigma. Coordination Chemistry Reviews 446, 214130. doi:10.1016/j.ccr.2021.214130

Donnelly C, Greuell W, Andersson J, Gerten D, Pisacane G, Roudier P, Ludwig F, 2017. Impacts of climate change on European hydrology at 1.5, 2 and 3 degrees mean global warming above preindustrial level. Climatic Change 143, 13–26.

Ekström P-A, 2017. Konvergens av probabilistiska beräkningar. SKBdoc 1581608 ver 1.0, Svensk Kärnbränslehantering AB. (In Swedish.)

Eliasson P, 1992. ”Genom helvetets port, men…” – skogsdikning som mål och medel. Aktuellt om historia 3–4, 46–60. (In Swedish.)

Eng T, Hudson J, Stephansson O, Skagius K, Wiborgh M, 1994. Scenario development methodologies. SKB TR 94-28, Svensk Kärnbränslehantering AB.

Engdahl A, Ternsell A, Hannu S, 2006. Oskarshamn site investigation. Chemical characterisation of deposits and biota. SKB P-06-320, Svensk Kärnbränslehantering AB.

Erichsen A C, Konovalenko L, Møhlenberg F, Closter R M, Bradshaw C, Aquilonius K, Kautsky U, 2013. Radionuclide transport and uptake in coastal aquatic ecosystems: a comparison of a 3D dynamic model and a compartment model. Ambio 42, 464–475.

Fredriksson D, 2004. Forsmark site investigation. Peatland investigation Forsmark. SKB P-04-127, Svensk Kärnbränslehantering AB.

Fuller A J, Shaw S, Peacock C L, Trivedi D, Small J S, Abrahamsen L G, Burke I T, 2014. Ionic strength and pH dependent multi-site sorption of Cs onto a micaceous aquifer sediment. Applied Geochemistry 40, 32–42.

Garnier-Laplace J, Gilbin R (eds), 2006. Derivation of predicted-no-effect-dose-rate values for ecosystems (and their sub-organisational levels) exposed to radioactive substances. Report D5 of the ERICA project, European Commission.

Garnier-Laplace J, Della-Vedova C, Andersson P, Copplestone D, Cailes C, Beresford N A, Howard B J, Howe P, Whitehouse P, 2010. A multi-criteria weight of evidence approach for deriving ecological benchmarks for radioactive substances. Journal of Radiological Protection 30, 215–233.

Gentzschein B, Levén J, Follin S, 2007. A comparison between well yield data from the site investigation in Forsmark and domestic wells in northern Uppland. SKB P-06-53, Svensk Kärnbränslehantering AB.

Gosling S N, Taylor R G, Arnell N W, Todd M C, 2011. A comparative analysis of projected impacts of climate change on river runoff from global and catchment-scale hydrological models. Hydrology and Earth System Science 15, 279–294.

Gosling S, Müller Schmied H, Betts R, Chang J, Ciais P, Dankers R, Döll P, Eisner S, Flörke M, Gerten D, Grillakis M, Hanasaki N, Hagemann S, Huang M, Huang Z, Jerez S, Kim H, Koutroulis A, Leng G, Liu X, Masaki Y, Montavez P, Morfopoulos C, Oki T, Papadimitriou L, Pokhrel Y, Portmann F T, Orth R, Ostberg S, Satoh Y, Seneviratne S, Sommer P, Stacke T, Tang Q, Tsanis I, Wada Y, Zhou T, Büchner M, Schewe J, Zhao F, 2019. ISIMIP2a Simulation Data from Water (global) Sector (V. 1.1). GFZ Data Services. Available at: https://doi.org/10.5880/PIK.2019.003

Green M, 2019. Fågelövervakning i Forsmark 2018. SKB P-19-02, Svensk Kärnbränslehantering AB. (In Swedish.)

Grolander S, 2013. Biosphere parameters used in radionuclide transport modelling and dose calculations in SR-PSU. SKB R-13-18, Svensk Kärnbränslehantering AB.

Grolander S, Jaeschke B, 2019. Biosphere parameters used in radionuclide transport modelling and dose calculations in SE-SFL. SKB R-19-18, Svensk Kärnbränslehantering AB

Gunia K, Gunia M, Seppänen A, Strömgren M, 2021. Terrain and ecosystem modelling for Forsmark area. Comparison of the regolith-lake development model and the Untamo model. SKB R-20-09, Svensk Kärnbränslehantering AB.

Gustafsson B G, 2004. Millennial changes of the Baltic Sea salinity. Studies of the sensitivity of the salinity to climate change. SKB TR-04-12, Svensk Kärnbränslehantering AB.

Gustafsson J P, 2012. Visual MINTEQ 3.0. Available at: https://vminteq.com

Gustafsson J P, Tiberg C, 2015. Molybdenum binding to soil constituents in acid soils: An XAS and modelling study. Chemical Geology 417, 279–288.

Haddeland I, Clark D B, Franssen W, Ludwig F, Voß F, Arnell N W, Bertrand N, Best M, Folwell S, Gerten D, Gomes S, Gosling S N, Hagemann S, Hanasaki N, Harding R, Heinke J, Kabat P, Koirala S, Oki T, Polcher J, Stacke T, Viterbo P, Weedon G P, Yehm P, 2011. Multimodel estimate of the global terrestrial water balance: Setup and first results. Journal of Hydrometeorology 12, 869–884.

Hall A M, Ebert K, Goodfellow B W, Hättestrand C, Heyman J, Krabbendam M, Moon S, Stroeven A P, 2019. Past and future impact of glacial erosion in Forsmark and Uppland. Final report. SKB TR-19-07, Svensk Kärnbränslehantering AB.

Hamrén U, Collinder P, 2010. Vattenverksamhet i Forsmark. Ekologisk fältinventering och naturvärdesklassificering samt beskrivning av skogsproduktionsmark. SKB R-10-16, Svensk Kärnbränslehantering AB. (In Swedish.)

Hannu S, Karlsson S, 2006. Forsmark site investigation. Chemical characterisation of deposits and biota. SKB P-06-220, Svensk Kärnbränslehantering AB.

Harrison F L, Anderson S L, 1996. Taxonomic and development aspects of radiosensitivity. In Amiro B, Avadhanula R, Johansson G, Larsson C M, Luning M (eds). Proceedings of the International Symposium in Ionizing Radiation, Stockholm, 20–24 May 1996. Stockholm: Swedish Radiation Protection Institute (SSI), 65–88.

Harrison J P, Hudson J A, 2006. Comprehensive hazard identification in rock engineering using interaction matrix mechanism pathways. In Golden Rocks 2006: the 41st U.S. Symposium on Rock Mechanics (USRMS), Golden, Colorado, 17–21 June 2006. Golden, CO: Colorado School of Mines.

Hartikainen J, Kouhia R, Wallroth T, 2010. Permafrost simulations at Forsmark using a numerical 2D thermo-hydro-chemical model. SKB TR-09-17, Svensk Kärnbränslehantering AB.

Hedenström A, Sohlenius G, 2008. Description of the regolith at Forsmark. Site descriptive modelling, SDM-Site. SKB R-08-04, Svensk Kärnbränslehantering AB.

Helz G R, Bura-Nakic E, Mikac N, Ciglenecki I, 2011. New model for molybdenum behavior in euxinic waters. Chemical Geology 284, 323–332.

Hjertstedt H, 1946. De organogena odlingsjordarnas beskaffenhet i olika län med avseende på torvslag, förmultningsgrad och reaktion samt innehåll av kalk och kväve, kali och fosforsyra, organisk substans, seskvioxider och svavelsyra. Svenska Vall- och Mossekulturföreningens kvartalsskrift 8, 255–277. (In Swedish.)

Hoch A R, 2014. Uptake of gaseous carbon-14 in the biosphere: development of an assessment model. AMEC/004041/007, AMEC, UK.

Hongxia Z, Zheng D, Zuyi T, 2006. Sorption of thorium(IV) ions on gibbsite: Effects of contact time, pH, ionic strength, concentration, phosphate and fulvic acid, Colloids and Surfaces A: Physicochemical and Engineering Aspects 278, 46–52.

Howard B J, Larsson C-M, 2008. The ERICA Integrated Approach and its contribution to protection of the environment from ionising radiation. Journal of Environmental Radioactivity 99, 1361–1363.

Hyenstrand Å, 1994. Kulturminnen och kulturmiljövård. In Selinge K-G (ed). Sveriges nationalatlas. Kulturminnen och kulturmiljövård. Stockholm: SNA. (In Swedish.)

IAEA, 2003. "Reference Biospheres" for solid radioactive waste disposal: Report of BIOMASS Theme 1 of the BIOsphere Modelling and ASSessment (BIOMASS) Programme. IAEA-BIOMASS-6, International Atomic Energy Agency, Vienna.

IAEA, 2009. Quantification of radionuclide transfers in terrestrial and freshwater environments for radiological assessments. Vienna: International Atomic Energy Agency. (IAEA TECDOC-1616)

IAEA, 2010. Handbook of parameter values for the prediction of radionuclide transfer in terrestrial and freshwater environments. Vienna: International Atomic Energy Agency. (IAEA Technical Reports Series 472)

IAEA, 2011. Wildlife transfer parameter database. International Atomic Energy Agency and International Union of Radioecologists. Available at: https://www.wildlifetransferdatabase.org [February 2011].

IAEA, 2012. The safety case and safety assessment for the disposal of radioactive waste. Vienna: International Atomic Energy Agency. (IAEA Safety Standard Series SSG-23)

IAEA, 2015. Wildlife transfer parameter database. International Atomic Energy Agency and International Union of Radioecologists. Available at: https://www.wildlifetransferdatabase.org [April 2015].

IAEA, 2018. Prospective radiological environmental impact assessment for facilities and activities. Vienna: International Atomic Energy Agency. (IAEA Safety Standards Series GSG-10)

Icenhower J P, Qafoku N P, Zachara J M, Martin W J, 2010. The Biogeochemistry of Technetium: A Review of the Behavior of an Artificial Element in the Natural Environment. American Journal of Science 310, 721–752.

ICRP, 1991. 1990 Recommendations of the International Commission on Radiological Protection. Oxford: Pergamon. (ICRP Publication 60; Annals of the ICRP 21)

ICRP, 2000. Radiation protection recommendations as applied to the disposal of long-lived solid radioactive waste. Oxford: Pergamon. (ICRP Publication 81; Annals of the ICRP 28)

ICRP, 2003. A Framework for Assessing the Impact of Ionising Radiation on Non-human Species. Oxford: Pergamon. (ICRP Publication 91; Annals of the ICRP 33)

ICRP, 2006. Assessing dose of the representative person for the purpose of radiation protection of the public and the optimisation of radiological protection: broadening the process. Amsterdam: Elsevier. (ICRP Publication 101; Annals of the ICRP 36)

ICRP, 2007. The 2007 Recommendations of the International Commission on Radiological Protection. Amsterdam: Elsevier. (ICRP Publication 103; Annals of the ICRP 37)

ICRP, 2008. Environmental Protection – the Concept and Use of Reference Animals and Plants. Amsterdam: Elsevier. (ICRP Publication 108; Annals of the ICRP 38)

ICRP, 2009. Environmental Protection: Transfer Parameters for Reference Animals and Plants. Amsterdam: Elsevier. (ICRP Publication 114; Annals of the ICRP 39)

ICRP, 2012. Compendium of dose coefficients based on ICRP Publication 60. Amsterdam: Elsevier (ICRP Publication 119; Annals of the ICRP 41(Suppl.))

ICRP, 2014. Protection of the environment under different exposure situations. SAGE. (ICRP Publication 124; Annals of the ICRP 43)

ICRP, 2015. Wildlife transfer parameter database. International Commission on Radiological Protection. Available at: https://www.wildlifetransferdatabase.org [April 2015].

ICRP, 2017. Dose coefficients for non-human biota environmentally exposed to radiation. SAGE. (ICRP Publication 136; Annals of the ICRP 46)

Ikonen A T K, 2022. A review of sources, transport and losses of methane in the biosphere. SKB R-21-20, Svensk Kärnbränslehantering AB.

Ingmar T, Moreborg K, 1976. The leaching and original content of calcium carbonate in northern Uppland, Sweden. Geologiska Föreningen i Stockholm Förhandlingar 98, 120–132.

IPCC, 2013. Working Group I contribution to the IPCC Fifth Assessment Report Climate Change 2013: The Physical Science Basis, Summary for Policymakers. Available at: http://www.ipcc.ch

Jaeschke B, Grolander S, 2017. Additional considerations for the non-human biota dose assessment in the SR-PSU. SKBdoc 1581297 ver 1.0, Svensk Kärnbränslehantering AB.

Jaeschke B, Smith K, Nordén S, Alfonso B, 2013. Assessment of risk to non-human biota from a repository for the disposal of spent nuclear fuel at Forsmark. Supplementary information. SKB TR-13-23, Svensk Kärnbränslehantering AB.

Jaremalm M, Köhler S, Lidman F, 2013. Precipitation of barite in the biosphere and its consequences for the mobility of Ra in Forsmark and Simpevarp. SKB TR-13-28, Svensk Kärnbränslehantering AB.

Johansson E, Sassner M, 2019. Development of methodology for flow path analysis in the surface system – Numerical modelling in MIKE SHE for Laxemar. A report for the safety evaluation SE-SFL. SKB R-19-04, Svensk Kärnbränslehantering AB.

Johansson M, Christensen T, Åkerman J, Callaghan T V, 2006. What determines the current presence or absence of permafrost in the Torneträsk region, a sub-arctic landscape in Northern Sweden? Ambio 35, 190–197.

Johansson P-O, 2008. Description of surface hydrology and near-surface hydrogeology at Forsmark. Site descriptive modelling, SDM-Site Forsmark. SKB R-08-08, Svensk Kärnbränslehantering AB.

Johansson P-O, Werner K, Bosson E, Berglund S, Juston J, 2005. Description of climate, surface hydrology, and near-surface hydrogeology. Preliminary site description Forsmark area – version 1.2. SKB R-05-06, Svensk Kärnbränslehantering AB.

Johansson W, 1973. Method using meteorological data for estimation of soil moisture content and soil moisture changes in cultivated land. Grundförbättring 26, 57–153. (In Swedish with summary in English.)

Johansson W, Klingspor P, 1977. Bevattning inom lantbruket 1976 : bevattnad areal, vattenåtgång och vattentäkter. Uppsala: Lantbrukshögskolan. (In Swedish.)

Kardell L, 2018. Ett försök med myrslåtter i Klövsjö samt något om mad- och myrslåtter i allmänhet. Uppsala: Sveriges lantbruksuniversitet. (In Swedish.)

Karlsson A, Eriksson C, Borell Lövstedt C, Liungman O, Engqvist A, 2010. High-resolution hydrodynamic modelling of the marine environment at Forsmark between 6500 BC and 9000 AD. SKB R-10-09, Svensk Kärnbränslehantering AB.

Kautsky U (ed), 2001. The biosphere today and tomorrow in the SFR area. SKB R-01-27, Svensk Kärnbränslehantering AB.

Kjellström E, Strandberg G, Brandefelt J, Näslund J-O, Smith B, Wohlfarth B, 2009. Climate conditions in Sweden in a 100 000-year time perspective. SKB TR-09-04, Svensk Kärnbränslehantering AB.

Konstantinova M, Prokopčiuk N, Gudelis A, Butkus D, 2015. Radiological assessment of ionizing radiation impact on the terrestrial non-human biota in Lithuania. Journal of Environmental Engineering and Landscape Management 23, 295–301.

Krall L, Evins L Z, Kooijman E, Whitehouse M, Tullborg E-L, 2019. Tracing the palaeoredox conditions at Forsmark, Sweden, using uranium mineral geochronology. Chemical Geology 506, 68–78.

Langmuir D, Herman J S, 1980. The mobility of thorium in natural waters at low temperatures. Geochimica et Cosmochimica Acta 44, 1753–1766.

Larsson U, Elmgren R, Wulff F, 1985. Eutrophication and the Baltic Sea: causes and consequences. Ambio 14, 9–14.

Lidman F, 2022. Biogeochemistry of nickel and molybdenum in the biosphere of Forsmark and Simpevarp. SKB TR-22-03, Svensk Kärnbränslehantering AB.

Lidman F, Källström K, Kautsky U, 2017. Mo-93 from the grave to the cradle. Report from a workshop on molybdenum in radioactive waste and in the environment. SKB P-16-22, Svensk Kärnbränslehantering AB.

Limer L, Klos R, Shaw G, Walke R, 2013. Terrestrial biosphere modelling of ^{14}C research. Report 2013:20, Swedish Radiation Safety Authority.

Lindborg T (ed), 2008. Surface system Forsmark. Site descriptive modelling, SDM-Site Forsmark. SKB R-08-11, Svensk Kärnbränslehantering AB.

Lindborg T (ed), 2010. Landscape Forsmark – data, methodology and results for SR-Site. SKB TR-10-05, Svensk Kärnbränslehantering AB.

Lindborg T (ed), 2018. BIOPROTA. BIOMASS 2020: Interim report. BIOPROTA report, produced in association with IAEA MODARIA II working group 6. SKB R-18-02, Svensk Kärnbränslehantering AB.

Lindborg T, Rydberg J, Tröjbom M, Berglund S, Johansson E, Löfgren A, Saetre P, Nordén S, Sohlenius G, Andersson E, Petrone J, Borgiel M, Kautsky U, Laudon H, 2016. Biogeochemical data from terrestrial and aquatic ecosystems in a periglacial catchment, West Greenland. Earth System Science Data 8, 439–459.

Lindborg T, Rydberg J, Andersson E, Löfgren A, Lindborg E, Saetre P, Sohlenius G, Berglund S, Kautsky U, Laudon H, 2020. A carbon mass-balance budget for a periglacial catchment in West Greenland – Linking the terrestrial and aquatic systems. Science of The Total Environment 711, 134561. doi:10.1016/j.scitotenv.2019.134561

Lindborg T, Brown J, Griffault L, Ikonen A T K, Kautsky U, Sanae S, Smith G, Smith K, Thorne M, Walke R, 2022. Safety assessments undertaken using the BIOMASS methodology: lessons learnt and methodological enhancements. Journal of Radiological Protection 42, 020503.

Lindgren M, Pettersson M, Karlsson S, Moreno L, 2001. Project SAFE. Radionuclide release and dose from the SFR repository. SKB R-01-18, Svensk Kärnbränslehantering AB.

Lindroth A, Lund M, Nilsson M, Aurela M, Christensen T R, Laurila T, Rinne J, Riutta T, Sagerfors J, Ström L, Tuovinen J-P, Vesala T, 2007. Environmental controls on the CO_2 exchange in north European mires. Tellus B 59, 812–825.

Loreth T, 2005. Quantification of one spring fish migration in a small coastal stream in the Forsmark area, Sweden. Uppsala: Institute of Limnology, Uppsala University. (Scripta Limnologica Upsaliensia 2005 B:7)

Lundberg C, Jakobsson B-M, Bonsdorff E, 2009. The spreading of eutrophication in the eastern coast of the Gulf of Bothnia, northern Baltic Sea – An analysis in time and space. Estuarine, Coastal and Shelf Science 82, 152–160.

Lundin L, Lode E, Stendahl J, Melkerud P-A, Björkvald L, Thorstensson A, 2004. Soils and site types in the Forsmark area. SKB R-04-08, Svensk Kärnbränslehantering AB.

Lundqvist G, 1963. Beskrivning till jordartskarta över Gävleborgs län (Quaternary deposits of Gävleborgs län, central Sweden). Karta i skala 1:200 000. (Sveriges Geologiska Undersökning Ca 42). (In Swedish.)

Löfgren A (ed), 2010. The terrestrial ecosystems at Forsmark and Laxemar-Simpevarp. SR-Site Biosphere. SKB TR-10-01, Svensk Kärnbränslehantering AB.

Löfgren A, 2011. Dissolved inorganic carbon and organic carbon in mires in the Forsmark area. A pilot study. SKB P-11-23, Svensk Kärnbränslehantering AB.

Löfroth M, 1991. Våtmarkerna och deras betydelse. (Wetlands and their importance). Rapport 3824, Naturvårdsverket (Swedish Environmental Protection Agency). (In Swedish.)

Maljanen M, Sigurdsson B D, Guðmundsson J, Óskarsson H, Huttunen J T, Martikainen P J, 2010. Greenhouse gas balances of managed peatlands in the Nordic countries – present knowledge and gaps. Biogeosciences 7, 2711–2738.

Marlow F W, 2005. Hunter-gatherers and human evolution. Evolutionary Antropology 14, 54–67.

Martino M, Turner A, Millward G E, 2003. Influence of organic complexation on the adsorption kinetics of nickel in river waters, Environmental Science & Technology 37, 2383–2388.

Mattsson E, Andersson J, Sabel U, Jakowlew G, Johansson T, Bollmark L, 2018. Jordbrukets behov av vattenförsörjning. Jordbruksverket, 2018:18.

Mayordomo N, Rodríguez D M, Schild D, Molodtsov K, Johnstone E V, Hübner R, Shams Aldin Azzam S, Brendler V, Müller, K, 2020. Technetium retention by gamma alumina nanoparticles and the effect of sorbed Fe^{2+}. Journal of Hazardous Materials 388, 122066. doi:10.1016/j.jhazmat.2020.122066

Meyer-Jacob C, Michelutti N, Paterson A M, Cumming B F, Keller W, Smol J P, 2019. The browning and re-browning of lakes: Divergent lake-water organic carbon trends linked to acid deposition and climate change. Scientific Reports 9, 16676. doi:10.1038/s41598-019-52912-0

Mikkonen A, Tummavuori J, 1993. Retention of molybdenum(VI) by three Finnish mineral soils. Acta Agriculturae Scandinavica, Section B – Soil & Plant Science 43, 206–212.

Millington R J, Quirk J P, 1961. Permeability of porous solids. Transactions of the Faraday Society 57, 1200–1207.

Mobbs S, Smith K, Thorne M, Smith G, 2014. Modelling approaches to C-14 in soil–plant systems and in aquatic environments. Report 2014:30, Swedish Radiation Safety Authority.

Moore T R, Bubier J L, Frolking S E, Lafleur P M, Roulet N T, 2002. Plant biomass and production and CO_2 exchange in an ombrotrophic bog. Journal of Ecology 90, 25–36.

Mäkilä M, Goslar T, 2008. The carbon dynamics of surface peat layers in southern and central boreal mires of Finland and Russian Karelia. Suo 59, 49–69.

Naour C L, Roques J, Den Auwer C, Moisy P, Aupiais J, 2019. Protactinium(V) in aqueous solution: a light actinide without actinyl moiety. Radiochimica Acta 107, 979–991.

NEA, 2012. Methods for safety assessment of geological disposal facilities for radioactive waste: outcomes of the NEA MeSA Initiative. Paris: OECD/NEA.

Nilsson A-C, Borgiel M, 2005. Forsmark site investigation. Sampling and analysis of near surface groundwater. Results from sampling of shallow soil monitoring wells, BAT pipes, a natural spring and private wells, May 2003–April 2005. SKB P-05-171, Svensk Kärnbränslehantering AB.

Nyberg J, Elhammer A, Sohlenius G, Kjellin B, Nordgren P, 2011. Results from marine geological investigations outside Forsmark. SKB P-11-39, Svensk Kärnbränslehantering AB.

Odén M, Follin S, Öhman J, Vidstrand P, 2014. SR-PSU Bedrock hydrogeology. Groundwater flow modelling methodology, setup and results. SKB R-13-25, Svensk Kärnbränslehantering AB.

Oertel C, Matschullat J, Zurba K, Zimmermann F, Erasmi S, 2016. Greenhouse gas emissions from soils – A review. Geochemistry 76, 327–352.

Osvald H, 1937. Myrar och myrodling. Stockholm: Kooperativa förbundets bokförlag. (In Swedish.)

Pedersen T R, 2004. Odlingsbeskrivningar – Spannmål. Jönköping: Jordbruksverket. (In Swedish.)

Pereira A R, Pruitt W O, 2004. Adaptation of the Thornthwaite scheme for estimating daily reference evapotranspiration. Agricultural Water Management 66, 251–257.

Pers K, Skagius K, Södergren S, Wiborgh M, Hedin A, Morén L, Sellin P, Ström A, Pusch R, Bruno J, 1999. SR 97 – Identification and structuring of processes. SKB TR-99-20, Svensk Kärnbränslehantering AB.

Petrone J, Strömgren M, 2020. Baseline Forsmark – Digital elevation model. SKB R-17-06, Svensk Kärnbränslehantering AB.

Petrone J, Sohlenius G, Ising J, 2020. Baseline Forsmark – Depth and stratigraphy of regolith. SKB R-17-07, Svensk Kärnbränslehantering AB.

Posiva, 2013. Safety case for the disposal of spent nuclear fuel at Olkiluoto. Terrain and ecosystems development modelling in the Biosphere assessment BSA-2012. Posiva 2012-29, Posiva Oy, Finland.

Posiva, 2014. Safety case for the disposal of spent nuclear fuel at Olkiluoto. Dose assessment for the plants and animals in the Biosphere assessment BSA-2012. Posiva 2012-32, Posiva Oy, Finland.

Påsse T, 2001. An empirical model of glacio-isostatic movements and shore-level displacement in Fennoscandia. SKB R-01-41, Svensk Kärnbränslehantering AB.

Qvarfordt S, Borgiel M, Berg C, 2010. Monitering Forsmark. Hydrochemical investigations in four calciferous lakes in the Forsmark area. Results from complementary investigations in the Forsmark area, 2008–2009. SKB P-10-25, Svensk Kärnbränslehantering AB.

Reinoso Maset E, Sidhu S H, Fisher A, Heydon A, Worsfold P J, Cartwright A J, Keith-Roach M J, 2006. Effect of organic co-contaminants on technetium and rhenium speciation and solubility under reducing conditions. Environmental Science & Technology 40, 5472–5477.

Rhén I, Follin S, Hermanson J, 2003. Hydrogeological Site Descriptive Model – a strategy for its development during Site Investigations. SKB R-03-08, Svensk Kärnbränslehantering AB.

Rönnback P, Åström M, Gustafsson J-P, 2008. Comparison of the behaviour of rare earth elements in surface waters, overburden groundwaters and bedrock groundwaters in two granitoidic settings, Eastern Sweden. Applied Geochemistry 23, 1862–1880.

Saetre P, Ekström P-A, 2016. Drainage of runoff water from 157_2 into 157_1 via a stream – Biosphere complementary information for SR-PSU. SKBdoc 1554499 ver 1.0, Svensk Kärnbränslehantering AB.

Saetre P, Ekström P-A, 2017a. Kompletterande beräkningar om biosfärsobjekt. SKBdoc 1571087 ver 1.0, Svensk Kärnbränslehantering AB. (In Swedish.)

Saetre P, Ekström P-A, 2017b. Kompletterande beräkningar för gasavgång. SKBdoc 1610560 ver 1.0, Svensk Kärnbränslehantering AB. (In Swedish.)

Saetre P, Lindgren M, 2017. Svar till SSM på begäran om komplettering av ansökan om utökad verksamhet vid SFR angående konsekvensanalys. SKBdoc 1601415, ver 3.0, Svensk Kärnbränslehantering AB. (In Swedish.)

Saetre P, Nordén S, Keesmann S, Ekström P-A, 2013a. The biosphere model for radionuclide transport and dose assessment in SR-PSU. SKB R-13-46, Svensk Kärnbränslehantering AB.

Saetre P, Valentin J, Lagerås P, Avila R, Kautsky U, 2013b. Land use and food intake of future inhabitants: outlining a representative individual of the most exposed group for dose assessment. Ambio 42, 488–496.

Sajih M, Bryan N D, Livens F R, Vaughan D J, Descostes M, Phrommavanh V, Nos J, Morris K, 2014. Adsorption of radium and barium on goethite and ferrihydrite: A kinetic and surface complexation modelling study. Geochimica et Cosmochimica Acta 146, 150–163.

Sassner M, Liakka J, Mayotte J M, 2022. Effects of a warmer climate on near-surface water balances of biosphere objects examined in the post-closure safety assessments for SFR. SKB P-22-05, Svensk Kärnbränslehantering AB.

SCB, 2017. Vattenuttag och vattenanvändning i Sverige 2015, Redovisning för vattendistrikt och län.

Schoning K, 2014. Torvtillväxt och kolackumulation hos unga torvmarker i Uppland. SGU-rapport 2014:35, Sveriges geologiska undersökning. (In Swedish.)

Schroeder L D, Sjoquist D L, Stephan P E, 1986. Understanding regression analysis: an introductory guide. Beverly Hills, CA: Sage.

SFS 1984:3. Lag om kärnteknisk verksamhet (Nuclear Activities Act). Stockholm: Ministry of the Environment. (In Swedish.)

SFS 1998:808. Miljöbalk (Environmental Code). Stockholm: Ministry of the Environment. (In Swedish.)

Shaw G G, Thorne M C, 2016. The oxidation of methane in soil as a factor in determining the radiological impact of a geological disposal facility. RWM005675, AMEC/200047/001 Issue 1, Radioactive Waste Management Limited.

Sheppard S C, 2011. Robust prediction of K_d from soil properties for environmental assessment. Human and Ecological Risk Assessment: An International Journal 17, 263–279.

Sheppard S, Long J, Sanipelli B, Sohlenius G, 2009. Solid/liquid partition coefficients (K_d) for selected soils and sediments at Forsmark and Laxemar-Simpevarp. SKB R-09-27, Svensk Kärnbränslehantering AB.

Sheppard S, Sohlenius G, Omberg L-G, Borgiel M, Grolander S, Nordén S, 2011. Solid/liquid partition coefficients (K_d) and plant/soil concentration ratios (CR) for selected soils, tills and sediments at Forsmark. SKB R-11-24, Svensk Kärnbränslehantering AB.

Sitch S, Smith B, Prentice I C, Arneth A, Bondeau A, Cramer W, Kaplan J O, Levis S, Lucht W, Sykes M T, Thonicke K, Venevsky S, 2003. Evaluation of ecosystem dynamics, plant geography and terrestrial carbon cycling in the LPJ dynamic global vegetation model. Global Change Biology 9, 161–185.

Sjörs H, Gunnarsson U, 2002. Calcium and pH in north and central Swedish mire waters. Journal of Ecology 90, 650–657.

Skagius K, Ström A, Wiborgh M, 1995. The use of interaction matrices for identification, structuring and ranking of FEPs in a repository system. Application on the far-field of a deep geological repository for spent fuel. SKB TR 95-22, Svensk Kärnbränslehantering AB.

SKB, 2016. Fud-program 2016. Program för forskning, utveckling och demonstration av metoder för hantering och slutförvaring av kärnavfall. Svensk Kärnbränslehantering AB. (In Swedish.)

SKB R-01-13. SKB 2001. Project SAFE. Scenario and system analysis. Svensk Kärnbränslehantering AB.

SKB R-07-34. SKB 2007. Forsmark site investigation. Programme for long-term observations of geosphere and biosphere after completed site investigations. Svensk Kärnbränslehantering AB.

SKB R-08-130. SKB 2008. Safety analysis SFR 1. Long-term safety. Svensk Kärnbränslehantering AB.

SKB R-13-43. SKB 2013. Components, features, processes and interactions in the biosphere. Svensk Kärnbränslehantering AB.

SKB R-14-02. SKB 2015. Handling of biosphere FEPs and recommendations for model development in SR-PSU. Svensk Kärnbränslehantering AB.

SKB TR-06-09. SKB 2006. Long-term safety for KBS-3 repositories at Forsmark and Laxemar – a first evaluation. Main report of the SR-Can project. Svensk Kärnbränslehantering AB.

SKB TR-08-05. SKB 2008. Site description of Forsmark at completion of the site investigation phase. SDM-Site Forsmark. Svensk Kärnbränslehantering AB.

SKB TR-10-09. SKB 2010. Biosphere analyses for the safety assessment SR-Site – synthesis and summary of results. Svensk Kärnbränslehantering AB.

SKB TR-11-01. SKB 2011. Long-term safety for the final repository for spent nuclear fuel at Forsmark. Main report of the SR-Site project. Svensk Kärnbränslehantering AB.

SKB TR-11-04. SKB 2013. Site description of the SFR area at Forsmark at completion of the site investigation phase. SDM-PSU Forsmark. Svensk Kärnbränslehantering AB.

SKB TR-13-18. SKB 2013. RD&D Programme 2013. Programme for research, development and demonstration of methods for the management and disposal of nuclear waste. Svensk Kärnbränslehantering AB.

SKB TR-14-01. SKB 2015. Safety analysis for SFR. Long-term safety. Main report for the safety assessment SR-PSU. Revised edition. Svensk Kärnbränslehantering AB.

SKB TR-14-06. SKB 2014. Biosphere synthesis report for the safety assessment SR-PSU. Svensk Kärnbränslehantering AB.

SKB TR-14-07. SKB 2014. FEP report for the safety assessment SR-PSU. Svensk Kärnbränslehantering AB.

SKB TR-14-09. SKB 2015. Radionuclide transport and dose calculations for the safety assessment SR-PSU. Revised edition. Svensk Kärnbränslehantering AB.

SKB TR-19-01. SKB 2019. Post-closure safety for a proposed repository concept for SFL. Main report for the safety evaluation SE-SFL. Svensk Kärnbränslehantering AB.

SKB TR-19-05. SKB 2019. Biosphere synthesis for the safety evaluation SE-SFL. Svensk Kärnbränslehantering AB.

SKB TR-19-06. SKB 2019. Radionuclide transport and dose calculations for the safety evaluation SE-SFL. Svensk Kärnbränslehantering AB.

SKB TR-19-24. SKB 2019. RD&D Programme 2019. Programme for research, development and demonstration of methods for the management and disposal of nuclear waste. Svensk Kärnbränslehantering AB.

Smedley P L, Kinniburgh D G, 2017. Molybdenum in natural waters: A review of occurrence, distributions and controls. Applied Geochemistry 84, 387–432.

SMHI, 2020. Ekvationer för medelvattenståndet i RH2000. Available at: https://www.smhi.se/hfa_coord/BOOS/dbkust/mwreg_MWekvationer_2020.pdf [28 March 2022]. (In Swedish.)

Soares M R, Casagrande J C, Mouta E R, 2011. Nickel adsorption by variable charge soils: effect of pH and ionic strength. Brazilian Archives of Biology and Technology 54, 207–220.

Sohlenius G, Strömgren M, Hartz F, 2013a. Depth and stratigraphy of regolith at Forsmark. SR-PSU Biosphere. SKB R-13-22, Svensk Kärnbränslehantering AB.

Sohlenius G, Saetre P, Nordén S, Grolander S, Sheppard S, 2013b. Inferences about radionuclide mobility in soils based on the solid/liquid partition coefficients and soil properties. Ambio 42, 414–424.

Sohlenius G, Schoning K, Baumgartner A, 2013c. Development, carbon balance and agricultural use of peatlands – overview and examples from Uppland, Sweden. SKB TR-13-20, Svensk Kärnbränslehantering AB.

Sonesten L, 2005. Chemical characteristics of surface waters in the Forsmark area. Evaluation of data from lakes, streams, and coastal sites. SKB R-05-41, Svensk Kärnbränslehantering AB.

SSM, 2008a. The Swedish Radiation Safety Authority's regulations and general advice concerning the protection of human health and the environment in connection with the final management of spent nuclear fuel and nuclear waste. Stockholm: Swedish Radiation Safety Authority. (SSMFS 2008:37)

SSM, 2008b. The Swedish Radiation Safety Authority's regulations and general advice concerning safety in connection with the disposal of nuclear material and nuclear waste. Stockholm: Swedish Radiation Safety Authority. (SSMFS 2008:21)

SSM, 2017. SSM's external experts' review of SKB's safety assessment SR-PSU – dose assessment, K_d-values, and safety analysis methodology. Report 2017:33, Swedish Radiation Safety Authority.

SSM, 2018. Strålsäkerhet efter slutförvarets förslutning. Beredning inför regeringens prövning Slutförvaring av använt kärnbränsle. Rapport 2018:07, Swedish Radiation Safety Authority. (In Swedish.)

SSM, 2019. Granskningsrapport – Utbyggnad och fortsatt drift av SFR. Rapport 2019:18, Swedish Radiation Safety Authority. (In Swedish.)

Stenberg K, Rensfeldt V, 2015. Estimating doses from exposure to contaminated air when burning peat or wood. SKB R-14-33, Svensk Kärnbränslehantering AB.

Stephens M B, Fox A, La Pointe P, Simeonov A, Isaksson H, Hermansson J, Öhman J, 2007. Geology Forsmark. Site descriptive modelling Forsmark stage 2.2. SKB R-07-45, Svensk Kärnbränslehantering AB.

Sternbeck J, Land M, Nilsson Ö, 2006. Oskarshamn and Forsmark site investigations. ^{210}Pb and ^{14}C dating of sediments and peat. Accumulation rates of carbon, nitrogen and phosphorus. SKB P-06-301, Svensk Kärnbränslehantering AB.

Strack M, Waddington J M, Turetsky M, Roulet N T, Byrne K A, 2008. Northern peatlands, greenhouse gas exchange and climate change. In Strack M (ed). Peatlands and climate change. Jyväskylä: International Peat Society, 44–69.

Strömgren M, Brydsten L, 2013. Digital elevation model of Forsmark. Site-descriptive modelling. SR-PSU Biosphere. SKB R-12-03, Svensk Kärnbränslehantering AB.

Strömgren M, Lindgren F, 2011. Mapping of reed in shallow bays. SFR-Site Forsmark. SKB P-11-09, Svensk Kärnbränslehantering AB.

Svanberg O, Vilborg I, 2001. Från surhål och mygghelvete till myllrande våtmarker: utvärdering av arbetet mot ett miljökvalitetsmål (From swampy pits and mosquito-hells to flourishing wetlands: an evaluation of work towards an environmental quality objective). Rapport 5146, Naturvårdsverket (Swedish Environmental Protection Agency). (In Swedish.)

Svensson T, Bastviken D, Löfgren A, 2021. Cl distribution in different terrestrial habitats along hill slope gradients in Forsmark. SKB R-21-04, Svensk Kärnbränslehantering AB.

Söderbäck B (ed), 2008. Geological evolution, palaeoclimate and historical development of the Forsmark and Laxemar-Simpevarp areas. Site descriptive modelling. SDM-Site. SKB R-08-19, Svensk Kärnbränslehantering AB.

Söderlund M, Hakanen M, Lehto J, 2016. Sorption of cesium on boreal forest soil I: the effect of grain size, organic matter and mineralogy. Journal of Radioanalytical and Nuclear Chemistry 309, 637–645.

Tiberg C, Sjöstedt C, Persson I, Gustafsson J P, 2013. Phosphate effects on copper(II) and lead(II) sorption to ferrihydrite. Geochimica et Cosmochimica Acta 120, 140–157.

Toraishi T, Tsuneda T, Tanaka S, 2006. Theoretical study on molecular property of protactinium(V) and uranium(VI) oxocations: why does protactinium(V) form monooxo cations in aqueous solution? The Journal of Physical Chemistry A 110, 13303–13309.

Torudd J, 2010. Long term radiological effects on plants and animals of a deep geological repository. SKB TR-10-08, Svensk Kärnberänslehantering AB.

Tröjbom M, Söderbäck B, 2006. Chemical characteristics of surface systems in the Forsmark area. Visualisation and statistical evaluation of data from shallow groundwater, precipitation, and regolith. SKB R-06-19, Svensk Kärnbränslehantering AB.

Tröjbom M, Grolander S, 2010. Chemical conditions in present and future ecosystems in Forsmark. Implications for selected radionuclides in the safety assessment SR-Site. SKB R-10-27, Svensk Kärnbränslehantering AB.

Tröjbom M, Nordén S, 2010. Chemistry data from surface ecosystems in Forsmark and Laxemar-Simpevarp. Site specific data used for estimation of CR and K_d-values in SR-Site. SKB R-10-28, Svensk Kärnbränslehantering AB.

Tröjbom M, Söderbäck B, Johansson P-O, 2007. Hydrochemistry in surface water and shallow groundwater. Site descriptive modelling, SDM-Site Forsmark. SKB R-07-55, Svensk Kärnbränslehantering AB.

Tröjbom M, Grolander S, Rensfeldt V, Nordén S, 2013. K_d and CR used for transport calculations in the biosphere in SR-PSU. SKB R-13-01, Svensk Kärnbränslehantering AB.

Ulanovsky A, 2017. Program BiotaDC (a complement to ICRP Publication 136). Available at: http://biotadc.icrp.org

UNSCEAR, 2011. Sources and effects of ionizing radiation. United Nations Scientific Committee on the Effects of Atomic Radiation (UNSCEAR). UNSCEAR 2008 Report to the General Assembly with Scientific Annexes – Volume II Scientific Annexes C, D and E. New York: United Nations.

US DOE, 2002. A graded approach for evaluating radiation doses to aquatic and terrestrial biota. Technical Standard DoE-STD-1153-2002, U.S. Department of Energy, Washington, DC.

van Vliet M, Donnelly C, Strömbäck L, Capell R, Ludwig F, 2015. European scale climate information services for water use sectors. Journal of Hydrology 528, 503–513.

Vasyukova E V, Pokrovsky O S, Viers J, Oliva P, Dupré B, Martin F, Candaudap F, 2010. Trace elements in organic- and iron-rich surficial fluids of the boreal zone: Assessing colloidal forms via dialysis and ultrafiltration. Geochimica and Cosmochimica Acta 74, 449–468.

Velasco H R, Ayub J J, Belli M, Sansone U, 2006. Interaction matrices as a first step toward a general model of radionuclide cycling: application to the ^{137}Cs behavior in a grassland ecosystem. Journal of Radioanalytical and Nuclear Chemistry 268, 503–509.

Wada Y, Wisser D, Eisner S, Flörke M, Gerten D, Haddeland I, Hanasaki N, Masaki Y, Portmann F T, Stacke T, Tessler Z, Schewe J, 2013. Multimodel projections and uncertainties of irrigation water demand under climate change. Geophysical Research Letters 40, 4626–4632.

Walke R, Limer L, Shaw G, 2017. In-depth review of key issues regarding biosphere models for specific radionuclides in SR-PSU. In SSM's external experts' review of SKB's safety assessment SR-PSU – dose assessment, K_d-values and safety analysis methodology. Main review phase. Report 2017-33, Swedish Radiation Safety Authority, Part 2.

Wazne M, Korfiatis G P, Meng X, 2003. Carbonate effects on hexavalent uranium adsorption by iron oxyhydroxide. Environmental Science & Technology 37, 3619–3624.

Welinder S, Pedersen E A, Widgren M, 1998. Det svenska jordbrukets historia. Band 1. Jordbrukets första femtusen år: 4000 f Kr – 1000 e Kr Stockholm: Natur och Kultur/LT. (In Swedish.)

Werner K, Johansson P-O, Brydsten L, Bosson E, Berglund S, Tröjbom M, Nyman H, 2007. Recharge and discharge of near-surface groundwater in Forsmark. Comparison of classification methods. SKB R-07-08, Svensk Kärnbränslehantering AB.

Werner K, Hamrén U, Collinder P, 2010. Vattenverksamhet i Forsmark (del I). Bortledande av grundvatten från slutförvarsanläggningen för använt kärnbränsle. SKB R-10-14, Svensk Kärnbränslehantering AB. (In Swedish.)

Werner K, Sassner M, Johansson E, 2013. Hydrology and near-surface hydrogeology at Forsmark – synthesis for the SR-PSU project. SR-PSU Biosphere. SKB R-13-19, Svensk Kärnbränslehantering AB.

Wesström I, Joel A, 2014. Bevattning och dränering. In Elmquist H, Arvidsson (eds). Höstvete mot nya höjder. Uppsala: Swedish University of Agricultural Sciences. (Rapporter från jordbearbetningen 129) (In Swedish.)

Weyhenmeyer G A, Müller R A, Norman M, Tranvik L J, 2016. Sensitivity of freshwaters to browning in response to future climate change. Climatic Change 134, 225–239.

Whicker F W, Schultz V, 1982. Radioecology: nuclear energy and the environment. Boca Raton, FL: CRC Press.

Wichard T, Mishra B, Myneni S C B, Bellenger J-P, Kraepiel A M L, 2009. Storage and bio-availability of molybdenum in soils increased by organic matter complexation. Nature Geoscience 2, 625–629.

Wikberger C, Johansson M, 2006. Konsumtion av livsmedel och dess näringsinnehåll. Statistikrapport 2006:2, Jordbruksverket, Stockholm. (In Swedish.)

Wilmot R, Robinson P, 2004. The issue of risk dilution in risk assessments. Management of uncertainty in safety cases and the role of risk: Proceedings of OECD/NEA Workshop, Stockholm, 2–4 February 2004. Paris: OECD/NEA.

Wirth S B, Gilli A, Niemann H, Dahl T W, Ravasi D, Sax N, Hamann Y, Peduzzi R, Peduzzi S, Tonolla M, Lehmann M F, Anselmetti F S, 2013. Combining sedimentological, trace metal (Mn, Mo) and molecular evidence for reconstructing past water-column redox conditions: The example of meromictic Lake Cadagno (Swiss Alps). Geochimica et Cosmochimica Acta 120, 220–238.

Xu N, Braida W, Christodoulatos C, Chen J, 2013. A review of molybdenum adsorption in soils/bed sediments: speciation, mechanism, and model applications. Soil and Sediment Contamination: An International Journal 22, 912–929.

Yoshida S, Muramatsu Y, Uchida S, 1992. Studies on the sorption of I^- (iodide) and IO_3^- (iodate) onto Andosols. Water, Air, and Soil Pollution 63, 321–329.

Yu Z, 2006. Holocene carbon accumulation of fen peatlands in boreal western Canada: a complex ecosystem response to climate variation and disturbance. Ecosystems 9, 1278–1288.

Zheng Z, Tokunaga T K, Wan J, 2003. Influence of calcium carbonate on U(VI) sorption to soils. Environmental Science & Technology 37, 5603–5608.

Åstrand P-G, Rasmusson M, Wessely O, 2022. Near-field radionuclide transport models for the post-closure safety assessment in PSAR SFR. SKB R-21-02, Svensk Kärnbränslehantering AB.

Åström M E, Peltola P, Rönnback P, Lavergren U, Bergback B, Tarvainen T, Backman B, Salminen R, 2009. Uranium in surface and groundwaters in Boreal Europe. Geochemistry: Exploration, Environment, Analysis 9, 51–62.

Öhman J, Odén M, 2017. TD15 Complementary simulation cases in support of SR-PSU. SKBdoc 1578373 ver 1.0, Svensk Kärnbränslehantering AB.

Öhman J, Odén M, 2018. SR-PSU (PSAR) Bedrock hydrogeology. TD18 – Temperate climate conditions. SKB P-18-02, Svensk Kärnbränslehantering AB.

Öhman J, Bockgård N, Follin S, 2012. Bedrock Hydrogeology. SFR Site investigation SFR. SKB R-11-03, Svensk Kärnbränslehantering AB.

Öhman J, Follin S, Odén M, 2014. SR-PSU Hydrogeological modelling. TD11 – Temperate climate conditions. SKB P-14-04, Svensk Kärnbränslehantering AB.

Appendix A

Terms and abbreviations

The present report contains terms and abbreviations that either are rarely used outside SKB, or can be regarded as specialised terminology within one or several of the scientific and modelling disciplines involved in the reported work. To facilitate the readability of the report, selected terms and abbreviations are explained in Table A-1.

Table A-1. Explanations of terms and abbreviations used in this report.

Name	Description
1–2BMA	Vaults for intermediate-level waste in SFR.
1–2BTF	Vaults for concrete tanks in SFR1.
1–5BLA	Vaults for low-level waste in SFR.
1BRT	Vault for reactor pressure vessels in SFR3.
2D	Two-dimensional.
3D	Three-dimensional.
Abiotic	Non-living physical or chemical component or process.
Absorbed dose rate	Amount of energy deposited in matter by ionizing radiation per unit mass and per unit time.
AD	Anno Domini.
Annual dose	Assessment endpoint calculated as the annual effective dose to an adult, where the annual effective dose is defined as the effective dose from external exposure in a year, plus the committed effective dose from intakes of radionuclides in that year.
Annual effective dose	The effective dose from external exposure in a year, plus the committed effective dose from intakes of radionuclides in that year.
Barrier	In the safety assessment context, a barrier is a physical feature, engineered or natural, which in one or several ways contributes to the containment and retention or prevention of dispersion of radioactive substances, either directly or indirectly by protecting other barriers.
Base case	The *base case* constitutes the basis for the radionuclide transport and dose calculations. The present-day climate calculation case is selected as the *base case* for the analysis of the main scenario. Models built and assumptions made for the other calculation cases are only described if they deviate from the *base case* and results from these cases are compared with those for the *base case*.
Basin	In the terminology used in this safety assessment for the drainage area of a biosphere object (cf below) minus the drainage area of any upstream object. When the basin is below sea level, the basin is identical to the biosphere object.
BC	Before Christ.
BE	Best estimate.
Bedrock	In the safety assessment context, the solid rock beneath the regolith also including the groundwater in the rock.
Best estimate	A single value for a parameter, describing a property or a process, used in deterministic calculations. Best estimates are typically derived from site and/or literature data and often correspond to mean values of the underpinning datasets.
BIOMASS	BIOsphere Modelling and ASSessment methods. An IAEA co-ordinated research programme and the methodology derived from that programme.
BIOPROTA	An international collaborative forum designed to support resolution of key issues in biosphere aspects of assessments of the long-term impact of contaminant releases associated with radioactive waste management (www.bioprota.org).
Biosphere object	A part of the landscape that will potentially receive radionuclides released from a repository, directly or indirectly via other biosphere objects.
Biosphere system	In the safety assessment context, refers to the part of the repository system that is above the geosphere, with all its abiotic and biotic processes and features, as well as humans and human behaviour. Synonymous with Surface system.
BioTEx	The Biosphere Transport and Exposure model. Used to calculate concentrations and subsequent transport of radionuclides in different environmental media in a biosphere object and potential doses to human and dose rates to non-human biota.
Biotic	Living ecosystem component or process involving living organisms.
Bulk density	The bulk density of a porous medium is defined as the mass of the solid particles that make up the medium divided by the total volume they occupy. The total volume includes particle volume, inter-particle void volume and internal pore volume.
Calculation case	Used for the quantitative assessment of the scenarios selected in the safety assessment, typically by calculating doses.

Table A-1. Continued.

Name	Description
Cautious	Indicates an expected overestimate of annual effective dose that follows from assumptions made, or models and parameter values selected, within the reasonably expected range of possibilities.
Central block	The volume of bedrock that is bounded to the northeast and southwest by two broad belts, the Northern boundary belt and the Southern boundary belt, of concentrated ductile and brittle deformation. The Central block is less affected by deformation than the bounding belts.
Climate domain	A climatically determined environment with a specific set of characteristic processes of importance for post-closure safety.
Climate variant	A climate development used in describing the range of possible future climate developments that may influence post-closure safety.
Collective dose	In the safety assessment context, equal to the collective effective dose, which is the sum of all the individual effective doses to members of a population. The special name of the unit of the collective effective dose is the man sievert (man Sv).
Conceptual model	A qualitative description of a physical system, including important processes and components and interactions between these components.
CR	Concentration ratio. Used to calculate uptake of radionuclides by biota, defined as the element-specific ratio between the concentration in biota and in the surrounding medium (soil or surface water).
DarcyTools	A computer code developed by SKB for simulation of flow and transport in porous and/or fractured media.
Data uncertainty	Uncertainties concerning all quantitative input data, that is parameter values, used in the assessment.
DCC	Dose conversion coefficient.
DCRL	Derived Consideration Reference Level. Used for screening of dose rates to animals and plants (non-human biota) to ensure protection of the environment.
DEM	Digital elevation model. Describes the topography and bathymetry of the modelled area.
DFN	Discrete fracture network.
DIC	Dissolved inorganic carbon.
Discharge locations/points	Locations/points/areas where groundwater reaches the surface ecosystem. In the safety assessment context, this term refers to discharge of groundwater that has passed though the repository volume in the geosphere and hence could bring radionuclides to the surface.
DM	Drained-mire farmers. Refers to self-sustained agriculture in which wetlands are drained and cultivated (both crop and fodder production). It is one of four potentially exposed groups (PEGs) in this safety assessment.
DOC	Dissolved organic carbon.
Ecosystem model	Conceptual or mathematical representation of an ecosystem, divided into compartments and its included processes.
Effective dose	Effective dose is a measure of dose designed to reflect the amount of radiation detriment likely to result from the dose. It is defined as a weighted summation of the tissue or organ equivalent doses, that is the summation of the absorbed dose in each tissue or organ multiplied by appropriate radiation weighting factor, each multiplied by the appropriate tissue weighting factor.
Emission scenario	Possible future pathways of anthropogenic greenhouse-gas and aerosol emissions.
ERICA	Environmental Risk from Ionising Contaminants – Assessment and management. EU-project that provided screening values to assess environmental risk.
ERICA Tool	A software system that has a structure based upon the tiered ERICA Integrated Approach to assessing the radiological risk to terrestrial, freshwater and marine biota.
EU	European Union.
Eustasy	Change in sea level due to, for example, changes in the volume and spatial distribution of sea water in the world's oceans.
Exposure	The act or condition of being subject to irradiation (not to be used as a synonym for dose, which is a measure of the effects of exposure).
External exposure	Exposure to radiation from a source outside the body.
FEP	Features, events and processes.
Functional group	A group of organisms with a common function in the ecosystem, e.g. primary producers or decomposers.
gC	Gram of carbon (used as a unit).
gdw	Gram dry weight.
Geosphere	The bedrock, including groundwater, surrounding the repository, bounded above by the surface system.
GIS	Geographical information system.
GP	Garden-plot households. Refers to a type of household that is self-sustained with respect to vegetables and root crops produced through small-scale horticulture. It is one of four potentially exposed groups (PEGs) in this safety assessment.

Table A-1. Continued.

Name	Description
Harmful effects	Cancer (fatal and non-fatal) as well as hereditary effects in humans caused by ionising radiation, in accordance with paragraphs 47–51 in ICRP Publication 60 (ICRP 1991).
HG	Hunter-gatherers. Refers to a community that uses the undisturbed surface ecosystems as living space and to obtain food. It is one of four potentially exposed groups (PEGs) in this safety assessment.
IAEA	International Atomic Energy Agency.
ICRP	International Commission on Radiological Protection.
IM	Interaction matrix. A tool used to identify processes, and interactions between processes, that have to be considered in quantitative analyses in the safety assessment.
Infilling	Infilling describes the combined process of sedimentation and organogenic deposition, which turns lakes into wetlands.
Initial state	The expected state of the repository and its environs at closure of the repository.
Insolation	The amount of solar radiation received per unit area at the top of the Earth's atmosphere.
Interaction matrix	A tool used to identify processes, and interactions between processes, that have to be considered in quantitative analyses in the safety assessment.
Intermediate-level waste	Radioactive waste that requires final disposal in a geological repository and shielding during handling. Cooling of the waste is not required.
Internal exposure	Exposure to radiation from a source within the body.
IO	Infield-outland farmers. Refers to a self-sustained agriculture in which infield farming of crops is dependent on nutrients from wetlands for haymaking (outland). It is one of four potentially exposed groups (PEGs) in this safety assessment.
IPCC	Intergovernmental Panel on Climate Change.
ISIMIP2	Inter-Sectoral Impact Model Intercomparison Project.
Isostasy	Vertical movement of the Earth's crust, which in Forsmark is dominated by isostatic rebound following the latest glaciation.
JJA	June, July, August (summer).
kgC	Kilogram of carbon (used as a unit).
kgdw	Kilogram dry weight.
kgfw	Kilogram fresh weight.
LDF	Landscape dose conversion factor. A radionuclide-specific dose conversion factor, expressed in Sv/a per Bq/a. It represents the mean annual effective dose to the PEG that receives the highest dose, resulting from a unit constant release rate to the biosphere.
Long-lived radionuclide	In the safety assessment context, radionuclides with a half-life exceeding 31 years.
Long-lived waste	In the safety assessment context, radioactive waste that contain significant levels of radionuclides with a half-life greater than 31 years.
Low-level waste	Radioactive waste that requires final disposal in a geological repository. Shielding during handling and cooling are not required.
LPJ-GUESS	A dynamic vegetation model.
Mathematical model	A quantitative description of a physical system, where important processes and components, and interactions between components, are represented by parameters and equations.
MIKE SHE	Computer code used to simulate groundwater and surface water flow.
Modelling uncertainty	Uncertainties arising from a necessarily imperfect understanding of the nature of processes involved in repository evolution which leads to imperfect conceptual models. The mathematical representation of conceptual models and imprecision in the numerical solution of mathematical models are other sources of uncertainty which fall into this category.
NEA	OECD Nuclear Energy Agency.
Near-field	Typically used for the model domain representing the repository, which may contain part of the nearby bedrock to obtain boundary conditions.
NEP	Net ecosystem production. The sum of gross primary production and ecosystem respiration.
NHB	Non-human biota.
NPP	Net primary production. The balance between gross primary production and plant respiration.
NPP	Nuclear power plant.
PDF	Probability density function.
Pessimistic	Indicates an expected overestimate of annual effective dose that follows from assumptions made, or models and parameter values selected, beyond the reasonably expected range of possibilities.
PET	Potential evapotranspiration.
Potentially exposed group	Groups of individuals potentially subjected to the highest exposure during any time of the assessment period.
PROTECT	Protection of the environment from ionising radiation in a regulatory context, an EC project that, among other things, provided screening values to assess environmental risk.

Table A-1. Continued.

Name	Description
Protective capability	The capability to protect human health and the environment from the harmful effects of ionising radiation.
PSAR	Preliminary Safety Analysis Report.
PSAR SFR	Preliminary Safety Analysis Report for the extended SFR.
QA	Quality assurance.
Radiotoxicity	The product of the activity of a radionuclide and it's corresponding dose coefficient for intake.
RCP4.5	Emission scenario from IPCC in which radiative forcing is stabilised at approximately 4.5 W m^{-2} at 2100 AD.
RCP6.0	Emission scenario from IPCC in which radiative forcing is stabilised at approximately 6.0 W m^{-2} at 2100 AD.
RCP8.5	Emission scenario from IPCC in which radiative forcing reaches approximately 8.5 W m^{-2} by 2100 AD and continues to rise for some time after that.
RD&D	Research, development and demonstration.
RDM	Regolith depth and stratigraphy model. A three-dimensional model of regolith extension.
Reference evolution	The probable post-closure evolution of the repository and its environs, including uncertainties in the evolution that may affect the protective capability of the repository.
Regolith	All matter overlying the bedrock. This includes both minerogenic and organogenic (i.e. derived from organic substances) deposits.
Relative sea level	The vertical position of the sea relative to land, as measured in the reference height system RH 2000. The relative sea level is determined by the net effect of eustasy and isostasy.
Repository	The disposed waste packages, the engineered barriers and other repository structures.
Repository system	The repository, the bedrock and the biosphere surrounding the repository. Synonymous with repository and its environs.
Risk	Refers in the post-closure safety assessment to the radiological risk, defined as the product of the probability of receiving a radiation dose and the harmful effects of that radiation dose.
Risk dilution	In the context of the radionuclide transport, dose and risk calculations, risk dilution in a broad sense refers to a situation in which an increase in the uncertainty of the values of important input parameters, or in the assumptions with respect to the timing of an event, leads to a decrease in the calculated annual dose and associated annual radiological risk.
RLDM	Regolith-lake development model. Used to project the future regolith depth and stratigraphy in the model area. Consists of a marine module describing sediment dynamics caused by waves action and a lake module that describes infilling of lakes.
RNT	Radionuclide transport.
RSL	Relative sea level.
SAFE	Post-closure safety assessment for SFR1 reported to the regulatory authorities in 2001.
Safety analysis	In the context of the present safety assessment, the distinction is generally not viewed as important and therefore safety analysis and safety assessment are used interchangeably. However, if the distinction is important, safety analysis should be used as a documented process for the study of safety and safety assessment should be used as a documented process for the evaluation of safety.
Safety assessment	The safety assessment is the systematic process periodically carried out throughout the life-time of the repository to ensure that all the relevant safety requirements are met and entails evaluating the performance of the repository system and quantifying its potential radiological impact on human health and the environment. The safety assessment corresponds to the term safety analysis in the Swedish Radiation Safety Authority's regulations.
SAR-08	Post-closure safety assessment for SFR1 reported to the regulatory authorities in 2008.
Scenario	A description of a potential evolution of the repository and its environs, given an initial state and specified external conditions and their development and how the protective capability of the repository is affected.
Scenario uncertainty	Uncertainties with respect to external conditions and internal processes in terms of type, degree and time sequence, resulting in an uncertainty in the future states of the repository system
SDM-Site	Site descriptive model for the Forsmark site for the spent nuclear fuel repository.
SE-SFL	The evaluation of post-closure safety for a proposed repository concept for SFL.
SFL	Final repository for long-lived radioactive waste.
SFR	Final repository for short-lived radioactive waste at Forsmark.
SFR1	The existing part of SFR.
SFR3	The extension part of SFR.
SGU	Geological Survey of Sweden.
Shoreline displacement	The movement of the shoreline, that is the variation in time of the spatial location of the shoreline.

Table A-1. Continued.

Name	Description
Shoreline regression	Migration of the coastline away from the land as the relative sea level decreases, which in turn increases the extent of the land area.
Shoreline transgression	Migration of the coastline away towards the land as the relative sea level increases, which in turn decreases the extent of the land area.
Short-lived radionuclide	In the safety assessment context, radionuclides with a half-life shorter than 31 years.
Silo	Cylindrical vault for intermediate-level waste (part of SFR1).
SKB	Swedish Nuclear Fuel and Waste Management Company.
SKBdoc	Internal document management system at SKB.
SMHI	Swedish Meteorological and Hydrological Institute.
Sorption coefficient	Element-specific sorption coefficient, defined as the ratio between the elemental concentrations in the solid and liquid phases.
SR-Can	Preliminary post-closure safety assessment for the planned spent nuclear fuel repository, published in 2006.
SR-PSU	Post-closure safety assessment that was a reference to the F-PSAR for the extended SFR, reported to the regulatory authority in 2014.
SR-Site	Post-closure safety assessment for a spent nuclear fuel repository in Forsmark, reported to the regulatory authority in 2011.
SSM	Swedish Radiation Safety Authority.
SSMFS	Regulations of the Swedish Radiation Safety Authority.
SVN	Subversion. A version handling system used for code and data in the PSAR SFR.
Sub-catchment	In the safety assessment context, defined as the drainage area of a biosphere object minus the drainage area of the inlets to the object. For objects without a stream inlet the sub-catchment is identical to the basin.
Surface ecosystem	The surface ecosystem refers to the part of the environment above the bedrock, with all its abiotic and biotic processes and features.
Surface system	In the safety assessment context, refers to the part of the repository system that is above the geosphere, with all its abiotic and biotic processes and features, as well as humans and human behaviour. Synonymous with Biosphere system.
System uncertainty	Uncertainties concerning comprehensiveness issues, i.e. the question of whether all aspects important for the safety evaluation have been identified and whether the assessment is capturing the identified aspects in a qualitatively correct manner.
Terrestrialisation	The transformation of an aquatic ecosystem (marine or limnic) to a terrestrial ecosystem.
UNSCEAR	United Nations Scientific Committee on the Effects of Atomic Radiation.
Waste package	The waste (form) and its packaging.
Waste type	SKB's systematic classification of wastes according to a developed code system.
Waste vault	Part of repository where waste is disposed.
Watershed	In the safety assessment it is used in the North American sense, defined as the drainage area of a biosphere object.

Appendix B

Map of the Forsmark area

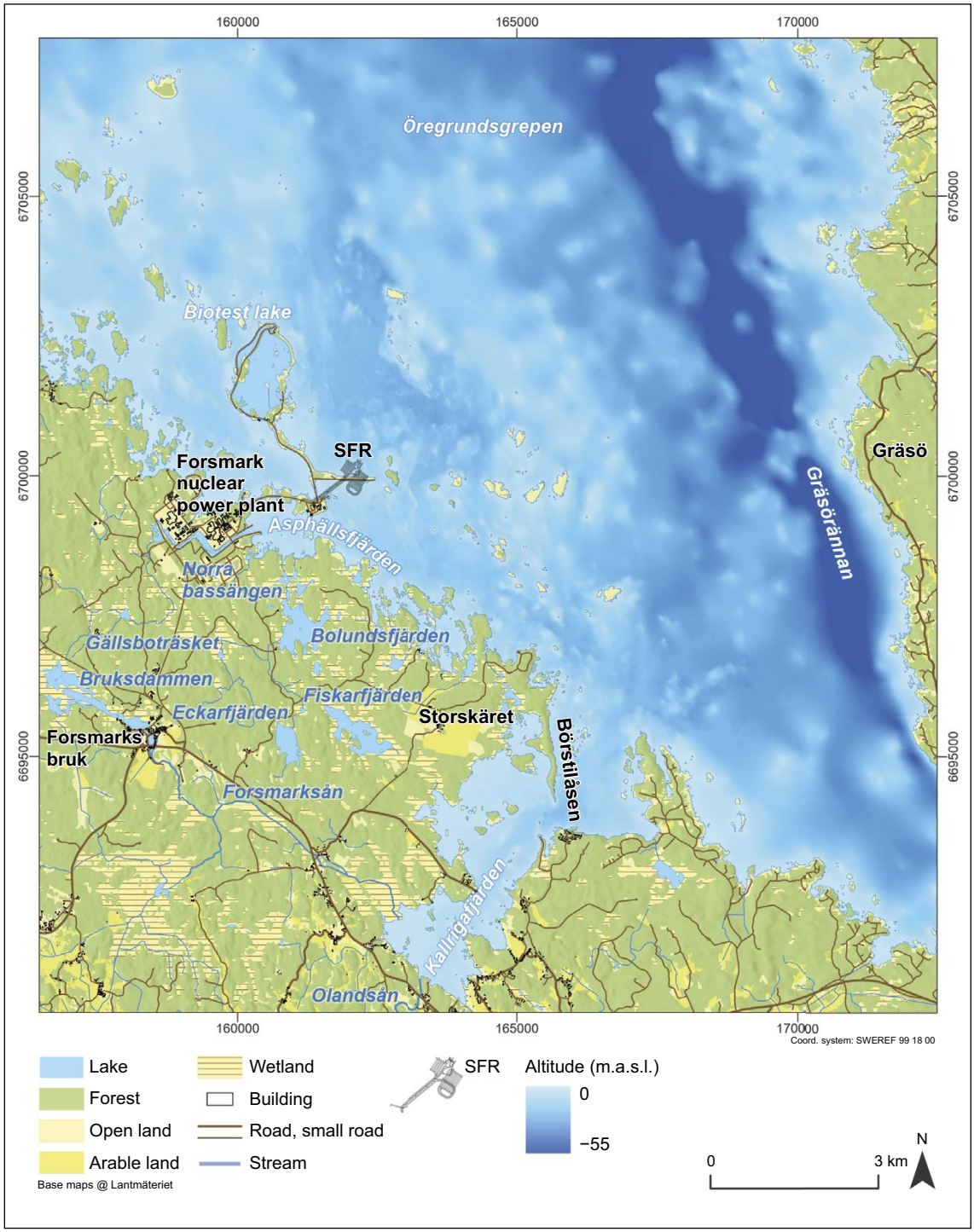

Figure B-1. *Overview map of the Forsmark area in the vicinity of the SFR facility. The geographical position of the Forsmark nuclear power plant, the esker Börstilsåsen and the farmland Storskäret, as well as lakes, streams and marine areas mentioned in the report are shown in the map.*

Appendix C

Landscape dose conversion factors

To quantify how data and model updates in the PSAR affect the assessment model performance, landscape dose conversion factors (LDF) have been calculated with the PSAR BioTEx model. The patterns of LDFs have previously been discussed in SR-PSU (SKB TR-14-06, Section 10.1). As the PSAR results are similar to those presented in the SR-PSU, this text primarily focuses on differences in LDFs between these two assessments. These differences are discussed in terms of model (Chapter 7) and parameter (Chapter 8) updates. In the last section of this appendix, LDFs in the PSAR from deterministic simulations are compared with LDFs derived from probabilistic simulations.

C1 Method

An annual dose or dose rate derived from a unit release rate to one or several biosphere objects is referred to as a landscape dose conversion factor (LDF). It represents an upper limit for the dose/dose rates that can be expected given a constant release rate of radionuclides to the surface systems over a defined assessment period. The fact that the endpoints from a constant release rate are dose conversion factors is evident from their units: Sv a^{-1} per Bq a^{-1}.

Following the method for LDF calculations used earlier in SR-PSU, a unit release rate for 51 radionuclides is analysed with the *base case* model setup. That is, the simulations are carried out with the updated PSAR version of BioTEx (Chapter 7) and with updated parameter values (Chapter 8) fixed at best estimates for a period of 18 000 years. The contributions from decay products are not included in the dose calculations.

These values are compared with the LDF values from SR-PSU (SKB TR-14-06, Table 10-1). In SR-PSU, the highest values resulted from exposure in the primary biosphere object, with the exception for Mo-93 for which the dose was marginally higher in the downstream object. For simplicity, the LDF calculations here in the PSAR are restricted to the primary discharge area (i.e. biosphere object 157_2).

To facilitate interpretation of results in the PSAR, the LDF values were also calculated with a version of the PSAR BioTEx model *without* increased discretisation in the two lowermost regolith compartments. Finally, the model setup was used for probabilistic simulations. There, the average LDF was calculated for each radionuclide based on 1 000 Monte-Carlo simulations, where the parameter values are varied randomly between simulations (for further details, see Section 6.4.1, Chapter 7 and Chapter 8).

C2 Results

C2.1 LDF comparison for deterministic calculations

The LDF values calculated with the PSAR settings generally agree well with those calculated earlier in SR-PSU. For 80 % of the radionuclides the difference in LDF values is within a factor of two (Figure C-1). The major exposure routes for radionuclides with half-lives longer than 1 000 years are still ingestion of food (C-14, Ca-41, Cl-36, Mo-93, Ni-59, Pd-107, Se-79) or ingestion of water (most other radionuclides) (Table C-1). The former dominating exposure route typically results from draining and cultivation of a mire (i.e. the drained-mire farmer exposure group), whereas high exposure via water typically results from a well drilled into the bedrock. This latter exposure pathway is associated with the garden-plot household exposure group (Section 6.2). Retardation of radionuclides in deep regolith layers that are not exposed when the mire is drained is a key factor for the relative importance of the main exposure routes. This is, radionuclides that result in highest exposure through the use of well water tend to sorb much more strongly in the till layer than radionuclides that result in the highest exposure through accumulation in mire ecosystems and subsequent food-chain exposure (SKB TR-14-06).

Although the overall results are similar in the two assessments, the simulated transport time through the two lowermost regolith compartments (RegoLow and RegoGL) has increased in the PSAR model. This is due to the finer sub-compartment discretisation used now for these compartments. This results in a smaller numerical dispersion and captures better the effects of slower groundwater flows in deeper sections of these two lowest regolith layers (Section 7.6). However, this effect of the discretisation is only significant for a few radionuclides. These include Tc-99 and Zr-93, for which slower transport results in increased radioactive decay. This reduces accumulation in upper regolith layers and causes the dominant exposure route to shift from ingestion of food to ingestion of well water. This shift also dampens the effect of the finer discretisation and limits the reduction in the LDF values to factors of 16 (Tc-99) and 10 (Zr-93), as compared with SR-PSU (Figure C-1).

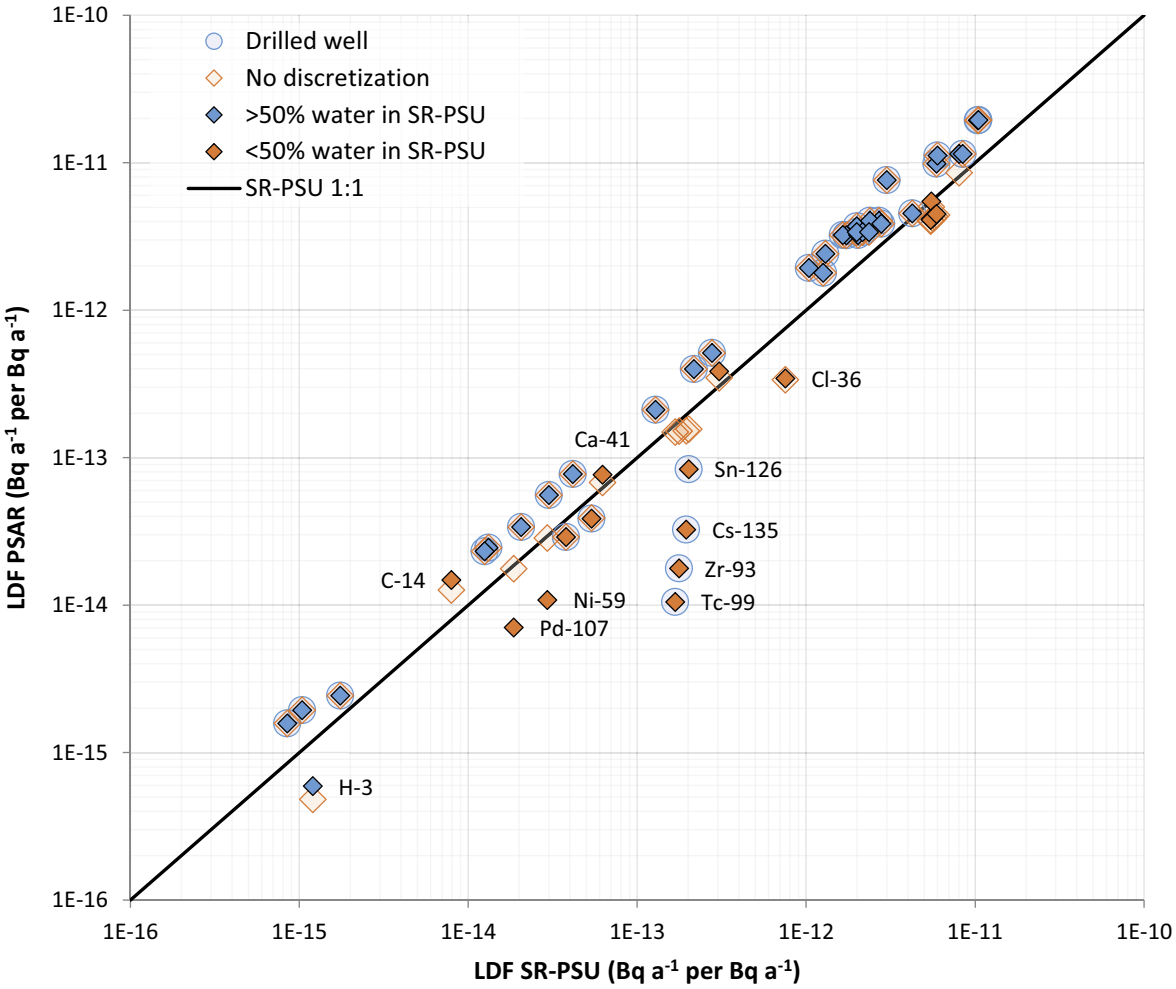

Figure C-1. *LDF values calculated with the updates in the BioTEx model and data introduced in the PSAR (this assessment) as compared with the earlier LDF values reported in SR-PSU (SKB TR-14-06, Table 10-1). To facilitate interpretations, the LDF values have been categorized both with respect to the dominating exposure route in the earlier SR-PSU assessment (blue colour indicating > 50 % of dose from drinking water, orange colour indicating < 50 % of dose from drinking water i.e. usually dominated by the dose from food) and with respect to exposure pathway now in the PSAR (a circle indicating that the exposure from the drilled well gave the highest dose). Moreover, transparent diamond symbols correspond to LDF values calculated with the PSAR model and data, but with the coarser discretization used in SR-PSU. If symbols fall on the line, the LDF values are the same in the two assessments. Radionuclides marked with names are discussed in the text.*

Table C-1. Maximum landscape dose conversion factors, LDF (Sv a^{-1} per Bq a^{-1}), calculated in a deterministic simulation using best-estimate parameters. "Exposure route" refers to the route of exposure for the exposed group with the highest LDF. Radionuclides are sorted according to decreasing half-life. There are two variants of garden-plot households, one that uses natural resources from the biosphere object (including a dug well) and one for which a well drilled into the bedrock in the well interaction area is the only source of radionuclides. For consistency with SR-PSU, the contributions of decay products are not included in the LDF values presented here.

Radionuclide	Half-life year	Exposed population	Max. dose Sv a^{-1}/Bq a^{-1}	Time year (AD)	Exposure route (% of total dose)			
					Ingestion of food	Ingestion of water	Inhalation	External
U-238	4.5×10^{9}	Garden plot	4.1×10^{-12}	20000	38.7	4.4	54.7	2.3
U-235	7.0×10^{8}	Garden plot	4.2×10^{-12}	19800	36.5	4.1	56.0	3.4
U-236	2.3×10^{7}	Garden plot	4.1×10^{-12}	19400	37.1	4.2	58.7	0.0
I-129	1.6×10^{7}	Drained mire	1.1×10^{-11}	3700	32.1	67.9	0.0	0.0
Pd-107	6500000	Drained mire	7.0×10^{-15}	20000	88.9	11.0	0.0	0.0
Cs-135	2300000	Garden plot (drilled well)	3.2×10^{-14}	3000	16.6	83.4	0.0	0.0
Np-237	2144000	Garden plot (drilled well)	1.8×10^{-12}	3000	16.1	83.9	0.0	0.0
Zr-93	1530000	Garden plot (drilled well)	1.8×10^{-14}	3000	16.0	84.0	0.0	0.0
Pu-242	375000	Garden plot (drilled well)	3.9×10^{-12}	3000	15.9	84.1	0.0	0.0
Cl-36	301000	Garden plot	3.4×10^{-13}	5600	99.0	1.0	0.0	0.0
Se-79	395000	Drained mire	3.9×10^{-13}	20000	72.3	27.6	0.0	0.0
U-234	245500	Garden plot	4.4×10^{-12}	19400	36.3	4.2	59.5	0.0
Sn-126	230000	Garden plot (drilled well)	8.4×10^{-14}	3000	15.5	82.1	0.0	2.3
Tc-99	211100	Garden plot (drilled well)	1.1×10^{-14}	3000	17.6	82.4	0.0	0.0
U-233	159200	Garden plot	4.5×10^{-12}	19800	36.8	4.2	59.0	0.0
Ca-41	102000	Drained mire	7.7×10^{-14}	20000	91.7	8.3	0.0	0.0
Ni-59	101000	Drained mire	1.1×10^{-14}	20000	88.4	11.6	0.0	0.0
Th-230	75380	Garden plot (drilled well)	3.4×10^{-12}	3000	15.9	84.1	0.0	0.0
Pa-231	32760	Garden plot (drilled well)	1.1×10^{-11}	3000	15.9	84.1	0.0	0.0
Pu-239	24110	Garden plot (drilled well)	4.0×10^{-12}	3000	15.9	84.1	0.0	0.0
Nb-94	20300	Garden plot (drilled well)	2.9×10^{-14}	3000	15.1	79.5	0.0	5.4
Cm-245	8500	Garden plot (drilled well)	3.4×10^{-12}	3000	15.9	84.1	0.0	0.0
Am-243	7370	Garden plot (drilled well)	3.2×10^{-12}	3000	15.9	84.1	0.0	0.0
Th-229	7340	Garden plot (drilled well)	9.9×10^{-12}	3000	15.9	84.1	0.0	0.0
Pu-240	6564	Garden plot (drilled well)	4.0×10^{-12}	3000	15.9	84.1	0.0	0.0
C-14	5700	Drained mire	1.5×10^{-14}	4900	92.8	7.2	0.0	0.0
Cm-246	4760	Garden plot (drilled well)	3.4×10^{-12}	3000	15.9	84.1	0.0	0.0
Mo-93	4000	Drained mire	5.5×10^{-12}	5000	98.0	2.0	0.0	0.0
Ra-226	1600	Garden plot (drilled well)	4.5×10^{-12}	3000	16.4	83.6	0.0	0.0
Ho-166m	1200	Garden plot (drilled well)	3.4×10^{-14}	3000	15.2	80.2	0.0	4.5
Am-241	432	Garden plot (drilled well)	3.2×10^{-12}	3000	15.9	84.1	0.0	0.0
Ag-108m	418	Garden plot (drilled well)	3.9×10^{-14}	3000	15.3	80.8	0.0	3.9
Am-242m	141	Garden plot (drilled well)	3.2×10^{-12}	3000	15.9	84.1	0.0	0.0

Table C-1. Continued.

Radionuclide	Half-life year	Exposed population	Max. dose Sv a^{-1}/Bq a^{-1}	Time year (AD)	Exposure route (% of total dose)			
					Ingestion of food	Ingestion of water	Inhalation	External
Ni-63	100	Garden plot (drilled well)	2.4×10^{-15}	3000	16.4	83.6	0.0	0.0
Sm-151	90	Garden plot (drilled well)	1.6×10^{-15}	3000	15.9	84.1	0.0	0.0
Pu-238	88	Garden plot (drilled well)	3.7×10^{-12}	3000	15.9	84.1	0.0	0.0
U-232	69	Garden plot (drilled well)	7.6×10^{-12}	3000	16.0	84.0	0.0	0.0
Cs-137	30	Garden plot (drilled well)	2.1×10^{-13}	3000	16.4	83.5	0.0	0.2
Cm-243	29	Garden plot (drilled well)	2.4×10^{-12}	3000	15.9	84.1	0.0	0.0
Sr-90	29	Garden plot (drilled well)	5.1×10^{-13}	3000	18.7	81.3	0.0	0.0
Pb-210	22	Garden plot (drilled well)	1.1×10^{-11}	3000	16.1	83.9	0.0	0.0
Ac-227	22	Garden plot (drilled well)	1.9×10^{-11}	3000	15.9	84.1	0.0	0.0
Cm-244	18	Garden plot (drilled well)	1.9×10^{-12}	3000	15.9	84.1	0.0	0.0
Nb-93m	16	Garden plot (drilled well)	1.9×10^{-15}	3000	16.0	84.0	0.0	0.0
Pu-241	14	Garden plot (drilled well)	7.7×10^{-14}	3000	15.9	84.1	0.0	0.0
Cd-113m	14	Garden plot (drilled well)	4.0×10^{-13}	3000	21.8	78.2	0.0	0.0
Eu-152	14	Garden plot (drilled well)	2.3×10^{-14}	3000	15.5	82.0	0.0	2.5
H-3	12	Drained mire	5.9×10^{-16}	3200	0.0	100.0	0.0	0.0
Ba-133	11	Garden plot (drilled well)	2.5×10^{-14}	3000	16.5	83.0	0.0	0.5
Co-60	5.3	Garden plot (drilled well)	5.6×10^{-14}	3000	16.0	82.8	0.0	1.2
Po-210	0.38	Garden plot (drilled well)	1.9×10^{-11}	3000	15.9	84.1	0.0	0.0

a) Contribution from decay products to U-238 and U-235 increase the LDF by 1 % and 120 %, respectively.

b) Contribution from decay products to U-234, U-233 and Th-230 increase the LDF by 24 %, 64 % and 55 %, and changes the most exposed group to drained mire farmers.

Several other radionuclides are also noticeably affected by the discretisation. For example, the main exposure pathway of Cs-135 and Sn-126 also shifts from cultivation of the drained mire to extraction of water from the drilled well, but the effects on the LDFs are modest for these radionuclides (i.e. within a factor of five, Figure C-1). The activity concentrations of Ni-59 and Pd-107 in regolith layers are reduced by the same mechanism. For Ni-59 and Pd-107 the limited reduction (by 60 %) does not change the dominant exposure pathway but reduces the LDF correspondingly. For Nb-94 the main exposure pathway is changed from external exposure to extraction of well water, but the shift has a marginal effect on the LDF value (reduction by ~25 %).

For radionuclides with (physical) half-lives shorter than 1 000 years, the dominating exposure route is always the ingestion of water, typically from the drilled well which is assessed in the garden-plot household exposure group. In the PSAR, the dose from these radionuclides is typically a factor of two larger than in SR-PSU. This is due to the combined effect of the changed handling of the drilled well and the updates in the representation of small-scale irrigation, as discussed below.

In the PSAR, the drilled well represents a well into the area in bedrock where the groundwater is expected to have the highest concentrations of radionuclides originating from SFR (i.e. *the well interaction area*, Section 5.5). The exposure from this well is only considered to be relevant for a small group. Thus, to make the dose comparable with that of other exposure groups, it is divided by a factor

of ten[70] (Section 7.5.4). In the LDF calculations, a deterministic value of 4.7 % is used for the fraction of the unit release that reaches the geosphere well[71]. In the earlier biosphere assessment of SR-PSU, drilled wells were only considered near an agricultural settlement, and in the LDF calculations 0.3 % of the geosphere release was considered to reach such sites[72]. Thus, the dose from drinking water from a drilled well is ~1.6 times higher in the PSAR as compared with SR-PSU, given a unit release rate. The well water is also used for irrigation, and the representation of this pathway was updated in SE-SFL (SKB TR-19-05, Section 8.2) and further incorporated in the PSAR. That is, now in the PSAR, the process of translocation of radionuclides intercepted on leaves further into edible parts of the crop is included, and the time between irrigation events has been shortened (allowing for less loss of intercepted activity prior to harvesting). These two updates combined result in a limited increase of the potential dose of most radionuclides with half-lives below 1 000 years, as well as of some of the radionuclides with longer half-lives, as seen as a band of blue diamond symbols overlaying blue circles above the 1:1 line in Figure C-1. The higher LDF values reflected in this band are independent of the increased discretisation in the lowermost regolith compartments but are a consequence of treating the drilled well as an exposure pathway in the base case. Moreover, the updates related to irrigation are considered to not overlook potentially important effects, thus making the corresponding exposure calculations more robust.

The LDFs of three other radionuclides differ between the PSAR and SR-PSU for partly other reasons than the increased discretisation or the handling of the drilled well. In Figure C-1 this is seen with off-diagonal transparent diamonds. For C-14, the new LDF in the PSAR is almost twice as large as earlier in SR-PSU, whereas for Cl-36 and H-3 the LDFs are halved.

The handling of C-14 has been updated in the PSAR, with the primary aim to allow a consistent handling of stable carbon and C-14 in probabilistic simulations. However, C-14 doses are also sensitive to the activity concentrations in and the amount of groundwater transported to the cultivated soil during the vegetation season, as this pathway is the primary source for C-14 once the mire is cultivated (Figure 9-10). Thus, the increased LDF is partly due to higher concentrations in groundwater associated with the finer discretization of the lowermost regolith layers and partly due to a higher rate of groundwater uptake during the vegetation season. In the PSAR, the parameter describing plant groundwater uptake is updated to reflect the water demand of all the crops postulated to be grown on the drained mire (Section 8.2.2). This has resulted in an increased parameter value, as the water demands of fodder and potatoes are greater than that of cereals (which was the only crop considered for the parametrisation in SR-PSU).

For Cl-36, two parameters are updated in the PSAR (Section 8.2.3) based on additional data from recent field studies in Forsmark (Svensson et al. 2021). This means that the data underlying the concentration ratio (CR) for mire vegetation have been significantly improved, and now in the PSAR the CR value is based on paired vegetation and soil samples. Earlier in SR-PSU, the fraction of plant Cl in inorganic form (i.e. the fraction released upon senescence) was estimated based on literature data. Now in the PSAR, this parameter is based on samples recently collected in Forsmark. These updated parameter values, that result in a lower accumulation of Cl-36 in peat, are considered to give a better representation of Cl cycling in mire ecosystems. Thus, the decrease in the LDF of Cl-36 by a factor two is considered to be well motivated.

The LDF for H-3 corresponds to drinking water from a dug well at the time when the highest point of biosphere object 157_2 has emerged 1 m above the sea. In SR-PSU, the area-specific groundwater flows in the object were assumed to be similar to flows under sea-covered conditions at this time. Whereas this is a reasonable assumption for the parts of the object covered by the sea, it is not plausible for the terrestrial parts of the object. In the PSAR, area-specific terrestrial groundwater flows are applied instead to the terrestrial part of the object directly after emergence (Section 7.5.5). These higher groundwater flows for the terrestrial areas result in more dilution and thus a lower LDF.

[70] A factor of 10 is equivalent to the ratio between the risk criteria appropriate for a small group (10^{-5}) and the regular regulatory risk criteria (10^{-6}).

[71] This value corresponds to the average fraction for all waste vaults and wells that received particles from SFR (Werner et al. 2013, Table X3).

[72] This fraction corresponds to two times the largest fraction observed in the particle release study to wells in agricultural settlements (Werner et al. 2013, Table X2).

C2.2 LDF comparison for probabilistic calculations

Mean LDF values from probabilistic calculations were reported as part of the parameter sensitivity and uncertainty analysis in SR-PSU (SKB TR-14-06, Section 10.9). As noted in that analysis, the uncertainty of parameters typically caused the arithmetic mean values from the probabilistic simulation to be equal to or higher than the corresponding values from a single simulation based on best estimate parameter values. This is also true for the PSAR (data not shown). In general, the mean LDF values calculated with the new PSAR settings agree well with those calculated in SR-PSU also when parameter uncertainty is accounted for. That is, for 75 % of the examined radionuclides, the difference in mean LDF values between the two assessments is within a factor of two (Figure C-2).

In general, it is the same radionuclides that deviate more than a factor of two in the probabilistic calculations as were observed in the comparison of deterministic LDFs above (cf e.g. Tc-99, Zr-93, Cs-135, Sn-126, Cl-36 and H-3 in Figure C-1 and Figure C-2). Moreover, apart from Cl-36 and H-3 (which are discussed already above), the differences in the probabilistically calculated mean LDFs can be explained almost entirely by the increased discretisation used in the PSAR (as indicated by the transparent diamonds falling on the diagonal for the radionuclides that deviate more than a factor of two).

However, there are a few additional features that are worth noticing. For example, the difference in the arithmetic mean LDFs between the PSAR and SR-PSU is much greater for Cs-135 when parameter uncertainties are accounted for than in the deterministic comparison. This is primarily due to the highly skewed LDF distribution in SR-PSU, where simulations with very low K_d-values for the lowest regolith layer (till) allowed Cs-135 to reach and accumulate in upper layers within the relatively short simulation time. In the more finely discretised PSAR model, the retardation of Cs-135 in the till is very effective even in realisations with K_d-values drawn from the lower region of the probability distribution function (PDF). Consequently, the drilled well is the main exposure pathway in the PSAR, and the mean LDFs for Cs-135 are insensitive to the highly variable K_d (the geometric standard deviation has been determined to be at 3 for Cs-135).

A similar explanation is applicable also to the cluster of Pu-239, Pu-242 and Ra-226, for which mean LDF values are systematically lower in the PSAR than in SR-PSU when parameter uncertainty is accounted for. Those LDF values did not deviate noticeably in deterministic calculations as the dominant exposure pathway was from well water in both SR-PSU and the PSAR (Table 10-1 in SKB TR-14-06 and Table C-1).

It can be noted that the mean LDF of C-14 in the PSAR is lower in relation to the deterministic LDF than the mean LDF calculated in SR-PSU (compare Figure C-1 and Figure C-2). This indicates that the PSAR model has reduced the uncertainties (or variation) associated with C-14 calculations noticeably. In SR-PSU, a parameter was used to characterise the given dissolved inorganic carbon (DIC) concentration in the soil pore water, whereas now in the PSAR the corresponding DIC concentration is calculated from the main source of stable carbon (i.e. soil respiration) and the rate of degassing. Also, in SR-PSU, the diffusivity which controls the degassing rate was the main uncertainty component for the C-14 dose. The distribution of the diffusivity was highly skewed and this caused the mean LDF from probabilistic calculations to exceed that from the deterministic calculations using best-estimate input values by a factor of 3.5 (SKB TR-14-06, Section 10.9). In the PSAR, the process of degassing affects the stable carbon and C-14 concentrations consistently. Consequently, the uncertainty with respect to degassing has a marginal effect on the specific activity in the soil pore water, and because of this also the dose from ingestion of crops is insensitive to the rate of degassing (Saetre and Ekström 2017b). This reduction of uncertainty can also be seen in the span between the 5th and 95th percentile of the C-14 dose, which is decreased by a factor of three in the PSAR as compared with SR-PSU (Figure 11-1, and Figure 10-34 in SKB TR-14-06). It can be concluded that the increased consistency in the handling of stable and radioactive carbon reduce the uncertainty (or variation) associated with C-14 calculations noticeably.

Finally, it can be noted that the shift in the handling of a well drilled in the bedrock, from a location in an agricultural settlement to a well drilled in the well interaction area also causes systematically higher mean LDF values in the PSAR than in SR-PSU when parameter uncertainties are considered. The differences are slightly larger in the probabilistic than in the deterministic calculation. This is expected as the uncertainties associated with the fraction of the release that reached the well were dealt with by a cautious deterministic assumption in SR-PSU and by a probability density function in the PSAR. The cautious assumption was the same in deterministic and probabilistic calculations in SR-PSU, but in the PSAR the variation in the fraction reaching the well caused a positively skewed distribution of the LDF values, with a mean higher than the deterministic best estimate. Regardless, the difference in the average LDF values between the two assessments is typically within a factor of two (Figure C-2).

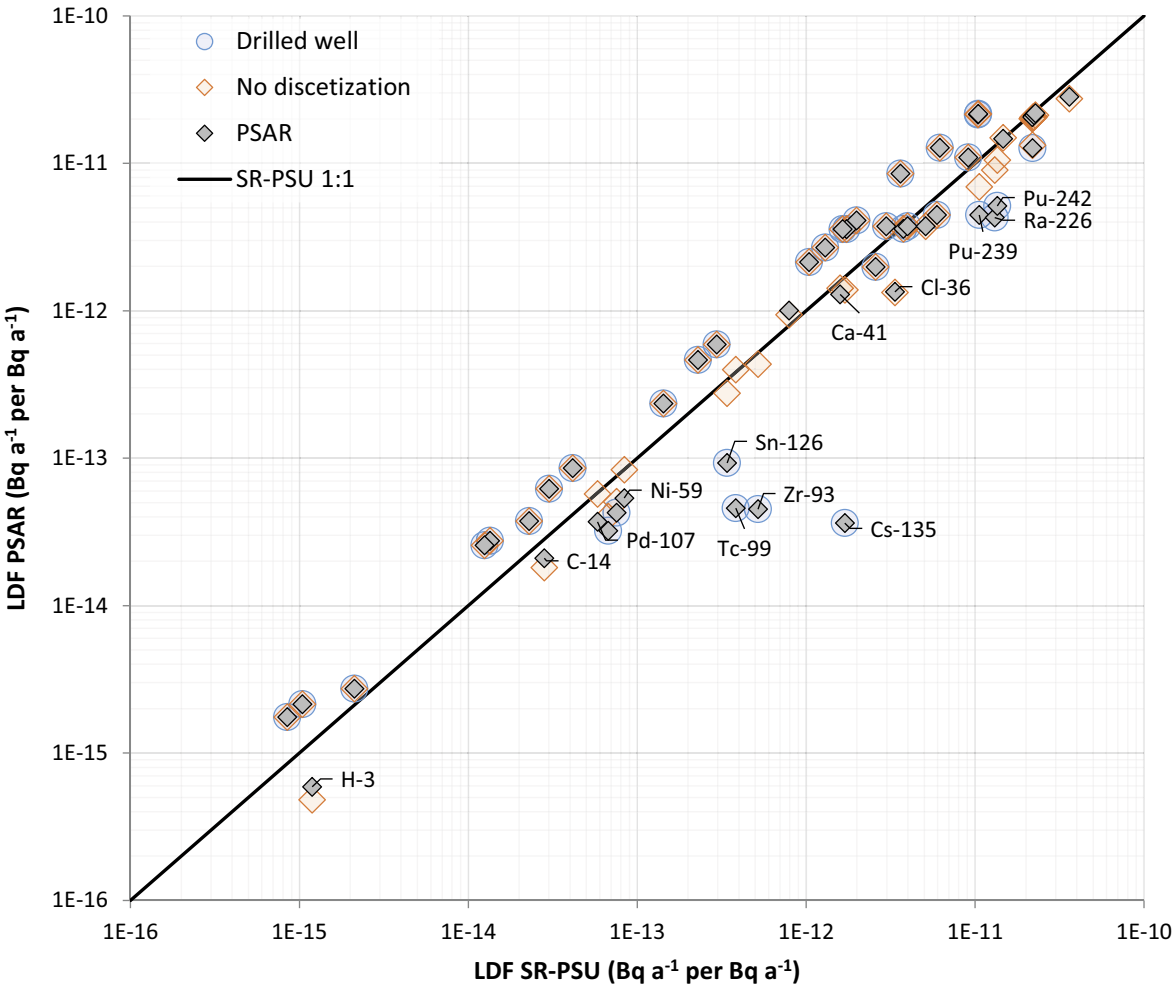

Figure C-2. *Arithmetic mean of LDF values calculated from 1 000 Monte-Carlo simulations with the updates introduced in the PSAR (vertical axis) as compared to the corresponding LDFs reported in SR-PSU (horizontal axis, Section 10.9 in SKB TR-14-06). In these simulations, parameter values are randomly drawn for each simulation (referred to as probabilistic calculations). To facilitate interpretation, the LDF values have been categorized with respect to exposure pathway in the PSAR (circle indicating that exposure from the drilled well gave the highest dose). Moreover, transparent diamonds correspond to LDF calculated with the PSAR model, but with the original coarser discretization used in SR-PSU. If symbols fall on the line, the LDF values are the same in the two assessments.*

Appendix D

Method to assess exposure of non-human biota

This appendix presents details of the ERICA Integrated Approach for calculating dose rates to non-human biota. The model code, and parameterisation including recent updates are described, including the implementation into BioTEx.

D1 Introduction

D1.1 The ERICA Tool

Dose rates to non-human biota from radioactive contamination are calculated using the mathematical formulae from the ERICA Tool (Brown et al. 2008), a software tool implementing the ERICA Integrated Approach (Howard and Larsson 2008).

The tool's latest release (v2.0, public release: November 2021) includes an updated methodology for deriving dose conversion coefficients, based on the ICRP's BiotaDC code (Ulanovsky 2017, ICRP 2017), which the tool uses to estimate doses from internal and external exposure. Details of the changes to the dose conversion coefficients resulting from the new derivation method, and their potential impact on the assessment outcome(s) are discussed separately in Section D4.1 and in Appendix E.

D1.2 Reference organisms in ERICA

A number of reference organisms are used to represent the range of species present at the site. The reference organism concept, included within ERICA, was designed to reflect the reference human concept employed in the radiation protection system for humans. The use of reference organisms has been tested and approved in studies of impacts on the environment in prior safety assessments by SKB in Sweden (Jaeschke et al. 2013, SKB TR-14-09), and in other international assessments (Aliyu et al. 2015a, b, ANSTO 2017, Konstantinova et al. 2015, Posiva 2014). The safety assessment for SKB's repository for spent nuclear fuel extensively compared ERICA reference organisms with site-specific species and determined that the reference organisms satisfactorily represented the species of interest at the site (Jaeschke et al. 2013).

ERICA reference organisms 'Marine Reptiles' and 'Sea anemones & True corals' represent biota that are not expected at the site now, nor in the future, and, thus, are not relevant for the present assessment and have been removed from consideration.

During the site-characterisation programme, microphytobenthos was identified as an 'organism type' that was present at the site but not suitably represented by any of the ERICA reference organisms. Microphytobenthos is a community of small photosynthesising organisms that occupy the bottom of the shallow lakes of the Forsmark area and, together with heterotrophic bacteria, form thick carpets on benthic sediments. Due to the shallowness of the water, these organisms have an important role as the predominant primary producers in the lake ecosystems (Andersson 2010). A user-defined organism was created for microphytobenthos with the same parameters as the reference organism 'Freshwater Phytoplankton', except the occupancy of the microphytobenthos has been changed from '*in water*' to '*on sediment*'.

Organisms are simplified in shape (simple ellipsoid) and are considered to be homogeneous, without distinct organs, etc. The reference organisms are assigned nominally representative values for their size and mass.

D1.3 The screening dose rate

The primary endpoint selected by SKB for demonstrating protection of non-human biota is absorbed dose rates to a set of reference organisms, in the following referred to as dose rates. The ERICA methodology, applied in the current assessment, proposes a screening dose rate at the ecosystem level of 10 μGy h^{-1} (Beresford et al. 2007, Brown et al. 2008), which has been further endorsed by the EU PROTECT project (Andersson et al. 2009). The ERICA screening dose rate was originally derived as a predicted no-effect-dose-rate value for ecosystems, based on a distribution analysis of mortality

and reproduction response to chronic exposure in a broad range of organisms (Garnier-Laplace and Gilbin 2006). Dose rates below the screening dose rate are considered to be unlikely to significantly negatively affect populations of organisms. The present, and previous SKB assessments for geological repositories for radioactive wastes, generally use the ERICA screening dose rate. In a few cases, the ICRP DCRLs (Derived Consideration Reference Levels), which have become advocated by the IAEA, are more restrictive than the ERICA screening dose rate (i.e. a lower band of 4 μSvh^{-1} is applied to some vertebrates and pine trees). These are described in more detail in Section 12.2 and are contrasted against the results in Section 12.8. Calculated dose rates that exceed the screening dose rate do not necessarily denote a significant radiological consequence, but rather serve as an indicator that a more detailed investigation and/or protective measures are warranted.

D1.4 Overview of the dose rate calculation methodology

Dose rates to non-human biota for each radionuclide are calculated from the activity concentrations in environmental media (ACs) and from the activity concentrations within the body of the organism. Activity concentrations for radionuclides within the body are estimated using transfer factors (concentration ratios, CRs) from those in the environmental media.

Dose conversion coefficients (DCCs) are then used to estimate external and internal dose rates for each radionuclide, which are adjusted using weighting factors for each relevant type of radiation (alpha, high- and low-energy beta, and gamma) and based on the organism's occupancy (OCC) in relation to environmental media. Unlike previous iterations of ERICA, the new version no longer differentiates between low-energy beta and high-energy beta/gamma radiations from external sources.

Internal and external dose rates are summed to give a total dose rate for each radionuclide. The total dose rates from each radionuclide are summed to give a final total dose rate to each organism type, which is then compared with a screening dose rate to assess the radiological consequence to populations of non-human biota.

D1.5 Incorporation of ERICA code into BioTEx

The Biosphere transport and exposure model (BioTEx) is the computer model employed by SKB for calculating radionuclide transport through the biosphere and doses/dose rates to humans and the environment (Chapter 7). This facilitates the automatic entry of input data (activity concentrations in environmental media: soil, sediment, water and air) directly from the transport sections of the model, facilitating multiple runs under various scenarios, time-series, etc.

Dose conversion coefficients for all organisms and radionuclides relevant to the assessment are calculated in ERICA (using the BiotaDC code) and subsequently imported into BioTEx. Relevant parameter data used in the calculations such as the occupancies of the reference organism (and user-generated organisms, such as microphytobenthos) are imported from ERICA to BioTEx. An overview of variables used in BioTEx implementation of ERICA 2.0 dosimetry models are given in Table D-1.

D2 Activity concentrations

ERICA version 2.0 can interchange freely between activity concentrations in water and in sediment, because one litre of water has a mass of approximately one kilogram (mass of seawater is very slightly more but is approximated to 1 kg l^{-1}). Consistently, the unit conversion in the BioTEx implementation (i.e., converting from cubic metres of water to kilogram dry weight) uses a constant value of 0.001 m^3 $kgdw^{-1}$. The conversion is applicable to concentrations, i.e. Bq m^{-3} to Bq kg^{-1}, but not from volume (m^3) to mass (kg).

Activity concentration variables used as input in the ERICA dose rate computations are calculated within the BioTEx model and mapped as described in the following subsections. In the description, BioTEx parameters and functions are indicated with italics.

D2.1 Terrestrial activity concentrations

Terrestrial activity concentrations are calculated from the year when the bay starts developing into a lake (i.e. the BioTEx-parameter $threshold_{start}$). Activity concentration in air (AC_{Air}) uses the activity concentration in air above the mire, calculated in the human exposure calculations, for the hunter & gatherer group (i.e. the BioTEx-variable $Forager.AC_{Air}$). Activity concentration in soil (AC_{Soil}) is set to the total activity concentration in the upper peat regolith layer in the mire (i.e. the BioTEx-variable $Ter.AC_{RegoUp,tot}$). Activity concentrations in terrestrial organisms (AC_{Org}) are calculated as the product between activity concentration in soil (AC_{Soil}) and the concentration ratio between organism and soil (cR_{soil}) for all radionuclides except for tritium and carbon-14. For tritium, the activity concentration of terrestrial organisms is calculated as the quotient of pore water activity concentration in the upper peat regolith layer in the mire (i.e. the BioTEx-variable $Ter.AC_{RegoUp,D}$) and density of water (i.e. the BioTEx-parameter $dens_{water}$) times the fraction of the organism that consists of water (i.e. one minus the fraction dry weight to fresh weight in organism, $f_{DW,org}$). For carbon-14, the activity concentration of terrestrial organisms is calculated as the product between the activity concentration in terrestrial primary producers on the mire (i.e. the BioTEx-variable $Ter.AC_{PP}$) and the fraction of carbon in organism per unit of fresh weight ($f_{C,org}$).

D2.2 Aquatic activity concentrations

For aquatic activity concentrations, the year the terrestrial part of the biosphere object is fully emerged (i.e. the BioTEx parameter $threshold_{isolation}$) separates the calculations of dose rates to marine organisms (before the threshold) and freshwater organisms (after the threshold), respectively. The activity concentration in water (AC_{Water}) corresponds to the total activity concentration in sea, lake or stream water, which includes activity sorbed on particles and activity in organic particles (i.e. the BioTEx-variable $Aqu.AC_{Water,tot}$), whereas activity concentration in filtered water ($AC_{Water,D}$) uses the dissolved fraction of the activity concentration in sea, lake or stream water (i.e. the BioTEx-variable $Aqu.AC_{Water,D}$). Activity concentration in sediment ($AC_{Sediment}$) uses the total activity concentration in the upper aquatic regolith layer (i.e. the BioTEx-variable $Aqu.AC_{RegoUp,tot}$). Activity concentrations in organisms (AC_{Org}) are calculated as the product between activity concentration in filtered water ($AC_{Water,D}$) and activity concentration ratio between organism and filtered water (cR_{water}) for all radionuclides except for tritium and carbon-14. For tritium, the activity concentration of aquatic organisms is calculated as the quotient of filtered water concentration ($AC_{Water,D}$) and the density of water (i.e. the BioTEx-parameter $dens_{water}$) times the fraction of the organism that consists of water (i.e. one minus the fraction dry weight to fresh weight in organism, $f_{DW,org}$). For carbon-14, the activity concentration of aquatic organisms is calculated as the quotient between the activity concentration in filtered water ($AC_{Water,D}$) and the concentration of dissolved inorganic carbon in sea or fresh water (i.e. the BioTEx-parameters $conc_{DIC,sea}$ or $conc_{DIC,lake}$ respectively) times the fraction of carbon in organism per fresh weight ($f_{C,org}$).

D3 Occupancy

The different external dose conversion coefficients apply differently for the different media types (soil, sediment, water and air) and the organism's relation to them. Terrestrial organisms may be '*in soil*', '*on soil*' or '*in air*', whereas aquatic organisms may be '*in sediment*', '*on sediment*', '*in water*' and '*on water*'.

Previously, organisms were considered to be externally exposed only to radionuclides in the soil, with '*in air*' organisms differentiated from '*on soil*' only by their separation from radionuclides in the soil – their 'height in air' determines their distance from the contaminants in soil, and, thus, the exposure therefrom. ERICA v2.0 introduced a calculation for organisms immersed in contaminated air, which permits the calculation of external doses from radioactive gases, such as radon, in the air surrounding the organism. As it is formed as a decay product from another modelled radionuclide, radon is not explicitly included in the calculation in BioTEx. To conform with the calculation methodology in BioTEx, the immersion dose in air from radon is applied to its parent radionuclide (which is based on the activity concentration in soil and the dust concentration in air). This is neither a realistic nor a cautious approach, as the main radon activity in air would originate from gaseous releases from the soil and is expected to be several orders of magnitude higher (~3–4). However, as the expected external exposure from the parent radionuclide in soil for the ERICA reference organisms is many orders of magnitude higher (~10–11) than the expected external exposure from radon isotopes in the air the simplified approach is considered reasonable.

In ERICA, where reasonably realistic, reference organisms are cautiously biased towards increased relationships with sediment/soil, where the dose rates are typically higher. This is because organisms that are in/on sediment or soil receive doses from radionuclides in both the sediment AND the water, or soil AND the air, whereas organisms '*in water*', '*on water*' or '*in air*' are less/not exposed to radionuclides in soil/sediment.

Furthermore, organisms are cautiously considered to be sedentary, meaning they remain in the same relationship with media as well as in the same area of the environment, i.e., they do not migrate or move from more- to less-contaminated areas.

D4 Dose conversion

D4.1 BiotaDC and decay chains

A new piece of software that enables the calculation of dose conversion coefficients (DCCs) for internal and external exposures of organisms and is called BiotaDC, was developed for the ICRP (ICRP 2017) to complement the updated methodology for calculating DCCs, superseding the method used in ICRP Publication 108 (ICRP 2008). BiotaDC was incorporated into the ERICA tool in v2.0. The BiotaDC software was used to calculate new DCC values for the present assessment, replacing values used in previous assessments that were based on ICRP Publication 108 (as detailed in Tröjbom et al. 2013). As not all radionuclides in decay chains are explicitly modelled in BioTEx, DCCs for these radionuclides are added to those of their parents' DCCs, assuming secular equilibrium, using the same method as for dose coefficients for humans in BioTEx (Grolander 2013, Section 3.3).

The BiotaDC code can also calculate the DCCs to include contributions from ingrown radioactive decay products during a set period (set to 1 year in ERICA v2.0), however, this was not used in the present assessment, in favour of the method already used when developing dose coefficients for humans, previously described in Grolander (2013, Section 3.3).

D4.2 Internal exposure

Weighted internal dose rate for an organism (μGy h^{-1}) is implemented in BioTEx as:

$$Dose_{rate,int} = AC_{Org} \times (w_{low,beta} \times DCC_{int,low,beta} + w_{alpha} \times DCC_{int,alpha} + w_{beta,gamma} \times DCC_{int,beta,gamma})$$

where

AC_{Org} is activity concentration in an organism (Bq $kgfw^{-1}$),

$w_{low,beta}$ is weighting factor of internal low-energy beta (-),

w_{alpha} is weighting factor of internal alpha (-),

$w_{beta,gamma}$ is weighting factor of internal high-energy beta radiation and gamma radiation (-),

$DCC_{int,low,beta}$ is dose conversion coefficient of internal low beta radiation (μGy h^{-1} per Bq $kgdw^{-1}$),

$DCC_{int,alpha}$ is dose conversion coefficient of internal alpha radiation (μGy h^{-1} per Bq $kgdw^{-1}$),

$DCC_{int,beta,gamma}$ is dose conversion coefficient of internal beta gamma radiation (μGy h^{-1} per Bq $kgdw^{-1}$).

In ERICA v2.0 radionuclide-specific weighting factors can be applied. However, due to incomplete data, and in order to be consistent with the calculations in SR-PSU, common weighting factors (based on the radiation-type released) are applied for all radionuclides (Saetre et al. 2013a, Section 10.2).

Note that in the BioTEx implementation, exposures from all sources have been combined into one equation; thus, for sources that are not necessarily applicable (e.g. beta and gamma radiation for radon isotopes and any internal radiation for other noble gases) the dose conversion coefficients are set to zero.

D4.3 External exposure in air

Weighted external dose rate for a terrestrial organism (μGy h^{-1}) is implemented in BioTEx as:

$$DoseRate_{ext} = AC_{Air}\, DCC_{imm,ext,in,air} + AC_{Soil} \times (OCC[\text{On-soil}] \times DCC_{ext,on,soil} + OCC[\text{In-soil}] \times DCC_{ext,in,soil} + OCC[\text{In-air}] \times DCC_{ext,in,air})$$

where

AC_{Soil} is activity concentration in soil (Bq $kgdw^{-1}$),

AC_{Air} is activity concentration in air (Bq m^{-3}),

OCC is occupancy factor for an organism in different habitats (-),

$DCC_{ext,on,soil}$ is dose conversion coefficient directly on soil (μGy h^{-1} per Bq $kgdw^{-1}$),

$DCC_{ext,in,soil}$ is dose conversion coefficient in soil (μGy h^{-1} per Bq $kgdw^{-1}$),

$DCC_{ext,in,air}$ is dose conversion coefficient in air – the organism is externally exposed to radionuclides in the soil but is separated by some distance (μGy h^{-1} per Bq $kgdw^{-1}$), and

$DCC_{imm,ext,in,air}$ is dose conversion coefficient of immersion external radiation in air – the organism is externally exposed by being within or near a radioactive cloud (μGy h^{-1} per Bq m^{-3}).

Note that in the BioTEx implementation, exposures from all sources have been combined into one equation; thus, for sources that are not necessarily applicable (e.g. the three first terms in the equation for gases) the dose conversion coefficients are set to zero.

D4.4 External exposure in water

Weighted external dose rate for an aquatic organism (μGy h^{-1}) is implemented in BioTEx as:

$$DoseRate_{ext} = AC_{Sediment} \times (OCC[\text{Sediment}] + 0.5 \times OCC[\text{Sediment-surface}])) \times DCC_{ext,in,water} + (\delta \times AC_{Water} \times (OCC[\text{Water}] + 0.5 \times OCC[\text{Water-surface}] + 0.5 \times OCC[\text{Sediment-surface}])$$

where

AC_{Water} is activity concentration in water (Bq m^{-3}),

$AC_{Sediment}$ is activity concentration in sediment (Bq $kgdw^{-1}$),

$DCC_{ext,in,water}$ is dose conversion coefficient in water (μGy h^{-1} per Bq $kgdw^{-1}$), and

δ is unit conversion constant (0.001 m^3 $kgdw^{-1}$).

Table D-1. Variables used in BioTEx implementation of ERICA 2.0 dosimetry models. Listed short names of dependencies correspond to: Org = organisms, Rns = radionuclides, M = marine, F = freshwater and T = terrestrial. "Probabilistic" parameters are those that are varied in a probabilistic assessment.

Variable	Unit	Dependencies	Type	Probabilistic
$Dose_{rate,int}$	µGy h^{-1}	Org, Rns, M, F, T	ERICA equation	Yes
$Dose_{rate,ext}$	µGy h^{-1}	Org, Rns, M, F, T	ERICA equation	Yes
$w_{low,beta}$	-	-	ERICA parameter	No
w_{alpha}	-	-	ERICA parameter	Yes
$w_{beta,gamma}$	-	-	ERICA parameter	No
$DCC_{int,low,beta}$	(µGy h^{-1})/(Bq $kgfw^{-1}$)	Org, Rns	ERICA parameter	No
$DCC_{int,alpha}$	(µGy h^{-1})/(Bq $kgfw^{-1}$)	Org, Rns	ERICA parameter	No
$DCC_{int,beta,gamma}$	(µGy h^{-1})/(Bq $kgfw^{-1}$)	Org, Rns	ERICA parameter	No
$DCC_{ext,in,water}$	(µGy h^{-1})/(Bq $kgdw^{-1}$)	Org, Rns, M, F	ERICA parameter	No
$DCC_{ext,on,soil}$	(µGy h^{-1})/(Bq $kgdw^{-1}$)	Org, Rns, T	ERICA parameter	No
$DCC_{ext,in,soil}$	(µGy h^{-1})/(Bq $kgdw^{-1}$)	Org, Rns, T	ERICA parameter	No
$DCC_{ext,in,air}$	(µGy h^{-1})/(Bq $kgdw^{-1}$)	Org, Rns, T	ERICA parameter	No
$DCC_{imm,ext,in,air}$	(µGy h^{-1})/(Bq m^{-3})	Org, Rns, T	ERICA parameter	No
OCC	-	Org, Habitat	ERICA parameter	No
cR_{soil}	(Bq $kgfw^{-1}$)/(Bq $kgdw^{-1}$)	Org, Element, T	ERICA parameter	Yes
cR_{water}	(Bq $kgfw^{-1}$)/(Bq m^{-3})	Org, Element, M, F	ERICA parameter	Yes
AC_{Org}	Bq $kgfw^{-1}$	Org, Rns, M, F, T	ERICA input equation	Yes
AC_{Air}	Bq m^{-3}	Rns, T	ERICA input variable	Yes
AC_{Soil}	Bq $kgdw^{-1}$	Rns, T	ERICA input variable	Yes
$AC_{Sediment}$	Bq $kgdw^{-1}$	Rns, M, F	ERICA input variable	Yes
$AC_{Water,D}$	Bq m^{-3}	Rns, M, F	ERICA input variable	Yes
AC_{Water}	Bg m^{-3}	Rns, M, F	ERICA input variable	Yes
δ	m^3 $kgdw^{-1}$	-	Unit conv. constant	No
$f_{DW,org}$	kgdw $kgfw^{-1}$	Org	Unit conv. parameter	No
$f_{C,org}$	kgC $kgfw^{-1}$	Org	Unit conv. parameter	No
$Forager.AC_{Air}$	Bq m^{-3}	Rns	BioTEx equation	Yes
$Ter.AC_{RegoUp,tot}$	Bq $kgdw^{-1}$	Rns	BioTEx equation	Yes
$Ter.AC_{PP}$	Bq kgC^{-1}	Rns	BioTEx equation	Yes
$Ter.AC_{Water,D}$	Bq m^{-3}	Rns	BioTEx equation	Yes
$Aqu.AC_{Water,D}$	Bq m^{-3}	Rns	BioTEx equation	Yes
$Aqu.AC_{Water}$	Bq m^{-3}	Rns	BioTEx equation	Yes
$area_{obj,ter}$	m^2	-	BioTEx lookup-table	No
$threshold_{start}$	a	-	BioTEx parameter	No
$threshold_{isolation}$	a	-	BioTEx parameter	No
$dens_{water}$	kg m^{-3}	M, F	BioTEx parameter	No
$conc_{DIC,sea}$, $conc_{DIC,lake}$	kgC m^{-3}	M, F	BioTEx parameter	Yes

Appendix E

Updated values for non-human biota concentration ratios, dose conversion coefficients and occupancy

This appendix includes the new values for non-human biota concentration ratios (NHB CR), dose conversion coefficients (DCC) and occupancy factors (OCC). For the PSAR, the NHB CR parameters are thoroughly revised due to significant updates to the Wildlife Transfer Database (WTD, IAEA 2015). This update affects geometric means and geometric standard deviations in many instances, and for all organisms, values for some of the elements are affected. Also values for DCC and OCC are updated due to new methods applied for calculating these (see Appendix D). This appendix also includes a more detailed description of the changes in NHB CR parameter values that are summarised in Chapter 8.

E1 Concentration ratios for non-human biota

E1.1 Selection of data source per parameter

In choosing data an assumption was made that site data is always more representative than literature data and therefore selected if sufficient amounts of observations were available from the site. Thus, the values for NHB CR parameters are based on site data if available, but as site data for many of the elements and organisms are missing, many of the values are based on literature data. The information on selection of the data is summarised in Table E-1. The WTD data used is from the IAEA table unless otherwise specified.

E1.2 Values for non-human biota concentration ratios and changes since SR-PSU

The NHB CR values for the PSAR are presented in Table E-2, where the changes in the values since SR-PSU are illustrated with red and blue highlights. Many of the updates on the NHB CR values are concentrated on a few elements and organisms, for which values have been updated either due to added (or removed) data in WTD. Generally, most of the changes in parameter values are within one order of magnitude.

For the elements Ag, Po, Pu and Tc, most of the values have been updated. For Ag, limnic plankton and microphytobenthos, and terrestrial flying insects have been assigned values that are more than one order of magnitude lower than in SR-PSU. The updates for most of the Ag parameters are due to discarded data in the updated versions of the WTD. In the PSAR, Cu is instead used as an element analogue in most cases since Cu is the most suitable analogue for Ag (Tröjbom et al. 2013). This is also the approach adopted in the ERICA Tool, version 1.2. In SR-PSU, data from arachnids (IAEA 2011) were used to derive a CR for terrestrial flying insects. Arachnids are not reported in WTD (IAEA 2015). Therefore, data from adult bees from WTD´s ICRP table (ICRP 2015) are instead used in the PSAR, and this causes a change in all CR values for flying insects.

For Po, the updated values differ from SR-PSU by more than one order of magnitude for ten organisms. For marine birds the difference is extremely large, more than eight orders of magnitude. This is mainly due to data from ICRP (2009) that are not included in the updated version of the WTD database. As no data are reported for marine birds by WTD, the CR value for marine fish is instead used as a parameter analogue for birds in the PSAR. The CR values for Po for terrestrial amphibians, birds and large mammals used in the PSAR are almost three orders of magnitude higher than values used in SR-PSU. In these cases, data for terrestrial mammals reported in WTD are used to replace the corresponding value that was previously reported in ERICA (Brown et al. 2008).

For Pu, differences are limited in most cases. However, for five of the organisms the difference is larger than one order of magnitude. In all these cases, updated data from WTD have been used to replace data from ICRP (2009) or ERICA (Brown et al. 2008). The updated CR values for marine benthic and pelagic fish increase, whereas the values for limnic vascular plants and terrestrial birds decrease. The updated CR value for Pu for freshwater birds is three orders of magnitude larger than the value used in SR-PSU (originating from ERICA, Brown et al. 2008).

Table E-1. Data sources for CR values and overlap of site and literature data. Green colour indicates that site-specific data are used, blue that literature data are used. Other colours indicate that neither site nor literature data are available for the specified organism-element combination. In these cases, values from an element analogue (yellow, EA), a parameter analogue (PA, orange) or a combination of the two (grey, EP) is used. If the selected analogue data is based on site data, this is marked as EA-SD, PA-SD or EP-SD, if the selected analogue data are based on literature data this is marked with EA-LD, PA-LD or EP-LD. For parameters that are based on primary site or literature data (i.e. blue or green) overlaps between different data sources are indicated by letters: SO = site data with > 50 % overlap with literature, SV = site data with < 50 % overlap with literature, SN = site data, no literature data available, SM = site data with large variation LO = literature data with overlap with other literature data, LV = literature data with no overlap with other literature data, LN = literature data, no other literature data available. Parameters with white colour (OV) indicates that values are selected by expert judgment rather than an automated process.

	Parameter	Organism	Ac	Ag	Am	Ba	Ca	Cd	Cl	Cm	Co	Cs	Eu	Ho	I	Mo	Nb	Ni	Np	Pa	Pb	Pd	Po	Pu	Ra	Se	Sm	Sn	Sr	Tc	Th	U	Zr
Freshwater	cR_Lake_amph_NHB	Amphibian	EP_SD	EP_SD	EP_SD	PA_SD	LO	PA_LD	PA_SD	EP_SD	PA_SD	PA_SD	EP_SD	PA_SD	PA_SD	PA_SD	PA_SD	PA_SD	EP_SD	EP_SD	LV	EP_SD	PA_LD	PA_LD	EP_SD	PA_SD	PA_SD	EP_SD	PA_SD	PA_LD	PA_LD	PA_SD	PA_SD
	cR_Lake_Fish_NHB	Benthic fish	EA_SD	EA_SD	EA_SD	SO	SO	LO	SV	EA_SD	SO	SV	EA_SD	SV	SO	SO	SV	SO	EA_SD	EA_SD	LO	EA_SD	LO	LO	EA_SD	SO	SV	EA_SD	SO	LO	LO	SM	SV
	cR_Lake_bird_NHB	Bird	EP_SD	EP_SD	EP_SD	LV	LO	LO	PA_SD	EP_SD	LO	LO	LO	PA_SD	LO	LO	LO	PA_SD	EP_SD	EP_SD	LV	EP_SD	PA_LD	LO	LV	LV	PA_SD	EP_SD	LO	PA_LD	PA_LD	LO	LO
	cR_Lake_bivalve_NHB	Mollusc – bivalve	EA_SD	SV	EA_SD	SV	SV	SV	SV	EA_SD	SV	SV	SV	SV	SV	SV	SO	SV	EA_SD	EA_SD	SO	EA_SD	LO	LO	EA_SD	SO	SV	EA_SD	SO	PA_LD	SV	SM	SO
	cR_Lake_crust_NHB	Crustacean	EP_SD	PA_SD	EP_SD	LO	LO	LO	PA_SD	EP_SD	LO	LO	PA_SD	PA_SD	PA_SD	LX	PA_SD	PA_SD	EP_SD	EP_SD	LV	EP_SD	LO	LO	LO	LO	PA_SD	LX	LO	PA_LD	PA_SD	LO	LO
	cR_Lake_gastr_NHB	Mollusc – gastropod	EP_SD	PA_SD	EP_SD	PA_SD	PA_SD	PA_SD	PA_SD	EP_SD	PA_SD	PA_SD	PA_SD	PA_SD	PA_SD	PA_SD	PA_SD	PA_SD	EP_SD	EP_SD	PA_SD	EP_SD	PA_LD	PA_LD	EP_SD	PA_SD	PA_SD	EP_SD	PA_SD	PA_LD	PA_SD	PA_SD	PA_SD
	cR_Lake_ins_larvae_NHB	Insect larvae	EP_SD	PA_SD	LO	PA_SD	LO	PA_SD	PA_SD	LV	PA_SD	LO	PA_SD	PA_SD	PA_SD	PA_SD	PA_SD	PA_SD	EP_SD	EP_SD	PA_SD	EP_SD	PA_LD	LV	EP_SD	LO	PA_SD	EP_SD	PA_SD	PA_LD	PA_SD	PA_SD	PA_SD
	cR_Lake_mammal_NHB	Mammal	EP_SD	EP_SD	EP_SD	LX	PA_SD	PA_LD	PA_SD	EP_SD	PA_SD	PA_SD	EP_SD	PA_SD	PA_SD	PA_SD	PA_SD	PA_SD	EP_SD	EP_SD	PA_LD	EP_SD	PA_LD	PA_LD	LO	PA_SD	PA_SD	EP_SD	PA_SD	PA_LD	PA_LD	PA_SD	PA_SD
	cR_Lake_Fish_NHB	Pelagic fish	EA_SD	EA_SD	EA_SD	SO	SO	LO	SV	EA_SD	SO	SV	EA_SD	SV	SO	SO	SV	SO	EA_SD	EA_SD	LO	EA_SD	LO	LO	EA_SD	SO	SV	EA_SD	SO	LO	LO	SM	SV
	cR_Lake_pp_plank_NHB	Phyto-plankton	EP_SD	EP_SD	EP_SD	PA_SD	LO	LO	PA_SD	EP_SD	LO	LO	PA_SD	PA_SD	PA_SD	PA_SD	PA_SD	PA_SD	EP_SD	EP_SD	PA_SD	EP_SD	LX	PA_LD	LO	PA_SD	PA_SD	EP_SD	LO	PA_LD	LO	LO	LO
	cR_Lake_pp_vasc_NHB	Vascular plant	EP_SD	EP_SD	EP_SD	PA_SD	PA_SD	PA_SD	PA_SD	EP_SD	PA_SD	PA_SD	PA_SD	PA_SD	PA_SD	PA_SD	PA_SD	PA_SD	EP_SD	EP_SD	PA_SD	EP_SD	LO	LO	EP_SD	PA_SD	PA_SD	EP_SD	PA_SD	PA_LD	PA_SD	PA_SD	PA_SD
	cR_Lake_reptile_NHB	Reptile	EA_LD	EP_SD	LX	LX	LX	LX	PA_SD	LX	LX	LX	EA_LD	EA_LD	PA_SD	LX	PA_SD	LX	PA_LD	EA_LD	LX	EP_SD	LX	LX	LX	LX	EA_LD	PA_LD	LX	PA_LD	LX	LX	LX
	cR_Lake_zoopl_NHB	Zoo-plankton	EP_SD	PA_SD	EP_SD	PA_SD	PA_SD	PA_SD	PA_SD	EP_SD	PA_SD	LO	PA_SD	PA_SD	PA_SD	PA_SD	PA_SD	PA_SD	EP_SD	EP_SD	PA_SD	EP_SD	PA_LD	LO	EP_SD	LO	PA_SD	EP_SD	LO	PA_LD	PA_SD	PA_SD	PA_SD

Table E-1. Continued.

	Parameter	Organism	Ac	Ag	Am	Ba	Ca	Cd	Cl	Cm	Co	Cs	Eu	Ho	I	Mo	Nb	Ni	Np	Pa	Pb	Pd	Po	Pu	Ra	Se	Sm	Sn	Sr	Tc	Th	U	Zr
Marine	cR_Sea_Fish_NHB	Benthic fish	EA_SD	LO	EA_SD	SO	SM	SV	SX	EA_SD	SO	SO	EA_SD	EA_SD	SX	SX	SX	SV	EA_SD	EA_SD	SM	EA_SD	LO	LO	EA_SD	SV	SX	SX	SV	EA_SD	SX	SV	SV
	cR_Sea_bent_moll_NHB	Mollusc – bivalve	EA_SD	LO	EA_SD	SV	SV	SO	SX	EA_SD	SO	SV	SO	SX	SV	SX	SV	SO	EA_SD	EA_SD	SM	EA_SD	LO	LO	LO	SO	SX	SX	EA_SD	LO	SV	SV	SO
	cR_Sea_bird_NHB	Bird	EP_SD	PA_LD	EP_SD	PA_SD	PA_SD	PA_SD	PA_SD	EP_SD	PA_SD	LO	EP_SD	EP_SD	PA_SD	PA_SD	PA_SD	PA_SD	EP_SD	EP_SD	PA_SD	EP_SD	PA_LD	LO	EP_SD	PA_SD	PA_SD	PA_SD	PA_SD	EP_SD	PA_SD	PA_SD	PA_SD
	cR_Sea_crust_NHB	Crustacean	EA_SD	PA_LD	EA_SD	SV	SV	SV	LV	EA_SD	SV	SV	SV	SX	PA_SD	SX	LV	SV	EA_SD	EA_SD	SM	EA_SD	LO	LO	LO	SX	SX	PA_SD	EA_SD	LV	SV	PA_SD	SX
	cR_Sea_mammal_NHB	Mammal	EP_SD	LO	EP_SD	PA_SD	PA_SD	LO	PA_SD	EP_SD	LO	LO	EP_SD	EP_SD	LV	PA_SD	PA_SD	PA_SD	EP_SD	EP_SD	LO	EP_SD	LO	LO	LX	LO	PA_SD	PA_SD	LO	LX	PA_SD	PA_SD	PA_SD
	cR_Sea_Fish_NHB	Pelagic fish	EA_SD	LO	EA_SD	SO	SM	SV	SX	EA_SD	SO	SO	EA_SD	EA_SD	SX	SX	SX	SV	EA_SD	EA_SD	SM	EA_SD	LO	LO	EA_SD	SV	SX	SX	SV	EA_SD	SX	SV	SV
	cR_Sea_polych_NHB	Polychaete worm	EP_SD	LV	EP_SD	PA_SD	PA_SD	LV	PA_SD	EP_SD	LO	LO	PA_SD	PA_SD	PA_SD	PA_SD	PA_SD	LV	EP_SD	EP_SD	LO	EA_LD	LO	LO	PA_LD	LV	PA_SD	PA_SD	EA_LD	PA_LD	PA_SD	PA_SD	PA_SD
	cR_Sea_pp_macro_NHB	Macroalgae	EP_SD	LO	EP_SD	PA_SD	PA_SD	PA_SD	PA_SD	EP_SD	PA_SD	PA_SD	PA_SD	PA_SD	PA_SD	PA_SD	PA_SD	PA_SD	EP_SD	EP_SD	PA_SD	EP_SD	LO	LO	EP_SD	PA_SD	PA_SD	PA_SD	PA_SD	LO	PA_SD	PA_SD	PA_SD
	cR_Sea_pp_plank_NHB	Phyto-plankton	EP_SD	LV	LV	PA_SD	PA_SD	LO	PA_SD	LV	LO	LO	PA_SD	PA_SD	LV	PA_SD	PA_SD	LO	LO	EP_SD	LV	EP_SD	LV	LO	LO	LO	LO	PA_SD	PA_SD	PA_SD	LV	LV	LO	LO
	cR_Sea_pp_vasc_NHB	Vascular plant	EP_SD	PA_LD	EP_SD	PA_SD	PA_SD	PA_SD	PA_SD	EP_SD	PA_SD	PA_SD	PA_SD	PA_SD	PA_SD	PA_SD	PA_SD	PA_SD	EP_SD	EP_SD	PA_SD	EP_SD	PA_LD	PA_LD	EP_SD	PA_SD	PA_SD	PA_SD	PA_SD	PA_LD	PA_SD	PA_SD	PA_SD
	cR_Sea_zoopl_NHB	Zoo-plankton	EA_SD	LO	EA_SD	SV	SV	SO	PA_SD	EA_SD	OV	OV	SX	SX	SX	SX	EA_SD	SX	LV	EA_SD	SM	EA_SD	LO	LO	LO	SV	SX	EA_SD	LO	EP_SD	OV	LO	SV
Terrestrail	cR_Ter_amph_NHB	Amphibian	EP_SD	EP_SD	EP_SD	EA_LD	EA_LD	LO	PA_SD	EP_SD	PA_SD	LO	EP_SD	EP_SD	PA_SD	PA_SD	PA_SD	PA_SD	EP_SD	EP_SD	LO	EP_SD	PA_LD	PA_LD	PA_SD	PA_SD	PA_SD	PA_SD	LO	LO	PA_SD	PA_SD	PA_SD
	cR_Ter_bird_NHB	Bird	EP_SD	EP_SD	EP_SD	EP_SD	EP_SD	PA_SD	PA_SD	EP_SD	PA_SD	LO	EP_SD	EP_SD	PA_SD	PA_SD	PA_SD	PA_SD	EP_SD	EP_SD	LO	EP_SD	PA_LD	LO	LO	PA_SD	PA_SD	PA_SD	LO	LV	LO	LV	PA_SD
	cR_Ter_detr_inv_NHB	Arthropod – detritivorous	EA_LD	LO	LO	LO	LO	LO	LO	EA_LD	LO	LO	LO	EA_LD	LO	LO	LO	LO	EP_LD	EA_LD	LO	EA_LD	LV	LO	EA_LD	LO	EA_LD	LO	LO	EA_LD	LO	LO	LO
	cR_Ter_fl_ins_NHB	Flying insects	EA_LD	LV	EA_LD	LO	LO	LV	PA_LD	EA_LD	LO	LO	LO	EA_LD	LX	LO	LV	LO	EA_LD	EA_LD	LV	LV	PA_LD	LO	LX	LO	EA_LD	LO	LO	EA_LD	LV	LV	LO
	cR_Ter_gastr_NHB	Mollusc – gastropod	EA_LD	PA_LD	LO	EA_LD	EA_LD	LO	LO	EA_LD	PA_LD	LO	EA_LD	EA_LD	LO	EP_LD	PA_LD	LO	EA_LD	EA_LD	LO	EA_LD	PA_LD	LO	LO	LO	EA_LD	EP_LD	LO	EP_LD	PA_LD	PA_LD	PA_LD
	cR_Ter_mammal_NHB	Mammal – large Mammal	EA_SD	EA_SD	EA_SD	SO	SV	SO	SX	EA_SD	SO	SM	EA_SD	EA_SD	SX	SV	SV	SV	EA_SD	EA_SD	SO	EA_SD	LO	LO	SO	SO	SX	SX	SV	PA_LD	SV	SV	SV
	cR_Ter_mammal_NHB	Mammal – small-burrowing	EA_SD	EA_SD	EA_SD	SO	SV	SO	SX	EA_SD	SO	SM	EA_SD	EA_SD	SX	SV	SV	SV	EA_SD	EA_SD	SO	EA_SD	LO	LO	SO	SO	SX	SX	SV	PA_LD	SV	SV	SV
	cR_Ter_pp_NHB	Grasses & Herbs	EA_SD	PA_SD	EA_SD	SO	SV	SO	SO	EA_SD	SO	SM	SO	SV	SO	SO	SO	SO	EA_SD	EA_SD	SV	EA_SD	EP_SD	EA_SD	SV	PA_SD	SO	SO	SO	EP_SD	SV	SV	SO
	cR_Ter_pp_NHB	Lichen & bryophytes	EA_SD	PA_	EA_SD	SO	SV	SO	SO	EA_SD	SO	SM	SO	SV	SO	SO	SO	SO	EA_SD	EA_SD	SV	EA_SD	EP_	EA_	SV	PA_	SO	SO	SO	EP_SD	SV	SV	SO
	cR_Ter_pp_NHB	Shrub	EA_SD	PA_SD	EA_SD	SO	SV	SO	SO	EA_SD	SO	SM	SO	SV	SO	SO	SO	SO	EA_SD	EA_SD	SV	EA_SD	EP_SD	EA_SD	SV	PA_SD	SO	SO	SO	EP_SD	SV	SV	SO
	cR_Ter_pp_NHB	Tree	EA_SD	PA_SD	EA_SD	SO	SV	SO	SO	EA_SD	SO	SM	SO	SV	SO	SO	SO	SO	EA_SD	EA_SD	SV	EA_SD	EP_SD	EA_SD	SV	PA_SD	SO	SO	SO	EP_SD	SV	SV	SO
	cR_Ter_rept_NHB	Reptile	EA_LD	EP_SD	LX	PA_SD	EA_LD	PA_SD	PA_SD	EA_LD	PA_SD	LX	EA_LD	EA_LD	PA_SD	PA_SD	PA_SD	LX	EA_LD	EA_LD	LX	EA_LD	LX	LX	PA_SD	PA_SD	EA_LD	PA_SD	LX	PA_LD	LX	LX	PA_SD
	cR_Ter_soil_inv_NHB	Annelid	EA_LD	LO	LO	EA_LD	LO	LO	LO	EP_LD	LO	LO	LO	EA_LD	LO	LO	LO	LO	EA_LD	EA_LD	LO	LO	PA_LD	LO	LX	LO	LO	LO	LO	LX	LO	LO	LO

For Tc the new value for marine zooplankton is more than one order of magnitude lower than the value in SR-PSU and for marine mammals and terrestrial bryophytes and lichen the differences are more than two orders of magnitude higher and lower, respectively. The change in CR value for marine mammals is due to updated values in the database. For terrestrial bryophytes and lichen, ERICA data were used in SR-PSU. The CR values presently listed in ERICA (version 1.2) reflect the highest reported values for plants. As there are site data for this organism with respect to Mo, the use of these as an element analogue is considered to be a better choice in the PSAR.

Organisms with many noticeable changes include freshwater zooplankton, terrestrial detritivorous invertebrates, terrestrial gastropods, terrestrial reptiles and flying insects. Additionally, freshwater reptile is added as data for this organism are now available in WTD. For freshwater zooplankton, no site data are available and literature data are available only for a few elements. Therefore, data for marine zooplankton were used in SR-PSU. In ERICA (version 1.2) it is recommended that data from a different ecosystem should not be used as analogues. Thus, in the PSAR, site data from freshwater bivalve are used as a parameter analogue in all cases where literature data on freshwater zooplankton are missing. For Nb and Ra, the new values are two orders of magnitude higher and for Zr two orders of magnitude lower than in SR-PSU, but for the other elements the changes are limited to one order of magnitude or less.

For terrestrial detritivorous invertebrates, new literature data have been compiled for many elements. These data are used in the PSAR to replace the previous values that were taken from ERICA. The differences between the PSAR and SR-PSU are small in general, except for Nb; for this element the updated value is approximately two orders of magnitude higher in the PSAR.

For flying insect, values for bees reported by WTD (ICRP 2015) are used in the PSAR. These data were not available in earlier versions of the WTD, and consequently the CR values for most elements are updated. For Ac, Am, Ho, Np, Pa and Sm, the values are two orders of magnitude lower than in SR-PSU, and for Sn the value is two orders of magnitude higher. For Cd and Cm, the values are closer to three orders of magnitude lower.

WTD reports data on terrestrial molluscs that are used for terrestrial gastropods. This resulted in updated values for almost all elements. The differences are small for most elements, but two orders of magnitude higher in the PSAR for Eu and Nb.

For soil invertebrates, WTD reported new data on annelids that were used when possible. This resulted in updated values for almost all elements. The differences are around one order of magnitude for all elements, except for Nb, for which the difference is two orders of magnitude.

For terrestrial reptiles, CR values in the PSAR are frequently three orders of magnitude higher than in SR-PSU. This is due to a shift towards more representative data. In SR-PSU, site-specific mammalian data for La were used for Ac, Am, Cm, Eu, Ho, Np, Pa and Sm. In the PSAR, data for terrestrial reptiles are used instead, with Am as an analogue for the other elements.

For freshwater birds, CR values in the PSAR are frequently two orders of magnitude higher than in SR-PSU. This is because new data on birds are used to replace previous values that were based on freshwater fish. The update affects CR values for Ba, Eu, Mo, Nb, Pu, Ra, Se and U.

Table E-2. NHB CR values for marine, freshwater and terrestrial organisms used in the PSAR. Values on a white background have not changed since SR-PSU, while fully saturated red and blue backgrounds correspond to an increase or decrease, respectively, of at least one order of magnitude since SR-PSU. Paler colours represent smaller corresponding changes. Freshwater Reptile is a new organism in the PSAR (indicated by grey colour).

Eco.	Organism		Ac	Ag	Am	Ba	Ca	Cd	Cl	Cm
Marine (m^3 $kgfw^{-1}$)	Bird	GM	3.0×10^{-3}	8.1×10^{0}	3.0×10^{-3}	9.7×10^{-3}	2.0×10^{-2}	4.7×10^{-1}	1.4×10^{-4}	3.0×10^{-3}
		GSD	5	5	5	5	6.2	5	5	5
	Benthic fish	GM	3.0×10^{-3}	8.1×10^{0}	3.0×10^{-3}	9.7×10^{-3}	2.0×10^{-2}	4.7×10^{-1}	1.4×10^{-4}	3.0×10^{-3}
		GSD	5	3	5	3.4	6.2	3	3	5
	Mollusc – bivalve	GM	3.4×10^{0}	1.6×10^{1}	3.4×10^{0}	1.9×10^{-1}	1.8×10^{0}	4.2×10^{1}	3.1×10^{-4}	3.4×10^{0}
		GSD	3	3.6	3	3	3	3.3	4.1	3
	Crustacean	GM	8.2×10^{0}	1.6×10^{1}	8.2×10^{0}	1.2×10^{0}	3.8×10^{0}	3.3×10^{2}	5.6×10^{-5}	8.2×10^{0}
		GSD	5	5	5	5	5	5	5	5
	Macroalgae	GM	6.4×10^{-1}	2.1×10^{0}	6.4×10^{-1}	6.1×10^{-1}	2.9×10^{-2}	6.0×10^{0}	1.7×10^{-3}	6.4×10^{-1}
		GSD	7.4	3	7.4	3.8	3	3.3	3	7.4
	Mammal	GM	3.0×10^{-3}	1.6×10^{1}	3.0×10^{-3}	9.7×10^{-3}	2.0×10^{-2}	3.2×10^{0}	1.4×10^{-4}	3.0×10^{-3}
		GSD	5	3	5	5	6.2	3	5	5
	Pelagic fish	GM	3.0×10^{-3}	8.1×10^{0}	3.0×10^{-3}	9.7×10^{-3}	2.0×10^{-2}	4.7×10^{-1}	1.4×10^{-4}	3.0×10^{-3}
		GSD	5	3	5	3.4	6.2	3	3	5
	Phytoplankton	GM	6.4×10^{-1}	4.4×10^{1}	1.5×10^{2}	6.1×10^{-1}	2.9×10^{-2}	4.7×10^{-1}	1.7×10^{-3}	2.1×10^{2}
		GSD	7.4	3	3	5	5	3	5	3
	Polychaete worm	GM	3.4×10^{0}	2.7×10^{1}	3.4×10^{0}	1.9×10^{-1}	1.8×10^{0}	1.5×10^{0}	3.1×10^{-4}	3.4×10^{0}
		GSD	5	5	5	5	5	5	5	5
	Vascular plant	GM	6.4×10^{-1}	2.1×10^{0}	6.4×10^{-1}	6.1×10^{-1}	2.9×10^{-2}	6.0×10^{0}	1.7×10^{-3}	6.4×10^{-1}
		GSD	7.4	3	7.4	3.8	3	3.3	3	7.4
	Zooplankton	GM	3.3×10^{1}	3.2×10^{0}	3.3×10^{1}	7.2×10^{-1}	2.8×10^{-1}	5.8×10^{1}	1.4×10^{-4}	3.3×10^{1}
		GSD	5	5	5	5	5	5	5	5
Freshwater (m^3 $kgfw^{-1}$)	Amphibian	GM	9.9×10^{-4}	2.7×10^{-1}	9.9×10^{-4}	2.5×10^{-2}	8.7×10^{-1}	3.3×10^{-1}	2.4×10^{-2}	9.9×10^{-4}
		GSD	5	5	5	5	3	6.8	5	5
	Benthic fish	GM	9.9×10^{-4}	2.7×10^{-1}	9.9×10^{-4}	2.5×10^{-2}	7.1×10^{-1}	3.3×10^{-1}	2.4×10^{-2}	9.9×10^{-4}
		GSD	3	3	3	3	3	6.8	3.2	3
	Bird	GM	9.9×10^{-4}	2.7×10^{-1}	9.9×10^{-4}	3.4×10^{0}	5.5×10^{-1}	2.4×10^{-1}	2.4×10^{-2}	9.9×10^{-4}
		GSD	5	5	5	3	3	3	5	5
	Mollusc – bivalve	GM	3.0×10^{0}	2.7×10^{0}	3.0×10^{0}	4.5×10^{0}	5.1×10^{-1}	7.9×10^{1}	5.4×10^{-2}	3.0×10^{0}
		GSD	3	5	3	3	3	3	4	3
	Crustacean	GM	3.0×10^{0}	2.7×10^{0}	3.0×10^{0}	1.1×10^{0}	6.4×10^{-1}	2.3×10^{1}	5.4×10^{-2}	3.0×10^{0}
		GSD	5	5	5	3	3	3	5	5
	Mollusc – gastropod	GM	3.0×10^{0}	2.7×10^{0}	3.0×10^{0}	4.5×10^{0}	5.1×10^{-1}	7.9×10^{1}	5.4×10^{-2}	3.0×10^{0}
		GSD	5	5	5	5	5	5	5	5
	Insect larvae	GM	3.0×10^{0}	2.7×10^{0}	1.8×10^{0}	4.5×10^{0}	3.0×10^{-2}	7.9×10^{1}	5.4×10^{-2}	2.5×10^{-1}
		GSD	5	5	5	5	3	5	5	5
	Mammal	GM	9.9×10^{-4}	2.7×10^{-1}	9.9×10^{-4}	9.3×10^{-2}	7.1×10^{-1}	2.4×10^{-1}	2.4×10^{-2}	9.9×10^{-4}
		GSD	5	5	5	5	5	5	5	5
	Microphytobenthos	GM	1.4×10^{0}	1.4×10^{0}	1.4×10^{0}	1.3×10^{0}	7.1×10^{-1}	2.1×10^{0}	2.2×10^{-2}	1.4×10^{0}
		GSD	6.9	4	6.9	4	4	4	7.1	6.9
	Pelagic fish	GM	9.9×10^{-4}	2.7×10^{-1}	9.9×10^{-4}	2.5×10^{-2}	7.1×10^{-1}	3.3×10^{-1}	2.4×10^{-2}	9.9×10^{-4}
		GSD	3	3	3	3	3	6.8	3.2	3
	Phytoplankton	GM	1.4×10^{0}	1.4×10^{0}	1.4×10^{0}	1.3×10^{0}	1.1×10^{-1}	1.3×10^{0}	2.2×10^{-2}	1.4×10^{0}
		GSD	7	7	7	7	4	4	7.1	7
	Reptile	GM	3.2×10^{0}	2.7×10^{-1}	3.2×10^{0}	1.4×10^{-1}	5.0×10^{-1}	1.3×10^{0}	2.4×10^{-2}	7.7×10^{-2}
		GSD	7	5	7	7	7	4	5	7
	Vascular plant	GM	1.4×10^{0}	1.4×10^{0}	1.4×10^{0}	1.3×10^{0}	7.1×10^{-1}	2.1×10^{0}	2.2×10^{-2}	1.4×10^{0}
		GSD	6.9	4	6.9	4	4	4	7.1	6.9
	Zooplankton	GM	3.0×10^{0}	2.7×10^{0}	3.0×10^{0}	4.5×10^{0}	5.1×10^{-1}	7.9×10^{1}	5.4×10^{-2}	3.0×10^{0}
		GSD	5	5	5	5	5	5	5	5

Table E-2. Continued.

Eco.	Organism		Ac	Ag	Am	Ba	Ca	Cd	Cl	Cm
Terrestrial (kgdw kgfw^{-1})	Amphibian	GM	5.3×10^{-5}	9.6×10^{-2}	5.3×10^{-5}	8.9×10^{-1}	8.9×10^{-1}	1.3×10^{-2}	1.8×10^{1}	5.3×10^{-5}
		GSD	7	7	7	4	4	4	7	7
	Bird	GM	5.3×10^{-5}	9.6×10^{-2}	5.3×10^{-5}	3.4×10^{-3}	3.4×10^{-3}	3.4×10^{-2}	1.8×10^{1}	5.3×10^{-5}
		GSD	7	7	7	7	7	7	7	7
	Arthropod – detritivorous	GM	9.0×10^{-2}	3.8×10^{-1}	9.0×10^{-2}	1.2×10^{-2}	1.8×10^{-1}	3.3×10^{0}	1.7×10^{-1}	9.0×10^{-2}
		GSD	4	7	4	7	7	4	4	4
	Flying insects	GM	4.3×10^{-4}	2.2×10^{-2}	4.3×10^{-4}	8.1×10^{-3}	8.3×10^{-2}	2.7×10^{-2}	1.7×10^{-1}	4.3×10^{-4}
		GSD	4	7	4	7	7	4	7	7
	Mollusc – gastropod	GM	1.0×10^{-1}	3.8×10^{-1}	1.0×10^{-1}	3.4×10^{-2}	8.7×10^{-2}	5.4×10^{-1}	1.4×10^{-1}	1.0×10^{-1}
		GSD	4	7	4	4	4	4	4	4
	Grasses & Herbs	GM	3.9×10^{-4}	4.6×10^{-3}	3.9×10^{-4}	1.1×10^{-1}	1.9×10^{-1}	7.5×10^{-2}	4.9×10^{1}	3.9×10^{-4}
		GSD	7	7	7	7	7	7	7	7
	Lichen & Bryophytes	GM	1.4×10^{-2}	3.1×10^{-1}	1.4×10^{-2}	2.4×10^{-1}	2.7×10^{-1}	2.1×10^{-1}	1.1×10^{1}	1.4×10^{-2}
		GSD	4.4	4	4.4	4	4	4	7	4.4
	Mammal – large	GM	5.3×10^{-5}	9.6×10^{-2}	5.3×10^{-5}	1.6×10^{-3}	1.9×10^{-2}	3.4×10^{-2}	1.8×10^{1}	5.3×10^{-5}
		GSD	7	7	7	7	7	7	7	7
	Mammal – small-burrowing	GM	5.3×10^{-5}	9.6×10^{-2}	5.3×10^{-5}	1.6×10^{-3}	1.9×10^{-2}	3.4×10^{-2}	1.8×10^{1}	5.3×10^{-5}
		GSD	7	7	7	7	7	7	7	7
	Reptile	GM	5.5×10^{-2}	9.6×10^{-2}	5.5×10^{-2}	1.6×10^{-3}	2.2×10^{-1}	3.4×10^{-2}	1.8×10^{1}	5.5×10^{-2}
		GSD	7	7	7	7	7	7	7	7
	Shrub	GM	3.9×10^{-4}	4.6×10^{-3}	3.9×10^{-4}	1.1×10^{-1}	1.9×10^{-1}	7.5×10^{-2}	4.9×10^{1}	3.9×10^{-4}
		GSD	7	7	7	7	7	7	7	7
	Annelid	GM	9.0×10^{-2}	3.8×10^{-1}	9.0×10^{-2}	4.2×10^{-2}	1.8×10^{-1}	3.3×10^{0}	1.7×10^{-1}	9.0×10^{-2}
		GSD	4	7	4	7	7	4	4	7
	Tree	GM	3.9×10^{-4}	4.6×10^{-3}	3.9×10^{-4}	1.1×10^{-1}	1.9×10^{-1}	7.5×10^{-2}	4.9×10^{1}	3.9×10^{-4}
		GSD	7	7	7	7	7	7	7	7

Table E-2. Continued. NHB CR values for marine, freshwater and terrestrial organisms used in the PSAR. Values on a white background have not changed since SR-PSU, while fully saturated red and blue backgrounds correspond to an increase or decrease, respectively, of at least one order of magnitude since SR-PSU. Paler colours represent smaller corresponding changes. Freshwater Reptile is a new organism in the PSAR (indicated by grey colour).

Eco.	Organism		Co	Cs	Eu	Ho	I	Mo	Nb	Ni
Marine (m^3 kgfw^{-1})	Bird	GM	1.3×10^{-1}	2.9×10^{-1}	3.0×10^{-3}	3.0×10^{-3}	2.1×10^{-2}	2.5×10^{-3}	1.6×10^{-2}	2.1×10^{-2}
		GSD	5	3	5	5	5	5	5	5
	Benthic fish	GM	1.3×10^{-1}	2.4×10^{-1}	3.0×10^{-3}	3.0×10^{-3}	2.1×10^{-2}	2.5×10^{-3}	1.6×10^{-2}	2.1×10^{-2}
		GSD	3.7	3	5	5	3	3	5	3
	Mollusc – bivalve	GM	4.8×10^{0}	1.2×10^{-1}	7.4×10^{-1}	3.8×10^{-1}	6.8×10^{-2}	8.1×10^{-2}	2.7×10^{-1}	4.8×10^{-1}
		GSD	3	3	3	3	3	3	5	3
	Crustacean	GM	5.8×10^{1}	5.9×10^{-1}	6.6×10^{-1}	1.3×10^{0}	6.8×10^{-2}	1.9×10^{-1}	1.0×10^{-1}	5.7×10^{0}
		GSD	5	5	5	5	5	5	5	5
	Macroalgae	GM	6.4×10^{0}	4.9×10^{-1}	3.0×10^{-1}	2.9×10^{-1}	6.3×10^{-1}	4.7×10^{-2}	1.5×10^{0}	1.3×10^{0}
		GSD	6.1	4.8	6	6.7	3	3.1	5	3.1
	Mammal	GM	1.7×10^{-1}	8.4×10^{-2}	3.0×10^{-3}	3.0×10^{-3}	6.4×10^{-4}	2.5×10^{-3}	1.6×10^{-2}	2.1×10^{-2}
		GSD	4.4	3.9	5	5	3	5	5	5
	Pelagic fish	GM	1.3×10^{-1}	2.4×10^{-1}	3.0×10^{-3}	3.0×10^{-3}	2.1×10^{-2}	2.5×10^{-3}	1.6×10^{-2}	2.1×10^{-2}
		GSD	3.7	3	5	5	3	3	5	3
	Phytoplankton	GM	1.8×10^{0}	3.6×10^{-3}	3.0×10^{-1}	2.9×10^{-1}	9.5×10^{-1}	4.7×10^{-2}	1.5×10^{0}	3.5×10^{-1}
		GSD	3	3.7	6	6.7	5	5	5	5
	Polychaete worm	GM	5.3×10^{0}	1.3×10^{-1}	7.4×10^{-1}	3.8×10^{-1}	6.8×10^{-2}	8.1×10^{-2}	2.7×10^{-1}	4.2×10^{0}
		GSD	5	3	5	5	5	5	5	5
	Vascular plant	GM	6.4×10^{0}	4.9×10^{-1}	3.0×10^{-1}	2.9×10^{-1}	6.3×10^{-1}	4.7×10^{-2}	1.5×10^{0}	1.3×10^{0}
		GSD	6.1	4.8	6	6.7	3	3.1	5	3.1
	Zooplankton	GM	2.9×10^{0}	6.7×10^{-2}	6.5×10^{0}	5.6×10^{0}	1.2×10^{0}	3.8×10^{-1}	2.0×10^{1}	3.0×10^{0}
		GSD	2.8	3.2	5	5	5	5	5	5

Table E-2. Continued.

Eco.	Organism		Co	Cs	Eu	Ho	I	Mo	Nb	Ni
Freshwater (m^3 $kgfw^{-1}$)	Amphibian	GM	2.7×10^{-2}	2.1×10^{0}	9.9×10^{-4}	1.3×10^{-2}	4.9×10^{-2}	9.5×10^{-3}	8.8×10^{-3}	8.9×10^{-3}
		GSD	5	5	5	5	5	5	5	5
	Benthic fish	GM	2.7×10^{-2}	2.1×10^{0}	9.9×10^{-4}	1.3×10^{-2}	4.9×10^{-2}	9.5×10^{-3}	8.8×10^{-3}	8.9×10^{-3}
		GSD	3	4.9	3	5	3	3	3	5
	Bird	GM	7.0×10^{-1}	9.2×10^{-1}	5.7×10^{0}	1.3×10^{-2}	3.9×10^{-2}	1.4×10^{0}	4.3×10^{0}	8.9×10^{-3}
		GSD	3	3.8	3	5	3	3	3	5
	Mollusc – bivalve	GM	2.6×10^{0}	4.8×10^{-1}	2.5×10^{0}	4.4×10^{-1}	1.5×10^{-1}	2.9×10^{-1}	5.2×10^{-1}	2.5×10^{-1}
		GSD	3	3	3	3	3	3	3	3
	Crustacean	GM	1.7×10^{0}	1.5×10^{0}	2.5×10^{0}	4.4×10^{-1}	1.5×10^{-1}	8.1×10^{-2}	5.2×10^{-1}	2.5×10^{-1}
		GSD	3	3	5	5	5	3	5	5
	Mollusc – gastropod	GM	2.6×10^{0}	4.8×10^{-1}	2.5×10^{0}	4.4×10^{-1}	1.5×10^{-1}	2.9×10^{-1}	5.2×10^{-1}	2.5×10^{-1}
		GSD	5	5	5	5	5	5	5	5
	Insect larvae	GM	2.6×10^{0}	1.4×10^{0}	2.5×10^{0}	4.4×10^{-1}	1.5×10^{-1}	2.9×10^{-1}	5.2×10^{-1}	2.5×10^{-1}
		GSD	5	3	5	5	5	5	5	5
	Mammal	GM	2.7×10^{-2}	2.1×10^{0}	9.9×10^{-4}	1.3×10^{-2}	4.9×10^{-2}	9.5×10^{-3}	8.8×10^{-3}	8.9×10^{-3}
		GSD	5	5	5	5	5	5	5	5
	Microphytobenthos	GM	1.8×10^{0}	8.7×10^{-1}	1.4×10^{0}	6.3×10^{-1}	3.3×10^{-1}	2.5×10^{-1}	1.1×10^{0}	4.5×10^{-1}
		GSD	4	4	6.1	7.7	4	6	7	4
	Pelagic fish	GM	2.7×10^{-2}	2.1×10^{0}	9.9×10^{-4}	1.3×10^{-2}	4.9×10^{-2}	9.5×10^{-3}	8.8×10^{-3}	8.9×10^{-3}
		GSD	3	4.9	3	5	3	3	3	5
	Phytoplankton	GM	2.5×10^{-1}	6.9×10^{-2}	1.4×10^{0}	6.3×10^{-1}	3.3×10^{-1}	2.5×10^{-1}	1.1×10^{0}	4.5×10^{-1}
		GSD	4	4	7	7.7	7	7	7	7
	Reptile	GM	5.9×10^{-3}	2.0×10^{0}	3.2×10^{0}	3.2×10^{0}	4.9×10^{-2}	8.7×10^{-1}	8.8×10^{-3}	9.5×10^{-1}
		GSD	4	4	7	7	5	7	5	7
	Vascular plant	GM	1.8×10^{0}	8.7×10^{-1}	1.4×10^{0}	6.3×10^{-1}	3.3×10^{-1}	2.5×10^{-1}	1.1×10^{0}	4.5×10^{-1}
		GSD	4	4	6.1	7.7	4	6	7	4
	Zooplankton	GM	2.6×10^{0}	7.3×10^{-2}	2.5×10^{0}	4.4×10^{-1}	1.5×10^{-1}	2.9×10^{-1}	5.2×10^{-1}	2.5×10^{-1}
		GSD	5	3	5	5	5	5	5	5
Terrestrial ($kgdw$ $kgfw^{-1}$)	Amphibian	GM	3.0×10^{-3}	2.2×10^{-1}	5.3×10^{-5}	5.3×10^{-5}	3.3×10^{-2}	1.2×10^{-2}	4.5×10^{-4}	5.5×10^{-3}
		GSD	7	4	7	7	7	7	7	7
	Bird	GM	3.0×10^{-3}	2.1×10^{-1}	5.3×10^{-5}	5.3×10^{-5}	3.3×10^{-2}	1.2×10^{-2}	4.5×10^{-4}	5.5×10^{-3}
		GSD	7	4.1	7	7	7	7	7	7
	Arthropod – detritivorous	GM	1.9×10^{-2}	3.7×10^{-2}	5.7×10^{-3}	9.0×10^{-2}	1.4×10^{-1}	2.3×10^{-1}	1.4×10^{-1}	5.0×10^{-2}
		GSD	7	4	7	4	4	7	7	4
	Flying insects	GM	6.2×10^{-3}	4.2×10^{-3}	4.3×10^{-4}	4.3×10^{-4}	2.8×10^{-1}	1.3×10^{-1}	9.5×10^{-4}	6.4×10^{-3}
		GSD	4	4	7	4	7	7	7	7
	Mollusc – gastropod	GM	1.9×10^{-2}	3.2×10^{-2}	1.0×10^{-1}	1.0×10^{-1}	1.7×10^{-1}	3.5×10^{-1}	1.4×10^{-1}	1.5×10^{-2}
		GSD	7	4	4	4	4	7	7	4
	Grasses & Herbs	GM	5.6×10^{-3}	3.8×10^{-2}	7.6×10^{-4}	7.7×10^{-4}	1.9×10^{-2}	3.3×10^{-2}	9.9×10^{-4}	1.7×10^{-2}
		GSD	7	7.2	7	7	7	7	7	7
	Lichen & Bryophytes	GM	3.2×10^{-2}	9.3×10^{-2}	1.3×10^{-2}	1.3×10^{-2}	6.7×10^{-2}	5.5×10^{-2}	3.5×10^{-2}	4.7×10^{-2}
		GSD	4	5.3	5.2	4.1	7	4	4.8	4
	Mammal – large	GM	3.0×10^{-3}	1.4×10^{-1}	5.3×10^{-5}	5.3×10^{-5}	3.3×10^{-2}	1.2×10^{-2}	4.5×10^{-4}	5.5×10^{-3}
		GSD	7	7.4	7	7	7	7	7	7
	Mammal – small-burrowing	GM	3.0×10^{-3}	1.4×10^{-1}	5.3×10^{-5}	5.3×10^{-5}	3.3×10^{-2}	1.2×10^{-2}	4.5×10^{-4}	5.5×10^{-3}
		GSD	7	7.4	7	7	7	7	7	7
	Reptile	GM	3.0×10^{-3}	2.8×10^{-1}	5.5×10^{-2}	5.5×10^{-2}	3.3×10^{-2}	1.2×10^{-2}	4.5×10^{-4}	3.0×10^{-1}
		GSD	7	7	7	7	7	7	7	7
	Shrub	GM	5.6×10^{-3}	3.8×10^{-2}	7.6×10^{-4}	7.7×10^{-4}	1.9×10^{-2}	3.3×10^{-2}	9.9×10^{-4}	1.7×10^{-2}
		GSD	7	7.2	7	7	7	7	7	7
	Annelid	GM	1.9×10^{-2}	3.7×10^{-2}	5.7×10^{-3}	9.0×10^{-2}	1.4×10^{-1}	2.3×10^{-1}	1.4×10^{-1}	5.0×10^{-2}
		GSD	7	4	7	4	4	7	7	4
	Tree	GM	5.6×10^{-3}	3.8×10^{-2}	7.6×10^{-4}	7.7×10^{-4}	1.9×10^{-2}	3.3×10^{-2}	9.9×10^{-4}	1.7×10^{-2}
		GSD	7	7.2	7	7	7	7	7	7

Table E-2. Continued. NHB CR values for marine, freshwater and terrestrial organisms used in the PSAR. Values on a white background have not changed since SR-PSU, while fully saturated red and blue backgrounds correspond to an increase or decrease, respectively, of at least one order of magnitude since SR-PSU. Paler colours represent smaller corresponding changes. Freshwater Reptile is a new organism in the PSAR (indicated by grey colour).

Eco.	Organism		Np	Pa	Pb	Pd	Po	Pu	Ra	Se
Marine (m^3 $kgfw^{-1}$)	Bird	GM	3.0×10^{-3}	3.0×10^{-3}	1.8×10^{-1}	2.1×10^{-2}	3.2×10^{1}	3.9×10^{-1}	9.7×10^{-3}	3.9×10^{0}
		GSD	5	5	6.3	5	5	3	5	5
	Benthic fish	GM	3.0×10^{-3}	3.0×10^{-3}	1.8×10^{-1}	2.1×10^{-2}	3.2×10^{1}	3.4×10^{-1}	9.7×10^{-3}	3.9×10^{0}
		GSD	5	5	6.3	3	3.9	5.5	3.4	3
	Mollusc – bivalve	GM	3.4×10^{0}	3.4×10^{0}	1.5×10^{0}	4.8×10^{-1}	3.8×10^{1}	7.0×10^{-1}	4.7×10^{-2}	1.1×10^{0}
		GSD	3	3	7	3	3	3	3	3
	Crustacean	GM	8.2×10^{0}	8.2×10^{0}	5.2×10^{0}	5.7×10^{0}	9.8×10^{1}	9.7×10^{-2}	7.3×10^{-2}	1.5×10^{0}
		GSD	5	5	6.8	5	3.5	3	3	5
	Macroalgae	GM	6.4×10^{-1}	6.4×10^{-1}	2.8×10^{0}	1.3×10^{0}	1.7×10^{0}	1.7×10^{0}	6.1×10^{-1}	6.9×10^{-1}
		GSD	7.4	7.4	7.9	3.1	3	3.7	3.8	3
	Mammal	GM	3.0×10^{-3}	3.0×10^{-3}	1.5×10^{1}	2.1×10^{-2}	4.3×10^{1}	9.2×10^{-1}	6.8×10^{-2}	7.9×10^{0}
		GSD	5	5	3	5	3	3	3.8	3
	Pelagic fish	GM	3.0×10^{-3}	3.0×10^{-3}	1.8×10^{-1}	2.1×10^{-2}	3.2×10^{1}	3.4×10^{-1}	9.7×10^{-3}	3.9×10^{0}
		GSD	5	5	6.3	3	3.9	5.5	3.4	3
	Phytoplankton	GM	1.3×10^{-1}	6.4×10^{-1}	2.2×10^{2}	1.3×10^{0}	2.9×10^{1}	8.3×10^{1}	1.2×10^{-1}	9.7×10^{-1}
		GSD	3	7.4	3.4	5	3	3	8.3	5.1
	Polychaete worm	GM	3.4×10^{0}	3.4×10^{0}	4.0×10^{1}	4.2×10^{0}	4.2×10^{2}	8.4×10^{-1}	7.3×10^{-2}	4.5×10^{0}
		GSD	5	5	3	5	3	5	5	5
	Vascular plant	GM	6.4×10^{-1}	6.4×10^{-1}	2.8×10^{0}	1.3×10^{0}	1.7×10^{0}	1.7×10^{0}	6.1×10^{-1}	6.9×10^{-1}
		GSD	7.4	7.4	7.9	3.1	3	3.7	3.8	3
	Zooplankton	GM	1.7×10^{-2}	3.3×10^{1}	1.8×10^{1}	3.0×10^{0}	8.7×10^{1}	3.5×10^{0}	3.6×10^{-2}	2.6×10^{1}
		GSD	5	5	7.5	5	3	3	3.6	5
Freshwater (m^3 $kgfw^{-1}$)	Amphibian	GM	9.9×10^{-4}	9.9×10^{-4}	5.3×10^{-3}	8.9×10^{-3}	5.9×10^{-1}	1.4×10^{-1}	2.5×10^{-2}	9.5×10^{-1}
		GSD	5	5	5	5	5	6.6	5	5
	Benthic fish	GM	9.9×10^{-4}	9.9×10^{-4}	1.0×10^{-1}	8.9×10^{-3}	5.9×10^{-1}	1.4×10^{-1}	2.5×10^{-2}	9.5×10^{-1}
		GSD	3	3	4.9	5	4.8	6.6	3	3
	Bird	GM	9.9×10^{-4}	9.9×10^{-4}	2.4×10^{-1}	8.9×10^{-3}	5.9×10^{-1}	2.1×10^{0}	6.3×10^{0}	6.9×10^{-3}
		GSD	5	5	3	5	5	5	5	3
	Mollusc – bivalve	GM	3.0×10^{0}	3.0×10^{0}	3.5×10^{0}	2.5×10^{-1}	1.1×10^{2}	2.3×10^{0}	4.5×10^{0}	3.0×10^{0}
		GSD	3	3	3	3	3	3.7	3	3
	Crustacean	GM	3.0×10^{0}	3.0×10^{0}	6.0×10^{0}	2.5×10^{-1}	6.3×10^{0}	5.4×10^{-1}	1.4×10^{-1}	4.3×10^{-1}
		GSD	5	5	3	5	3	3	3.1	3
	Mollusc – gastropod	GM	3.0×10^{0}	3.0×10^{0}	3.5×10^{0}	2.5×10^{-1}	1.1×10^{2}	2.3×10^{0}	4.5×10^{0}	3.0×10^{0}
		GSD	5	5	5	5	5	5	5	5
	Insect larvae	GM	3.0×10^{0}	3.0×10^{0}	3.5×10^{0}	2.5×10^{-1}	1.1×10^{2}	2.5×10^{0}	4.5×10^{0}	2.8×10^{0}
		GSD	5	5	5	5	5	3	5	3
	Mammal	GM	9.9×10^{-4}	9.9×10^{-4}	1.0×10^{-1}	8.9×10^{-3}	5.9×10^{-1}	1.4×10^{-1}	1.7×10^{-4}	9.5×10^{-1}
		GSD	5	5	5	5	5	6.6	5	5
	Microphytobenthos	GM	1.4×10^{0}	1.4×10^{0}	2.6×10^{0}	4.5×10^{-1}	1.1×10^{0}	5.7×10^{-1}	1.3×10^{0}	5.0×10^{-1}
		GSD	6.9	6.9	5	4	4	4	4	4
	Pelagic fish	GM	9.9×10^{-4}	9.9×10^{-4}	1.0×10^{-1}	8.9×10^{-3}	5.9×10^{-1}	1.4×10^{-1}	2.5×10^{-2}	9.5×10^{-1}
		GSD	3	3	4.9	5	4.8	6.6	3	3
	Phytoplankton	GM	1.4×10^{0}	1.4×10^{0}	2.6×10^{0}	4.5×10^{-1}	1.3×10^{0}	2.6×10^{1}	2.7×10^{-1}	5.0×10^{-1}
		GSD	7	7	7	7	7	14	4	7
	Reptile	GM	1.0×10^{-2}	3.2×10^{0}	2.5×10^{-1}	8.9×10^{-3}	3.1×10^{0}	5.5×10^{0}	3.5×10^{-1}	1.9×10^{0}
		GSD	7.2	7	4	5	4	4	4	4
	Vascular plant	GM	1.4×10^{0}	1.4×10^{0}	2.6×10^{0}	4.5×10^{-1}	1.1×10^{0}	5.7×10^{-1}	1.3×10^{0}	5.0×10^{-1}
		GSD	6.9	6.9	5	4	4	4	4	4
	Zooplankton	GM	3.0×10^{0}	3.0×10^{0}	3.5×10^{0}	2.5×10^{-1}	1.1×10^{2}	2.4×10^{-1}	4.5×10^{0}	5.7×10^{0}
		GSD	5	5	5	5	5	3.6	5	5

Table E-2. Continued.

Eco.	Organism		Np	Pa	Pb	Pd	Po	Pu	Ra	Se
Terrestrial (kgdw kgfw^{-1})	Amphibian	GM	5.3×10^{-5}	5.3×10^{-5}	2.7×10^{-2}	5.5×10^{-3}	1.4×10^{0}	3.5×10^{-3}	5.9×10^{-2}	7.8×10^{-2}
		GSD	7	7	5.6	7	7	7	7	7
	Bird	GM	5.3×10^{-5}	5.3×10^{-5}	2.0×10^{-2}	5.5×10^{-3}	1.4×10^{0}	9.8×10^{-4}	2.1×10^{-2}	7.8×10^{-2}
		GSD	7	7	4.4	7	7	4	4	7
	Arthropod – detritivorous	GM	1.0×10^{-1}	9.0×10^{-2}	2.6×10^{-1}	5.0×10^{-2}	9.6×10^{-2}	2.1×10^{-2}	1.2×10^{-2}	2.8×10^{0}
		GSD	7	4	4	4	4	4	7	4
	Flying insects	GM	4.3×10^{-4}	4.3×10^{-4}	2.8×10^{-3}	2.8×10^{-3}	9.6×10^{-2}	2.2×10^{-2}	3.5×10^{-2}	8.8×10^{-2}
		GSD	4	7	7	7	7	4	7	7
	Mollusc – gastropod	GM	1.0×10^{-1}	1.0×10^{-1}	3.6×10^{-3}	1.5×10^{-2}	9.6×10^{-2}	9.7×10^{-2}	3.4×10^{-2}	2.6×10^{-2}
		GSD	4	4	4	4	7	4	4	4
	Grasses & Herbs	GM	3.9×10^{-4}	3.9×10^{-4}	4.1×10^{-3}	1.7×10^{-2}	7.2×10^{-4}	1.4×10^{-4}	6.9×10^{-3}	6.2×10^{-3}
		GSD	5.6	7	7	7	7	5.6	7	7
	Lichen & Bryophytes	GM	1.4×10^{-2}	1.4×10^{-2}	1.2×10^{-1}	4.7×10^{-2}	1.8×10^{0}	1.3×10^{-1}	3.1×10^{-2}	1.0×10^{-1}
		GSD	4.4	4.4	4	4	4	7	7	7
	Mammal – large	GM	5.3×10^{-5}	5.3×10^{-5}	5.6×10^{-3}	5.5×10^{-3}	1.4×10^{0}	3.5×10^{-3}	5.9×10^{-2}	7.8×10^{-2}
		GSD	5.8	7	7	7	4	4	7	7
	Mammal – small-burrowing	GM	5.3×10^{-5}	5.3×10^{-5}	5.6×10^{-3}	5.5×10^{-3}	3.4×10^{-2}	2.8×10^{-3}	5.9×10^{-2}	7.8×10^{-2}
		GSD	5.8	7	7	7	4	5.7	7	7
	Reptile	GM	5.5×10^{-2}	5.5×10^{-2}	9.1×10^{-3}	3.0×10^{-1}	1.3×10^{-1}	3.6×10^{-3}	5.9×10^{-2}	7.8×10^{-2}
		GSD	7	7	7	7	7	7	7	7
	Shrub	GM	3.9×10^{-4}	3.9×10^{-4}	4.1×10^{-3}	1.7×10^{-2}	7.2×10^{-4}	1.4×10^{-4}	6.9×10^{-3}	6.2×10^{-3}
		GSD	5.6	7	7	7	7	5.6	7	7
	Annelid	GM	9.0×10^{-2}	9.0×10^{-2}	2.6×10^{-1}	1.2×10^{-2}	9.6×10^{-2}	2.1×10^{-2}	4.2×10^{-2}	2.8×10^{0}
		GSD	4	4	4	7	7	4	7	7
	Tree	GM	3.9×10^{-4}	3.9×10^{-4}	4.1×10^{-3}	1.7×10^{-2}	7.2×10^{-4}	1.4×10^{-4}	6.9×10^{-3}	6.2×10^{-3}
		GSD	5.6	7	7	7	7	5.6	7	7

Table E-2. Continued. NHB CR values for marine, freshwater and terrestrial organisms used in the PSAR. Values on a white background have not changed since SR-PSU, while fully saturated red and blue backgrounds correspond to an increase or decrease, respectively, of at least one order of magnitude since SR-PSU. Paler colours represent smaller corresponding changes. Freshwater Reptile is a new organism in the PSAR (indicated by grey colour).

Eco.	Organism		Sm	Sn	Sr	Tc	Th	U	Zr
Marine (m^3 kgfw^{-1})	Bird	GM	1.5E−2	4.5E−1	1.0E−3	2.5E−3	3.5E−1	1.8E−4	3.7E−1
		GSD	5.0	5.0	5.0	5.0	5.0	5.0	5.0
	Benthic fish	GM	1.5E−2	4.5E−1	1.0E−3	2.5E−3	3.5E−1	1.8E−4	3.7E−1
		GSD	5.0	5.0	5.0	3.0	3.0	5.0	3.5
	Mollusc – bivalve	GM	2.0E+0	4.5E−1	1.8E+0	5.5E+0	5.8E+0	2.7E−1	3.0E+0
		GSD	3.0	5.0	3.0	3.0	4.4	5.0	4.4
	Crustacean	GM	2.0E+0	4.5E−1	3.8E+0	1.1E+1	2.3E+1	2.7E−1	1.1E+1
		GSD	5.0	5.0	5.0	3.0	5.0	5.0	5.0
	Macroalgae	GM	6.5E−1	8.1E−1	4.8E−2	3.5E+1	1.3E+1	9.1E−2	9.4E+0
		GSD	9.6	5.0	5.0	3.0	11.3	5.0	6.5
	Mammal	GM	1.5E−2	4.5E−1	6.8E−2	1.1E+1	3.5E−1	1.8E−4	3.7E−1
		GSD	5.0	5.0	3.8	3.0	5.0	5.0	5.0
	Pelagic fish	GM	1.5E−2	4.5E−1	1.0E−3	2.5E−3	3.5E−1	1.8E−4	3.7E−1
		GSD	5.0	5.0	5.0	3.0	3.0	5.0	3.5
	Phytoplankton	GM	6.5E−1	8.1E−1	4.8E−2	3.3E−3	5.1E+2	1.5E−1	1.7E+1
		GSD	9.6	5.0	5.0	3.0	3.0	3.0	3.1
	Polychaete worm	GM	2.0E+0	4.5E−1	4.6E−4	1.1E+1	5.8E+0	2.7E−1	3.0E+0
		GSD	5.0	5.0	5.0	5.0	5.0	5.0	5.0
	Vascular plant	GM	6.5E−1	8.1E−1	4.8E−2	3.5E+1	1.3E+1	9.1E−2	9.4E+0
		GSD	9.6	5.0	5.0	3.0	11.3	5.0	6.5
	Zooplankton	GM	2.0E+1	2.0E+1	4.8E−2	2.5E−3	5.0E+0	2.3E−3	2.0E+1
		GSD	5.0	5.0	3.0	5.0	2.4	5.0	5.0

Table E-2. Continued.

Eco.	Organism		Sm	Sn	Sr	Tc	Th	U	Zr
Freshwater (m^3 $kgfw^{-1}$)	Amphibian	GM	2.8E−3	2.4E−2	1.5E−1	7.1E−2	1.2E−1	3.0E−4	2.4E−2
		GSD	5.0	5.0	5.0	5.0	6.7	5.0	5.0
	Benthic fish	GM	2.8E−3	2.4E−2	1.5E−1	7.1E−2	1.2E−1	3.0E−4	2.4E−2
		GSD	5.0	3.0	3.0	5.0	6.7	5.0	3.0
	Bird	GM	2.8E−3	2.4E−2	7.3E+0	7.1E−2	1.2E−1	5.3E−2	3.0E−2
		GSD	5.0	5.0	3.0	5.0	6.7	3.0	3.0
	Mollusc – bivalve	GM	9.5E−1	1.5E−1	3.7E−1	7.1E−2	3.9E−1	9.9E−2	1.5E−1
		GSD	3.0	3.0	3.0	5.0	3.0	5.6	3.0
	Crustacean	GM	9.5E−1	3.0E−1	7.9E−1	7.1E−2	3.9E−1	1.1E−1	4.1E−1
		GSD	5.0	3.0	3.0	5.0	5.0	3.1	3.7
	Mollusc – gastropod	GM	9.5E−1	1.5E−1	3.7E−1	7.1E−2	3.9E−1	9.9E−2	1.5E−1
		GSD	5.0	5.0	5.0	5.0	5.0	5.6	5.0
	Insect larvae	GM	9.5E−1	1.5E−1	3.7E−1	7.1E−2	3.9E−1	9.9E−2	1.5E−1
		GSD	5.0	5.0	5.0	5.0	5.0	5.6	5.0
	Mammal	GM	2.8E−3	2.4E−2	1.5E−1	7.1E−2	1.2E−1	3.0E−4	2.4E−2
		GSD	5.0	5.0	5.0	5.0	6.7	5.0	5.0
	Microphytobenthos	GM	8.4E−1	2.5E−1	2.2E−1	5.5E−3	4.5E−1	1.6E−1	2.5E−1
		GSD	7.0	4.6	4.0	4.9	6.3	4.7	4.6
	Pelagic fish	GM	2.8E−3	2.4E−2	1.5E−1	7.1E−2	1.2E−1	3.0E−4	2.4E−2
		GSD	5.0	3.0	3.0	5.0	6.7	5.0	3.0
	Phytoplankton	GM	8.4E−1	2.5E−1	7.1E−2	5.5E−3	7.1E+0	4.8E−2	1.2E+0
		GSD	7.0	7.0	4.0	7.0	4.0	4.0	4.0
	Reptile	GM	3.2E+0	4.0E−1	2.8E+0	7.1E−2	8.7E−1	9.0E−2	1.2E+0
		GSD	7.0	5.0	5.5	5.0	4.0	4.0	7.0
	Vascular plant	GM	8.4E−1	2.5E−1	2.2E−1	5.5E−3	4.5E−1	1.6E−1	2.5E−1
		GSD	7.0	4.6	4.0	4.9	6.3	4.7	4.6
	Zooplankton	GM	9.5E−1	1.5E−1	3.6E+0	7.1E−2	3.9E−1	9.9E−2	1.5E−1
		GSD	5.0	5.0	3.0	5.0	5.0	5.6	5.0
Terrestrial (kgdw $kgfw^{-1}$)	Amphibian	GM	6.5E−5	3.1E−2	8.9E−1	3.5E−1	2.6E−3	3.0E−4	6.2E−3
		GSD	7.0	7.0	4.0	4.0	7.0	7.0	7.0
	Bird	GM	6.5E−5	3.1E−2	4.9E−1	1.7E−1	3.8E−4	7.9E−4	6.2E−3
		GSD	7.0	7.0	4.0	7.0	7.0	7.0	7.0
	Arthropod – detritivorous	GM	9.0E−2	1.1E−2	6.4E−2	2.3E−1	7.3E−3	2.8E−2	8.0E−3
		GSD	4.0	7.0	7.0	7.0	4.0	4.0	7.0
	Flying insects	GM	4.3E−4	7.9E−2	9.4E−3	1.3E−1	4.2E−4	8.9E−4	5.7E−3
		GSD	4.0	7.0	7.0	7.0	7.0	7.0	7.0
	Mollusc – gastropod	GM	1.0E−1	8.0E−3	8.7E−2	2.3E−1	7.3E−3	2.8E−2	8.0E−3
		GSD	4.0	7.0	4.0	7.0	7.0	7.0	7.0
	Grasses & Herbs	GM	4.1E−4	1.4E−2	1.4E−1	7.1E−3	1.4E−3	1.4E−4	3.4E−3
		GSD	7.0	7.0	7.0	7.0	7.0	7.0	7.0
	Lichen & Bryophytes	GM	1.3E−2	8.5E−2	2.8E−1	5.5E−2	1.5E−2	2.5E−2	1.3E−1
		GSD	4.7	4.0	4.0	7.0	4.8	8.9	4.4
	Mammal – large	GM	6.5E−5	3.1E−2	3.4E−3	3.5E−1	2.6E−3	3.0E−4	6.2E−3
		GSD	7.0	7.0	7.0	7.0	7.0	7.0	7.0
	Mammal – small-burrowing	GM	6.5E−5	3.1E−2	3.4E−3	3.5E−1	2.6E−3	3.0E−4	6.2E−3
		GSD	7.0	7.0	7.0	7.0	7.0	7.0	7.0
	Reptile	GM	5.5E−2	3.1E−2	2.2E−1	3.5E−1	2.2E−3	3.2E−3	6.2E−3
		GSD	7.0	7.0	7.0	7.0	7.0	7.0	7.0
	Shrub	GM	4.1E−4	1.4E−2	1.4E−1	7.1E−3	1.4E−3	1.4E−4	3.4E−3
		GSD	7.0	7.0	7.0	7.0	7.0	7.0	7.0
	Annelid	GM	5.4E−3	1.1E−2	6.4E−2	3.5E−1	7.3E−3	2.8E−2	8.0E−3
		GSD	7.0	7.0	7.0	7.0	7.0	7.0	7.0
	Tree	GM	4.1E−4	1.4E−2	1.4E−1	7.1E−3	1.4E−3	1.4E−4	3.4E−3
		GSD	7.0	7.0	7.0	7.0	7.0	7.0	7.0

E2 Occupancy factors and dose conversion coefficients

Following updates in ERICA with respect to reference organisms and their associated habitats, the occupancy factors are updated in the PSAR (Table E-3).

Dose rates to non-human biota are in the PSAR calculated using organism-, radionuclide- and radiation type-specific dose conversion coefficients (DCC) according to the updated methodology used in ERICA tool version 2.0, that is based on the ICRP's BiotaDC code (Ulanovsky 2017, ICRP 2017). This is, in the PSAR, the DCC calculations are updated, following this methodology in the new version of the ERICA tool. This update also includes an adjustment of how DCCs are applied in the assessment. In SR-PSU, the DCC values were calculated with default settings in the BiotaDC tool, including the contributions from radioactive decay products generated during one year. In the PSAR, the contribution of decay products is implicitly modelled by assuming secular equilibrium with the parent radionuclide. This change is done to increase the consistency of the assessment, as it is the methodology used to calculate dose coefficients for humans.

ERICA version 2.0 introduced a calculation for organisms immersed in contaminated air, which permits the calculation of external doses from radioactive gases, such as radon, in the air surrounding the organism. As it is formed as a decay product from another modelled radionuclide, radon is not explicitly included in the calculation in BioTEx and so the immersion dose in air from radon is applied to its parent radionuclide assuming secular equilibrium with its radon decay product in the environmental media (Table E-4, see Appendix D3 for further discussion about this simplified approach).

The combined effects of the updates introduced in the PSAR lead to internal and external DCC values that deviate from the corresponding values in SR-PSU. The DCCs used in the PSAR (Tables E-5 to E-6) are similar to those used in SR-PSU for most radionuclides and exposure modes. However, for some radionuclides and organisms, the new DCCs deviate by more than one order of magnitude (as indicated by the fully saturated colours in Tables E-5 and E-6).

In general, DCCs for radionuclides with short-lived decay products with high-energy radiation increase. The main reason for this is the new more cautious assumption of decay products being in secular equilibrium with their parents, which generates significantly more radiation than the previously assumed ingrowth of only one year. An example of this is Ac-227, which has internal and external DCCs that are two to three orders of magnitude higher than in SR-PSU. Similarly, the DCCs of Cm-246, Np-237, Pu-241, Th-229, U-232 and U-238 increase in the PSAR for the same reason.

Extremely high increases (several orders of magnitude) are seen in DCCs for external exposure in the habitats 'In-air' and 'On-soil' for Ca-41 and Ni-59. The reason for this is that the DCCs used in SR-PSU were very small (practically zero).

As for organism-specific updates, there is a general decrease in DCCs for external exposure in water for phytoplankton and microphytobenthos by several orders of magnitude. However, the DCCs for internal exposure to beta and gamma radiation have simultaneously increased by up to six orders of magnitude. These changes are due to the updated ERICA methodology and assumptions in the DCC calculations. Another example of an organism with a large increase in the DCC is 'Lichen & Bryophytes' for which the external exposure in the habitat 'On-soil' has increased between four to six orders of magnitude for several radionuclides, mainly due to corrections in the DCC values (Brown et al. 2016).

Calculating external exposure from radionuclides when the organism is immersed in air is part of the updated ERICA methodology. The corresponding DCCs are presented in Table E-4.

Table E-3. Selected ERICA v2.0 reference organisms, plus the added freshwater organism 'Microphytobenthos', implemented in the BioTEx-model with occupancy factors (OCC) defining habitats.

Marine	Habitat	OCC	Freshwater	Habitat	OCC	Terrestrial	Habitat	OCC
Benthic fish	Sediment-surface	1	Amphibian	Water	1	Amphibian	In-soil	1
Bird	Water	1	Benthic fish	Sediment-surface	1	Annelid	In-soil	1
Crustacean	Sediment-surface	1	Bird	Water	1	Arthropod – detritivorous	In-soil	1
Macroalgae	Sediment-surface	1	Crustacean	Sediment-surface	1	Bird	On-soil	1
Mammal	Water	1	Insect larvae	Sediment	1	Flying insects	On-soil	1
Mollusc – bivalve	Sediment-surface	1	Mammal	Water	1	Grasses & Herbs	On-soil	1
Pelagic fish	Water	1	Microphytobenthos	Sediment-surface	1	Lichen & Bryophytes	On-soil	1
Phytoplankton	Water	1	Mollusc-bivalve	Sediment-surface	1	Mammal – large	On-soil	1
Polychaete worm	Sediment	1	Mollusc – gastropod	Sediment-surface	1	Mammal – small-burrowing	In-soil	1
Vascular plant	Sediment-surface	1	Pelagic fish	Water	1	Mollusc-gastropod	On-soil	1
Zooplankton	Water	1	Phytoplankton	Water	1	Reptile	In-soil	1
			Reptile	Sediment	0.5	Shrub	On-soil	1
			Reptile	Water	0.5	Tree	On-soil	1
			Vascular plant	Sediment-surface	1			
			Zooplankton	Water	1			

Table E-4. External dose conversion coefficients (DCC, (μGy h^{-1})/(Bq m^{-3})) for organisms immersed in air.

$DCC_{imm,ext,in,air}$	Ac-227	Ra-226	U-232
Amphibian (terrestrial)	1.7×10^{-5}	1.2×10^{-7}	1.7×10^{-7}
Arthropod – detritivorous	1.7×10^{-5}	1.2×10^{-7}	1.6×10^{-7}
Bird (terrestrial)	1.7×10^{-5}	1.2×10^{-7}	1.7×10^{-7}
Flying insects	1.7×10^{-5}	1.2×10^{-7}	1.7×10^{-7}
Lichen & Bryophytes	1.7×10^{-5}	1.2×10^{-7}	1.6×10^{-7}
Mammal – large	9.2×10^{-6}	7.0×10^{-8}	9.9×10^{-8}
Mammal – small-burrowing	1.6×10^{-5}	1.2×10^{-7}	1.6×10^{-7}
Mollusc – gastropod (terrestrial)	1.7×10^{-5}	1.2×10^{-7}	1.7×10^{-7}
Reptile (terrestrial)	1.6×10^{-5}	1.1×10^{-7}	1.6×10^{-7}

Table E-5. External dose conversion coefficients (DCC, (μGy h^{-1})/(Bq $kgdw^{-1}$)) for non-human biota. White background indicates no change from SR-PSU, fully saturated red and blue backgrounds correspond to an increase or decrease, respectively, of at least one order of magnitude since SR-PSU. Paler colours represent smaller corresponding changes. Grey background specifies no data in SR-PSU.

	Ac-227	Ag-108m	Am-241	Am-242m	Am-243	Ba-133	C-14	Ca-41	Cd-113m	Cl-36	Cm-243	Cm-244	Cm-245	Cm-246	Co-60	Cs-135	Cs-137
$DCC_{ext,in,air}$																	
Bird (terrestrial)	6.8×10^{-5}	2.9×10^{-4}	1.6×10^{-6}	2.3×10^{-6}	3.4×10^{-5}	6.6×10^{-5}		1.6×10^{-11}	1.3×10^{-8}	3.3×10^{-8}	2.1×10^{-5}	1.1×10^{-8}	1.4×10^{-5}	6.5×10^{-7}	4.7×10^{-4}		1.2×10^{-4}
Flying insects	7.8×10^{-5}	3.2×10^{-4}	2.1×10^{-6}	3.1×10^{-6}	3.9×10^{-5}	7.7×10^{-5}		4.9×10^{-9}	1.6×10^{-8}	3.7×10^{-8}	2.4×10^{-5}	7.6×10^{-8}	1.7×10^{-5}	6.4×10^{-7}	4.4×10^{-4}		1.3×10^{-4}
$DCC_{ext,in,water}$																	
Amphibian (freshwater)	2.4×10^{-4}	9.0×10^{-4}	1.3×10^{-5}	1.3×10^{-5}	1.3×10^{-4}	2.2×10^{-4}	5.9×10^{-8}	6.6×10^{-9}	1.8×10^{-6}	4.1×10^{-6}	7.1×10^{-5}	3.6×10^{-7}	5.6×10^{-5}	2.5×10^{-6}	1.4×10^{-3}	2.8×10^{-7}	3.1×10^{-4}
Benthic fish (freshwater)	1.9×10^{-4}	8.0×10^{-4}	1.0×10^{-5}	9.2×10^{-6}	1.1×10^{-4}	1.9×10^{-4}	1.7×10^{-8}	1.8×10^{-9}	5.6×10^{-7}	1.3×10^{-6}	6.2×10^{-5}	1.4×10^{-7}	4.9×10^{-5}	2.0×10^{-6}	1.3×10^{-3}	8.6×10^{-8}	2.8×10^{-4}
Benthic fish (marine)	2.1×10^{-4}	8.5×10^{-4}	1.2×10^{-5}	1.0×10^{-5}	1.2×10^{-4}	2.0×10^{-4}	1.8×10^{-8}	2.0×10^{-9}	7.1×10^{-7}	1.8×10^{-6}	6.6×10^{-5}	2.0×10^{-7}	5.2×10^{-5}	2.2×10^{-6}	1.3×10^{-3}	9.3×10^{-8}	3.0×10^{-4}
Bird (freshwater)	1.9×10^{-4}	8.0×10^{-4}	1.0×10^{-5}	9.2×10^{-6}	1.1×10^{-4}	1.9×10^{-4}	1.8×10^{-8}	1.9×10^{-9}	5.8×10^{-7}	1.3×10^{-6}	6.2×10^{-5}	1.4×10^{-7}	4.8×10^{-5}	2.0×10^{-6}	1.3×10^{-3}	9.0×10^{-8}	2.8×10^{-4}
Bird (marine)	1.9×10^{-4}	8.0×10^{-4}	1.0×10^{-5}	9.2×10^{-6}	1.1×10^{-4}	1.9×10^{-4}	1.8×10^{-8}	1.9×10^{-9}	5.8×10^{-7}	1.3×10^{-6}	6.2×10^{-5}	1.4×10^{-7}	4.8×10^{-5}	2.0×10^{-6}	1.3×10^{-3}	9.0×10^{-8}	2.8×10^{-4}
Crustacean (freshwater)	5.4×10^{-4}	9.6×10^{-4}	1.6×10^{-5}	3.8×10^{-5}	1.5×10^{-4}	2.3×10^{-4}	9.1×10^{-7}	5.6×10^{-8}	2.4×10^{-5}	5.3×10^{-5}	8.2×10^{-5}	8.4×10^{-7}	6.3×10^{-5}	3.7×10^{-6}	1.4×10^{-3}	4.4×10^{-6}	3.7×10^{-4}
Crustacean (marine)	2.0×10^{-4}	8.2×10^{-4}	1.1×10^{-5}	9.7×10^{-6}	1.2×10^{-4}	1.9×10^{-4}	2.1×10^{-8}	2.3×10^{-9}	6.8×10^{-7}	1.6×10^{-6}	6.4×10^{-5}	1.6×10^{-7}	5.0×10^{-5}	2.1×10^{-6}	1.3×10^{-3}	1.1×10^{-7}	2.9×10^{-4}
Insect larvae	5.3×10^{-4}	9.6×10^{-4}	1.6×10^{-5}	3.7×10^{-5}	1.5×10^{-4}	2.3×10^{-4}	8.2×10^{-7}	5.4×10^{-8}	2.3×10^{-5}	5.0×10^{-5}	8.2×10^{-5}	8.3×10^{-7}	6.3×10^{-5}	3.6×10^{-6}	1.4×10^{-3}	4.0×10^{-6}	3.7×10^{-4}
Macroalgae	3.1×10^{-4}	9.2×10^{-4}	1.4×10^{-5}	1.8×10^{-5}	1.3×10^{-4}	2.2×10^{-4}	2.2×10^{-7}	6.4×10^{-9}	5.9×10^{-6}	1.4×10^{-5}	7.4×10^{-5}	4.3×10^{-7}	5.8×10^{-5}	2.8×10^{-6}	1.4×10^{-3}	9.7×10^{-7}	3.3×10^{-4}
Mammal (freshwater)	1.7×10^{-4}	7.3×10^{-4}	8.7×10^{-6}	7.9×10^{-6}	9.9×10^{-5}	1.7×10^{-4}	1.2×10^{-8}	1.3×10^{-9}	4.2×10^{-7}	9.6×10^{-7}	5.5×10^{-5}	9.5×10^{-8}	4.3×10^{-5}	1.8×10^{-6}	1.2×10^{-3}	6.3×10^{-8}	2.6×10^{-4}
Mammal (marine)	8.4×10^{-5}	4.0×10^{-4}	3.3×10^{-6}	3.5×10^{-6}	4.5×10^{-5}	8.4×10^{-5}	3.6×10^{-9}	3.9×10^{-1}	1.3×10^{-7}	3.0×10^{-7}	2.6×10^{-5}	3.0×10^{-8}	1.9×10^{-5}	1.1×10^{-6}	7.2×10^{-4}	1.8×10^{-8}	1.4×10^{-4}
Microphytobenthos	6.7×10^{-4}	9.6×10^{-4}	1.6×10^{-5}	5.7×10^{-5}	1.7×10^{-4}	2.3×10^{-4}	1.7×10^{-6}	6.4×10^{-8}	4.5×10^{-5}	9.2×10^{-5}	8.8×10^{-5}	8.8×10^{-7}	6.5×10^{-5}	3.8×10^{-6}	1.5×10^{-3}	8.0×10^{-6}	4.0×10^{-4}
Mollusc – bivalve (freshwater)	2.3×10^{-4}	8.8×10^{-4}	1.3×10^{-5}	1.2×10^{-5}	1.3×10^{-4}	2.1×10^{-4}	4.5×10^{-8}	5.1×10^{-9}	1.4×10^{-6}	3.2×10^{-6}	7.0×10^{-5}	3.0×10^{-7}	5.5×10^{-5}	2.4×10^{-6}	1.4×10^{-3}	2.2×10^{-7}	3.1×10^{-4}
Mollusc – bivalve (marine)	2.5×10^{-4}	9.0×10^{-4}	1.4×10^{-5}	1.4×10^{-5}	1.3×10^{-4}	2.2×10^{-4}	7.2×10^{-8}	8.2×10^{-9}	2.2×10^{-6}	5.0×10^{-6}	7.2×10^{-5}	4.0×10^{-7}	5.7×10^{-5}	2.6×10^{-6}	1.4×10^{-3}	3.5×10^{-7}	3.2×10^{-4}
Mollusc – gastropod (freshwater)	2.7×10^{-4}	9.2×10^{-4}	1.4×10^{-5}	1.6×10^{-5}	1.3×10^{-4}	2.3×10^{-4}	1.2×10^{-7}	1.4×10^{-8}	3.5×10^{-6}	8.1×10^{-6}	7.4×10^{-5}	5.2×10^{-7}	5.8×10^{-5}	2.8×10^{-6}	1.4×10^{-3}	5.5×10^{-7}	3.3×10^{-4}
Pelagic fish (freshwater)	2.0×10^{-4}	8.1×10^{-4}	1.1×10^{-5}	9.4×10^{-6}	1.1×10^{-4}	1.9×10^{-4}	1.8×10^{-8}	1.9×10^{-9}	5.9×10^{-7}	1.3×10^{-6}	6.3×10^{-5}	1.5×10^{-7}	4.9×10^{-5}	2.0×10^{-6}	1.3×10^{-3}	9.0×10^{-8}	2.8×10^{-4}
Pelagic fish (marine)	2.0×10^{-4}	8.3×10^{-4}	1.1×10^{-5}	1.0×10^{-5}	1.2×10^{-4}	2.0×10^{-4}	2.3×10^{-8}	2.5×10^{-9}	7.4×10^{-7}	1.7×10^{-6}	6.5×10^{-5}	1.8×10^{-7}	5.1×10^{-5}	2.1×10^{-6}	1.3×10^{-3}	1.1×10^{-7}	2.9×10^{-4}
Phytoplankton (freshwater)	6.7×10^{-4}	9.6×10^{-4}	1.6×10^{-5}	5.7×10^{-5}	1.7×10^{-4}	2.3×10^{-4}	1.7×10^{-6}	6.4×10^{-8}	4.5×10^{-5}	9.2×10^{-5}	8.8×10^{-5}	8.8×10^{-7}	6.5×10^{-5}	3.8×10^{-6}	1.5×10^{-3}	8.0×10^{-6}	4.0×10^{-4}
Phytoplankton (marine)	6.7×10^{-4}	9.6×10^{-4}	1.6×10^{-5}	5.7×10^{-5}	1.7×10^{-4}	2.3×10^{-4}	1.7×10^{-6}	6.4×10^{-8}	4.5×10^{-5}	9.2×10^{-5}	8.8×10^{-5}	8.8×10^{-7}	6.5×10^{-5}	3.8×10^{-6}	1.5×10^{-3}	8.0×10^{-6}	4.0×10^{-4}
Polychaete worm	2.7×10^{-4}	9.2×10^{-4}	1.4×10^{-5}	1.6×10^{-5}	1.3×10^{-4}	2.2×10^{-4}	7.2×10^{-8}	9.8×10^{-9}	3.2×10^{-6}	8.5×10^{-6}	7.3×10^{-5}	4.8×10^{-7}	5.8×10^{-5}	2.7×10^{-6}	1.4×10^{-3}	3.7×10^{-7}	3.2×10^{-4}
Reptile (freshwater)	1.9×10^{-4}	8.0×10^{-4}	1.1×10^{-5}	9.4×10^{-6}	1.1×10^{-4}	1.9×10^{-4}	2.0×10^{-8}	2.1×10^{-9}	6.2×10^{-7}	1.4×10^{-6}	6.3×10^{-5}	1.4×10^{-7}	4.9×10^{-5}	2.0×10^{-6}	1.3×10^{-3}	9.7×10^{-8}	2.8×10^{-4}
Vascular plant (freshwater)	4.8×10^{-4}	9.5×10^{-4}	1.6×10^{-5}	4.1×10^{-5}	1.6×10^{-4}	2.3×10^{-4}	1.1×10^{-6}	5.2×10^{-8}	2.9×10^{-5}	5.4×10^{-5}	8.4×10^{-5}	8.1×10^{-7}	6.3×10^{-5}	3.5×10^{-6}	1.4×10^{-3}	5.7×10^{-6}	3.7×10^{-4}
Vascular plant (marine)	2.4×10^{-4}	9.0×10^{-4}	1.4×10^{-5}	1.4×10^{-5}	1.3×10^{-4}	2.2×10^{-4}	6.2×10^{-8}	7.1×10^{-9}	1.9×10^{-6}	4.5×10^{-6}	7.2×10^{-5}	3.8×10^{-7}	5.7×10^{-5}	2.5×10^{-6}	1.4×10^{-3}	3.0×10^{-7}	3.2×10^{-4}
Zooplankton (freshwater)	6.3×10^{-4}	9.6×10^{-4}	1.6×10^{-5}	5.0×10^{-5}	1.6×10^{-4}	2.3×10^{-4}	1.3×10^{-6}	6.0×10^{-8}	3.7×10^{-5}	7.9×10^{-5}	8.6×10^{-5}	8.6×10^{-7}	6.4×10^{-5}	3.7×10^{-6}	1.5×10^{-3}	6.3×10^{-6}	3.9×10^{-4}
Zooplankton (marine)	4.4×10^{-4}	9.5×10^{-4}	1.6×10^{-5}	2.7×10^{-5}	1.4×10^{-4}	2.3×10^{-4}	4.3×10^{-7}	4.0×10^{-8}	1.3×10^{-5}	3.0×10^{-5}	7.9×10^{-5}	7.6×10^{-7}	6.1×10^{-5}	3.5×10^{-6}	1.4×10^{-3}	2.1×10^{-6}	3.5×10^{-4}

Table E-5. Continued.

	Ac-227	Ag-108m	Am-241	Am-242m	Am-243	Ba-133	C-14	Ca-41	Cd-113m	Cl-36	Cm-243	Cm-244	Cm-245	Cm-246	Co-60	Cs-135	Cs-137
$DCC_{ext,in,soil}$																	
Amphibian (terrestrial)	1.6×10^{-4}	8.5×10^{-4}	5.6×10^{-6}	6.3×10^{-6}	8.0×10^{-5}	1.8×10^{-4}		7.8×10^{-9}	2.9×10^{-8}	7.4×10^{-8}	4.9×10^{-5}	1.5×10^{-7}	3.2×10^{-5}	1.9×10^{-6}	1.3×10^{-3}		3.0×10^{-4}
Annelid	1.7×10^{-4}	8.6×10^{-4}	5.7×10^{-6}	6.4×10^{-6}	8.1×10^{-5}	1.8×10^{-4}		8.1×10^{-9}	3.0×10^{-8}	7.5×10^{-8}	5.0×10^{-5}	1.5×10^{-7}	3.2×10^{-5}	2.0×10^{-6}	1.3×10^{-3}		3.0×10^{-4}
Arthropod – detritivorous	1.7×10^{-4}	8.6×10^{-4}	5.8×10^{-6}	6.4×10^{-6}	8.2×10^{-5}	1.8×10^{-4}		8.3×10^{-9}	3.0×10^{-8}	7.6×10^{-8}	5.0×10^{-5}	1.6×10^{-7}	3.2×10^{-5}	2.0×10^{-6}	1.3×10^{-3}		3.0×10^{-4}
Mammal – small-burrowing	1.6×10^{-4}	8.0×10^{-4}	5.2×10^{-6}	5.9×10^{-6}	7.7×10^{-5}	1.7×10^{-4}		6.5×10^{-9}	2.8×10^{-8}	7.0×10^{-8}	4.7×10^{-5}	1.3×10^{-7}	3.0×10^{-5}	1.8×10^{-6}	1.2×10^{-3}		2.8×10^{-4}
Mollusc – gastropod (terrestrial)	1.7×10^{-4}	8.6×10^{-4}	5.7×10^{-6}	6.4×10^{-6}	8.2×10^{-5}	1.8×10^{-4}		8.2×10^{-9}	3.0×10^{-8}	7.6×10^{-8}	5.0×10^{-5}	1.6×10^{-7}	3.2×10^{-5}	2.0×10^{-6}	1.3×10^{-3}		3.0×10^{-4}
Reptile (terrestrial)	1.5×10^{-4}	7.7×10^{-4}	4.9×10^{-6}	5.6×10^{-6}	7.4×10^{-5}	1.6×10^{-4}		5.6×10^{-9}	2.7×10^{-8}	6.8×10^{-8}	4.5×10^{-5}	1.1×10^{-7}	2.9×10^{-5}	1.8×10^{-6}	1.2×10^{-3}		2.7×10^{-4}
$DCC_{ext,on,soil}$																	
Amphibian (terrestrial)	7.8×10^{-5}	3.3×10^{-4}	2.0×10^{-6}	2.9×10^{-6}	3.8×10^{-5}	7.6×10^{-5}		1.6×10^{-9}	1.5×10^{-8}	3.7×10^{-8}	2.4×10^{-5}	4.7×10^{-8}	1.6×10^{-5}	7.2×10^{-7}	5.1×10^{-4}		1.4×10^{-4}
Arthropod – detritivorous	7.8×10^{-5}	3.2×10^{-4}	2.2×10^{-6}	3.1×10^{-6}	3.9×10^{-5}	7.7×10^{-5}		6.3×10^{-9}	1.6×10^{-8}	3.7×10^{-8}	2.4×10^{-5}	8.2×10^{-8}	1.7×10^{-5}	5.9×10^{-7}	4.0×10^{-4}		1.3×10^{-4}
Bird (terrestrial)	7.4×10^{-5}	3.1×10^{-4}	1.8×10^{-6}	2.6×10^{-6}	3.6×10^{-5}	7.2×10^{-5}		4.9×10^{-1}	1.4×10^{-8}	3.5×10^{-8}	2.2×10^{-5}	2.1×10^{-8}	1.5×10^{-5}	7.1×10^{-7}	5.1×10^{-4}		1.3×10^{-4}
Flying insects	7.8×10^{-5}	3.2×10^{-4}	2.1×10^{-6}	3.1×10^{-6}	3.9×10^{-5}	7.7×10^{-5}		4.9×10^{-9}	1.6×10^{-8}	3.7×10^{-8}	2.4×10^{-5}	7.6×10^{-8}	1.7×10^{-5}	6.4×10^{-7}	4.4×10^{-4}		1.3×10^{-4}
Grasses & Herbs	7.1×10^{-5}	3.2×10^{-4}	3.0×10^{-6}	3.4×10^{-6}	3.9×10^{-5}	7.4×10^{-5}		1.0×10^{-8}	1.3×10^{-8}	2.9×10^{-8}	2.3×10^{-5}	1.2×10^{-7}	1.7×10^{-5}	7.6×10^{-7}	4.8×10^{-4}		1.1×10^{-4}
Lichen & Bryophytes	7.8×10^{-5}	3.2×10^{-4}	2.2×10^{-6}	3.1×10^{-6}	3.9×10^{-5}	7.7×10^{-5}		6.3×10^{-9}	1.6×10^{-8}	3.7×10^{-8}	2.4×10^{-5}	8.2×10^{-8}	1.7×10^{-5}	5.9×10^{-7}	4.0×10^{-4}		1.3×10^{-4}
Mammal – large	4.4×10^{-5}	2.0×10^{-4}	7.5×10^{-7}	1.4×10^{-6}	2.0×10^{-5}	4.2×10^{-5}		6.4×10^{-11}	8.3×10^{-9}	2.2×10^{-8}	1.3×10^{-5}	5.8×10^{-9}	8.4×10^{-6}	5.0×10^{-7}	3.5×10^{-4}		8.4×10^{-5}
Mammal – small-burrowing	7.6×10^{-5}	3.2×10^{-4}	1.9×10^{-6}	2.7×10^{-6}	3.7×10^{-5}	7.4×10^{-5}		7.7×10^{-1}	1.5×10^{-8}	3.6×10^{-8}	2.3×10^{-5}	2.9×10^{-8}	1.6×10^{-5}	7.2×10^{-7}	5.1×10^{-4}		1.4×10^{-4}
Mollusc – gastropod (terrestrial)	7.8×10^{-5}	3.3×10^{-4}	2.1×10^{-6}	3.0×10^{-6}	3.9×10^{-5}	7.7×10^{-5}		4.0×10^{-9}	1.5×10^{-8}	3.7×10^{-8}	2.4×10^{-5}	7.1×10^{-8}	1.6×10^{-5}	6.6×10^{-7}	4.7×10^{-4}		1.4×10^{-4}
Reptile (terrestrial)	7.5×10^{-5}	3.2×10^{-4}	1.8×10^{-6}	2.6×10^{-6}	3.7×10^{-5}	7.3×10^{-5}		5.8×10^{-1}	1.4×10^{-8}	3.6×10^{-8}	2.3×10^{-5}	2.4×10^{-8}	1.6×10^{-5}	7.2×10^{-7}	5.1×10^{-4}		1.3×10^{-4}
Shrub	6.6×10^{-5}	3.1×10^{-4}	2.6×10^{-6}	2.8×10^{-6}	3.6×10^{-5}	7.0×10^{-5}		7.4×10^{-1}	1.2×10^{-8}	2.7×10^{-8}	2.2×10^{-5}	5.5×10^{-8}	1.5×10^{-5}	6.7×10^{-7}	4.5×10^{-4}		1.1×10^{-4}
Tree	5.6×10^{-5}	2.6×10^{-4}	1.9×10^{-6}	2.2×10^{-6}	3.0×10^{-5}	5.8×10^{-5}		2.2×10^{-13}	9.8×10^{-9}	2.3×10^{-8}	1.8×10^{-5}	1.3×10^{-8}	1.3×10^{-5}	5.5×10^{-7}	3.9×10^{-4}		9.0×10^{-5}

Table E-5. Continued. External dose conversion coefficients (DCC, (μGy h^{-1})/(Bq $kgdw^{-1}$)) for non-human biota. White background indicates no change from SR-PSU, fully saturated red and blue backgrounds correspond to an increase or decrease, respectively, of at least one order of magnitude since SR-PSU. Paler colours represent smaller corresponding changes. Grey background specifies no data in SR-PSU.

	Eu-152	H-3	Ho-166m	I-129	Mo-93	Nb-93m	Nb-94	Ni-59	Ni-63	Np-237	Pa-231	Pb-210	Pd-107	Po-210	Pu-238	Pu-239	Pu-240
$DCC_{ext,in,air}$																	
Bird (terrestrial)	2.1×10^{-4}		3.2×10^{-4}	6.9×10^{-7}	5.3×10^{-8}	9.6×10^{-9}	3.1×10^{-4}	3.6×10^{-9}		3.5×10^{-5}	5.8×10^{-6}	1.1×10^{-7}		2.2×10^{-9}	1.0×10^{-8}	1.4×10^{-8}	1.1×10^{-8}
Flying insects	2.1×10^{-4}		3.5×10^{-4}	1.5×10^{-6}	5.8×10^{-7}	1.1×10^{-7}	3.3×10^{-4}	1.1×10^{-8}		4.1×10^{-5}	7.0×10^{-6}	2.4×10^{-7}		2.4×10^{-9}	9.4×10^{-8}	5.2×10^{-8}	8.9×10^{-8}
$DCC_{ext,in,water}$																	
Amphibian (freshwater)	6.5×10^{-4}	2.6×10^{-12}	9.0×10^{-4}	1.2×10^{-5}	2.4×10^{-6}	4.3×10^{-7}	8.6×10^{-4}	8.7×10^{-8}	4.0×10^{-9}	1.4×10^{-4}	2.1×10^{-5}	1.1×10^{-5}	5.3×10^{-1}	5.4×10^{-9}	3.7×10^{-7}	1.9×10^{-7}	3.6×10^{-7}
Benthic fish (freshwater)	5.9×10^{-4}	3.9×10^{-13}	8.1×10^{-4}	7.4×10^{-6}	7.8×10^{-7}	1.4×10^{-7}	7.8×10^{-4}	3.0×10^{-8}	1.1×10^{-9}	1.2×10^{-4}	1.7×10^{-5}	3.8×10^{-6}	1.5×10^{-1}	4.9×10^{-9}	1.3×10^{-7}	8.5×10^{-8}	1.3×10^{-7}
Benthic fish (marine)	6.2×10^{-4}	8.1×10^{-13}	8.5×10^{-4}	9.3×10^{-6}	1.2×10^{-6}	2.1×10^{-7}	8.2×10^{-4}	3.2×10^{-8}	1.1×10^{-9}	1.3×10^{-4}	1.9×10^{-5}	6.2×10^{-6}	1.5×10^{-1}	5.1×10^{-9}	1.9×10^{-7}	1.1×10^{-7}	1.8×10^{-7}
Bird (freshwater)	5.8×10^{-4}	3.8×10^{-13}	8.0×10^{-4}	7.2×10^{-6}	7.8×10^{-7}	1.4×10^{-7}	7.7×10^{-4}	3.1×10^{-8}	1.2×10^{-9}	1.2×10^{-4}	1.7×10^{-5}	3.9×10^{-6}	1.6×10^{-1}	4.8×10^{-9}	1.3×10^{-7}	8.4×10^{-8}	1.3×10^{-7}
Bird (marine)	5.8×10^{-4}	3.8×10^{-13}	8.0×10^{-4}	7.2×10^{-6}	7.8×10^{-7}	1.4×10^{-7}	7.7×10^{-4}	3.1×10^{-8}	1.2×10^{-9}	1.2×10^{-4}	1.7×10^{-5}	3.9×10^{-6}	1.6×10^{-1}	4.8×10^{-9}	1.3×10^{-7}	8.4×10^{-8}	1.3×10^{-7}
Crustacean (freshwater)	7.0×10^{-4}	3.3×10^{-13}	9.5×10^{-4}	1.5×10^{-5}	5.6×10^{-6}	1.1×10^{-6}	9.2×10^{-4}	6.7×10^{-7}	5.9×10^{-8}	1.6×10^{-4}	2.5×10^{-5}	1.1×10^{-4}	1.4×10^{-8}	5.6×10^{-9}	9.8×10^{-7}	4.5×10^{-7}	9.3×10^{-7}
Crustacean (marine)	6.0×10^{-4}	9.8×10^{-15}	8.2×10^{-4}	8.0×10^{-6}	9.3×10^{-7}	1.7×10^{-7}	7.9×10^{-4}	3.5×10^{-8}	1.7×10^{-9}	1.2×10^{-4}	1.8×10^{-5}	4.5×10^{-6}	3.5×10^{-1}	4.9×10^{-9}	1.6×10^{-7}	9.5×10^{-8}	1.5×10^{-7}
Insect larvae	7.0×10^{-4}	3.2×10^{-13}	9.5×10^{-4}	1.5×10^{-5}	5.6×10^{-6}	1.1×10^{-6}	9.2×10^{-4}	6.5×10^{-7}	5.6×10^{-8}	1.6×10^{-4}	2.5×10^{-5}	1.1×10^{-4}	1.3×10^{-8}	5.6×10^{-9}	9.7×10^{-7}	4.4×10^{-7}	9.2×10^{-7}
Macroalgae	6.7×10^{-4}	2.3×10^{-9}	9.1×10^{-4}	1.3×10^{-5}	2.8×10^{-6}	5.3×10^{-7}	8.8×10^{-4}	8.1×10^{-8}	2.1×10^{-8}	1.4×10^{-4}	2.1×10^{-5}	3.4×10^{-5}	6.4×10^{-9}	5.5×10^{-9}	4.5×10^{-7}	2.2×10^{-7}	4.3×10^{-7}
Mammal (freshwater)	5.4×10^{-4}	2.9×10^{-13}	7.3×10^{-4}	5.3×10^{-6}	5.3×10^{-7}	9.5×10^{-8}	7.1×10^{-4}	2.3×10^{-8}	7.8×10^{-1}	1.0×10^{-4}	1.5×10^{-5}	2.9×10^{-6}	9.5×10^{-11}	4.4×10^{-9}	9.1×10^{-8}	6.4×10^{-8}	8.7×10^{-8}
Mammal (marine)	3.2×10^{-4}	3.6×10^{-14}	4.1×10^{-4}	1.6×10^{-6}	1.5×10^{-7}	2.7×10^{-8}	4.1×10^{-4}	8.3×10^{-9}	1.8×10^{-1}	5.1×10^{-5}	7.4×10^{-6}	8.9×10^{-7}	1.9×10^{-11}	2.6×10^{-9}	2.7×10^{-8}	2.3×10^{-8}	2.6×10^{-8}
Microphytobenthos	7.1×10^{-4}	1.9×10^{-1}	9.6×10^{-4}	1.6×10^{-5}	5.8×10^{-6}	1.2×10^{-6}	9.3×10^{-4}	7.6×10^{-7}	1.2×10^{-7}	1.7×10^{-4}	2.6×10^{-5}	1.7×10^{-4}	1.6×10^{-8}	5.7×10^{-9}	1.0×10^{-6}	4.9×10^{-7}	9.9×10^{-7}
Mollusc – bivalve (freshwater)	6.4×10^{-4}	1.6×10^{-12}	8.9×10^{-4}	1.1×10^{-5}	1.9×10^{-6}	3.5×10^{-7}	8.5×10^{-4}	6.9×10^{-8}	3.0×10^{-9}	1.3×10^{-4}	2.0×10^{-5}	8.7×10^{-6}	4.1×10^{-1}	5.3×10^{-9}	3.1×10^{-7}	1.6×10^{-7}	2.9×10^{-7}
Mollusc – bivalve (marine)	6.6×10^{-4}	3.0×10^{-12}	9.0×10^{-4}	1.2×10^{-5}	2.6×10^{-6}	4.8×10^{-7}	8.7×10^{-4}	1.1×10^{-7}	4.9×10^{-9}	1.4×10^{-4}	2.1×10^{-5}	1.3×10^{-5}	6.6×10^{-1}	5.4×10^{-9}	4.2×10^{-7}	2.1×10^{-7}	4.0×10^{-7}
Mollusc – gastropod (freshwater)	6.7×10^{-4}	6.3×10^{-14}	9.2×10^{-4}	1.3×10^{-5}	3.5×10^{-6}	6.3×10^{-7}	8.8×10^{-4}	1.7×10^{-7}	9.8×10^{-9}	1.4×10^{-4}	2.2×10^{-5}	2.1×10^{-5}	2.2×10^{-9}	5.5×10^{-9}	5.5×10^{-7}	2.7×10^{-7}	5.2×10^{-7}
Pelagic fish (freshwater)	6.0×10^{-4}	3.8×10^{-13}	8.2×10^{-4}	7.8×10^{-6}	8.4×10^{-7}	1.5×10^{-7}	7.9×10^{-4}	3.1×10^{-8}	1.2×10^{-9}	1.2×10^{-4}	1.7×10^{-5}	4.0×10^{-6}	1.6×10^{-1}	4.9×10^{-9}	1.4×10^{-7}	8.9×10^{-8}	1.4×10^{-7}
Pelagic fish (marine)	6.1×10^{-4}	1.1×10^{-14}	8.4×10^{-4}	8.7×10^{-6}	1.1×10^{-6}	2.0×10^{-7}	8.1×10^{-4}	3.8×10^{-8}	1.8×10^{-9}	1.2×10^{-4}	1.8×10^{-5}	5.0×10^{-6}	3.9×10^{-1}	5.0×10^{-9}	1.8×10^{-7}	1.1×10^{-7}	1.7×10^{-7}
Phytoplankton (freshwater)	7.1×10^{-4}	1.9×10^{-1}	9.6×10^{-4}	1.6×10^{-5}	5.8×10^{-6}	1.2×10^{-6}	9.3×10^{-4}	7.6×10^{-7}	1.2×10^{-7}	1.7×10^{-4}	2.6×10^{-5}	1.7×10^{-4}	1.6×10^{-8}	5.7×10^{-9}	1.0×10^{-6}	4.9×10^{-7}	9.9×10^{-7}
Phytoplankton (marine)	7.1×10^{-4}	1.9×10^{-1}	9.6×10^{-4}	1.6×10^{-5}	5.8×10^{-6}	1.2×10^{-6}	9.3×10^{-4}	7.6×10^{-7}	1.2×10^{-7}	1.7×10^{-4}	2.6×10^{-5}	1.7×10^{-4}	1.6×10^{-8}	5.7×10^{-9}	1.0×10^{-6}	4.9×10^{-7}	9.9×10^{-7}
Polychaete worm	6.7×10^{-4}	3.0×10^{-12}	9.2×10^{-4}	1.3×10^{-5}	3.2×10^{-6}	5.8×10^{-7}	8.8×10^{-4}	1.3×10^{-7}	4.9×10^{-9}	1.4×10^{-4}	2.2×10^{-5}	2.2×10^{-5}	6.5×10^{-1}	5.5×10^{-9}	5.1×10^{-7}	2.5×10^{-7}	4.8×10^{-7}
Reptile (freshwater)	5.9×10^{-4}	8.8×10^{-15}	8.1×10^{-4}	7.5×10^{-6}	8.4×10^{-7}	1.5×10^{-7}	7.8×10^{-4}	3.3×10^{-8}	1.5×10^{-9}	1.2×10^{-4}	1.7×10^{-5}	4.2×10^{-6}	3.2×10^{-1}	4.9×10^{-9}	1.4×10^{-7}	8.9×10^{-8}	1.4×10^{-7}
Vascular plant (freshwater)	7.0×10^{-4}	1.8×10^{-9}	9.5×10^{-4}	1.5×10^{-5}	5.4×10^{-6}	1.1×10^{-6}	9.2×10^{-4}	6.2×10^{-7}	6.4×10^{-8}	1.6×10^{-4}	2.5×10^{-5}	9.6×10^{-5}	9.7×10^{-9}	5.6×10^{-9}	9.3×10^{-7}	4.4×10^{-7}	8.9×10^{-7}
Vascular plant (marine)	6.6×10^{-4}	2.8×10^{-12}	9.0×10^{-4}	1.2×10^{-5}	2.5×10^{-6}	4.6×10^{-7}	8.7×10^{-4}	9.2×10^{-8}	4.2×10^{-9}	1.4×10^{-4}	2.1×10^{-5}	1.2×10^{-5}	5.6×10^{-1}	5.4×10^{-9}	4.0×10^{-7}	2.0×10^{-7}	3.8×10^{-7}
Zooplankton (freshwater)	7.1×10^{-4}	1.3×10^{-1}	9.5×10^{-4}	1.6×10^{-5}	5.7×10^{-6}	1.2×10^{-6}	9.3×10^{-4}	7.2×10^{-7}	9.1×10^{-8}	1.7×10^{-4}	2.6×10^{-5}	1.5×10^{-4}	1.3×10^{-8}	5.6×10^{-9}	1.0×10^{-6}	4.7×10^{-7}	9.6×10^{-7}
Zooplankton (marine)	6.9×10^{-4}	2.2×10^{-13}	9.4×10^{-4}	1.4×10^{-5}	5.1×10^{-6}	9.7×10^{-7}	9.1×10^{-4}	4.8×10^{-7}	3.7×10^{-8}	1.5×10^{-4}	2.4×10^{-5}	7.2×10^{-5}	8.6×10^{-9}	5.6×10^{-9}	8.6×10^{-7}	4.0×10^{-7}	8.2×10^{-7}
$DCC_{ext,in,soil}$																	
Amphibian (terrestrial)	5.8×10^{-4}		8.3×10^{-4}	3.5×10^{-6}	9.6×10^{-7}	1.7×10^{-7}	8.2×10^{-4}	1.0×10^{-7}		1.0×10^{-4}	1.6×10^{-5}	6.0×10^{-7}		5.1×10^{-9}	1.6×10^{-7}	9.0×10^{-8}	1.5×10^{-7}
Annelid	5.9×10^{-4}		8.4×10^{-4}	3.6×10^{-6}	1.0×10^{-6}	1.8×10^{-7}	8.3×10^{-4}	1.0×10^{-7}		1.0×10^{-4}	1.6×10^{-5}	6.1×10^{-7}		5.2×10^{-9}	1.7×10^{-7}	9.3×10^{-8}	1.6×10^{-7}
Arthropod – detritivorous	6.0×10^{-4}		8.4×10^{-4}	3.6×10^{-6}	1.0×10^{-6}	1.8×10^{-7}	8.4×10^{-4}	1.1×10^{-7}		1.0×10^{-4}	1.6×10^{-5}	6.2×10^{-7}		5.2×10^{-9}	1.7×10^{-7}	9.5×10^{-8}	1.6×10^{-7}
Mammal – small-burrowing	5.6×10^{-4}		7.9×10^{-4}	3.1×10^{-6}	8.1×10^{-7}	1.5×10^{-7}	7.8×10^{-4}	8.5×10^{-8}		9.7×10^{-5}	1.5×10^{-5}	5.4×10^{-7}		4.9×10^{-9}	1.4×10^{-7}	7.9×10^{-8}	1.3×10^{-7}
Mollusc – gastropod (terrestrial)	5.9×10^{-4}		8.4×10^{-4}	3.6×10^{-6}	1.0×10^{-6}	1.8×10^{-7}	8.4×10^{-4}	1.1×10^{-7}		1.0×10^{-4}	1.6×10^{-5}	6.2×10^{-7}		5.2×10^{-9}	1.7×10^{-7}	9.4×10^{-8}	1.6×10^{-7}
Reptile (terrestrial)	5.4×10^{-4}		7.5×10^{-4}	2.8×10^{-6}	6.9×10^{-7}	1.2×10^{-7}	7.5×10^{-4}	7.3×10^{-8}		9.3×10^{-5}	1.4×10^{-5}	4.9×10^{-7}		4.7×10^{-9}	1.2×10^{-7}	7.0×10^{-8}	1.1×10^{-7}

Table E-5. Continued.

	Eu-152	H-3	Ho-166m	I-129	Mo-93	Nb-93m	Nb-94	Ni-59	Ni-63	Np-237	Pa-231	Pb-210	Pd-107	Po-210	Pu-238	Pu-239	Pu-240
$DCC_{ext,on,soil}$																	
Amphibian (terrestrial)	2.3×10^{-4}		3.6×10^{-4}	1.3×10^{-6}	3.2×10^{-7}	6.1×10^{-8}	3.4×10^{-4}	6.4×10^{-9}		4.1×10^{-5}	6.8×10^{-6}	1.8×10^{-7}		2.5×10^{-9}	5.2×10^{-8}	3.3×10^{-8}	5.0×10^{-8}
Arthropod – detritivorous	2.0×10^{-4}		3.4×10^{-4}	1.5×10^{-6}	6.3×10^{-7}	1.2×10^{-7}	3.2×10^{-4}	1.3×10^{-8}		4.1×10^{-5}	7.1×10^{-6}	2.5×10^{-7}		2.3×10^{-9}	1.0×10^{-7}	5.7×10^{-8}	9.8×10^{-8}
Bird (terrestrial)	2.3×10^{-4}		3.5×10^{-4}	9.2×10^{-7}	1.2×10^{-7}	2.2×10^{-8}	3.3×10^{-4}	4.6×10^{-9}		3.8×10^{-5}	6.3×10^{-6}	1.4×10^{-7}		2.4×10^{-9}	2.1×10^{-8}	1.9×10^{-8}	2.0×10^{-8}
Flying insects	2.1×10^{-4}		3.5×10^{-4}	1.5×10^{-6}	5.8×10^{-7}	1.1×10^{-7}	3.3×10^{-4}	1.1×10^{-8}		4.1×10^{-5}	7.0×10^{-6}	2.4×10^{-7}		2.4×10^{-9}	9.4×10^{-8}	5.2×10^{-8}	8.9×10^{-8}
Grasses & Herbs	2.2×10^{-4}		3.2×10^{-4}	2.0×10^{-6}	7.9×10^{-7}	1.4×10^{-7}	3.1×10^{-4}	1.2×10^{-7}		4.6×10^{-5}	7.1×10^{-6}	4.1×10^{-7}		1.9×10^{-9}	1.3×10^{-7}	6.7×10^{-8}	1.3×10^{-7}
Lichen & Bryophytes	2.0×10^{-4}		3.4×10^{-4}	1.5×10^{-6}	6.3×10^{-7}	1.2×10^{-7}	3.2×10^{-4}	1.3×10^{-8}		4.1×10^{-5}	7.1×10^{-6}	2.5×10^{-7}		2.3×10^{-9}	1.0×10^{-7}	5.7×10^{-8}	9.8×10^{-8}
Mammal – large	1.5×10^{-4}		2.2×10^{-4}	2.3×10^{-7}	2.0×10^{-8}	3.8×10^{-9}	2.2×10^{-4}	2.5×10^{-9}		2.3×10^{-5}	3.7×10^{-6}	4.6×10^{-8}		1.6×10^{-9}	4.2×10^{-9}	7.4×10^{-9}	4.4×10^{-9}
Mammal – small-burrowing	2.3×10^{-4}		3.5×10^{-4}	1.1×10^{-6}	1.8×10^{-7}	3.3×10^{-8}	3.4×10^{-4}	5.1×10^{-9}		3.9×10^{-5}	6.5×10^{-6}	1.5×10^{-7}		2.5×10^{-9}	3.0×10^{-8}	2.3×10^{-8}	2.9×10^{-8}
Mollusc – gastropod (terrestrial)	2.2×10^{-4}		3.5×10^{-4}	1.5×10^{-6}	5.4×10^{-7}	1.0×10^{-7}	3.4×10^{-4}	9.8×10^{-9}		4.1×10^{-5}	7.0×10^{-6}	2.2×10^{-7}		2.4×10^{-9}	8.6×10^{-8}	4.8×10^{-8}	8.2×10^{-8}
Reptile (terrestrial)	2.3×10^{-4}		3.5×10^{-4}	1.0×10^{-6}	1.4×10^{-7}	2.6×10^{-8}	3.3×10^{-4}	4.8×10^{-9}		3.9×10^{-5}	6.4×10^{-6}	1.4×10^{-7}		2.4×10^{-9}	2.4×10^{-8}	2.1×10^{-8}	2.3×10^{-8}
Shrub	2.1×10^{-4}		3.0×10^{-4}	1.6×10^{-6}	3.6×10^{-7}	6.3×10^{-8}	2.9×10^{-4}	1.2×10^{-8}		4.2×10^{-5}	6.3×10^{-6}	2.1×10^{-7}		1.8×10^{-9}	5.6×10^{-8}	3.3×10^{-8}	5.3×10^{-8}
Tree	1.8×10^{-4}		2.6×10^{-4}	8.9×10^{-7}	5.2×10^{-8}	9.3×10^{-9}	2.5×10^{-4}	2.5×10^{-9}		3.5×10^{-5}	5.2×10^{-6}	1.4×10^{-7}		1.5×10^{-9}	1.0×10^{-8}	1.2×10^{-8}	9.8×10^{-9}

Table E-5. Continued. External dose conversion coefficients (DCC, (μGy h^{-1})/(Bq $kgdw^{-1}$)) for non-human biota. White background indicates no change from SR-PSU, fully saturated red and blue backgrounds correspond to an increase or decrease, respectively, of at least one order of magnitude since SR-PSU. Paler colours represent smaller corresponding changes. Grey background specifies no data in SR-PSU.

	Pu-241	Pu-242	Ra-226	Se-79	Sm-151	Sn-126	Sr-90	Tc-99	Th-229	Th-230	U-232	U-233	U-234	U-235	U-236	U-238	Zr-93
$DCC_{ext,in,air}$																	
Bird (terrestrial)	7.0×10^{-1}	2.2×10^{-8}	3.0×10^{-4}		8.7×10^{-11}	4.1×10^{-4}	7.3×10^{-12}	7.3×10^{-11}	5.2×10^{-5}	5.2×10^{-8}	2.7×10^{-4}	3.9×10^{-8}	1.8×10^{-8}	2.8×10^{-5}	1.0×10^{-8}	4.7×10^{-6}	
Flying insects	8.2×10^{-1}	8.8×10^{-8}	2.9×10^{-4}		5.3×10^{-1}	4.5×10^{-4}	5.5×10^{-11}	8.7×10^{-11}	5.9×10^{-5}	9.7×10^{-8}	2.2×10^{-4}	8.5×10^{-8}	9.6×10^{-8}	3.2×10^{-5}	8.0×10^{-8}	5.1×10^{-6}	
$DCC_{ext,in,water}$																	
Amphibian (freshwater)	2.7×10^{-9}	3.5×10^{-7}	1.0×10^{-3}	6.7×10^{-8}	8.4×10^{-9}	1.1×10^{-3}	6.3×10^{-5}	3.8×10^{-7}	1.9×10^{-4}	4.1×10^{-7}	8.6×10^{-4}	2.9×10^{-7}	3.7×10^{-7}	1.0×10^{-4}	3.0×10^{-7}	6.3×10^{-5}	4.7×10^{-9}
Benthic fish (freshwater)	2.3×10^{-9}	1.5×10^{-7}	8.9×10^{-4}	2.0×10^{-8}	2.7×10^{-9}	1.0×10^{-3}	2.1×10^{-5}	1.2×10^{-7}	1.6×10^{-4}	2.4×10^{-7}	7.7×10^{-4}	1.7×10^{-7}	1.5×10^{-7}	8.6×10^{-5}	1.2×10^{-7}	3.0×10^{-5}	1.3×10^{-9}
Benthic fish (marine)	2.5×10^{-9}	2.0×10^{-7}	9.5×10^{-4}	2.0×10^{-8}	3.2×10^{-9}	1.1×10^{-3}	5.0×10^{-5}	1.3×10^{-7}	1.7×10^{-4}	2.8×10^{-7}	8.1×10^{-4}	2.0×10^{-7}	2.0×10^{-7}	9.2×10^{-5}	1.6×10^{-7}	5.1×10^{-5}	1.3×10^{-9}
Bird (freshwater)	2.3×10^{-9}	1.5×10^{-7}	8.9×10^{-4}	2.1×10^{-8}	2.7×10^{-9}	9.9×10^{-4}	2.0×10^{-5}	1.2×10^{-7}	1.6×10^{-4}	2.4×10^{-7}	7.6×10^{-4}	1.7×10^{-7}	1.5×10^{-7}	8.5×10^{-5}	1.2×10^{-7}	2.9×10^{-5}	1.4×10^{-9}
Bird (marine)	2.3×10^{-9}	1.5×10^{-7}	8.9×10^{-4}	2.1×10^{-8}	2.7×10^{-9}	9.9×10^{-4}	2.0×10^{-5}	1.2×10^{-7}	1.6×10^{-4}	2.4×10^{-7}	7.6×10^{-4}	1.7×10^{-7}	1.5×10^{-7}	8.5×10^{-5}	1.2×10^{-7}	2.9×10^{-5}	1.4×10^{-9}
Crustacean (freshwater)	3.2×10^{-9}	8.6×10^{-7}	1.3×10^{-3}	1.0×10^{-6}	8.7×10^{-8}	1.4×10^{-3}	4.5×10^{-4}	5.7×10^{-6}	3.7×10^{-4}	9.3×10^{-7}	1.2×10^{-3}	6.2×10^{-7}	9.5×10^{-7}	1.1×10^{-4}	8.3×10^{-7}	3.7×10^{-4}	7.0×10^{-8}
Crustacean (marine)	2.4×10^{-9}	1.7×10^{-7}	9.1×10^{-4}	2.4×10^{-8}	3.5×10^{-9}	1.0×10^{-3}	2.3×10^{-5}	1.4×10^{-7}	1.6×10^{-4}	2.6×10^{-7}	7.8×10^{-4}	1.8×10^{-7}	1.7×10^{-7}	8.8×10^{-5}	1.3×10^{-7}	3.1×10^{-5}	1.9×10^{-9}
Insect larvae	3.2×10^{-9}	8.5×10^{-7}	1.3×10^{-3}	9.4×10^{-7}	8.2×10^{-8}	1.4×10^{-3}	4.4×10^{-4}	5.3×10^{-6}	3.6×10^{-4}	9.2×10^{-7}	1.1×10^{-3}	6.2×10^{-7}	9.4×10^{-7}	1.1×10^{-4}	8.2×10^{-7}	3.7×10^{-4}	6.6×10^{-8}
Macroalgae	5.0×10^{-9}	4.2×10^{-7}	1.1×10^{-3}	2.4×10^{-7}	3.1×10^{-8}	1.2×10^{-3}	1.9×10^{-4}	1.3×10^{-6}	2.3×10^{-4}	4.7×10^{-7}	9.5×10^{-4}	3.3×10^{-7}	4.3×10^{-7}	1.0×10^{-4}	3.6×10^{-7}	1.6×10^{-4}	2.5×10^{-8}
Mammal (freshwater)	2.1×10^{-9}	1.1×10^{-7}	8.2×10^{-4}	1.4×10^{-8}	1.9×10^{-9}	9.0×10^{-4}	1.4×10^{-5}	8.5×10^{-8}	1.4×10^{-4}	2.0×10^{-7}	7.1×10^{-4}	1.4×10^{-7}	1.1×10^{-7}	7.6×10^{-5}	8.4×10^{-8}	2.3×10^{-5}	9.2×10^{-1}
Mammal (marine)	9.1×10^{-1}	4.5×10^{-8}	4.9×10^{-4}	4.1×10^{-9}	4.8×10^{-1}	5.0×10^{-4}	4.2×10^{-6}	2.4×10^{-8}	7.0×10^{-5}	7.9×10^{-8}	4.5×10^{-4}	5.7×10^{-8}	3.9×10^{-8}	3.6×10^{-5}	2.7×10^{-8}	9.7×10^{-6}	2.2×10^{-1}
Microphytobenthos	3.8×10^{-9}	9.1×10^{-7}	1.4×10^{-3}	1.9×10^{-6}	1.7×10^{-7}	1.5×10^{-3}	5.4×10^{-4}	1.1×10^{-5}	4.6×10^{-4}	1.1×10^{-6}	1.2×10^{-3}	6.7×10^{-7}	1.1×10^{-6}	1.2×10^{-4}	9.3×10^{-7}	4.4×10^{-4}	1.4×10^{-7}
Mollusc – bivalve (freshwater)	2.7×10^{-9}	3.0×10^{-7}	9.9×10^{-4}	5.1×10^{-8}	6.6×10^{-9}	1.1×10^{-3}	4.9×10^{-5}	2.9×10^{-7}	1.8×10^{-4}	3.7×10^{-7}	8.4×10^{-4}	2.6×10^{-7}	3.1×10^{-7}	9.7×10^{-5}	2.5×10^{-7}	5.2×10^{-5}	3.5×10^{-9}
Mollusc – bivalve (marine)	2.8×10^{-9}	3.9×10^{-7}	1.0×10^{-3}	8.2×10^{-8}	1.0×10^{-8}	1.1×10^{-3}	7.7×10^{-5}	4.6×10^{-7}	2.0×10^{-4}	4.4×10^{-7}	8.7×10^{-4}	3.2×10^{-7}	4.1×10^{-7}	1.0×10^{-4}	3.4×10^{-7}	7.4×10^{-5}	5.8×10^{-9}
Mollusc – gastropod (freshwater)	2.9×10^{-9}	5.0×10^{-7}	1.1×10^{-3}	1.3×10^{-7}	1.7×10^{-8}	1.2×10^{-3}	1.2×10^{-4}	7.4×10^{-7}	2.1×10^{-4}	5.3×10^{-7}	9.1×10^{-4}	3.8×10^{-7}	5.3×10^{-7}	1.0×10^{-4}	4.5×10^{-7}	1.1×10^{-4}	1.1×10^{-8}
Pelagic fish (freshwater)	2.4×10^{-9}	1.6×10^{-7}	9.0×10^{-4}	2.1×10^{-8}	2.8×10^{-9}	1.0×10^{-3}	2.3×10^{-5}	1.2×10^{-7}	1.6×10^{-4}	2.5×10^{-7}	7.7×10^{-4}	1.8×10^{-7}	1.6×10^{-7}	8.7×10^{-5}	1.2×10^{-7}	3.1×10^{-5}	1.4×10^{-9}
Pelagic fish (marine)	2.5×10^{-9}	1.9×10^{-7}	9.3×10^{-4}	2.7×10^{-8}	3.9×10^{-9}	1.0×10^{-3}	2.7×10^{-5}	1.5×10^{-7}	1.7×10^{-4}	2.8×10^{-7}	7.9×10^{-4}	2.0×10^{-7}	1.9×10^{-7}	9.1×10^{-5}	1.5×10^{-7}	3.5×10^{-5}	2.1×10^{-9}
Phytoplankton (freshwater)	3.8×10^{-9}	9.1×10^{-7}	1.4×10^{-3}	1.9×10^{-6}	1.7×10^{-7}	1.5×10^{-3}	5.4×10^{-4}	1.1×10^{-5}	4.6×10^{-4}	1.1×10^{-6}	1.2×10^{-3}	6.7×10^{-7}	1.1×10^{-6}	1.2×10^{-4}	9.3×10^{-7}	4.4×10^{-4}	1.4×10^{-7}
Phytoplankton (marine)	3.8×10^{-9}	9.1×10^{-7}	1.4×10^{-3}	1.9×10^{-6}	1.7×10^{-7}	1.5×10^{-3}	5.4×10^{-4}	1.1×10^{-5}	4.6×10^{-4}	1.1×10^{-6}	1.2×10^{-3}	6.7×10^{-7}	1.1×10^{-6}	1.2×10^{-4}	9.3×10^{-7}	4.4×10^{-4}	1.4×10^{-7}
Polychaete worm	2.8×10^{-9}	4.6×10^{-7}	1.1×10^{-3}	8.2×10^{-8}	1.0×10^{-8}	1.2×10^{-3}	1.1×10^{-4}	5.0×10^{-7}	2.1×10^{-4}	4.9×10^{-7}	9.0×10^{-4}	3.6×10^{-7}	4.8×10^{-7}	1.0×10^{-4}	4.1×10^{-7}	1.0×10^{-4}	5.7×10^{-9}
Reptile (freshwater)	2.4×10^{-9}	1.6×10^{-7}	9.0×10^{-4}	2.2×10^{-8}	3.2×10^{-9}	1.0×10^{-3}	2.1×10^{-5}	1.3×10^{-7}	1.6×10^{-4}	2.5×10^{-7}	7.7×10^{-4}	1.7×10^{-7}	1.6×10^{-7}	8.7×10^{-5}	1.2×10^{-7}	3.0×10^{-5}	1.8×10^{-9}
Vascular plant (freshwater)	5.0×10^{-9}	8.2×10^{-7}	1.3×10^{-3}	1.3×10^{-6}	1.0×10^{-7}	1.4×10^{-3}	3.7×10^{-4}	7.7×10^{-6}	3.5×10^{-4}	9.5×10^{-7}	1.1×10^{-3}	6.0×10^{-7}	9.5×10^{-7}	1.1×10^{-4}	8.1×10^{-7}	3.0×10^{-4}	7.5×10^{-8}
Vascular plant (marine)	2.8×10^{-9}	3.7×10^{-7}	1.0×10^{-3}	7.1×10^{-8}	8.9×10^{-9}	1.1×10^{-3}	6.9×10^{-5}	4.0×10^{-7}	1.9×10^{-4}	4.2×10^{-7}	8.6×10^{-4}	3.1×10^{-7}	3.9×10^{-7}	1.0×10^{-4}	3.2×10^{-7}	6.8×10^{-5}	5.0×10^{-9}
Zooplankton (freshwater)	3.6×10^{-9}	8.8×10^{-7}	1.4×10^{-3}	1.5×10^{-6}	1.4×10^{-7}	1.5×10^{-3}	5.1×10^{-4}	8.5×10^{-6}	4.3×10^{-4}	1.0×10^{-6}	1.2×10^{-3}	6.5×10^{-7}	1.0×10^{-6}	1.2×10^{-4}	8.9×10^{-7}	4.2×10^{-4}	1.1×10^{-7}
Zooplankton (marine)	3.0×10^{-9}	7.6×10^{-7}	1.2×10^{-3}	4.9×10^{-7}	5.5×10^{-8}	1.4×10^{-3}	3.6×10^{-4}	2.8×10^{-6}	3.0×10^{-4}	8.0×10^{-7}	1.1×10^{-3}	5.5×10^{-7}	8.3×10^{-7}	1.1×10^{-4}	7.2×10^{-7}	3.0×10^{-4}	4.4×10^{-8}
$DCC_{ext,in,soil}$																	
Amphibian (terrestrial)	1.6×10^{-9}	1.7×10^{-7}	8.8×10^{-4}		1.0×10^{-9}	1.0×10^{-3}	1.2×10^{-1}	1.7×10^{-1}	1.3×10^{-4}	2.1×10^{-7}	7.3×10^{-4}	1.6×10^{-7}	1.7×10^{-7}	7.0×10^{-5}	1.4×10^{-7}	1.2×10^{-5}	
Annelid	1.6×10^{-9}	1.7×10^{-7}	8.9×10^{-4}		1.0×10^{-9}	1.0×10^{-3}	1.2×10^{-1}	1.7×10^{-1}	1.4×10^{-4}	2.1×10^{-7}	7.4×10^{-4}	1.6×10^{-7}	1.7×10^{-7}	7.1×10^{-5}	1.4×10^{-7}	1.2×10^{-5}	
Arthropod – detritivorous	1.6×10^{-9}	1.8×10^{-7}	8.9×10^{-4}		1.1×10^{-9}	1.1×10^{-3}	1.3×10^{-1}	1.7×10^{-1}	1.4×10^{-4}	2.2×10^{-7}	7.4×10^{-4}	1.7×10^{-7}	1.8×10^{-7}	7.1×10^{-5}	1.5×10^{-7}	1.2×10^{-5}	
Mammal – small-burrowing	1.5×10^{-9}	1.5×10^{-7}	8.4×10^{-4}		8.6×10^{-1}	9.8×10^{-4}	1.0×10^{-1}	1.6×10^{-1}	1.3×10^{-4}	1.9×10^{-7}	7.0×10^{-4}	1.4×10^{-7}	1.5×10^{-7}	6.6×10^{-5}	1.2×10^{-7}	1.1×10^{-5}	
Mollusc – gastropod (terrestrial)	1.6×10^{-9}	1.8×10^{-7}	8.9×10^{-4}		1.1×10^{-9}	1.0×10^{-3}	1.2×10^{-1}	1.7×10^{-1}	1.4×10^{-4}	2.2×10^{-7}	7.4×10^{-4}	1.7×10^{-7}	1.8×10^{-7}	7.1×10^{-5}	1.5×10^{-7}	1.2×10^{-5}	
Reptile (terrestrial)	1.5×10^{-9}	1.3×10^{-7}	8.1×10^{-4}		7.4×10^{-1}	9.4×10^{-4}	8.9×10^{-11}	1.5×10^{-1}	1.2×10^{-4}	1.7×10^{-7}	6.7×10^{-4}	1.3×10^{-7}	1.3×10^{-7}	6.3×10^{-5}	1.0×10^{-7}	1.1×10^{-5}	

Table E-5. Continued.

	Pu-241	Pu-242	Ra-226	Se-79	Sm-151	Sn-126	Sr-90	Tc-99	Th-229	Th-230	U-232	U-233	U-234	U-235	U-236	U-238	Zr-93
$DCC_{ext,on,soil}$																	
Amphibian (terrestrial)	8.0×10^{-1}	5.7×10^{-8}	3.3×10^{-4}		3.4×10^{-1}	4.6×10^{-4}	3.1×10^{-11}	8.4×10^{-11}	5.9×10^{-5}	7.7×10^{-8}	2.8×10^{-4}	6.3×10^{-8}	5.5×10^{-8}	3.1×10^{-5}	4.3×10^{-8}	5.3×10^{-6}	
Arthropod – detritivorous	8.2×10^{-1}	9.4×10^{-8}	2.6×10^{-4}		5.8×10^{-1}	4.4×10^{-4}	6.0×10^{-11}	8.7×10^{-11}	5.8×10^{-5}	1.0×10^{-7}	1.9×10^{-4}	9.1×10^{-8}	1.1×10^{-7}	3.2×10^{-5}	8.9×10^{-8}	4.9×10^{-6}	
Bird (terrestrial)	7.5×10^{-1}	3.2×10^{-8}	3.3×10^{-4}		1.5×10^{-1}	4.4×10^{-4}	1.5×10^{-11}	7.9×10^{-11}	5.6×10^{-5}	6.1×10^{-8}	2.9×10^{-4}	4.7×10^{-8}	2.8×10^{-8}	3.0×10^{-5}	1.9×10^{-8}	5.1×10^{-6}	
Flying insects	8.2×10^{-1}	8.8×10^{-8}	2.9×10^{-4}		5.3×10^{-1}	4.5×10^{-4}	5.5×10^{-11}	8.7×10^{-11}	5.9×10^{-5}	9.7×10^{-8}	2.2×10^{-4}	8.5×10^{-8}	9.6×10^{-8}	3.2×10^{-5}	8.0×10^{-8}	5.1×10^{-6}	
Grasses & Herbs	8.1×10^{-1}	1.2×10^{-7}	3.3×10^{-4}		8.7×10^{-1}	4.0×10^{-4}	9.4×10^{-11}	9.4×10^{-11}	5.7×10^{-5}	1.4×10^{-7}	2.6×10^{-4}	1.1×10^{-7}	1.4×10^{-7}	3.2×10^{-5}	1.2×10^{-7}	5.0×10^{-6}	
Lichen & Bryophytes	8.2×10^{-1}	9.4×10^{-8}	2.6×10^{-4}		5.8×10^{-1}	4.4×10^{-4}	6.0×10^{-11}	8.7×10^{-11}	5.8×10^{-5}	1.0×10^{-7}	1.9×10^{-4}	9.1×10^{-8}	1.1×10^{-7}	3.2×10^{-5}	8.9×10^{-8}	4.9×10^{-6}	
Mammal – large	4.1×10^{-1}	1.4×10^{-8}	2.3×10^{-4}		2.9×10^{-11}	2.8×10^{-4}	5.8×10^{-12}	4.0×10^{-11}	3.4×10^{-5}	2.9×10^{-8}	2.1×10^{-4}	2.3×10^{-8}	9.1×10^{-9}	1.7×10^{-5}	5.0×10^{-9}	3.2×10^{-6}	
Mammal – small-burrowing	7.8×10^{-1}	3.9×10^{-8}	3.3×10^{-4}		2.2×10^{-1}	4.5×10^{-4}	2.0×10^{-11}	8.1×10^{-11}	5.8×10^{-5}	6.7×10^{-8}	2.9×10^{-4}	5.2×10^{-8}	3.6×10^{-8}	3.1×10^{-5}	2.6×10^{-8}	5.2×10^{-6}	
Mollusc – gastropod (terrestrial)	8.1×10^{-1}	8.2×10^{-8}	3.0×10^{-4}		4.9×10^{-1}	4.6×10^{-4}	5.1×10^{-11}	8.6×10^{-11}	5.9×10^{-5}	9.3×10^{-8}	2.4×10^{-4}	8.1×10^{-8}	8.8×10^{-8}	3.2×10^{-5}	7.3×10^{-8}	5.2×10^{-6}	
Reptile (terrestrial)	7.6×10^{-1}	3.4×10^{-8}	3.3×10^{-4}		1.8×10^{-1}	4.5×10^{-4}	1.6×10^{-11}	8.0×10^{-11}	5.7×10^{-5}	6.3×10^{-8}	2.9×10^{-4}	4.9×10^{-8}	3.1×10^{-8}	3.0×10^{-5}	2.1×10^{-8}	5.1×10^{-6}	
Shrub	7.4×10^{-1}	5.8×10^{-8}	3.1×10^{-4}		3.5×10^{-1}	3.7×10^{-4}	4.1×10^{-11}	8.5×10^{-11}	5.3×10^{-5}	7.9×10^{-8}	2.5×10^{-4}	6.1×10^{-8}	5.9×10^{-8}	3.0×10^{-5}	4.7×10^{-8}	4.6×10^{-6}	
Tree	6.2×10^{-1}	2.0×10^{-8}	2.7×10^{-4}		9.5×10^{-11}	3.2×10^{-4}	8.5×10^{-12}	7.0×10^{-11}	4.5×10^{-5}	4.6×10^{-8}	2.2×10^{-4}	3.5×10^{-8}	1.8×10^{-8}	2.5×10^{-5}	1.1×10^{-8}	3.9×10^{-6}	

Table E-6. Internal dose conversion coefficients (DCC, (μGy h^{-1})/(Bq $kgfw^{-1}$)) for non-human biota. White background indicates no change from SR-PSU, fully saturated red and blue backgrounds correspond to an increase or decrease, respectively, of at least one order of magnitude since SR-PSU. Paler colours represent smaller corresponding changes. Grey background specifies no data in SR-PSU.

	Ac-227	Ag-108m	Am-241	Am-242m	Am-243	Ba-133	C-14	Ca-41	Cd-113m	Cl-36	Cm-243	Cm-244	Cm-245	Cm-246	Co-60	Cs-135	Cs-137
$DCC_{int,\alpha}$	1.5×10^{-2}		3.2×10^{-3}	3.0×10^{-3}	3.1×10^{-3}						3.4×10^{-3}	3.4×10^{-3}	3.1×10^{-3}	3.2×10^{-3}			
$DCC_{int,low,\beta}$	1.5×10^{-5}	1.8×10^{-6}	3.3×10^{-6}	4.8×10^{-6}	9.5×10^{-6}	4.3×10^{-6}	3.1×10^{-7}	1.6×10^{-6}	9.3×10^{-8}	6.3×10^{-8}	7.1×10^{-6}	5.5×10^{-7}	4.2×10^{-6}	4.4×10^{-7}	1.9×10^{-7}	1.9×10^{-7}	3.4×10^{-7}
$DCC_{int,\beta,\gamma}$																	
Amphibian	6.2×10^{-4}	7.9×10^{-5}	2.2×10^{-5}	1.3×10^{-4}	1.7×10^{-4}	4.1×10^{-5}	2.8×10^{-5}	2.8×10^{-7}	1.0×10^{-4}	1.5×10^{-4}	7.7×10^{-5}	4.6×10^{-6}	4.9×10^{-5}	4.8×10^{-6}	1.1×10^{-4}	5.1×10^{-5}	1.5×10^{-4}
Annelid	5.8×10^{-4}	5.2×10^{-5}	2.0×10^{-5}	1.3×10^{-4}	1.6×10^{-4}	3.4×10^{-5}	2.8×10^{-5}	2.7×10^{-7}	1.0×10^{-4}	1.5×10^{-4}	7.4×10^{-5}	4.4×10^{-6}	4.7×10^{-5}	4.4×10^{-6}	7.7×10^{-5}	5.1×10^{-5}	1.4×10^{-4}
Arthropod – detritivorous	4.7×10^{-4}	3.2×10^{-5}	1.9×10^{-5}	1.2×10^{-4}	1.5×10^{-4}	2.9×10^{-5}	2.8×10^{-5}	2.5×10^{-7}	9.6×10^{-5}	1.3×10^{-4}	7.0×10^{-5}	4.3×10^{-6}	4.5×10^{-5}	3.9×10^{-6}	5.9×10^{-5}	5.0×10^{-5}	1.2×10^{-4}
Benthic fish (freshwater)	6.7×10^{-4}	1.7×10^{-4}	2.5×10^{-5}	1.4×10^{-4}	1.8×10^{-4}	6.9×10^{-5}	2.8×10^{-5}	2.9×10^{-7}	1.1×10^{-4}	1.6×10^{-4}	8.6×10^{-5}	4.9×10^{-6}	5.7×10^{-5}	5.3×10^{-6}	2.3×10^{-4}	5.1×10^{-5}	1.9×10^{-4}
Benthic fish (marine)	6.5×10^{-4}	1.2×10^{-4}	2.4×10^{-5}	1.4×10^{-4}	1.8×10^{-4}	5.6×10^{-5}	2.8×10^{-5}	2.9×10^{-7}	1.1×10^{-4}	1.6×10^{-4}	8.2×10^{-5}	4.8×10^{-6}	5.4×10^{-5}	5.1×10^{-6}	1.7×10^{-4}	5.1×10^{-5}	1.7×10^{-4}
Bird	6.7×10^{-4}	1.8×10^{-4}	2.5×10^{-5}	1.4×10^{-4}	1.8×10^{-4}	7.1×10^{-5}	2.8×10^{-5}	2.9×10^{-7}	1.1×10^{-4}	1.6×10^{-4}	8.7×10^{-5}	4.9×10^{-6}	5.8×10^{-5}	5.3×10^{-6}	2.4×10^{-4}	5.1×10^{-5}	1.9×10^{-4}
Crustacean (freshwater)	3.2×10^{-4}	1.8×10^{-5}	1.9×10^{-5}	1.1×10^{-4}	1.4×10^{-4}	2.7×10^{-5}	2.7×10^{-5}	2.3×10^{-7}	8.2×10^{-5}	1.0×10^{-4}	6.6×10^{-5}	4.2×10^{-6}	4.3×10^{-5}	3.7×10^{-6}	5.1×10^{-5}	4.7×10^{-5}	9.6×10^{-5}
Crustacean (marine)	6.6×10^{-4}	1.6×10^{-4}	2.4×10^{-5}	1.4×10^{-4}	1.8×10^{-4}	6.5×10^{-5}	2.8×10^{-5}	2.9×10^{-7}	1.1×10^{-4}	1.6×10^{-4}	8.5×10^{-5}	4.9×10^{-6}	5.6×10^{-5}	5.3×10^{-6}	2.1×10^{-4}	5.1×10^{-5}	1.8×10^{-4}
Flying insects	5.3×10^{-4}	4.1×10^{-5}	2.0×10^{-5}	1.3×10^{-4}	1.6×10^{-4}	3.1×10^{-5}	2.8×10^{-5}	2.7×10^{-7}	1.0×10^{-4}	1.4×10^{-4}	7.2×10^{-5}	4.3×10^{-6}	4.6×10^{-5}	4.2×10^{-6}	6.5×10^{-5}	5.0×10^{-5}	1.3×10^{-4}
Grasses & Herbs	5.7×10^{-4}	5.0×10^{-5}	2.0×10^{-5}	1.3×10^{-4}	1.6×10^{-4}	3.3×10^{-5}	2.8×10^{-5}	2.7×10^{-7}	1.0×10^{-4}	1.5×10^{-4}	7.3×10^{-5}	4.4×10^{-6}	4.7×10^{-5}	4.4×10^{-6}	7.4×10^{-5}	5.1×10^{-5}	1.4×10^{-4}
Insect larvae	3.3×10^{-4}	1.8×10^{-5}	1.9×10^{-5}	1.1×10^{-4}	1.4×10^{-4}	2.7×10^{-5}	2.7×10^{-5}	2.3×10^{-7}	8.4×10^{-5}	1.1×10^{-4}	6.6×10^{-5}	4.2×10^{-6}	4.3×10^{-5}	3.7×10^{-6}	5.2×10^{-5}	4.7×10^{-5}	9.8×10^{-5}
Lichen & Bryophytes	4.4×10^{-4}	2.9×10^{-5}	1.9×10^{-5}	1.2×10^{-4}	1.5×10^{-4}	2.9×10^{-5}	2.8×10^{-5}	2.5×10^{-7}	9.2×10^{-5}	1.3×10^{-4}	6.9×10^{-5}	4.2×10^{-6}	4.4×10^{-5}	3.9×10^{-6}	5.6×10^{-5}	4.9×10^{-5}	1.2×10^{-4}
Macroalgae	5.5×10^{-4}	5.7×10^{-5}	2.1×10^{-5}	1.3×10^{-4}	1.6×10^{-4}	3.7×10^{-5}	2.8×10^{-5}	2.8×10^{-7}	1.0×10^{-4}	1.4×10^{-4}	7.4×10^{-5}	4.5×10^{-6}	4.8×10^{-5}	4.5×10^{-6}	8.7×10^{-5}	5.0×10^{-5}	1.4×10^{-4}
Mammal (freshwater)	6.9×10^{-4}	2.5×10^{-4}	2.6×10^{-5}	1.4×10^{-4}	2.0×10^{-4}	9.1×10^{-5}	2.8×10^{-5}	2.9×10^{-7}	1.1×10^{-4}	1.6×10^{-4}	9.3×10^{-5}	4.9×10^{-6}	6.3×10^{-5}	5.5×10^{-6}	3.3×10^{-4}	5.1×10^{-5}	2.1×10^{-4}
Mammal (marine)	7.8×10^{-4}	5.7×10^{-4}	3.2×10^{-5}	1.4×10^{-4}	2.5×10^{-4}	1.8×10^{-4}	2.8×10^{-5}	2.9×10^{-7}	1.1×10^{-4}	1.6×10^{-4}	1.2×10^{-4}	5.0×10^{-6}	8.7×10^{-5}	6.2×10^{-6}	7.8×10^{-4}	5.1×10^{-5}	3.3×10^{-4}
Mammal – large	7.9×10^{-4}	6.1×10^{-4}	3.2×10^{-5}	1.4×10^{-4}	2.6×10^{-4}	1.8×10^{-4}	2.8×10^{-5}	2.9×10^{-7}	1.1×10^{-4}	1.6×10^{-4}	1.2×10^{-4}	5.0×10^{-6}	8.9×10^{-5}	6.3×10^{-6}	8.5×10^{-4}	5.1×10^{-5}	3.4×10^{-4}
Mammal – small-burrowing	6.5×10^{-4}	1.3×10^{-4}	2.3×10^{-5}	1.4×10^{-4}	1.7×10^{-4}	5.6×10^{-5}	2.8×10^{-5}	2.9×10^{-7}	1.1×10^{-4}	1.6×10^{-4}	8.2×10^{-5}	4.8×10^{-6}	5.3×10^{-5}	5.1×10^{-6}	1.7×10^{-4}	5.1×10^{-5}	1.7×10^{-4}
Mollusc – bivalve (freshwater)	6.3×10^{-4}	9.2×10^{-5}	2.2×10^{-5}	1.3×10^{-4}	1.7×10^{-4}	4.5×10^{-5}	2.8×10^{-5}	2.8×10^{-7}	1.1×10^{-4}	1.5×10^{-4}	7.8×10^{-5}	4.7×10^{-6}	5.1×10^{-5}	4.9×10^{-6}	1.2×10^{-4}	5.1×10^{-5}	1.6×10^{-4}
Mollusc – bivalve (marine)	6.1×10^{-4}	7.1×10^{-5}	2.1×10^{-5}	1.3×10^{-4}	1.6×10^{-4}	3.9×10^{-5}	2.8×10^{-5}	2.8×10^{-7}	1.0×10^{-4}	1.5×10^{-4}	7.6×10^{-5}	4.6×10^{-6}	4.9×10^{-5}	4.7×10^{-6}	9.8×10^{-5}	5.1×10^{-5}	1.5×10^{-4}
Mollusc – gastropod (freshwater)	5.9×10^{-4}	5.5×10^{-5}	2.1×10^{-5}	1.3×10^{-4}	1.6×10^{-4}	3.4×10^{-5}	2.8×10^{-5}	2.8×10^{-7}	1.0×10^{-4}	1.5×10^{-4}	7.4×10^{-5}	4.5×10^{-6}	4.7×10^{-5}	4.5×10^{-6}	7.9×10^{-5}	5.1×10^{-5}	1.4×10^{-4}
Mollusc – gastropod (terrestrial)	5.6×10^{-4}	4.7×10^{-5}	2.0×10^{-5}	1.3×10^{-4}	1.6×10^{-4}	3.3×10^{-5}	2.8×10^{-5}	2.7×10^{-7}	1.0×10^{-4}	1.5×10^{-4}	7.3×10^{-5}	4.4×10^{-6}	4.6×10^{-5}	4.3×10^{-6}	7.1×10^{-5}	5.1×10^{-5}	1.4×10^{-4}
Pelagic fish (freshwater)	6.6×10^{-4}	1.6×10^{-4}	2.4×10^{-5}	1.4×10^{-4}	1.8×10^{-4}	6.7×10^{-5}	2.8×10^{-5}	2.9×10^{-7}	1.1×10^{-4}	1.6×10^{-4}	8.5×10^{-5}	4.9×10^{-6}	5.7×10^{-5}	5.3×10^{-6}	2.1×10^{-4}	5.1×10^{-5}	1.8×10^{-4}
Pelagic fish (marine)	6.6×10^{-4}	1.4×10^{-4}	2.4×10^{-5}	1.4×10^{-4}	1.8×10^{-4}	6.0×10^{-5}	2.8×10^{-5}	2.9×10^{-7}	1.1×10^{-4}	1.6×10^{-4}	8.3×10^{-5}	4.8×10^{-6}	5.5×10^{-5}	5.2×10^{-6}	1.9×10^{-4}	5.1×10^{-5}	1.8×10^{-4}
Phytoplankton & Microphytobenthos	2.0×10^{-4}	1.0×10^{-5}	1.9×10^{-5}	8.8×10^{-5}	1.3×10^{-4}	2.5×10^{-5}	2.7×10^{-5}	2.3×10^{-7}	6.1×10^{-5}	6.5×10^{-5}	6.0×10^{-5}	4.1×10^{-6}	4.1×10^{-5}	3.5×10^{-6}	4.5×10^{-5}	4.3×10^{-5}	6.6×10^{-5}
Polychaete worm	5.9×10^{-4}	5.9×10^{-5}	2.1×10^{-5}	1.3×10^{-4}	1.6×10^{-4}	3.6×10^{-5}	2.8×10^{-5}	2.8×10^{-7}	1.0×10^{-4}	1.5×10^{-4}	7.5×10^{-5}	4.5×10^{-6}	4.8×10^{-5}	4.6×10^{-6}	8.5×10^{-5}	5.1×10^{-5}	1.4×10^{-4}
Reptile (freshwater)	6.7×10^{-4}	1.7×10^{-4}	2.5×10^{-5}	1.4×10^{-4}	1.8×10^{-4}	6.9×10^{-5}	2.8×10^{-5}	2.9×10^{-7}	1.1×10^{-4}	1.6×10^{-4}	8.6×10^{-5}	4.9×10^{-6}	5.7×10^{-5}	5.3×10^{-6}	2.3×10^{-4}	5.1×10^{-5}	1.9×10^{-4}
Reptile (terrestrial)	6.4×10^{-4}	1.1×10^{-4}	2.3×10^{-5}	1.4×10^{-4}	1.7×10^{-4}	5.3×10^{-5}	2.8×10^{-5}	2.9×10^{-7}	1.1×10^{-4}	1.6×10^{-4}	8.1×10^{-5}	4.8×10^{-6}	5.3×10^{-5}	5.0×10^{-6}	1.5×10^{-4}	5.1×10^{-5}	1.7×10^{-4}
Shrub	5.7×10^{-4}	5.0×10^{-5}	2.0×10^{-5}	1.3×10^{-4}	1.6×10^{-4}	3.3×10^{-5}	2.8×10^{-5}	2.7×10^{-7}	1.0×10^{-4}	1.5×10^{-4}	7.3×10^{-5}	4.4×10^{-6}	4.7×10^{-5}	4.4×10^{-6}	7.4×10^{-5}	5.1×10^{-5}	1.4×10^{-4}
Tree	7.8×10^{-4}	5.7×10^{-4}	3.2×10^{-5}	1.4×10^{-4}	2.6×10^{-4}	1.8×10^{-4}	2.8×10^{-5}	2.9×10^{-7}	1.1×10^{-4}	1.6×10^{-4}	1.3×10^{-4}	5.0×10^{-6}	9.0×10^{-5}	6.2×10^{-6}	7.3×10^{-4}	5.1×10^{-5}	3.2×10^{-4}
Vascular plant (freshwater)	3.8×10^{-4}	2.4×10^{-5}	1.9×10^{-5}	1.0×10^{-4}	1.4×10^{-4}	2.7×10^{-5}	2.7×10^{-5}	2.4×10^{-7}	7.8×10^{-5}	1.0×10^{-4}	6.4×10^{-5}	4.2×10^{-6}	4.2×10^{-5}	3.8×10^{-6}	5.2×10^{-5}	4.6×10^{-5}	9.8×10^{-5}
Vascular plant (marine)	6.2×10^{-4}	7.4×10^{-5}	2.1×10^{-5}	1.3×10^{-4}	1.6×10^{-4}	4.0×10^{-5}	2.8×10^{-5}	2.8×10^{-7}	1.0×10^{-4}	1.5×10^{-4}	7.6×10^{-5}	4.6×10^{-6}	4.9×10^{-5}	4.8×10^{-6}	1.0×10^{-4}	5.1×10^{-5}	1.5×10^{-4}
Zooplankton (freshwater)	2.3×10^{-4}	1.2×10^{-5}	1.9×10^{-5}	9.5×10^{-5}	1.3×10^{-4}	2.6×10^{-5}	2.7×10^{-5}	2.3×10^{-7}	6.9×10^{-5}	7.8×10^{-5}	6.3×10^{-5}	4.1×10^{-6}	4.2×10^{-5}	3.6×10^{-6}	4.8×10^{-5}	4.5×10^{-5}	7.6×10^{-5}
Zooplankton (marine)	4.2×10^{-4}	2.7×10^{-5}	1.9×10^{-5}	1.2×10^{-4}	1.5×10^{-4}	2.9×10^{-5}	2.8×10^{-5}	2.5×10^{-7}	9.4×10^{-5}	1.3×10^{-4}	6.9×10^{-5}	4.2×10^{-6}	4.4×10^{-5}	3.8×10^{-6}	5.6×10^{-5}	4.9×10^{-5}	1.2×10^{-4}

Table E-6. Continued. Internal dose conversion coefficients (DCC, (μGy h^{-1})/(Bq $kgfw^{-1}$)) for non-human biota. White background indicates no change from SR-PSU, fully saturated red and blue backgrounds correspond to an increase or decrease, respectively, of at least one order of magnitude since SR-PSU. Paler colours represent smaller corresponding changes. Grey background specifies no data in SR-PSU.

	Eu-152	H-3	Ho-166m	I-129	Mo-93	Nb-93m	Nb-94	Ni-59	Ni-63	Np-237	Pa-231	Pb-210	Pd-107	Po-210	Pu-238	Pu-239	Pu-240
$DCC_{int,\alpha}$										2.8×10^{-3}	2.9×10^{-3}	3.7×10^{-9}		3.1×10^{-3}	3.2×10^{-3}	3.0×10^{-3}	3.0×10^{-3}
$DCC_{int,low,\beta}$	3.3×10^{-6}	2.2×10^{-6}	4.9×10^{-6}	4.8×10^{-6}	1.4×10^{-6}	1.2×10^{-6}	1.0×10^{-7}	2.6×10^{-6}	1.0×10^{-6}	1.2×10^{-5}	7.8×10^{-6}	5.2×10^{-6}	1.5×10^{-6}	4.6×10^{-13}	6.7×10^{-7}	1.4×10^{-6}	6.3×10^{-7}
$DCC_{int,\beta,\gamma}$																	
Amphibian	9.6×10^{-5}	1.1×10^{-6}	1.2×10^{-4}	3.5×10^{-5}	5.5×10^{-6}	1.7×10^{-5}	1.3×10^{-4}	1.3×10^{-6}	9.0×10^{-6}	1.6×10^{-4}	2.8×10^{-5}	2.3×10^{-4}	4.0×10^{-6}	2.8×10^{-1}	6.3×10^{-6}	3.4×10^{-6}	6.2×10^{-6}
Annelid	7.8×10^{-5}	1.1×10^{-6}	9.7×10^{-5}	3.4×10^{-5}	4.0×10^{-6}	1.6×10^{-5}	1.1×10^{-4}	1.2×10^{-6}	9.0×10^{-6}	1.6×10^{-4}	2.7×10^{-5}	2.2×10^{-4}	4.0×10^{-6}	1.5×10^{-1}	6.0×10^{-6}	3.3×10^{-6}	5.9×10^{-6}
Arthropod – detritivorous	6.2×10^{-5}	1.1×10^{-6}	8.2×10^{-5}	3.3×10^{-5}	2.8×10^{-6}	1.6×10^{-5}	9.4×10^{-5}	9.3×10^{-7}	9.0×10^{-6}	1.5×10^{-4}	2.5×10^{-5}	1.9×10^{-4}	4.0×10^{-6}	6.6×10^{-11}	5.8×10^{-6}	3.2×10^{-6}	5.7×10^{-6}
Benthic fish (freshwater)	1.6×10^{-4}	1.1×10^{-6}	2.1×10^{-4}	4.0×10^{-5}	7.2×10^{-6}	1.7×10^{-5}	2.1×10^{-4}	1.3×10^{-6}	9.0×10^{-6}	1.8×10^{-4}	3.2×10^{-5}	2.4×10^{-4}	4.0×10^{-6}	7.9×10^{-1}	6.6×10^{-6}	3.5×10^{-6}	6.4×10^{-6}
Benthic fish (marine)	1.3×10^{-4}	1.1×10^{-6}	1.6×10^{-4}	3.8×10^{-5}	6.8×10^{-6}	1.7×10^{-5}	1.7×10^{-4}	1.3×10^{-6}	9.0×10^{-6}	1.7×10^{-4}	3.1×10^{-5}	2.4×10^{-4}	4.0×10^{-6}	5.3×10^{-1}	6.5×10^{-6}	3.5×10^{-6}	6.4×10^{-6}
Bird	1.6×10^{-4}	1.1×10^{-6}	2.2×10^{-4}	4.0×10^{-5}	7.2×10^{-6}	1.7×10^{-5}	2.2×10^{-4}	1.3×10^{-6}	9.0×10^{-6}	1.8×10^{-4}	3.2×10^{-5}	2.4×10^{-4}	4.0×10^{-6}	8.3×10^{-1}	6.6×10^{-6}	3.5×10^{-6}	6.4×10^{-6}
Crustacean (freshwater)	4.8×10^{-5}	1.1×10^{-6}	7.1×10^{-5}	3.2×10^{-5}	2.3×10^{-6}	1.6×10^{-5}	7.9×10^{-5}	7.0×10^{-7}	9.0×10^{-6}	1.4×10^{-4}	2.4×10^{-5}	1.3×10^{-4}	4.0×10^{-6}	2.6×10^{-11}	5.7×10^{-6}	3.1×10^{-6}	5.6×10^{-6}
Crustacean (marine)	1.5×10^{-4}	1.1×10^{-6}	2.0×10^{-4}	3.9×10^{-5}	7.1×10^{-6}	1.7×10^{-5}	2.0×10^{-4}	1.3×10^{-6}	9.0×10^{-6}	1.8×10^{-4}	3.1×10^{-5}	2.4×10^{-4}	4.0×10^{-6}	7.1×10^{-1}	6.5×10^{-6}	3.5×10^{-6}	6.4×10^{-6}
Flying insects	7.0×10^{-5}	1.1×10^{-6}	8.8×10^{-5}	3.3×10^{-5}	3.4×10^{-6}	1.6×10^{-5}	1.0×10^{-4}	1.1×10^{-6}	9.0×10^{-6}	1.5×10^{-4}	2.6×10^{-5}	2.1×10^{-4}	4.0×10^{-6}	9.8×10^{-11}	5.9×10^{-6}	3.2×10^{-6}	5.8×10^{-6}
Grasses & Herbs	7.6×10^{-5}	1.1×10^{-6}	9.5×10^{-5}	3.4×10^{-5}	3.9×10^{-6}	1.6×10^{-5}	1.1×10^{-4}	1.2×10^{-6}	9.0×10^{-6}	1.6×10^{-4}	2.7×10^{-5}	2.2×10^{-4}	4.0×10^{-6}	1.4×10^{-1}	6.0×10^{-6}	3.3×10^{-6}	5.9×10^{-6}
Insect larvae	4.9×10^{-5}	1.1×10^{-6}	7.2×10^{-5}	3.2×10^{-5}	2.3×10^{-6}	1.6×10^{-5}	8.1×10^{-5}	7.1×10^{-7}	9.0×10^{-6}	1.4×10^{-4}	2.4×10^{-5}	1.4×10^{-4}	4.0×10^{-6}	2.7×10^{-11}	5.7×10^{-6}	3.1×10^{-6}	5.6×10^{-6}
Lichen & Bryophytes	5.9×10^{-5}	1.1×10^{-6}	7.9×10^{-5}	3.3×10^{-5}	2.6×10^{-6}	1.6×10^{-5}	8.9×10^{-5}	8.4×10^{-7}	9.0×10^{-6}	1.5×10^{-4}	2.5×10^{-5}	1.8×10^{-4}	4.0×10^{-6}	5.7×10^{-11}	5.8×10^{-6}	3.2×10^{-6}	5.7×10^{-6}
Macroalgae	8.1×10^{-5}	1.1×10^{-6}	1.0×10^{-4}	3.5×10^{-5}	4.8×10^{-6}	1.6×10^{-5}	1.2×10^{-4}	1.3×10^{-6}	9.0×10^{-6}	1.6×10^{-4}	2.7×10^{-5}	2.1×10^{-4}	4.0×10^{-6}	1.9×10^{-1}	6.2×10^{-6}	3.3×10^{-6}	6.1×10^{-6}
Mammal (freshwater)	2.1×10^{-4}	1.1×10^{-6}	2.9×10^{-4}	4.2×10^{-5}	7.5×10^{-6}	1.7×10^{-5}	2.8×10^{-4}	1.3×10^{-6}	9.0×10^{-6}	2.0×10^{-4}	3.4×10^{-5}	2.4×10^{-4}	4.0×10^{-6}	1.2×10^{-9}	6.6×10^{-6}	3.5×10^{-6}	6.5×10^{-6}
Mammal (marine)	4.3×10^{-4}	1.1×10^{-6}	6.1×10^{-4}	4.6×10^{-5}	7.8×10^{-6}	1.7×10^{-5}	5.9×10^{-4}	1.4×10^{-6}	9.0×10^{-6}	2.5×10^{-4}	4.2×10^{-5}	2.4×10^{-4}	4.0×10^{-6}	3.1×10^{-9}	6.7×10^{-6}	3.6×10^{-6}	6.5×10^{-6}
Mammal – large	4.7×10^{-4}	1.1×10^{-6}	6.5×10^{-4}	4.6×10^{-5}	7.8×10^{-6}	1.7×10^{-5}	6.3×10^{-4}	1.4×10^{-6}	9.0×10^{-6}	2.5×10^{-4}	4.2×10^{-5}	2.4×10^{-4}	4.0×10^{-6}	3.4×10^{-9}	6.7×10^{-6}	3.6×10^{-6}	6.5×10^{-6}
Mammal – small-burrowing	1.3×10^{-4}	1.1×10^{-6}	1.7×10^{-4}	3.8×10^{-5}	6.7×10^{-6}	1.7×10^{-5}	1.7×10^{-4}	1.3×10^{-6}	9.0×10^{-6}	1.7×10^{-4}	3.0×10^{-5}	2.4×10^{-4}	4.0×10^{-6}	5.4×10^{-1}	6.5×10^{-6}	3.5×10^{-6}	6.4×10^{-6}
Mollusc – bivalve (freshwater)	1.1×10^{-4}	1.1×10^{-6}	1.3×10^{-4}	3.6×10^{-5}	6.0×10^{-6}	1.7×10^{-5}	1.4×10^{-4}	1.3×10^{-6}	9.0×10^{-6}	1.7×10^{-4}	2.9×10^{-5}	2.4×10^{-4}	4.0×10^{-6}	3.5×10^{-1}	6.4×10^{-6}	3.4×10^{-6}	6.2×10^{-6}
Mollusc – bivalve (marine)	9.1×10^{-5}	1.1×10^{-6}	1.1×10^{-4}	3.5×10^{-5}	5.2×10^{-6}	1.6×10^{-5}	1.3×10^{-4}	1.3×10^{-6}	9.0×10^{-6}	1.6×10^{-4}	2.8×10^{-5}	2.3×10^{-4}	4.0×10^{-6}	2.4×10^{-1}	6.2×10^{-6}	3.4×10^{-6}	6.1×10^{-6}
Mollusc – gastropod (freshwater)	8.0×10^{-5}	1.1×10^{-6}	9.9×10^{-5}	3.4×10^{-5}	4.3×10^{-6}	1.6×10^{-5}	1.1×10^{-4}	1.2×10^{-6}	9.0×10^{-6}	1.6×10^{-4}	2.7×10^{-5}	2.2×10^{-4}	4.0×10^{-6}	1.6×10^{-1}	6.1×10^{-6}	3.3×10^{-6}	6.0×10^{-6}
Mollusc – gastropod (terrestrial)	7.4×10^{-5}	1.1×10^{-6}	9.3×10^{-5}	3.4×10^{-5}	3.8×10^{-6}	1.6×10^{-5}	1.1×10^{-4}	1.1×10^{-6}	9.0×10^{-6}	1.6×10^{-4}	2.6×10^{-5}	2.2×10^{-4}	4.0×10^{-6}	1.2×10^{-1}	6.0×10^{-6}	3.3×10^{-6}	5.9×10^{-6}
Pelagic fish (freshwater)	1.5×10^{-4}	1.1×10^{-6}	2.0×10^{-4}	3.9×10^{-5}	7.2×10^{-6}	1.7×10^{-5}	2.1×10^{-4}	1.3×10^{-6}	9.0×10^{-6}	1.8×10^{-4}	3.2×10^{-5}	2.4×10^{-4}	4.0×10^{-6}	7.4×10^{-1}	6.5×10^{-6}	3.5×10^{-6}	6.4×10^{-6}
Pelagic fish (marine)	1.4×10^{-4}	1.1×10^{-6}	1.8×10^{-4}	3.9×10^{-5}	6.9×10^{-6}	1.7×10^{-5}	1.9×10^{-4}	1.3×10^{-6}	9.0×10^{-6}	1.8×10^{-4}	3.1×10^{-5}	2.4×10^{-4}	4.0×10^{-6}	6.2×10^{-1}	6.5×10^{-6}	3.5×10^{-6}	6.4×10^{-6}
Phytoplankton & Microphytobenthos	3.6×10^{-5}	1.1×10^{-6}	6.3×10^{-5}	3.1×10^{-5}	2.1×10^{-6}	1.6×10^{-5}	6.1×10^{-5}	6.0×10^{-7}	8.9×10^{-6}	1.3×10^{-4}	2.3×10^{-5}	8.0×10^{-5}	4.0×10^{-6}	9.0×10^{-12}	5.6×10^{-6}	3.1×10^{-6}	5.5×10^{-6}
Polychaete worm	8.3×10^{-5}	1.1×10^{-6}	1.0×10^{-4}	3.4×10^{-5}	4.4×10^{-6}	1.6×10^{-5}	1.2×10^{-4}	1.2×10^{-6}	9.0×10^{-6}	1.6×10^{-4}	2.7×10^{-5}	2.2×10^{-4}	4.0×10^{-6}	1.8×10^{-1}	6.1×10^{-6}	3.3×10^{-6}	6.0×10^{-6}
Reptile (freshwater)	1.6×10^{-4}	1.1×10^{-6}	2.1×10^{-4}	4.0×10^{-5}	7.2×10^{-6}	1.7×10^{-5}	2.1×10^{-4}	1.3×10^{-6}	9.0×10^{-6}	1.8×10^{-4}	3.2×10^{-5}	2.4×10^{-4}	4.0×10^{-6}	7.9×10^{-1}	6.5×10^{-6}	3.5×10^{-6}	6.4×10^{-6}
Reptile (terrestrial)	1.2×10^{-4}	1.1×10^{-6}	1.6×10^{-4}	3.7×10^{-5}	6.5×10^{-6}	1.7×10^{-5}	1.6×10^{-4}	1.3×10^{-6}	9.0×10^{-6}	1.7×10^{-4}	3.0×10^{-5}	2.4×10^{-4}	4.0×10^{-6}	4.7×10^{-1}	6.4×10^{-6}	3.5×10^{-6}	6.3×10^{-6}
Shrub	7.6×10^{-5}	1.1×10^{-6}	9.5×10^{-5}	3.4×10^{-5}	3.9×10^{-6}	1.6×10^{-5}	1.1×10^{-4}	1.2×10^{-6}	9.0×10^{-6}	1.6×10^{-4}	2.7×10^{-5}	2.2×10^{-4}	4.0×10^{-6}	1.4×10^{-1}	6.0×10^{-6}	3.3×10^{-6}	5.9×10^{-6}
Tree	4.2×10^{-4}	1.1×10^{-6}	6.1×10^{-4}	4.6×10^{-5}	7.9×10^{-6}	1.7×10^{-5}	5.7×10^{-4}	1.4×10^{-6}	9.0×10^{-6}	2.5×10^{-4}	4.2×10^{-5}	2.4×10^{-4}	4.0×10^{-6}	3.0×10^{-9}	6.7×10^{-6}	3.6×10^{-6}	6.5×10^{-6}
Vascular plant (freshwater)	5.2×10^{-5}	1.1×10^{-6}	7.3×10^{-5}	3.2×10^{-5}	2.4×10^{-6}	1.6×10^{-5}	7.6×10^{-5}	7.5×10^{-7}	9.0×10^{-6}	1.3×10^{-4}	2.4×10^{-5}	1.5×10^{-4}	4.0×10^{-6}	4.7×10^{-11}	5.7×10^{-6}	3.1×10^{-6}	5.6×10^{-6}
Vascular plant (marine)	9.3×10^{-5}	1.1×10^{-6}	1.2×10^{-4}	3.5×10^{-5}	5.3×10^{-6}	1.6×10^{-5}	1.3×10^{-4}	1.3×10^{-6}	9.0×10^{-6}	1.6×10^{-4}	2.8×10^{-5}	2.3×10^{-4}	4.0×10^{-6}	2.6×10^{-1}	6.2×10^{-6}	3.4×10^{-6}	6.1×10^{-6}
Zooplankton (freshwater)	4.0×10^{-5}	1.1×10^{-6}	6.6×10^{-5}	3.2×10^{-5}	2.2×10^{-6}	1.6×10^{-5}	6.8×10^{-5}	6.5×10^{-7}	8.9×10^{-6}	1.3×10^{-4}	2.3×10^{-5}	9.6×10^{-5}	4.0×10^{-6}	1.3×10^{-11}	5.7×10^{-6}	3.1×10^{-6}	5.6×10^{-6}
Zooplankton (marine)	5.8×10^{-5}	1.1×10^{-6}	7.9×10^{-5}	3.3×10^{-5}	2.7×10^{-6}	1.6×10^{-5}	9.0×10^{-5}	8.8×10^{-7}	9.0×10^{-6}	1.5×10^{-4}	2.5×10^{-5}	1.7×10^{-4}	4.0×10^{-6}	5.2×10^{-11}	5.8×10^{-6}	3.2×10^{-6}	5.7×10^{-6}

Table E-6. Continued. Internal dose conversion coefficients (DCC, (μGy h^{-1})/(Bq $kgfw^{-1}$)) for non-human biota. White background indicates no change from SR-PSU, fully saturated red and blue backgrounds correspond to an increase or decrease, respectively, of at least one order of magnitude since SR-PSU. Paler colours represent smaller corresponding changes. Grey background specifies no data in SR-PSU.

	Pu-241	Pu-242	Ra-226	Se-79	Sm-151	Sn-126	Sr-90	Tc-99	Th-229	Th-230	U-232	U-233	U-234	U-235	U-236	U-238	Zr-93
$DCC_{int,\alpha}$	7.0×10^{-8}	2.9×10^{-3}	1.1×10^{-2}						1.9×10^{-2}	2.7×10^{-3}	1.8×10^{-2}	2.8×10^{-3}	2.8×10^{-3}	2.6×10^{-3}	2.6×10^{-3}	2.5×10^{-3}	
$DCC_{int,low,\beta}$	2.0×10^{-6}	5.4×10^{-7}	2.0×10^{-6}	2.8×10^{-7}	9.4×10^{-7}	3.7×10^{-6}	9.3×10^{-8}	1.6×10^{-7}	1.7×10^{-5}	7.9×10^{-7}	5.1×10^{-6}	6.9×10^{-7}	9.9×10^{-7}	1.4×10^{-5}	9.0×10^{-7}	2.2×10^{-6}	8.2×10^{-7}
$DCC_{int,\beta,\gamma}$																	
Amphibian	1.0×10^{-6}	5.3×10^{-6}	5.5×10^{-4}	3.0×10^{-5}	1.1×10^{-5}	4.9×10^{-4}	5.9×10^{-4}	5.8×10^{-5}	5.1×10^{-4}	8.2×10^{-6}	5.3×10^{-4}	3.2×10^{-6}	7.7×10^{-6}	1.2×10^{-4}	6.4×10^{-6}	4.7×10^{-4}	1.0×10^{-5}
Annelid	1.0×10^{-6}	5.1×10^{-6}	4.8×10^{-4}	3.0×10^{-5}	1.1×10^{-5}	4.2×10^{-4}	5.2×10^{-4}	5.8×10^{-5}	4.9×10^{-4}	8.1×10^{-6}	4.7×10^{-4}	3.0×10^{-6}	7.4×10^{-6}	1.2×10^{-4}	6.2×10^{-6}	4.1×10^{-4}	1.0×10^{-5}
Arthropod – detritivorous	1.0×10^{-6}	4.9×10^{-6}	3.6×10^{-4}	3.0×10^{-5}	1.1×10^{-5}	3.1×10^{-4}	3.5×10^{-4}	5.6×10^{-5}	4.3×10^{-4}	7.9×10^{-6}	3.5×10^{-4}	2.9×10^{-6}	7.2×10^{-6}	1.1×10^{-4}	6.0×10^{-6}	2.8×10^{-4}	1.0×10^{-5}
Benthic fish (freshwater)	1.0×10^{-6}	5.5×10^{-6}	6.6×10^{-4}	3.0×10^{-5}	1.1×10^{-5}	6.2×10^{-4}	6.3×10^{-4}	5.8×10^{-5}	5.5×10^{-4}	8.4×10^{-6}	6.2×10^{-4}	3.3×10^{-6}	7.9×10^{-6}	1.4×10^{-4}	6.6×10^{-6}	5.0×10^{-4}	1.0×10^{-5}
Benthic fish (marine)	1.0×10^{-6}	5.4×10^{-6}	6.0×10^{-4}	3.0×10^{-5}	1.1×10^{-5}	5.5×10^{-4}	6.0×10^{-4}	5.8×10^{-5}	5.3×10^{-4}	8.4×10^{-6}	5.7×10^{-4}	3.3×10^{-6}	7.8×10^{-6}	1.3×10^{-4}	6.5×10^{-6}	4.8×10^{-4}	1.0×10^{-5}
Bird	1.0×10^{-6}	5.5×10^{-6}	6.7×10^{-4}	3.0×10^{-5}	1.1×10^{-5}	6.3×10^{-4}	6.3×10^{-4}	5.8×10^{-5}	5.5×10^{-4}	8.4×10^{-6}	6.3×10^{-4}	3.3×10^{-6}	7.9×10^{-6}	1.4×10^{-4}	6.6×10^{-6}	5.0×10^{-4}	1.0×10^{-5}
Crustacean (freshwater)	1.0×10^{-6}	4.8×10^{-6}	2.4×10^{-4}	2.9×10^{-5}	1.1×10^{-5}	1.9×10^{-4}	2.0×10^{-4}	5.3×10^{-5}	3.4×10^{-4}	7.7×10^{-6}	2.3×10^{-4}	2.8×10^{-6}	7.1×10^{-6}	1.1×10^{-4}	5.8×10^{-6}	1.5×10^{-4}	1.0×10^{-5}
Crustacean (marine)	1.0×10^{-6}	5.5×10^{-6}	6.5×10^{-4}	3.0×10^{-5}	1.1×10^{-5}	6.0×10^{-4}	6.3×10^{-4}	5.8×10^{-5}	5.4×10^{-4}	8.4×10^{-6}	6.1×10^{-4}	3.3×10^{-6}	7.9×10^{-6}	1.3×10^{-4}	6.6×10^{-6}	5.0×10^{-4}	1.0×10^{-5}
Flying insects	1.0×10^{-6}	5.0×10^{-6}	4.3×10^{-4}	3.0×10^{-5}	1.1×10^{-5}	3.7×10^{-4}	4.3×10^{-4}	5.7×10^{-5}	4.6×10^{-4}	8.0×10^{-6}	4.1×10^{-4}	3.0×10^{-6}	7.3×10^{-6}	1.1×10^{-4}	6.1×10^{-6}	3.5×10^{-4}	1.0×10^{-5}
Grasses & Herbs	1.0×10^{-6}	5.0×10^{-6}	4.7×10^{-4}	3.0×10^{-5}	1.1×10^{-5}	4.1×10^{-4}	5.1×10^{-4}	5.7×10^{-5}	4.8×10^{-4}	8.0×10^{-6}	4.6×10^{-4}	3.0×10^{-6}	7.4×10^{-6}	1.2×10^{-4}	6.1×10^{-6}	4.0×10^{-4}	1.0×10^{-5}
Insect larvae	1.0×10^{-6}	4.8×10^{-6}	2.5×10^{-4}	2.9×10^{-5}	1.1×10^{-5}	2.0×10^{-4}	2.1×10^{-4}	5.3×10^{-5}	3.4×10^{-4}	7.7×10^{-6}	2.4×10^{-4}	2.8×10^{-6}	7.1×10^{-6}	1.1×10^{-4}	5.9×10^{-6}	1.6×10^{-4}	1.0×10^{-5}
Lichen & Bryophytes	1.0×10^{-6}	4.8×10^{-6}	3.4×10^{-4}	3.0×10^{-5}	1.1×10^{-5}	2.9×10^{-4}	3.2×10^{-4}	5.5×10^{-5}	4.1×10^{-4}	7.8×10^{-6}	3.3×10^{-4}	2.9×10^{-6}	7.2×10^{-6}	1.1×10^{-4}	5.9×10^{-6}	2.5×10^{-4}	1.0×10^{-5}
Macroalgae	1.0×10^{-6}	5.2×10^{-6}	4.6×10^{-4}	3.0×10^{-5}	1.1×10^{-5}	4.0×10^{-4}	4.7×10^{-4}	5.7×10^{-5}	4.7×10^{-4}	8.1×10^{-6}	4.4×10^{-4}	3.1×10^{-6}	7.5×10^{-6}	1.2×10^{-4}	6.3×10^{-6}	3.7×10^{-4}	1.0×10^{-5}
Mammal (freshwater)	1.0×10^{-6}	5.5×10^{-6}	7.4×10^{-4}	3.0×10^{-5}	1.1×10^{-5}	7.1×10^{-4}	6.4×10^{-4}	5.8×10^{-5}	5.6×10^{-4}	8.5×10^{-6}	6.8×10^{-4}	3.3×10^{-6}	7.9×10^{-6}	1.5×10^{-4}	6.6×10^{-6}	5.1×10^{-4}	1.0×10^{-5}
Mammal (marine)	1.0×10^{-6}	5.6×10^{-6}	1.1×10^{-3}	3.0×10^{-5}	1.1×10^{-5}	1.1×10^{-3}	6.5×10^{-4}	5.8×10^{-5}	6.3×10^{-4}	8.6×10^{-6}	9.4×10^{-4}	3.4×10^{-6}	8.0×10^{-6}	1.9×10^{-4}	6.7×10^{-6}	5.2×10^{-4}	1.0×10^{-5}
Mammal – large	1.0×10^{-6}	5.6×10^{-6}	1.1×10^{-3}	3.0×10^{-5}	1.1×10^{-5}	1.2×10^{-3}	6.5×10^{-4}	5.8×10^{-5}	6.4×10^{-4}	8.6×10^{-6}	9.8×10^{-4}	3.4×10^{-6}	8.0×10^{-6}	1.9×10^{-4}	6.7×10^{-6}	5.2×10^{-4}	1.0×10^{-5}
Mammal – small-burrowing	1.0×10^{-6}	5.4×10^{-6}	6.1×10^{-4}	3.0×10^{-5}	1.1×10^{-5}	5.6×10^{-4}	6.2×10^{-4}	5.8×10^{-5}	5.3×10^{-4}	8.4×10^{-6}	5.8×10^{-4}	3.3×10^{-6}	7.8×10^{-6}	1.3×10^{-4}	6.5×10^{-6}	4.9×10^{-4}	1.0×10^{-5}
Mollusc – bivalve (freshwater)	1.0×10^{-6}	5.3×10^{-6}	5.7×10^{-4}	3.0×10^{-5}	1.1×10^{-5}	5.1×10^{-4}	6.0×10^{-4}	5.8×10^{-5}	5.2×10^{-4}	8.3×10^{-6}	5.5×10^{-4}	3.2×10^{-6}	7.7×10^{-6}	1.2×10^{-4}	6.4×10^{-6}	4.8×10^{-4}	1.0×10^{-5}
Mollusc – bivalve (marine)	1.0×10^{-6}	5.2×10^{-6}	5.4×10^{-4}	3.0×10^{-5}	1.1×10^{-5}	4.7×10^{-4}	5.7×10^{-4}	5.8×10^{-5}	5.1×10^{-4}	8.2×10^{-6}	5.2×10^{-4}	3.1×10^{-6}	7.6×10^{-6}	1.2×10^{-4}	6.3×10^{-6}	4.5×10^{-4}	1.0×10^{-5}
Mollusc – gastropod (freshwater)	1.0×10^{-6}	5.1×10^{-6}	4.9×10^{-4}	3.0×10^{-5}	1.1×10^{-5}	4.3×10^{-4}	5.3×10^{-4}	5.8×10^{-5}	4.9×10^{-4}	8.1×10^{-6}	4.8×10^{-4}	3.1×10^{-6}	7.5×10^{-6}	1.2×10^{-4}	6.2×10^{-6}	4.2×10^{-4}	1.0×10^{-5}
Mollusc – gastropod (terrestrial)	1.0×10^{-6}	5.0×10^{-6}	4.6×10^{-4}	3.0×10^{-5}	1.1×10^{-5}	4.0×10^{-4}	4.9×10^{-4}	5.7×10^{-5}	4.8×10^{-4}	8.0×10^{-6}	4.5×10^{-4}	3.0×10^{-6}	7.4×10^{-6}	1.2×10^{-4}	6.1×10^{-6}	3.9×10^{-4}	1.0×10^{-5}
Pelagic fish (freshwater)	1.0×10^{-6}	5.5×10^{-6}	6.5×10^{-4}	3.0×10^{-5}	1.1×10^{-5}	6.1×10^{-4}	6.3×10^{-4}	5.8×10^{-5}	5.4×10^{-4}	8.4×10^{-6}	6.1×10^{-4}	3.3×10^{-6}	7.9×10^{-6}	1.3×10^{-4}	6.6×10^{-6}	5.0×10^{-4}	1.0×10^{-5}
Pelagic fish (marine)	1.0×10^{-6}	5.4×10^{-6}	6.3×10^{-4}	3.0×10^{-5}	1.1×10^{-5}	5.8×10^{-4}	6.2×10^{-4}	5.8×10^{-5}	5.4×10^{-4}	8.4×10^{-6}	5.9×10^{-4}	3.3×10^{-6}	7.9×10^{-6}	1.3×10^{-4}	6.5×10^{-6}	4.9×10^{-4}	1.0×10^{-5}
Phytoplankton & Microphytobenthos	1.0×10^{-6}	4.7×10^{-6}	1.5×10^{-4}	2.8×10^{-5}	1.0×10^{-5}	1.3×10^{-4}	1.2×10^{-4}	4.8×10^{-5}	2.5×10^{-4}	7.5×10^{-6}	1.6×10^{-4}	2.8×10^{-6}	6.9×10^{-6}	1.0×10^{-4}	5.8×10^{-6}	9.2×10^{-5}	1.0×10^{-5}
Polychaete worm	1.0×10^{-6}	5.1×10^{-6}	5.0×10^{-4}	3.0×10^{-5}	1.1×10^{-5}	4.4×10^{-4}	5.4×10^{-4}	5.8×10^{-5}	4.9×10^{-4}	8.1×10^{-6}	4.9×10^{-4}	3.1×10^{-6}	7.5×10^{-6}	1.2×10^{-4}	6.2×10^{-6}	4.3×10^{-4}	1.0×10^{-5}
Reptile (freshwater)	1.0×10^{-6}	5.5×10^{-6}	6.6×10^{-4}	3.0×10^{-5}	1.1×10^{-5}	6.2×10^{-4}	6.3×10^{-4}	5.8×10^{-5}	5.4×10^{-4}	8.4×10^{-6}	6.2×10^{-4}	3.3×10^{-6}	7.9×10^{-6}	1.4×10^{-4}	6.6×10^{-6}	5.0×10^{-4}	1.0×10^{-5}
Reptile (terrestrial)	1.0×10^{-6}	5.4×10^{-6}	5.9×10^{-4}	3.0×10^{-5}	1.1×10^{-5}	5.4×10^{-4}	6.0×10^{-4}	5.8×10^{-5}	5.3×10^{-4}	8.3×10^{-6}	5.6×10^{-4}	3.2×10^{-6}	7.8×10^{-6}	1.3×10^{-4}	6.5×10^{-6}	4.7×10^{-4}	1.0×10^{-5}
Shrub	1.0×10^{-6}	5.0×10^{-6}	4.7×10^{-4}	3.0×10^{-5}	1.1×10^{-5}	4.1×10^{-4}	5.1×10^{-4}	5.7×10^{-5}	4.8×10^{-4}	8.0×10^{-6}	4.6×10^{-4}	3.0×10^{-6}	7.4×10^{-6}	1.2×10^{-4}	6.1×10^{-6}	4.0×10^{-4}	1.0×10^{-5}
Tree	1.0×10^{-6}	5.6×10^{-6}	1.0×10^{-3}	3.0×10^{-5}	1.1×10^{-5}	1.1×10^{-3}	6.5×10^{-4}	5.8×10^{-5}	6.4×10^{-4}	8.6×10^{-6}	9.2×10^{-4}	3.4×10^{-6}	8.0×10^{-6}	1.9×10^{-4}	6.7×10^{-6}	5.2×10^{-4}	1.0×10^{-5}
Vascular plant (freshwater)	1.0×10^{-6}	4.8×10^{-6}	2.9×10^{-4}	2.9×10^{-5}	1.0×10^{-5}	2.6×10^{-4}	2.8×10^{-4}	5.1×10^{-5}	3.6×10^{-4}	7.7×10^{-6}	2.9×10^{-4}	2.8×10^{-6}	7.1×10^{-6}	1.1×10^{-4}	5.9×10^{-6}	2.3×10^{-4}	1.0×10^{-5}
Vascular plant (marine)	1.0×10^{-6}	5.2×10^{-6}	5.4×10^{-4}	3.0×10^{-5}	1.1×10^{-5}	4.8×10^{-4}	5.8×10^{-4}	5.8×10^{-5}	5.1×10^{-4}	8.2×10^{-6}	5.2×10^{-4}	3.1×10^{-6}	7.6×10^{-6}	1.2×10^{-4}	6.3×10^{-6}	4.6×10^{-4}	1.0×10^{-5}
Zooplankton (freshwater)	1.0×10^{-6}	4.7×10^{-6}	1.8×10^{-4}	2.9×10^{-5}	1.0×10^{-5}	1.5×10^{-4}	1.4×10^{-4}	5.0×10^{-5}	2.8×10^{-4}	7.6×10^{-6}	1.8×10^{-4}	2.8×10^{-6}	7.0×10^{-6}	1.1×10^{-4}	5.8×10^{-6}	1.1×10^{-4}	1.0×10^{-5}
Zooplankton (marine)	1.0×10^{-6}	4.8×10^{-6}	3.3×10^{-4}	3.0×10^{-5}	1.1×10^{-5}	2.7×10^{-4}	2.9×10^{-4}	5.5×10^{-5}	4.0×10^{-4}	7.8×10^{-6}	3.1×10^{-4}	2.9×10^{-6}	7.2×10^{-6}	1.1×10^{-4}	5.9×10^{-6}	2.3×10^{-4}	1.0×10^{-5}

Appendix F

Hydrological simulations with MIKE SHE

This appendix present parameter values derived from MIKE SHE simulations for the *base case* (Section 8.2.4), and for the warm and cold climate cases (see surface and groundwater flow in Sections 8.3.1 and 8.3.2). The appendix also includes the MIKE SHE water balances underlying the parameters for the two variants of the *warm climate calculation case* (Sassner et al. 2022).

F1 Hydrological parameter values

Table F-1. Parameters describing area specific ground and surface water flows for the sea (dark blue), limnic (lake/stream, light blue) and mire (ter, orange) stages in the three biosphere objects 157_2, 157_1 and 116 (m a^{-1}). Parameters were derived from MIKE SHE simulations presented in Werner et al. 2013. New parameters in bold. The values in the first three columns are used in the *base case*, whereas the last column (no stream) is used in one variant of the *alternative landscape configuration calculation case*.

Parameter name	Water flux in biosphere object				Description of water flux (phase)
	157_2[2]	157_1[3]	116[3]	No stream[3,4]	
q_bedrock_low_sea[1]	1.8×10^{-2}	1.1×10^{-3}	2.2×10^{-3}		bedrock to lower regolith (sea)
q_low_bedrock_sea[1]	1.1×10^{-2}	9.9×10^{-4}	1.8×10^{-3}		lower regolith to bedrock (sea)
q_low_gl_sea	2.8×10^{-2}	3.7×10^{-3}	9.5×10^{-3}		lower regolith to glacial clay(sea)
q_gl_low_sea	2.1×10^{-2}	3.6×10^{-3}	9.0×10^{-3}		glacial clay to lower regolith (sea)
q_gl_pg_sea	2.9×10^{-2}	2.0×10^{-2}	3.3×10^{-2}		glacial clay to post glacial clay (sea)
q_pg_gl_sea	2.2×10^{-2}	2.0×10^{-2}	3.2×10^{-2}		post glacial clay to glacial clay (sea)
q_pg_up_sea	3.1×10^{-2}	2.3×10^{-2}	3.8×10^{-2}		post glacial clay to upper sediment (sea)
q_up_pg_sea	2.4×10^{-2}	2.3×10^{-2}	3.7×10^{-2}		upper sediment to post glacial clay (sea)
q_up_wat_sea	3.1×10^{-2}	2.3×10^{-2}	3.8×10^{-2}		upper sediment to water column (sea)
q_wat_up_sea	2.4×10^{-2}	2.3×10^{-2}	3.7×10^{-2}		water column to upper sediment (sea)
q_bedrock_low_lake/stream[1]	1.4×10^{-1}	5.8×10^{-3}	7.3×10^{-3}		bedrock to lower regolith for aquatic part (limnic)
q_low_bedrock_lake/stream[1]	2.8×10^{-2}	2.3×10^{-4}	4.5×10^{-3}		lower regolith to bedrock for aquatic part (limnic)
q_low_gl_lake/stream	1.8×10^{-1}	1.0×10^{-2}	1.8×10^{-2}		lower regolith to glacial clay for aquatic part (limnic)
q_gl_low_lake/stream	4.2×10^{-2}	6.1×10^{-4}	1.7×10^{-2}		glacial clay to lower regolith for aquatic part (limnic)
q_gl_pg_lake/stream	2.2×10^{-1}	1.7×10^{-2}	2.6×10^{-2}		glacial clay to post glacial clay for aquatic part (limnic)
q_pg_gl_lake/stream	7.3×10^{-2}	2.6×10^{-3}	2.6×10^{-2}		post glacial clay to glacial clay for aquatic part (limnic)
q_pg_up_lake/stream	6.4×10^{-1}	1.3×10^{0}	2.2×10^{0}		post glacial clay to upper sediment for aquatic part (limnic)
q_up_pg_lake/stream	4.3×10^{-1}	1.2×10^{0}	2.1×10^{0}		upper sediment to post glacial clay for aquatic part (limnic)
q_up_wat_lake/stream	6.4×10^{-1}	1.3×10^{0}	2.2×10^{0}		upper sediment to water column for aquatic part (limnic)
q_wat_up_lake/stream	4.3×10^{-1}	1.2×10^{0}	2.1×10^{0}		water column to upper sediment for aquatic part (limnic)
q_bedrock_low_ter_iso	1.4×10^{-1}	1.2×10^{-2}	1.3×10^{-2}	1.4×10^{-1}	bedrock to lower regolith for terrestrial part (limnic)
q_low_bedrock_ter_iso	2.8×10^{-2}	5.0×10^{-4}	2.0×10^{-3}	2.8×10^{-2}	lower regolith to bedrock for terrestrial part (limnic)
q_low_gl_ter_iso	1.8×10^{-1}	2.2×10^{-2}	2.8×10^{-2}	1.8×10^{-1}	lower regolith to glacial clay for terrestrial part (limnic)
q_gl_low_ter_iso	4.2×10^{-2}	1.8×10^{-3}	8.9×10^{-3}	4.2×10^{-2}	glacial clay to lower regolith for terrestrial part (limnic)
q_gl_pg_ter_iso	2.2×10^{-1}	4.3×10^{-2}	5.9×10^{-2}	2.2×10^{-1}	glacial clay to post glacial clay for terrestrial part (limnic)
q_pg_gl_ter_iso	7.3×10^{-2}	8.8×10^{-3}	2.6×10^{-2}	7.2×10^{-2}	post glacial clay to glacial clay for terrestrial part (limnic)

Table F-1. Continued.

Parameter name	Water flux in biosphere object				Description of water flux (phase)
	157_2[2]	157_1[3]	116[3]	No stream[3,4]	
q_pg_peat_ter_iso	5.1×10^{-1}	4.8×10^{-2}	6.8×10^{-2}	5.0×10^{-1}	post glacial clay to peat for terrestrial part (limnic)
q_peat_pg_ter_iso	3.2×10^{-1}	1.1×10^{-2}	3.1×10^{-2}	3.1×10^{-1}	peat to post glacial clay for terrestrial part (limnic)
q_peat_up_ter_iso	6.4×10^{-1}	1.4×10^{-1}	1.0×10^{-1}	6.6×10^{-1}	peat to upper peat for terrestrial part (limnic)
q_up_peat_ter_iso	4.3×10^{-1}	1.6×10^{-1}	1.2×10^{-1}	4.1×10^{-1}	upper peat to peat for terrestrial part (limnic)
q_up_wat_ter_iso	1.2×10^{0}	1.1×10^{0}	9.8×10^{-1}	1.2×10^{0}	upper peat to water column for terrestrial part (limnic)
q_wat_up_ter_iso	0.0×10^{0}	1.1×10^{-3}	1.7×10^{-3}	0.0×10^{0}	water column to upper peat for terrestrial part (limnic)
q_downstream_iso	1.2×10^{0}	3.4×10^{0}	1.5×10^{0}	1.2×10^{0}	water column downstream (limnic)
q_bedrock_low_ter_end[1]	1.4×10^{-1}	1.2×10^{-2}	1.0×10^{-2}	1.7×10^{-1}	bedrock to lower regolith for terrestrial part (mire)
q_low_bedrock_ter_end[1]	2.8×10^{-2}	2.5×10^{-4}	2.2×10^{-3}	3.5×10^{-2}	lower regolith to bedrock for terrestrial part (mire)
q_low_gl_ter_end	1.8×10^{-1}	1.7×10^{-2}	1.9×10^{-2}	2.2×10^{-1}	lower regolith to glacial clay for terrestrial part (mire)
q_gl_low_ter_end	4.2×10^{-2}	8.6×10^{-4}	7.9×10^{-3}	4.8×10^{-2}	glacial clay to lower regolith for terrestrial part (mire)
q_gl_pg_ter_end	2.2×10^{-1}	3.1×10^{-2}	3.0×10^{-2}	2.4×10^{-1}	glacial clay to post glacial clay for terrestrial part (mire)
q_pg_gl_ter_end	7.3×10^{-2}	5.2×10^{-3}	1.4×10^{-2}	6.2×10^{-2}	post glacial clay to glacial clay for terrestrial part (mire)
q_pg_peat_ter_end	5.1×10^{-1}	3.3×10^{-2}	3.3×10^{-2}	5.3×10^{-1}	post glacial clay to peat for terrestrial part (mire)
q_peat_pg_ter_end	3.2×10^{-1}	6.1×10^{-3}	1.5×10^{-2}	2.8×10^{-1}	peat to post glacial clay for terrestrial part (mire)
q_peat_up_ter_end	6.4×10^{-1}	2.3×10^{-1}	1.0×10^{-1}	6.9×10^{-1}	peat to upper peat for terrestrial part (mire)
q_up_peat_ter_end	4.3×10^{-1}	2.0×10^{-1}	7.1×10^{-2}	3.9×10^{-1}	upper peat to peat for terrestrial part (mire)
q_up_wat_ter_end	1.2×10^{0}	1.2×10^{0}	1.3×10^{0}	1.3×10^{0}	upper peat to water column for terrestrial part (mire)
q_wat_up_ter_end	0.0×10^{0}	2.6×10^{-3}	1.1×10^{-3}	0.0×10^{0}	water column to upper peat for terrestrial part (mire)
q_downstream_end	1.2×10^{0}	4.3×10^{0}	1.7×10^{0}	1.3×10^{0}	water column downstream in stream phase

1 The flows from and to the bedrock are calculated from the original water balances (Figures A1-31,34, 35 in Werner et al. 2013).

2 The parameters for 157_2 in the terrestrial stage are derived from one water balance with a stream (Figure A1-56 in Werner et al. 2013). Thus, flows at isolation (_iso) and mire completion (_end) have the same values.

3 Data from Grolander 2013 (Table D-1).

4 Parameters for object 157_2 without a stream (corresponding to the *base case* in SR-PSU). Parameter values for sea stage identical to object 157_2 (1st column).

Table F-2. Parameters describing area-specific ground and surface water flows (m a^{-1}) for the warm and cold climate calculation cases. All data are new for the PSAR except the flows in the two taliks (objects 157_1 and 114) in the cold climate case (Grolander 2013, Tables D2 and D3).

	Warm, high percip.			Warm, low precip.			Cold climate		
Parameter name	**157_2**	**157_1**	**116**	**157_2**	**157_1**	**116**	**157_1**	**114**	**157_2**
q_bedrock_low_lake/stream	0.14	0.02	0.01	0.12	0.02	0.01	0.03	0.01	0.00
q_low_bedrock_lake/stream	0.03	0.00	0.00	0.03	0.00	0.01	0.00	0.00	0.00
q_low_gl_lake/stream	0.18	0.03	0.02	0.16	0.03	0.02	0.03	0.01	0.00
q_gl_low_lake/stream	0.04	0.01	0.02	0.04	0.01	0.02	0.00	0.00	0.00
q_gl_pg_lake/stream	0.21	0.04	0.03	0.17	0.04	0.03	0.03	0.01	0.006
q_pg_gl_lake/stream	0.07	0.01	0.03	0.05	0.01	0.03	0.00	0.00	0.006
q_pg_up_lake/stream	0.49	0.84	2.09	0.42	0.80	2.00	0.40	0.06	0.14
q_up_pg_lake/stream	0.35	0.73	2.03	0.26	0.72	1.96	0.02	0.04	0.02
q_up_wat_lake/stream	0.49	0.84	2.09	0.42	0.80	2.00	0.40	0.06	0.14
q_wat_up_lake/stream	0.35	0.73	2.03	0.26	0.72	1.96	0.02	0.04	0.02
q_downstream	0.87	2.80	1.24	0.56	1.82	0.83	4.03	98.8	1.48
q_bedrock_low_ter	0.14	0.01	0.01	0.12	0.01	0.01	0.03		0.00
q_low_bedrock_ter	0.03	0.00	0.00	0.03	0.00	0.00	0.00		0.00
q_low_gl_ter	0.18	0.02	0.03	0.16	0.02	0.03	0.03		0.00
q_gl_low_ter	0.04	0.00	0.01	0.04	0.01	0.01	0.00		0.00
q_gl_pg_ter	0.21	0.04	0.06	0.17	0.05	0.06	0.03		0.006
q_pg_gl_ter	0.07	0.02	0.03	0.05	0.02	0.04	0.00		0.006
q_pg_peat_ter	0.45	0.05	0.07	0.33	0.05	0.07	0.03		0.008
q_peat_pg_ter	0.27	0.02	0.04	0.19	0.03	0.04	0.00		0.006
q_peat_up_ter	0.49	0.14	0.11	0.42	0.12	0.08	0.40		0.14
q_up_peat_ter	0.35	0.17	0.13	0.26	0.14	0.09	0.02		0.02
q_up_wat_ter	0.87	0.88	0.82	0.56	0.57	0.56	3.29		1.48
q_wat_up_ter	0.00	0.00	0.00	0.00	0.00	0.00	0.00		0.00

Table F-3. The fraction of particles released from each waste vault that is captured by a drilled well. The particle capturing ratios were determined from forward particle tracking using a water withdrawal rate of 700 L/day. Data from Table A3-2 and A3-3 in Werner et al. (2013).

	SFR1					SFR3					
Well	**1BTF**	**2BTF**	**1BLA**	**1BMA**	**Silo**	**2BLA**	**3BLA**	**4BLA**	**5BLA**	**2BMA**	**1BRT**
28	0 %	0 %	0.01 %	0.1 %	0 %	0 %	0 %	0 %	0 %	0 %	0 %
21	0 %	0 %	0 %	0 %	0 %	0.001 %	0.02 %	0.1 %	1 %	4 %	0.0004 %
24	0 %	0.03 %	1 %	5 %	0 %	0 %	0 %	0 %	0 %	0 %	0.0001 %
22	0 %	0 %	0 %	0 %	0 %	1 %	1 %	2 %	2 %	1 %	0.1 %
27	1 %	0.01 %	0 %	0 %	7 %	6 %	5 %	4 %	4 %	2 %	3 %
26	2 %	2 %	2 %	2 %	5 %	6 %	3 %	2 %	2 %	2 %	8 %
25	5 %	6 %	6 %	5 %	10 %	9 %	4 %	2 %	2 %	2 %	13 %
23	5 %	1 %	0.5 %	0.02 %	17 %	12 %	10 %	6 %	4 %	3 %	12 %
29	23 %	32 %	31 %	17 %	1 %	2 %	0.4 %	0.1 %	0.04 %	0.04 %	6 %

F2 MIKE SHE modelling results for future warmer conditions

F2.1 Water balances for warm climate with high summer precipitation (5000 AD)

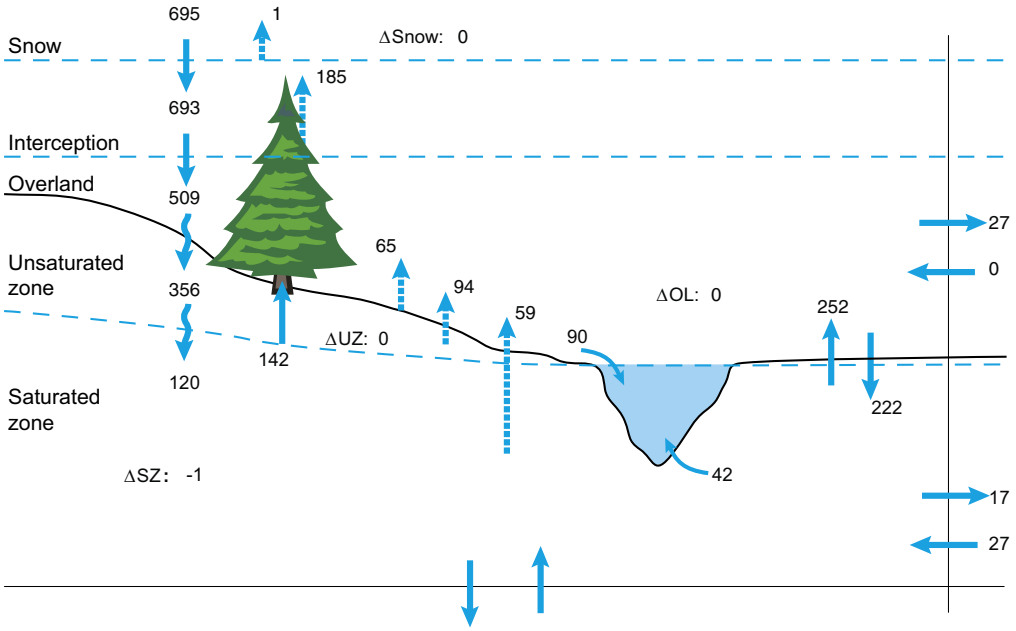

Figure F-1. Water balance (mm a^{-1}) for land areas in the MIKE SHE local model area at 5000 AD for a warm climate with high summer precipitation. Total evapotranspiration is 546 and runoff is 149 (mm a^{-1}).

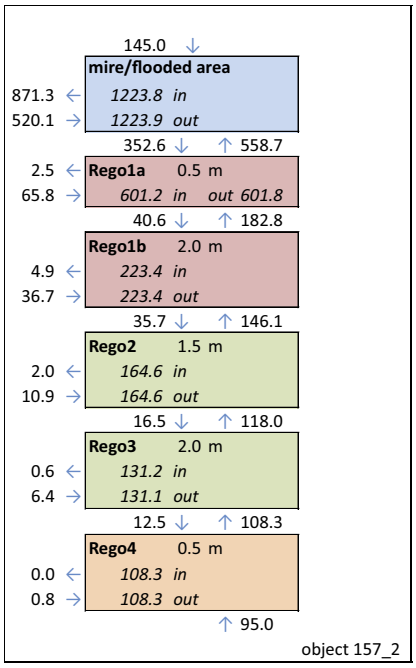

Figure F-2. Water balance (mm a^{-1}) for biosphere object 157_2 at 5000 AD (warm climate with high summer precipitation.

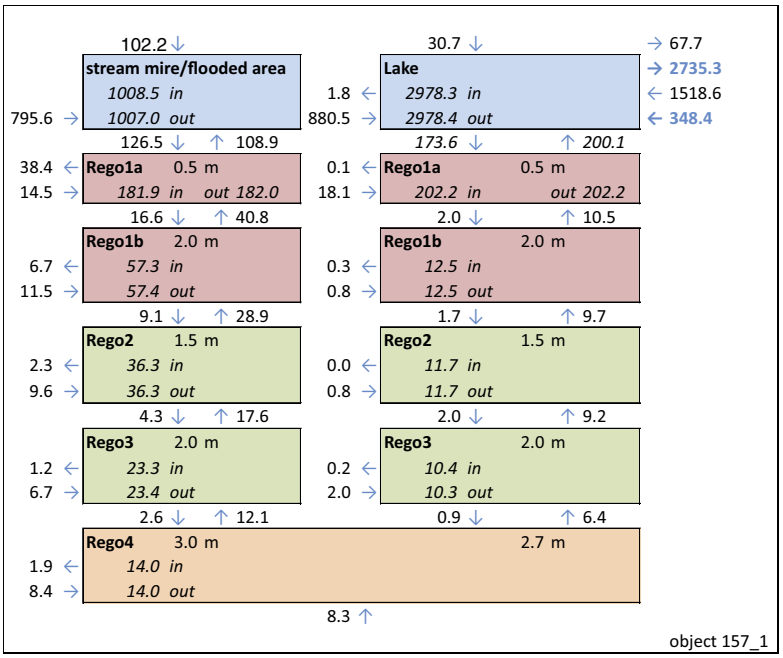

Figure F-3. *Water balance (mm a^{-1}) for biosphere object 157_ 1 at 5000 AD (warm climate with high summer precipitation).*

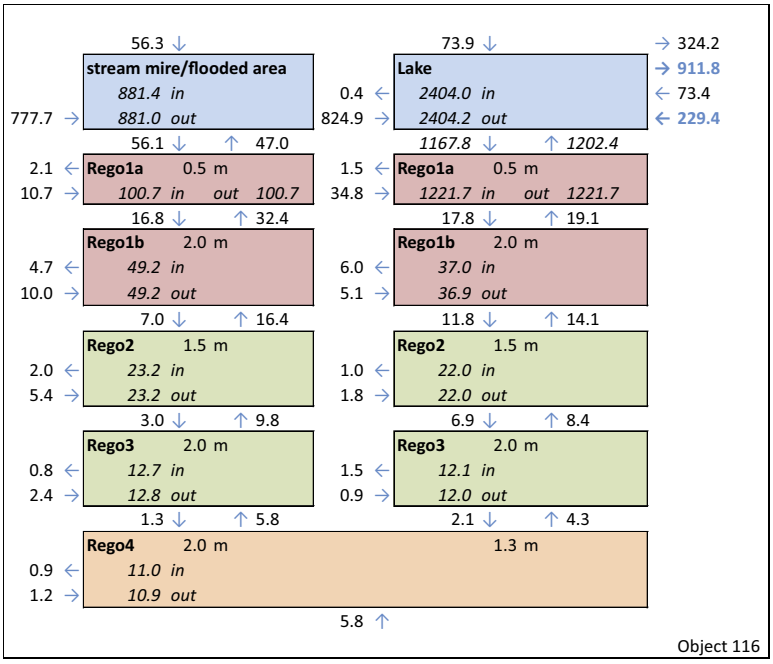

Figure F-4. *Water balance (mm a^{-1}) for biosphere object 116 at 5000 AD (warm climate with high summer precipitation).*

F2.2 Water balances for the warm climate with low summer precipitation (5000 AD)

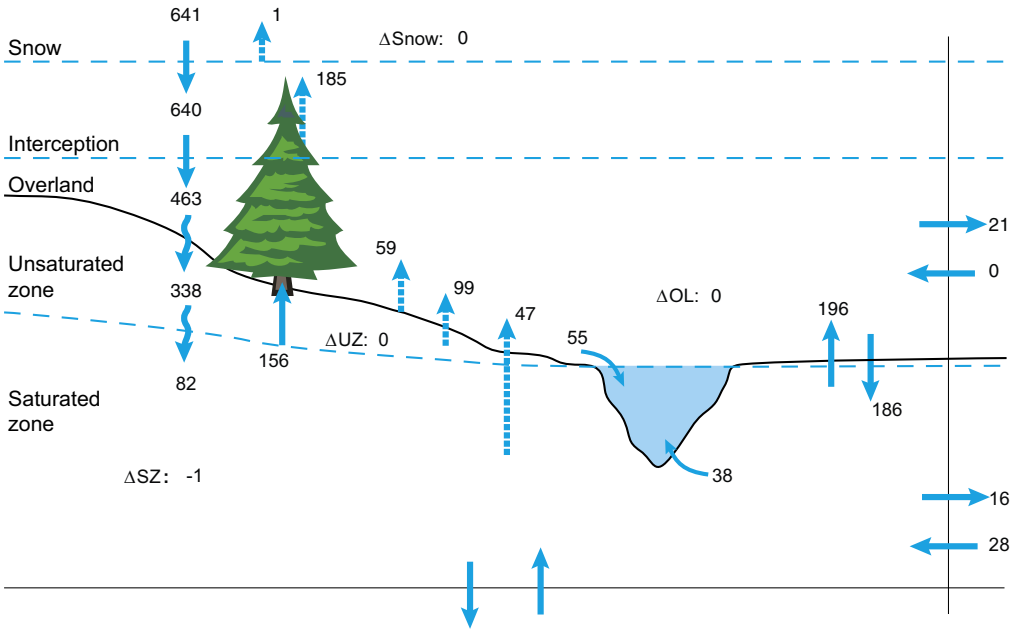

Figure F-5. *Water balance (mm a^{-1}) for land areas in the MIKE SHE local model area at 5000 AD for a warm climate with low summer precipitation. Total evapotranspiration is 540 and runoff is 101 (mm a^{-1}).*

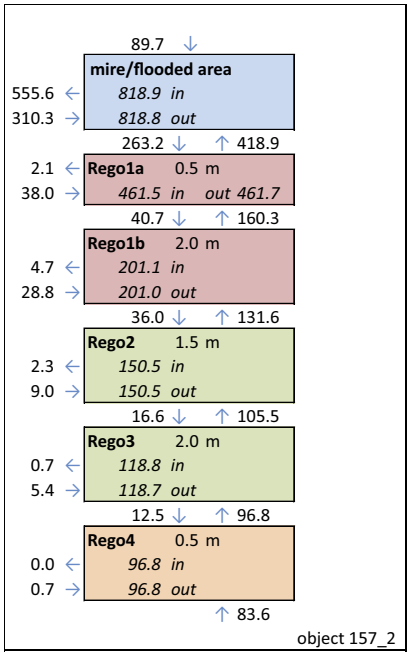

Figure F-6. *Water balance (mm a^{-1}) for biosphere object 157_2 at 5000 AD (warm climate with low summer precipitation.*

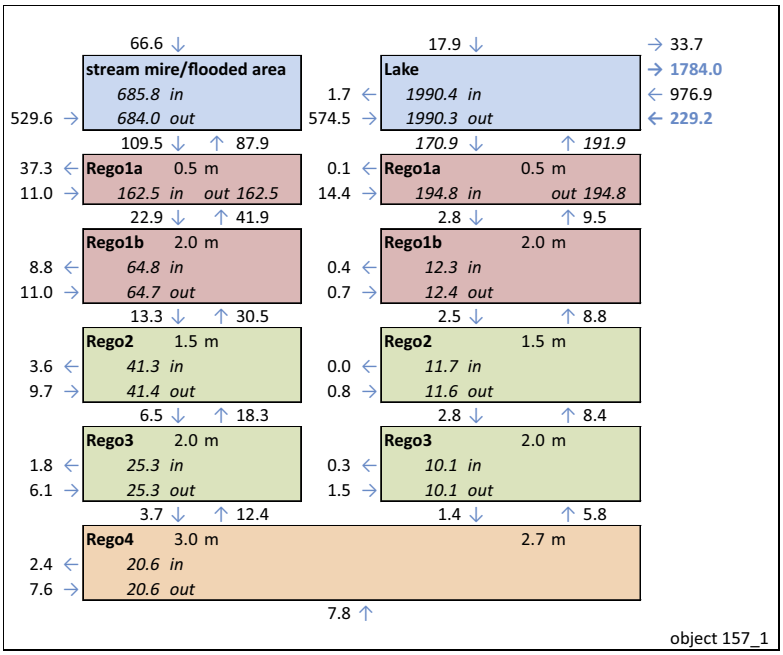

Figure F-7. *Water balance (mm a^{-1}) for biosphere object 157_ 1 at 5000 AD (warm climate with low summer precipitation).*

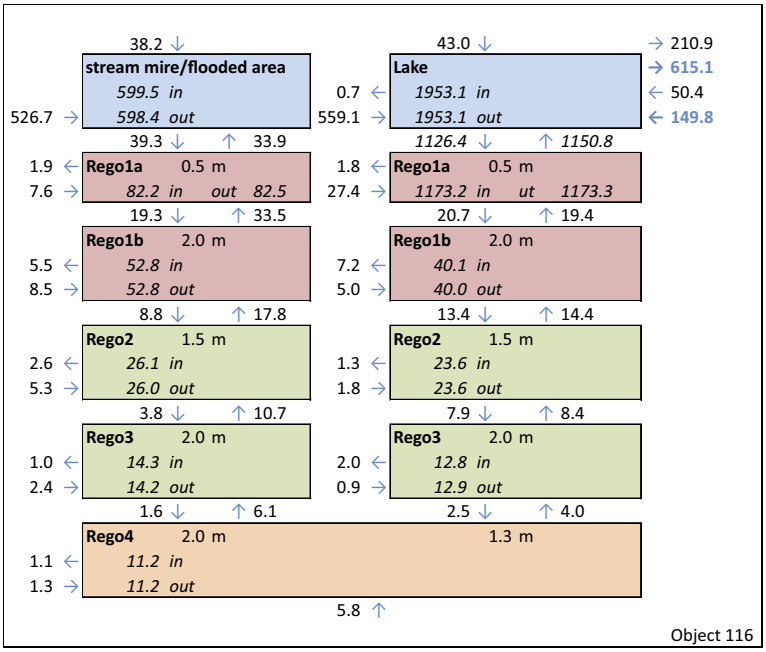

Figure F-8. *Water balance (mm a^{-1}) for biosphere object 116 at 5000 AD (warm climate with low summer precipitation).*

Appendix G

Multi-model projections and uncertainties of irrigation water demand in a warmer climate

G1 Introduction

Global warming is expected to cause large-scale changes to the terrestrial water cycle, affecting, for example, future runoff and crop water demand. In a situation with moderate carbon emissions (comparable to IPCC emission scenario RCP4.5), the annual average temperature at Forsmark may increase by up to 5 °C within this millennium (**Climate report**, Chapter 4). In a scenario, where carbon emissions increase substantially and are maintained at high levels during this and the next century (corresponding to IPCC emission scenario RCP8.5), average temperatures at Forsmark may increase by 7 °C or more within the coming thousands of years.

Potential changes in Europe's water resources due to climate change have been assessed in several studies (e.g. van Vliet et al. 2015, Donnelly et al. 2017). The results indicate substantial variations in hydrological indicators among hydrological models and different climate projections used to force those hydrological models. Due to the large and model-specific uncertainty, several studies, including e.g. Gosling et al. (2011) and Haddeland et al. (2011), have suggested a multi-model approach when climate change impacts are assessed.

Following this recommendation, data for twelve combinations of global climate and hydrological models are used in the PSAR to project the future irrigation demand, as a function of changes in summer temperature and precipitation. The derived relationships are then applied to the postulated conditions in the *warm climate calculation case*, to project future crop water demand, and to assign an uncertainty to the estimates.

G2 Method

Data for this evaluation are provided by the second phase of the Inter-Sectoral Impact Model Intercomparison Project (ISIMIP2, available at https://www.isimip.org/). ISIMIP is an international network of climate-impact modellers that offers a framework for comprehensive and consistent projections of the impacts of climate change across affected sectors and spatial scales.

For this study, temperature and precipitation data from four climate models (*gfdl-esm2m*, *hadgem2-es*, *ipsl-cm5a-lr* and *miroc5*) under RCP8.5 are analysed for two periods; 1981–2005 representing a 25-year historical reconstruction period, and 2080–2099 representing the furthermost 20-year period of the available projections. Three of the hydrological models used (*h08*, *lpjml* and *watergap*) provide estimates of crop water demand (CWD), as described by potential irrigation water consumption. However only one of the hydrological models (*watergap*) provided numerical results for the 0.5° × 0.5° grid cell including Forsmark. Thus, in addition to the local scale, data for all the three models are also extracted at the level of Scandinavia (5°E–35°E; 55°N–70°N).

The average difference in annual CWD between the projection and the historical period was calculated for each combination of the climate and hydrological model. Similarly, the corresponding changes in the explanatory variables, summer (June, July and August) temperature and summer precipitation were calculated. Changes in temperature are expressed as °C, whereas changes in precipitation and CWD are expressed relative (in %) to the values in the historical period. Using one observation per model combination ensures that all data points can be treated as independent in the following statistical analyses.

First, linear models were used to contrast the amount of systematic variation that can be attributed to climate and hydrological models, respectively. In this analysis, climate and hydrological models were fixed categorical factors, and the analysis was carried out with response on the level of Scandinavia. To see whether the response due to climatic change could be attributed to change in summer temperature and precipitation, the factor of climate model was replaced by these two quantitative variables (used as regressors in the model).

In the final mixed model, data from Forsmark were added, and the additional variable scale (Scandinavia vs Forsmark) was included as a fixed categorical factor. As in the model above, summer temperature and precipitation change were included as regressors. Finally, the factor hydrological model was included as a random variable. This allows the variation caused by the hydrological model to be summed with that of the stochastic (or residual) variation. This model was then used to predict the response in CWD expected due to the projected changes in the temperature and precipitation in the two variants of the *warm climate calculation case*, which are derived from the *warm climate variant* (Table 4-2). All statistical analyses were performed with JMP 15.0 (SAS Institute, Carey, North Carolina, USA).

G3 Results

About 30 % of the variation in the modelled response of the crop water demand (CWD) in Scandinavia can be explained by systematic differences between the driving climate models. The projected future water demand increases for all four climate models. For three of four models, the response is modest and the average increase does not exceed 20 %. However, the response is substantially stronger for the *hadgem2-es* model, and the projected increase in water demand averages 70 % for these climate projections. The differences in response between the climate models can be explained as linear effects of temperature and precipitation changes (> 95 % of between model variation). Thus the 70 % increase in water demand observed in the *hadgem2-es* simulations corresponds to a relatively large projected increase in summer temperature (7 °C) and a 15 % decrease in summer precipitation, whereas summer precipitation increases in all other climate projections.

Systematic differences between the hydrological models explain more than 60 % of the variation in the crop water demand response projected in Scandinavia. This is consistent with the results for the studied period (2080–2099) for other parts of the world (Wada et al. 2013). For two of the hydrological models (*h08* and *water gap*), the water demand increases substantially (~50 %), whereas it on average decreases by 20 % for the *lpjml* hydrological model. The reduced water demand in *lpjml* is likely related to the assumption that crop water use efficiency increases with elevated atmospheric CO_2 levels.

As stated above, most of the differences in crop water demand response between climate models can be explained by changes in the average summer temperature and precipitation. As only one model projected provided numerical results of crop water demand for the grid cell encompassing Forsmark, these results (4 simulations) are combined with results from Scandinavia (12 simulations) into one analysis[73]. The regression model can estimate the response in crop water demand from the simulations with a relatively good precision ($r^2 = 0.92$, left panel in Figure G-1). In this linear approximation, water demand increases with temperature ($\Delta CWD/\delta T = 6$ % per °C) and decreases with increasing summer precipitation ($\Delta CWD/\delta P = -1.4$ % per %). Moreover, the analysis shows that the increase in water demand in Forsmark was 26 % higher than in the rest of Scandinavia[74].

The regression model was then used to calculate the projected change in CWD for the *warm climate calculation case* at the Forsmark grid cell (using the average output from all three hydrological models) (Right panel in Figure G-1). That is, the summer temperature is assumed to increase by 4.1 °C, and the summer precipitation increases by 17 % or decreases by 13 % (*low summer precipitation* variant) (see Section 10.2). This results in an increased CWD of 28 % in the first case, whereas the corresponding increase in the *low summer precipitation* variant is 71 %. The random variation due to hydrological models is nine times larger than that of stochastic (or residual) variation. Adding the two variance components results in a standard deviation of the response in crop water demand of 45 %.

[73] To derive estimates that are unbiased, hydrological model and spatial scale of results are also included in the statistical model.

[74] The regression used to predict the change in crop water demand in Forsmark was thus: $\Delta CWD\ (\%) = 28 + 6 \times \Delta T\ (\%) - 1.4 \times \Delta P\ (\%)$, where ΔT and ΔP is changes in temperature and precipitation, respectively.

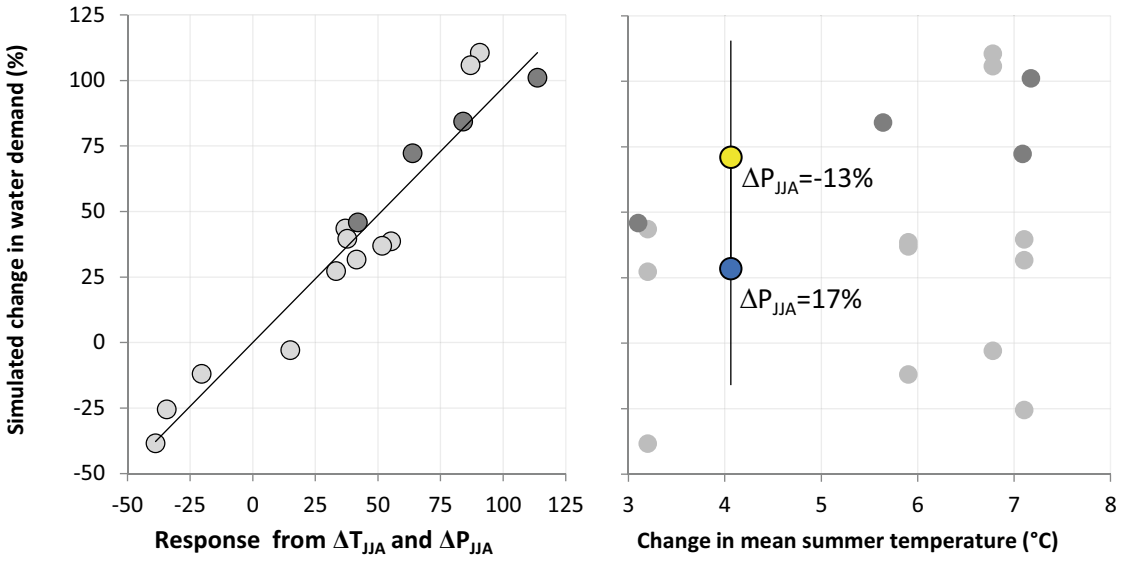

Figure G-1. *Response in crop water demand as a function of change in summer temperature and summer precipitation. Left: fit of regression model shown by plotting the simulated water demand from twelve combinations of climate and hydrology models against the predicted response (r^2 = 0.92). Light grey circles represent simulation results from Scandinavia, whereas dark grey circles represent results from the Forsmark grid cell. Right: coloured circles show the projected change in water demand for the two variants of the warm climate calculation case. The blue circle represents a climate with increased summer precipitation, whereas the yellow circle represents a climate with decreased summer precipitation. Error bars represent the standard deviation, which primarily reflects the uncertainty in projections between hydrological models (see text for details). Lighter and darker grey circles correspond to the change in water demand in the simulations shown in the left panel.*

Appendix H

Parameter files used in the BioTex model

This appendix lists all parameter files used in the BioTex model for the *base case*. The parameters are organized in files according to their context and the files are stored at SVN at SKB.

In folder svn\SFR\SR-PSU15\Synthesis\Parameters are the following files:

File "AquaticEcosystem.xlsm"

The file comprises of parameters related to aquatic ecosystems. These include parameters related to fish and crayfish, mineralization rate, gas exchange, and concentration and/or fraction of chlorine, carbon, suspended matter and organic matter.

File "Drilled_well.xlsm"

The file comprises of parameters strictly related to a well drilled into the bedrock. These include the water extraction rate, and parameters describing the fractions of the release reaching the well from individual SFR waste vaults.

File "ElementSpecific.xlsm"

The file comprises of all the parameters that have specific values for the individual elements. These include sorption coefficients (K_d) and organism concentration ratios (*CR*), as well as diffusion coefficients, and transfer coefficients (*TC*) to meat and milk.

File "HumanCharac.xlsm"

The file comprises of parameters related to different potentially exposed groups postulated to inhabit the Forsmark area including garden-plot household, drained-mire and infield-outland farming and foragers. The file includes parameters such as group size, fraction of different foods in the diet, area needed to support the groups and food and water ingestion rate.

File "IngrowthMatrix.xlsx

The file includes tables for the relative ingrowth of decay products for three potentially exposed groups; Drained-mire farmers and garden-plot household (50 years), and infield-outland farmers (500 years).

File "lobj_10_Grepen_lobj_1_Baltic_sea.xlsm"

The file includes parameters related to the properties of Öregrundsgrepen and the Baltic Sea, such as water volume, area and depth.

File "OS_lt.xlsx"

The file comprises of object specific and time dependent parameters that describes the landscape development. The parameter values are primary output from the regolith lake development model (RLDM) or have been calculated from this output. The parameters include geometric properties, e.g. areas of terrestrial and aquatic ecosystems, water depth, and thickness of clay-gyttja and peat, and rates for sedimentation, resuspension and lateral peat ingrowth. Biomasses and net primary production of benthic and pelagic organisms have been calculated for aquatic ecosystems.

File "OS_q.xlsm"

The file comprises of object specific hydrological parameters. These parameters have been derived from water balances generated with the MIKE SHE tool and describe area specific water flows between different regolith compartments, and to and from the water column. The flows are listed separately for three ecosystems (sea, lake, mire), and for the mire ecosystems, values for two time points are included.

File "OS_tt.xlsm"

The file includes object specific parameters (that do not vary in time). These are related to the area of the objects in the terrestrial stage, and to regolith thicknesses that do not change over time (e.g. till and glacial clay). The file also contains time points when shifts in ecosystems (marine-lake-mire) are initiated and/or completed, and times describing when a well can be dug and the mire drained for cultivation.

File "Regolith.xlsm"

The file comprises of parameters connected to regolith properties, including, density, porosity, and water saturation. For cultivation of a drained mire, soil compaction and trenching depth are also listed.

File "TerrestrialEcosystem.xlsm"

The file comprises of parameters related to terrestrial ecosystems, including mire ecosystems and cultivated land. The parameters describe the basic structure (e.g. plant biomass, canopy height, leaf area index and soil depth), and function of ecosystems (e.g. primary production, translocation, respiration, mineralization and gas exchange), and human utilization of the ecosystems (e.g. wood fuel consumption, sustainable yield of plants, game and crops, as well as irrigation practices). The file also contains carbon concentrations, ingestion rates of cattle and rudimentary hydrological parameters for arable land (e.g. groundwater uptake from the saturated zone and percolation).

File "WF_landscape.xslx"

The file includes object specific and time dependent parameters that describe the water flow between neighbouring sea basins (including exchange with Öregrundsgrepen and the Baltic Sea). The data is the primary output from oceanographic flow modelling with the MIKE 3 FM tool.

In folder svn://svn.skb.se/PSU/PSAR/RNT-Data/Independent-of-system/ is the following file:

File "DCC.xlsx"

The file includes radionuclide specific parameters for dose coefficients with respect to external exposure, inhalation and ingestion.

In folder svn://svn.skb.se/PSU/PSAR/RNT-Data/Independent-of-system/Radionuclides are the following files:

File "DecayPairs.xlsx"

The file has the information on parent radionuclides and decay products used in the model.

File "Radionuclides.xlsx"

The file has a list of all radionuclides used in the model.

File "halfLife.xlsm"

The file has the half-lives of all radionuclides used in the model.

Arkitektkopia AB, Bromma, 2023

SKB is responsible for managing spent nuclear fuel and radioactive waste produced by the Swedish nuclear power plants such that man and the environment are protected in the near and distant future.

skb.se